**UNIVERSITY OF SOUTHAMPTON**

Faculty of Natural and Environmental Sciences

Chemistry

# The Application of Physics-Based Rescoring in Drug Design

by

**Ioannis Haldoupis**

Thesis for the degree of Doctor of Philosophy

December 2014

UNIVERSITY OF SOUTHAMPTON

**ABSTRACT**

FACULTY OF NATURAL AND ENVIRONMENTAL
SCIENCES SCHOOL OF CHEMISTRY

Doctor of Philosophy

# THE APPLICATION OF PHYSICS-BASED RESCORING IN DRUG DESIGN

By Ioannis Haldoupis

Most drugs exert their action by binding to a macromolecule target, e.g. a protein. Hence estimating the binding affinity, using computer programs, is of utmost importance in the drug design process. Approximate free energy methods such as MM-PBSA/GBSA appear as attractive alternatives to rigorous free energy methodology. Recently, simplified versions of MM-PBSA/GBSA have been shown to give encouraging results for use as a fast rescoring tool of docked poses in the lead optimisation stage. The primary aim of this work is to ascertain the capability of the method in this context. First the reproducibility of a published all-in-one (docking and MM-GBSA rescoring) protocol was assessed. Following this the same five protein-ligand systems as in the published work, were subjected to multiple tests involving a range of docking tools and rescoring protocols with varying solvent models. Robust comparisons using statistical analysis, revealed the method performed overall poorly and inconsistently, showing, amongst other things, a strong sensitivity to starting system configuration. The effect of additional sampling on the performance of the method was investigated by generating Molecular Dynamics (MD) trajectories using both implicit and explicit solvent models. The first was shown to introduce considerable noise in the calculations, meanwhile, for the latter, the computational overhead was not justified. Overall we found that MM-PBSA/GBSA does not appear as promising in for routine use in the lead optimisation context, however it may have potential applications in the lead identification stage of drug discovery.

## ACKNOWLEDGMENTS

First and foremost, I would like to thank my academic supervisor and mentor Professor Jonathan W. Essex for his continuous guidance and rigorous scientific training over the course of my PhD studies. Besides being a dedicated teacher, his support, patience and trust he has shown throughout our collaboration, but also the freedom and space to do my research, has been an invaluable experience, that has helped me improve my presentation and communication skills, but one that has also taught me how to work independently and has shaped who I am today. Jon's quality as a person has been an inspiration to me and it has been a great honour having the opportunity to know him and work under his guidance.

I would like to say a special thanks to my industrial supervisor Dr. Xavier Fradera for always been helpful and finding time to assist me with my research. I also want to thank him for his ideas and thoughts and guidance throughout my PhD and our fruitful scientific discussions. I am also grateful for the help of Dr. Brad Sherborne in the early stages of my PhD, but also for giving me the unique opportunity to spend three months as an intern in Boston with Merck&Co. Furthermore, I would also like to thank Dr. Daniel McMasters for his discussions over the time I spent during my internship. Finally, none of this work would have been possible without the generous funding provided by the Merck&Co. company.

I was very fortunate to work in group with many bright individuals who I consider now my friends. I am deeply thankful to everyone in the group. Specifically I would like to thank Dr. Samuel Genheden, Dr. Richard Bradshaw, Dr. Greg Ross, Dr. Christopher Bull, Dr. Michael Carter, Dr. Chris Cave-Ayland, Zohra Ouaray, Michael Criddle, Ana Cabedo Martinez and Donna Goreham for their helpful discussions and for the comfort and encouragement at difficult times.

I would like to thank all my friends along the way who have, each one in their own way, helped. These include in no particular order: Nikos Papadakis,

Athanasios Margiolakis, Dimitris Tsagarakis, Matt Pateman, Katharine Aston, Dr. Alvaro Ruiz Serrano, Samuel Golten, Tonia Minou, Stefanos Maragkos, Ally Hou, Shizuo and Mikiko, Dr. Georgios Orfanoudakis and Dr. Charalampos Tsourakakis. Along with my friends I would like to thank my uncle and auntie, John and Diane Eptas for their support and love over the years.

I am eternally grateful to my parents for everything they offered without asking anything in return. Without their guidance and support I would not be where I am today and most likely I would not have chosen to do a PhD. I could not thank them enough for giving me the education, and personal qualities required to pursue my post-graduate studies.

The next person I would like to thank is my best friend and brother Emmanuel, for always being there when I needed him and for his unconditional love and support. I am deeply honoured and grateful to have him as a brother.

The last paragraph I kept for you Yuki. I thank you for giving a higher meaning in my life and for your selfless love, compassion and support ever since we met. You have been a blessing in my life and I am eternally grateful to have met you. I thank you for believing in me and for making me happy. This PhD would not have been possible without you. Arigatou gozaimashita.

# Contents

# Chapter 1

# Introduction

## 1.1 Introduction

The use of computational methods is common in modern drug discovery.[1] The incremental increase in computer power over the last couple of decades has made possible the study of drug effects at the atomistic level, including the perturbation or modification of a biomolecule such as a protein or a cell membrane. There has been considerable interest from academia and the pharmaceutical industry in methods that can predict the affinity between a small organic molecule (drug or ligand) and a target biomolecule (receptor), for the discovery and optimization of new medications or biological probes.[2, 3]

Traditionally, experimental high-throughput screening (HTS) is used to find active molecules, or hits, that can be subsequently optimized into leads with the required potency, solubility, etc. Typically, attractive lead molecules are the basis of lead optimization programs, where many analogues are synthesized and tested to try to arrive at a drug candidate with optimal pharmacological properties. The whole process from hit to lead, and lead to drug candidate, can be costly and lengthy. Thus, computational approaches

that could predict the binding affinity of new ligands before they are synthesized could be of great value in this context.

Crystal structure determination of the complex (receptor and ligand), usually from x-ray crystallography, has given rise to structure-based drug design (SBDD) as an essential component of drug discovery.[4] Structural data can be used to design tightly binding small molecules that modulate the function of a target biomolecule.[5] Statistical mechanics and the principles of thermodynamics and quantum mechanics are the theoretical bases for methods dealing with such interactions. The application of these principles to computer models has shown a trade-off between rigor and time. This trade-off limits the routine use of more rigorous methods in the pharmaceutical industry. Consequently there is need for the use of simplified, less realistic models, which are nonetheless able to provide useful insights.

Protein-ligand docking methods attempt to predict the binding mode of ligands into the active site of a protein. There are two main aspects to this. The first is to generate a number of protein-ligand configurations, or poses, that explore the available degrees of freedom of the ligand, and optionally the protein. This is often a difficult task due to the large amount of possible ligand and receptor configurations. Secondly, the poses generated, need to be ranked using a simplified scoring function. Poses with a highest ranking should be more likely to correspond to the experimental binding mode of the ligand. Docking methods can be useful to predict binding modes in the absence of structural data for the ligands of interest, and can also be applied in a virtual screening scenario, to prioritize ligands which are more likely to bind to the protein of interest. However, they are not accurate enough for the prediction of binding affinities, and more rigorous approaches are needed for this.

Unfortunately, despite the latest computational advancements, it is still very difficult to use free energy calculations routinely. They are comparatively time-consuming. The large number of degrees of freedom of the flexible protein and ligand make it difficult to complete the sampling and convergence

of the results. Thus, long simulations are required to obtain reliable results. In addition, the size and the complexity of the protein-ligand systems make evaluation of the energy of the system even more expensive. The reason for this is that a substantial portion of the target protein along with surrounding solvent molecules needs to be modelled for meaningful results to be obtained.

The aforementioned reasons make the routine use of free energy calculations on medium or large libraries of compounds impossible. Docking methods can be used at low computational cost, but cannot provide useful estimates of free energies of binding. One of the main reasons for this is that the scoring functions commonly used in docking are not designed for the prediction of free energies and arguably are too simple for this kind of calculations.

As an alternative to rigorous free energy methods, approximate end-point methods were developed. These methods reduce the computational cost by a number of ways, but most importantly by considering only the end states. The most popular of these methods is the methodology studied in this thesis: MM-PBSA/GBSA, developed over a decade ago.[6-8] Owing to methodological challenges, the method was soon simplified further, to be used for qualitative predictions with experiment, in earlier stages of drug design, such as high throughput screening and early stages of lead optimisation.

In recent years, MM-PBSA/GBSA has been used in the refinement of docking outcomes in what has come to be called, physics-based rescoring of docked poses. A number of publications have reported encouraging results, that such an application of the method could play a promising role in early stages of lead optimisation, in qualitatively estimating the binding affinity, but also in improving the ranking of the affinities for a congeneric series of ligands.[9-22]

Our research focused on the application and critical assessment of MM-PBSA/GBSA in the context of a fast physics-based tool for rescoring docked poses in the lead optimisation stage of drug discovery. The methodology was applied on a range of five protein-ligand systems, using different docking

tools, rescoring protocols, and continuum solvation models. Comparisons were performed against experiment and between the various rescoring protocols and solvent models. Statistics was used throughout the thesis to critically assess and quantify the aforementioned comparisons. The effect of sampling was also investigated by running implicit and explicit solvent simulations.

In the course of our investigations, we were able to better understand the workings of the method. We provide an unbiased comparison of a number of solvent models. Furthermore, we elucidate the challenges associated with the application of the method in this context, and ascertain the ability and consistency of the method to qualitatively estimate binding affinities with respect to experiment, and, finally, to determine its capability as a rescoring tool of docked poses.

## 1.2 Thesis outline

The present Ph. D. dissertation is organised into eight chapters (including this chapter). Chapter 2 contains the underlying theory of the methods used in this thesis, and shows how the Boltzmann distribution underlies much of computational chemistry. Chapter 3 is then dedicated to the MM-GBSA methodology. First, each of the components of the method are described, followed by an overview of the literature with respect to the application of the method in drug design from when the method was first conceived, to the present day. Then in chapter 4 the datasets are presented. For each protein-ligand system, an overview of the biological relevance, mechanism of activity in relation to structural characterisation, binding mode architecture and characteristics of the ligand series, will be provided. The results of our research are presented and discussed in Chapters 5-7. In Chapter 5 we show our results from attempting to reproduce an all-in-one published protocol, which claims to be an automated tool in lead optimisation. Having shown the challenges associated with attempting to reproduce one such published work, in Chapter 6, we set out to make a thorough comparison of different solvent

models and rescoring protocols, in a range of docking tools. This is followed by evaluation of the effect of additional sampling described in Chapter 7. Finally in Chapter 8, the thesis is concluded by summarising what we have achieved with our investigations and outline work for future developments. Appendices A and B include information and additional analysis that was not possible to include in the main body of the thesis. Appendix C includes rigorous free energy calculations applied on the systems of Thrombin and HIV-1 Protease. Owing to time constraints full analysis and further investigation of the data was not possible, therefore the results are included in the appendix section of this thesis.

# Chapter 2

# Computational Methods

## 2.1 Introduction

The use of computers and computational methods is common in modern drug discovery.[1] The steady increase in computer power over the last couple of decades has made possible the study of drug effects at the atomistic level. These effects include the perturbation or modification of a biomolecule such as a protein or a cell membrane. This chapter will provide a brief overview of the computational methods that are used to simulate this complex process. The basic physical and mathematical concepts that connect the microscopic world to the macroscopic will be discussed followed by the basics of molecular mechanics and protein-ligand docking. Having established that, the sampling techniques used to simulate protein-ligand systems including Molecular Dynamics (MD) and Monte Carlo (MC), and the associated algorithms, will be summarised. Last, an overview of established methodologies for estimating the free energy of binding will be explored.

## 2.2 Statistical Mechanics

### 2.2.1 Concepts and postulates of statistical mechanics

The discipline of classical thermodynamics has its foundations back in the 1600s with the first vacuum pumps and steam engines. The universe is treated as if it were made up of large-scale continua ignoring the presence of atoms and molecules or other smaller particles. A system, defined by its particles and their average motions, interacts with its surrounding in a certain way. Thermodynamics is a science that deals with macroscopic quantities such as heat, work, entropy of a system and its surroundings. An example of this is the precursor of the ideal gas law by Boyle, introduced in 1661, which related the product of the pressure and volume of a gas to its temperature. Although, thermodynamics leads to a great understanding of the behaviour of the world, owing to its macroscopic theme, it lacks the perception of fine detail to appreciate quantities of the order of magnitude of single particles.[23]

At the other end of the spectrum from thermodynamics, lies the theory of quantum mechanics. This theory accepts that the universe comprises by microscopic particles such as atoms, electrons, protons, etc. The particle behaviour is described probabilistically via the concept of the wave function. Using the Schrödinger equation one can in theory obtain a complete description of the particle behaviour. However in practice, an exact solution is only possible for the hydrogen atom, while when more particles are considered the computational cost increases exponentially, and the problem becomes quickly insoluble.

Statistical mechanics can be used to bridge the classical subject of thermodynamics and the non-classical quantum mechanics. This is done by trying to explain the laws of thermodynamics (macroscopic world) from the mechanical properties of collections of molecules (microscopic world). The linkage between the macroscopic observation and the atomistic reality was

the triumph of physicists Maxwell, Gibbs and, especially Boltzmann, who laid the foundations of statistical mechanics.[23]

To illustrate this theory we can consider a system of interest comprised of a box containing a gas of N particles. In a 6N dimensional space called the phase space and under a given set of conditions (for example, constant volume of the box and constant temperature), the particles can freely adopt different positions and momenta, leading to different microstates. The collection of all these microstates forms an ensemble. In equilibrium, the microstates in that ensemble are distributed according to a probability density of the unique phase-space point comprised of the position and momenta of each N particle. This assertion relies on two important assumptions[24]:

1. The equal *a priori* probability postulate: This postulate states two microstates with equal energy are equally probable.

2. The postulate of *ergodicity*: This postulate states that the time average of a property of a system equals the ensemble average of that property.

### 2.2.2 The Boltzmann Distribution

Much of the following described in this section is taken from pages 560-565 of *Physical Chemistry* by Atkins.[25]

A system of N non-interacting particles is assumed. Each molecule, $n$, may exist in a different state of energy. The configuration of the system changes with time, however some configurations are more likely than others. The microstates of the system increase as N increases. As the microstates increase, so do the microstates within the most probable macrostates. This was expressed numerically by Boltzmann, as the configurational weight of the configuration:

$$W = \frac{N!}{n_0!\, n_1!\, n_2! \ldots} \tag{2.2.1}$$

Where W is the number of microstates in a macrostate, N is the number of particles, and n is the number of particles occupying a specific region of the box.

The question we are interested in answering is which are the most probable configurations of the system, i.e. which configurations contribute the most to the properties observed. To answer this we need to first make two assumptions: a) that any configuration in the same system will have the same total energy, E and, b), the same number of particles. These constraints are shown below:

$$\sum_i n_i \varepsilon_i = E \tag{2.2.2}$$

$$\sum_i n_i = N \tag{2.2.3}$$

Using these constraints and Lagrange's method of undetermined multipliers we can differentiate W with respect to all the populations in the system which gives the following equation:

$$\frac{\partial \ln W}{\partial n_i} + \alpha - \beta \varepsilon_i = 0 \tag{2.2.4}$$

Where $\alpha$ and $\beta$ are constants. Equation (2.2.4) can be solved using Sterling's approximation ($\ln x! \approx x \ln x - x$). Combining this with (2.2.1) gives:

$$\ln W \approx \ln N! - \sum_i (n_i \ln n_i - n_i) \tag{2.2.5}$$

Estimation of the solution for equation (2.2.4) can now begin:

$$\frac{\partial \ln W}{\partial n_i} = -\ln n_i \tag{2.2.6}$$

Substituting the above to (2.2.4), we obtain:

$$-\ln n_i + \alpha - \beta\varepsilon_i = 0 \tag{2.2.7}$$

This gives the most probable population of the state of energy $\varepsilon_i$ as:

$$n_i = e^{\alpha - \beta\varepsilon_i} \tag{2.2.8}$$

Using constraint that any configuration of the system will have the same number of particles ((2.2.3)) we get:

$$N = \sum_i n_i = e^{\alpha} \sum_i e^{-\beta\varepsilon_i} \tag{2.2.9}$$

Finally from the two previous equations we can obtain the Boltzmann distribution:

$$n_i = e^{-\beta\varepsilon_i} e^{\alpha} = \frac{N e^{-\beta\varepsilon_i}}{\sum_i e^{-\beta\varepsilon_i}} \tag{2.2.10}$$

where β is equal to:

$$\frac{1}{k_b T} \tag{2.2.11}$$

where $k_b$ is the Boltzmann constant and T the temperature.

### 2.2.3 The Ensembles of Statistical Mechanics

An *ensemble* is called the collection of all, or a representative subset of, the possible configurations (microstates) of a system. When statistical mechanics is used it is important to define a system ensemble. These ensembles are

constrained by different properties and are commonly categorised as the *canonical* ensemble, the *grand canonical*, *isothermal-isobaric* and *microcanonical* ensemble. Each ensemble has a characteristic state function from which a partition function can be calculated. This function is of utmost importance as all of the thermodynamic variables of a system can be expressed from it.

The *canonical* ensemble, or in other words the constant NVT ensemble, is one where the number of particles, volume and temperature of the system are kept constant, allowing the energy and the pressure to fluctuate. The characteristic state function of this ensemble is the Helmholtz free energy (A).

The *grand canonical* ensemble allows the exchange in particles with a reservoir, fixing the chemical potential, volume and temperature (symbolised by μVT).

The *isothermal-isobaric* (NPT ensemble) although similar to the *canonical* ensemble, in this case the pressure is constrained. This particular ensemble is commonly used in simulations during equilibration for the adjustment of volume. The characteristic state function for this ensemble is the Gibbs free energy (G).

Finally, in the *microcanonical* ensemble the system is isolated from the outside environment (symbolised by NVE). This means the system cannot exchange energy with the environment and due to the second law of thermodynamics the entropy will only increase until equilibrium is reached. This ensemble is also called NVE and is useful for simulation when density equilibration is desired. The characteristic state function for this ensemble is the entropy (S).

### 2.2.4 The Partition Function

The focus on the rest of this section will be on the *canonical* or NVT ensemble (described in the previous section). The main tools of statistical mechanics are the Boltzmann distribution and the partition function. Dividing

the first by the latter gives an expression for the probability density π. The probability distribution for the NVT ensemble is given by the following formula:

$$\pi_{NVT}(i) = \frac{1}{Q_{NVT}} exp(-\beta\varepsilon_i) \tag{2.2.12}$$

Where $\varepsilon_i$ is the energy of state i. The exponential term is a weighting term of an individual state in the ensemble and is known as the Boltzmann factor. This term is normalised when divided by the partition symbolised by $Q_{NVT}$. The distribution described by (2.2.12) is commonly referred to as the Boltzmann distribution. As defined in the previous section, for a finite number of states, the partition function is equal to the sum of all the Boltzmann factors of each state of the system, given by the equation below:

$$Q_{NVT} = \sum_i exp(-\beta\varepsilon_i) \tag{2.2.13}$$

However, for a very large number of states, classical treatment requires continuous properties for the particles, and therefore the configurational integral is defined by:

$$Q_{NVT} = \frac{1}{N!}\frac{1}{h^{3N}} \iint d\boldsymbol{p}^N d\boldsymbol{r}^N exp\big(-\beta E(\boldsymbol{p}^N, \boldsymbol{r}^N)\big) \tag{2.2.14}$$

Where $\boldsymbol{p}^N$ and $\boldsymbol{r}^N$ are the momenta and position of the each particle respectively. The term $\frac{1}{N!}$ is valid when indistinguishable particles are used, as in this case. The variable $h$ is the Planck constant.

The energy consists of the kinetic energy (K) part due to the momenta, and the potential (U) part due to the positions. Since K is a quadratic function of the momenta it can be solved analytically, but this is not the case for U. With the exception of simple cases, U is evaluated through numerical methods, which are mentioned later in this chapter.

Based on the postulates earlier in this section, an observable quantity (macroscopic property) can be taken to be equal to the ensemble average (microscopic property), and therefore one can obtain thermodynamic properties *ab initio*.

## 2.3 Classical Force Fields

Good models for the systems under investigation are required for computer simulations. These models need to be developed in a practical manner. This means to be accurate, yet not too computationally expensive, and to be transferable to a variety of systems[26]. The most accurate models are obtained through Quantum Mechanical (QM) methods. Unfortunately these methods are very slow for our interests in biomolecular modelling, and Molecular Mechanics Force Field are a better choice.

Force fields are the complete set of molecular mechanics terms required to model a system. Such terms include stretching of bonds, angles, torsions and non-bonded interactions. There are a number of force fields developed for biomolecules including OPLS[27], AMBER[28], and CHARMm[29] for example. All are based on similar components, however, differently parameterized. The functional form of a simple force field (there may be additional terms depending on the type of forcefield) contains the following four terms:

$$E_{total} = \sum E_{bond} + \sum E_{angle} + \sum E_{torsion} + \sum E_{non-bonded} \quad (2.3.1)$$

$$\sum E_{non-bonded} = \sum E_{electrostatics} + \sum E_{vdW} \quad (2.3.2)$$

In many cases the first three terms are grouped together to form the bonded term (covalent bonds). The fourth term is usually broken down as in equation (2.3.2)[30]. Each term of the equation is defined below.

Harmonic potentials are usually used to model bond and angle contributions:

$$E_{bond} = \sum_{bonds} k_r(r - r_0)^2 \tag{2.3.3}$$

$$E_{angle} = \sum_{angles} k_\theta(\theta - \theta_0)^2 \tag{2.3.4}$$

where $r$ and $\theta$ represent the bond lengths and valence angles respectively. $r_0$ and $\theta_0$ are the reference values. These are the values that the bond or angle adopt when all the other force field terms are ignored and the isolated term is in equilibrium[30]. The terms $k_r$ and $k_\theta$ are force constants. The energy change caused by a rotation of a dihedral angle is described by the following equation.

$$E_{torsions} = \sum_{torsions} k_n(1 + cos(n\phi - \delta)) \tag{2.3.5}$$

where $\phi$ is the dihedral angle, $k_n$ is a force constant, $\delta$ is the phase angle and $n$ is the multiplicity, which gives the number of minima in the function as angle $\phi$ changes from 0° to 360°. Finally the two terms of the non-bonded interactions are shown combined in equation (2.3.6). The first part of the equation corresponds to the electrostatic potential (Coulomb potential), while the second to the van der Waals (vdW) potential (Lennard-Jones potential).

$$E_{non-bonded} = \sum_{i}^{N-1} \sum_{j=i+1}^{N} \left\{ \frac{q_i q_j}{4\pi\epsilon_0 r_{ij}} + 4\epsilon_{ij} \left[ \left( \frac{\sigma_{ij}}{r_{ij}} \right)^{12} - \left( \frac{\sigma_{ij}}{r_{ij}} \right)^{6} \right] \right\} \tag{2.3.6}$$

where $i$ and $j$ are each pair of atoms, $q_i$ and $q_j$ the corresponding charges, $\varepsilon_0$ the permittivity of free space, $\epsilon_{ij}$ is the Lennard-Jones well-depth energy, $\sigma_{ij}$ the distance between the atoms when their interaction energy is zero and $r_{ij}$ their interatomic distance. The term to the power of 12 corresponds to the repulsive interaction while the term to the power of 6 the attractive interaction; as $r$ gets very small the energy increases sharply and as $r$ is

increased an attractive interaction is observed which then, as $r$ keeps increasing, decreases relatively slowly.

The combination of force-fields is rarely performed, since parameters used within force-fields are commonly derived differently. The Generalised Amber Force Field (GAFF) obtains its parameters through a combination of empirical and quantum mechanical means.[31] Partial charges are typically obtained using a high level quantum theory such as Hartree-Fock calculations, whilst bond lengths are typically obtained by a combination of experimental methods (such as X-ray crystallography) and high level ab initio calculations. Angle bending and torsional terms are obtained using a similar procedure. Other force-fields can be purely empirical, such as the GROMOS force-field in which case non-bonded terms are parameterised to fit experimental properties such as the free energy of hydration, while bonded terms are parameterised purely against crystallographic and spectroscopic data.[32]

***Periodic boundary conditions***

In a protein system there is a vast volume of water and other molecules that need to be taken into account. This increases the complexity and time of simulations. Periodic boundary conditions offer a solution to this by allowing the use of relatively small number of particles when calculating the bulk properties of a system. This is done by placing solute and solvent molecules in a box, which is then replicated in all directions through space. If one particle is to leave the box from one side, it is replaced by an image particle on the opposite side, allowing for the number of molecules in the box to remain the same. Each particle's position is replicated infinitely by multiplying each of its positional vector components (x, y, and z) with integers (i, j, and k). In this manner, surface effects, such as solvent molecules leaving the box, are eliminated.

## 2.4 Simulation sampling methodologies

Having established how to calculate the energy between atoms in the system we now can discuss the methodology that allows us to sample the phase space. The two major sampling methodologies are the MD and MC methods.

### 2.4.1 Molecular Dynamics

Molecular dynamics (MD) is a method used to generate an ensemble of time dependent configurations of the system. This is achieved by generating a trajectory of the simulated system. A starting configuration at a specific point on the energy surface is chosen, and time dependencies calculated by solving Newton's laws of motion. This requires the calculation of 3N coupled, second order differential equations, with N the number of atoms in the system, making analytical methods impossible. Fortunately, numerical integration methods may be used, which allow for repeated integration of the forces over small time intervals to yield a trajectory. The most commonly used algorithms are the velocity Verlet or Verlet *leapfrog* algorithms. The first is considered more complete, as it is able to calculate the velocities and positions at the same time step. The velocity Verlet algorithm is summarised in the following four equations:

$$\boldsymbol{r}\big(t+\delta(t)\big) = \boldsymbol{r}(t) + \ \boldsymbol{v}(t)\delta t + \frac{1}{2}\boldsymbol{\alpha}(t)\delta t^2, \tag{2.4.1}$$

$$\boldsymbol{v}\left(t+\frac{\delta t}{2}\right) = \boldsymbol{v}(t) + \frac{1}{2}\boldsymbol{\alpha}(t)\delta t, \tag{2.4.2}$$

$$\boldsymbol{\alpha}(t+\delta t) = -\frac{1}{m}\nabla U\big(\boldsymbol{r}(t+\delta t)\big), \tag{2.4.3}$$

$$\boldsymbol{v}\ (t+\delta t) = \boldsymbol{v}\left(t+\frac{\delta t}{2}\right) + \frac{1}{2}\boldsymbol{\alpha}(t+\delta t)\delta t. \tag{2.4.4}$$

Where, $r$ is the position of a particle, $v$ is the velocity of the particle, and $\alpha$ is the acceleration of the particle. Considering that using Newton's laws the energy should be conserved, the trajectories are sampled under the NVE ensemble. To sample at a constant temperature (NVT ensemble) or at constant pressure (NVP ensemble) a thermostat or barostat is needed, respectively. According to one of the fundamental axioms of statistical mechanics, the assumption of ergodicity, the time trajectory will be equal to the ensemble average, after sufficient time.

The timestep is an important variable to take into consideration. Time step is defined by the smallest oscillation period in the system. The values that the time step takes are therefore in the femtosecond range to account for the oscillation of hydrogen bond atoms, which in the case of organic molecules is the smallest oscillation period. If the chosen value for the timestep is very large, the integrator will not be stable (as the forces will change too quickly), leading to loss of energy conservation. If too small the sampling of the system will be insufficient. Usually (including in this work) a 2 fs (femtosecond) is used, enabled by the SHAKE algorithm[33] which, in our implementation of the algorithm, applies a constraint on bonds involving hydrogen, as these have a higher vibrational frequency. The value of the timestep is therefore a limiting factor regarding the timescales that can be achieved. This means MD simulations are in danger of being stuck in local energy minima, which can be very difficult to get out of in the simulation time available. Despite this, MD being deterministic, i.e. that the preceding configurations can be found from the current configuration, it is able to give dynamic information, for example diffusion constant, unlike the stochastic MC calculations.

### 2.4.2 Monte Carlo

Another method that is aimed towards generating an ensemble of configurations is Monte Carlo (MC). In contrast to the deterministic approach of MD, MC is stochastic. That means that it randomly generates many

configurations of the system which are then weighted according to their probability of occurring.

### 2.4.3 Metropolis Monte Carlo

There are many methods that calculate the probabilities of the generated configurations, however, one of the most important ones is the Metropolis method[34]. In fact it is so important that an MC simulation is chemistry usually refers to a Metropolis MC simulation. The algorithm works as follows:

1. Start in state i and calculate the energy at the present configuration
2. Make a random change to i giving configuration j with a probability $p_{ij}$
3. Calculate the energy at the new configuration j
4. Accept the move with a probability of $\alpha_{ij} = min(1, \chi)$ where $\chi = (\pi_i/\pi_j)$
5. If the move is accepted set i = j, otherwise i = i
6. Add energy to average and return to 1
7. Terminate after a number of iterations or when the average is converged

To yield a Boltzmann distribution of states by MC, the probability of moving from configuration i to j before weighting by $\pi_i$ and $\pi_j$ is equal to the probability of moving form j to i. This is referred to as observing detailed balance or as microscopic reversibility [35]. When this is followed the acceptance test of moving from state i to j is:

$$\frac{\pi_j}{\pi_i} = \frac{exp(-\beta U_j)/Z_{N,NVT}}{exp(-\beta U_i)/Z_{N,NVT}} = \exp\left(-\beta(U_j - U_i)\right) \qquad (2.4.5)$$

If the energy of the new configuration j is lower than i, then the new state is accepted. On the other hand, if this is not the case, a random number between 0 and 1 is obtained, the ratio of Boltzmann factor of state j over state i is calculated and compared to that number. If the ratio is smaller than that number then the move is accepted, otherwise add the energy of the previous state to the average and proceed by generating a new configuration from that previous state. The process is repeated until the maximum number of iterations is met.

## 2.5 Docking and scoring in structure based drug design

Docking methodology attempts to provide solutions to the problem of predicting the binding mode of a small molecule, within the active site of a target protein.[36] Used in virtual screening, large datasets (thousands or even millions) of lead-like molecules are screened against a receptor of interest, to yield a smaller set for further analysis. Docking can be viewed as a multi-step process with two major aims: accurate prediction of binding modes, and correct ranking of diverse ligands. First, a quick search of the conformational space is performed by generating large numbers of conformations for each molecule. Docking is computationally a really challenging process and this step is certainly not an exception. Even small organic molecules can have large numbers of degrees of freedom and hence sampling these configurations accurately and quickly for thousands of molecules can be challenging. The problem is more complex when incorporating flexibility of the ligand and the protein. Proposed solutions for the latter include: a pragmatic multiple conformation approach (create an ensemble of dockings on distinct, experimentally derived proteins and choose the best pose), an automatic or *de novo* prediction of small sidechain movements, or prediction of large-scale

movements in cases where conformational changes are associated with the mechanism of the protein and known to occur in related proteins[4]. However, protein flexibility is often ignored due to the huge increase in search space which translates to higher computation times. There are numerous algorithms developed to treat ligand flexibility which can be grouped into three categories: systematic (incremental construction, conformational search, databases); stochastic methods (Monte Carlo, genetic algorithms, tabu search); and simulation methods (molecular dynamics, energy minimization)[37]. It is then determined whether these conformations, in various orientations, can fit in the active site. This is called *posing*.

A *scoring function* is a function that can estimate the interaction between ligand and protein. They are used within the docking algorithm to generate a number of poses for each ligand, providing a rough estimation of the position of a ligand in the binding site. Ranking, the second step, is the ordering of a number of the poses obtained from the first stage, using the same scoring function, or a second one specific to this. Depending on the implementation, a wide range of scoring functions exist, but can typically be classified in three main categories: force-field-based, empirical and knowledge-based scoring functions.

### 2.5.1 Force Field based scoring functions

Existing molecular mechanics force fields are employed to estimate the internal conformational energy of the ligand and interactions between a ligand and a receptor. Both of these contributions are based on van der Waals and electrostatic terms. There are significant limitations that come with these methods. Some include the exclusion of entropic contributions and desolvation effects, but also cut-offs have to be applied for non-bonded interactions which results in increased complexity of the treatment of long range interactions. Additionally minimisations are required before scoring can be applied, due to the rugged energy landscape associated with the force field potentials, which

adds to the computation time.[4] An attempt to tackle some of these issues, is the specific generation of force field parameters. Recent functions also include a torsional entropy term for ligands in G-Score[38] and the addition of explicit hydrogen bonding terms in Gold[39] and Autodock[40] which are thought to increase the potential for molecular recognition.[37]

### 2.5.2 Empirical scoring functions

The thinking behind these functions is based on the idea that the free energy of binding can be approximated as a sum of a number of chemically relevant contributions. Each term is multiplied by its own coefficient (weight) derived from regression analysis using experimental binding free energies.[4] An inherent drawback of any regression-based scoring function is the dependence of the weights on the dataset used for the regression. As a consequence recombination of terms from different scoring functions into a new scoring function can be difficult. These functions are similar (but typically simplified) to a non-bonded force field potential including hydrogen bonding terms, ionic interactions, hydrophobic effects and the internal energy of the ligand. The additive rationale of these methods results in larger ligands scoring better than smaller ones, which also applies to forcefield based methods. However larger ligands, due to increased number of rotatable bonds, have higher entropic penalties in the bound state. Some scoring functions like ChemScore[41] include additional terms such as ligand rotational entropy or terms to account for desolvation penalty such as in Fresno.[32] However, only incomplete descriptions of these effects are provided by current functions.[37] When compared to forcefield methods, due to their simple energy terms, these methods perform much faster in calculating the scores.

### 2.5.3 Knowledge based scoring functions

Essentially these potentials are formed by extracting statistical information about protein-ligand binding modes from structural data. These binding

modes are then correlated to the free energy of binding using statistical mechanics. These potentials are generally called potentials of mean force (PMF). The attractiveness of these methods is due to: computational simplicity enabling the processing of large data sets; and that, PMF potentials capture binding effects implicitly using a term to take into account volume occupied by the ligand. The disadvantage is that using limited sets of protein-ligand complex structures, the diversity of protein binding sites and ligand functional groups is not reflected. Additionally, other disadvantages include that pairwise additivity of free energy contributions is assumed, and that the Boltzmann inversion used to extract the PMF from the distance distributions, assumes the distances are all derived from the same ensemble, which is not true. DrugScore[42] is an example of a PMF method which is derived from protein-ligand complexes from the PDB Date Bank.

### 2.5.4 Consensus scoring

*Consensus scoring*[43] is a pragmatic approach to improve scoring accuracy by combining two or more scoring functions for the same data set to balance out the errors from the individual functions and reduce the number of false positives. They work well when the combined scoring functions describe different aspects of the binding and are of comparable quality.[4] In contrast, errors can be intensified when terms in different scoring functions are highly correlated.[37]

Owing to the diversity of docking algorithms a rigorous comparison can be difficult.[44] Although, docking can give very different binding conformations of ligands, there have been tests that show that on average 70% of the time the binding modes correlate well with experiment (in this study the core of the ligands is kept rigid to the crystal structure and therefore similar binding modes are expected).[36] The combination of docking with early scoring functions and the speed of this method make it a good tool for the search of new inhibitors and for differentiating good binding ligands from poor binders

or non-binders. On the other hand, this is not the case when having to calculate affinity differences between related ligands.[42] The scoring functions presented previously fail to produce accurate binding free energies.[45] This is mainly due the fact that they are simple functions trying to provide a solution for a very complicated problem. Apart from the numerous issues associated, such as the treatment of water molecules, overestimated charge-charge interactions, scoring functions, lack proper consideration of solvation and entropic effects. A recent assessment of docking and scoring programs shows clearly and unambiguously that significant improvements are necessary before compound ranking by docking algorithms will become a reliable method for lead optimization[46]. This could become a reality *in silico* if there were a method to provide accurate and consistent binding affinities at a low computational cost. Recent methods attempt this by rescoring the docking score using a more physics-based approach.

## 2.6 Free Energy Methods

### 2.6.1 Calculating the free energy

The free energy is perhaps the most important quantity of all thermodynamic quantities. It is the driving force behind chemical processes, determining the direction of spontaneous change. The benefits of being able to predict this quantity cannot be overstated. It allows the ability to predict properties such as solvation, binding of a ligand to a host, stabilities, environmental effect on reactions and many other properties.

In the case of protein-ligand binding, experimental affinities are measured via the association constant ($K_a$). At equilibrium and under standard conditions the free energy is related to the equilibrium constant:

$$\Delta G = -RT \ln K_a \tag{2.6.1}$$

Where R is the gas constant and T the absolute temperature. Usually the limit for usable data is an error of 1 kcal $mol^{-1}$, which corresponds to an error in $K_a$ of less than one order of magnitude.

In this thesis $\Delta G$ is used as a general notation, irrespectively if it is a Helmholtz free energy or a Gibbs free energy.

In the case of the canonical ensemble the free energy is given by the following integral:

$$exp(-\beta A) = \frac{1}{N!\,h^{3N}} \int_{-\infty}^{+\infty} exp\Big(-\beta H(\boldsymbol{p}^N, \boldsymbol{r}^N)\Big) d\boldsymbol{p}^N d\boldsymbol{r}^N \qquad (2.6.2)$$

Where h is Plank's constant, $\mathbf{p}$ is the momentum of particle $N$ and $\boldsymbol{r}$ the position of the particle $N$.

Unfortunately solution to the integral above is not possible with the current sampling methods and computational resources. Also, since MD and MC mostly sample low energy regions of the phase space, high energy states that contribute to the binding free energy are not sampled adequately.

Thus special methods have been devised that can be used to calculate the relative free energy differences between two systems instead of the absolute free energy change. These methods can be broadly grouped into two categories, the rigorous free energy methods and the approximate free energy methods. Each will be discussed in the rest of this chapter.

### 2.6.2 Rigorous free energy methods

#### Free Energy Perturbation

Zwanzig derived a method of calculating the free energy differences between two systems from the partition functions of each system as follows[47]:

$$\Delta G_{A \to B} = G_B - G_A$$

$$= \left(-\frac{1}{\beta}\ln Q_B\right) - \left(-\frac{1}{\beta}\ln Q_A\right)$$

$$= -\frac{1}{\beta}\ln\left[\frac{Q_B}{Q_A}\right]$$

$$= -\frac{1}{\beta}\ln\left[\frac{\int \exp\left(-\beta U_B(r^N)\right)dr^N}{\int \exp\left(-\beta U_A(r^N)\right)dr^N}\right]$$

multiplying by $1 = \exp\left(-\beta U_A(r^N)\right)\exp\left(\beta U_A(r^N)\right)$

$$= -\frac{1}{\beta}\ln\left[\frac{\int \exp\left(-\beta U_B(r^N)\right)dr^N \times \exp\left(-\beta U_A(r^N)\right)\exp\left(\beta U_A(r^N)\right)}{\int \exp\left(-\beta U_A(r^N)\right)dr^N}\right]$$

$$= -\frac{1}{\beta}\left[\int \frac{exp\left(-\beta U_A(r^N)\right)}{Q_A} \times exp\left(-\beta \Delta U_{AB}(r^N)\right)dr^N\right]$$

$$= -\frac{1}{\beta}\left[\int \pi_A(r^N) \times exp\left(-\beta \Delta U_{AB}(r^N)\right)dr^N\right]$$

$$= -\frac{1}{\beta}\ln\left\langle exp\left(-\beta \Delta U_{AB}(r^N)\right)\right\rangle_A \tag{2.6.3}$$

Where $\pi_A(r^N)$ is the Boltzmann probability of configuration q in the ensemble state A, $\Delta U_{AB}$ is the difference in energy between system A and B and $<>_A$ symbolises the ensemble average over system A and $\Delta U_{AB}$ represents the difference between potentials $U_B$ and $U_A$.

The computational implementation of this equation is called free energy perturbation (FEP).[5] The difference between the potential energy of the systems A and B can be found by either using single or dual topology.[5] The first is the case where a molecule A is morphed to molecule B, while the latter describes the case where both molecules are present and one is switched on as the other is switched off. Single topology is accurate only when small transformations occur, and dual topology can in theory be used with any two

molecules. However, the system may interact differently with each molecule, causing increased noise in the potential energy difference.

A difficulty that arises when using the Zwanzig equation is when the phase space of systems A and B is too different. If the low energy regions of B are in portions of phase space corresponding to high energy regions of A, then a simulation run with potential $U_A$ will rarely generate the significant configurations of potential $U_B$. As a result, the free energy change $\Delta G_{A \to B}$ is likely to be overestimated. Any difference between those two values is termed as hysteresis. Large hysteresis is diagnostic for a poor approximation of the free energy difference between the two systems.

The way to tackle this is to ensure that there is a good overlap of the phase space between systems A and B. This is achieved by linking the transition from one system to the other to a parameter λ. This parameter takes intermediate values from 0, which corresponds to system A, to 1, which corresponds to system B. Therefore, the Zwanzig equation can be rewritten as the sum of the resulting free energy differences. The FEP is then described by the following equation:

$$G_B - G_A = \Delta G = \sum_{\lambda=0}^{1} -\frac{1}{\beta} \ln \langle exp\{-\beta \Delta U_{AB}(r^N)\} \rangle_{\lambda_k} \tag{2.6.4}$$

### Thermodynamic integration

In the thermodynamic integration approach (TI) the change of free energy is calculated across the λ trajectory and is equal to the ensemble average of the gradient of force field, as per the formula below:

$$G_{\lambda=1} - G_{\lambda=0} = \int_0^1 \left(\frac{\partial G}{\partial \lambda}\right)_\lambda d\lambda = \int_0^1 \left\langle \frac{\partial U}{\partial \lambda} \right\rangle_\lambda d\lambda \tag{2.6.5}$$

The resulting integral can then be evaluated numerically, e.g. using the trapezium rule.

### Finite Difference Thermodynamic Integration

Instead of calculating the ensemble average of the gradient of the force field analytically, one can do this numerically via the finite difference which is essentially a combination of FEP and TI. Instead of the partial derivative of the free energy of gradient, the finite difference approximation is used, calculating the gradient at λ+Δλ and at state λ-Δλ; where the Δλ is normally given a small value, for example 0.001.

Performing this, the following formula is obtained:

$$\Delta G = \int_0^1 \langle \frac{\Delta U}{\Delta \lambda} \rangle_\lambda \; d\lambda \tag{2.6.6}$$

Similarly as in TI, the total free energy change is obtained by numerically integrating over the computed values.

### Replica Exchange Thermodynamic Integration

Replica exchange thermodynamic integration (RETI) is the development of combining FDTI with Hamiltonian replica exchange moves between λ window simulations adjacent on the λ coordinate.[48, 49] For detailed balance to apply, the λ moves are accepted or rejected based on the following metropolis test:

$$exp\{\beta[U_B(j) - U_B(i) - U_A(j) + U_A(i)]\} \geq rand(0,1) \tag{2.6.7}$$

Where $i$ and $j$ are the configurations being exchanged and A and B are the Hamiltonians of the replicas exchanging.

RETI increases sampling especially of the solvent by providing the possibility of configurations making large jumps in phase space. Also, as simulations are able to move freely across λ, configurations which are more favourable to a particular area of λ may migrate there .[48, 49]

### 2.6.3 Approximate free energy methods

Thus far in this chapter we have concentrated on the rigorous free energy methods for estimating the binding affinity of protein ligand systems. These methods are deemed rigorous on the basis they remain theoretically loyal to the principles of statistical mechanics. On the downside, their set up and application can be tedious and time consuming. As a result there has been an interest in the development of approximate methodology to estimate the free energy of binding. Such methods are also called end-point method utilising the fact that the free energy is a state function and thus only consider the start and end of the change. Two of the most known methods are Linear Interaction Energy (LIE) and MM-PBSA/GBSA. In this chapter only LIE will be covered as a detailed account of the latter appears in the next chapter.

#### Linear interaction energy

The Linear Interaction Energy method (LIE) [50], allows the estimation of the absolute binding free energy of a ligand to a protein based on just two simulations. One is of the ligand free in solution, and the other is of the ligand bound to the protein. The absolute binding free energy, ΔG, is estimated using the following equation:

$$\Delta G = 0.5\langle \Delta U_{elec} \rangle + \alpha \langle \Delta U_{vdw} \rangle \qquad (2.6.8)$$

Where $\langle \Delta U_{elec} \rangle$ and $\langle \Delta U_{vdw} \rangle$ are the averages of the difference in electrostatic and van der Waals energy, respectively, between the ligand and the environment in the two simulations. The Linear Response approximations provides the factor 0.5.[50] The linear relationship with the van der Waals energy was justified by the linear relationship between the number of carbons in an n-alkane, and its free energy of solvation. The value of the parameter $\alpha$ in equation (2.6.8) was originally determined by a fit to the experimental binding free energy of a series of endothiapepsin inhibitors and a value of 0.161 was thus derived.[50]

Though the method has shown positive results in some cases, the overall consensus is there are no universal parameters that can predict the binding free energies of different protein ligand complexes.[1, 51] Thus the equation would need to be retrained for each system studied, which is an expensive procedure with the prerequisite of a large number of pre-determined experimental protein-ligand binding free energies.

## 2.7 Summary

This chapter has provided an overview of available computational methods including the ones used in this study. The ultimate basis of all this work is the theory of statistical mechanics, which, with its postulates, enables our computational models to be related to experimental observations.

Both MD and MC methodologies are utilised in this work taking into account the advantages and disadvantages of each. MD, since it is easily parallelised, is used to introduce sampling in the rescoring techniques used in this thesis, while MC's ability to perform novel sampling schemes, due to its stochastic nature, is utilised in the rigorous free energy methodology applied here (see appendix C).

The next chapter is devoted to the methodological details of the method mostly used in this work (MM-PBSA/GBSA) including a review of the

current literature. The origins of the methodology will be shown and the motivation behind this work will be discussed.

# Chapter 3

# MM-PBSA/GBSA: Background and Review

## 3.1 Introduction

In the previous chapter, the underlying methodological basis for the work presented in the thesis was introduced. Along with the foundations of computer simulations, such as statistical mechanics, and common simulation sampling methods, such as molecular dynamics (MD) and Monte Carlo (MC) methods, a short review of existing methods for obtaining absolute and relative protein-ligand binding affinity estimates was discussed. Free energy methods were split in rigorous and approximate methods, of which, for the latter, one popular method, namely linear interaction method (LIE), was given as an example. In this chapter, the most well-known end-point implicit solvent method, the molecular mechanics with Poisson-Boltzmann or Generalised Born and surface-area solvation (MM-PBSA/GBSA) will be thoroughly discussed. First, the polar and non-polar components of implicit solvation utilised in this methodology will be addressed followed by a detailed account of the various ways this method can be applied to estimate the free

energy of binding. Having established the theoretical background of MM-PBSA/GBSA, a review of its application in drug design, from when it was first used in 1998[52] to the current date, will be presented, followed by an overview of the limitations and the motivation for the work conducted in this thesis. Owing to the vast amount of literature available on this subject, the review will be concise highlighting only the most important developments. It should also be noted at this point that although both MM-PBSA and MM-GBSA will be discussed, the emphasis will be on the latter, considering it was the method used for the majority of this thesis.

## 3.2 Continuum solvation

Many biomolecular functions occur in an aqueous environment. Accurate computer simulation methods, such as the free energy perturbation (FEP) and thermodynamic integration (TI) methods, discussed in the previous chapter, represent the solvent with a large number of molecules, or in other words explicitly. The number of water molecules is in the thousands for a protein to be properly solvated, resulting in the majority of the simulation time being spent on computing non-bonded interactions for solvent molecules. This makes such calculations very computationally expensive, which is complimented by the use of complicated methodology such as periodic boundary conditions and Ewald summation for the purpose of avoiding artificial boundary effects[30]. One of the most common methods to reduce the computational cost and improve the convergence is to treat solvent effects implicitly, using continuum solvent methods.

In this case the solvent is considered as a high-dielectric continuum (with dielectric constant $\varepsilon$=78 or 80) interacting with charges that are embedded in solute molecules of lower dielectric ($\varepsilon_i$=1). The solute response to the reaction field of the solvent dielectric can then be modelled by applying laws of classical electrostatics.[35] There are commonly two ways to model these electrostatic interactions; the more regorous Poisson-Boltzmann (PB)

equation, and the more approximate generalised Born (GB) approach, giving rise to the so-called MM-PBSA and MM-GBSA variants, respectively.

Both of these approaches were adopted in this work and are presented in the next sections.

### 3.2.1 The Poisson-Boltzmann equation

The PB model method is one of the most accurate ways to investigate the electrostatic properties of biological molecules such as proteins and DNA[53]. The Poisson equation relates the variation in the potential $\boldsymbol{\phi}$ at a given point $\boldsymbol{r}$, within a homogeneous medium with dielectric constant $\boldsymbol{\varepsilon}$ to the charge density $\rho$ i.e. the distribution of charge throughout the system:

$$\nabla^2\phi(\boldsymbol{r}) = -\frac{4\pi\rho(\boldsymbol{r})}{\varepsilon} \tag{3.2.1}$$

For a set of point charges under a constant dielectric the equation resembles Coulomb's law[30]. In the case where the dielectric is not constant and varies with the position $\boldsymbol{r}$, the Poisson equation is correctly written as:

$$\nabla\varepsilon(\mathbf{r}) \bullet \nabla\phi(\mathbf{r}) = -4\pi\rho(\mathbf{r}) \tag{3.2.2}$$

However, the Poisson equation is valid under conditions of zero ionic strength and must therefore, in the case where mobile ions are present, be modified to account for the dispersal of those ions as a result of the electric field. The ion distribution is described by the following Boltzmann distribution:

$$n(\boldsymbol{r}) = \mathcal{N}\exp(-\mathcal{V}(\mathbf{r})/\mathrm{k_B T}) \tag{3.2.3}$$

Where $n(\boldsymbol{r})$, $\mathcal{N}$, $\mathcal{V}(\boldsymbol{r})$, $\mathrm{k_B}$, $T$ represent the number density of ions at a particular location $\boldsymbol{r}$, the bulk number density and the energy change when

bringing the ion from infinity to position $\boldsymbol{r}$, the Boltzmann's constant, and the temperature respectively. Incorporation of these effects in the Poisson equation results to the Poisson-Boltzmann equation:

$$\nabla\varepsilon(\mathbf{r}) \bullet \nabla\phi(\mathbf{r}) - \varepsilon(\mathbf{r})\ \lambda(\boldsymbol{r})\kappa^2 \frac{k_B T}{q} \sinh\left[\frac{q\phi(\boldsymbol{r})}{k_B T}\right] = -4\pi\rho(\mathbf{r}) \qquad (3.2.4)$$

Where, $q$ is the magnitude of the charge of the electrolyte ions, $\boldsymbol{\lambda}$ is a switching function controlling the regions accessible to the electrolyte, and $\boldsymbol{\kappa^2}$ is the Debye-Hückel parameter equal to:

$$\kappa^2 = \frac{8\pi q^2 I}{\varepsilon\ \mathrm{k_B} T} \qquad (3.2.5)$$

Where $I$ is the ionic strength of the electrolyte solution. The inverse of $k$ is also known as Debye length[54].

The hyperbolic sine function in equation (3.2.4) can be expanded as a Taylor series, and by taking only the first term in the expansion gives the linearised Poisson-Boltzmann equation[30] as shown below:

$$\nabla\varepsilon(\mathbf{r}) \bullet \nabla\phi(\boldsymbol{r}) - \varepsilon(\boldsymbol{r})\ \lambda(\boldsymbol{r})\ \kappa^2\ \phi(\boldsymbol{r}) = -4\pi\ \rho(\boldsymbol{r}) \qquad (3.2.6)$$

Having an equation to estimate the electrostatic interactions between a solute molecule and solvent is important, but what is more important is solving it, which is where the challenge lies with equation (3.2.6). Initially, prior to the advancement of computers, spherical geometry was used to solve the equation analytically. Models such as spheres were used for proteins, cylinders for DNA, planes for membranes.[8, 30] Following the development of computational techniques numerical solutions were possible, including finite element, boundary element, and finite difference methods. The latter is commonly used and was first applied on a grid of proteins in 1982[55] to solve the Poisson equation, and later the Honig group used it to solve the Poisson-

Boltzmann equation for systems with different ionic strengths[56], which was incorporated in the popular DelPhi program.

In such a method, the charge distribution and the dielectric constant are discretised over a cubic lattice which is superimposed onto the solute and the surrounding solvent. There are a number of finite difference methods that have been used to numerically solve the PB equation[55, 56], however what they all have in common is that they are computationally intensive. This is mainly due to the slow convergence of the procedure and the very large number of grid points.[53] A technique called *focusing*[30], i.e. using $\alpha$ multi-grid[8, 57], deals with the latter, which enables better estimates of the potential values at the boundary (between the solute and solvent) to be obtained. Despite attempts to make this method more convenient, it still remains computationally expensive for medium throughput calculations like those explored in this thesis.

One of the more efficient and approximate methods proposed as a less computationally demanding, but less accurate, alternative to PB is the GB method. The following section will showcase the origins of this method, the Born equation.

### 3.2.2 The Born equation

In 1920, Born described the electrostatic component of the free energy of solvation by placing a charge within a spherical solvent cavity.[58] He showed that an equation to obtain the electrostatic energy of an isolated ion, can be derived directly from classical electrostatic theory. The derivation presented here was taken from the first chapter of Classical Electrodynamics by John David Jackson.[59]

The electrostatic energy in a dielectric medium is defined by the following equation:

$$G = \frac{1}{8\pi}\int_V \vec{E}\vec{D}dV \tag{3.2.7}$$

With:

$$\vec{D} = \varepsilon\vec{E} \tag{3.2.8}$$

Where $\vec{D}$ is the electric displacement, $\vec{E}$ the electric field, $\varepsilon$ the dielectric constant, and $dV$ an element of volume.

Gauss's Law can be used to relate the electric field to the total charge Q that lies within a closed surface $\vec{S}$, using the following integral:

$$\int_S \vec{E}d\vec{S} = \frac{Q}{\varepsilon} \tag{3.2.9}$$

Now let us assume a sphere of radius $\alpha$ with an interior dielectric of $\varepsilon_{vac}$. Using equations (3.2.8) and (3.2.9) one can obtain the following if $r < \alpha$:

$$\vec{E}_{int} = 0 \quad and \quad \vec{D}_{int} = 0 \tag{3.2.10}$$

and if $r > \alpha$:

$$\vec{E}_{out} = \frac{kq}{\varepsilon_{vac}r^3}\vec{r} \quad and \quad \vec{D}_{out} = \frac{kq}{r^3}\vec{r} \tag{3.2.11}$$

Where $k$ is the Coulomb constant, which is equal to $\frac{1}{4\pi\varepsilon_o}$.

The total electrostatic energy of the system can be obtained by substituting equations (3.2.10) and (3.2.11) in equation (3.2.7), which gives:

$$G_{vac} = \frac{k^2}{8\pi\varepsilon_{vac}}\int_{out}\frac{q^2}{r^4}dV \tag{3.2.12}$$

This can be integrated from $\alpha$ to infinity to give:

$$G_{vac} = \frac{q^2 k^2}{2\varepsilon_{vac}\alpha} \tag{3.2.13}$$

A similar relationship as equation (3.2.13) is obtained if the same sphere has an exterior dielectric of $\varepsilon_{solv}$ with the subscript 'vac' replaced by 'solv'. The electrostatic energy required to transfer a charged ion with radius $\alpha$ from a medium dielectric $\varepsilon_{vac}$ to a dielectric of $\varepsilon_{solv}$ is given by taking the difference between the energies at those two dielectric mediums, and is called the Born Equation:

$$\Delta G_{born} = -\frac{q^2 k^2}{2\alpha}\left(\frac{1}{\varepsilon_{vac}} - \frac{1}{\varepsilon_{solv}}\right) \tag{3.2.14}$$

### 3.2.3 The generalised Born model

The generalized Born model treats each atom as a sphere of a radius $\alpha_i$, a charge $q_i$, and dielectric $\varepsilon_i$. Assuming that the atoms appear as point charges (separated by a large enough distance) the total electrostatic free energy of such a system is the sum of the Coulomb energy and Born solvation energy:

$$G_{tot} = \sum_{i=1}^{N}\sum_{j=i+1}^{N}\frac{q_i q_j}{\varepsilon r_{ij}} - \frac{1}{2}\left(\frac{1}{\varepsilon_{vac}} - \frac{1}{\varepsilon_{solv}}\right)\sum_{i=1}^{N}\frac{q_i^2}{a_i} \tag{3.2.15}$$

However equation (3.2.15) is not applicable for molecular systems where it is common for radii and distances to be very small. To overcome this, Still[60] suggested breaking the Coulomb term into two, one term in *vacuo* and a second term in a dielectric of value $(1 - 1/\varepsilon)$. The second term and the Born solvation free energy term (the second term in (3.2.15)) can be combined in one term to give:

$$\Delta G_{Genborn} = -\frac{1}{2}\left(\frac{1}{\varepsilon_{vac}} - \frac{1}{\varepsilon_{solv}}\right)\sum_{i=1}^{N}\sum_{j=1}^{N}\frac{q_i q_j}{f(r_{ij}, B_{ij})} \tag{3.2.16}$$

Where $r_{ij}$ is the interatomic distance, $q$ the charge of each ion, $\varepsilon_{solv}$ the medium dielectric and $B_{ij}$ the *effective* Born radii (similar to the quantity $\alpha_i$ in previous equations). The function $f$ is defined as:

$$f(r_{ij}, B_{ij}) = \sqrt{r_{ij}^2 + B_{ij}^2 e^{-D}} \tag{3.2.17}$$

Where:

$$B_{ij} = \sqrt{B_i B_j} \quad \text{and} \quad D = r_{ij}^2/(2B_{ij})^2 \tag{3.2.18}$$

Depending on the values of $i$, $j$, and the interatomic distance in comparison to the Born radii, $f$ alters between the Born expression (as r approaches 0), and the Coulomb equation (as r approaches infinity)[61]. The most challenging term to compute is the *effective* Born radius of an atom. This corresponds to the radius that would give the electrostatic energy of the system according to the Born equation if all the remaining atoms in the molecule were unchanged.

Still et al. developed a numerical method to calculate the Born radii, which can be summarised in the following equation:

$$\frac{1}{B_i} = \sum_{x=1}^{N}\frac{A_x}{4\pi r_x^2}\left[\left(\frac{1}{r_x - 0.5T_x}\right) - \left(\frac{1}{r_x + 0.5T_x}\right)\right] + \frac{1}{r_{N+1} - 0.5T_{M+1}} \tag{3.2.19}$$

This algorithm can be described in the following 4 steps:

1. Assume the van der Waals surface of an atom $x$ is surrounded by a shell of thickness $T_x$.

2. Weight the interior radius of this shell by a factor of $r_x - 0.5T_x$ and the exterior radius by $r_x + 0.5T_x$ using the solvent accessible surface

area $A_x$ divided by the actual surface area, and compute their difference.

3. Sum all the differences from the previous step, for equivalent shells N, until the van der Waals surface is reached.

4. There is no weight added for shell N, but rather the radius is added to the sum from the previous step. The resulting value is the effective Born radius that is consequently substituted in (3.2.16).

However, the method described above is time consuming and for this reason various approximate analytical approaches have been developed. One such method is the Pairwise Descreening Approximation (PDA) which is the first of the GB models implemented in AMBER ($GB^{HCT}$ – option igb = 1).[62] It is not within the scope of this review to detail the workings of this method, however it should be mentioned that a scaling factor is used to correct systematic errors because PDA over-estimates the Born radius by not taking into account that two spheres can overlap.[61] However this single parameter correction proved insufficient for small molecules, and the re-scaling of the effective radii was proposed so that the re-scaling parameters be proportional to the degree of the atom's burial[63]. This lead to replacing the original expression for calculating the effective radii by a new function that apart from a scaling factor contains three ($\alpha$, $\beta$, and $\gamma$) adjustable dimensionless parameters, as with most GB models, optimised to reproduce PB results. This describes two more models used in this work; the Onufriev Bashford and Case models 1 and 2 (OBC 1 – option igb = 2, and OBC 2 – option igb = 5).[63] The choosing of appropriate parameters for $\alpha$, $\beta$, and $\gamma$, differentiates one OBC model from the other. The relevant parameters are provided in section 6.2.2.

The models discussed in this section have a common limitation. That is that they neglect cavitation free energy terms and any hydrophobic effects. These effects will be discussed in the next section.

### 3.2.4 The nonpolar solvation term

Except from the electrostatic contribution to the solvation energy, one has to consider other effects namely, the cavitation, dispersion and repulsion contributions. The first related to the cavity that is created when a solute is inserted inside a solvent, while the latter two relate to the van der Waals forces between the solute and solvent atoms.

Although there are more theoretically rigorous methods available, the most popular method to compute the non-polar solvation free energy is to relate all contributions to the solvent accessible surface area (SASA) of the solute molecule.[64]

$$G_{non-polar} = \gamma SASA + b \tag{3.2.20}$$

The parameters $\gamma$ (this is different from the $\gamma$ used in the OBC models as discussed in previous page) and $b$ are empirical and fitted to experimental solvation free energies of hydrocarbons. SASA is the surface from which solvent is excluded after a solute is inserted. It is obtained by sliding a probe sphere (typically with a radius of that of the van der Waals radius of water – 1.4 Å) over the van der Waals surface of the solute, as shown in Figure 3.1.

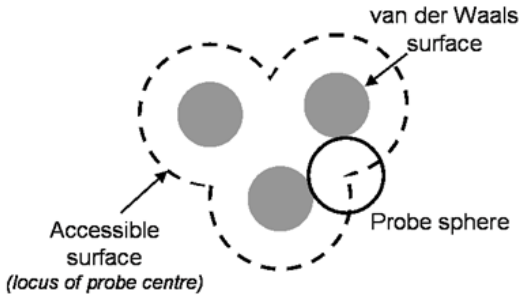


Figure 3.1: Depiction of the surface accessible surface area (SASA) of a solute. The probe sphere represents a water molecule (van der Waals radius of 1.4 Å). Taken from[65]

## 3.3 The MM-PBSA/GBSA method

The method of molecular mechanics using the Poisson-Boltzmann or generalized Born Surface Area (MM-PBSA/GBSA), described in the previous sections of this chapter, was co-developed by the Kollman and Case labs in the late 1990s[6, 8, 66]. The amount of attention it has received is due to the following reasons:[8, 67] It is more physically rigorous compared to scoring functions; depends less on empirical factors; it can handle more structurally dissimilar ligands; and is less computationally demanding when compared to the more rigorous methods.

$$\Delta G_{bind} = G_{complex} - (G_{protein} + G_{ligand}) \tag{3.3.1}$$

$$G = E_{MM} + G_{pol} + G_{np} - TS_{solute} \tag{3.3.2}$$

$$E_{MM} = E_{int} + E_{ele} + E_{vdW} \tag{3.3.3}$$

The free energy $G$ of a molecule is given by the sum of its gas-phase energy, the solvation free energy, and a contribution for the configurational entropy of the solute upon binding. The gas-phase contribution ($E_{MM}$) is obtained from the molecular mechanics energy of the molecule and consists of bond, angle and torsion energy terms ($E_{int}$), and electrostatic ($E_{ele}$), and van der Waals interactions ($E_{vdW}$). The polar contribution of solvation i.e. the transfer of a molecule from gas-phase to solvent, is given by the $G_{pol}$ term. When the method was first conceived the term was determined by solution of the Poisson-Boltzmann (PB) equation while later the less computationally demanding Generalized Born (GB) model was used.[68] The non-polar solvation free energy is given by the $G_{np}$ term discussed in the previous section. The $TS_{solute}$ term in equation (3.3.2) is used to estimate the configurational entropy of the solute by applying either normal mode analysis[52] or the

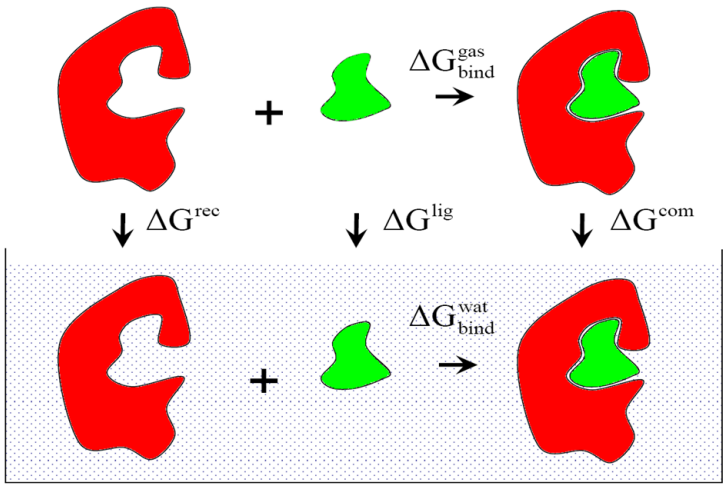


Figure 3.2: Thermodynamic cycle for calculating a binding free energy.

quasiharmonic approximation.[69] This term is one of the most criticised terms[70], associated with large errors, and frequently neglected when relative free energies of binding of similar ligands is of interest.[67]

Having obtained a free energy for each of the interacting molecules, a binding free energy can be obtained by calculating the difference between the free energy of the complex and the sum of the free energies of the individual components, in this case the ligand and the protein (see equation (3.3.1)). Figure 3.2 shows the thermodynamic cycle used to compute the binding free energy. As shown, it is equivalent to the sum of energy associated with the formation of the complex in the gas-phase, and the difference in solvation between the complex and the unbound molecules (equation(3.3.1)).[67]

Although MM-PBSA/GBSA calculations can be performed based on single structures, for example minimised structures[9, 10, 71, 72] or crystal structures[73] it is commonly used on a molecular dynamics (MD) generated conformational ensemble. MD simulations, typically in explicit solvent, because they have shown to give better results[74], are applied on the protein-ligand complex, the unbound protein and the unbound ligand in explicit solvent; this approach is known as the three-trajectory approach.[11, 67] An ensemble of conformations is then obtained by extracting a number of

snapshots from the MD trajectory. The snapshots are post-processed by replacing the explicit solvent with an implicit one (PBSA or GBSA models), which is followed by turning off the interactions between the protein-ligand atoms. The energies calculated for each snapshot are averaged and their difference gives the first, second and third terms in equation (3.3.2). The entropic contribution is obtained by the minimization of one or a few of the snapshots of the unbound and bound structure followed by quasiharmonic or normal mode analysis, as mentioned above.

To date the MM-PBSA/GBSA method has been applied to several protein-ligand systems and has undergone various alterations.[11, 12, 14, 75-81] The first modification of the original method was to perform molecular dynamics simulations for only the protein-ligand complex. This would mean the cancellation of the internal energy term during the calculation of the binding affinity, leading to significantly lower error as sampling and force field errors cancel. However, such simplification is only possible in closely related derivatives and in cases where no large structural changes upon binding are expected.[11, 67] Later the method was further simplified by replacing the explicit solvation model during molecular dynamics simulations with the implicit generalised Born (GB) model.[12, 76, 77] While positive results have been reported in some cases[12, 76, 77] large scale studies tend to indicate that the method is accurate for distinguishing weak and strong binders that differ by 2-3 orders of magnitude in $IC_{50}$ only[11]. Other studies have shown MM-PBSA to perform no better than some common scoring functions.[79] Huang *et al.* developed a simplified MM-GBSA method as a rescoring method that is an intermediary step between high-throughput docking methods and more rigorous molecular-mechanics-based methods.[14, 80] The major modification to the original method is that the molecular dynamics simulations of the complex and the isolated protein and ligand in explicit solvent are replaced by simple minimizations in implicit GB solvent model. This study is used as the

basis for the publications of Guimaraes and Cardozo[15] and Pierce et al.[16] which were the starting point of the research presented in this thesis.

The next section focuses on the application of the method in drug design, highlighting the most notable examples from literature.

## 3.4 Application in Drug Design

MM-PBSA/GBSA methodology is not limited to applications in drug design. It has been applied in a range of free energy studies on biomacromolecules. Some examples include the study of the stability of DNA, RNA, and protein conformers to differentiate the native fold from a set of decoy structures, prediction of disulphide connectivity in proteins, and the specificity of protein-protein, protein-DNA and protein-RNA interactions by utilising techniques such as alanine scanning proposed to identify hot-spots.[6, 52, 67] However, work in this thesis is specifically related to the application of the method in protein-ligand binding affinity prediction, and therefore the focus of this review will be solely on its application in different stages of drug design and mostly on the context the method was utilised in this work, i.e. as a physics-based rescoring tool of dock poses.

Estimation of the binding free energy both on qualitative and quantitative scales, as well as accurate and consistent rank-ordering of compounds based on their affinity, are of utmost importance in various stages of drug design process, ranging from early stages such as lead identification to lead optimisation and further refinement of a few dozen compounds.

Methods such as free energy perturbation (FEP) and thermodynamic integration (TI) have been developed to accurately predict absolute and relative free energies.[5] However, these pathway methods require long sampling times which classify them impractical for the context of lead optimization in industry. Hence an endpoint method such as MM-PBSA/GBSA, that only considers the unbound and bound states of the protein-ligand complex (i.e. without sampling intermediate steps), appears as an attractive alternative as

a tool for large-scale *in silico* lead optimization. However, the method is designed to calculate both absolute and relative binding affinities which still makes it prohibitively expensive for this context; MD simulations in explicit water are costly.

The work by Kuhn et al. in 2005[11] gave rise to the possibility of this method becoming usable for re-scoring docked poses. A comparison of obtaining the complex coordinates by minimization of one structure in explicit solvent or by generating an ensemble of molecular conformations is reported in this extensive study involving a large number of ligands and eight different protein targets. It was shown that applying the MM-PBSA method in a single, relaxed structure is an adequate and sometimes better approach than averaging over molecular dynamics snapshots. In addition there were no signs of significant improvement by performing longer MD runs or by minimizing the extracted snapshots from the MD trajectory, before free energy averaging. However, their results showed that including water molecules explicitly from the first solvation shell into the free energy expression is more appropriate than the use of the continuum description. Finally they classify the method as a valuable post-docking filter, a helpful tool to prioritize de Novo design tool and for distinguishing between good and weak binders that differ by 2-3 orders of magnitude in $IC_{50}$.

The first method devised specifically as a post-docking filter came from Huang et al. in 2006.[13, 14] The compounds of interest are docked using DOCK 3.5.54 and the top 25% of the docking results are submitted for further processing (most known binders were typically ranked in the top 25%). The re-scoring protocol consists of three minimizations (ligand, protein and complex) in implicit GB solvent using the Protein Local Optimization (PLOP)[82] program with the OPLS all atom force field.[83] PLOP implements the multiscale truncated-Newton (MSTN) minimisation algorithm.[84] The protein is kept rigid and the entropic contributions are ignored. The method was initially developed with the aim of being used for enrichment studies and

despite its limitations (incorrect docking poses, fixed protein) it can be a promising approach for improving the discrimination between known ligands and decoys in large-scale virtual screening (the maximum enrichment factors observed increased for all nine of the test cases by a factor of 6).

Lyne et al.[17] was the first to apply this method in the context of lead optimization for four different kinases. A different docking approach was used but the rest of the protocol remained the same. Overall the method was proven promising in the lead optimization stage of chemical series for inhibition of protein kinases; however, it is highly dependent on how good the predicted poses are and it was suggested that the GB parameters may not be of high enough quality to give reliable results for certain functional groups.[17]

In a different, study the same method was implemented on poorly docked poses and a total of 33 molecules highly ranked by MM-GBSA were tested experimentally.[18] The method performed well when the initial docking geometry resembled the crystallographic pose, but fell short when large conformational changes occurred during ligand binding. Specifically 23 molecules which were false negatives by the docking, were rescued by the re-scoring, and the 10 remaining were true negatives by the docking while false positives by the re-scoring. This introduction of false positives is a real caveat of the method, limiting its applicability to good docking predictions or non-flexible binding pockets. This represents a major challenge for the method, where a number of studies[10, 19, 85] have shown the same problem.

In both the Ferrari et al.[19], and the Rastelli[10] methods four different minimization protocols were tested, and solvation free energies were obtained from three different models. The minimization techniques trialled were: (a) minimization in explicit solvent, (b) minimization with the GBSA solvent, (c) distance-dependent dielectric constant ($\varepsilon = 4r$) and (d) same minimization as in (c) followed by MD simulation of the ligand and a final re-minimization. The Delphi[86] PBSA, and the PBSA and GBSA as implemented in AMBER[87] were used to obtain the free energies of solvation. The non-polar contributions were calculated with Molsurf of AMBER and the entropy was ignored.

Overall they obtain very good correlations of binding affinities to experimental data and in particular AMBER PBSA combined with the distance-dependent dielectric minimization gave a similar correlation with the energies obtained from the minimization with explicit waters (AMBER PBSA $R^2 = 0.80$ vs 0.81 for explicit solvent minimisation). In addition, the Rastelli et al.[10] study confirmed the Kuhn[11] study, by showing that the results of a single minimized structure had high similarity with the ones obtained after averaging over multiple MD snapshots. However, it should be noted that all the data sets in these studies have orientations and conformations validated with crystallography.

In the method by Guimaraes and Cardozo[15] conformational analysis of the unbound ligand is first attempted by the use of a so-called Monte Carlo multiple method (MCMM) as implemented in MacroModel[88], and proceed to obtain an entropic contribution from a Boltzmann distribution and minimize the best pose for each inhibitor in the bound state to better account for protein flexibility. The entropy term of the bound state was ignored. Despite encouraging results (improvement over docking results) they also stressed the issue that rigid compounds are more appropriate for use in this method. In addition, in the same publication, a comparison study between obtaining the entropy through penalizing each rotatable bond by 0.65 kcal $mol^{-1}$ (a common approach in scoring functions) and through a Boltzmann distribution was performed. This comparison led to the conclusion that the entropic contribution should not be important for rank ordering and even more so for congeneric series, since according to the Boltzmann distribution method the overall penalty is small and similar for all compounds, even for dissimilar ligands.

Another way the MM-PB(GB)SA method has been employed to fit the time restrictions of lead optimization is by replacing the explicit solvent with that of an implicit (usually a GB model). Rizzo et al.[12] were the first to implement this modification. The motivations of this study were the expected

increased sampling for the ligand and protein and therefore shorter simulations might be employed to compute thermodynamic and structural quantities that could only be obtained from much longer MD runs with explicit solvent. They obtained good correlations with experimental binding affinities ($R^2 = 0.71$ for six thiadiazole urea ligands with stromelysin-1 and gelatinase-A which improved to $R^2 = 0.74$ by removal of solute entropy contributions) and the results appeared well converged, despite the limitation of the lack of detailed solute solvent interactions. Although this study focused on the quantitative estimation of binding free energies rather than being a quick post-docking filter, it provided a potential opportunity.

This opportunity was exploited by Brown and Muchmore[81, 89, 90] who have developed a high throughput formulation of the MM-PBSA (htMM-PBSA) based on a distributed computer paradigm. Excluding entropic contributions, they performed GB-MD simulations and an efficient PB solver as implemented in the ZAP module from OpenEye Scientific Software[91] to calculate solvation free energies. Employing implicit solvation MD simulations is expected to obtain convergence by shortening of the MD steps by one order of magnitude compared to MD simulations with explicit waters.[81] The PB solver employs a diffuse representation of the dielectric boundary, rather than the more common discrete transition between solute and solvent. It also alleviates a number of grid related problems present in other PB treatments, such as the discontinuity of the dielectric at the boundary between the solvent and solute.[92] This method was applied on a set of 308 small-molecule ligands across three protein targets. The process completed overnight with a simple submission across 400 desktop computers. It is important to note that the parameterization of the complexes in addition with the deployment and reconciliation processes, were automated. They observed good correlations with experimental data with correlation coefficients in the range of 0.72 and 0.83 (which correspond to $R^2$ of 0.52 and 0.69 respectively).

To this stage, all the MM-PBSA/GBSA methods developed and applied rely on computer generated conformations or conformational ensembles which

are open to defective computational methods and errors. A study to tackle this issue was performed by Li et al.[93]. To achieve this, 24 diverse protein-ligand complexes, each of which has a set of multiple NMR resolved structures, were tested. With the entropic term calculated through nMode in AMBER[87] binding affinities of a single structure and an ensemble of structures were estimated through both MM-PBSA and MM-GBSA. The results once again, as in Kuhn[11], favoured the energies obtained from the single structure representation. The respective correlation coefficient ranges obtained were 0.72-0.79 and 0.61-0.74 for the single structure and the ensemble. It is emphasized that the methods fail when computing absolute free energies and are rather more reliable for estimating relative binding affinities. Again, as in previous reports, these methods fail on protein-ligand complexes which undergo substantial conformational changes upon binding. Finally, it was shown in their tests that the MM-GBSA method produced more accurate and converged results than the MM-PBSA method.

If one were to revert the scope of this method to its original aim, i.e. the quantitative estimation of free energies of binding it is worth mentioning a seminal study by Weis et al.[74]. In this study the dependence of the method on the simulation methods used and the force fields applied was evaluated. The simulation methods tested range from simulations with explicit solvent and periodic boundary conditions, via GB implicit solvent, to vacuum simulations with a constant or distance-dependent dielectric constant. As with regard to the force fields, the four AMBER force fields were implemented: ff94[94], ff99[95], ff03[96] and ff02 (first three are non-polarizable).[97] The complex of Avidin-Biotin was carefully chosen in order to allow concentration on electrostatics, solvation and van der Waals. It is well characterized by x-ray crystallography, a wide range of experimental binding free energies exist (to avoid obtaining trends by chance), it has been investigated by a number of theoretical methods (FEP, LIE and MM-PBSA), does not involve any metals and shows little change in the structure of the protein upon binding. The outcomes of

this method are worth taking into consideration when performing MM-PBSA/GBSA calculations, and are therefore outlined below:

- Mixing force fields for geometry generation and energy calculations is not recommended.
- The $GB^{OBC}$ of AMBER 8 that was used here provided poor simulated structures for a high cost and poor absolute binding affinities compared to PB. The GB performance on different proteins appears to vary.
- Explicit waters in MD simulations must be used, but the size of the system and the boundary conditions are of less importance.
- Non-polarizable force fields tested give similar results. A polarizable force field would give a more consistent treatment of the solvation.
- The MM-PBSA/GBSA is insensitive to the total charge of the protein and surface charges distant from the binding pocket. The method also worked well for both neutral and charged ligands (using PB in Delphi but not with AMBER 8.0).
- Generally single geometry minimizations can provide good results instead of ensemble averages obtained from MD simulations. On the other hand, in other cases they are entirely wrong; therefore some filtering is needed.
- The entropic term has the largest variation amongst the other terms of the equation and is also the most computationally demanding.

Their study concluded that the method is an attractive method to calculate absolute free energies, in particular for cases where the expected spread of the affinities is high. The standard deviation of the energies was high, 5-15 kJ $mol^{-1}$ which could explain the poor results obtained by Pearlman[79] where the spread of the binding affinities was only 10 kJ $mol^{-1}$.

## 3.5 Limitations

Although encouraging results have been reported in literature, MM-PBSA/GBSA suffers from a plethora of methodological limitations that hamper it from being used routinely in the drug design process. The most major and relevant sources or error/limitations will be covered in this section.

The first and most major shortcoming of the method is the calculation of the solute entropy. This is particularly important in cases where quantitative agreement with experiment is of interest, or in cases where significant conformational changes occur upon binding. In cases where ligands are very similar and relative free energies are of interest entropy is commonly ignored. Anharmonic contributions are ignored when normal mode analysis is used to estimate changes in vibrational entropy which can lead to systematic errors. In fact, significant fluctuations in the range of 5 kcal $mol^{-1}$ have been previously reported for entropy estimates.[7, 67] On the other hand, quasiharmonic analysis may include some anharmonic effects[98], but convergence is not possible within the current timescales.[68]

Another major underlying methodological limitation of MM-PBSA/GBSA, which was mentioned earlier in this chapter, is the difficulty in obtaining accurate solvation free energies for charged and/or buried solutes in the interior of proteins. The more polar the studied compounds the higher is the uncertainty[73] in the estimation of the solvation free energy, and therefore in cases where the key binding interactions are electrostatic, i.e. there are very few hydrophobic interactions, it is difficult to obtain reasonable results. Attempts have been made to tackle this by increasing the value of the dielectric constant for more polar solutes.[20, 99] Although this approach has a rational basis and in the aforementioned cases seems to improve agreement with experiment (although in the case of Hou et.al.[20] the results are still fairly poor) it seems more a way of fiddling with results until the desired results is obtained rather a rigorous solution to a serious underlying methodological

limitation. In addition, it is impractical if the method is to be applied routinely for the ranking of inhibitors.

Furthermore, a source of error not unique to this method, is that of sampling and statistical convergence. As discussed in the previous section it has been shown that for the single-trajectory approach longer MD simulations do not necessarily provide better results, which is probably due to introduced noise, and hence obtaining an accurate value with increased fluctuations becomes an even greater challenge. However, a greater problem with MM-PBSA/GBSA is the large standard deviation, that is commonly not reported, which arises from the large variations between the terms in equations (3.3.2) and (3.3.3).[68, 74, 79, 100] This poses a serious limitation when attempting to use the method to differentiate two similar analogues in a typical lead optimisation experiment. A way to obtain statistically converged results has been devised by Genheden et al.[101], which rather than relying on one long MD simulation, one shall perform a large number of independent (by assigning a random initial velocity) MD runs and average the results. Although it was shown that statistically converged MM-PBSA/GBSA results are possible, that study reported poor performance with experiment with largely overestimated energies (systematically more negative than experiment).

Another concern that is particularly important if the method is to be used as a fast post-docking filter, i.e., minimising a single geometry, is potentially a strong dependence on the starting configuration, or in other words the method is highly sensitive to small structural differences. There have been studies that have shown good performance following simply minimising a single structure [11, 102], while others have shown contradicting results with cases giving better results than using MD ensembles, while in other cases they were completely wrong.[74] Interestingly, Feher and Williams[103] who tested minimisation-based binding energy calculations, found that as minute perturbations to the input structures as 0.01 Å resulted to solutions that differ by as much as 0.8 Å in atom displacement and up to 17 kcal $mol^{-1}$ in binding energy. They also observed that in many cases different ligand poses

were obtained with different hydrogen bonding patterns. Furthermore, following investigation of highly similar structures they found the barriers between different poses appeared fractal-like, making it difficult to predict a solution from the input structure.

Finally, there is a plethora of PB solvers, and GB models with varying parameters and selected radii available. This can give rise to potentially positive results which could simply be obtained by a fortuitous combination of all these parameters. Usually the model that performs best for a certain protein target and data set gets reported and when occasionally such comparisons arise, they tend to lack the statistical rigour required.

## 3.6 Conclusions

MM-PBSA/GBSA is an attractive method that could potentially play an important role in future research in drug design. Its main advantage lies with the wide spectrum of applications and range of stages in drug design for which it is suitable. Furthermore, it can be considerably more efficient on resources (especially the GBSA variant) when compared to state of the art rigorous free energy methodology. There have been encouraging results throughout its various applications, and in particular at the early stages of lead optimisation. Here qualitative agreement with experiment is sufficient and correct ranking of compounds is of utmost importance. Since 2005[11] and 2007[102] there have been a number of papers reporting encouraging results by applying the methodology as a fast rescoring tool of dock poses. Despite these claims, the method suffers from severe methodological limitations and sources of errors, and the aforementioned studies tend to be of small data sets, in some cases systems that are known to do well with simple scoring functions, and in most cases they lack the statistical rigour allowing room for fortuitous results.

In this thesis, we present a systematic evaluation of the ability and consistency of MM-PBSA/GBSA methodology to qualitatively estimate binding affinities with respect to experiment, and ultimately to determine its capability as a rescoring tool of dock poses. First, we attempt to reproduce a published all-in-one protocol, and then the methodology is applied on a range of protein-ligand systems, using different docking tools, rescoring protocols and continuum solvent models. A statistically rigorous comparison between these protocols and solvents is performed, followed by assessment of additional conformational sampling both in the form of long implicit solvent molecular dynamics simulations (MD), and multiple shorter explicit MD calculations.

In the following chapter the biological relevance and structural characterisation of the protein-ligand systems used in this work will be discussed.

# Chapter 4

# Protein-ligand systems

## 4.1 Introduction

Before presenting the research conducted in this work and its findings, it is important to familiarise the reader with the protein-ligand systems studied. In the work presented in this thesis, a dataset consisting of 63 ligands across 5 protein targets was studied. The proteins used were Thrombin, β-Secretase, Factor Xa, HIV-1 protease, and Src tyrosine kinase, corresponding to the crystal structures with Protein Data Bank (PDB) codes, 1ETT, 2P4J, 1FJS, 2PQZ, and 2BDJ respectively. To ensure valid comparisons and for consistency, the same protein structures and series of data with the published studies of E-Novo[16] and Guimaraes and Cardozo[15] publications were used. For each system an overview of the biological relevance, mechanism of activity in relation to structural characterisation, binding mode architecture and characteristics of the ligand series, will be provided.

## 4.2 Thrombin

Hemostasis comes from the Greek *hema* meaning blood and *stasis* meaning standing still or stop. In other words, it is the body's mechanism, as the first step to wound healing, for the arrest of bleeding from an injured vessel. This involves a complex 'waterfall' of enzymatic reactions which can be categorised in to three sets of factors: vascular, platelet, and plasma factors. Vascular factors reduce blood loss by vasoconstriction, or narrowing of wounded vessels, to reduce overflow of blood into surrounding tissues. Under the conditions of an injury, platelet factors participate in a process of collecting platelets in the damaged intima following their activation. Platelets provide the surface for the step coagulation to occur, guided by plasma coagulation factors, ultimately producing fibrin and therefore strong clot formation, completing the action of hemostasis.

The cascade presented above, in a normal individual, is closely regulated to counterbalance the inappropriate formation of clots. Abnormalities of these mechanisms can lead to either excessive bleeding or thrombosis. The latter is the cause of many cardiovascular diseases present in the industrialised world, including myocardial infarction, pulmonary embolism, deep vein thrombosis and stroke.[104] The principal factor in this cascade is thrombin, more specifically α-thrombin, which generates fibrin from fibrinogen (see Figure 4.1). Thrombin, as a procoagulant, it also acts as an activator of the fibrin-linking factor XIII (FXIII), and stimulates platelet aggregation.[105] In contrast, thrombin can also act as anticoagulant in the presence of thrombomodulin, which enables the activation of protein C, an anticoagulant zymogen, along with the plasma metallo-carboxypeptidase thrombin-activatable-fibrinolysis inhibitor (TAFI).[105] Therefore, the key roles thrombin plays in thrombosis make it an attractive pharmaceutical target; however, interference with the process of hemostasis, such as the platelet function, and presence of many trypsin-like serine proteases sharing high sequence homology with thrombin,

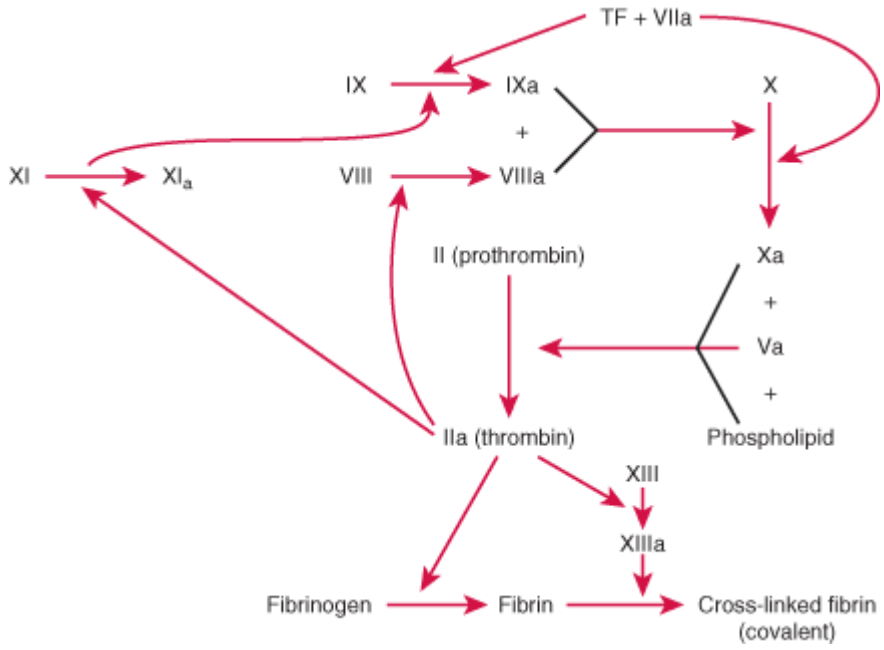


Figure 4.1: Blood coagulation pathways. Taken from the Merck Manual[106].

are some of the factors that make the development of antithrombotic pharmaceuticals challenging.

The human procoagulant α-thrombin is a trypsin-like serine protease, which consists of a 36 residue A-chain and a 259 residue B-chain; the two chains are linked covalently via a disulphide bridge. As shown in Figure 4.2a chain B is organised in two adjacent β-barrels. The active site residues Ser195, His57, and Asp102 fall at the meeting point of those β-barrels, at which point the active site cleft extends in a perpendicular manner. Part of the high specificity of thrombin is attributed to loops 60 and 149 (see Figure 4.2b) which mediate access of the catalytic residues to substrates and inhibitors. Another characteristic of the thrombin structure is a sodium ($Na^+$) binding site, along with two exosites (Figure 4.2). The $Na^+$ binding site is responsible for a number of allosteric effects; however, it is not within the scope of this chapter, but more details can be found in an excellent review by Di Cera.[107] Exosite1 is a positively charged surface pocket (shown to the right of Figure 4.2b) known to be the binding site of fibrinogen and

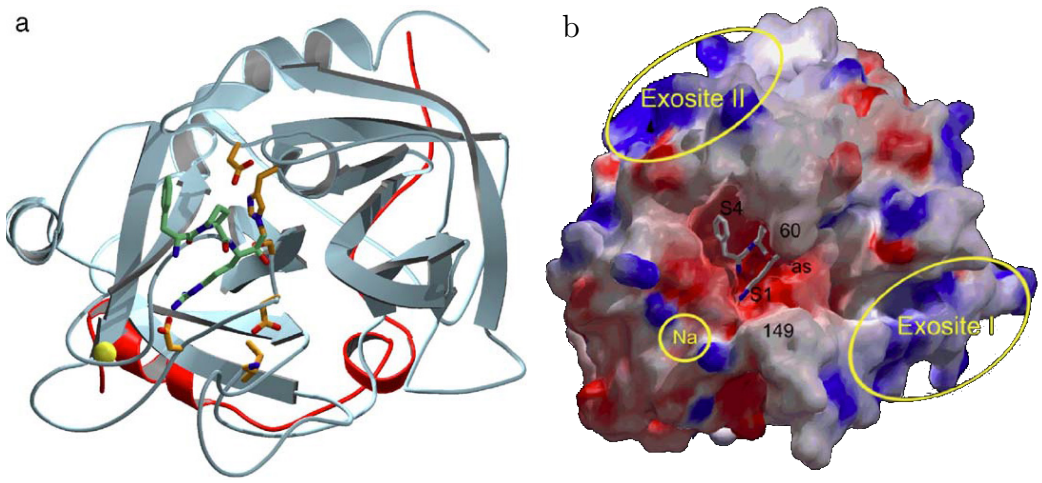


Figure 4.2: Human α-thrombin in complex with inhibitor PPACK. (a) Chains A (red) and B (cyan) in cartoon representation. PPACK inhibitor shown in green, $Na^+$ shown as a yellow sphere, and key active site residues highlighted in orange. (b) Surface representation coloured according to the electrostatic potential (red: negative; blue: positive). The inhibitor is shown in stick representation and parts of the active site and surface areas are highlighted accordingly. These images are taken and partly adapted from Bode, 2006.[105] Pockets S1 and S2 shown in figure (b).

thrombomodulin and commonly referred to as anion-binding exosite 1 (ABE1). Similarly, the second exosite is also positively charged and due to binding of heparin, is known as heparin-binding site or as anion-binding exosite 2 (ABE2).

Figure 4.2 shows the crystal structure of α-thrombin (PDB code: 1PPB; resolution: 1.9 Å) bound with the D-Phe-Pro-Arg choloromethylketone (PPACK) inhibitor. The deep S1 specificity pocket can be found to the left of the active site residues. At the bottom of this deep pocket is found the acidic Asp189, a similarity with trypsin. The specificity of the thrombin binding site is additionally complemented by the polar residue Glu192 positioned at the entrance of the S1 pocket. On top of this pocket are the non-polar pockets S2 and S4 (aryl-binding site), separated by the 60 loop (delimited by residue Trp60). Pocket S1' is a small polar pocket to the right of the active site bordered by Lys60. Inhibitor PPACK consists of a D-Phe-Pro-Arg peptide fragment and a methyl-ketone linking group. At the left-most part of the

inhibitor molecule, the benzyl side chain of the D-Phe1$_{PPACK}$ is located at the non-polar S4 pocket interacting with Trp60 on the top, and Trp215 on the bottom. The hydrophobic pentameric Pro2$_{PPACK}$ ring fills the narrow S2 cavity, whereas the Arg side chain (the other end of the molecule) extends into the S1 pocket and is found to form hydrogen bonds with Asp189, Gly219, and a buried water molecule. The hemiketal group of the carbonyl moiety of the C-terminus of Arg3$_{PPACK}$ is covalently linked to Ser195, whereas the methylene group of the same moiety is found to be covalently bonded to His57. Finally the peptidyl moiety forms three hydrogen bonds along the residues Ser214 and Glu217. Indeed the majority of the substrates that bind in the active site, tend to have similar groups possessing a bulky hydrophobic residue at the P4 position (the position of the molecule to occupy the S4 binding pocket or aryl pocket), a Pro at P2 position, an Arg at the P1, a hydrophobic group at P2', and a basic group at the P3' position.[105]

In this study a bovine thrombin is used with PDB code 1ETT and resolution 2.50 Å (see Figure 4.3). This is the same protein used in the E-Novo publication.[16] The crystal structure consists of the protein bound to inhibitor $N^{\alpha}$-(4-toluene-sulphonyl)-DL-p-amidinophenylanyl-piperidine (4-TAPAP). As in the human thrombin, there are two chains, but chain-A has 49 residues instead of 36. Despite some residues appearing in different sequence, the structural differences between human thrombin bound to PPACK and bovine thrombin bound to 4-TAPAP are miniscule (α-carbon RMSD of 0.5 Å).[108] Most importantly, the binding mode is similar with the toluene group of the inhibitor placed in the aryl site (S4 pocket), then the middle of the molecule (one of the sulphonyl oxygens) is within hydrogen bond distance to the Gly219 nitrogen atom. The piperidine ring is placed in the S2 pocket, between the toluene ring and the imidazole ring of His57, leaving space for additional substituents to be added. The amidino group appears to interact with the Asp189 (at the bottom of S1 pocket) only via one of its nitrogens; however both oxygens of Asp189 are in equal distance from

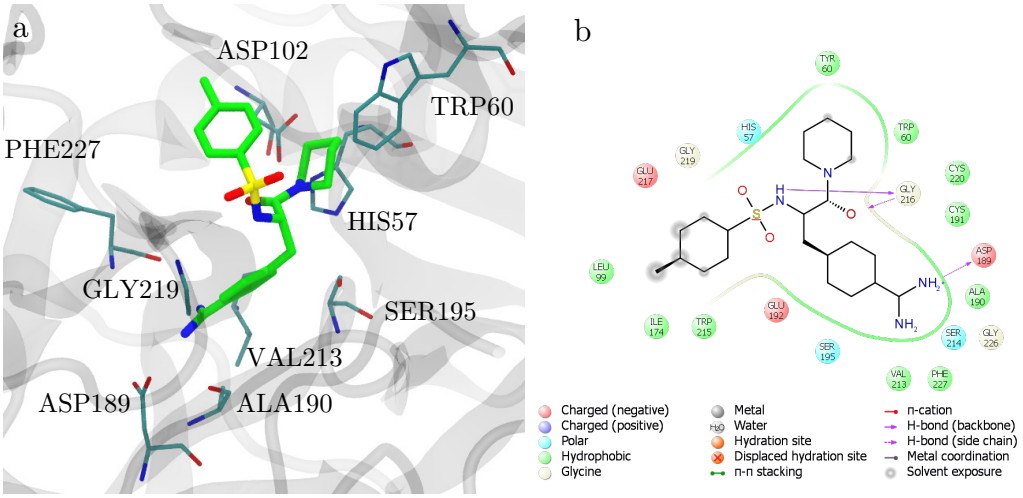


Figure 4.3: Bovine thrombin (PDB: 1ETT) bound to inhibitor 4-TAPAP. (a) Binding site with key residues, and (b) interaction diagram including residues up to 4 Å away from ligand (double bonds are not shown). Picture generated using Maestro[109]. Hydrogens are excluded for clarity.

the nitrogen of the amidino group. The other nitrogen forms van der Waals interactions with Ala190, Val213, and Phe227.

The inhibitor 4-TAPAP was used as the basis for the construction of the scaffold for all the ligand of the series studied in this work. A schematic representation of this scaffold is shown in Figure 4.4. In red are the three R-groups filled by different substituent for the different ligands listed in Table 4.1.

For reasons of consistency, all datasets in this thesis, were taken to be the same as in the E-Novo study[16], who in turn obtained the dataset form Guimaraes and Cardozo.[15] It should be noted here that in the E-Novo study the numbering of the ligands were different (as indicated in the brackets in Table 4.1). Cross-referencing with the Guimaraes and Cardozo study[15] it was found Pearce et al. (E-Novo study) removed the intermediate ligands, without giving the reasons in the published paper. The discrepancy was discovered when noticing that the numbers in the table provided in the supporting information of the paper, did not follow a continuous sequence from 1 to 12. No information regarding this omission was provided. At this stage it should

also be noted that ligand 7 has a much lower binding affinity than the rest of the ligands in the series, and a very different R3 group. From the published results of Guimaraes and Cardozo[15] ligand 7 is a clear leveraging point, benefiting the correlation. This could therefore justify why it was chosen. Our results, where appropriate, will reflect this assertion.

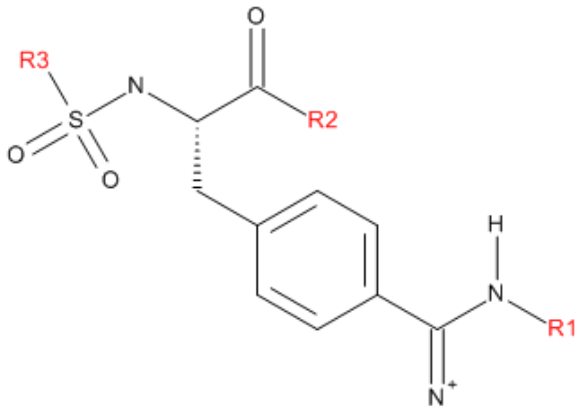


Figure 4.4: Structure of the scaffold used to generate the Thrombin inhibitors.

Table 4.1: Experimental activity of the 4-TAPAP analogues against thrombin (PDB: 1ETT). Numbers in brackets reflect the numbering in the E-Novo publication (see main text for details).

| Ligand No. | R1 | R2 | R3 | pKi |
|---|---|---|---|---|
| 1 | H | 1-cycloheptylamino | 2-Naphthyl | 7.28 |
| 2 | $CH_3$ | 1-cycloheptylamino | 2-Naphthyl | 7.34 |
| 3 | $NH_2$ | 1-cycloheptylamino | 2-Naphthyl | 8.82 |
| 4 | $NH_2$ | NMe(Cyclopropyl) | 2-Naphthyl | 6.61 |
| 5 | $NH_2$ | NMe(Cyclopentyl) | 2-Naphthyl | 8.96 |
| 6 | $NH_2$ | NMe(Cyclohexyl) | 2-Naphthyl | 6.82 |
| 7 | $NH_2$ | N-Piperazinyl-N'-ethoxycarbonyl | 2-Naphthyl | 5.48 |
| 8 (9) | $NH_2$ | NMe(Cyclopentyl) | 2(6,7,8,9-tetrahydro-5H-benzo[7]annulene) | 10.35 |
| 9 (10) | $NH_2$ | NMe(Cyclopentyl) | 1-Naphtyl | 8.1 |
| 10 (12) | $NH_2$ | NMe(Cyclopentyl) | Bz | 7.74 |
| 11 (13) | $NH_2$ | NMe(Cyclopentyl) | 2-Athracyl | 10 |
| 12 (14) | $NH_2$ | NMe(Cyclopentyl) | 1-Naphthyl-5-dimethylamino | 9.52 |

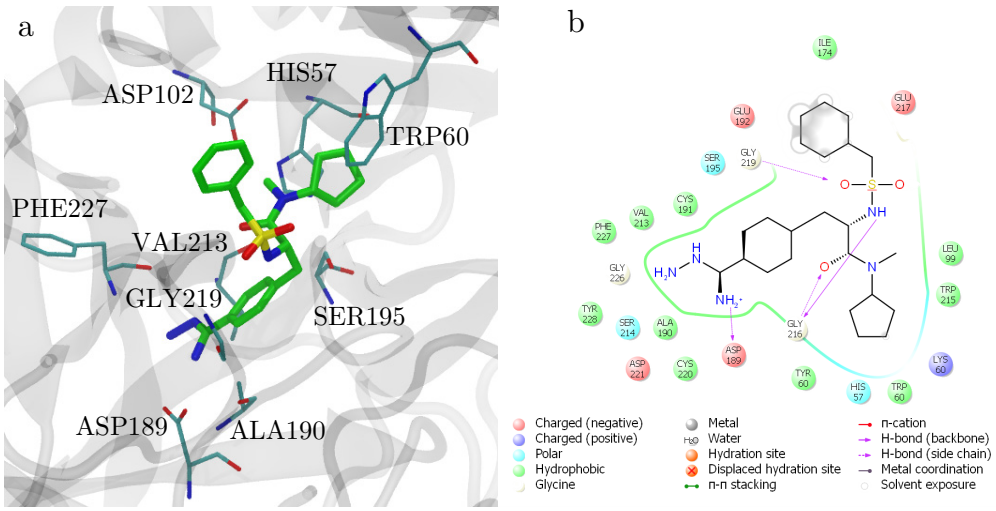


Figure 4.5: Bovine thrombin (PDB: 1ETT) bound to the 4-TAPAP analogue ligand 10. (a) Binding site with key residues, and (b) interaction diagram including residues up to 4 Å away from ligand (double bonds are not shown). Picture generated using Maestro.[109] Hydrogens are excluded for clarity.

The binding site of Ligand 10, the closest analogue to the natural substrate of the protein, 4-TAPAP is shown in Figure 4.5.

## 4.3 β-Secretase

Dementia is the term commonly used to describe a collection of diseases or conditions related to the death or abnormal function of brain nerve cells.[110] The most prevalent form of dementia is Alzheimer's disease (AD).[110] It was first identified more than 100 years ago, but it is only in the last 30 years that research and treatment has gained momentum.[110] Despite this however, little is known regarding the intricate details of processes that occur in the brain resulting in the development of AD. As of 2013 there are an estimated 44.4 million people globally who suffer from a form of dementia, from which 5.2 million have been diagnosed with AD in the United States of America alone, 200,000 of whom are below the age of 65.[110] Naturally, apart from the social impact, AD and dementia in general are associated, with a cost of $600 billion

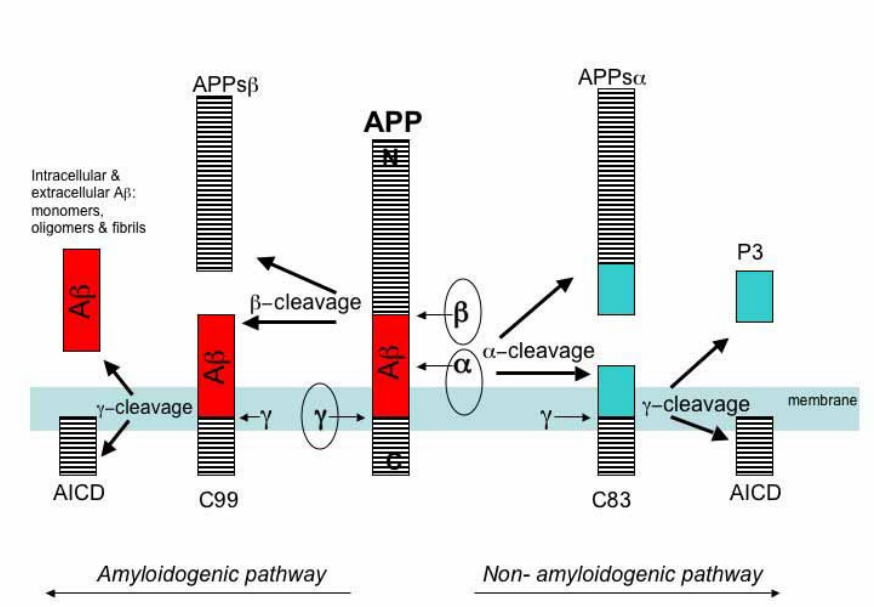


Figure 4.6: Metabolism of APP by the Secretase enzymes. Taken from Cole S.L. and Vassar R. [111].

globally (Alzheimer's Disease International).[110] Therefore, there are clear social and economic benefits from mitigating the progression of AD, or, ideally, from preventing it altogether.

AD is a neurodegenerative disease of the brain characterised by the accumulation of amyloid beta peptide (Aβ), as fibrillary tangles and insoluble plaques.[111, 112] Evidence shows that aggregates of Aβ are the trigger for a complex cascade that results in degeneration of neurons.[111] This critical peptide is generated by the sequential processing of β-amyloid precursor protein (APP), as shown in Figure 4.6. There are three proteins that have been found to cleave APP, namely: α, β, and γ secretases. Genesis of Aβ is avoided if APP is first cleaved by α-Secretase, ultimately giving $APP_{s\alpha}$, and C83, as shown in non-amyloidogenic pathway in Figure 4.6. However, β-Secretase is the first to cleave APP at the β-site giving the N-terminal domain $APP_{s\beta}$, and following further cleavage of the C-terminal by γ-Secretase, producing AICD and amyloid peptide Aβ. Since β-Secretase initiates the

genesis of Aβ, it is considered a major therapeutic target for the treatment and/or prevention of the Alzheimer's disease.

β-Secretase is a transmembrane aspartyl protease. Figure 4.7 shows the overall structure of the protein used in this study (PDB: 2P4J). The active site is located in the extracellular domain of the protein, and comprises of two aspartate residues: Asp32 and Asp228. On top of the active site is located a β-hairpin loop consisting of residues 67 through 77 and commonly known as the *flap*; it remains in the open conformation when the protein is inactive, but the closed conformation is preferred when the protein is bound to a substrate or inhibitor. Finally another key characteristic of β-Secretase is the so-called 10s loop. It is located in the S3 pocket and consists of residues 9 through 14. Though this loop is largely flexible, allowing substrates/inhibitors of varying size to bind, it is stabilised via Gly11, which can form a hydrogen bond with the ligand.

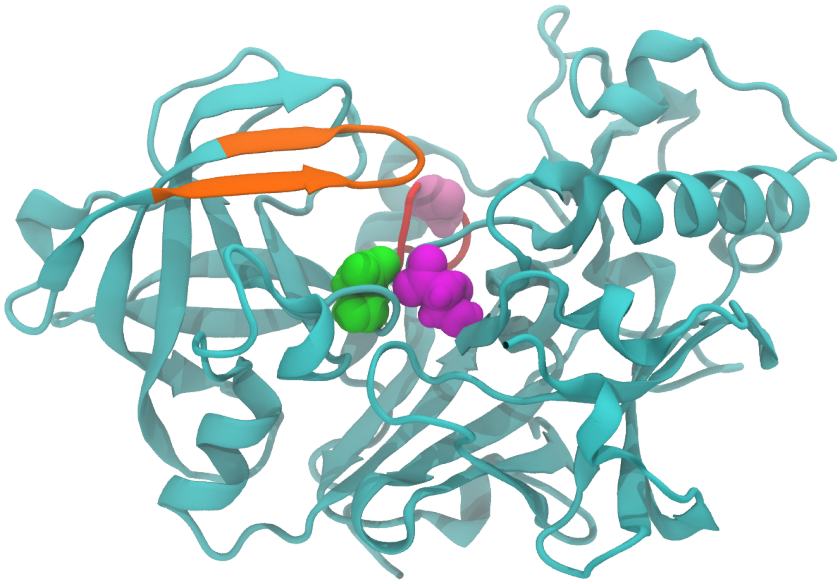

Figure 4.7: Structure of β-Secretase (PDB: 2P4J). The *flap* shown in orange. Asp32 and Asp228 in green and magenta (vdW representation) respectively. 10s loop shown in red, and residue Gly11 in mauve (vdW representation).

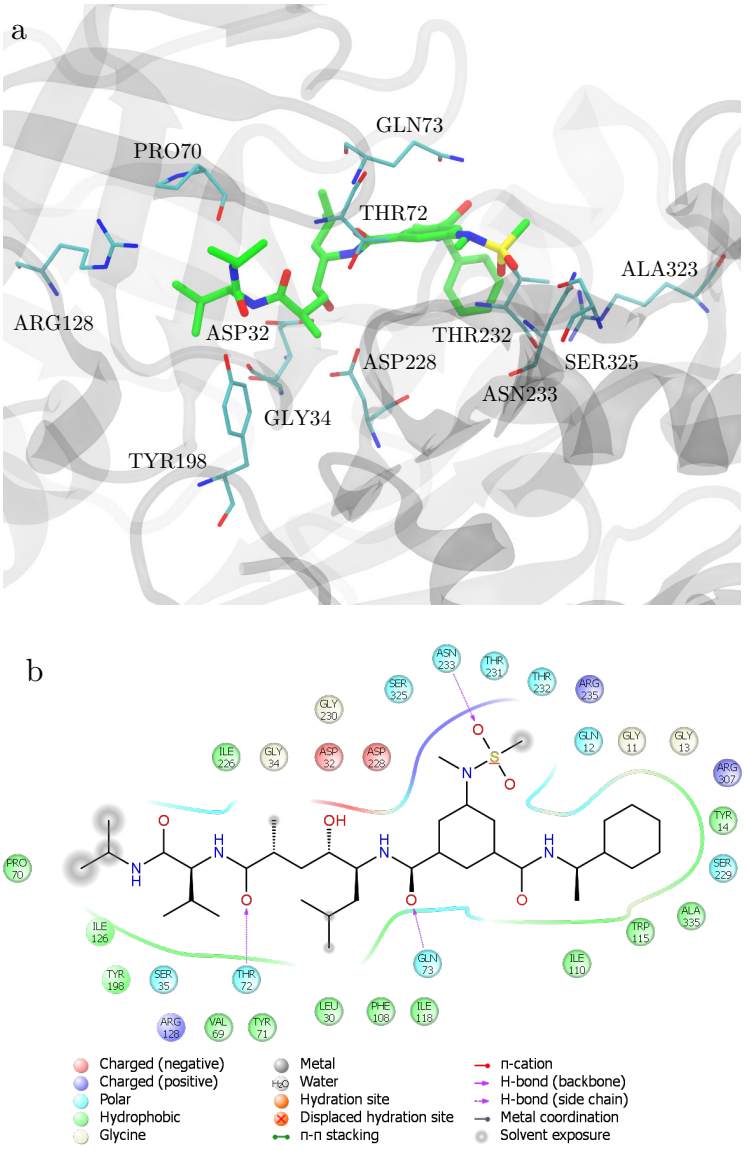


Figure 4.8: Crystal structure of β-Secretase (PDB: 2P4J) bound to ligand 4 (5d) shown in green. (a) Binding site with key residues, and (b) interaction diagram including residues up to 4 Å away from ligand (double bonds are not shown). Picture generated using Maestro.[109] Hydrogens are excluded for clarity.

A description of the interactions between important amino acids in the binding site and ligand 4 (5d) is presented in Figure 4.8 for the crystal structure with PDB code 2P4J and resolution 2.5 Å. The hydroxyl group of the Leu-Ala isostere part of the ligand, interacts with the aspartates forming tight hydrogen bonds. Interactions are seen between the *flap* residues Thr72

and Gln73 with the carbonyl group in the middle of the ligand. The phenyl group of the ligand occupies the S3 pocket (which contains the 10s loop) and forms contacts with residues Thr232, Arg307 and Ala335. The sulphonamide group is positioned in the S2 pocket with the oxygens in hydrogen bond distance with residues Asn233, Ser325, Arg235, and Thr232. The isopropyl group is found in the apolar S2´ pocket forming van der Waals interactions with residues Pro70, Thr72, and Arg128.

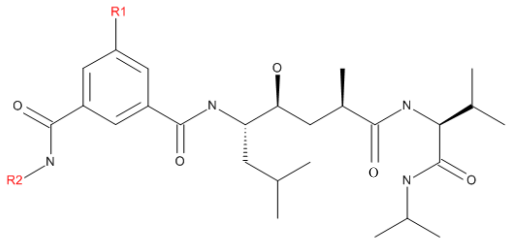


Figure 4.9: Structure of the scaffold used to generate the β-Secretase inhibitors.

Table 4.2: Experimental activity of the β-Secretase analogues. Numbers in brackets correspond to the compound number in the experimental study.[113]

| Ligand No. | R1 | R2 | pKi |
|---|---|---|---|
| 1 (5a) | 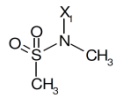 | 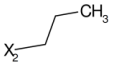 | 7.24 |
| 2 (5b) | 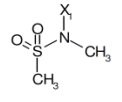 | 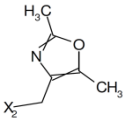 | 8.74 |
| 3 (5c) | 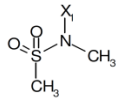 |  | 6.87 |
| 4 (5d) | 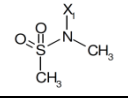 | 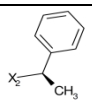 | 8.96 |
| 5(5e) | 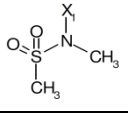 | 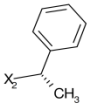 | 6.5 |
| 6 (5f) | 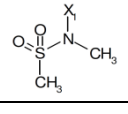 | 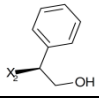 | 6.36 |
| 7 (22) | H |  | 6.1 |

The scaffold on which all the analogues in the series are based, is shown in Figure 4.9. Different substitutions on the R1 and R2 positions are listed in Table 4.2. Numbering in brackets corresponds to the compound numbering in the experimental study.[113] Herein a simple numbering from 1 to 7 was used. The range of experimental is around three orders of magnitude. Derivative 2 (5b) showed a much higher potency compared to inhibitor 1 (5a). This could possibly be attributed to R2 group (dimethyloxazole) which appears to fill almost entirely the hydrophobic S3 pocket. Similarly the smaller R2 group of 3 (5c) resulted in significantly reduced potency. In addition, experimental data show that R-configuration of the α-methylbenzyl R2 moiety in 4 (5d) is preferred over the S-configuration in ligand 5 (5e).

## 4.4 Factor Xa

Earlier in this chapter thrombin and its important role in hemostasis and thrombosis was discussed. Another key enzyme in the blood coagulation pathway is factor Xa (fXA). This enzyme, combined with its cofactor (factor Va) and calcium on the platelet phopsholipid membrane surface, form a prothrombinase complex, which then goes to activate prothrombin into thrombin.[114] Therefore, fXA is a prerequisite for thrombin. fXA is a more attractive drug candidate than thrombin for a number of reasons. First, fXA is not as multifunctional as thrombin and therefore poses a lower risk. In addition, targeting fXA can be more efficient than targeting thrombin considering that, due to the nature of the coagulation cascade, many molecules of thrombin are generated by a small amount of fXA.[114-116] Moreover, unlike thrombin inhibitors, targeting fXA does not prevent hemostasis, therefore posing a lower bleeding risk which translates to a wider therapeutic index.

fXA is a trypsin-like serine protease. It comprises a light and a heavy chain. The latter contains the binding site and catalytic domain. Like trypsin, the heavy chain, shares a globular catalytic domain of two β-barrel

subdomains. The surface cleft formed at the junction of those subdomains forms the binding site for substrate peptides and inhibitors. There the catalytic triad Asp102, His57, and Ser195 is located. In addition to these similarities with trypsin, fXA shares similarities in the binding site, such as the deep S1 pocket and aryl S4 pocket. Considering these similarities and that serine proteases participate in a variety of biological pathways, for example the important digestive enzyme trypsin, designing inhibitors with high selectivity towards fXA is of utmost importance and poses a significant challenge.

Figure 4.10: Crystal structure of factor XA (PDB: 1FJS). Heavy chain in cyan and light in yellow. In orange the catalytic triad, magenta Asp189, green the aromatic box, and yellow Glu97.

Figure 4.10 shows the crystal structure of fXa that was used in this study (PDB: 1FJS).[114] The two chains are shown in different colours. The β-barrels in chain A (heavy chain) are noticeable and key binding site residues are highlighted, including the catalytic triad (carbons in orange), aspartate 189 in the bottom of pocket S1 (magenta), residues Trp215, Tyr99 and Phe174 in the hydrophobic pocket S4, commonly known as the hydrophobic box (green

carbons), and residue Glu97 at the top of S4. The latter is also known as the cation hole due to the proximity of the carboxylate of Glu97, which allows, in addition to hydrophobic groups, for positively charged moieties to bind.[117]

The crystal structure of fXA with PDB 1FJS is bound to inhibitor ZK-807834, which shows >2500-fold selectivity for fXA compared to trypsin and other coagulation factors.[114] Figure 4.11 shows the binding site for this inhibitor and the key interactions with fXA. Similarly to many potent fXA inhibitors, ZK-807834 shares the architecture of an arylamidine connected by a linker to a basic group and adopting an L-shaped conformation when bound. The proximal ring (benzamidine) occupies the same position as the normal substrate of prothrombin in the S1 pocket. The amidine is hinged into position by four hydrogen bonds: two with Asp189, one with Gly218, and one to a water molecule, which is bonded to Ile227. The hydroxyl on the proximal ring forms a strong hydrogen bond with Ser195. The pyridine ring in close contact with residue Gln192, whereas the sarcosine (off the pyridine ring) is indirectly in contact with fXA via a water molecule (HOH712). The phenoxy group (distal ring) extends towards the S4 pocket forming interactions with the aromatic box residues. Finally, the methyl of the imidazoline group attached to the phenoxy ring, is positioned in the bottom of the S4 pocket in proximity to Trp215, whereas the imidazoline forms weak electrostatic interactions with the cation hole residues (Glu97 is 5 Å from the inhibitor).[114]

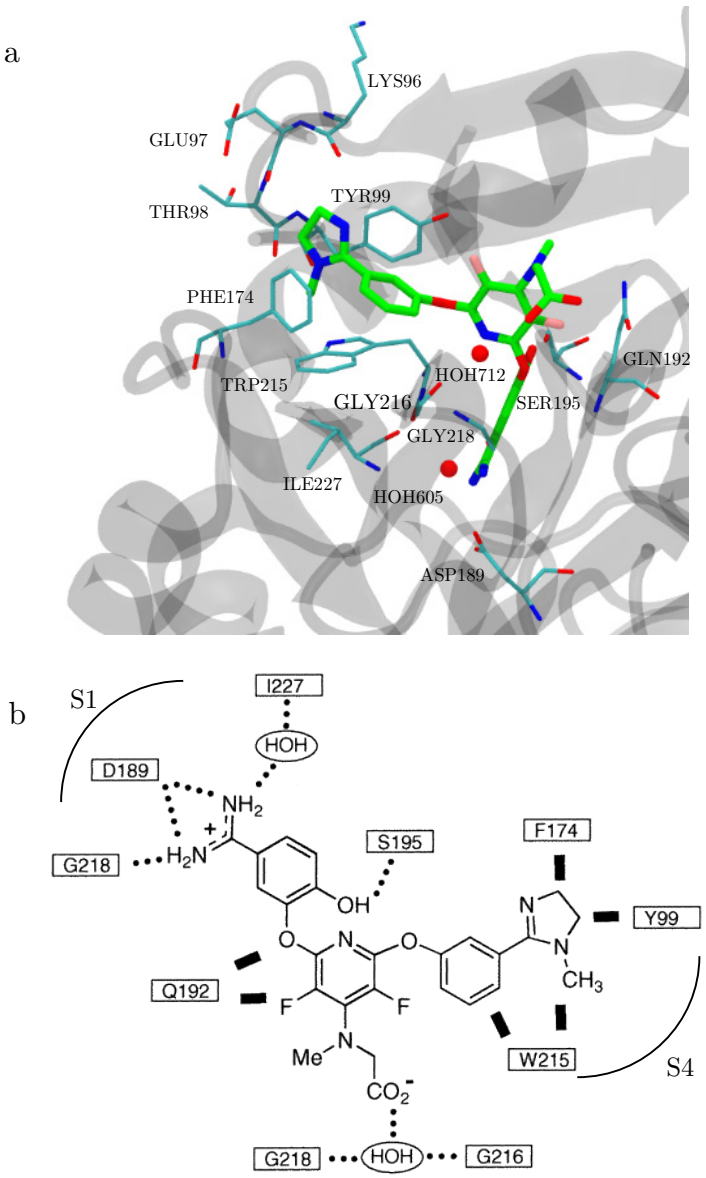


Figure 4.11: Crystal structure of fXA (PDB:1FJS) bound to the inhibitor ZK-807834. (a) Binding site with key residues, and (b) interaction diagram of binding site adapted from [114] showing major contacts with fXA. Dotted lines represent hydrogen bonds, while close contacts are shown with thick lines.

The data series used for this study was taken from a different publication [118], than the crystal structure of the protein.[114] The scaffold used as the basis to construct all the ligands in the series is shown in Figure 4.12. The central core of the ligand that includes the proximal ring (benzamidine), the pyridine with the fluorine atoms, and the distal ring (phenoxy moiety) is the same as the inhibitor ZK-807834 bound to the crystal structure with PDB code 1FJS. However, rather than the sarcosine moiety attached in the central pyridine ring at position 4, a methyl group was used in this set of ligands. Considering this group does not form direct contacts with the protein (as shown above in the description of the binding site) this should not cause large deviation from the binding mode observed in the crystal structure. Indeed similar docked poses to the crystal structure were obtained for the ligands in this series, as will be shown in later chapters.

Table 4.3 shows the 22 different inhibitors obtained by different combinations of moieties attached to the 4 positions indicated in red in Figure 4.12. A clear distinction in potency is observed when the group R1 is substituted by a polar moiety such as $NH_2$ or OH for ligands 17, 18, 20, and 21, with these ligands being the most potent in the series. This is an indication of the important role the interaction with the catalytic triad residue Ser195 plays with regard to the potency of the inhibitors.

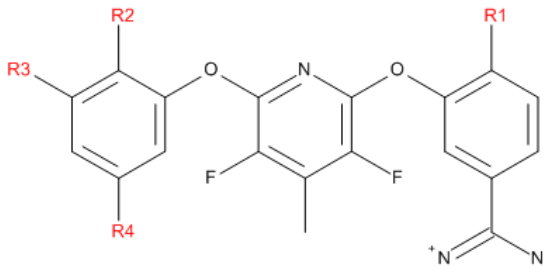


Figure 4.12: Structure of the scaffold used to generate the Factor-Xa inhibitors

Table 4.3: Experimental activities of the factor Xa analogues.

| Ligand No. | R1 | R2 | R3 | R4 | pKi |
|---|---|---|---|---|---|
| 1 | H | H | H | CONH2 | 6.55 |
| 2 | H | H | H | C=ONHMe | 5.92 |
| 3 | H | H | H | $C{=}O(NMe)_2$ | 7.1 |
| 4 | H | H | H | COMe | 5.85 |
| 5 | H | H | H | $NO_2$ | 5.6 |
| 6 | H | H | H | $NH_2$ | 5.48 |
| 7 | H | H | H | $NMe_2$ | 6.8 |
| 8 | H | H | H | NHCH2CH3 | 6.28 |
| 9 | H | H | H | OMe | 5.87 |
| 10 | H | H | H | OCF3 | 5.74 |
| 11 | H | H | H | F | 5.49 |
| 12 | H | H | H | Cl | 5.77 |
| 13 | H | H | H | OH | 5.3 |
| 14 | H | H | H | $CF_3$ | 5.8 |
| 15 | H | H | OMe | $C{=}O(NMe)_2$ | 6.85 |
| 16 | H | $CH_3$ | H | $C{=}O(NMe)_2$ | 6.49 |
| 17 | $NH_2$ | H | H | $NMe_2$ | 7.85 |
| 18 | OH | H | H | $NMe_2$ | 8.74 |
| 19 | $CH_3$ | H | H | $NMe_2$ | 5.92 |
| 20 | $NH_2$ | H | H | $NMe_2$ | 7.19 |
| 21 | OH | H | H | $NMe_2$ | 8.52 |
| 22 | OMe | H | H | $NMe_2$ | 5.85 |

## 4.5 HIV-1 Protease

Human immunodeficiency virus (HIV) is a lentivirus that leads to the acquired immune deficiency syndrome (AIDS), which is a disease affecting the human immune system. Since the start of the epidemic about 35 years ago, there have been an estimated 36 million deaths.[106] According to the World Health Organisation (WHO), as of 2013, 35 million people are infected with HIV, with 2.1 million new infections in that year alone.[106] The HIV virus appears in two forms: HIV-1 and the less virulent and infective, and hence less common HIV-2. Unfortunately, to this date a vaccine has not been developed. On the other hand, successful structure-based drug design has led to the highly active antiretroviral therapy (HAART). This involves the intake of a combination of drugs that inhibit two viral proteins: a) the reverse transcriptase, and b) the protease. The latter is the HIV-1 protease (HIVP) which is an aspartic protease and performs an essential step in the life cycle of HIV-1. It cleaves precursor polypeptides, including gag and pol, into mature viral proteins (step 13 in Figure 4.13). This step is critical for the development of the virus to its infectious form. By inhibiting HIV-1 protease the virus perishes, which makes this protease an excellent target for drug discovery. To date there have been ten drugs approved by the FDA.[119]

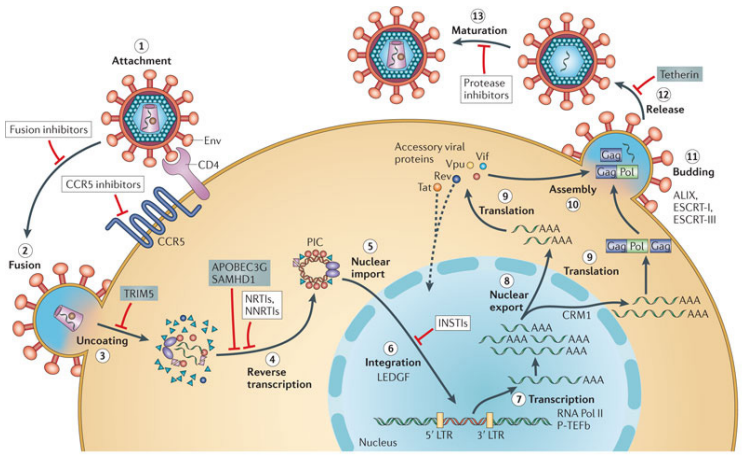


Figure 4.13: The replication cycle of HIV-1 virus. Taken from Engleman A. and Cherepanov P. 2012.[120]

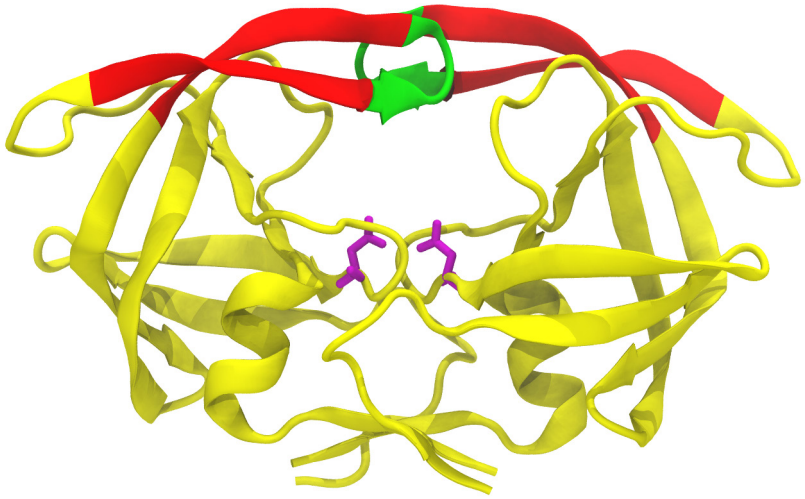

Figure 4.14: Structure of HIV-1 protease (ligand removed for clarity) with PDB code 2PQZ. In red are the flap regions, and in green the flap tips. In magenta is the catalytic dyad comprised of aspartates 25A and 25B.

Figure 4.14 shows the structure of HIV-1 protease (PDB: 2PQZ). HIVP is a symmetric homo-dimer. Each subunit contains 99 residues and at their junction they form a tunnel which comprises the active site. At the bottom of the tunnel is positioned the dual Asp25-Thr26-Gly27 catalytic triad, but what makes this a protease is the catalytic dyad of aspartates 25A and 25B, which with the help of a water molecule cleave the peptide bond of the substrate. At the top of the tunnel (in the opposite direction from the aspartates) lies the so called flap region (residues 43 to 58). The flaps open so that the substrate can interact with the catalytic dyad.

The series of inhibitors investigated in this study were based on a pyrrolidine scaffold (Figure 4.15). Electrostatic calculations reported by Czodrowsk P. et al. 2007[121] indicate the amino functionality of the pyrrolidine should be protonated with both of the aspartates deprotonated. The series of inhibitors are shown in Table 4.4.

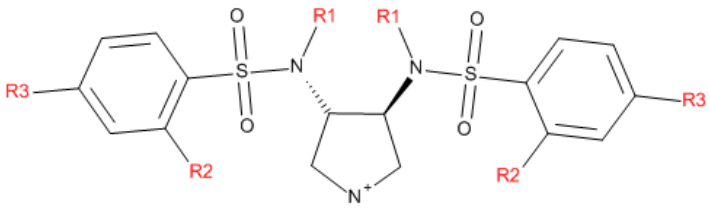


Figure 4.15: Structure of the scaffold used to generate the HIV-1 Protease inhibitors

Table 4.4: Experimental activities of the HIV-1 protease analogues. Compound name shown in bracket as per experimental study [122].

| Ligand No. | R1 | R2 | R3 | pKi |
|---|---|---|---|---|
| 1 (6aa) | Allyl | H | H | 4.91 |
| 2 (6ab) | $CH_2(=CH_2)CH_3$ | H | H | 4.13 |
| 3 (6ac) | $CH_2CH=C(CH_3)_2$ | H | H | 5.8 |
| 4 (6ad) | Bz | H | H | 5.67 |
| 5 (6ae) | $CH_2(4\text{-}BrC6H_4)$ | H | H | 6.34 |
| 6 (6af) | $CH_2(4\text{-}IC6H_4)$ | H | H | 6.41 |
| 7 (6ag) | $CH_2(4\text{-}CF_3C6H_4)$ | H | H | 6.1 |
| 8 (6bd) | Benzyl | $CH_3$ | H | 6.17 |
| 9 (6cd) | Benzyl | Cl | H | 6.11 |
| 10 (6dd) | Benzyl | H | $NO_2$ | 5.76 |
| 11 (6fd) | Benzyl | H | $CONH_2$ | 6.59 |
| 12 (6fg) | $CH_2(4\text{-}CF_3C_6H_4)$ | H | $CONH_2$ | 7.15 |
| 13 (6gd) | Benzyl | H | $NH_2$ | 6.57 |

The crystal structure bound with ligand 6ad showed (Figure 4.16), as expected, that the pyrrolidine amino nitrogen forms a pivotal hydrogen bond network with the two aspartates. Only one of the two sulphonamides was found to interact with the protein. More specifically each of the two sulphonyl oxygens, on one of the sulphonamide, was found within hydrogen bond distance from the isoleucines of each of the flap tips. The benzyl and phenyl substituents were found to occupy pockets S1/S1´, and S2/S2´ respectively, and form van der Waals contacts with protein residues. The findings from the crystal structure enabled the design of the rest of the compounds in the series based on compound 6ad.

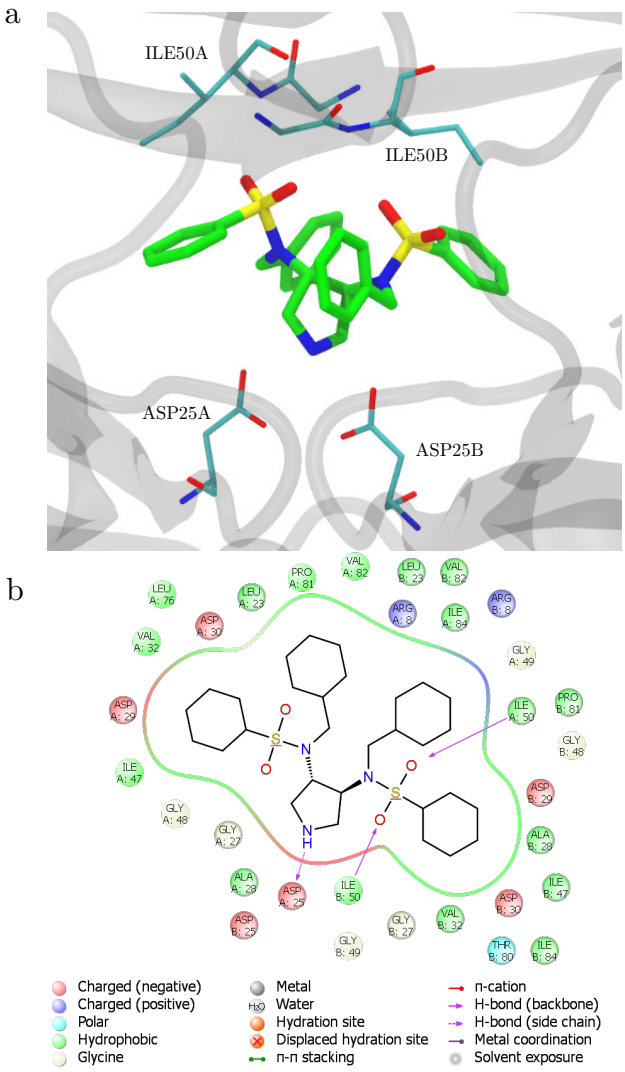


Figure 4.16: Crystal structure of HIVP (PDB: 2PQZ) bound to the inhibitor 4(6ad). (a) Binding site with key residues (Asp25A, Asp25B, Ile50A, Ile50B), and (b) interaction diagram including residues up to 4 Å away from ligand (double bonds are not shown). Picture generated using Maestro.[109] Hydrogens are excluded for clarity.

## 4.6 Src Tyrosine Kinase

Protein tyrosine kinases (PTKs) are a collection of enzymes that are involved in tyrosine phosphorylation by catalysing the transfer of the γ phosphate of adenosine triphosphate (ATP) to tyrosine residues on protein substrates.[123] PTKs are separated in two classes: the receptor tyrosine kinases (RTKs) and the nonreceptor tyrosine kinases (NRTKs). The RTKs are

transmembrane glycoproteins that partake in autophosphorylation and are involved in a number of signalling pathways, such as cell proliferation, differentiation, and migration. This family of kinases includes receptors for insulin and range of growth factors. The Src (from sarcoma) family falls under the umbrella of NRTKs, which are a crucial component of signal transduction pathways generated by various receptors including RTKs, and G protein coupled receptors.[123] There are nine Src family members in total including c-Yes, Fyn, Lyn, Lck, Hck, Blk, Fgr, Yrk, and c-Src. C-Src is a prototypical member of the Src family kinases, that is often overexpressed and/or abnormally activated in a variety of epithelial and non-epithelial cancers.[124] In addition to their involvement in many cancers, such as colorectal and breast cancers, they have been linked to diseases including osteoporosis, and stroke-induced vascular permeability.[125] The involvement of Src kinases in this vast range of normal signalling pathways, in conjunction with the ability of active forms of the proteins to transform cells, has made Src a well-defined therapeutic target.

Figure 4.17 shows the crystal structure of a c-Src kinase with PDB code 2SRC, bound to the ATP analogue phosphoaminophosphonic acid-adenylate ester (AMP-PNP) in its inactive downregulated conformation. Src kinases consist of a myristylated N-terminal unique domain (not shown in the crystal structure), which differentiates family members from each other.[126] After this domain is the SH3 domain, followed by the SH2, which is linked via a short polyproline type II helix to the tyrosine kinase domain or catalytic domain, followed by a short C-terminal tail. All of these parts are essential for the function of the protein, and work closely with each other.[126] The key to the transition between the inactive and active form is a tyrosine (pTyr527) in the C-terminal tail. The moment this residue is phosphorylated it interacts favourably with SH2 domain gluing the complex shut. This, in cooperation with intramolecular interactions with the linker and SH3 domain, results in the activation loop forming an α-helix, which in turn stabilises the inactive

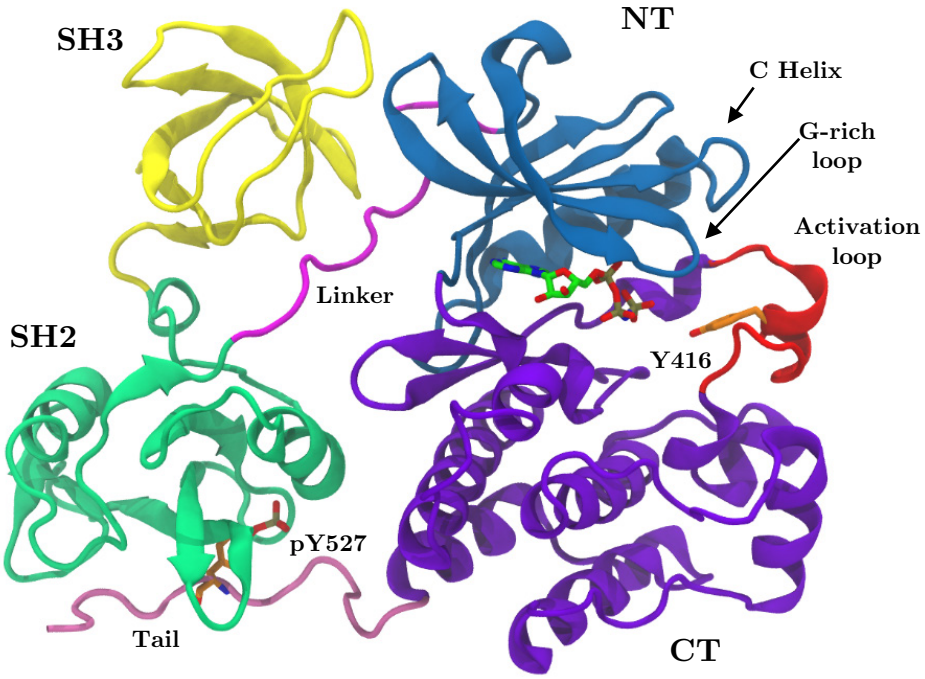


Figure 4.17: Crystal structure of downregulated c-Src (PDB: 2SRC) bound to inhibitor AMP-PNP. The amino and C-terminal (CT) lobes are shown in blue and violet respectively. The activation loop is shown in red with Tyr416 in orange. Domains SH2 and SH3 are shown in green and yellow respectively, the N-terminal (NT) and SH2 linker (PPII helix) is shown in magenta, and the C-terminal tail is shown in pink with the mutated pTry527 in orange. The ligand is shown with green carbons between the CT and NT.

conformation of the catalytic domain, blocking phosphorylation of Tyr416 (orange and attached to the activation loop; unlike many other Src crystal structures, the tyrosine and flanking residues adopt an ordered conformation), which positively regulates catalytic activity and ultimately block the peptide substrate-binding site. Additionally, the folding of the protein limits accessibility of the binding surfaces of the SH3 and SH2 domains further regulating participation of these complexes in cellular signalling.[124] If dephosphorylation of pTyr527 occurs then the molecule unfolds, freeing the SH3 binding site, which in turn can wrap itself around protein chains, and with the now activated kinase active site, signalling can commence. Clearly if this is unregulated it can lead to, amongst other things, uncontrollable cell growth, and cancer.

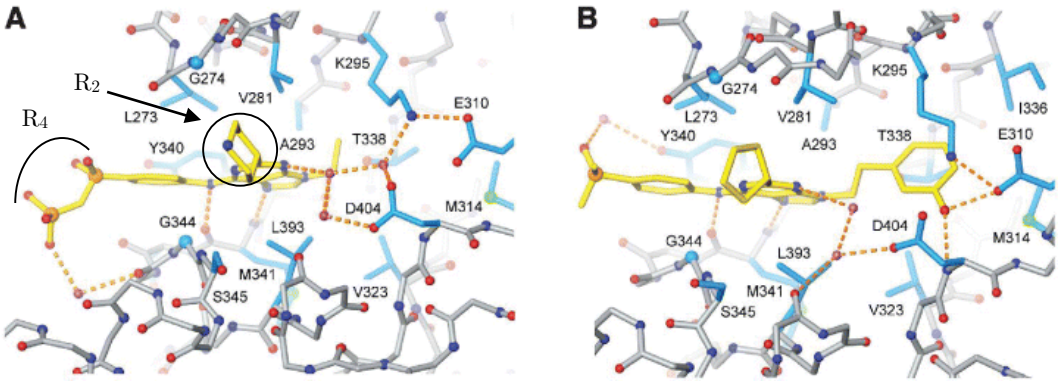


Figure 4.18: Binding site of Src kinase with two purine-based inhibitors. Protein backbone shown in grey, side chains that interact with the ligand in light blue, and oxygens of x-ray water molecules are in purple. Ligand phosphorus is orange, nitrogen blue, sulphur green and oxygen red. (A) X-ray structure with PDB code 2BDF (resolution 2.10 Å) bound with ligand 9 (see Table 4.5 below), and (B) structure with PDB code 2BDJ (resolution 2.50 Å) bound with ligand 6. Image taken from Dalgarno D. et al. 2005.[125]

The dataset used with this target is a set of purine-based analogues designed by Dalgarno and co-workers.[125] A tri-substituted purine template core (see Figure 4.19) was utilised to construct a series of 9 potent inhibitors shown in Table 4.5. The protonation states of the $R_4$ group of ligands 7, 8, and 9, are discussed in Chapter 5.

Two crystal structures of the tyrosine kinase domain only (Tyr416 and part of the activation loop was disordered), were presented in the Dalgarno paper, bound with ligands 9 (PDB: 2BDF), and 6 (PDB: 2BDJ). To remain consistent with the E-Novo work, the latter protein structure was used for our studies.

The binding sites of those two crystal structures with ligands 9 and 6 is shown in Figure 4.18 A and B respectively. Both inhibitors present similar binding modes. Substituents in the R4 position do not make direct contact with protein substituents. The middle of the ring and the substituent in position R2 form hydrophobic interactions with residues surrounding the ligand (see Figure 4.18). Perhaps the main difference arises from the substituent in position R1. Ligand 6 contains a longer group

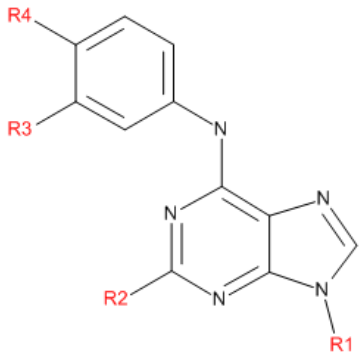


Figure 4.19: Structure of scaffold used to generate the Src Tyrosine kinase inhibitors

Table 4.5: Experimental activities of the Src kinase purine-based analogues.

| Ligand No. | R1 | R2 | R3 | R4 | pIC50 |
|---|---|---|---|---|---|
| 1 | 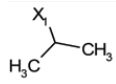 | 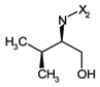 | Cl | H | 6.6 |
| 2 | 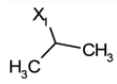 | 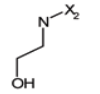 | Cl | H | 5.8 |
| 3 | 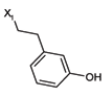 | 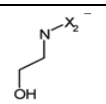 | Cl | H | 7.6 |
| 4 | 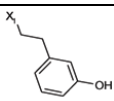 | 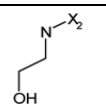 | H | H | 7.6 |
| 5 | 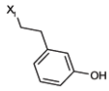 | 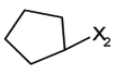 | H | H | 7.5 |
| 6 | 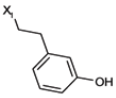 | 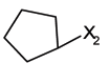 | H | 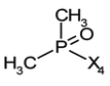 | 9.3 |
| 7 | 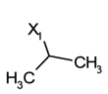 | 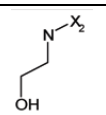 | H | 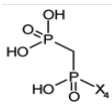 | 5.7 |
| 8 | 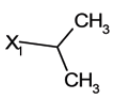 | 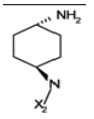 | H | 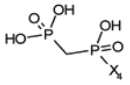 | 6.6 |
| 9 | 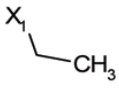 | 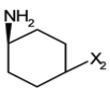 | H | 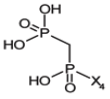 | 7.2 |

(3 hydroxyphenethyl) in this position, which penetrates deeply into the pocket forming intricate hydrogen bonding interactions with inhibitors Lys295, Glu310, and Asp404. It should be noted that both ligands bind a little differently than the natural ligand ATP. The R1 moiety is projecting towards the rear of the binding site, whereas the R2 towards the position occupied by the ribose in ATP. The authors found similar binding modes with CDK2 and purine based inhibitors.[125]

## 4.7 Summary

In this chapter the five protein-ligand systems used in this thesis including Thrombin, β-Secretase, factor XA, HIV-1 protease, and Src kinase, were introduced. A short background of the biological relevance for each target protein, and the motivation behind the efforts of producing pharmaceutical compounds to inhibit their action, was outlined. Where applicable, statistics were provided regarding the socio-economic impact the relevant disease has in the world, as in the case of Alzheimer's disease or dementia. The mechanism of each of the proteins was briefly discussed in conjunction with the presentation of key structural motifs. Then, an overview of the binding site with key protein-ligand interactions were discussed, followed by an outline of the series of the congeneric inhibitors included in this study, along with comparison of their potencies where necessary.

Having established the basics of the principles behind the methodology used in the present study, the motivation for conducting this research, and an understanding of the importance and challenges associated with the systems on which the study was conducted, the reader is ready to be presented with the details and the findings of this research. The next chapter will focus on an attempt to reproduce a published all-in-one workflow for physics-based rescoring of protein-ligand docking poses in the setting of lead-optimisation.

# Chapter 5

# Assessing a Published Workflow for Lead Optimization

## 5.1 Introduction

In the previous chapter the protein-ligand systems used in this study were introduced. These systems were included in a published protocol, targeted as a tool for lead optimization in structure-based drug design, where a set of ligands are prepared, docked and later rescored using MM-GBSA.

This section details the work performed on attempting to reproduce that workflow. The aim of doing this was to first see if such a method is indeed reproducible and how successfully it works, and second to assess the advantages and disadvantages of the method. In this chapter the protocol and a detailed account of the steps involved are initially described, along with a description of the systems tested. Comparison of the results of this study and the published results with experiment is performed, followed by an individual investigation of the docking and rescoring steps. Finally conclusions are drawn regarding the reproducibility of the protocol and the ways to move forward are presented.

## 5.2 E-Novo Protocol

### 5.2.1 Introducing the workflow

The E-Novo method proposed by Pearce, et al.[16] is designed to be a convenient "all-in-one" protocol to be used as a structure-based lead optimization tool. This is performed through a three-stage semi-automated process where compounds of choice are enumerated, core-constrained docked and finally re-scored with a more accurate scoring function. These stages were employed as separate sub-protocols in Pipeline Pilot (PP)[127] using modules as implemented in Discovery Studio (DS).[127] A summary of the workflow is shown in Figure 5.1.

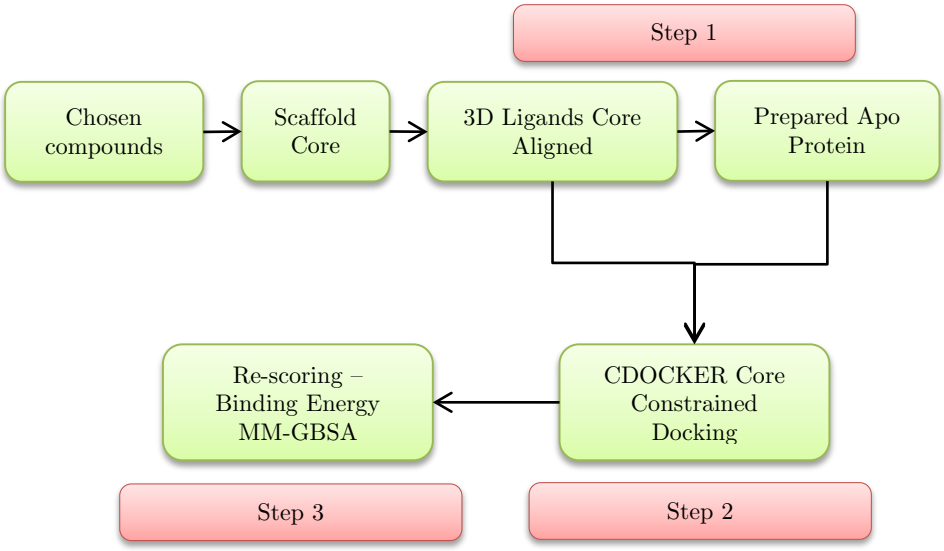


Figure 5.1: Schematic representation of the of the E-Novo protocol steps

The required input files for the protocol to run are: the prepared protein target structure file, the 3D scaffold and the set of compounds chosen for evaluation. Initially, X-ray structures of the complexes are downloaded from the PDB database and loaded into DS to be prepared. The protein is separated from the bound ligand and crystallographic waters. The command "clean" is then executed on the protein alone to add hydrogens, fix missing

side chains, and determine the protonation state of ionisable side chains and terminal groups residue protonation at a neutral pH, and, finally, saved in a PDB file format. The ligand initially bound to the protein in the x-ray structure, is processed into the scaffold file; this is given a file format of R-group or RG format under Symyx draw[128], which is essentially a coordinate file that consists of the core (scaffold) of the ligand, used as a basis to derive the candidate ligands by changing only certain groups (R-groups). The desired scaffold framework is obtained by stripping of all hydrogens from the ligand and then adding them back again with the exception of those selected for the position of the R-groups. Finally, a structure data file is obtained for each of the ligands of interest.

The three sub-protocols are namely: 1. Ligand Enumeration and setup (LES), 2. Core-Constrained Docking (CCD), and 3. Calculate Binding Energy (CBE). Below, a detailed account of these sub-protocols is presented.

### 5.2.2 Ligand Enumeration and Setup (LES)

The compounds of interest can be from screening results or from a generated virtual library or both. In this step the structure data file of the ligands and the RG file of the scaffold are utilized to enumerate all possible ligands for the docking step that follows. Ionization and tautomer states are controlled by two distinct components within this sub-protocol, with the option of being set active or inactive. The ionization component (named in PP as "enumerate ionization states") uses a lookup table within PP to estimate possible ionization states. The desired pH can be adjusted but the default is 7.0. However, individual inspection of the protonation states of the ligands is required before proceeding. Published work of the model used in this component has demonstrated a good $pK_a$ predictive ability for 28 chemically diverse compounds of pharmaceutical interest, when compared to experiment ($R^2 = 0.85$, RMSE = 0.90).[129] Conversion of the enumerated two-dimensional ligands to 3D occurs, followed by cleanup minimization using the "clean force

field" within PP. Based on the attachment point defined in the RG file, R-groups are fragmented from the ligands using a "Generate RGroups" component. These groups are then re-attached in all possible conformations through the use of an "RG reader" component. Unique desired molecules are retained by cross-referencing the canonical smiles of these structures with the ones obtained from the enumerated 2D structures. A structure data file with all the desired ligands aligned to the crystal structure geometry is written out into the input directory for the next step.

In the published E-Novo protocol the tautomer enumerator was switched off, and therefore the same choice was made in our study for purposes of reproducibility. The authors of E-Novo reported longer run times and poorer fitting data for the alternate tautomers, when the enumerator was turned on.[16]

### 5.2.3 Core-Constrained Docking (CCD)

In this protocol diverse conformations of the ligands from the previous step are generated and docked in the protein of interest keeping the core constrained to the coordinates of the crystal structure.

The docking algorithm implemented is CDOCKER[130] a CHARMm-based MD simulation scheme for docking ligands in a receptor binding site. Constrain command lines are added into the force field script to constrain the core. Atom types and partial atomic charges for the ligand default to the ones in the general purpose Quanta®3.2/CHARMm force field.[131] CDOCKER is a grid based docking algorithm with the active site being defined as residues at a given distance from the centre of mass of the core scaffold; the default is 8 Å. Initially the ligand is run through an adopted basis Newton-Raphson (ABNR) minimization stage.[29] With the core constrained and in the absence of the protein, conformations are generated with the use of high-temperature (1000 K) MD simulations (default 20 simulations). The resulting conformations are then docked into the protein and minimized using the

steepest descent (SD) algorithm. With the core unconstrained, the docked poses are further refined in the receptor active site using a short simulated annealing protocol and then minimized using steepest descent combined with conjugate gradient. Nonbonded interactions (van der Waals and electrostatic potentials) are softened during docking and the initial refinement phase, but not in the final minimization. The protein is held rigid throughout the entirety of the procedure. In a 41-member protein-ligand validation study a substantial improvement in accuracy (docking success rate from 66% to 76%) was achieved if explicit all-atom forcefield is used in a final minimisation step with the aim to refine the docking poses.[130] The top five lowest dock scored poses are selected and saved for the final rescoring step.

### 5.2.4 Calculate Binding Energy (CBE)

Here, a physics-based scoring function with the use of implicit solvent is employed to rank the top five poses of each ligand. The method implemented here is Molecular Mechanics using Generalized-Born Simple Switching as implicit solvent (MM-GBSW). It falls under one of the four different GB and GB-like methods that are applied in CHARMm. In this method a van der Waals surface with a smooth dielectric boundary is parameterized based on various smoothing lengths against the exact Born radii of a small protein (PDB code 1AJJ).[132] Free energies are obtained from three structures: the bound complex, the unbound protein and unbound ligand. Each calculated energy contains an electrostatic term (Coulombic interactions), a nonpolar term (van der Waals and hydrophobic interactions) and an internal strain term which evaluates the strain upon binding of ligand with the receptor; internal strain energy reflecting protein deformation upon ligand binding is omitted since the protein is held fixed. Entropic contributions are completely ignored in this protocol based on the assumption that they are similar for a congeneric series of ligands binding to the same protein and will cancel when relative comparisons are made. Finally, the relative free energy of binding is

calculated by subtracting the energies of the free protein and free ligand from the bound complex.

The next section focuses on our attempt to reproduce the E-Novo results. First the details of preparing the protein-ligand systems is presented along with the difficulties faced. This is followed by a direct comparison of our results with the published versus experiment. The outcomes taken from that comparison lead to a closer investigation and critical assessment of the docking and rescoring steps. Finally we present our conclusions about the method along with suggestions to move forward.

## 5.3 Assessing E-Novo

### 5.3.1 System preparation

The systems were prepared in line with the published work as described in paragraph 5.2.1 in this chapter. The exact PP protocols used in the original publication were obtained from Accelrys, where they have become available for further testing and development. A set of the input files for one of the target sets was also provided as a guide. Unfortunately, at the time this study was conducted, the available program versions were different from the ones that were used in the published E-Novo work. The work in this thesis was conducted using versions 7.5 and 2.5 of PP and DS respectively, instead of 6.02 and 1.7 in the published work. Such software is typically executed as a "black box" making it difficult to identify differences between versions. Some of the parameters used by default in our implementation of E-Novo are shown in Figure A.1 and Figure A.2 for the docking and for the rescoring step respectively.

Initially the reproducibility of the published protocol was tested. In the next section our results obtained by running E-Novo, are compared against the published study and presented accordingly for each system.

### 5.3.2 Comparison with published results

Table 5.1 illustrates the comparison between the published and the calculated scores of the rescoring sub-protocol on all cases. The $R^2$ is shown, with the corresponding p-value for a two tailed t-test. To give a quantitative perspective of the differences between the energy prediction of the two sets of data (published and calculated), the average energy difference and the range of the energy differences between free energies of each ligand, is also shown.

This table will be referred to throughout the rest of this chapter.

Table 5.1: Comparison of Published binding Energies with Calculated (rescoring protocol). The p-value is shown as $P_R^2$. The statistical significance is set at 5%.

| System | $R^2$ Published vs Calculated | $P_R^2$ | Average Energy Difference (kcal $mol^{-1}$) | Energy Difference Range (kcal $mol^{-1}$) |
|---|---|---|---|---|
| **Src Kinase** | 0.56 | 0.02 | 20.45 | 12.37 |
| **β-Secretase** | 0.60 | 0.04 | 31.22 | 11.58 |
| **Factor Xa** | 0.05 | 0.30 | 13.29 | 17.68 |
| **HIV Protease** | 0.00 | 0.83 | 27.49 | 37.30 |
| **Thrombin** | 0.43 | 0.02 | 6.94 | 13.84 |

#### *Src Tyrosine Kinase*

The predicted binding energies of the 9 analogues against the experimental pIC50s are shown on Figure 5.4. A shift between predicted energies of this study and the published study, was observed. This was consistent across all the targets. Unfortunately, due to the "black box" nature of the software it was not possible to determine the origin of this issue.

The coefficient of determination $r^2$ for the published results was 0.76 and for the calculated results 0.56.

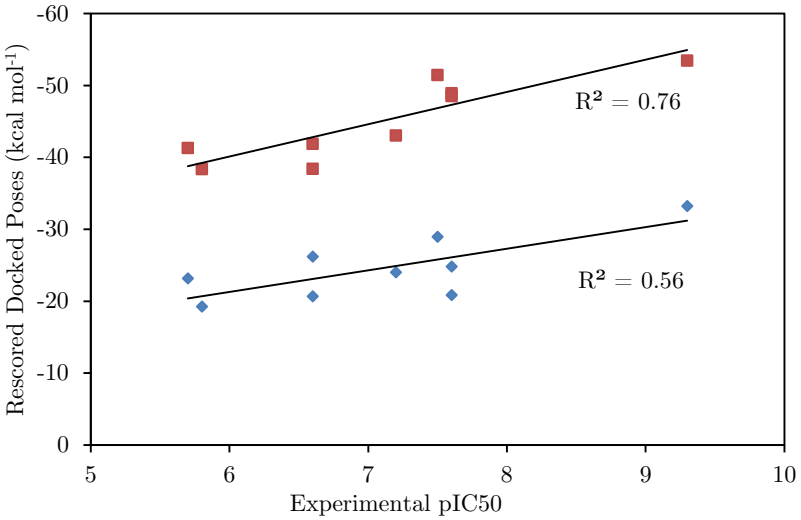


Figure 5.2: Correlation between experimental pIC50 for Src Tyrosine Kinase and calculated (diamonds) and published (squares) binding energies.

This result is not as poor compared to the results obtained for the rest of the systems, however, it is inferior to the published result, considering the same method and force field was used. According to the authors of the published work, the good correlation observed, was attributed to nonpolar energy contributions considering the pocket is narrow with buried protein-ligand interactions. This was justified by a good coefficient of determination of 0.67 between the nonpolar surface area (NPSA) and experiment. In addition, the R4 group of ligands 7, 8, and 9 (see Figure 4.19

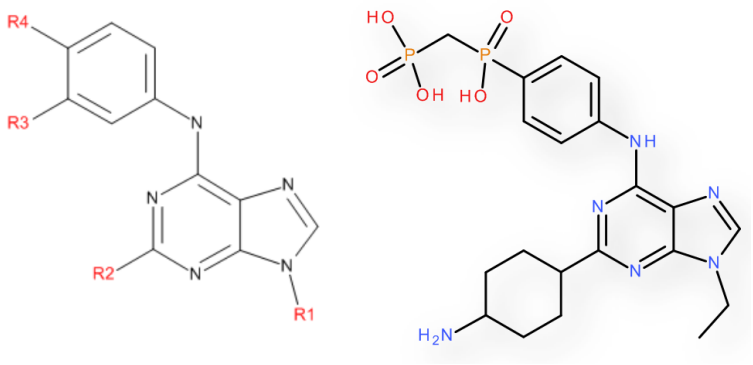


Figure 5.3: The ligand scaffold of Src Tyrosine Kinase system is seen on the left while ligand number 9 is shown on the right. The R4 group corresponds to phosphonomethylphosphinyl (PMP) group and amidine to R2 group.

and Table 4.5), consists of a phosphonomethylphosphinyl (PMP) moiety facing the solvent exposed part of the pocket, while the R2 group of ligands 8 and 9 contains an amine buried in the protein bonding pocket.

Realistically one would expect both these groups to be charged, however the contrary is seen in the published work. All correlations reported throughout all systems in the E-Novo article, with the exception of Thrombin, consist of neutral ligands. This choice was made based on a single study [133] of a series of β-Secretase inhibitors. This study concluded that using GBSA solvation models, ligand binding correlated better with van der Waals interactions and less with Coulombic/solvation terms, while charged ligands caused large deviations in the same terms. Although, it is known that charges increase complexity significantly, it is highly unrealistic to run such calculations using the neutral form of ligands and one runs the risk of biasing the results. This is even more evident in the case where charged moieties of the ligands may form key interactions with the protein. An example of this, which will be described in more detail later, is the binding site of HIV Protease where the pyrolidine of the ligands should be doubly protonated (i.e. be charged) to interact with the two aspartates of the catalytic dyad. on closer investigation it appears the motivation behind chosen protonation states was purely based on the improved correlations observed against

experiment. The results published were those with the protonation states that gave best agreement with experiment, thus presenting a better overall performance of E-Novo. Specifically, for the case of Src Kinase, choosing neutral ligands over charged ligands, improved the correlation of determination from 0.69 to 0.76.

An $R^2$ of 0.56 was obtained between published and calculated data, suggesting some relationship between the data which was significant at a 5% significance level; however it is not a sufficiently high correlation to denote the method as robust and reproducible. The latter is further indicated by the average difference between the two energies of 20.45 kcal $mol^{-1}$. The differences between the two sets of energies for the set of 9 ligands vary from 15.67 to 28.04 kcal $mol^{-1}$ (see Table 5.1).

### *β-Secretase*

The next system investigated consisted of 7 similar ligands. The correlations with experiment for this study and the original E-Novo study are shown in Figure 5.6 and are 0.10 and 0.21 respectively.

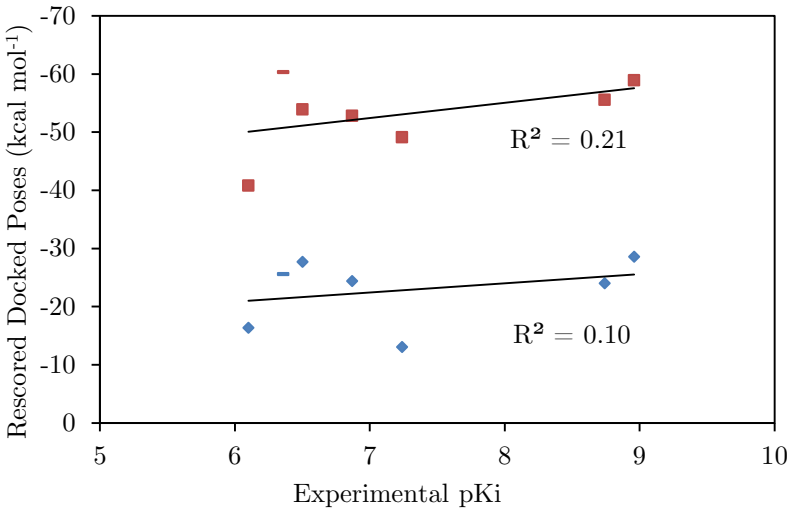


Figure 5.4: Correlation between experimental pKi for β-Secretase and calculated (diamonds) and published (squares) binding energy. The dash depicts outlier ligand 6(5f). Ligand 5(5e) is seen as the utmost bottom left point in each series.

In the study by Pearce et al., the correlation was improved to 0.58 by removal of outlier ligand 6 (5f in E-Novo) and to 0.80 by removal of ligand 5 (5e in E-Novo). In the latter the authors of the published work noted a rotation of the sulphonamide by 120 degrees (Figure 5.5). This was not observed in this study, with the poses of ligands 5 and 6 being identical (Figure 5.6). Ligands 6 and 5 were not outliers in the calculated results. It should be noted that ligand 5 does not appear as a clear outlier in the plot of the published data either. The improved coefficient of determination observed upon its removal only seems coincidental. That combined with the observation of the rotated sulphonamide classified it conveniently as an outlier. Correlations in our study when removing ligand 6 and then ligand 5 are: 0.17 and 0.45 respectively.

According to Table 5.1, the calculated data explains 60% of the variability in the published data which is borderline significant with a p-value of 0.04 (for a 5%significance limit). Though better than the rest of the systems, this correlation is not sufficient to conclude the method is robustly reproducible. Quantitatively the two versions gave very different results.

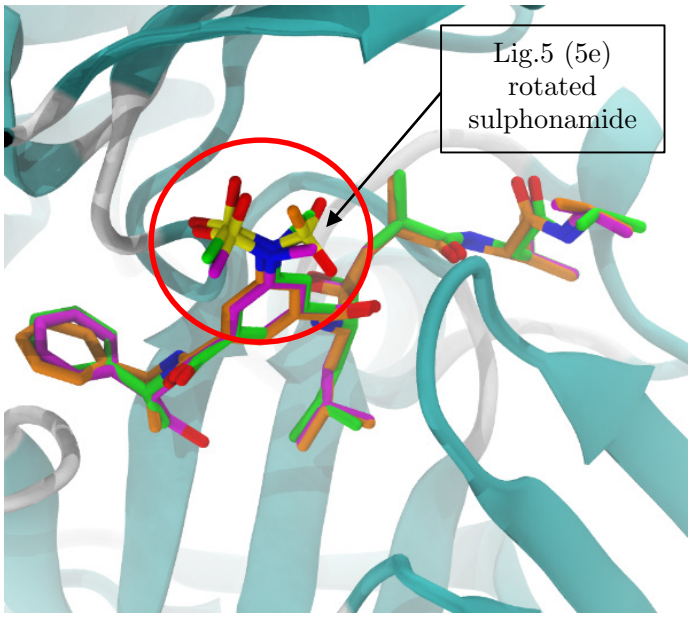


Figure 5.5: From published E-Novo protocol. Top re-scored poses for ligands 5 (5e) and 6 (5f) shown with orange and magenta carbons respectively. The molecule with green carbons corresponds to the crystal structure for compound 4(5d) with PDB code 2P4J. Hydrogens are removed for clarity.

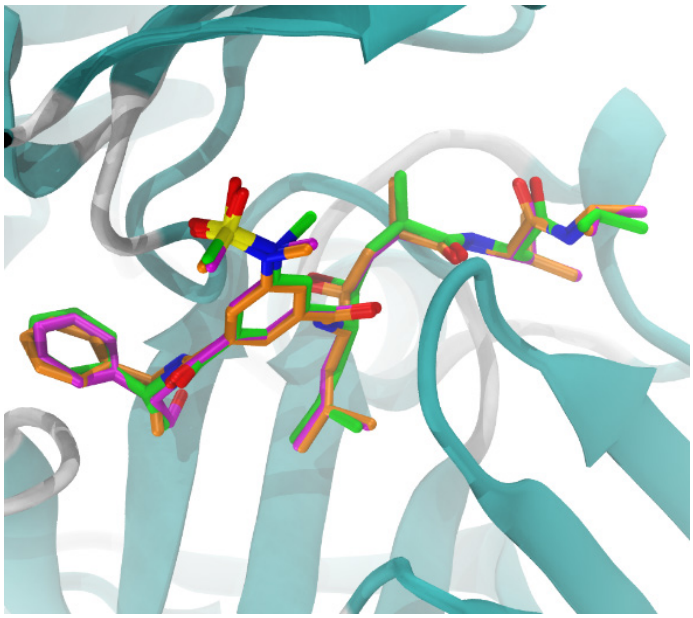

Figure 5.6: From calculated E-Novo protocol. Top re-scored poses for ligands 5 (5e) and 6 (5f) shown with orange and magenta carbons respectively. The molecule with green carbons corresponds to the crystal structure for compound 4(5d) with PDB code 2P4J. Hydrogens are removed for clarity.

### *Factor Xa*

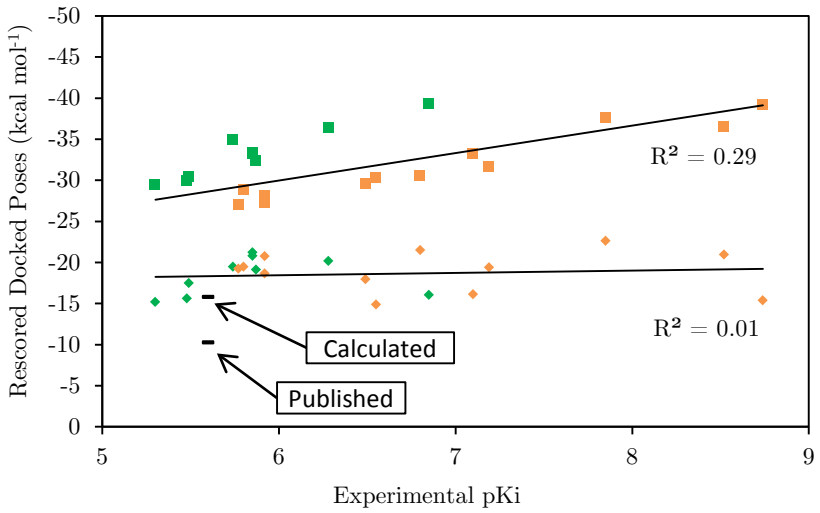


Figure 5.7: Correlation between experimental pKi for Factor Xa and calculated (diamonds) and published (squares) binding energy. Colored green and orange are the individual series observed in published results.

This system consisted of the largest dataset in the study with a total of 22 compounds. In this case, there was no correlation between our adopted protocol and the original published results (Figure 5.7). Again the average difference of the two sets of energies, and the range of difference, indicate that the protocol is not reproducible both quantitatively and qualitatively. Additionally no correlation was observed with experimental data ($R^2 = 0.01$). Poor correlation with experiment was also reported in the published work ($r^2 = 0.29$), however this was improved to 0.43 by removal of ligand 5; a clear outlier as indicated in Figure 5.9. Insufficient explanation was provided as to why such a large deviation from the rest of the dataset was observed for this ligand. This was not an outlier in our study (see Figure 5.7) and neither was it in the Amgen[134] study that used the same dataset. In fact, the poses of ligand 5 from our study against the published study are nearly identical with only a slight shift of one of the oxygen of the nitrogen dioxide R5 group

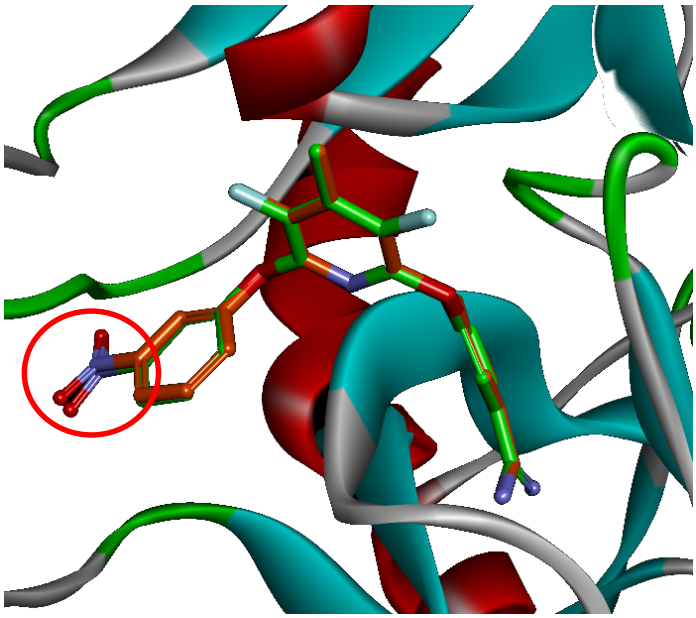

Figure 5.8: Comparison between the re-scored pose of outlier ligand 5 in the published study (green) and the calculated study (orange). For this ligand R1, R2 and R3 are a hydrogen while R4, shown in with a red circle, a $NO_2$ (see Table 4.3).

(Figure 5.8). This is an indicator that the rescoring protocol works differently. A more detailed discussion follows later in this chapter. The authors of E-Novo also observed the split of the dataset into two series depicted as green and orange in Figure 5.7, which showed high correlations with experiment; 0.91 (improved to 0.98 by removal of ligand 10 – no explanation provided) and 0.93 respectively. We observed no indication of such series and neither did researchers in the Amgen study.[134]

### *HIV-1 Protease*

The binding pocket of HIV Protease is highly flexible and since the protein is held rigid throughout the entirety of this protocol, it is a challenging test case. A key interaction between the protein and all of the ligands in the series is the salt bridge between the pyrrolidine moiety (part of the scaffold) and the catalytic dyad ASP25A and ASP25B. Hence one would expect the nitrogen of the pyrrolidine to be positively charged to form these key interactions.

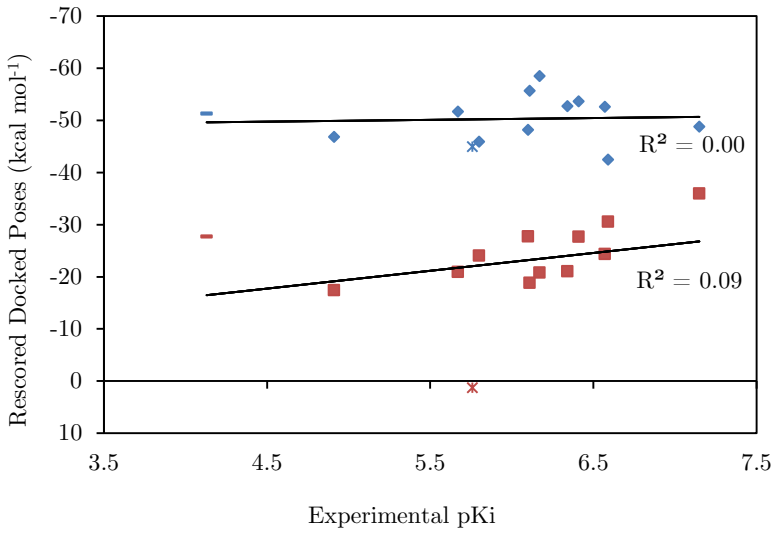


Figure 5.9: Correlation between experimental pKi for HIV Protease and calculated (diamonds) and published (squares) binding energy.

However, the authors of the published article used the neutral form of the ligands (singly protonated pyrolidine) on the basis they observed stronger correlations with experiment. For purposes of reproducibility the author of this thesis decided to use the doubly protonated pyrrolidine form for the calculations. Extremely large deviations in predicted energies were observed while for some ligands even large positive energies were obtained which the author could not explain.

Presented here are the results from the more realistic model of the protonated nitrogen of the pyrolidine. This would explain the large average energy differences and range of differences shown in Table 5.1. The comparison with experiment is particularly poor. Again certain outliers, symbolised in Figure 5.9 by a dash and a star, improved the $R^2$ from 0.09 to 0.60 for the published results, but were not observed in our study.

### *Thrombin*

The correlation of the calculated binding energies for the series of Thrombin versus published binding energies is 0.43, which with a p-value of 0.02 is significant (see Table 5.1). At 6.94 kcal $mol^{-1}$ the average energy difference is

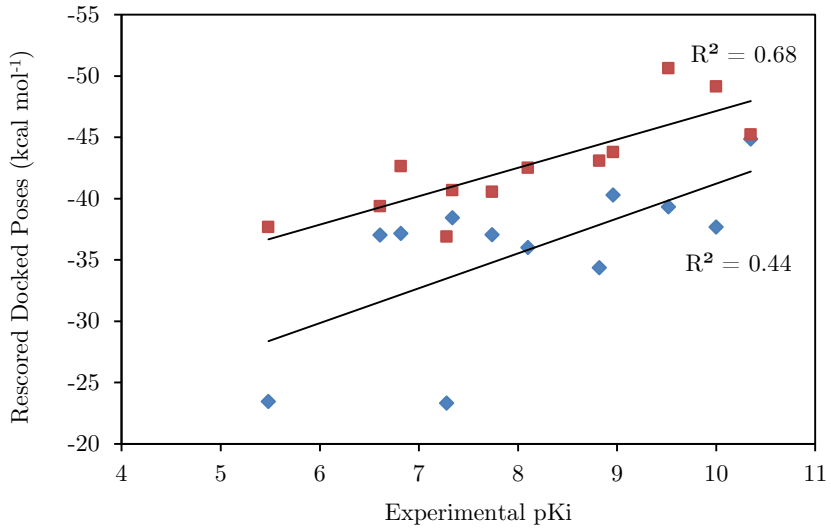


Figure 5.10: Correlation between experimental pKi for Thrombin and calculated (diamonds) and published (squares) binding energy.

the smallest amongst the targets, but the range still remains high at 13.84 kcal $mol^{-1}$. Considering such changes and poor $R^2$ are observed for the same method and ligands when only the software versions are different, is worrying. The binding energies with experimental pKi are shown in Figure 5.12. Here, unlike the previous targets, the authors of E-Novo kept the charged form of amidine claiming slightly better results compared to the neutral form. We were unable yet again to reproduce the published results. Our results showed a greater variation, with the $R^2$ reaching 0.44. This value is sustained only due to ligand 7 (far bottom - left point in Figure 5.10 with pKi = 5.48). When ligand 7 is removed, the correlation plummets to 0.24. Based on a 5% significance level for the size of this dataset, any value of $R^2$ above 0.33 can be accepted as statistically significant.

### 5.3.3 Analysis of docking step

Thus far, we have shown that E-Novo protocol was undeniably non-reproducible. However, we have not discussed the reasons for this. To

perfectly pinpoint what has changed between the code versions proved impossible. Instead it is possible to investigate which step of the protocol generates the majority of the error.

We compared our docking results with the results of Pearce et al., in three ways: the coefficient of determination relating the calculated top docked poses with the published poses, the average absolute difference between dock scores for each ligand in each series, and by constructing an all-poses-with-all-poses Root Mean Square Deviation (RMSD) matrix between the top 5 docked poses output by CDOCKER for the calculations of this study and the published E-Novo study.

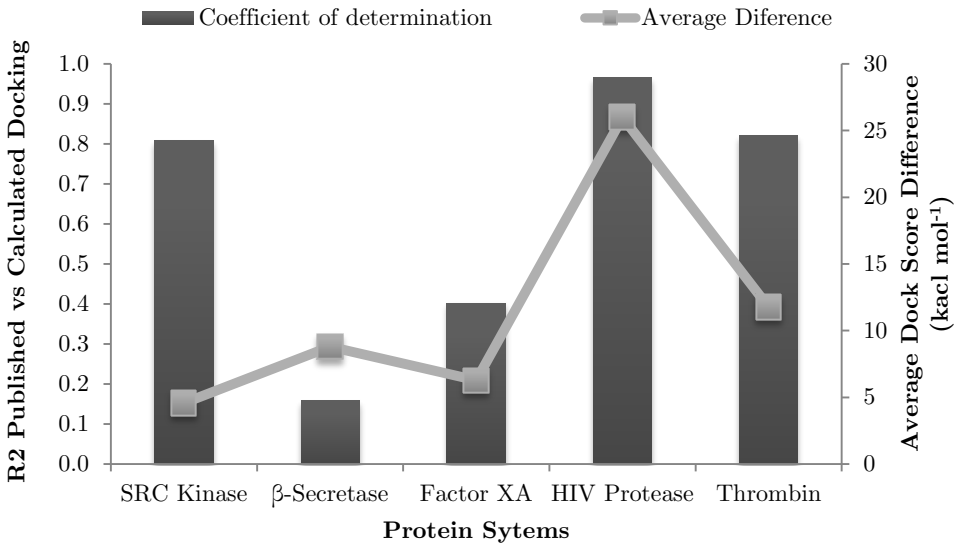


Figure 5.61: Comparison between the published dock scores and the calculated dock scores in our version of the protocol for all 5 systems. The quantities plotted are the coefficient of determination between the dock scores and the average absolute difference between the score values.

Clearly (Figure 5.11) there is significant correlation between docking scores for 3 out of the 5 targets, while less for Factor Xa and even less for β-

Secretase. The average absolute differences between the two sets of scores for the 5 protein-ligand systems varies form 4.58 kcal $mol^{-1}$ to 25.99 kcal $mol^{-1}$.

The differences in the scores could be due to either changes in the parameters relating to scoring between the two versions, or to different poses. The latter was investigated with the use of the RMSD matrix mentioned previously. Overall RMSDs of less than 2 Å were observed for the majority of poses across all 5 systems. There were a few exceptions with higher RMSDs where an alternative binding mode was predicted by the docking algorithm. Such an example is the highest scored pose of the 5 dock poses for the Thrombin ligand 9 (ligand 10 in published E-Novo) shown in Figure 5.12 (the different numbering of the ligands is explained in section 4.2). Both are reasonable orientations that would give different results in most rescoring methods. This comparison indicates that although the scores were not reproducible, reasonable poses were predicted and the results were qualitatively equivalent, prompting an investigation of the rescoring protocol.

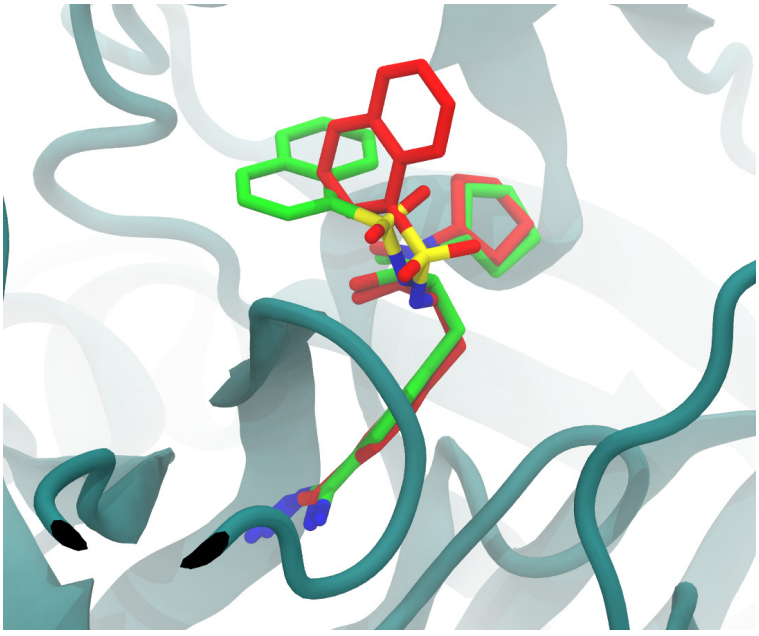

Figure 5.72: Comparison between the top CDOCKER scored posed of ligand 9 (in E-Novo ligand 10) for the published (green) and the calculated (red), for Thrombin.

### 5.3.4 Analysis of rescoring step

The comparison of the published MM-GBSA scores against the scores obtained by rescoring the published docked poses using our version of the software is illustrated in Figure 5.13. For this we are thankful to the authors of E-Novo for willingly sharing their data to assist with our investigation. The hypothesis here is that for the rescoring step to be reliable and consistent, the use of identical input structures should produce exactly the same results. It is clear, however, that the two rescoring sub-protocols work differently. Owing to the nature of the software we were unable to identify precisely what was different. The average absolute differences between the two sets of energies for the 5 systems, ranged from 4.91 kcal $mol^{-1}$ in Thrombin to as high as 34.00 kcal $mol^{-1}$ in β-Secretase.

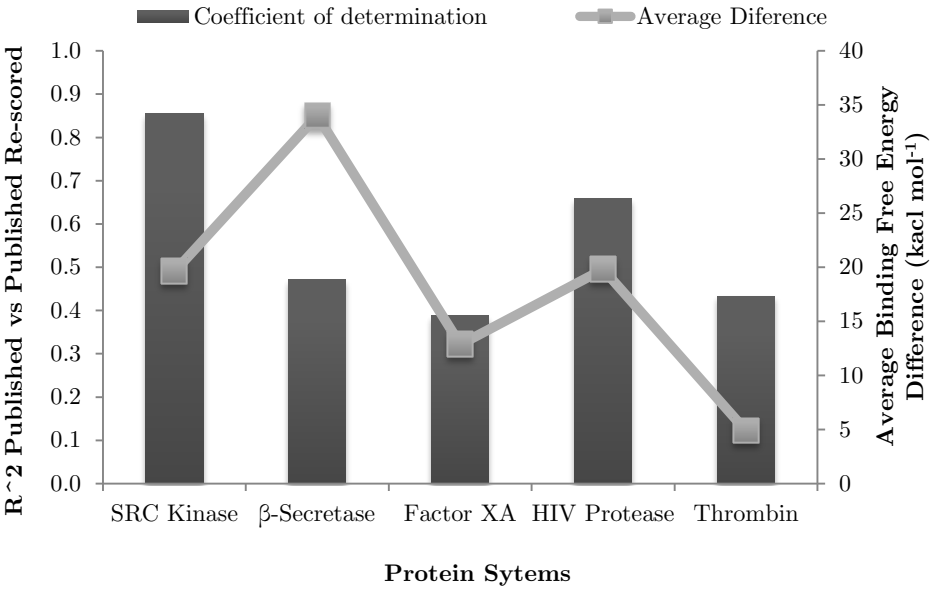


Figure 5.13: Comparison between the originally published binding energies and the published binding energies rescored in our version of the protocol for all 5 systems. The quantities plotted are the coefficient of determination between the binding energies and the average absolute difference between binding energy values.

## 5.4 Conclusions

This chapter focused on a fair assessment of a published all-in-one PP protocol targeted as an efficient tool for structure-based lead optimization. It was clearly and unambiguously shown that the published work is not reproducible. This was mainly due to undocumented software changes. The nature of the protocol made it impossible to attain knowledge of what the differences of the versions were. Our results using the available software were generally poor across all targets, while the published results were marginally better. However, arbitrary assignment of outliers, for which poor or no explanation was provided, were a major contribution to some of the better published results. In addition, the protonation states of the ligands were chosen on the basis of the correlation of the predicted energies with experiment, rather than what would make chemical sense. This suggests that the better performance observed was either by manipulation of the data or simply by luck. Overall E-Novo is an attractive method but it is far from being an efficient structure based lead optimization tool, as proposed by the authors of the published article.

There are a number of recent publications reporting encouraging results regarding the use of physics-based rescoring of docked poses using this method or variations.[10-12, 14, 15, 17-19, 21, 80] Although disproving a rescoring protocol is an important finding, on its own it is not sufficient to confidently denounce the performance of this method. Numerous questions arise such as: How well do different MM-GBSA implementations perform on the same system i.e. on the same input structures? What agreement with experiment is obtained when the same rescoring methodology is applied on docked poses of a system derived from different docking algorithms i.e. the sensitivity of binding energy calculations on initial structures? What is the performance of the method across a range of systems? Are consistent results obtained? Is there an indication of an implementation of the method that provides reasonable predictions with experiment across all systems or an indication of

which implementation to use for a particular system? To adequately assess the performance of MM-GBSA as a fast physics-based post-docking filter, we would need to investigate these questions by testing the methodology (that is docking followed by MM-GBSA rescoring) in a range of software using a range of Generalised Born implementations. The details of the protocols used, along with the results and our findings are discussed in the next chapter.

# Chapter 6

# Application of MM-GBSA as a rescoring tool of docked poses in a range of software

## 6.1 Introduction

In the previous chapter, a published "all-in-one" – molecule set-up, docking and MM-GBSA rescoring – protocol was critically assessed. For consistency matters the exact same set-up and configurations were chosen; however, at the time of testing different software versions were available, something that should not pose an issue for a method to be robust. The testing showed that the protocol was not only unreproducible, but also performed poorly at generating qualitative results with experiment. In fact, a closer investigation into the published data suggested human intervention or simple chance as the reasons behind the observed positive results. Assessment of the individual steps of the protocol showed a qualitatively equivalent performance for docking pose prediction across the published and re-produced data, with the

main differences arising from the rescoring sub-protocol. Based on these results and on a number of encouraging publications on the use of MM-GBSA as a fast rescoring tool of dock poses[9, 10, 15, 16, 20, 22], several questions arise: Is the poor performance observed thus far due to the software used in the E-Novo study? Is the way MM-GBSA is implemented in Charmm[131] the problem? How sensitive is the underlying methodology to different starting geometries? Is the methodology system-dependent or can it produce valuable results for a range of systems? Are consistent results obtained across a range of GB models?

To address these issues, we have tested the methodology in a range of software, some of which are widely used in the pharmaceutical industry, employing a number of protocols. This involved generating additional dock poses to the CDOCKER poses, for each one of the five systems investigated in the previous chapter. Three different dock poses were obtained for each protein ligand system using different initial parameters. These, including the CDOCKER poses were then re-scored in four different protocols using a range of GB models as implemented in a range of software, both industrial and academic. In this chapter, the specific details of the protocols is first presented. Then, comparison of our results between the various protocols and methods are reported in an attempt to tackle the aforementioned questions. Furthermore, to assess issues relating to lack of sampling due to the use of minimised structures, we run short MD runs in implicit solvent, remaining within the context of the application of this method, which is in the early stages of lead optimization, where speed and qualitative agreement with experiment is desired over quantitative agreement that comes with the added computational overhead. MM-GBSA energies were calculated by post-processing snapshots generated from the MD simulations with and without an intermediate minimisation step. This chapter only discusses results using MM-GBSA. A comparison between MM-GBSA and MM-PBSA methods is presented in the following chapter (Chapter 7).

## 6.2 Tests conducted in this study

To fully assess the performance of a simplified MM-GBSA method as a fast rescoring tool of docked poses, the same dataset as for CDOCKER was tested in a range of software employing a range of protocols. The tests conducted are shown in Figure 6.1.

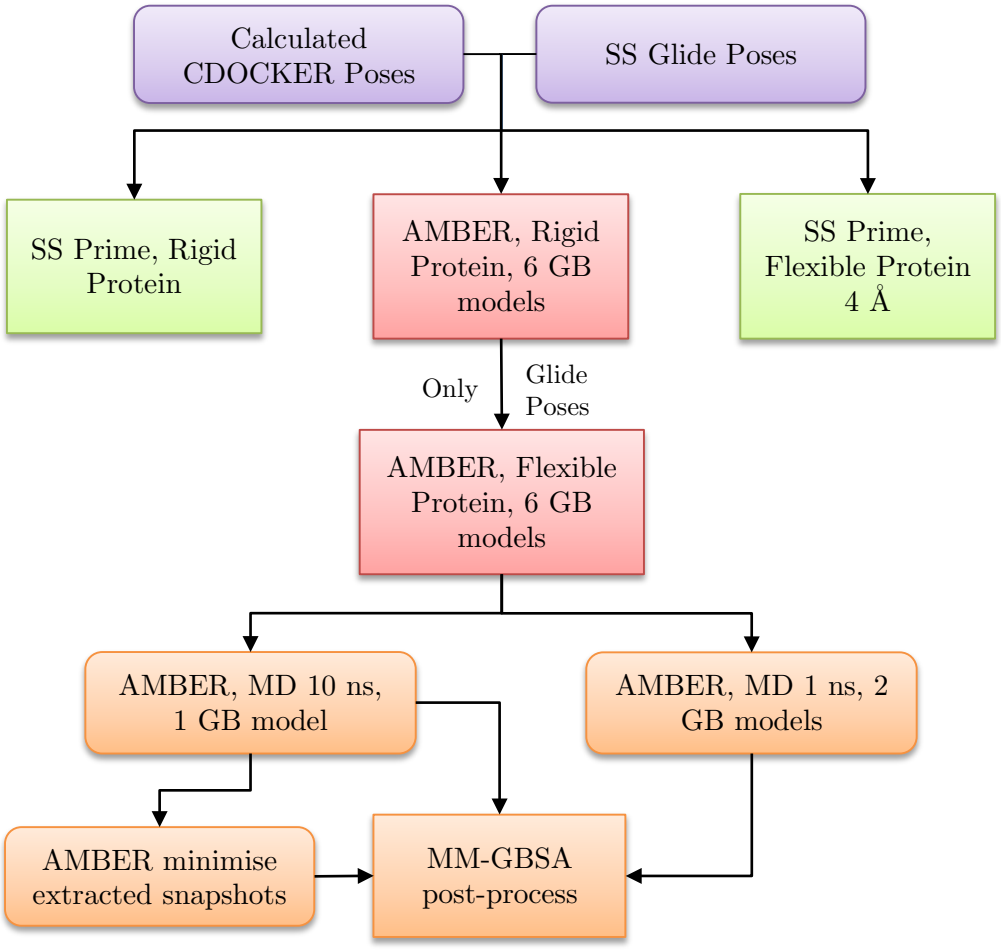


Figure 6.1: Schematic representation of the range of tests conducted in this study along with the software used. SS corresponds to Schrodinger Suite 2010, AMBER to AMBER 10 molecular dynamics package, GB to Generalised Born solvent model and MD to Molecular Dynamics. Glide poses comprise of three different docked poses per ligand. Square shaped boxes indicate where MM-GBSA rescoring is done.

Initially docked poses were generated using the Glide docking algorithm as implemented in the Schrodinger Suite 2010 (SS2010).[135] Three different docking jobs were performed on each protein-ligand system, giving three individual docked poses. Each of those three poses in Glide along with the top CDOCKER poses from our attempt to reproduce the E-Novo protocol were subsequently utilised as test cases for the MM-GBSA rescoring methodology, i.e. four poses per protein-ligand system. Rescoring was performed in the academic package AMBER 10[28] and the industrial package Prime[136] as part of the SS2010.[135] In both software packages the systems were simply minimised in GBSA solvent before obtaining a MM-GBSA binding energy. Two protocols were devised in Prime; one where the protein was kept rigid (constrained), while on the other protein residues within 4 Å of the ligand were allowed to be flexible. AMBER allowed a more elaborate investigation. Here again two main protocols were used; one with the protein being kept rigid (in this case the protein was restrained by applying a weight of 500 kcal $mol^{-1}$ $Å^{-2}$ for the entire minimization) and one where the protein was allowed to be fully flexible. However, in each case calculations were performed in all GB flavours offered in AMBER namely: $GB^{HCT}$, $GB^{OBC1}$, $GB^{OBC2}$, and GB*n*. The OBC models were applied with two different set of *bondii radii* (bondi and mbondi2), giving a total of six GB models.

A potentially serious limitation of simply minimising the system is the lack of sufficient sampling. That is, the dependence of the final result on a single structure rather than an average over a number of different conformations of the system. In other words following minimisation, if a system is stuck in an unfavourable orientation it could have a direct effect on the quality of the correlations obtained in comparison with experiment. To investigate the effect of sampling and whether it improves results, molecular dynamics simulations were performed in the AMBER package. To remain within the context of early stages of lead optimization, the simulations were run using implicit solvent and the calculation of entropy was ignored. This is

a common occurrence in literature when the method is applied on a congeneric set of ligands[20, 68, 74, 75]. Simulations were performed on all three Glide jobs, but not on the CDOCKER poses. Finally, the snapshots generated from the MD simulations were further minimised and MM-GBSA energies recalculated. The purpose of this was to eliminate the case of any "bad" contacts and observe what effect that would have on the results.

The following subsections present the technical details of each of the tests conducted in this study, starting with the generation of dock poses in Glide, moving on to the MM-GBSA rescoring protocols in Prime and AMBER, and, finally, detailing the setup of the MD simulations.

### 6.2.1 Generating dock poses

The LigPrep[137] utility in SS2010 was used to prepare the ligands. More specifically the structure data file of the ligands used in the Pipeline Pilot (PP) protocol (described in section 5.2.2) was converted to chemical table file format (SDF) which in turn was imported into LigPrep to be processed into a 3D structure. The prepared target and ligand files were stored in a Maestro (.mae) file. This was the input file used for docking.

The protein was taken exactly as prepared in Discovery Studio (DS), and for reasons of compatibility with the SS2010 software was minimized with OPLS-AA force field[27] to a maximum RMSD of 0.3 Å under the preparation wizard in Maestro.[109]

The docking calculations were performed in Glide version 5.6 by the Glide 5.0 XP scoring function. Just like in the E-Novo protocol, the core of the inhibitors was held rigid, allowing flexibility for the surrounding R-groups; however, in this case three docking jobs were performed. They differed by how much the ligand is allowed to deviate from the pose of the crystal structure. This was set to a maximum RMSD of 1 Å, 1.5 Å and 2 Å for jobs

1, 2, and 3 respectively. This choice was made in order to assess the sensitivity of the method on the initial pose.

Docking cannot be initiated before generating a potential energy grid for the receptor. For this stage the "prepared" protein structure along with a ligand is loaded using the Receptor Grid Generation panel in Maestro. The force field used for grid generation is OPLS_2005. The ligand is picked and in that way excluded from the receptor grid generation. Receptor flexibility is not allowed in Glide (apart from hydroxyl rotations), however the option of scaling van der Waals radii of non-polar atoms is available, which decreases penalties for close contacts allowing for some "giving", in part of the protein, the ligand or both, during binding. Non-polar atoms are defined as any atom with an absolute value of atomic partial charge that is less than or equal to a specified number; the default value of 0.25 was used. In the manual it is recommended that for ordinary docking, for example in cases where the active site is not tight, no protein scaling should occur, but rather the ligand radii should be altered. For this case the van der Waals radii of non-polar receptor atoms were multiplied by the default value of 1.00, leaving the protein radii unchanged. The next step is to determine the positioning of the scoring grids. In Glide, this is calculated using two boxes: the *outer box* or *grid box* and the *ligand centre box* or *inner box*. The first is the space where the grids themselves are calculated, along with the area within which all the ligand atoms are contained. The latter, provides a truer measure of the effective size of the search space where the ligand centre lies, although the ligands are allowed to move out of this box during grid minimisation. The centre of the ligand is defined as the point half way along the vector of the two most widely separated atoms. In our case where part of the ligand is flexible, the centre is calculated in a similar way with the difference that the two most widely separated atoms of the ligand scaffold are used instead. It is important to note that the *grid box* must be large enough to accommodate the length of the inner box plus the maximum length of any ligand (the maximum size of

the grid box is 50 Å). Both boxes share the same centre. The defaults were used for choosing the centre and size of the *grid box*; that is at the centre of the centroid of the chosen ligand and according to the size of the ligand, respectively. An example of the *grid box* (purple), *inner box* (bright green), and centre of the box (set of coordinate axis coloured bright green) are illustrated in Figure 6.2.

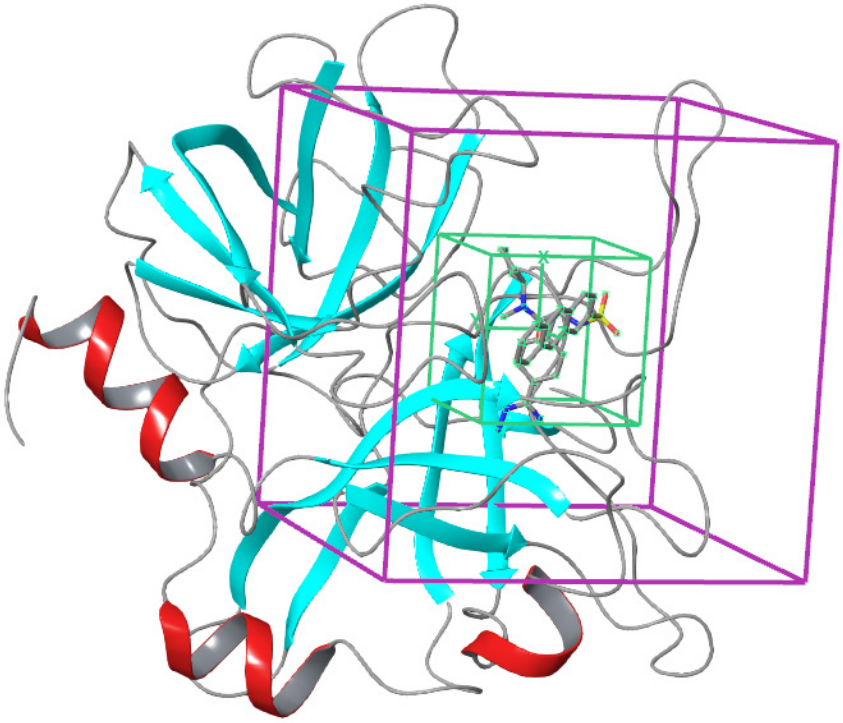

Figure 6.2: Representation of a typical receptor grid in Glide. The *grid box* is shown in purple, the *inner box* in bright green, and the *centre of the box* as a set of coordinate axis coloured bright green.

Once the receptor grid is generated docking can commence. Glide (grid-based ligand docking with energetics) is designed to perform as thorough a search of the orientational, positional and conformational space of the ligand as possible, for it to be sufficiently computationally inexpensive to screen large libraries.[138] A collection of hierarchical filters are applied to search for

all likely locations of the ligand in the receptor's active site (Figure 6.3). The aim is to score as accurately as possible the predicted poses of the ligand. A pose is defined as a set of values for its position and orientation with respect to the receptor, core conformation, and rotamer group conformations. The first step of the process is the generation of ligand conformations. Glide performs an exhaustive conformational search evaluating the torsion-angle space of the various ligand minima. Considering the number of rotatable bonds this can amount to thousands or tens of thousands conformations to be docked. These conformations are fed into an initial screening which is comprised of 5 steps as per Figure 6.3: (1) "Site-points" are selected on an equally spaced 2Å grid that fills the active-site of the protein , (2a) ligand diameter test of clashes with the receptor, (2b) a subset of atoms that as the ligand is rotated about its diameter form hydrogen bonds with the receptor is scored, (2c) following this score if it surpasses a certain threshold all interactions with the receptor are scored, hence the name Greedy score, and finally, (2d) the ligand as one entity is allowed to translate by a predefined distance (±1 Å) in Cartesian coordinates. After the completion of this initial refinement the remaining poses (usually in the range of 250 to 500) are minimised in the protein grid using the OPLS-AA[83] with a distance dependent dielectric model. Then, a Monte Carlo procedure that examines nearby torsional minima, is applied to the three to six lowest-energy minimised poses. The docking procedure is completed by rescoring these poses using a composite energy model called Emodel. This comprises the ligand strain energy (for flexible docking), the protein-ligand interaction energy, and the GlideScore scoring function; derived from the empirically based ChemScore function developed by Eldridge et al.,[41] and comes in two forms: the GlideScore Standard-Precision (SP), and the GlideScore Extra-Precision (XP). The former is designed as a more forgiving function aimed at minimising false negatives and hence more appropriate in large database screening applications, while the later (used in here), in contrast, is aimed at

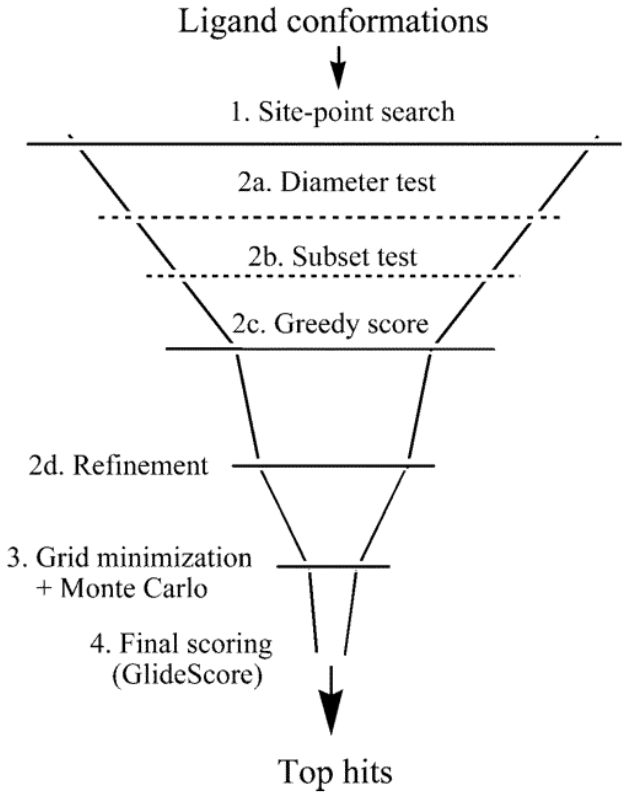


Figure 6.3: The Glide hierarchy in a "funnel" representation. Picture taken from[138].

minimising false positives by applying harsher penalties for poses that violate physicochemical principles, making it useful in lead optimization studies.

There are two key novel features marking the GlideScore XP function: (1) the application of large desolvation penalties to both protein and ligand polar and charged groups when appropriate, and (2) the identification of specific structural motifs that provide very large contributions to enhanced binding affinity.[139] In both SP and XP, solvation is modelled by a combination of an explicit-water methodology on a series of protein-ligand complexes known to receive a good GlideScore, and a set of descriptors that are used to ascertain the physical state of the complex. Penalties are then applied to structures following statistical analysis of charged and polar groups of the ligand and protein that are not sufficiently solvated. The XP scoring function includes additional terms compared to the SP scoring function, and more robust

treatment of some SP terms. A major advantage of XP over SP is the enhanced sampling algorithms which allow XP to assign significantly higher penalties when violations of physical principles are observed. The second novel characteristic of the XP function is enabled by the addition of the hydrophobic enclosure term. This term rewards occupancy of well-defined hydrophobic pockets by hydrophobic ligand groups. This overcomes underestimation of hydrophobic effects as in the cases where simple pair terms, such as, lipophilic-lipophilic, are used (as in ChemScore and SP). In addition, the hydrophobic term in GlideScore XP also includes improvements on the neutral-neutral and charged-charged hydrogen bond motifs, and π-cation and π-stacking interactions.[139]

In our study we used the GlideScore XP scoring function. Flexible ligand was chosen with the options of sampling nitrogen inversions, ring conformations and biasing sampling of torsions for amides only, switched on. The default value of 2.5 kcal $mol^{-1}$ was used as the threshold after which ring conformations were discarded. Default values were also used for the selection of initial poses and for the energy minimisation step. This translated to keeping a maximum of 5000 poses passing from the initial geometric screens to the grid refinement calculation, from which survive only those that score within 100 kcal $mol^{-1}$ of the best pose (the one with the lowest i.e. most negative score), while the maximum number of poses that will be minimised in the OPLS-AA non-bonded interaction grid were limited to a maximum of 800. The effective dielectric "constant" was obtained via a distant-dependent dielectric model, where the default constant number of 2.0 is multiplied by the distance between the interacting pair of atoms. Then, 100 steps of conjugate gradient minimisation were performed. The van der Waals radii and partial charges of nonpolar atoms of the ligand were scaled by a factor of 0.8 and 0.15 respectively. Core constraint was performed here as in the E-Novo study by specifying a tolerance RMSD to the reference position, that of the crystal structure. This value was set to 1, 1.5, and 2 Å, generating three

distinct docked poses per protein-ligand system. For the full force-field post-docking minimisation step, the default of 10 poses per ligand was chosen with a convergence threshold of 0.5 kcal $mol^{-1}$. Finally, to be consistent with the E-Novo study we chose to report a maximum of 5 poses per ligand. To avoid duplicate poses, Glide recognises changes such as 180° rotation of a phenyl group. Additionally, ligand poses are compared to those reported in the output. The default values of 0.5 and 1.3 Å were used for the RMSD threshold and maximum atomic displacement between new generated poses and previously selected for inclusion poses, respectively.

It should be noted that at most two poses were reported per ligand in contrast to the five poses in the E-Novo study, while for some protein-ligand systems not a single pose was written in the output file. This resulted in cases where (these will be detailed in each target system in the later sub-chapters) a system did not have a complete data set for all three docking jobs. This was confirmed by re-running docking calculations and obtaining the same result. According to the Glide manual the poses that pass all the filters are reported. In this case this would probably mean that for some instances the filters may have been too stringent for a pose to be obtained. However, owing to time constraints, the exact cause of this remains unclear.

The software and protocols used to re-score the docked poses using MM-GBSA are detailed in the following section.

### 6.2.2 MM-GBSA rescoring protocols

Rescoring of CDCOKER and Glide poses was performed in the Prime suite[136] and the AMBER 10 simulation package.[28]

*Prime*

The *prime_mmgbsa* version 1.41 in the Prime package was used to re-score the docked poses obtained from the E-Novo protocol and Glide docking program. Two rescoring calculations were performed for each docked pose.

One with the entire receptor atoms frozen (the default option in Prime), and one where any atom within 4Å of the first ligand, is allowed full flexibility. The OPLS-AA forcefield and the surface-area-based version of the GB model (SGB)[140] were used to calculate the molecular mechanics term and the polar solvation term, respectively.

The SGB model introduced by Ghosh et al. (1998)[140] employs a surface integral formulation unlike the volume-based-integration approach used in the original GB version devised by Still et al. (1990).[60] In the SGB paper it is shown that the two formulations (the surface and the volume) are mathematically equivalent which was confirmed by observing quantitative agreement between the calculated predictions from the two models. However, by applying empirical corrections to the SGB model, the authors of the SGB paper managed to obtain significant improvement to the deviations of the absolute energies and the mean square deviations of relative energies, in comparison with PB results.[140]

The solvation energy consists of the polar and non-polar components. The polar SGB element is combined with a nonpolar hydration free energy estimator to form the SGB/NP model.[141] In addition to the commonly used solvent accessible surface area term (see Chapter 3), this model contains a component describing the solute-solvent dispersion interactions that is not zero even for buried atoms up to certain distance from the solute solvent-exposed surface. This distance is determined by using a switching function and the Born radius as a measure of how deeply an atom is buried; a choice defined by a range of factors including the sensitivity of the Born radius to the geometry of the solvent that surrounds solute atoms, the well-defined limiting values and the fact the Born radii are pre-calculated during the evaluation of the electrostatic term (SGB). Reportedly this novel non-polar term was credited with improving the accuracy of the model, especially for cyclic and hydrogen bonding compounds.

Gallicchio et al. (2002)[141] achieve improved accuracy for cyclic and hydrogen bonding compounds with their added nonpolar component, when compared with experimental hydration free energies of small organic molecules. However, the question as to whether the description of hydrophobicity between small molecules in bulk solvent, and large macromolecules such as proteins, might be qualitatively different, is not addressed. Zhu et al. (2006)[142] attempt to approach this issue by investigating the application of hydrophobic models in the context of protein-ligand docking functions. Therefore, Zhu et al. (2006)[142], incorporated an additional term to model the energy gained by the placement of a hydrophobic ligand group into a hydrophobic area of the protein. A modified implementation of the ChemScore[41] scoring function term used to describe protein-ligand hydrophobic interactions in GOLD docking program[143], was used. The authors reported qualitative agreement over the original model, but concluded that further optimisation of the parameters was needed. Further particulars on this, along with details on making the model more computationally efficient can be found elsewhere.[142, 144]

The result of the aforementioned parameterisations corresponds to the SGB/NP model employed in the SS2010 Prime package.

*AMBER 10*

PDB files were obtained for the proteins and the docked poses from both docking programs. The proteins as prepared in DS and SS2010 were matched with the CDOCKER and Glide docked poses respectively and were run through the LEaP module of the AMBER tools package to ensure naming conventions and to generate the necessary topology and coordinate files.

The AMBER99 Stony Brook (AMBER99SB) forcefield[145] is used to describe the protein throughout all calculations (minimisations and molecular dynamics simulations) in AMBER.

Inhibitors were passed to the antechamber program also from the AmberTools software suite, which was used to assign charges using the

AM1BCC[146] method, and generate parameters from the General Amber Forcefield (GAFF).[31] Semi-empirical (AM1) population charges are first used to capture underlying electronic structure characteristics, including formal charge and electron delocalization, while bond charge correction (BCC) is then applied, which is parameterized against a training set of HF/6-31G* electrostatic potential (ESP)[147] derived charges. Protonation states were kept consistent with the docked poses. Missing parameters were checked using the parmchk program, also in the AmberTools package, until it was free from any warnings.

The systems were then minimised (rescored) using the sander program from the AMBER simulation package. A total of 5000 minimisation steps were run of which 1000 using steepest descent algorithm and the remaining 4000 using conjugate gradient. To be consistent with the previous protocols (E-Novo and Prime) all protein atoms were restrained using a force constant of 500 kcal $mol^{-1}Å^{-2}$ (constraints are not allowed when GB is enabled). The electrostatic solvation energy was calculated using all GB models included in AMBER 10, including their variations; the GB method of Hawkins, Cramer, Truhlar ($GB^{HCT}$, option igb=1 with the default modified Bondi radii)[62], the method developed by Onufriev, Bushford and Case model I ($GB^{OBCI}$, option igb = 2 with $\alpha = 0.8$, $\beta = 0.0$ and $\gamma = 2.91$, and with Bondi radii and with the second modification of the Bondi radii – mbondi2), model II ($GB^{OBCII}$, option igb = 5, with $\alpha$, $\beta$, and $\gamma$ set to 1.0, 0.8, and 4.85, respectively, and again with the same radii as model I)[61], and the model by Mongan et al.(2006) (GBn, option igb=7 with Bondi radii)[148], giving a total of six solvation models. The Glide poses were additionally minimized allowing the protein to be fully flexible. The same number of minimization steps was executed with all six GB models. The default convergence criterion for the energy gradient of 1.0E-4 kcal $mol^{-1}$ $Å^{-1}$ was used. In cases where on completion of the total minimisation steps, the energy criterion was not reached, the energies were manually checked to confirm they remained stable.

### 6.2.3 Implicit solvent molecular dynamics simulations

Following the MM-GBSA rescoring in AMBER molecular dynamics simulations were performed only on the Glide docked poses, also in AMBER. A Langevin thermostat was employed with a collision frequency of 1 $ps^{-1}$. A time step of 2 fs was possible with the use of SHAKE algorithm to constrain bonds involving hydrogen atoms. Implicit waters were used in all simulations with the application of the $GB^{HCT}$ solvation model. Following the two minimisations (first rigid protein, then flexible) totalling 10,000 steps, the systems were first equilibrated in three runs of 100 ps each, gradually raising the temperature from 0 K to 300 K. This was followed by a production run of 10 ns at constant temperature of 300 K, saving a total of 100 snapshots, i.e. every 100 ps.

The MM-GBSA energies were obtained by post-processing of the snapshots using the mm_pbsa.pl script in AMBER with the $GB^{HCT}$ model and non-polar solvation parameters as described previously in Chapter 3.

Each snapshot extracted from the 10 ns trajectory, was then minimised for a further 5000 steps (1000 steepest descent and 4000 conjugate gradient) with fully flexible protein to eliminate the possibility of "bad" contacts that could have a negative effect in the calculated energies. The minimised snapshots were then combined to a trajectory that was also post-processed using the mm_pbsa.pl script in the same way to calculate the MM-GBSA energies (see Figure 6.1).

Owing to the lack of explicit waters, the simulation could be described as "frictionless", which could mean that during the course of the 10 ns simulation the system could drift to an unrealistic state quicker than using explicit solvation. For this reason we investigated the first ns. However, with 100 snapshots across 10 ns this left only a small number of snapshots for analysis. Molecular dynamics simulations were re-run from the output of flexible protein minimisations in AMBER, i.e. the same initial structure as the 10 ns

MD simulation, but with a different random seed. Snapshots were saved every 5 ps, leading to 200 snapshots during a 1 ns trajectory. The post-processing analysis was performed in the same way, with the only difference of calculating energies not only using the $GB^{HCT}$ model, but also with the $GB^{OBCI}$ model utilising the second modified Bondi radii (option mbondi2). As has been previously (Chapter 3) noted, the former is the oldest implementation in AMBER, and hence arguably the best parameterised[62], while the latter although newer, has been used extensively in recent publications and has proven to provide encouraging results.[20, 149]

## 6.3 Thrombin

### 6.3.1 System preparation

The same protein preparation and simulation protocols as described in section 6.2.2 were followed, using the PDB structure 1ETT (resolution = 2.50 Å).[108]

### 6.3.2 Rescoring results

***Comparison with experiment***

The performance (correlation of calculated binding free energy versus experiment, i.e. $R^2$) of the rescoring protocols is presented in Figure 6.4 and Figure 6.6, grouped by docking job and rescoring protocol respectively, and the data are summarised in Table 6.1. The significance level for the $R^2$ was set to 5% and shown as a black line across the bar charts. This is based on a two-tailed test since we are interested in how well the model correlates with experiment regardless of the direction. Docking scores are included in the plots and table for comparison purposes. Owing to the questionable quality of the CDOCKER poses we only performed rigid-protein calculations in AMBER.

Table 6.1: Coefficient of determination of calculated binding energies versus experiment for each rescoring protocol. Statistically significant results based on a two tailed test, shown in bold.

| | **$R^2$ of Calculated Energies versus Experiment** | | | |
|---|---|---|---|---|
| **Protocol** | **CDOCKER** | **Glide 1** | **Glide 2** | **Glide 3** |
| **Docking** | 0.00 | **0.58** | **0.72** | **0.67** |
| **E-Novo** | 0.44 | | | |
| **Prime Rigid** | 0.20 | 0.16 | 0.09 | **0.44** |
| **Prime Flex** | 0.23 | 0.22 | 0.04 | **0.54** |
| **Prime Rigid L.** | | 0.07 | 0.10 | 0.27 |
| **Prime Flex L.** | | **0.52** | 0.05 | 0.23 |
| **$GB^{HCT}$ Rigid** | 0.21 | 0.06 | 0.28 | 0.04 |
| **$GB^{OBC1}$ bondi Rigid** | 0.15 | 0.04 | **0.43** | 0.02 |
| **$GB^{OBC1}$ mbondi2 Rigid** | 0.16 | 0.18 | 0.31 | 0.08 |
| **$GB^{OBC2}$ bondi Rigid** | 0.24 | 0.31 | **0.44** | 0.13 |
| **$GB^{OBC2}$ mbondi2 Rigid** | 0.15 | 0.09 | 0.22 | 0.07 |
| **Gbn Rigid** | 0.24 | **0.33** | **0.43** | 0.08 |
| **$GB^{HCT}$ Flex** | | 0.09 | **0.60** | **0.46** |
| **$GB^{OBC1}$ bondi Flex** | | 0.00 | **0.39** | 0.32 |
| **$GB^{OBC1}$ mbondi2 Flex** | | 0.01 | **0.50** | **0.44** |
| **$GB^{OBC2}$ bondi Flex** | | 0.04 | 0.31 | **0.47** |
| **$GB^{OBC2}$ mbondi2 Flex** | | 0.00 | **0.40** | **0.39** |
| **Gbn Flex** | | 0.17 | **0.38** | 0.33 |

It is noted there are two sets of results for the Prime Rigid and Prime Flexible protocols. As mentioned earlier in section 6.2.1, for some ligands there were two dock poses reported in the final docking output. In the AMBER rescoring protocol the dock pose with the lowest energy (i.e. most potent) for each ligand was used. However, it was later observed that the lowest Prime scores did not always correspond to the lowest energy dock pose. Therefore, here both the originally obtained Prime scores, labelled as Prime Rigid and Prime Flex., and the Prime scores when the lowest energy dock pose is considered, labelled as Prime Rigid L. and Prime Flex. L., are included.

The coefficient of determination ($R^2$) of the rescoring protocols against experimental data ranged from as low as 0.00 to 0.60 for the Glide poses and

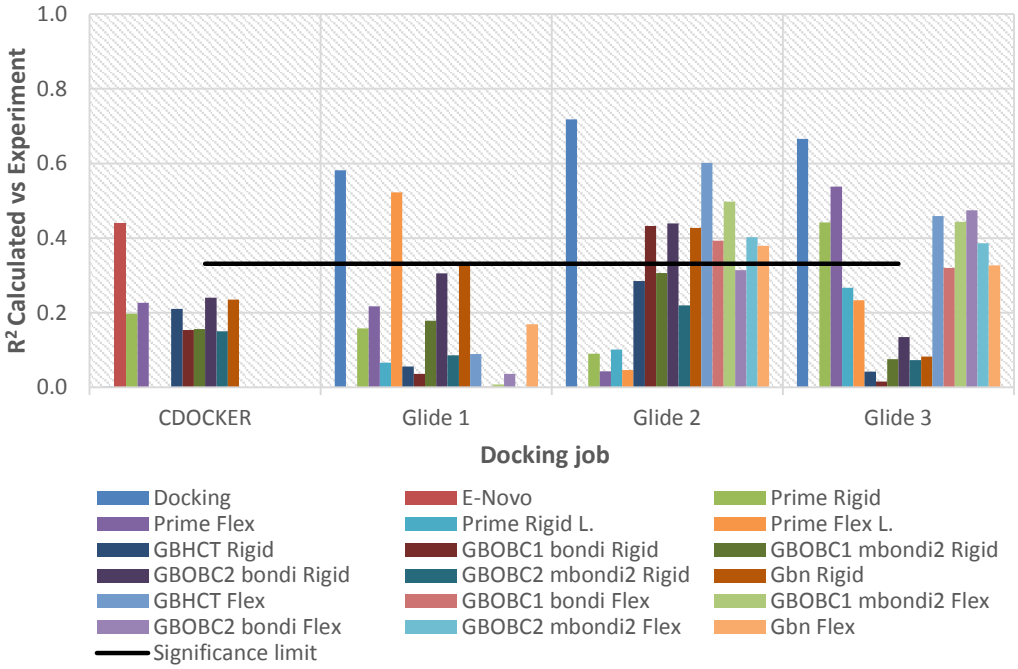


Figure 6.4: Coefficient of determination of rescoring protocols with experiment grouped by docking jobs (CDOCKER, Glide 1, Glide 2, Glide 3). Each rescoring protocol is shown by a differently coloured bar. The 'L.' for Prime jobs stands for the Prime score based on the lowest (more negative) docking score, in the case of two dock poses obtained for one ligand. 'Rigid' and 'Flex' refer to protein flexibility, with the latter fully flexible for Amber calculations, while only 4 Å for Prime calculations. No flexible protein calculations performed with CDOCKER poses. Glide poses not tested on Pipeline Pilot. Correlation with docking provided for comparison purposes. The black line shows the 5% significance level for the number of observations (12 ligands).

0.15 to 0.24 for the CDOCKER poses (Table 6.1). For the Glide poses this is a particularly large variation showing large inconsistencies across the various models when compared with experiment. This is even more evident when looking at Figure 6.4.

In the case of rigid AMBER minimizations it can be seen that the same initial pose can give very different $R^2$ across the different protocols; this is observed even when the same GB model is used, but with slightly different bondi radii as in the cases of $GB^{OBC1}$mbondi2 and $GB^{OBC1}$bondi, and $GB^{OBC2}$mbondi2 and $GB^{OBC2}$bondi. For the rigid minimisation the $R^2$ ranged from a descent correlation of 0.43 ($GB^{OBC2}$bondi for Glide 2 job) to an

insignificant correlation of 0.02 ($GB^{OBC1}$bondi for Glide 3 job). Although the $GB^{OBC}$ models with bondi radii appear to perform slightly better than the rest of the models in Glide job 2 and the model GBn in Glide jobs 1 and 2, there does not seem to be one model that stands out from the crowd.

A similar trend was observed for the AMBER flexible minimisations. Here the correlations ranged from 0.60 ($GB^{HCT}$ for Glide 2 job) to 0.00 ($GB^{OBC2}$mdondi2 for Glide 1 job). Predictions for Glide 1 job appear significantly poorer when compared to the rigid protein calculations, while an improvement is observed for both jobs 2 and 3. The best performance is seen on the second Glide job. However, even in this case a large variation across the different methods is seen. The range of $R^2$ here was 0.29, or in other words as much as 29% more of the variation in experiment can be explained by one $GB^{HCT}$ model over $GB^{OBC2}$bondi.

Unlike the rigid protein calculations, where the input structure was the docked pose, the starting ligand configuration between each solvent model for the flexible calculations differed. This poses the question that perhaps the varied correlations could be attributed to differences in starting conformations. To validate this argument we set out to calculate the heavy atom ligand-ligand RMSD between solvent models, for every possible combination, at the end of the rigid protein minimisations (i.e. starting pose of flexible protein minimisations).

This RMSD comparison, of the starting ligand configurations for the flexible protein minimisations between each solvent model, will be used to assess the effect difference in structures have on $R^2$ between estimated binding free energies and experiment.

Since the energy reported from minimisations is that of the final minimised structure, we will also be comparing the relevant heavy atom ligand-ligand RMSD of the ligand structures obtained at the end of the flexible minimisations between each solvent model.

As the name suggests in rigid protein minimisations, the protein remains fixed throughout the minimisation, meaning the input structure for flexible minimisations will be the same for all models and therefore the protein RMSD comparison is not applicable in this case; however, the protein structures at the end of the flexible minimisations will be different and therefore it is necessary we calculate the RMSD between protein structures of different solvent model minimisations.

Figure 6.5 displays the distributions of RMSD values with respect to different ligand configurations, across all possible combinations of GB models and all Glide jobs combined. With a total of six GB models, corresponding to 15 combinations, three Glide jobs and twelve ligands, a total of 540 values is displayed in each histogram. Plot A (Figure 6.5) shows the RMSD distribution at the end of rigid-protein minimisations prior to commencing flexible-protein minimisations, or in other words the initial structures for the aforementioned calculations. It is clear that with roughly 66.5% (359 out of 540) RMSD calculations under 0.1 Å, and with the majority of them below 0.8 Å, the poses are near identical. Similarly the structures considered when calculating the binding free energy (plot B and C Figure 6.5) displayed an equivalent trend. Both the ligand and protein backbone RMSD were significantly low indicating yet again that the GB models are highly sensitive, with subtle conformational changes having a profound effect on the calculated energies.

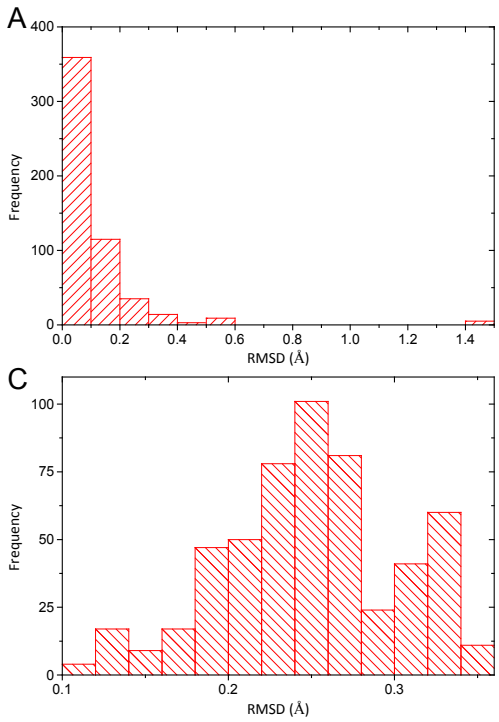


| Average RMSD (Å) | | | |
|---|---|---|---|
| | Glide 1 | Glide 2 | Glide 3 |
| Ligand - R.Min. | 0.115 | 0.127 | 0.103 |
| Ligand - Fl.Min. | 0.224 | 0.283 | 0.236 |
| Protein - Fl.Min. | 0.249 | 0.253 | 0.246 |

Figure 6.5: Ligand-ligand (A, B) and protein-protein backbone (C) RMSD distribution between Amber GB models in all possible combinations for each Glide job 1, prior (A) and after (B, C) protein flexible minimisations. The average RMSD values for each Glide job shown in table (D). Only heavy atoms are considered and only the backbone of the protein. R.Min. and Fl. Min., correspond to the output for rigid protein and flexible protein minimisations, respectively.

Preliminary results show poor and inconsistent performance of the various rescoring protocols applied here, in terms of predicting experimental results. In addition, a model needs to be robust, or in other words to be able to provide similar results, to within error, when initial conditions differ, as in the likes of this case, where three slightly different docking protocols are considered. Therefore it is important to investigate each rescoring protocol independently. In Figure 6.6 the results are grouped by rescoring protocol displaying the $R^2$ across the three Glide jobs. Although results from docking appear to not differ by much for the three dock poses, this is not evident in the rescoring protocols. Correlations with experiment ranged by an average $R^2$ of 0.35. The highest at 0.51 was observed for $GB^{HCT}$ Flex, with the likes of Prime Flex, Prime Flex L., $GB^{OBC1}$bondi Rigid, $GB^{OBC1}$mbondi2 Flex,

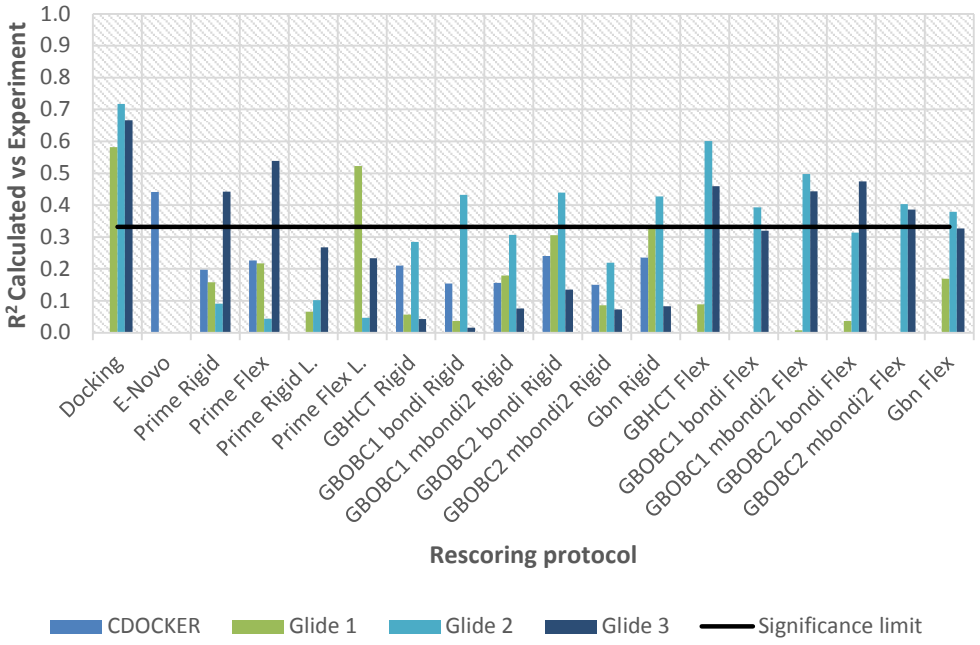


Figure 6.6: Coefficient of determination of rescoring protocols with experiment grouped by each protocol. The colour in each bar corresponds to the docking protocol re-scored (blue for CDOCKER, green for Glide 1, light blue for Glide 2 and dark blue for Glide 3). Naming of protocols as described in Figure 6.4. No flexible protein calculations performed with CDOCKER poses. Glide poses not tested on Pipeline Pilot. Correlation with docking provided for comparison purposes. The black line shows the 5% significance level for the number of observations (12 ligands).

$GB^{OBC2}$bondi Flex, and $GB^{OBC2}$mbondi Flex having a range of $R^2$ more than 0.40.

These results are disappointing but cannot be conclusive without considering the structural differences amongst the three Glide dock pose sets. For this the ligand-ligand and protein-protein backbone RMSD (for heavy atoms in all cases only) of the structures for each solvent model between the three Glide poses was calculated for the following cases: (a) after docking, that is prior to rigid protein minimisations, (b) at the end of rigid-protein minimisations – structures based for calculating the rigid protein energies but also input for the flexible minimisations – and (c) at the end of the flexible-protein minimisations – structures used to determine the final energies.

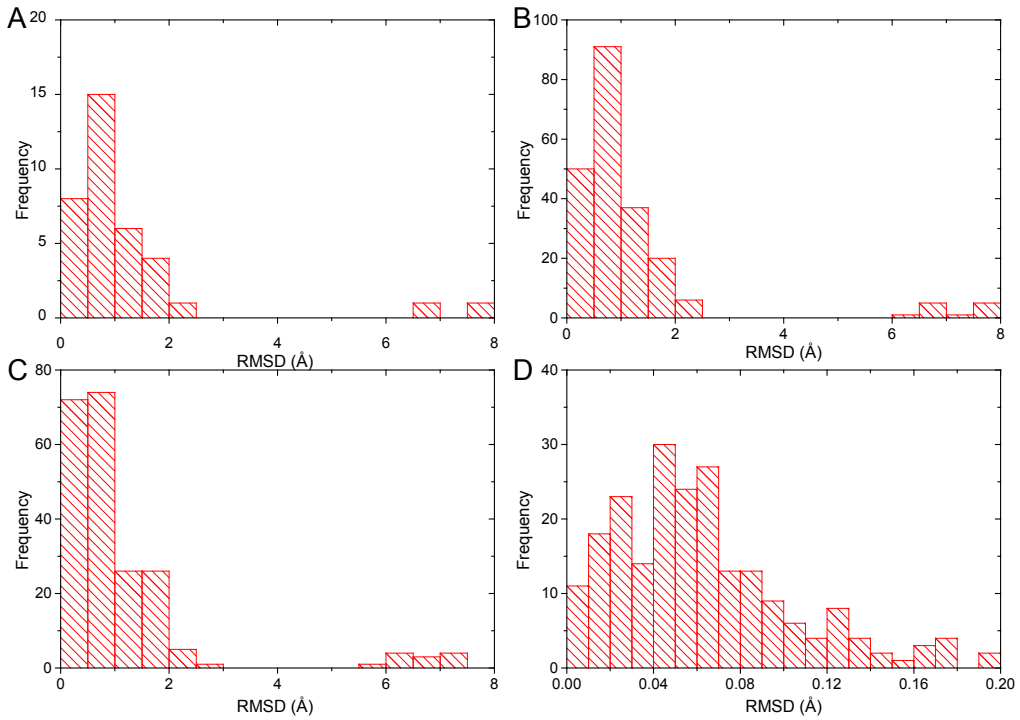


Figure 6.7: Ligand-ligand (A, B, C) and protein-protein backbone (D) RMSD distributions across the different Glide poses in all possible combinations (Glide 1-2, 1-3, and 2-3) for each solvent model. Plot A: Dock poses. Plot B and C: end of rigid-protein and flexible-protein minimisations, respectively. Plot D: protein-protein backbone RMSD at end of flexible-protein minimisations. All reported RMSD are obtained using heavy atoms.

To avoid confusion, it should be made clear that previously RMSDs were calculated between structures from different GB models for each Glide pose set, whereas now, RMSDs are calculated between the structures of the three different Glide poses for the each GB solvent model. For example, RMSD values are calculated for the structure of ligand 1 that was minimised using model $GB^{HCT}$ between docked poses 1 and 2, or 1 and 3, or 2 and 3, as opposed to calculating the RMSD between ligand 1 of docked pose 1 minimised using $GB^{HCT}$ and ligand 1 of the same docked pose using $GB^{OBC1}$mbondi2.

Results of the RMSD analysis are summarised in Figure 6.7, Figure 6.12, and Figure 6.13. All calculations were performed using heavy atoms only. Since three Glide poses were met, there are three possible combinations for

comparison, corresponding to the differences between docking jobs 1 and 2, 1 and 3, and finally 2 and 3, referred to, respectively, as job1-2, job1-3 and job2-3. With 12 ligands per docking protocol corresponding to 36 measurements, 33 fall under the 2 Å RMSD threshold of what is normally perceived as an acceptable difference[42, 71] (plot A in Figure 6.7). In fact, what is not clear from the figure is the values reach 1.63 Å, and not 2 Å. This corresponds to the difference of the structures of ligand 4 between job2-3. Pictured in Figure 6.8, coloured cyan is docking job 2 while lime shows job 3.

The RMSD value (1.63 Å) arises from movements in the hydrophobic parts of the ligand. A rotation of the amide bond between the nitrogen and cyclopropyl group is shown. This group occupies the hydrophobic S2 pocket of Thrombin or in other words the P-pocket (proximal to the active site serine) defined by Leu99, His57, Tyr60, Lys60, and, lastly, Trp60 which occludes the pocket. Owing to its size, cyclopropyl unlike other groups in the series, for example the cyclopentyl group, does not form tight van der Waals interactions with the aforementioned residues, and therefore there is more space resulting in the two observed, and both plausible conformations. The other source of difference in the RMSD originates from the flip and slight twist of the naphthyl group. This aromatic group occupies the solvent exposed S3 pocket or as commonly referred to as the D-pocket (distal to the active site serine), forming contacts with Ile174 and π-interactions with Trp215 and Tyr60. The solvent exposed pocket and its size again allow room for the kind of movements seen, and without breaking key interactions, both conformations would be acceptable. What is worth noting, however, is that despite the observed fluctuations in parts of the molecule the amidino group occupying the specificity pocket S1, remains unchanged between the two docking poses (something observed for all ligands). This is important because unlike the other fluctuations occurring in hydrophobic pockets, this is a key buried polar interaction, between one of the nitrogens of the amidino group and Asp189 residue anchoring the ligand in place. Such interactions are

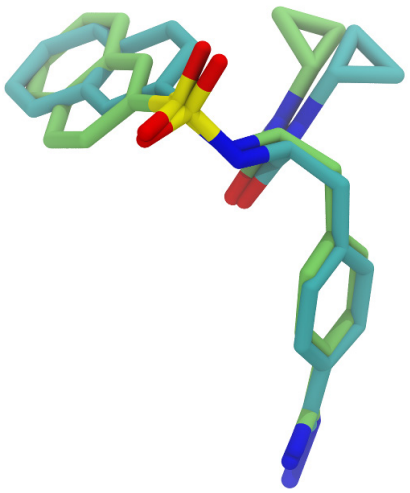

Figure 6.8: Ligand 4 dock poses. Cyan: Glide job 2. Lime: Glide job 3. Hydrogens removed for clarity. RMSD is 1.63 Å.

exactly of the type that pose significant challenge for implicit solvent models.[67, 73] It is therefore encouraging that there is a lack of fluctuation in that part of the molecule as it enables a better comparison across the different models.

Figure 6.7 plot A, contains three outliers with values 2.41 Å, 6.58 Å, and 7.76 Å. These correspond to ligand 7 job1-2, job1-3, and job2-3 respectively, pictured in Figure 6.9. As in ligand 4, the amidino part of the molecule remains unchanged, however this time significant movement is seen on the other groups. Comparing job1 with job2 there is a small movement of the naphthyl group that occupies the aryl binding site of Thrombin. A larger movement is seen at the S2 pocket with the piperazinyl-ethoxycarbonyl moiety. In job 1, one of the ethoxycarbonyl oxygens is within hydrogen bond distance (3.5 Å) to the Lys60 nitrogen, while the entire group appears to nicely fit in the space between Trp60, Lys60, His57 and Tyr60. On the other hand, the same group in job 2 is seen to have shifted to the right, with the ethoxycarbonyl oxygens within hydrogen bond distance to both Lys60 and Gly193, at 2.9 Å and 3.8 Å respectively. The ligand in job3 is shown to have a completely different binding mode. Here, the piperazinyl-ethoxycarbonyl

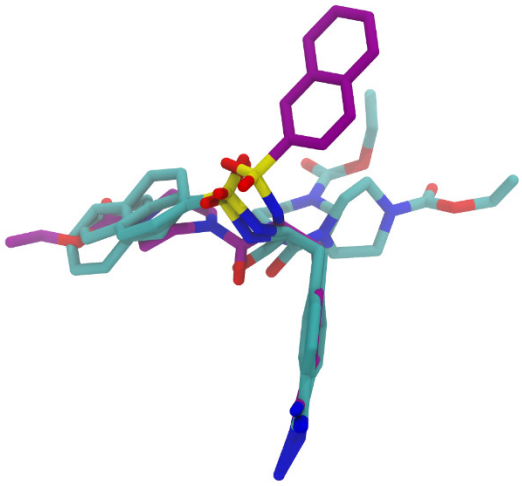

Figure 6.9: Ligand 7 dock poses. Cyan: Glide jobs 1 (far back of the image) and 2. Purple: Glide job 3. Hydrogens removed for clarity. RMSD is 2.41, 6.58, and 7.76 Å for job1-2, job1-3, and job2-3 respectively.

group has taken the place of the naphthyl group, whereas the latter is found shifted to the right, outside of pocket S2 and between residues Trp60 and Trp148. This binding mode is very different to the crystal structure where the naphthyl group is positioned in the S3 pocket. Although this pose may be wrong, it is likely under a docking experiment. With one subpocket long, narrow and with buried interactions (where the amidino group sits), and the rest of the pockets as large hydrophobic and partially solvent exposed cavities, it is more of a challenge for the docking algorithm. Large deviations and flexibility are possible as will be shown later in the MD studies.

Similarly to the dock poses, the majority of RMSD values fall under the 2 Å threshold, for both the structures at the end of rigid protein and flexible protein minimisations, plots B and C in Figure 6.7 respectively. In addition, ligand 7 consistently appears as an outlier. This is not surprising considering not much sampling is in effect. Finally, investigation of the protein backbone revealed nearly no change between dock poses, with all values below 0.2 Å, and the majority below 0.08 Å.

In such cases as ligand 7, it would be expected that most rescoring protocols would perform differently. What is perhaps more interesting, is the fluctuations observed in binding energy. Although, it would be expected that Glide job 1 and 2 (similar binding mode) would have similar energies while job3 (different binding mode) would differ, this was not the case. It was observed that job2 and job3 had similar energies while job1 differed. This was the case for the AMBER protocols. For Prime, job 1 and 3 gave similar binding energies, while job2 differed. In fact Prime exhibited the largest differences with job 1, 2, and 3 giving -37.5, -75.2, and -41.1 kcal $mol^{-1}$ binding energy for the rigid protocol, and -64.9, -100.9, -62.2 kcal $mol^{-1}$ for the flexible protocol, respectively.

It should be noted here that ligand 7 job1 was one of the cases where two dock poses were reported in the docking output. The results discussed so far include the lowest energy docked pose corresponding to Prime Rigid L., and Prime Flex. L. scores. Similar observation was made when the original Prime scores are considered, i.e. when the higher energy docked pose from job 1 is used. In fact, in this case the RMS deviation between job1-2 is even smaller, indicating even more evidently how a small structural difference can have dramatic effects in the performance of a rescoring protocol, while larger differences can give profoundly similar results. This is shown in Figure 6.10 and Figure 6.11. Plots A and B in Figure 6.11, show job1-2 rigid protein minimised poses, and job 3 and 4-TAPAP found in the crystal structure with PDB code 1ETT (shown here as a comparison of the x-ray structure pose), respectively. The RMSD between job1-2 was 1.21 Å, however this corresponds to an energy difference of about 30 kcal $mol^{-1}$ (pink and yellow points on Figure 6.10). On the other hand the RMSD between job1-3 was 7.46 Å, giving a completely different binding mode (green in Figure 6.11 plot B). Here the energy difference was only about 4 kcal $mol^{-1}$. Unfortunately, it was not possible to identify the source of this observation, but it is sufficient to

highlight important limitations of the method, including dependence on starting configuration and structural sensitivity.

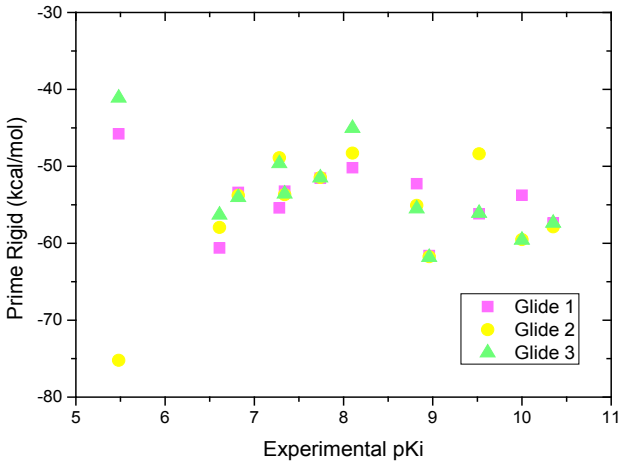


Figure 6.10: Scatter plot of predicted Prime rigid binding free energy against experimental pKi.

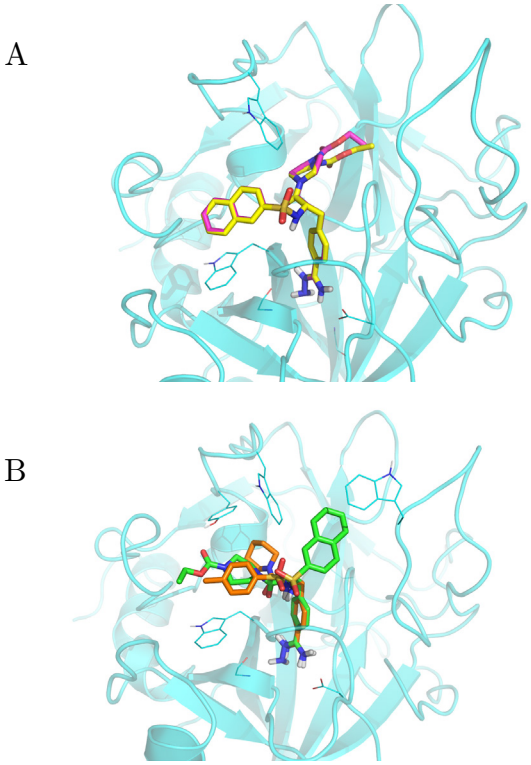


Figure 6.11: Rigid protein minimised ligand 7 poses when job 1 higher energy dock pose is considered. Jobs 1, 2, and 3 are coloured as pink (plot A), yellow (plot A)

and green (plot B). 4-TAPAP inhibitor bound in the crystal structure is shown in orange. Only ligand polar hydrogens are shown.

Table 6.2: Coefficient of determination of calculated binding energies versus experiment for each rescoring protocol **excluding ligand 7**. Statistically significant results based on a two tailed test, shown in bold.

| | $R^2$ of Calculated Energies versus Experiment | | | |
|---|---|---|---|---|
| **Protocol** | **CDOCKER** | **Glide 1** | **Glide 2** | **Glide 3** |
| **Docking** | 0.02 | **0.41** | **0.68** | **0.77** |
| **E-Novo** | 0.24 | | | |
| **Prime Rigid** | 0.33 | 0.01 | 0.09 | 0.23 |
| **Prime Flex** | **0.47** | 0.32 | **0.42** | 0.34 |
| **Prime Rigid L.** | | 0.00 | 0.05 | 0.07 |
| **Prime Flex L.** | | **0.37** | **0.42** | 0.08 |
| **$GB^{HCT}$ Rigid** | 0.34 | **0.56** | 0.22 | 0.09 |
| **$GB^{OBC1}$ bondi Rigid** | 0.26 | 0.18 | 0.32 | 0.02 |
| **$GB^{OBC1}$ mbondi2 Rigid** | 0.24 | 0.31 | 0.30 | 0.03 |
| **$GB^{OBC2}$ bondi Rigid** | **0.38** | 0.35 | **0.44** | 0.10 |
| **$GB^{OBC2}$ mbondi2 Rigid** | 0.29 | 0.31 | 0.24 | 0.07 |
| **Gbn Rigid** | 0.29 | 0.21 | 0.17 | 0.13 |
| **$GB^{HCT}$ Flex** | | 0.22 | **0.47** | **0.38** |
| **$GB^{OBC1}$ bondi Flex** | | 0.22 | 0.23 | 0.12 |
| **$GB^{OBC1}$ mbondi2 Flex** | | **0.44** | **0.55** | **0.42** |
| **$GB^{OBC2}$ bondi Flex** | | **0.47** | **0.48** | 0.27 |
| **$GB^{OBC2}$ mbondi2 Flex** | | 0.18 | 0.28 | 0.18 |
| **Gbn Flex** | | 0.18 | 0.31 | 0.20 |

It has been discussed previously (Chapter 5), how ligand 7 is structurally different from the rest of the ligand series with a smaller pKi acting as a leverage point. Therefore, depending on how well this point is predicted, determines the quality of the correlation observed. This is also seen in Figure 6.10 where job3 (green points) $R^2$ is 0.44 when including ligand 7, but plummets to 0.23 when removed. The correlations for job1 and job2 with

experiment were poor in both cases. Therefore in this case the best correlation is the one obtained with a different binding mode from experiment, i.e. right answer for the wrong reason.

Results of the coefficient of determination with experiment excluding the clear outlier, ligand 7, are shown in Table 6.2. The values here range from 0.00 to 0.56 for Glide poses and 0.24 to 0.47 for CDOCKER poses. When comparing this with the results inclusive of ligand 7 (Table 6.2) the overall number of significant correlations was almost the same (17 vs 19 when all ligands are considered), however the per pose set performance ($R^2$) varied.

In an attempt to quantify the effect of varying poses on the $R^2$ we compare the average variation of ligand structures with respect to the change in $R^2$ amongst the three sets of Glide poses. This is shown in Figure 6.12 (includes all ligands) and Figure 6.13 (excludes ligand 7). Each of these figures are split into two plots. Plot A shows rigid protein rescoring data and plot B data from flexible protein minimisations. Each of these plots shows comparisons between the three Glide poses, i.e. Glide 1-2, Glide 1-3, and Glide 2-3. The bar charts represent the change in $R^2$ for each pair compared, or in other words, the absolute difference between the two $R^2$. Above each plot is shown the average RMSD value between the ligands for each pair of Glide poses. These values are shown for the starting (top) and final (bottom) ligand configurations for each rescoring case. As stated earlier in this section, for the rigid protein minimisations (plot A) the starting conformations are the docked poses, and the final conformations the end structures of the rigid protein minimisations. The latter comprise the starting configurations for the flexible protein minimisations (plot B) with the final structure of these calculations to naturally correspond to the final ligand configurations for this case.

Overall, the results indicate that very small structural differences (low RMSD values) between ligands can result in dramatic changes in the correlation of predicted energies against experiment. Although there are some

cases where the difference in $R^2$ is small, this is not the case for the majority of the tests. Most importantly we observe a largely varied and inconsistent performance between the various solvent models.

Figure 6.12 shows a noticeable worsening when transitioning from plot A to plot B. However such an observation cannot be made when ligand 7 is excluded (Figure 6.13). Also, when the two plots B are compared, exclusion of ligand 7 lowers the $R^2$ difference, i.e. gives more stable results. Although this does not mean better results are obtained by removal of ligand 7 (the $R^2$ difference may be small but the individual $R^2$ may also be small), it highlights the effect one ligand, with a different binding affinity to the rest of the group, can have on the results. In lead optimisation, where small datasets are commonplace and inhibitor affinity may not always be evenly distributed, such sensitivity in initial structure constitutes a significant limitation in the application of the method as a fast rescoring tool in this setting.

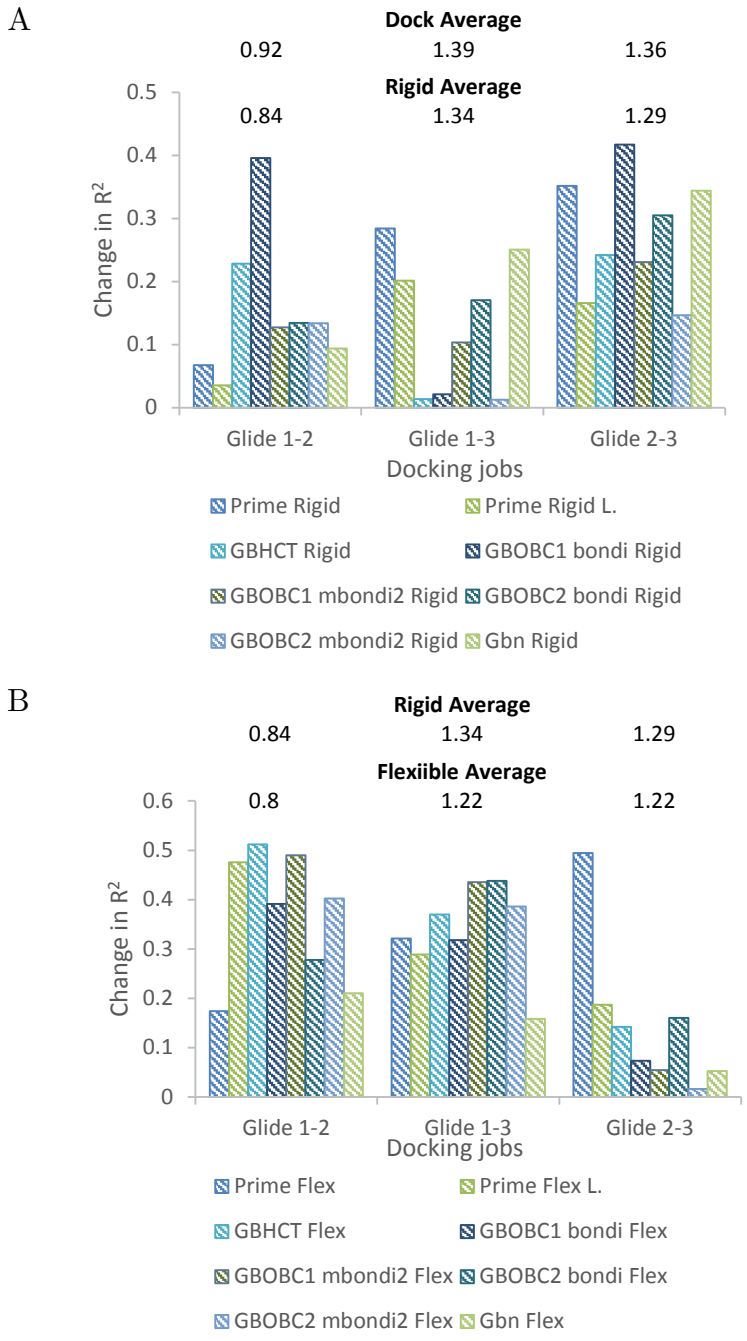


Figure 6.12: Variation of $R^2$ with respect to average docking, and rigid and flexible protein minimisations, RMSD between Glide jobs 1-2, 1-3, and 2-3. Rigid protein minimisation data including average dock pose RMSD shown in plot A. Flexible-protein minimisation data displayed in plot B.

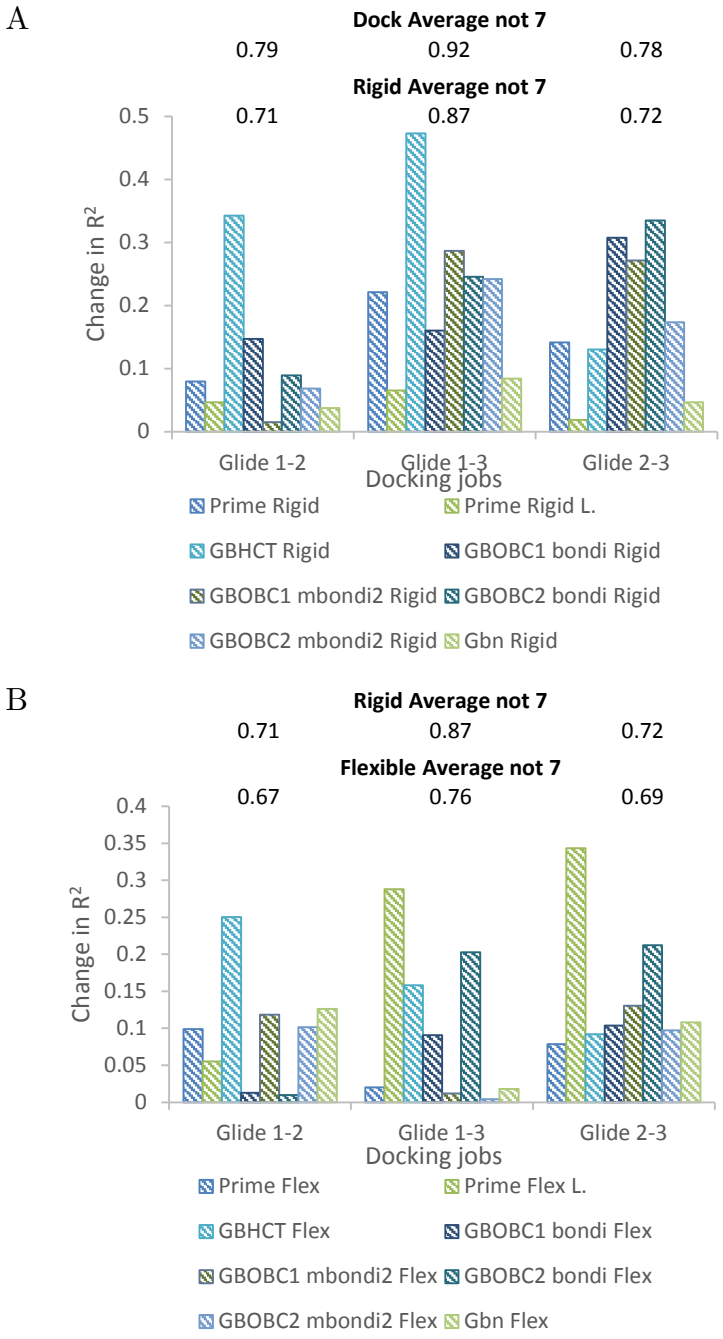


Figure 6.13: Variation of $R^2$ with respect to average docking, and rigid and flexible protein minimisations, RMSD between Glide jobs 1-2, 1-3, and 2-3. Rigid protein minimisation data including average dock pose RMSD shown in plot A. Flexible-protein minimisation data displayed in plot B. Data updated to reflect exclusion of ligand 7.

To further quantify the results obtained thus far, we calculated Kendall's tau (τ) rank correlation coefficient[150]; a nonparametric, i.e. a distribution free, statistical test that provides a measure of the extent to which the order of the observations in quantity X varies with that in quantity Y. The τ coefficient is defined as:

$$\tau = \frac{n_c - n_d}{1/2\, n(n-1)} \tag{6.3.1}$$

where $n_c$ is the number of concordant pairs, $n_d$ the number of discordant pairs and $n$ the total number of pairs. Concordant are the pairs where the rank of both elements agree, while if the opposite occurs they are classified as discordant, shown in equations (6.3.2) and (6.3.3) respectively, for a set of experimental values ($E_{(i)}$), and corresponding predicted scores ($P_{(i)}$).

$$\frac{E_{(j)} - E_{(i)}}{P_{(j)} - P_{(i)}} > 0 \tag{6.3.2}$$

$$\frac{E_{(j)} - E_{(i)}}{P_{(j)} - P_{(i)}} < 0 \tag{6.3.3}$$

If $P_{(j)} - P_{(i)} = 0$ or $E_{(j)} - E_{(i)} = 0$ then the pair is neither concordant nor discordant. The values of τ range from -1, indicating 100% negative association, to +1, 100% positive association, with 0 indicating predictions that are completely random.

To accurately measure the statistical significance of our results, or lack thereof, we calculated the p-values for both the $R^2$ and τ using a two-tailed test in the R programming language. The results are shown in Figure 6.14 when all ligands are considered and Figure 6.15 when ligand 7 is excluded.

R^2

| | Docking | Prime R | Prime F | Prime R L | Prime F L | $GB^{HCT}$ R | $GB^{OBC1}$ B R | $GB^{OBC1}$ MB2 R | $GB^{OBC2}$ B R | $GB^{OBC2}$ MB2 R | GBn R | $GB^{HCT}$ F | $GB^{OBC1}$ B F | $GB^{OBC1}$ MB2 F | $GB^{OBC2}$ B F | $GB^{OBC2}$ MB2 F | GBn F |
|---|---|---|---|---|---|---|---|---|---|---|---|---|---|---|---|---|---|
| Glide 1 | 0.58 | 0.16 | 0.22 | 0.07 | 0.52 | 0.06 | 0.04 | 0.18 | 0.31 | 0.09 | 0.33 | 0.09 | 0.00 | 0.01 | 0.04 | 0.00 | 0.17 |
| | 0.00 | 0.20 | 0.13 | 0.42 | 0.01 | 0.46 | 0.55 | 0.17 | 0.06 | 0.36 | 0.05 | 0.35 | 0.90 | 0.78 | 0.55 | 0.95 | 0.18 |
| Glide 2 | 0.72 | 0.09 | 0.04 | 0.10 | 0.05 | 0.28 | 0.43 | 0.31 | 0.44 | 0.22 | 0.43 | 0.60 | 0.39 | 0.50 | 0.31 | 0.40 | 0.38 |
| | 0.00 | 0.34 | 0.51 | 0.31 | 0.50 | 0.07 | 0.02 | 0.06 | 0.02 | 0.12 | 0.02 | 0.00 | 0.03 | 0.01 | 0.06 | 0.03 | 0.03 |
| Glide 3 | 0.67 | 0.44 | 0.54 | 0.27 | 0.23 | 0.04 | 0.02 | 0.08 | 0.13 | 0.07 | 0.08 | 0.46 | 0.32 | 0.44 | 0.47 | 0.39 | 0.33 |
| | 0.00 | 0.02 | 0.01 | 0.09 | 0.11 | 0.52 | 0.70 | 0.39 | 0.24 | 0.39 | 0.36 | 0.02 | 0.06 | 0.02 | 0.01 | 0.03 | 0.05 |
| CDOCKER | 0.00 | 0.20 | 0.23 | | | 0.21 | 0.15 | 0.16 | 0.24 | 0.15 | 0.24 | | | | | | |
| | 0.90 | 0.15 | 0.12 | | | 0.13 | 0.21 | 0.20 | 0.11 | 0.21 | 0.11 | | | | | | |

Kendall tau

| | Docking | Prime R | Prime F | Prime R L | Prime F L | $GB^{HCT}$ R | $GB^{OBC1}$ B R | $GB^{OBC1}$ MB2 R | $GB^{OBC2}$ B R | $GB^{OBC2}$ MB2 R | GBn R | $GB^{HCT}$ F | $GB^{OBC1}$ B F | $GB^{OBC1}$ MB2 F | $GB^{OBC2}$ B F | $GB^{OBC2}$ MB2 F | GBn F |
|---|---|---|---|---|---|---|---|---|---|---|---|---|---|---|---|---|---|
| Glide 1 | 0.58 | 0.21 | 0.55 | 0.12 | 0.67 | 0.30 | 0.12 | 0.30 | 0.39 | 0.24 | 0.42 | 0.18 | 0.21 | 0.24 | 0.24 | 0.15 | 0.36 |
| | 0.01 | 0.38 | 0.01 | 0.64 | 0.00 | 0.20 | 0.64 | 0.20 | 0.09 | 0.31 | 0.06 | 0.46 | 0.38 | 0.31 | 0.31 | 0.55 | 0.12 |
| Glide 2 | 0.61 | -0.09 | 0.21 | -0.21 | 0.24 | 0.52 | 0.52 | 0.45 | 0.69 | 0.55 | 0.52 | 0.61 | 0.42 | 0.64 | 0.36 | 0.42 | 0.45 |
| | 0.01 | 0.74 | 0.38 | 0.38 | 0.31 | 0.02 | 0.02 | 0.04 | 0.00 | 0.01 | 0.02 | 0.01 | 0.06 | 0.00 | 0.12 | 0.06 | 0.04 |
| Glide 3 | 0.82 | 0.42 | 0.58 | 0.24 | 0.45 | 0.24 | 0.15 | 0.48 | 0.42 | 0.39 | 0.09 | 0.48 | 0.21 | 0.52 | 0.52 | 0.45 | 0.48 |
| | 0.00 | 0.06 | 0.01 | 0.31 | 0.04 | 0.31 | 0.55 | 0.03 | 0.06 | 0.09 | 0.74 | 0.03 | 0.38 | 0.02 | 0.02 | 0.04 | 0.03 |
| CDOCKER | 0.00 | 0.33 | 0.24 | | | 0.39 | 0.21 | 0.24 | 0.30 | 0.15 | 0.30 | | | | | | |
| | 1.00 | 0.15 | 0.31 | | | 0.09 | 0.38 | 0.31 | 0.20 | 0.55 | 0.20 | | | | | | |

Figure 6.14: The correlation of determination ($R^2$) and Kendall tau rank correlation coefficient ($\tau$) across all rescoring tests (including the docking score) for each docking protocol. The coloured boxes represent the p-values (from a two-tailed test) for each statistic ($R^2$ and Kendall's tau) with green any value below 5% (statistical significance limit), while red anything above that threshold. R, F, B, MB2 stand for Rigid, Flexible (4 Å around ligand for Prime – full flexibility for Amber), Bondi radii, and MBondi2 radii respectively. The table should be read in pairs of colourless (statistic) and coloured cells (p-value).

The null hypothesis here is defined as such that any relationship we observe between experimental measurements and predicted energies is entirely by chance. The statistical significance threshold was set at 5%. In other words, any p-value obtained below the value of 0.05 means the null hypothesis can be rejected and that the correlation we observed is statistically significant, i.e. not by chance. In contrast any p-value above 0.05 means the null hypothesis cannot be rejected, i.e. the observed $R^2$ is not statistically significant and there is high probability it is random. Naturally any value in Figure 6.14 and below the threshold is coloured green while anything above is red. The results reported are from a two tailed test.

R^2

| | Docking | Prime R | Prime F | Prime R L | Prime F L | $GB^{HCT}$ R | $GB^{OBC1}$ B R | $GB^{OBC1}$ MB2 R | $GB^{OBC2}$ B R | $GB^{OBC2}$ MB2 R | GBn R | $GB^{HCT}$ F | $GB^{OBC1}$ B F | $GB^{OBC1}$ MB2 F | $GB^{OBC2}$ B F | $GB^{OBC2}$ MB2 F | GBn F |
|---|---|---|---|---|---|---|---|---|---|---|---|---|---|---|---|---|---|
| Glide 1 | 0.41 | 0.01 | 0.32 | 0.00 | 0.37 | 0.56 | 0.18 | 0.31 | 0.35 | 0.31 | 0.21 | 0.22 | 0.22 | 0.44 | 0.47 | 0.18 | 0.18 |
| | 0.03 | 0.79 | 0.07 | 0.85 | 0.05 | 0.01 | 0.20 | 0.07 | 0.06 | 0.08 | 0.16 | 0.14 | 0.15 | 0.03 | 0.02 | 0.20 | 0.19 |
| Glide 2 | 0.68 | 0.09 | 0.42 | 0.05 | 0.42 | 0.22 | 0.32 | 0.30 | 0.44 | 0.24 | 0.17 | 0.47 | 0.23 | 0.55 | 0.48 | 0.28 | 0.31 |
| | 0.00 | 0.38 | 0.03 | 0.50 | 0.03 | 0.15 | 0.07 | 0.08 | 0.03 | 0.12 | 0.20 | 0.02 | 0.14 | 0.01 | 0.02 | 0.10 | 0.08 |
| Glide 3 | 0.77 | 0.23 | 0.34 | 0.07 | 0.08 | 0.09 | 0.02 | 0.03 | 0.10 | 0.07 | 0.13 | 0.38 | 0.12 | 0.42 | 0.27 | 0.18 | 0.20 |
| | 0.00 | 0.14 | 0.06 | 0.43 | 0.40 | 0.38 | 0.70 | 0.64 | 0.33 | 0.44 | 0.28 | 0.04 | 0.29 | 0.03 | 0.10 | 0.19 | 0.17 |
| CDOCKER | 0.02 | 0.33 | 0.47 | | | 0.34 | 0.26 | 0.24 | 0.38 | 0.29 | 0.29 | | | | | | |
| | 0.65 | 0.06 | 0.02 | | | 0.06 | 0.11 | 0.12 | 0.04 | 0.09 | 0.09 | | | | | | |

Kendall tau

| | Docking | Prime R | Prime F | Prime R L | Prime F L | $GB^{HCT}$ R | $GB^{OBC1}$ B R | $GB^{OBC1}$ MB2 R | $GB^{OBC2}$ B R | $GB^{OBC2}$ MB2 R | GBn R | $GB^{HCT}$ F | $GB^{OBC1}$ B F | $GB^{OBC1}$ MB2 F | $GB^{OBC2}$ B F | $GB^{OBC2}$ MB2 F | GBn F |
|---|---|---|---|---|---|---|---|---|---|---|---|---|---|---|---|---|---|
| Glide 1 | 0.49 | 0.05 | 0.60 | -0.05 | 0.60 | 0.56 | 0.27 | 0.42 | 0.38 | 0.45 | 0.35 | 0.27 | 0.45 | 0.49 | 0.49 | 0.38 | 0.42 |
| | 0.04 | 0.88 | 0.01 | 0.88 | 0.01 | 0.02 | 0.28 | 0.09 | 0.12 | 0.06 | 0.16 | 0.28 | 0.06 | 0.04 | 0.04 | 0.12 | 0.09 |
| Glide 2 | 0.53 | 0.09 | 0.45 | -0.05 | 0.49 | 0.45 | 0.45 | 0.42 | 0.67 | 0.53 | 0.42 | 0.53 | 0.31 | 0.64 | 0.49 | 0.35 | 0.42 |
| | 0.03 | 0.76 | 0.06 | 0.88 | 0.04 | 0.06 | 0.06 | 0.09 | 0.00 | 0.03 | 0.09 | 0.03 | 0.22 | 0.01 | 0.04 | 0.16 | 0.09 |
| Glide 3 | 0.78 | 0.31 | 0.49 | 0.09 | 0.38 | 0.38 | 0.16 | 0.45 | 0.42 | 0.38 | 0.13 | 0.45 | 0.09 | 0.49 | 0.42 | 0.35 | 0.42 |
| | 0.00 | 0.22 | 0.04 | 0.76 | 0.12 | 0.12 | 0.54 | 0.06 | 0.09 | 0.12 | 0.65 | 0.06 | 0.76 | 0.04 | 0.09 | 0.16 | 0.09 |
| CDOCKER | 0.13 | 0.42 | 0.38 | | | 0.49 | 0.31 | 0.27 | 0.38 | 0.31 | 0.35 | | | | | | |
| | 0.65 | 0.09 | 0.12 | | | 0.04 | 0.22 | 0.28 | 0.12 | 0.22 | 0.16 | | | | | | |

Figure 6.15: The correlation of determination ($R^2$) and Kendall tau rank correlation coefficient ($\tau$) across all rescoring tests (including the docking score) for each docking protocol, **excluding ligand 7**. The coloured boxes represent the p-values (from a two tailed test) for each statistic ($R^2$ and Kendall's tau) with green any value below 5% (statistical significance limit), while red anything above that threshold. R, F, B, MB2 stand for Rigid, Flexible (4 Å around ligand for Prime – full flexibility for Amber), Bondi radii, and MBondi2 radii respectively. The table should be read in pairs of colourless (statistic) and coloured cells (p-value).

The $R^2$ is shown largely inconsistent across the different protocols. In particular for Glide 1 job (Figure 6.14) only 3 out of the 16 models provide statistically significant results. In total 28.6% of the data when all ligands are considered, and 25% when ligand 7 is excluded, is significant. This becomes worse when taking into account that the best correlation obtained was 0.6, while docking outperformed all rescoring protocols. However, most worryingly, a similar observation can be made for the rank ordering of the inhibitors. The ranking is mostly poor with statistically significantly correct ranking for a third of the cases (33.9%), and even fewer (25%) when ligand 7 (the leveraging point) is excluded. This is an important observation considering

the method is to be applied at early stages of lead optimisation. Failing to predict the correct ordering of different analogues is a considerable limitation.

Scatter plots of predicted against experimental binding affinities are shown in Figure 6.16 and Figure 6.17 for all solvent models for rigid and flexible minimisations respectively. The data is shown for Glide poses only. Each scatter plot contains the data from all three Glide sets of poses for the respective solvent model. Thus far in this chapter a number of metrics have been used to analyse the data. Although useful, these metrics reduce the data to a single number. In this way here, the reader is able to view how the data is distributed, and thus obtain a more complete picture of how the predicted energies compare with the experimental values.

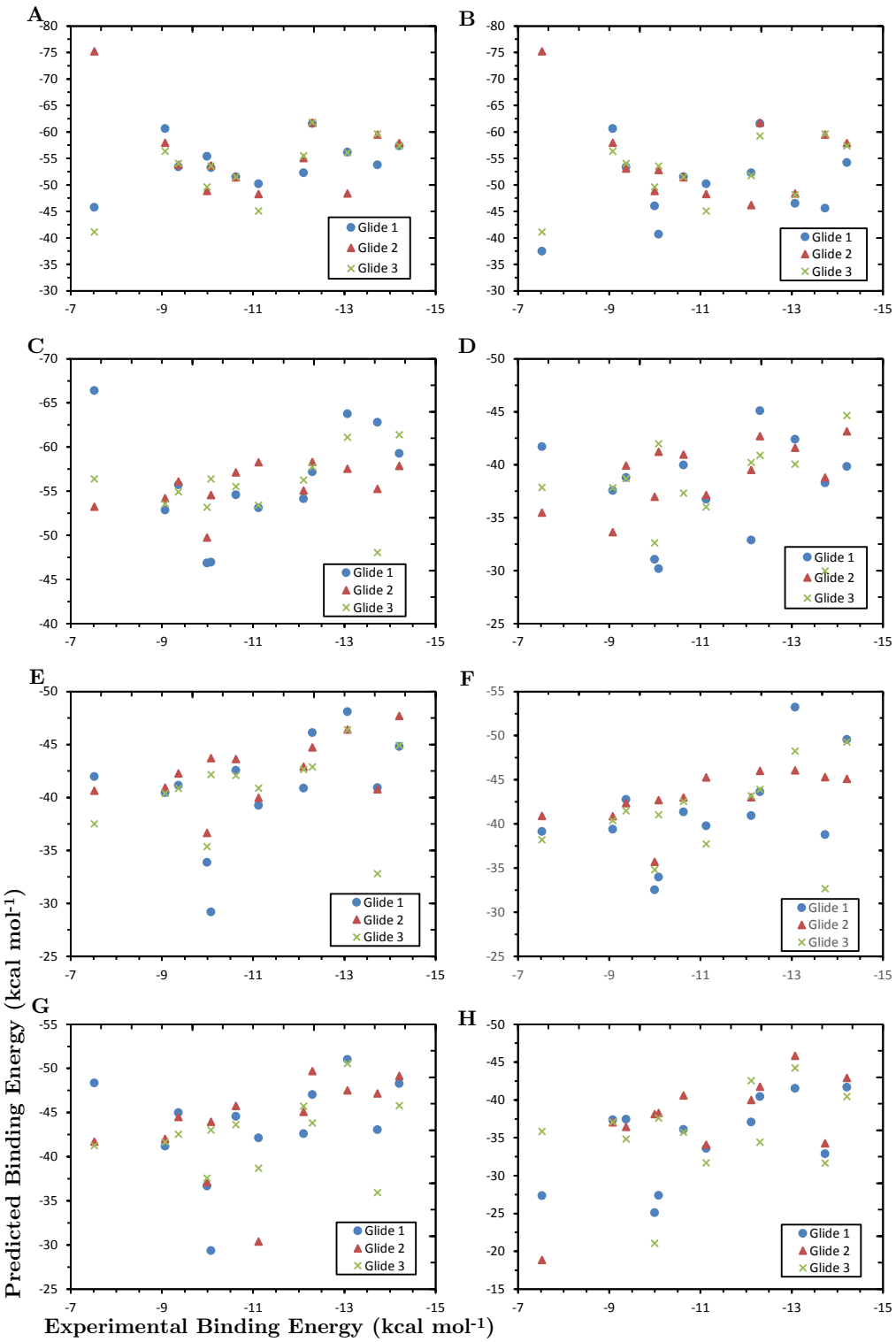


Figure 6.16: Scatter plots of the predicted and experimental binding affinities for Thrombin. The plots correspond to the solvent models, A: Prime Rigid, B: Prime Rigid L., C: $GB^{HCT}$ Rigid, D: $GB^{OBC1}$ bondi Rigid, E: $GB^{OBC1}$ mbondi2 Rigid, F: $GB^{OBC2}$ bondi Rigid, G: $GB^{OBC2}$ mbondi2 Rigid, H: Gbn Rigid.

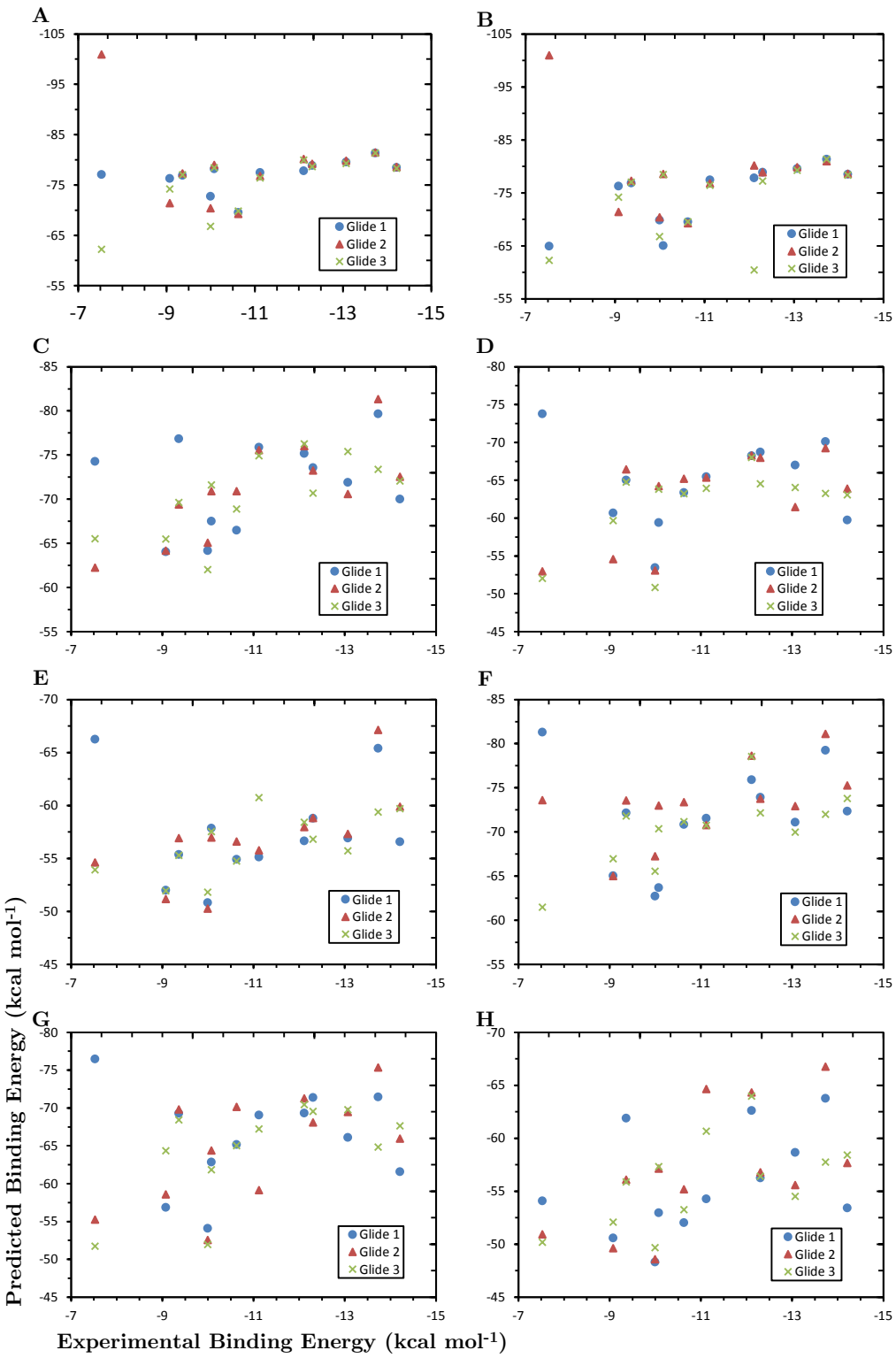


Figure 6.17: Scatter plots of the predicted and experimental binding affinities for Thrombin. The plots correspond to the solvent models, A: Prime Flex, B: Prime Flex L., C: $GB^{HCT}$ Flex, D: $GB^{OBC1}$ bondi Flex, E: $GB^{OBC1}$ mbondi2 Flex, F: $GB^{OBC2}$ bondi Flex, G: $GB^{OBC2}$ mbondi2 Flex, H: Gbn Flex.

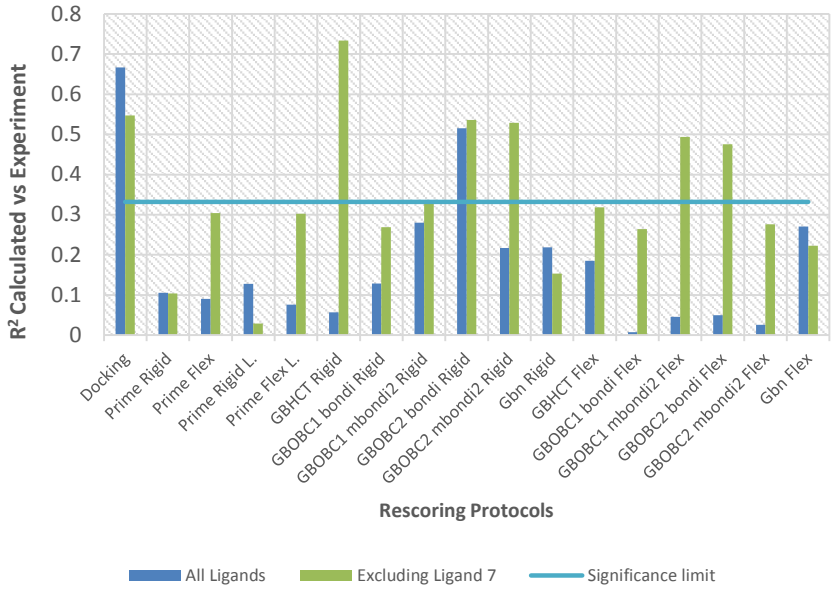


Figure 6.18: Summary of $R^2$ with experiment for each protocol when the lowest energy poses from the three Glide jobs is considered. Shown in blue is all ligands, in green ligand 7 is excluded and the light blue indicates the significance level for a two-tailed test.

Next, we consider the agreement of the lowest (most stable) binding free energy for each rescoring model with the experimental data. The results are summarised in Figure 6.18 and Figure 6.19.

Our assumption that the lowest energy structure, hence the most stable structure, would correspond to improved agreement with experiment, proved futile. A similar trend is observed with some border-line significant correlations and poor ranking. A general $R^2$ improvement is seen when ligand 7 is excluded, mostly noticeable in the case of $GB^{HCT}$ Rigid, where ligand 7 energy is overestimated causing an imbalance in the correlation when included. We found that the lowest energy structures failed to describe more of the variance in experimental measurements, than the results from each individual Glide pose.

R^2

| | Docking | Prime R | Prime F | Prime R L | Prime F L | $GB^{HCT}$ R | $GB^{OBC1}$ B R | $GB^{OBC1}$ MB2 R | $GB^{OBC2}$ B R | $GB^{OBC2}$ MB2 R | GBn R | $GB^{HCT}$ F | $GB^{OBC1}$ B F | $GB^{OBC1}$ MB2 F | $GB^{OBC2}$ B F | $GB^{OBC2}$ MB2 F | GBn F |
|---|---|---|---|---|---|---|---|---|---|---|---|---|---|---|---|---|---|
| All Ligands | 0.67 | 0.11 | 0.09 | 0.13 | 0.08 | 0.06 | 0.13 | 0.28 | 0.52 | 0.22 | 0.22 | 0.19 | 0.01 | 0.05 | 0.05 | 0.03 | 0.27 |
| | 0.00 | 0.30 | 0.34 | 0.25 | 0.38 | 0.46 | 0.25 | 0.08 | 0.01 | 0.13 | 0.13 | 0.16 | 0.79 | 0.50 | 0.49 | 0.62 | 0.08 |
| Excluding 7 | 0.55 | 0.10 | 0.30 | 0.03 | 0.30 | 0.73 | 0.27 | 0.33 | 0.54 | 0.53 | 0.15 | 0.32 | 0.26 | 0.49 | 0.48 | 0.28 | 0.22 |
| | 0.01 | 0.33 | 0.08 | 0.61 | 0.08 | 0.00 | 0.10 | 0.07 | 0.01 | 0.01 | 0.23 | 0.07 | 0.11 | 0.02 | 0.02 | 0.10 | 0.14 |

Kendall tau

| | Docking | Prime R | Prime F | Prime R L | Prime F L | $GB^{HCT}$ R | $GB^{OBC1}$ B R | $GB^{OBC1}$ MB2 R | $GB^{OBC2}$ B R | $GB^{OBC2}$ MB2 R | GBn R | $GB^{HCT}$ F | $GB^{OBC1}$ B F | $GB^{OBC1}$ MB2 F | $GB^{OBC2}$ B F | $GB^{OBC2}$ MB2 F | GBn F |
|---|---|---|---|---|---|---|---|---|---|---|---|---|---|---|---|---|---|
| All Ligands | 0.61 | 0.00 | 0.24 | -0.18 | 0.27 | 0.42 | 0.27 | 0.38 | 0.73 | 0.42 | 0.48 | 0.24 | 0.21 | 0.33 | 0.24 | 0.18 | 0.39 |
| | 0.01 | 1.00 | 0.31 | 0.46 | 0.25 | 0.06 | 0.25 | 0.09 | 0.00 | 0.06 | 0.03 | 0.31 | 0.38 | 0.15 | 0.31 | 0.46 | 0.09 |
| Excluding 7 | 0.53 | 0.20 | 0.49 | -0.02 | 0.53 | 0.71 | 0.38 | 0.40 | 0.75 | 0.60 | 0.45 | 0.31 | 0.45 | 0.56 | 0.49 | 0.42 | 0.35 |
| | 0.03 | 0.45 | 0.04 | 1.00 | 0.03 | 0.00 | 0.12 | 0.09 | 0.00 | 0.01 | 0.06 | 0.22 | 0.06 | 0.02 | 0.04 | 0.09 | 0.16 |

Figure 6.19: The correlation of determination ($R^2$) and Kendall tau rank correlation coefficient ($\tau$) across of the lowest predicted energy for all rescoring tests (including the docking score). Results shown for all ligands and for when ligand 7 is excluded. The table should be read in pairs of colourless (statistic) and coloured cells (p-value). Green cells denote p-values below the 5% significance limit, i.e. are statistically significant.

Before ending this subsection, the correlation of number of heavy atoms (NHA) and molecular weight (MW) with experiment will be considered. Except for key protein-ligand interactions, ligands are also designed to occupy cavities within binding sites. A recent study has shown comparable correlations with experiment between NHA and a range of scoring functions.[151] Although low correlations were observed in a different study where heavy atoms are compared with solvent–accessible surface in a dataset comprised from various different proteins[152], it is suspected this is because NHA correlation really becomes noticeable in single-protein data sets, and, in particular, congeneric series.

The results for the correlation $R^2$ and rank correlation coefficient $\tau$ for NHA and MW with experiment, are summarised in Table 6.3. This shows an improved $R^2$ with experiment compared to the results of the majority of the rescoring protocols, when ligand 7 is excluded. Considering the structural dissimilarity of the R2-group (Figure 4.5) of ligand 7 from the rest of the data set, the better agreement with experiment when it is excluded is justifiable. Similar observations were made for Kendall's tau rank correlation coefficient.

Table 6.3: Coefficient of determination and Kendall's tau rank correlation coefficient for heavy atoms and molecular weight with experiment. Data presented for both the whole dataset and excluding ligand 7. *P*-values resulting from a two tailed test.

| | $R^2$ | $P_{R^2}$ | Kendall tau (τ) | $p_\tau$ |
|---|---|---|---|---|
| **Heavy Atoms** | 0.04 | 0.55 | -0.23 | 0.33 |
| **MW** | 0.04 | 0.56 | -0.26 | 0.24 |
| **Heavy Atoms Excluding 7** | 0.41 | 0.03 | -0.47 | 0.05 |
| **MW Excluding 7** | 0.47 | 0.02 | -0.52 | 0.03 |

Thus far we have presented a thorough comparison and assessment of the qualitative performance for a range of MM-GBSA rescoring protocols of a number of docked poses, against experimental binding affinities. With a handful of exceptions, overall performance ($R^2$ and Kendal tau) was poor across all solvent models and protocols. In addition, we found a largely inconsistent performance between the different solvent models even though the starting ligand configurations were near identical. Besides this, even when the same solvent model was used to rescore slightly different docked poses, results varied, indicating even further the sensitivity to the initial configuration. Though this could be related to a number of methodological limitations, which will be discussed further in the conclusions section (section 6.8), potential experimental errors could have played a significant role.

For one to use the methodology routinely to rescore docked poses, it needs to be robust. Thus, a qualitative and quantitative comparison of the GB models with respect to each other was carried out and is presented in the following section.

### *Comparison between rescoring protocols*

Herein, we set out to identify how similarly the models behave when compared to one another. This could elucidate further the robustness, or lack thereof, of MM-GBSA as a rescoring tool for docking poses; that is, how

consistent are the predicted energies amongst a range of software and protocols. Although comparisons with experiment may have proven poor, for a model to be robust one should expect changes in software or small changes in the model itself not to have a major effect on the predicted values. To ascertain this, a rigorous comparison between the binding energies predicted from each model was carried out. It should be noted here, that although for a rescoring method only qualitative agreement with experiment is to be expected, for the methods to behave similarly there should exist quantitative agreement when one method is compared to another.

First, a qualitative assessment was undertaken by calculating the $R^2$ and Kendall tau ($\tau$). With 16 rescoring protocols (tests conducted only on Glide poses), this resulted in 120 pairwise comparisons. P-values for the statistics were obtained from a two-tailed test. For each statistic and each Glide protocol, a matrix was constructed that contained the statistic and p-value of each comparison. The results for Glide job 1 are summarised in Table 6.5 and Table 6.6 for $R^2$ and $\tau$, respectively. For expediency, Glide job 2 and 3 results are included in the appendix B (Table B.1, Table B.2, for job 2, and Table B.3, Table B.4, for job 3). Descriptive statistics of the two coefficients ($R^2$ and $\tau$) amongst all pairwise comparisons for each docking job are shown in Table 6.4.

Table 6.4: Descriptive statistics of $R^2$ and Kendall $\tau$ across all pairwise comparisons for each Glide job. Percentage of statistics ($R^2$, $\tau$) with p-value below 0.05 is shown (%SIG).

| | | MIN | MAX | MEAN | STDEV | % SIG. |
|---|---|---|---|---|---|---|
| **Glide 1** | $R^2$ | 0.00 | 0.93 | 0.28 | 0.25 | 35.83 |
| | $\tau$ | -0.27 | 0.82 | 0.32 | 0.26 | 32.5 |
| **Glide 2** | $R^2$ | 0.00 | 1.00 | 0.26 | 0.26 | 35.83 |
| | $\tau$ | -0.21 | 0.97 | 0.30 | 0.25 | 33.33 |
| **Glide 3** | $R^2$ | 0.00 | 0.89 | 0.30 | 0.28 | 37.50 |
| | $\tau$ | -0.12 | 0.91 | 0.36 | 0.22 | 32.50 |

Table 6.5: Coefficient of determination ($R^2$) matrix between rescoring models for Glide 1. P–values from a two-tailed test shown. Significant correlations highlighted in bold.

| | | Prime Rigid | Prime Flex | Prime Rigid L. | Prime Flex L. | GBHCT Rigid | GBOBC1 bondi Rigid | GBOBC1 mbondi2 Rigid | GBOBC2 bondi Rigid | GBOBC2 mbondi2 Rigid | Gbn Rigid | GBHCT Flex | GBOBC1 bondi Flex | GBOBC1 mbondi2 Flex | GBOBC2 bondi Flex | GBOBC2 mbondi2 Flex | Gbn Flex |
|---|---|---|---|---|---|---|---|---|---|---|---|---|---|---|---|---|---|
| **Prime Rigid** | $R^2$ | 1.0000 | 0.0311 | **0.5586** | 0.2574 | 0.0402 | 0.0354 | 0.0562 | 0.0753 | 0.0012 | 0.2903 | 0.1149 | 0.1406 | 0.1844 | 0.1829 | 0.2466 | 0.0148 |
| **Prime Rigid** | p | -- | 0.5833 | **0.0052** | 0.0923 | 0.5322 | 0.5581 | 0.4580 | 0.3881 | 0.9147 | 0.0707 | 0.2811 | 0.2297 | 0.1636 | 0.1655 | 0.1005 | 0.7063 |
| **Prime Flex** | $R^2$ | | 1.0000 | 0.0029 | 0.2769 | 0.2041 | 0.0361 | 0.0450 | 0.1064 | 0.0319 | 0.0681 | **0.3967** | 0.2085 | 0.2886 | 0.1647 | 0.1719 | **0.3655** |
| **Prime Flex** | p | | -- | 0.8691 | 0.0789 | 0.1404 | 0.5542 | 0.5081 | 0.3009 | 0.5788 | 0.4125 | **0.0282** | 0.1356 | 0.0717 | 0.1906 | 0.1803 | **0.0373** |
| **Prime Rigid L.** | $R^2$ | | | 1.0000 | **0.3569** | 0.0273 | 0.1035 | 0.1821 | 0.1004 | 0.0616 | **0.5134** | 0.0140 | 0.0190 | 0.2416 | 0.0262 | 0.0506 | 0.0000 |
| **Prime Rigid L.** | p | | | -- | **0.0403** | 0.6081 | 0.3079 | 0.1666 | 0.3155 | 0.4368 | **0.0088** | 0.7142 | 0.6689 | 0.1046 | 0.6153 | 0.4822 | 0.9884 |
| **Prime Flex L.** | $R^2$ | | | | 1.0000 | 0.0933 | 0.1313 | **0.3645** | **0.3374** | 0.2296 | **0.5582** | 0.2279 | 0.0469 | 0.0023 | 0.0667 | 0.0118 | **0.3345** |
| **Prime Flex L.** | p | | | | -- | 0.3344 | 0.2472 | **0.0376** | **0.0477** | 0.1150 | **0.0052** | 0.1165 | 0.4990 | 0.8813 | 0.4176 | 0.7370 | **0.0488** |
| **GBHCT Rigid** | $R^2$ | | | | | 1.0000 | **0.5816** | **0.5670** | **0.3778** | **0.6902** | 0.1234 | 0.3206 | **0.6065** | **0.5319** | **0.6816** | **0.4450** | 0.2183 |
| **GBHCT Rigid** | p | | | | | -- | **0.0039** | **0.0047** | **0.0335** | **0.0008** | 0.2628 | 0.0550 | **0.0028** | **0.0071** | **0.0009** | **0.0178** | 0.1256 |
| **GBOBC1 bondi Rigid** | $R^2$ | | | | | | 1.0000 | **0.7775** | **0.4760** | **0.7515** | **0.3684** | 0.0997 | **0.3444** | 0.1378 | 0.2979 | 0.2536 | 0.0372 |
| **GBOBC1 bondi Rigid** | p | | | | | | -- | **0.0001** | **0.0130** | **0.0003** | **0.0364** | 0.3174 | **0.0449** | 0.2349 | 0.0664 | 0.0951 | 0.5483 |
| **GBOBC1 mbondi2 Rigid** | $R^2$ | | | | | | | 1.0000 | **0.7408** | **0.9258** | **0.6391** | 0.1152 | 0.2836 | 0.0413 | 0.3068 | 0.1545 | 0.1220 |
| **GBOBC1 mbondi2 Rigid** | p | | | | | | | -- | **0.0003** | **0.0000** | **0.0018** | 0.2805 | 0.0747 | 0.5263 | 0.0617 | 0.2063 | 0.2657 |
| **GBOBC2 bondi Rigid** | $R^2$ | | | | | | | | 1.0000 | **0.6624** | **0.7437** | 0.0569 | 0.0885 | 0.0032 | 0.0961 | 0.0431 | 0.1084 |
| **GBOBC2 bondi Rigid** | p | | | | | | | | -- | **0.0013** | **0.0003** | 0.4554 | 0.3476 | 0.8622 | 0.3267 | 0.5175 | 0.2960 |
| **GBOBC2 mbondi2 Rigid** | $R^2$ | | | | | | | | | 1.0000 | **0.4292** | 0.1549 | 0.3271 | 0.0835 | **0.4097** | 0.2146 | 0.1061 |
| **GBOBC2 mbondi2 Rigid** | p | | | | | | | | | -- | **0.0208** | 0.2056 | 0.0520 | 0.3623 | **0.0250** | 0.1294 | 0.3015 |
| **Gbn Rigid** | $R^2$ | | | | | | | | | | 1.0000 | 0.0344 | 0.0405 | 0.0228 | 0.0339 | 0.0092 | 0.1291 |
| **Gbn Rigid** | p | | | | | | | | | | -- | 0.5638 | 0.5307 | 0.6395 | 0.5668 | 0.7666 | 0.2513 |
| **GBHCT Flex** | $R^2$ | | | | | | | | | | | 1.0000 | **0.5950** | **0.4212** | **0.6410** | **0.7058** | **0.7300** |
| **GBHCT Flex** | p | | | | | | | | | | | -- | **0.0033** | **0.0224** | **0.0018** | **0.0006** | **0.0004** |
| **GBOBC1 bondi Flex** | $R^2$ | | | | | | | | | | | | 1.0000 | **0.6229** | **0.8141** | **0.8879** | **0.4183** |
| **GBOBC1 bondi Flex** | p | | | | | | | | | | | | -- | **0.0023** | **0.0001** | **0.0000** | **0.0230** |
| **GBOBC1 mbondi2 Flex** | $R^2$ | | | | | | | | | | | | | 1.0000 | **0.6688** | **0.6364** | 0.2307 |
| **GBOBC1 mbondi2 Flex** | p | | | | | | | | | | | | | -- | **0.0012** | **0.0019** | 0.1140 |
| **GBOBC2 bondi Flex** | $R^2$ | | | | | | | | | | | | | | 1.0000 | **0.7832** | **0.4093** |
| **GBOBC2 bondi Flex** | p | | | | | | | | | | | | | | -- | **0.0001** | **0.0251** |
| **GBOBC2 mbondi2 Flex** | $R^2$ | | | | | | | | | | | | | | | 1.0000 | **0.4116** |
| **GBOBC2 mbondi2 Flex** | p | | | | | | | | | | | | | | | -- | **0.0245** |
| **Gbn Flex** | $R^2$ | | | | | | | | | | | | | | | | 1.0000 |
| **Gbn Flex** | p | | | | | | | | | | | | | | | | -- |

Table 6.6: Kendall tau (τ) rank correlation coefficient matrix between rescoring models for Glide 1. P–values from a two-tailed test shown. Significant correlations highlighted in bold.

| | | Prime Rigid | Prime Flex | Prime Rigid L. | Prime Flex L. | GBHCT Rigid | GBOBC1 bondi Rigid | GBOBC1 mbondi2 Rigid | GBOBC2 bondi Rigid | GBOBC2 mbondi2 Rigid | Gbn Rigid | GBHCT Flex | GBOBC1 bondi Flex | GBOBC1 mbondi2 Flex | GBOBC2 bondi Flex | GBOBC2 mbondi2 Flex | Gbn Flex |
|---|---|---|---|---|---|---|---|---|---|---|---|---|---|---|---|---|---|
| **Prime Rigid** | τ | 1.0000 | 0.2424 | **0.5455** | 0.3636 | 0.0000 | 0.1212 | 0.1818 | 0.2121 | 0.0606 | 0.4242 | -0.1818 | -0.1515 | -0.0606 | -0.1212 | -0.2727 | -0.0606 |
| **Prime Rigid** | p | -- | 0.2726 | **0.0136** | 0.0998 | 1.0000 | 0.5833 | 0.4106 | 0.3371 | 0.7839 | 0.0549 | 0.4106 | 0.4929 | 0.7839 | 0.5833 | 0.2171 | 0.7839 |
| **Prime Flex** | τ | | 1.0000 | -0.0303 | **0.6970** | 0.3939 | 0.1515 | 0.2727 | 0.2424 | 0.2727 | 0.2727 | 0.2727 | 0.3636 | **0.5758** | 0.3333 | 0.3030 | 0.5152 |
| **Prime Flex** | p | | -- | 0.8909 | **0.0016** | 0.0746 | 0.4929 | 0.2171 | 0.2726 | 0.2171 | 0.2171 | 0.2171 | 0.0998 | **0.0092** | 0.1314 | 0.1702 | 0.0197 |
| **Prime Rigid L.** | τ | | | 1.0000 | 0.2727 | -0.0303 | 0.2121 | 0.2727 | 0.4242 | 0.1515 | **0.6364** | -0.0909 | -0.1212 | -0.2727 | 0.0303 | -0.1212 | -0.0303 |
| **Prime Rigid L.** | p | | | -- | 0.2171 | 0.8909 | 0.3371 | 0.2171 | 0.0549 | 0.4929 | **0.0040** | 0.6808 | 0.5833 | 0.2171 | 0.8909 | 0.5833 | 0.8909 |
| **Prime Flex L.** | τ | | | | 1.0000 | 0.3939 | 0.2121 | 0.3939 | 0.4242 | 0.3333 | 0.4546 | 0.2121 | 0.3636 | 0.2727 | 0.3333 | 0.2424 | **0.4546** |
| **Prime Flex L.** | p | | | | -- | 0.0746 | 0.3371 | 0.0746 | 0.0549 | 0.1314 | **0.0397** | 0.3371 | 0.0998 | 0.2171 | 0.1314 | 0.2726 | **0.0397** |
| **GBHCT Rigid** | τ | | | | | 1.0000 | **0.5758** | **0.6364** | **0.5455** | **0.8182** | 0.3333 | 0.3333 | **0.6061** | **0.5758** | **0.6364** | **0.5455** | 0.3939 |
| **GBHCT Rigid** | p | | | | | -- | **0.0092** | **0.0040** | **0.0136** | **0.0002** | 0.1314 | 0.1314 | **0.0061** | **0.0092** | **0.0040** | **0.0136** | 0.0746 |
| **GBOBC1 bondi Rigid** | τ | | | | | | 1.0000 | **0.8182** | **0.4849** | **0.7576** | **0.3939** | 0.0909 | 0.3636 | 0.2727 | 0.3333 | 0.3030 | 0.1515 |
| **GBOBC1 bondi Rigid** | p | | | | | | -- | **0.0002** | **0.0282** | **0.0006** | **0.0746** | 0.6808 | 0.0998 | 0.2171 | 0.1314 | 0.1702 | 0.4929 |
| **GBOBC1 mbondi2 Rigid** | τ | | | | | | | 1.0000 | **0.6667** | **0.8182** | **0.5152** | 0.0303 | 0.3030 | 0.2727 | 0.3333 | 0.2424 | 0.2121 |
| **GBOBC1 mbondi2 Rigid** | p | | | | | | | -- | **0.0026** | **0.0002** | **0.0197** | 0.8909 | 0.1702 | 0.2171 | 0.1314 | 0.2726 | 0.3371 |
| **GBOBC2 bondi Rigid** | τ | | | | | | | | 1.0000 | **0.6667** | **0.7879** | 0.0606 | 0.1515 | 0.1212 | 0.1818 | 0.0909 | 0.2424 |
| **GBOBC2 bondi Rigid** | p | | | | | | | | -- | **0.0026** | **0.0004** | 0.7839 | 0.4929 | 0.5833 | 0.4106 | 0.6808 | 0.2726 |
| **GBOBC2 mbondi2 Rigid** | τ | | | | | | | | | 1.0000 | **0.4546** | 0.1515 | 0.4242 | 0.3939 | **0.4546** | 0.3636 | 0.2727 |
| **GBOBC2 mbondi2 Rigid** | p | | | | | | | | | -- | **0.0397** | 0.4929 | 0.0549 | 0.0746 | **0.0397** | 0.0998 | 0.2171 |
| **Gbn Rigid** | τ | | | | | | | | | | 1.0000 | -0.0303 | 0.0000 | -0.0303 | 0.0909 | -0.0606 | 0.1515 |
| **Gbn Rigid** | p | | | | | | | | | | -- | 0.8909 | 1.0000 | 0.8909 | 0.6808 | 0.7839 | 0.4929 |
| **GBHCT Flex** | τ | | | | | | | | | | | 1.0000 | **0.4849** | 0.3939 | **0.5758** | **0.6061** | **0.7576** |
| **GBHCT Flex** | p | | | | | | | | | | | -- | **0.0282** | 0.0746 | **0.0092** | **0.0061** | **0.0006** |
| **GBOBC1 bondi Flex** | τ | | | | | | | | | | | | 1.0000 | **0.6061** | **0.7273** | **0.8182** | **0.5455** |
| **GBOBC1 bondi Flex** | p | | | | | | | | | | | | -- | **0.0061** | **0.0010** | **0.0002** | **0.0136** |
| **GBOBC1 mbondi2 Flex** | τ | | | | | | | | | | | | | 1.0000 | **0.6364** | **0.6667** | **0.4546** |
| **GBOBC1 mbondi2 Flex** | p | | | | | | | | | | | | | -- | **0.0040** | **0.0026** | **0.0397** |
| **GBOBC2 bondi Flex** | τ | | | | | | | | | | | | | | 1.0000 | **0.7879** | **0.5758** |
| **GBOBC2 bondi Flex** | p | | | | | | | | | | | | | | -- | **0.0004** | **0.0092** |
| **GBOBC2 mbondi2 Flex** | τ | | | | | | | | | | | | | | | 1.0000 | **0.6061** |
| **GBOBC2 mbondi2 Flex** | p | | | | | | | | | | | | | | | -- | **0.0061** |
| **Gbn Flex** | τ | | | | | | | | | | | | | | | | 1.0000 |
| **Gbn Flex** | p | | | | | | | | | | | | | | | | -- |

The calculated values of $R^2$ and $\tau$ are found to spread over a large range from zero correlation to nearly 100% correlation for both statistical measurements and across the three docking jobs. The average correlation ranged from 0.26 (Glide 2 $R^2$) to 0.36 (Glide 3 Kendall tau), with the standard deviation found to be about a quarter of the size of the statistic. Taking into account the calculated *p-values*, between 32.50% and 37.50% of the measurements were found to be statistically significant (to within 95% certainty).

Though this is relatively low (see %SIG. in Table 6.4), we found an overall tendency (see Table 6.5 and Table 6.6) for significant correlations between rigid-rigid and flexible-flexible AMBER GB models. A similar observation can be made for the ranking coefficient ($\tau$), although its performance was slightly worse. This is somewhat encouraging, indicating that indeed there appears to be some similarity between the models. However, with the exception of a few cases (model $GB^{HCT}$ Rigid Glide 1 compared to flexible GB Amber models), the correlation diminishes when rigid and flexible models are compared with each other. In addition, the same models that may be highly correlated when rescoring the poses of one docked job, appear uncorrelated when the poses of another docking job are considered. Such an example is $GB^{HCT}$ Rigid and $GB^{OBC2}$mbondi2 Rigid, where the coefficient of determination is 0.78 for Glide pose 3, drops to 0.69 for Glide 1, and plummets to 0.1 for Glide 2. In contrast model $GB^{OBC1}$mbondi2 Rigid that is better behaved when compared to $GB^{HCT}$ Rigid, it still fluctuates from an $R^2$ 0.52 (Glide2) to 0.76 (Glide3).

Closer investigation reveals that although there is undeniably a strong relationship between some of the models, there are numerous correlations ($R^2$ and $\tau$) which range from around 0.3 to 0.6. These correlations, although significant in the current test and sample size, would be considered low. Much higher correlations should be anticipated from a robust model. It is fair to say there are some strongly significant correlations present, however the small

changes from method to method, and minute structural differences in ligand starting configurations appear to have an obvious undesirable impact on the behaviour of the models. Just by how much the models differ we aim to quantify in the remainder of this subsection.

To evaluate quantitatively the different methods with regard to each other, box plots were constructed for each set of rescored dock poses (Figure 6.20, Figure 6.21, Figure 6.22, and Figure 6.23). The primary interest of this investigation is the elucidation of the general performance of the methods, and so outliers are not shown. Box plots inclusive of outliers are found in Appendix B (Figure B.1, Figure B.2, Figure B.3, and Figure B.4), and will be briefly discussed later in the main text.

First we consider the case of CDOCKER poses. It was found that the CHARMm based MM-GBSA model in E-Novo (see Figure 6.20), although having the highest (less negative) median, also has one of the lowest variation throughout its binding free energy estimates. Prime Flex showed the lowest median at about 20 kcal $mol^{-1}$ more negative than Prime Rigid and 40 kcal $mol^{-1}$ more negative than the E-Novo result. Perhaps the protein flexibility in Prime Flex allows for a more stable configuration, however it is interesting how different a result can be obtained compared to Prime Rigid, when only 4 Å protein flexibility around the ligand is introduced. Overall, the AMBER models share a similar spread of binding affinities, and the OBC models show similar medians ranging from -44.96 to -53.65, but the HCT model data is about 10 kcal $mol^{-1}$ more negative. The box plot for this case, tells us that closely related GB models (OBC)) from the same code (AMBER), can give similar quantitative results, but a different model in the same code, and even more so models from different software, can give very different results.

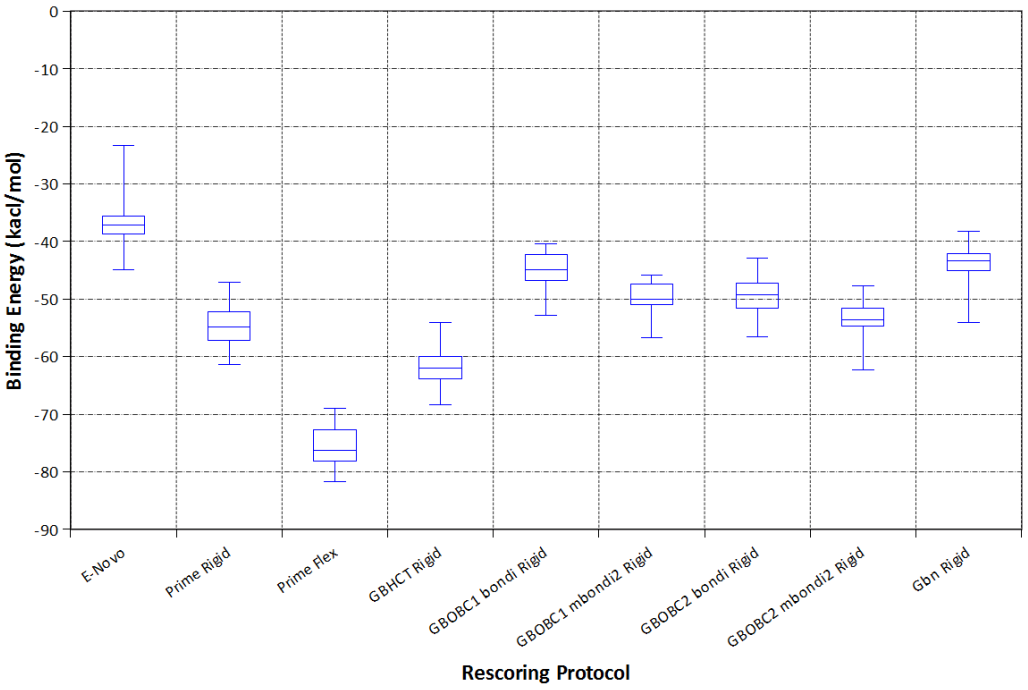


Figure 6.20: Box Plot of predicted binding free energies (kcal $mol^{-1}$) of CDOCKER poses for each rescoring protocol. The whiskers represent the minimum and maximum values, the box corresponds to the range of values between the 1st and 3rd quartiles, and the line through the box represents the median value of the binding free energies.

A similar trend was found for the OBC Rigid models for Glide 1 as in CDOCKER poses, and $GB^{HCT}$ having different median in comparison to the rest GB Rigid models (see Figure 6.21). Flexible minimisations in both software (AMBER and PRIME) gave more negative results compared to rigid minimisations. Again this is expected however perhaps not in the scale found here. In Prime, in both cases when the more negative docked poses were rescored, the spread of the binding affinities was greater, indicating yet again the sensitivity to the starting configuration. It was also found that flexible AMBER minimisations are less stable than their rigid counterparts, with larger variation between the models in both spread of the data (interquartile range – ICR) and values of median. This could suggest that inclusion of protein

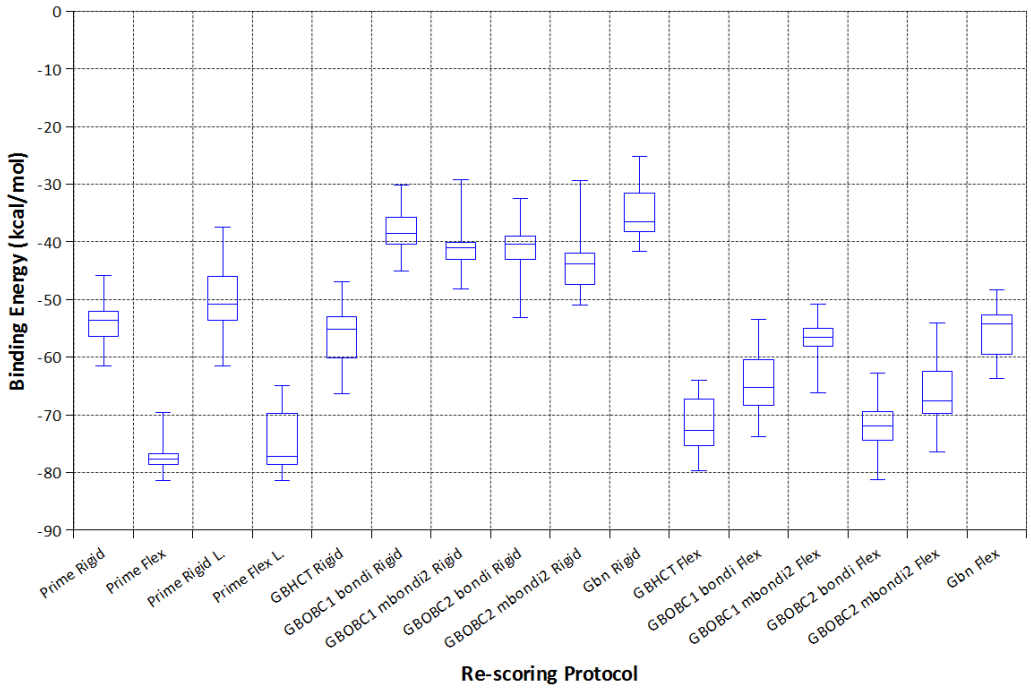


Figure 6.21: Box Plot of predicted binding free energies (kcal $mol^{-1}$) of Glide 1 poses for each rescoring protocol. The whiskers represent the minimum and maximum values, the box corresponds to the range of values between the 1st and 3rd quartiles, and the line through the box represents the median value of the binding energies.

flexibility adds considerable noise to the calculations and perhaps should be avoided.

As shown previously, Prime Rigid and Flex, differ vastly (Figure 6.22), however this time, ligand 7 is especially overestimated, acting as a clear outlier (Figure B.3). The same ligand was an outlier for Gbn Rigid, however instead of a high negative value, this time it was about 80 kcal $mol^{-1}$ larger (less negative) than Prime jobs. Similar observations were made as in Glide 1 with respect to rigid and flexible minimisations in AMBER.

Overall the same observations as in the previous sets of Glide poses, can be also made for Glide 3 poses (see Figure 6.23). Predictions between Prime and AMBER vary, and when rigid and flexible minimisations in AMBER are compared, the former appear much more similar.

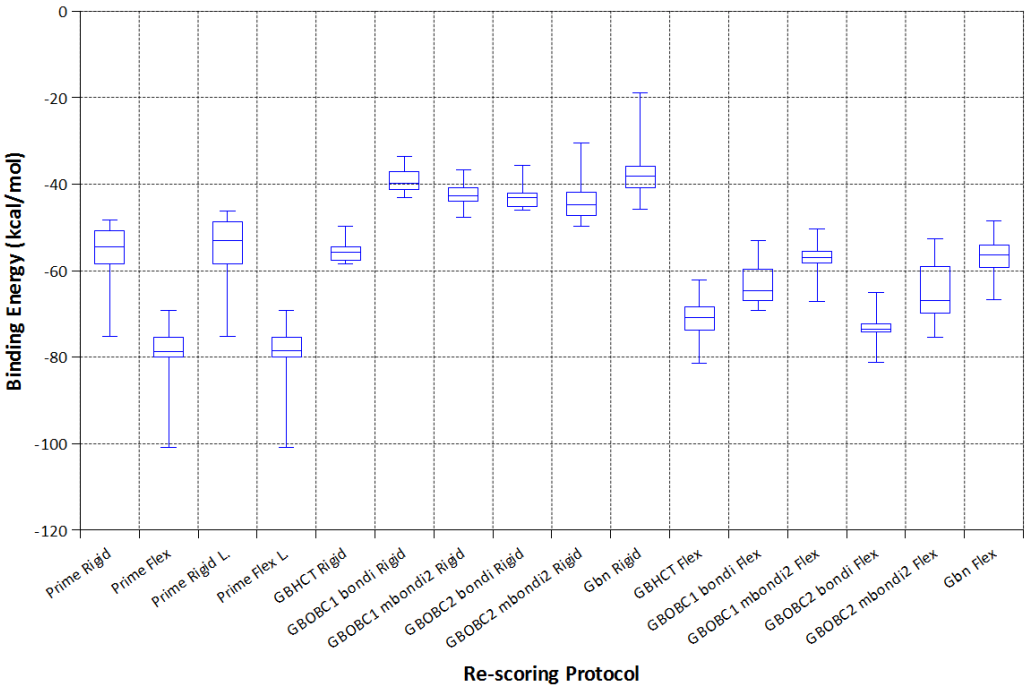


Figure 6.22: Box Plot of predicted binding free energies (kcal $mol^{-1}$) of Glide 2 poses for each rescoring protocol. The whiskers represent the minimum and maximum values, the box corresponds to the range of values between the 1st and 3rd quartiles, and the line through the box represents the median value of the binding energies.

Glide 3 contained the most outliers (10 out of the 16 models exhibited at least one outlier - as seen in Figure B.4). Ligands 1, 3, 7, 11, and 12, where amid the outliers. Although, many are mild outliers, what this reveals is the risk with using this method routinely. Although across all Glide jobs the same ligands were determined as outliers (ligands 1, 3, 7, 8, 11, 12), they were not consistently identified as outliers in particular solvent models, but rather sprang into appearance randomly. Without delving further into their significance, they can serve evidence of inconsistencies encountered between different solvent models, different rescoring protocols of the same solvent model, and also, same solvent models with different, but in reality almost identical, starting ligand configurations.

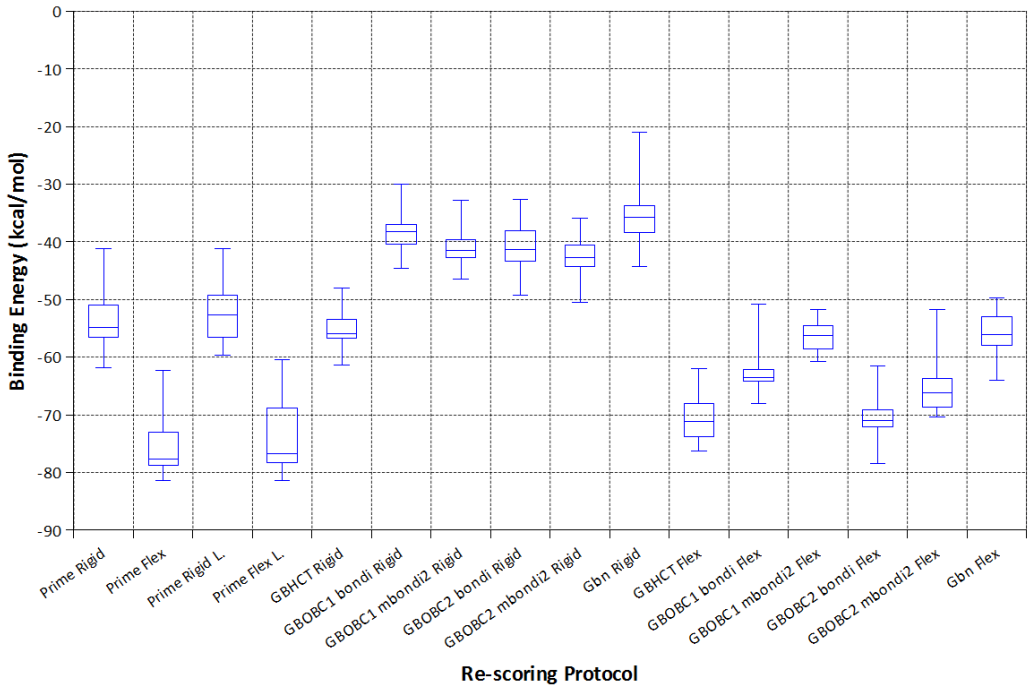


Figure 6.23: Box Plot of predicted binding free energies (kcal $mol^{-1}$) of Glide 3 poses for each rescoring protocol. The whiskers represent the minimum and maximum values, the box corresponds to the range of values between the 1st and 3rd quartiles, and the line through the box represents the median value of the binding energies.

Overall, box plots give only an overview of the distribution of the data of each rescoring method, but, they do highlight some interesting differences in the behaviour of the models, and provide an important stepping stone from which to commence further analysis.

The question arises: how much do the models differ and are the differences we find significant, and if so do they have a practical effect? To identify the significance of the observations made thus far, a rigorous assessment of the differences of the models is needed. Therefore an appropriate statistical test must be chosen. Considering the methods are paired (all performed on the same protein structure) a paired test is appropriate. A commonly used test in such cases to determine if two sets of data are significantly different, is a paired t-test. However, in the case where multiple comparisons are needed, as in our case, multiple paired sample t-

tests would result in an increased probability of committing a type I error (see Table 6.7), i.e., concluding the means are different when in reality they are not (rejecting the null hypothesis when it is true). The result of this is inflated significance rates, and is commonly referred to as multiple comparisons problem or simply as multiplicity.[153-155]

Table 6.7: Error types in hypothesis testing. The null hupothesis ($H_o$) here is that the means of the samples, i.e. binding free energy predictions for each solvent model per Glide pose, are equal.

| | $H_o$ True | $H_o$ False |
|---|---|---|
| Reject $H_o$ | Type I error - False positive | Correct result - Negative |
| Fail to reject $H_o$ | Correct result - Positive | Type II error – False negative |

A more appropriate test, therefore, is Analysis of Variance (ANOVA). In particular since our data is paired, we used the so-called Repeated Measures ANOVA (RM-ANOVA), which adds two additional terms: One to account for the variability of *subjects* (in this case the different ligands) from measurement to measurement (in this case the different solvent models), and another to account for the variability of error, which is equal to the first term subtracted from the variability within subjects (ligands).

ANOVA calculates an F statistic (Fisher distribution) that aims to describe whether or not two means are equal. In this way it can be useful in comparing three or more means for statistical significance. Results of RM-ANOVA are shown in Table 6.8, for both when all ligands are included, and when ligand 7 is excluded. One of the key assumptions of ANOVA, sphericity (variances of the differences amongst all possible pairs of models are equal), was violated, meaning it cannot be assumed, in which case the statistic F

Table 6.8: Repeated measures ANOVA results. $SS_b$ is the Sum of Squares between measures, df is the degrees of freedom, and $MS_b$, the Mean Square($SS_b/df\ model$). The * indicates exclusion of ligand 7.

| | $SS_b$ | df model | df error | $MS_b$ | F | p |
|---|---|---|---|---|---|---|
| Glide1 | 34614.56 | 2.97 | 32.70 | 11643.3 | 127.75 | 4.33E-18 |
| Glide1* | 31141.22 | 3.40 | 34.04 | 9149.69 | 154.44 | 1.62E-20 |
| Glide 2 | 33372.73 | 2.13 | 23.41 | 15680.47 | 83.70 | 1.37E-11 |
| Glide 2* | 28468.54 | 3.73 | 37.26 | 7639.87 | 164.38 | 9.66E-23 |
| Glide 3 | 30951.43 | 3.78 | 41.62 | 8180.16 | 147.94 | 1.12E-23 |
| Glide 3* | 29760.15 | 4.10 | 40.96 | 7265.21 | 157.68 | 1.91E-24 |

becomes too liberal, resulting in false positives. Hence, all results reported here, are from the Greenhouse-Geisser[156] correction of degrees of freedom.

We found very low p-values, indicating the null hypothesis can be rejected with a very high significance, i.e. the means of binding affinities between solvent models are significantly different. All Glide poses showed similar significance level, although Glide 3 poses were found a little more significantly different (highest F value).

RM-ANOVA, although useful, only provides information on whether or not the mean of the subjects are significantly different. To identify which differ significantly or not, post-hoc analysis should follow. There exist numerous tests one can apply.[157-160] The Holm-Šidák method was applied in our study.[157, 158, 161-163] This method is less conservative (i.e. reduced chance of obtaining false negatives – type II error) and more powerful (utilising a step-down approach) compared to other post-hoc single step tests including Šidák (on its own), Bonferroni or Tukey tests. First, a set of t-tests and corresponding p-values are computed. These differ from a regular t-test in the manner that the standard deviation (SD) is not calculated from only the two

groups compared, but instead pooled from all the groups, which is essentially equal to the square root of the $MS_b$ term (defined in the legend of Table 6.8) obtained from RM-ANOVA. Following this, the generated p-values are corrected to reduce the probability of a type I error (false positives). The aforementioned methods (and the majority ANOVA post-hoc methods for that matter), do this, by controlling what is called the *experimentwise* or *familywise* error rate called: familywise alpha, α[PF]; that is the probability of making at least one type I error across all the tests or in other words *family* of tests. Thereby, setting the familywise alpha to the standard value of 5%, an alpha value per test (α[PT]) needs to be recalculated. This is the point where in an attempt to suppress the type I error, the danger of increasing a type II error arises (a false negative, i.e. concluding the means are not different when they are). Stepwise tests manage to reduce this effect resulting in a more powerful method.

In Holm-Šidák, the calculated p-values are ranked most significant (lowest p-values) to least significant (highest p-values), and are then sequentially rejected or accepted based on the null hypothesis. This way instead of setting a global α[PT], a different value is set for each iteration, used as a control to accept or reject the current p-value. When a p-value is rejected the testing ends. It should be noted at this point, that when such methods (that supress type I error) are used there is always the risk of false negatives and it is something to take into consideration when interpreting results, although this is more evident for a large number of comparisons. Although there are more powerful methods available such as permutation (bootstrap-adjusted p-values) or even methods that do not control the familywise error but rather the false discovery rate (FDR, pFDR, etc,), the latter usually applied in genomics studies where a large number of data needs to be analysed, they were not deemed necessary for the scope of this work. The current tests conducted in this section in conjunction with the box-plots discussed previously, are

sufficient to elucidate the performance of a range of GB models and rescoring protocols.

Table 6.9 summarises the Holm-Šidák post-hoc results for Glide job 1 including all ligands. For practicality, the results for the other two Glide jobs (both all ligands and excluding ligand 7) are summarised in similar tables in the appendix ranging from Table B.8 to Table B.12). The models are ranked according to p-value from lowest to highest as explained in the previous paragraph. Measures provided include, an index number relating to the pair number, the mean of the differences (Mean Diff.), the standard error of the Mean Diff. (Std.Er.), the total degrees of freedom of the RM-ANOVA test (DF), the t-value of the t-test performed in the post-hoc analysis (|t|value), the p-value (Prob>|t|), the estimated alpha value per test or α[PT] (Alpha) as per the Holm-Šidák method, and finally the d index (d) as per the equation (6.3.7), which is explained further below. In bold (Prob>|t|) are highlighted any statistically significant differences of the mean, i.e. the pair for which the null hypothesis was rejected.

Table 6.9: Holm-Šidák results for Glide job 1. Names abbreviated for expediency. F., R., b., mb2, and d, correspond to Flexible, Rigid, bondi, mbondi2, and Cohen's d respectively. Significant differences shown in bold.

| Compared Models | Index | Mean Diff. | Std.Er. | DF | \|t\|value | Prob>\|t\| | Alpha | d |
|---|---|---|---|---|---|---|---|---|
| Prime F. Gbn R. | 22 | -42.20 | 1.74 | 165 | 24.32 | **1.95E-56** | 4.27E-04 | 3.00 |
| Prime F. L. Gbn R. | 47 | -39.85 | 1.74 | 165 | 22.96 | **2.94E-53** | 4.31E-04 | 2.99 |
| Prime F. GBOBC1 b. R. | 18 | -39.15 | 1.74 | 165 | 22.56 | **2.70E-52** | 4.35E-04 | 4.40 |
| Gbn R. GBOBC2 b. F. | 102 | 36.83 | 1.74 | 165 | 21.22 | **4.94E-49** | 4.38E-04 | 4.46 |
| Gbn R. GBHCT F. | 99 | 36.80 | 1.74 | 165 | 21.21 | **5.43E-49** | 4.42E-04 | 4.79 |
| Prime F. L. GBOBC1 b. R. | 43 | -36.79 | 1.74 | 165 | 21.21 | **5.48E-49** | 4.46E-04 | 4.38 |
| Prime F. GBOBC1 mb2 R. | 19 | -36.25 | 1.74 | 165 | 20.89 | **3.26E-48** | 4.50E-04 | 4.26 |
| Prime F. GBOBC2 b. R. | 20 | -35.77 | 1.74 | 165 | 20.61 | **1.64E-47** | 4.54E-04 | 4.33 |
| Prime F. L. GBOBC1 mb2 R. | 44 | -33.90 | 1.74 | 165 | 19.54 | **8.80E-45** | 4.58E-04 | 4.25 |
| GBOBC1 b. R. GBOBC2 b. F. | 72 | 33.78 | 1.74 | 165 | 19.47 | **1.35E-44** | 4.62E-04 | 8.89 |
| Prime F. GBOBC2 mb2 R. | 21 | -33.75 | 1.74 | 165 | 19.45 | **1.46E-44** | 4.66E-04 | 3.75 |
| GBOBC1 b. R. GBHCT F. | 69 | 33.75 | 1.74 | 165 | 19.45 | **1.49E-44** | 4.70E-04 | 6.64 |
| Prime F. L. GBOBC2 b. R. | 45 | -33.42 | 1.74 | 165 | 19.26 | **4.64E-44** | 4.75E-04 | 4.32 |
| Prime F. L. GBOBC2 mb2 R. | 46 | -31.40 | 1.74 | 165 | 18.10 | **4.98E-41** | 4.79E-04 | 3.73 |

| | | | | | | | | |
|---|---|---|---|---|---|---|---|---|
| Gbn R. GBOBC2 mb2 F. | 103 | 31.31 | 1.74 | 165 | 18.04 | **6.96E-41** | 4.84E-04 | 3.86 |
| GBOBC1 mb2 R. GBOBC2 b. F. | 81 | 30.88 | 1.74 | 165 | 17.80 | **3.08E-40** | 4.88E-04 | 7.18 |
| GBOBC1 mb2 R. GBHCT F. | 78 | 30.85 | 1.74 | 165 | 17.78 | **3.41E-40** | 4.93E-04 | 5.20 |
| GBOBC2 b. R. GBOBC2 b. F. | 89 | 30.40 | 1.74 | 165 | 17.52 | **1.72E-39** | 4.98E-04 | 8.28 |
| GBOBC2 b. R. GBHCT F. | 86 | 30.37 | 1.74 | 165 | 17.50 | **1.90E-39** | 5.03E-04 | 6.97 |
| Gbn R. GBOBC1 b. F. | 100 | 29.75 | 1.74 | 165 | 17.15 | **1.69E-38** | 5.08E-04 | 3.69 |
| GBOBC2 mb2 R. GBOBC2 b. F. | 96 | 28.38 | 1.74 | 165 | 16.36 | **2.31E-36** | 5.13E-04 | 6.01 |
| GBOBC2 mb2 R. GBHCT F. | 93 | 28.35 | 1.74 | 165 | 16.34 | **2.56E-36** | 5.18E-04 | 4.01 |
| GBOBC1 b. R. GBOBC2 mb2 F. | 73 | 28.26 | 1.74 | 165 | 16.28 | **3.65E-36** | 5.23E-04 | 4.53 |
| Prime F. Prime R. L. | 15 | -27.02 | 1.74 | 165 | 15.57 | **3.29E-34** | 5.29E-04 | 3.93 |
| GBOBC1 b. R. GBOBC1 b. F. | 70 | 26.70 | 1.74 | 165 | 15.39 | **1.04E-33** | 5.34E-04 | 5.13 |
| GBOBC1 mb2 R. GBOBC2 mb2 F. | 82 | 25.36 | 1.74 | 165 | 14.62 | **1.42E-31** | 5.40E-04 | 3.80 |
| GBOBC2 b. R. GBOBC2 mb2 F. | 90 | 24.88 | 1.74 | 165 | 14.34 | **8.54E-31** | 5.46E-04 | 4.00 |
| Prime R. L. Prime F. L. | 29 | 24.66 | 1.74 | 165 | 14.21 | **1.87E-30** | 5.51E-04 | 3.90 |
| GBOBC1 mb2 R. GBOBC1 b. F. | 79 | 23.81 | 1.74 | 165 | 13.72 | **4.45E-29** | 5.57E-04 | 3.80 |
| GBOBC2 b. R. GBOBC1 b. F. | 87 | 23.32 | 1.74 | 165 | 13.44 | **2.71E-28** | 5.64E-04 | 4.59 |
| GBOBC2 mb2 R. GBOBC2 mb2 F. | 97 | 22.86 | 1.74 | 165 | 13.18 | **1.50E-27** | 5.70E-04 | 4.08 |
| Prime R. Prime F. | 0 | 22.75 | 1.74 | 165 | 13.11 | **2.33E-27** | 5.76E-04 | 4.53 |
| Gbn R. GBOBC1 mb2 F. | 101 | 22.40 | 1.74 | 165 | 12.91 | **8.53E-27** | 5.83E-04 | 2.60 |
| Prime R. L. GBOBC2 b. F. | 39 | 21.65 | 1.74 | 165 | 12.47 | **1.40E-25** | 5.89E-04 | 2.25 |
| Prime R. L. GBHCT F. | 36 | 21.62 | 1.74 | 165 | 12.46 | **1.56E-25** | 5.96E-04 | 2.72 |
| GBHCT R. Gbn R. | 58 | -21.32 | 1.74 | 165 | 12.29 | **4.74E-25** | 6.03E-04 | 2.94 |
| GBOBC2 mb2 R. GBOBC1 b. F. | 94 | 21.31 | 1.74 | 165 | 12.28 | **4.88E-25** | 6.10E-04 | 2.99 |
| Prime F. Gbn F. | 28 | -21.29 | 1.74 | 165 | 12.27 | **5.26E-25** | 6.18E-04 | 2.24 |
| Gbn R. Gbn F. | 104 | 20.91 | 1.74 | 165 | 12.05 | **2.17E-24** | 6.25E-04 | 2.35 |
| Prime F. GBHCT R. | 17 | -20.88 | 1.74 | 165 | 12.03 | **2.41E-24** | 6.33E-04 | 2.68 |
| Prime R. Prime F. L. | 2 | 20.39 | 1.74 | 165 | 11.75 | **1.47E-23** | 6.41E-04 | 4.49 |
| Prime F. GBOBC1 mb2 F. | 25 | -19.80 | 1.74 | 165 | 11.41 | **1.32E-22** | 6.49E-04 | 2.61 |
| Prime R. Gbn R. | 8 | -19.45 | 1.74 | 165 | 11.21 | **4.81E-22** | 6.57E-04 | 1.41 |
| GBOBC1 b. R. GBOBC1 mb2 F. | 71 | 19.35 | 1.74 | 165 | 11.15 | **7.13E-22** | 6.66E-04 | 4.75 |
| Prime F. L. Gbn F. | 53 | -18.94 | 1.74 | 165 | 10.91 | **3.22E-21** | 6.75E-04 | 2.22 |
| Prime F. L. GBHCT R. | 42 | -18.53 | 1.74 | 165 | 10.68 | **1.45E-20** | 6.84E-04 | 2.67 |
| GBHCT R. GBOBC1 b. R. | 54 | -18.27 | 1.74 | 165 | 10.53 | **3.77E-20** | 6.93E-04 | 6.52 |
| GBOBC1 b. R. Gbn F. | 74 | 17.86 | 1.74 | 165 | 10.29 | **1.68E-19** | 7.02E-04 | 3.13 |
| Prime F. L. GBOBC1 mb2 F. | 50 | -17.45 | 1.74 | 165 | 10.06 | **7.43E-19** | 7.12E-04 | 2.59 |
| Prime R. GBOBC2 b. F. | 12 | 17.37 | 1.74 | 165 | 10.01 | **9.75E-19** | 7.22E-04 | 2.47 |
| Prime R. GBHCT F. | 9 | 17.35 | 1.74 | 165 | 10.00 | **1.08E-18** | 7.32E-04 | 3.05 |
| GBOBC1 mb2 R. GBOBC1 mb2 F. | 80 | 16.45 | 1.74 | 165 | 9.48 | **2.69E-17** | 7.43E-04 | 3.52 |
| Prime R. GBOBC1 b. R. | 4 | -16.40 | 1.74 | 165 | 9.45 | **3.23E-17** | 7.54E-04 | 1.92 |
| Prime R. L. GBOBC2 mb2 F. | 40 | 16.13 | 1.74 | 165 | 9.29 | **8.65E-17** | 7.65E-04 | 1.75 |
| GBOBC2 b. R. GBOBC1 mb2 F. | 88 | 15.97 | 1.74 | 165 | 9.20 | **1.52E-16** | 7.77E-04 | 4.65 |
| GBOBC2 b. F. Gbn F. | 118 | -15.92 | 1.74 | 165 | 9.17 | **1.80E-16** | 7.89E-04 | 4.19 |

| | | | | | | | | |
|---|---|---|---|---|---|---|---|---|
| GBHCT F. Gbn F. | 109 | -15.89 | 1.74 | 165 | 9.16 | **2.00E-16** | 8.01E-04 | 7.36 |
| GBHCT R. GBOBC2 b. F. | 62 | 15.51 | 1.74 | 165 | 8.94 | **7.63E-16** | 8.14E-04 | 4.16 |
| GBHCT R. GBHCT F. | 59 | 15.48 | 1.74 | 165 | 8.92 | **8.45E-16** | 8.27E-04 | 3.34 |
| GBHCT R. GBOBC1 mb2 R. | 55 | -15.37 | 1.74 | 165 | 8.86 | **1.23E-15** | 8.41E-04 | 6.22 |
| Prime R. L. Gbn R. | 35 | -15.18 | 1.74 | 165 | 8.75 | **2.41E-15** | 8.55E-04 | 1.30 |
| GBOBC1 mb2 R. Gbn F. | 83 | 14.96 | 1.74 | 165 | 8.62 | **5.11E-15** | 8.69E-04 | 2.37 |
| GBHCT R. GBOBC2 b. R. | 56 | -14.89 | 1.74 | 165 | 8.58 | **6.67E-15** | 8.84E-04 | 10.53 |
| Prime R. L. GBOBC1 b. F. | 37 | 14.57 | 1.74 | 165 | 8.40 | **1.98E-14** | 8.99E-04 | 1.86 |
| GBOBC2 b. R. Gbn F. | 91 | 14.48 | 1.74 | 165 | 8.34 | **2.73E-14** | 9.16E-04 | 3.13 |
| GBOBC1 mb2 F. GBOBC2 b. F. | 114 | 14.43 | 1.74 | 165 | 8.32 | **3.23E-14** | 9.32E-04 | 8.17 |
| GBHCT F. GBOBC1 mb2 F. | 106 | -14.40 | 1.74 | 165 | 8.30 | **3.56E-14** | 9.49E-04 | 4.73 |
| GBOBC2 mb2 R. GBOBC1 mb2 F. | 95 | 13.95 | 1.74 | 165 | 8.04 | **1.64E-13** | 9.67E-04 | 2.78 |
| Prime R. GBOBC1 mb2 R. | 5 | -13.51 | 1.74 | 165 | 7.79 | **7.26E-13** | 9.86E-04 | 1.66 |
| Prime R. GBOBC2 b. R. | 6 | -13.02 | 1.74 | 165 | 7.51 | **3.63E-12** | 1.01E-03 | 1.60 |
| GBHCT R. GBOBC2 mb2 R. | 57 | -12.87 | 1.74 | 165 | 7.42 | **5.90E-12** | 1.03E-03 | 2.28 |
| GBOBC2 mb2 R. Gbn F. | 98 | 12.46 | 1.74 | 165 | 7.18 | **2.22E-11** | 1.05E-03 | 1.70 |
| Prime F. GBOBC1 b. F. | 24 | -12.44 | 1.74 | 165 | 7.17 | **2.37E-11** | 1.07E-03 | 1.48 |
| Prime R. L. GBOBC1 b. R. | 31 | -12.13 | 1.74 | 165 | 6.99 | **6.44E-11** | 1.09E-03 | 1.72 |
| Prime R. GBOBC2 mb2 F. | 13 | 11.85 | 1.74 | 165 | 6.83 | **1.54E-10** | 1.11E-03 | 1.85 |
| Prime R. GBOBC2 mb2 R. | 7 | -11.01 | 1.74 | 165 | 6.34 | **2.06E-09** | 1.14E-03 | 1.54 |
| Prime F. GBOBC2 mb2 F. | 27 | -10.89 | 1.74 | 165 | 6.28 | **2.94E-09** | 1.17E-03 | 1.24 |
| GBOBC2 mb2 F. Gbn F. | 119 | -10.40 | 1.74 | 165 | 5.99 | **1.26E-08** | 1.19E-03 | 2.39 |
| Prime R. GBOBC1 b. F. | 10 | 10.30 | 1.74 | 165 | 5.94 | **1.67E-08** | 1.22E-03 | 1.99 |
| Prime F. L. GBOBC1 b. F. | 49 | -10.09 | 1.74 | 165 | 5.82 | **3.04E-08** | 1.25E-03 | 1.47 |
| GBHCT R. GBOBC2 mb2 F. | 63 | 9.99 | 1.74 | 165 | 5.76 | **4.08E-08** | 1.28E-03 | 1.56 |
| Prime R. L. GBOBC1 mb2 R. | 32 | -9.24 | 1.74 | 165 | 5.32 | **3.28E-07** | 1.31E-03 | 1.46 |
| GBOBC1 mb2 F. GBOBC2 mb2 F. | 115 | 8.91 | 1.74 | 165 | 5.14 | **7.87E-07** | 1.35E-03 | 1.82 |
| GBOBC1 b. F. Gbn F. | 113 | -8.84 | 1.74 | 165 | 5.10 | **9.35E-07** | 1.39E-03 | 1.71 |
| Prime R. L. GBOBC2 b. R. | 33 | -8.75 | 1.74 | 165 | 5.04 | **1.19E-06** | 1.42E-03 | 1.41 |
| Prime F. L. GBOBC2 mb2 F. | 52 | -8.54 | 1.74 | 165 | 4.92 | **2.07E-06** | 1.46E-03 | 1.23 |
| GBOBC2 mb2 R. Gbn R. | 92 | -8.44 | 1.74 | 165 | 4.87 | **2.64E-06** | 1.51E-03 | 1.21 |
| GBHCT R. GBOBC1 b. F. | 60 | 8.44 | 1.74 | 165 | 4.86 | **2.70E-06** | 1.55E-03 | 1.58 |
| GBOBC1 b. F. GBOBC1 mb2 F. | 110 | -7.36 | 1.74 | 165 | 4.24 | **3.72E-05** | 1.60E-03 | 1.82 |
| Prime R. L. GBOBC1 mb2 F. | 38 | 7.22 | 1.74 | 165 | 4.16 | **5.14E-05** | 1.65E-03 | 1.30 |
| GBOBC1 b. F. GBOBC2 b. F. | 111 | 7.07 | 1.74 | 165 | 4.08 | **7.09E-05** | 1.71E-03 | 2.54 |
| GBHCT F. GBOBC1 b. F. | 105 | -7.04 | 1.74 | 165 | 4.06 | **7.56E-05** | 1.77E-03 | 3.02 |
| Prime R. L. GBOBC2 mb2 R. | 34 | -6.74 | 1.74 | 165 | 3.88 | **1.49E-04** | 1.83E-03 | 1.32 |
| GBOBC2 b. R. Gbn R. | 85 | -6.43 | 1.74 | 165 | 3.71 | **2.87E-04** | 1.90E-03 | 1.01 |
| Prime R. L. GBHCT R. | 30 | 6.14 | 1.74 | 165 | 3.54 | **5.27E-04** | 1.97E-03 | 1.01 |
| GBOBC1 mb2 R. Gbn R. | 77 | -5.94 | 1.74 | 165 | 3.43 | **7.75E-04** | 2.05E-03 | 0.99 |
| Prime R. L. Gbn F. | 41 | 5.73 | 1.74 | 165 | 3.30 | **1.18E-03** | 2.13E-03 | 1.08 |
| GBOBC2 b. F. GBOBC2 mb2 F. | 117 | -5.52 | 1.74 | 165 | 3.18 | **1.75E-03** | 2.23E-03 | 1.75 |

| | | | | | | | | |
|---|---|---|---|---|---|---|---|---|
| GBHCT F. GBOBC2 mb2 F. | 108 | -5.49 | 1.74 | 165 | 3.16 | **1.85E-03** | 2.33E-03 | 1.31 |
| Prime F. GBHCT F. | 23 | -5.40 | 1.74 | 165 | 3.11 | **2.19E-03** | 2.44E-03 | 0.79 |
| GBOBC1 b. R. GBOBC2 mb2 R. | 67 | 5.39 | 1.74 | 165 | 3.11 | **2.22E-03** | 2.56E-03 | 2.39 |
| Prime F. GBOBC2 b. F. | 26 | -5.37 | 1.74 | 165 | 3.10 | **2.31E-03** | 2.70E-03 | 0.89 |
| Prime R. Prime R. L. | 1 | -4.27 | 1.74 | 165 | 2.46 | 1.49E-02 | 2.85E-03 | 0.34 |
| GBOBC1 b. R. GBOBC2 b. R. | 66 | 3.38 | 1.74 | 165 | 1.95 | 5.32E-02 | 0.00E+00 | 1.68 |
| GBOBC1 b. R. Gbn R. | 68 | -3.05 | 1.74 | 165 | 1.76 | 8.06E-02 | 0.00E+00 | 0.78 |
| Prime F. L. GBHCT F. | 48 | -3.05 | 1.74 | 165 | 1.76 | 8.09E-02 | 0.00E+00 | 0.79 |
| Prime F. L. GBOBC2 b. F. | 51 | -3.02 | 1.74 | 165 | 1.74 | 8.38E-02 | 0.00E+00 | 0.87 |
| Prime R. GBOBC1 mb2 F. | 11 | 2.94 | 1.74 | 165 | 1.70 | 9.16E-02 | 0.00E+00 | 1.15 |
| GBOBC1 b. R. GBOBC1 mb2 R. | 65 | 2.89 | 1.74 | 165 | 1.67 | 9.74E-02 | 0.00E+00 | 1.80 |
| GBOBC1 mb2 R. GBOBC2 mb2 R. | 76 | 2.50 | 1.74 | 165 | 1.44 | 1.52E-01 | 0.00E+00 | 0.97 |
| Prime F. Prime F. L. | 16 | -2.35 | 1.74 | 165 | 1.36 | 1.77E-01 | 0.00E+00 | 0.55 |
| GBOBC2 b. R. GBOBC2 mb2 R. | 84 | 2.01 | 1.74 | 165 | 1.16 | 2.47E-01 | 0.00E+00 | 0.82 |
| Prime R. GBHCT R. | 3 | 1.87 | 1.74 | 165 | 1.07 | 2.84E-01 | 0.00E+00 | 0.83 |
| GBOBC1 b. F. GBOBC2 mb2 F. | 112 | 1.55 | 1.74 | 165 | 0.90 | 3.72E-01 | 0.00E+00 | 1.33 |
| GBOBC1 mb2 F. Gbn F. | 116 | -1.49 | 1.74 | 165 | 0.86 | 3.92E-01 | 0.00E+00 | 1.00 |
| Prime R. Gbn F. | 14 | 1.46 | 1.74 | 165 | 0.84 | 4.03E-01 | 0.00E+00 | 1.05 |
| GBHCT R. GBOBC1 mb2 F. | 61 | 1.08 | 1.74 | 165 | 0.62 | 5.35E-01 | 0.00E+00 | 0.76 |
| GBOBC1 mb2 R. GBOBC2 b. R. | 75 | 0.49 | 1.74 | 165 | 0.28 | 7.80E-01 | 0.00E+00 | 0.80 |
| GBHCT R. Gbn F. | 64 | -0.41 | 1.74 | 165 | 0.24 | 8.14E-01 | 0.00E+00 | 1.00 |
| GBHCT F. GBOBC2 b. F. | 107 | 0.03 | 1.74 | 165 | 0.02 | 9.87E-01 | 0.00E+00 | 1.03 |

From the table above it is shown that the majority of the 120 pairs that are compared, have significantly different means. This was the case also for the other Glide jobs.

Table 6.10 shows percentage wise for how many of the pairwise comparisons per Glide job, the null hypothesis was rejected, at a 5% significance level. What we find is that in general a similar amount of comparisons was found to be significantly different.

Table 6.10: Percentage of significant differences (5% significance level) between rescoring methods, following post-hoc analysis of RM-ANOVA.

| | Glide 1 | Glide 2 | Glide 3 |
|---|---|---|---|

| | | | |
|---|---|---|---|
| All ligands | 85.0 | 76.6 | 80.8 |
| Excluding Lig. 7 | 83.3 | 80.0 | 81.7 |

However, what is the strength of these differences? Quantifying the size of the difference between two groups, or in other words knowing the magnitude of an effect, enables the researcher to ascertain the substantive significance of statistical significance. If a sample is large an observed effect may be statistically significant, but not have a practical significance, and vice versa, if the sample size is too small even a large effect may not be statistically significant. Therefore, we shall perform meta-analysis estimating the effect size of the observed differences. For this we will be using Cohen's d standardised test of the difference of two means[164]. The measurement is computed for each pair using the following formula:

$$d = \frac{\bar{x}_1 - \bar{x}_2}{S_{pooled}} \tag{6.3.4}$$

Where $\bar{x}_1$ and $\bar{x}_2$ are the means of the compared samples and $S_{pooled}$ is the pooled standard deviation given by:

$$S_{pooled} = \sqrt{\frac{(n_1 - 1)s_1^2 + (n_2 - 1)s_2^2}{n_1 + n_2 - 2}} \tag{6.3.5}$$

Where $n_1$ and $n_2$ is each sample size, and $S_1^2$ and $S_2^2$ the variances of each sample. In the case of same sample sizes, the above formula can be replaced by the more simplified equivalent:

$$S_{pooled} = \sqrt{\frac{S_1^2 + S_2^2}{2}} \tag{6.3.6}$$

However, although this form is widely used in the literature, it assumes independent (unpaired) samples and homogeneity of the data (equal variances). When these assumptions cannot be fulfilled, as in our case, then the following equation can be used instead:

$$d = \frac{\bar{x}_D}{S_D} \tag{6.3.7}$$

Where $\overline{x}_D$, is the mean of the differences of the compared rescoring protocols, and $S_D$ the standard deviation of those differences.

Apart from the simplicity of the calculation, what perhaps popularised Cohen's d index, was that Cohen (1992)[164] provided a set of interpretation guidelines, as per the following table:

Table 6.11: Cohen's interpretation guidelines.

| $d < 0.2$ | $d > 0.2$ | $d > 0.5$ | $d > 0.8$ |
|---|---|---|---|
| Trivial | Small | Medium | Large |

The following observations apply for all Glide jobs in both the cases of including all ligands or excluding ligand 7. Cohen's d guidelines, which were based on a thorough investigation on social science literature, should not be mindlessly invoked, but rather a personal value judgement is required. Here, all differences that were deemed statistically significant exhibited very high d-values (in some cases even more than 10) and in many cases these values were inflated when ligand 7 was not included, indicating its leveraging role in the dataset. This indicates the means are not only different according to a certain significance level, but also have a practical effect. In other words, the differences we observe are very strong.

With respect to the pairs after the test stopped (i.e. based on the previous description of the Holm-Šidák post-hoc analysis method, when the p-value

was rejected) the only conclusion that can be made is that the null hypothesis was not rejected. In other words, this means that it cannot be said that the difference between the means of the binding free energy for those pairs is statistically significant. Most of these pairs are between the AMBER rigid protocols, with a few extending across different software such as the Prime Rigid and $GB^{HCT}$Rigid rescoring protocols. Encouragingly we did find quantitative agreement across the three Glide poses, within standard error, as shown in Figure 6.24 (descriptive statistics for the means of each solvent model for each Glide pose shown in Table B.5 to Table B.7). Also within standard error, the pairs, for which the null hypothesis could not be rejected was, roughly the same across the three Glide poses (see comparison Table B.13).

The findings are on par with those from the box plots. Most of the models not relate well quantitatively with each other, with only the rigid OBC models showing consistent relationship amongst one another. Flexibility appears largely problematic and should be avoided in this setting of rescoring by simply minimising. This analysis enabled the quantification of the differences we observed in the box plots. We were able to show that most models differ significantly but also that these differences show a substantive significance.

A major limitation of these methods is the lack of sampling. In the next section we investigate the contribution of implicit MD simulations in the estimation binding free energies using the MM-GBSA methodology.

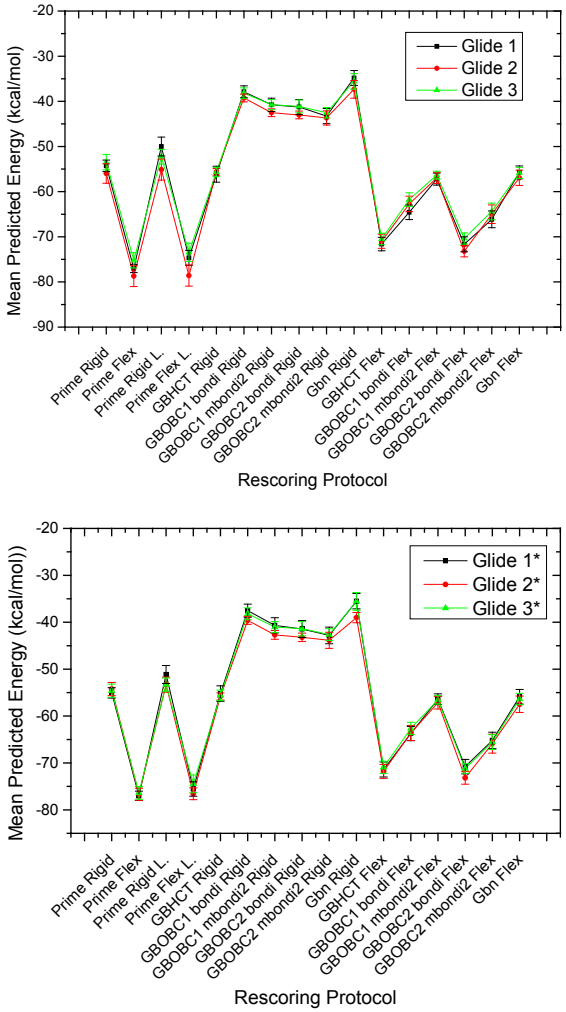


Figure 6.24: Line and symbol plot of means of each rescoring model for Glide jobs 1, 2, and 3. Top plot: All ligands. Bottom plot: Excluding ligand 7. Error bars correspond to the standard error of the mean $\left(s/\sqrt{n}\right)$.

### 6.3.3 Molecular dynamics results

Three independent MD simulations were performed using two different GB models in Amber: $GB^{HCT}$ and $GB^{OBC1}$mbondi2; the reason for this is described at the end of section 6.2.3. The first was used in two simulations; one was 10 ns long, saving snapshots every 100 ps (total 100 snapshots), while the other, 1 ns long, saving coordinates every 5 ps (total 200 snapshots). A 1 ns (collecting 200 snapshots) long MD simulation with implicit solvent was also run using the $GB^{OBC1}$mbondi2 model. The simulations were independent

of each other, i.e. starting at different points in the phase space, despite starting from the same conformation (output of flexible protein minimisations in AMBER). This is achieved by assigning random starting velocities to a Maxwell distribution through a random seed number generator (*ig* parameter in Amber). Further details of the simulation protocols can be found in section 6.2.3.

Figure 6.25 shows the results of predicted binding energies from the MD simulations versus experiment for the three docking sets of poses. The coefficient of determination ($R^2$) ranged from 0.00 ($GB^{HCT}$ job3 10 ns and 1 ns) to 0.31 ($GB^{OBC1}$ job 2 1ns). Based on a significance level of 5% (anything above $R^2 = 0.33$) none of the correlations obtained following rescoring with the use of MD simulations were significant. It can be seen in plots A through C in Figure 6.25 that the results from GB model OBC1 are quantitatively different from those obtained using the HCT model. The values obtained from the OBC1 model were consistently less negative (blue triangles in plots A through C in Figure 6.25). Although the results were similar both quantitatively and qualitatively for Glide jobs 1 and 2, they appeared more scattered for job 3, giving lower $R^2$ values across both GB models and both the longer and shorter MD simulations.

Ligand 7 (the least potent inhibitor discussed in more detail in the previous section) is consistently ranked wrongly across all GB models and Glide jobs. Removal of ligand 7 generally improves correlations (except for job 3), however not enough for statistically significant correlations to be obtained (see plot D in Figure 6.25).

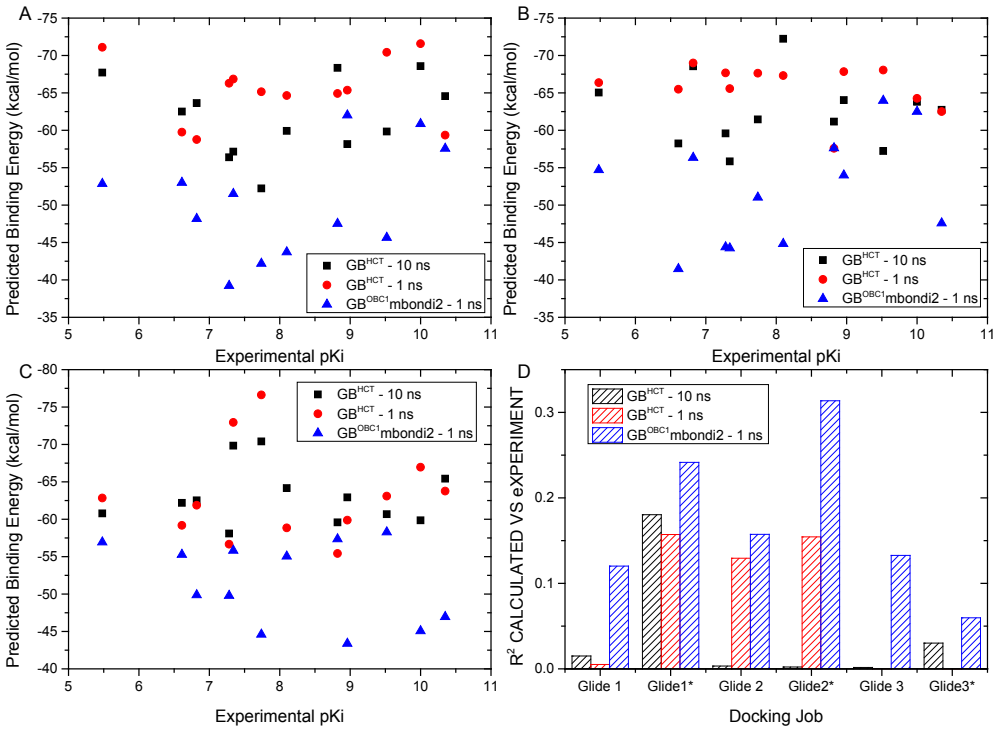


Figure 6.25: Summary of the three MD protocols (GB1 – 10ns, GB1 – 1ns, GB2mb – 1ns) versus experimental data. Glide job 1, 2, and 3 shown in plots A, B, and C respectively. Plot D: $R^2$ for each run across the three Glide jobs. The asterisk (*) corresponds to the correlation when ligand 7 is excluded.

Table 6.12 summarises the results of Kendall tau ($\tau$) rank correlation coefficient of predicted energies with experiment. As can be seen in Figure 6.25, this measurement confirms MM-GBSA rescoring using implicit solvent fails in this case to rank the ligands correctly. Very low ranking correlations were obtained with particularly high p-values (anything below 0.05 would be significant).

Table 6.12: Kendall tau (τ) and the corresponding p-values for the three MD calculations versus experimental data for each Glide job. The asterisk (*)

| | Glide 1 | | Glide 1* | | Glide 2 | | Glide 2* | | Glide 3 | | Glide 3* | |
|---|---|---|---|---|---|---|---|---|---|---|---|---|
| | τ | p | τ | p | τ | p | τ | p | τ | p | τ | p |
| $GB^{HCT}$ – 10ns | 0.12 | 0.64 | 0.27 | 0.28 | 0.00 | 1.00 | 0.13 | 0.65 | 0.06 | 0.84 | 0.02 | 1.00 |
| $GB^{HCT}$ – 1ns | 0.09 | 0.74 | 0.27 | 0.28 | -0.15 | 0.55 | -0.20 | 0.45 | 0.15 | 0.55 | 0.20 | 0.45 |
| $GB^{OBC1}$ – 1ns | 0.15 | 0.55 | 0.24 | 0.36 | 0.33 | 0.15 | 0.45 | 0.06 | -0.18 | 0.46 | -0.09 | 0.76 |

To eliminate bad contacts arising during the MD runs, each snapshot was minimised for a further 5000 steps (1000 steps using the steepest descent algorithm and 4000 steps using the conjugate gradient algorithm) with full protein flexibility. This was only performed on the 10 ns MD simulation. With small fluctuations, the $R^2$ were equivalent to the original results. In addition, it is possible in the beginning of an MD run that a system is still equilibrating, while in the end of the run the system may drift away to an unreasonable conformation. Therefore, to investigate the effect of this in the results, the data was reprocessed excluding a number of snapshots at the start and end of the simulation. We concluded this did not have an effect for this case.

The energy (Kinetic, potential and total for the system) for all systems remained stable throughout the simulations, and the temperature was kept constant at the desired value of 300 K, indicating the thermostat worked correctly. Figure 6.26 shows an example of this taken from the 1 ns – long trajectory of ligand 1, Glide job1, with the $GB^{HCT}$ model.

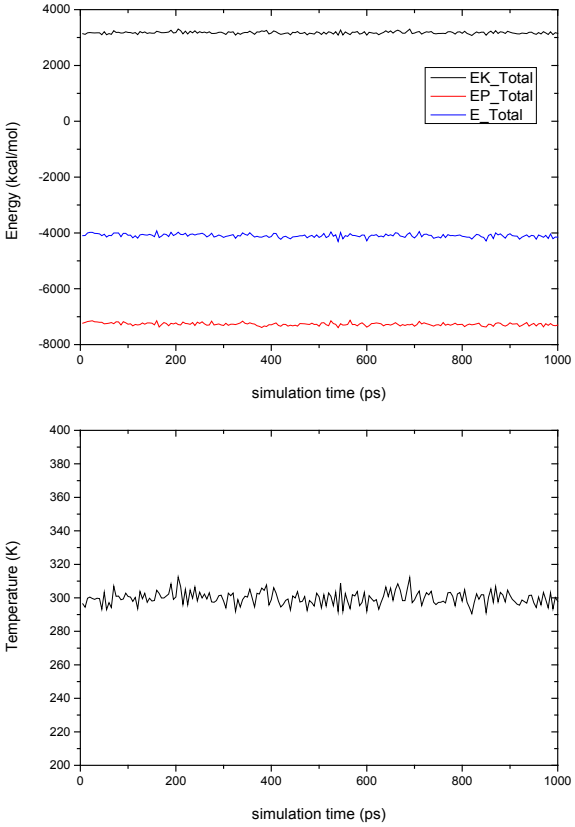


Figure 6.26: Kinetic energy (black line), potential energy (red line) and total system energy (blue line) for ligand 1 Glide job 1 during 1 ns MD using model $GB^{HCT}$. Bottom plot shows the temperature during the simulation.

The heavy atom root mean squared deviation (RMSD) of the protein backbone was overall stable for all protein-ligand systems and remained, in most cases, below the value of 2 Å. The ligand in all simulations remained in the binding site. More specifically the amidino part of the molecule remained fixed in the deep S1 pocket retaining key electrostatic interactions with Asp189, and van der Waals interactions with Ala190, Val213, and Phe227 (see section 4.2). However, other parts of the molecule showed large fluctuations reaching in some cases heavy atom RMSDs for the ligand of up to 6 Å. Although some movement of R2 group was observed, the majority of the fluctuations came from rotations of the mostly hydrophobic R3

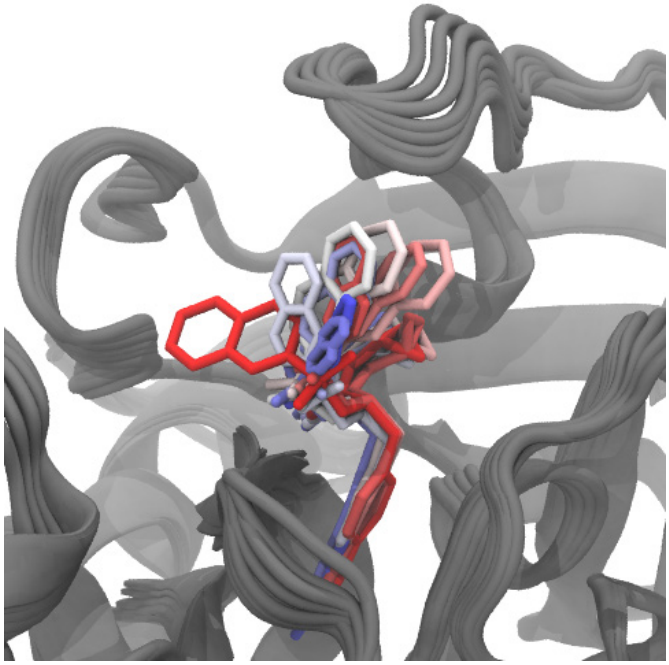

Figure 6.27: Ten equally spaced snapshots for the 10 ns trajectory of ligand 4 Glide job 1 using $GB^{HCT}$ implicit solvent. The ligand is coloured by the timestep colouring method where red is the start and blue the end of the simulation.

substituent around the sulphonamide (see section 4.2). An example of this is shown in Figure 6.27.

### 6.3.4 Summary

This section focused on the critical assessment of a range of MM-GBSA rescoring protocols in a range of software. None of the models performed better (gave higher $R^2$ with experiment) than docking (Thrombin was one of the proteins on which GlideScore was optimised), except for when the lowest energy of the three Glide dock poses per ligand was rescored with the model $GB^{HCT}$ (with protein rigid and excluding ligand 7). Thus far, it has been shown that in general simple rescoring protocols utilising the MM-GBSA methodology give poor results compared with experimental binding free energies. In addition, these results vary significantly from model to model,

and from software to software, when compared with experiment. Besides this, we found an unreasonably strong dependence on starting conformations (significant differences in $R^2$ and $\tau$ observed for trivial ligand-ligand RMSD differences). Results derived from rescoring docked poses with slightly different initial conditions gave very different qualitative results with experiment. Importantly, we were not able to identify one model which gave good agreement with experiment across all the different docked poses. Such poor results and inconsistencies were also found for the ranking of compounds ($\tau$ coefficient).

Rigorous head-to-head comparison between solvent models, showed overall poor qualitative and quantitative relationship. Although some of the models were found to be similar, models from different software, and protocols with flexible protein were found to be largely different. However, binding free energies amongst Glide poses for each solvent model were found to be almost equivalent to within the standard error of the mean.

Additional sampling utilising implicit MD simulations did not add value in this case. Correlations were worse than those obtained by rescoring using minimisation techniques. This could be attributed to noise during the simulations due to large ligand fluctuations exaggerated by the lack of physical waters.

## 6.4 β-Secretase

### 6.4.1 System preparation

The same protein preparation and simulation protocols as described in section 6.2, were followed, using the PDB structure 2P4J (resolution = 2.50 Å).[113]

### 6.4.2 Rescoring results

### *Comparison with experiment*

Table 6.13: Coefficient of determination of calculated binding energies versus experiment for each rescoring protocol.

| | $R^2$ of Calculated Energies versus Experiment | | | |
|---|---|---|---|---|
| **Protocol** | **CDOCKER** | **Glide 1** | **Glide 2** | **Glide 3** |
| **Docking** | 0.02 | 0.01 | 0.01 | 0.04 |
| **E-Novo** | 0.10 | | | |
| **Prime Rigid** | 0.31 | 0.24 | 0.36 | 0.15 |
| **Prime Flex** | 0.40 | 0.36 | 0.27 | 0.29 |
| **Prime Rigid L.** | | 0.30 | 0.19 | 0.18 |
| **Prime Flex L.** | | 0.04 | 0.16 | 0.33 |
| **$GB^{HCT}$ Rigid** | 0.07 | 0.29 | 0.18 | 0.07 |
| **$GB^{OBC1}$ bondi Rigid** | 0.07 | 0.10 | 0.13 | 0.05 |
| **$GB^{OBC1}$ mbondi2 Rigid** | 0.05 | 0.07 | 0.08 | 0.06 |
| **$GB^{OBC2}$ bondi Rigid** | 0.06 | 0.06 | 0.06 | 0.00 |
| **$GB^{OBC2}$ mbondi2 Rigid** | 0.06 | 0.14 | 0.09 | 0.00 |
| **Gbn Rigid** | 0.00 | 0.03 | 0.02 | 0.00 |
| **$GB^{HCT}$ Flex** | | 0.38 | 0.50 | 0.28 |
| **$GB^{OBC1}$ bondi Flex** | | 0.37 | 0.30 | 0.23 |
| **$GB^{OBC1}$ mbondi2 Flex** | | 0.15 | 0.08 | 0.12 |
| **$GB^{OBC2}$ bondi Flex** | | 0.16 | 0.17 | 0.17 |
| **$GB^{OBC2}$ mbondi2 Flex** | | 0.31 | 0.13 | 0.16 |
| **Gbn Flex** | | 0.16 | 0.12 | 0.18 |

The correlation of predicted binding affinities with experiment are shown in Figure 6.28 and Figure B.5, grouped by docking run and rescoring protocol respectively. The exact data for the correlations are shown in Table 6.13. The 5% significance level resulting from a two-tailed test is shown as a black line. Similarly as for Thrombin only rigid-protein calculations in AMBER were performed on the CDOCKER poses. Also, as in Thrombin, two sets of Prime rigid and flexible results are shown, for the cases were two docking poses were reported in the docking output. The 'L.' suffix corresponds to the correlations obtained using the lowest (most negative) dock-scored pose.

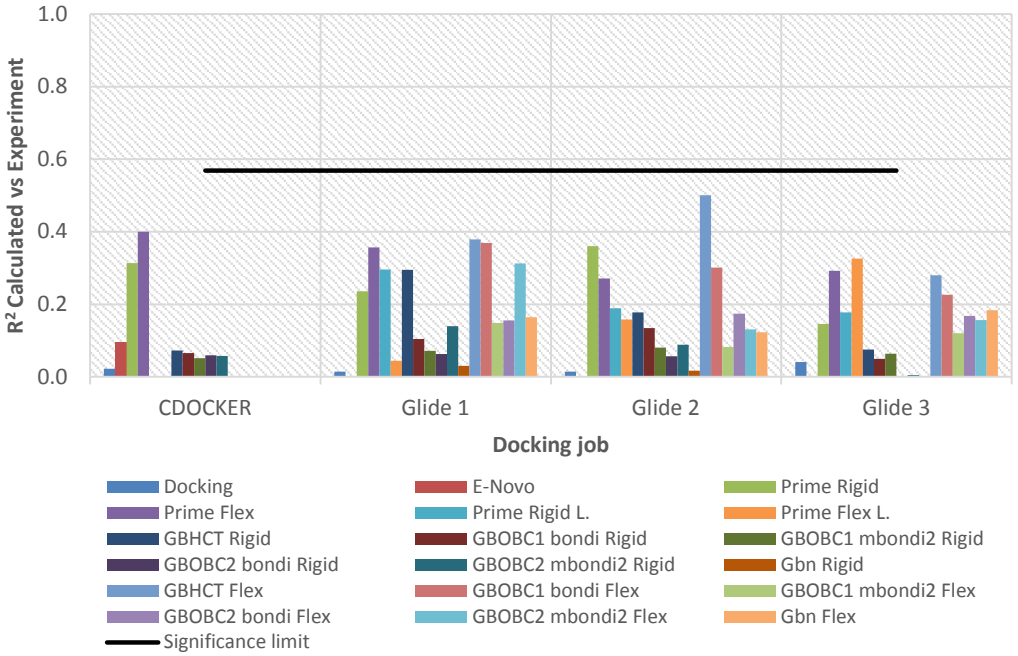


Figure 6.28: Coefficient of determination of rescoring protocols with experiment grouped by docking jobs (CDOCKER, Glide 1, Glide 2, Glide 3). Each rescoring protocol is shown by a differently coloured bar. The 'L.' for Prime jobs stands for the Prime score based on the lowest (more negative) docking score, in the case of two dock poses obtained for one ligand. 'Rigid' and 'Flex' refer to protein flexibility, with the latter fully flexible for Amber calculations, while only 4 Å for Prime calculations. No flexible protein calculations performed with CDOCKER poses. Glide poses not tested on Pipeline Pilot. Correlation with docking provided for comparison purposes. The black line shows the 5% significance level for the number of observations (7 ligands).

The $R^2$ of predicted energies with experiment ranged from 0.00 to 0.50 for Glide poses, and 0.00 to 0.40 for CDOCKER poses. Owing to the small data size the 5% significance threshold is higher than for Thrombin, at 0.57. At this level, none of the obtained correlations against experiment were found to be statistically significant. The large variation in $R^2$ between the different rescoring protocols is more evident in Figure 6.28.

Here, the docking scores are very poor. When compared to the rescoring protocols, some manage to improve the correlation with experiment, but overall were small and insignificant. Although AMBER with flexible protein

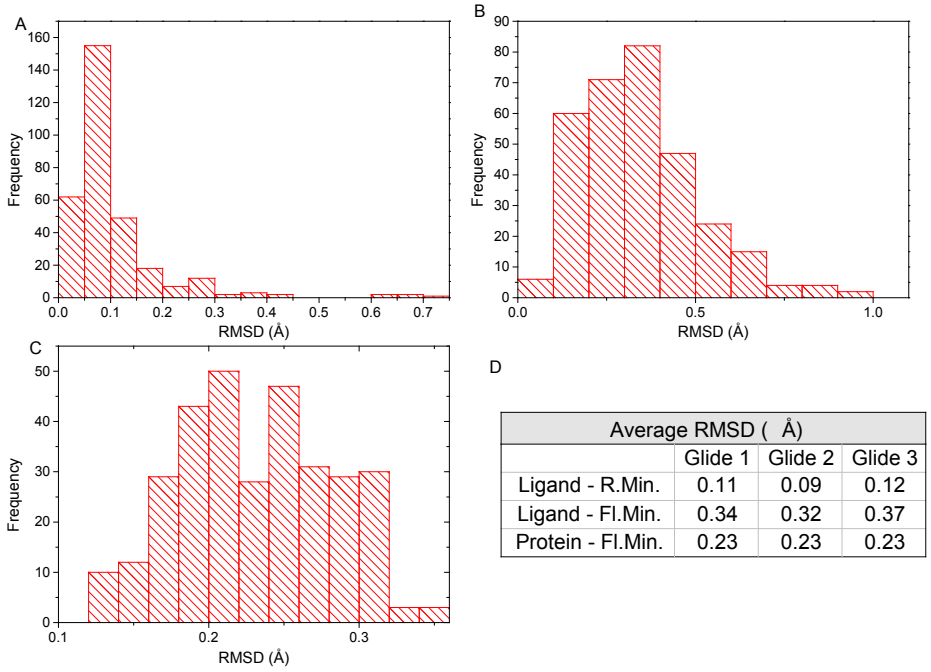


| Average RMSD ( Å) | | | |
|---|---|---|---|
| | Glide 1 | Glide 2 | Glide 3 |
| Ligand - R.Min. | 0.11 | 0.09 | 0.12 |
| Ligand - Fl.Min. | 0.34 | 0.32 | 0.37 |
| Protein - Fl.Min. | 0.23 | 0.23 | 0.23 |

Figure 6.29: Ligand-ligand (A, B) and protein-protein backbone (C) RMSD distribution between AMBER GB models in all possible combinations for each Glide job 1, prior (A) and after (B, C) protein flexible minimisations. The average RMSD values for each Glide job shown in table (D). Only heavy atoms are considered and only the backbone of the protein. R.Min. and Fl. Min., correspond to the output for rigid protein and flexible protein minimisations, respectively.

in particular the model $GB^{HCT}$ performed better than Prime, considering how insignificant the correlations are, any such observations are fortuitous.

Figure 6.29 shows the heavy atom ligand-ligand and protein-protein backbone RMSD across all possible combinations of solvent models and all Glide jobs combined into three histogram plots. From A to C each shows the ligand-ligand RMSD at the end of rigid minimisations, ligand-ligand RMSD and protein-protein backbone RMSD both at the end of flexible protein minimisations, respectively. With six GB models, corresponding to 15 combinations, three Glide jobs and seven ligands, a total of 315 values are shown in each plot. In all cases the RMSD values are very low (below 1 Å). This is to show that essentially identical structures give the random $R^2$ we see.

Considering the magnitude of the correlations with experiment for this dataset and how much lower from the 5% significance level they are (i.e. very high probability they occur at random), a similar analysis comparing the performance of the solvent models with experiment across Glide jobs, as performed in Thrombin, will not be presented here. However the plots showing the $R^2$ differences and the ligand-ligand RMSD between solvent models for the possible Glide job combinations are shown in appendix B (Figure B.5 and Figure B.6). Again the RMSD values were very small in the majority of the cases.

Below, in Figure 6.30, we show the statistical measures of $R^2$ and Kendall tau with p-values (from a two-tailed student t-test for a significance level of 5%) for each to accurately portray the statistical significance of our results. Correct ranking of the inhibitors was possible for only one out of 57 predictions. This poor ranking performance is a stark reminder of the limitations involved with applying MM-GBSA as a fast rescoring tool in lead optimisation.

For a complete picture of the data, scatter plots of the predicted versus the experimental binding affinities for the rigid and flexible protein minimisations, respectively, are shown in Figure B.7 and Figure B.8.

As in section 6.3.2, the lowest predicted energy structure was considered and the resulting values were compared with experiment. This did not improve results in this case either, although the trend of a slight improvement in $R^2$ for flexible-protein minimisations was again visible. Ranking was also particularly poor with all values not being statistically significant, and with the highest $\tau$ at 0.43 (see Figure B.9 and Figure B.10). In addition, there was no correlation found between number of heavy atoms (NHA) and molecular weight (MW) with experiment (Table B.14) for this case.

R^2

| | Docking | Prime R | Prime F | Prime R L | Prime F L | $GB^{HCT}$ R | $GB^{OBC1}$ B R | $GB^{OBC1}$ MB2 R | $GB^{OBC2}$ B R | $GB^{OBC2}$ MB2 R | GBn R | $GB^{HCT}$ F | $GB^{OBC1}$ B F | $GB^{OBC1}$ MB2 F | $GB^{OBC2}$ B F | $GB^{OBC2}$ MB2 F | GBn F |
|---|---|---|---|---|---|---|---|---|---|---|---|---|---|---|---|---|---|
| Glide 1 | 0.07 | 0.24 | 0.36 | 0.30 | 0.04 | 0.29 | 0.10 | 0.07 | 0.06 | 0.14 | 0.03 | 0.38 | 0.37 | 0.15 | 0.16 | 0.31 | 0.16 |
| | 0.56 | 0.27 | 0.16 | 0.21 | 0.65 | 0.21 | 0.48 | 0.56 | 0.59 | 0.41 | 0.71 | 0.14 | 0.15 | 0.39 | 0.38 | 0.19 | 0.37 |
| Glide 2 | 0.01 | 0.36 | 0.27 | 0.19 | 0.16 | 0.18 | 0.13 | 0.08 | 0.06 | 0.09 | 0.02 | 0.50 | 0.30 | 0.08 | 0.17 | 0.13 | 0.12 |
| | 0.79 | 0.15 | 0.23 | 0.33 | 0.38 | 0.35 | 0.42 | 0.54 | 0.61 | 0.52 | 0.78 | 0.08 | 0.20 | 0.53 | 0.35 | 0.43 | 0.44 |
| Glide 3 | 0.04 | 0.15 | 0.29 | 0.18 | 0.33 | 0.07 | 0.05 | 0.06 | 0.00 | 0.00 | 0.00 | 0.28 | 0.23 | 0.12 | 0.17 | 0.16 | 0.18 |
| | 0.67 | 0.40 | 0.21 | 0.35 | 0.18 | 0.55 | 0.63 | 0.58 | 0.94 | 0.89 | 0.99 | 0.22 | 0.28 | 0.45 | 0.36 | 0.38 | 0.34 |
| CDOCKER | 0.02 | 0.31 | 0.40 | | | 0.07 | 0.07 | 0.05 | 0.06 | 0.06 | 0.00 | | | | | | |
| | 0.75 | 0.19 | 0.13 | | | 0.56 | 0.58 | 0.63 | 0.60 | 0.60 | 0.99 | | | | | | |

Kendall tau

| | Docking | Prime R | Prime F | Prime R L | Prime F L | $GB^{HCT}$ R | $GB^{OBC1}$ B R | $GB^{OBC1}$ MB2 R | $GB^{OBC2}$ B R | $GB^{OBC2}$ MB2 R | GBn R | $GB^{HCT}$ F | $GB^{OBC1}$ B F | $GB^{OBC1}$ MB2 F | $GB^{OBC2}$ B F | $GB^{OBC2}$ MB2 F | GBn F |
|---|---|---|---|---|---|---|---|---|---|---|---|---|---|---|---|---|---|
| Glide 1 | 0.24 | 0.24 | 0.33 | 0.43 | 0.24 | 0.43 | 0.24 | 0.14 | 0.24 | 0.24 | 0.14 | 0.52 | 0.71 | 0.24 | 0.14 | 0.62 | 0.14 |
| | 0.56 | 0.56 | 0.38 | 0.24 | 0.56 | 0.24 | 0.56 | 0.77 | 0.56 | 0.56 | 0.77 | 0.14 | 0.03 | 0.56 | 0.77 | 0.07 | 0.77 |
| Glide 2 | 0.05 | 0.43 | 0.43 | 0.33 | 0.33 | 0.24 | 0.24 | 0.24 | 0.24 | 0.24 | 0.14 | 0.43 | 0.43 | 0.14 | 0.14 | 0.14 | 0.24 |
| | 1.00 | 0.24 | 0.24 | 0.38 | 0.38 | 0.56 | 0.56 | 0.56 | 0.56 | 0.56 | 0.77 | 0.24 | 0.24 | 0.77 | 0.77 | 0.77 | 0.56 |
| Glide 3 | -0.05 | 0.33 | 0.43 | 0.33 | 0.43 | 0.33 | 0.14 | 0.24 | 0.05 | 0.14 | 0.05 | 0.33 | 0.24 | 0.14 | 0.14 | 0.24 | 0.14 |
| | 1.00 | 0.38 | 0.24 | 0.38 | 0.24 | 0.38 | 0.77 | 0.56 | 1.00 | 0.77 | 1.00 | 0.38 | 0.56 | 0.77 | 0.77 | 0.56 | 0.77 |
| CDOCKER | 0.05 | 0.43 | 0.43 | | | 0.05 | 0.05 | 0.05 | 0.05 | 0.05 | -0.05 | | | | | | |
| | 1.00 | 0.24 | 0.24 | | | 1.00 | 1.00 | 1.00 | 1.00 | 1.00 | 1.00 | | | | | | |

Figure 6.30: The correlation of determination ($R^2$) and Kendall tau rank correlation coefficient ($\tau$) across all rescoring tests (including the docking score) for each docking protocol. The coloured boxes represent the p-values (from a two-tailed test) for each statistic ($R^2$ and Kendal's tau) with green any value below 5% (statistical significance limit), while red anything above that threshold. R, F, B, MB2 stand for Rigid, Flexible (4 Å around ligand for Prime – full flexibility for Amber), Bondi radii, and MBondi2 radii respectively. The table should be read in pairs of colourless (statistic) and coloured cells (p-value).

Thus overall performance with experiment was particularly poor, both when the models were compared with each other and when compared across the different docking jobs. Both the coefficient of determination and the ranking correlation coefficient were statistically insignificant for all cases (except for one for the latter). This is a clear example MM-GBSA is very system dependent and should be used with caution.

Although, the predictive performance of the method is important a model should also be robust, i.e. one should be able to obtain similar results when using different implementations of MM-GBSA if the method is to be used routinely. This is investigated in the next section.

***Comparison between rescoring protocols***

Following the poor results in the previous subsection an attempt to identify how the models behave with respect to each other is discussed herein. A rigorous comparison was carried out, first investigating the qualitative agreement of the methods, followed by assessment of their quantitative similarity.

The chosen statistical measures for our qualitative tests were the coefficient of determination ($R^2$), and Kendall's tau ($\tau$) rank correlation coefficient. Descriptive statistics for these measurements for all 120 pairwise comparisons (resulting form 16 rescoring models compared with respect to each other and not with experiment) for each Glide job, are summarised in Table 6.14. Overall, compared to Thrombin, a much greater agreement between models was observed. The average correlation ranged from 0.66 (Glide 2) to 0.74 (Glide 3). The $\tau$ values were lower in comparison to $R^2$and ranged from 0.59 (Glide 1) to 0.70 (Glide 3), however still improved over those obtained for Thrombin. What the data in the table below tell us is that overall the solvent models show a good qualitative agreement between them, but the ranking was found to be average.

Table 6.14: Descriptive statistics of $R^2$ and Kendall $\tau$ across all pairwise comparisons for each Glide job. Percentage of statistics ($R^2$, $\tau$) with p-value below 0.05 is shown (%SIG).

| | | MIN | MAX | MEAN | STDEV | % SIG. |
|---|---|---|---|---|---|---|
| **Glide 1** | $R^2$ | 0.19 | 0.99 | 0.73 | 0.18 | 84.17 |
| | $\tau$ | 0.14 | 1.00 | 0.59 | 0.20 | 36.67 |
| **Glide 2** | $R^2$ | 0.05 | 0.98 | 0.66 | 0.25 | 68.33 |
| | $\tau$ | 0.05 | 1.00 | 0.64 | 0.24 | 55.00 |
| **Glide 3** | $R^2$ | 0.31 | 0.99 | 0.74 | 0.17 | 80.83 |
| | $\tau$ | 0.33 | 1.00 | 0.70 | 0.16 | 60.83 |

Matrices containing the statistic and the corresponding *p-value*, for all pairwise comparisons for each statistical measure and for each Glide pose are included in appendix B (see Table B. 15 through Table B.20). Although here a much larger number of measurements were statistically significant, a similar trend as for Thrombin is observed, with an overall tendency for significant correlations within rigid and within flexible AMBER GB models. However, despite the improved results, we do find variation between different docked poses when we compare the same pairs of models. An example of that is Prime Flex L. and $GB^{OBC2}$bondi Rigid, where the $R^2$ is 0.88 for Glide 1, drops to 0.47 for Glide 3, and reduces even further to 0.24 for Glide 2.

In the remainder of this subsection we aim to quantify the agreement between the different models.

To evaluate the quantitative agreement of the different methods with regard to each other, box plots were constructed for each set of rescored dock poses (see Figure 6.31, Figure 6.32, Figure B.11, and Figure B.12).

Figure 6.31 shows the distributions of the predicted energies when the CDOCKER poses are used. In contrast with Thrombin, it was found E-Novo this time had the lowest (more negative) mean, while Prime Rigid was shown to have the highest, at about 30 kcal $mol^{-1}$ less negative than E-Novo and 10 kcal $mol^{-1}$ than Prime Flex. $GB^{HCT}$ does not appear much isolated from the rest of the AMBER GB models, which, here, share a similar distribution, but have mostly different median values. Ligand 1 was an outlier for E-Novo and ligand 7 for both Prime Rigid and Flex. In both cases the outlier is displayed by the least negative whisker. The R2 group in both of these ligands is highly flexible (see Table 4.2), and so this could potentially be a source of error. No outliers where observed for the Amber GB models.

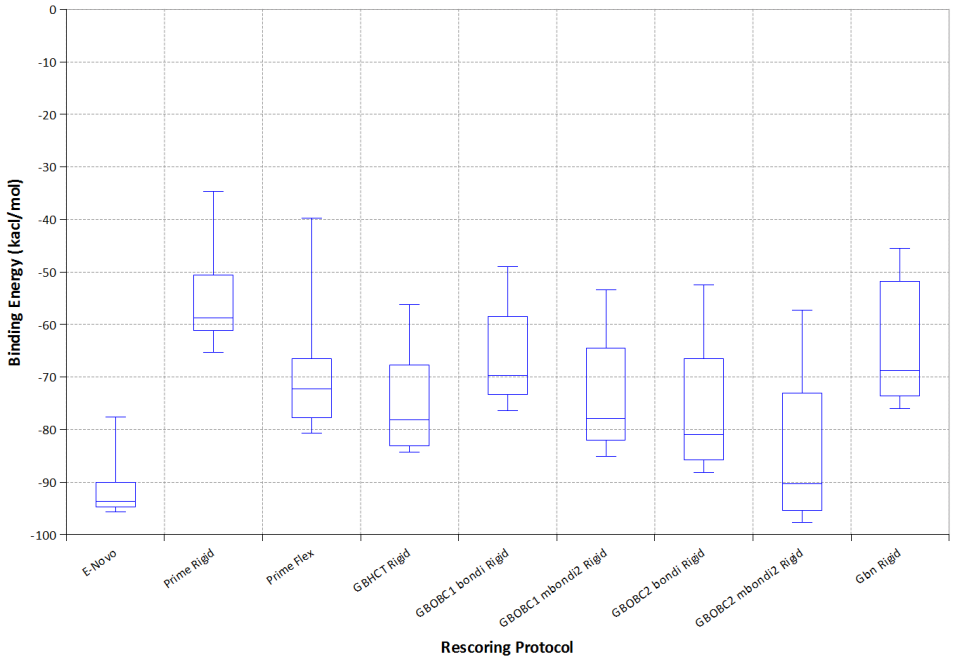


Figure 6.31: Box Plot of predicted binding free energies (kcal $mol^{-1}$) of CDOCKER poses for each rescoring protocol. The whiskers represent the minimum and maximum values, the box corresponds to the range of values between the 1st and 3rd quartiles, and the line through the box represents the median value of the binding energies.

Figure 6.32 shows the binding free energy distributions for each model for Glide job 1. Here the ICR and values for the median were quite different between all models, except between OBC1 bondi rigid and OBC2 mbondi2 rigid. A division of the data in two groups is noticeable in the plot, where all flexible protein minimisation results are consistently more negative. The reason for the large ranges observed for the AMBER flexible models. This outlier is again ligand 7 (also an outlier for Prime results using CDOCKER poses), however it is not an outlier for the remaining rescoring protocols, except for $GB^{HCT}$ Rigid. Visual inspection did not reveal any reasons justifying ligand 7 as an outlier, except for having a hydrogen in place of the sulphonamide R1 group when compared to the rest of the ligands in the group (Table 4.2). The fact it is not consistently an outlier in all models highlights the unreliability of the method.

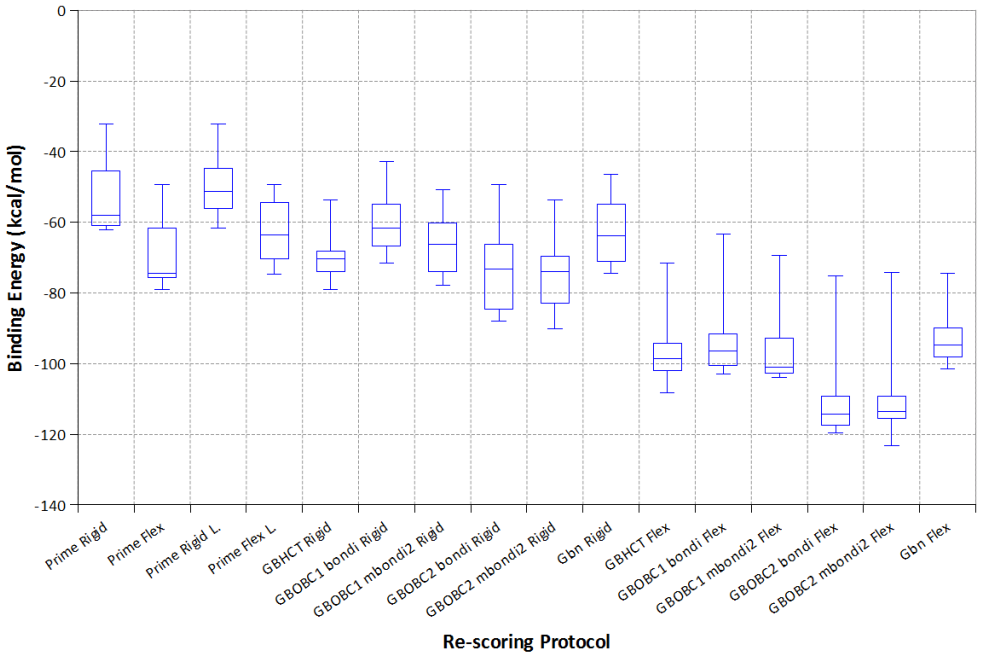


Figure 6.32: Box Plot of predicted binding free energies (kcal $mol^{-1}$) of Glide 1 poses for each rescoring protocol. The whiskers represent the minimum and maximum values, the box corresponds to the range of values between the 1st and 3rd quartiles, and the line through the box represents the median value of the binding energies.

The same observations were made for Glide jobs 2 (Figure B.11) and 3 (Figure B.12). In these cases ligand 7 was shown to be an outlier for the AMBER flexible rescoring models, but not for the other models, except for Glide 3 Prime Rigid protocol.

Results from a Repeated Measures ANOVA (RM-ANOVA) are summarised in Table 6.15 (technical details for the analysis in section 6.3.2). The null hypothesis (Table 6.7) can be rejected with a very high probability for all three Glide poses. The value of the F statistic indicates that Glide 1 contains the most significant differences, followed by Glide 3, and lastly by Glide 2.

Table 6.15: Repeated measures ANOVA results. $SS_b$ is the Sum of Squares between measures, df is the degrees of freedom, and $MS_b$, the Mean Square($SS_b/df\ model$).

| | $SS_b$ | df model | df error | $MS_b$ | F | p |
|---|---|---|---|---|---|---|
| Glide1 | 38823.11 | 2.68 | 16.08 | 14489.37634 | 100.26198 | 2.13E-10 |
| Glide 2 | 40642.82 | 2.00 | 12.00 | 20326.18 | 86.11 | 7.67E-8 |
| Glide 3 | 39754.42 | 2.51 | 15.03 | 15795.72 | 99.12 | 8.33E-10 |

To identify which methods differed the Holm-Šidák post-hoc analysis method was used. Overall a similar number of rejections of the null hypothesis was observed across all three Glide jobs with roughly 74% significant differences or about 89 out the 120 pairwise comparisons.

Table 6.16: Percentage of significant differences (5% significance level) between rescoring methods, following post-hoc analysis of RM-ANOVA.

| | %Sig. Diff. |
|---|---|
| Glide 1 | 75.00 |
| Glide 2 | 73.33 |
| Glide 3 | 73.33 |

To determine if these differences are meaningful, the effect size (d index) is calculated as per the formula (6.3.7). The results combined with the RM-ANOVA post-hoc analysis results are summarised in three tables (one for each Glide job) in appendix B (see Table B.24 to Table B.26). Large effect sizes were obtained for all cases where the null hypothesis was rejected, indicating that the differences are substantial. In addition large *d-values* and mean differences (as much as 8 kcal $mol^{-1}$) were also obtained for more than half of the cases where the null hypothesis could not be rejected (a

comparison between Glide poses for these pairs is shown in Table B.27). Owing to the small size of the data set, this could be an indication of a false negative, i.e. concluding two means are not different when in reality they are.

All this analysis shows that although earlier we found a qualitative agreement between the models, quantitatively they are mostly very different from each other. Therefore the choice of solvent model involves a great risk and there does not seem to be an indication to choose one over the other. On a positive note, it was found that overall a good overlap of the means across Glide poses exists (Figure 6.33), although compared to Thrombin, the standard errors were larger, owing to, perhaps, the smaller dataset.

In the next section the issue of sampling will be addressed by introducing molecular dynamics simulations.

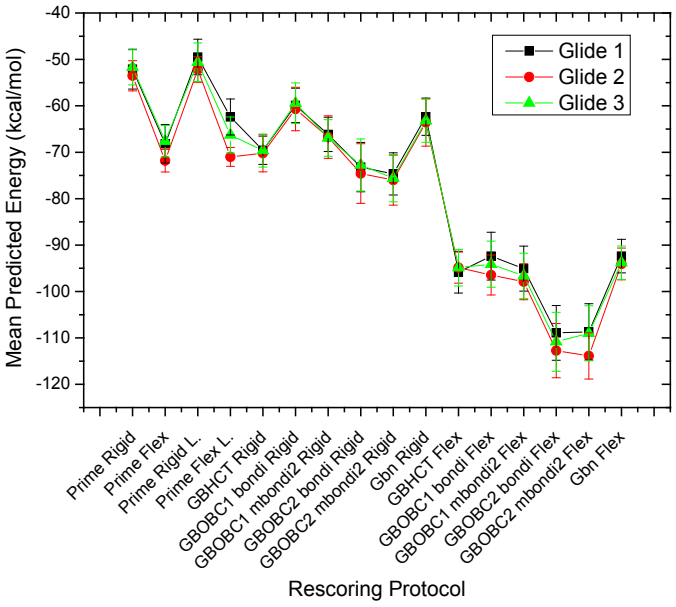


Figure 6.33: Line and symbol plot of means of each rescoring model for Glide jobs 1, 2, and 3. Error bars correspond to the standard error of the mean$\left(s/\sqrt{n}\right)$.

### 6.4.3 Molecular dynamics results

Molecular dynamics (MD) simulations were used with the purpose to investigate the effect sampling has on the results, and if there is an improvement over simply minimising docking poses. The same length of MD simulations were conducted with the same GB models as in Thrombin (section 6.3.3).

The results for the implicit molecular dynamics (MD) runs versus experiment for the three Glide jobs are shown in Figure 6.34. The $R^2$ between predicted and experimental binding free energies ranged from as low as 0.01 for job 2 $GB^{OBC1}$mbondi2 (1 ns), to 0.61 for job1 $GB^{HCT}$ (10 ns).

At a significance level of 5% ($R^2 = 0.57$) the only significant measurement is that of job1 $GB^{HCT}$ (10 ns) at 0.60 (see plot D Figure 6.34). The second best correlation was again obtained from using model $GB^{HCT}$ of job 2 (10 ns) at 0.53, however in job 3 (10 ns) it plummeted to 0.04. The plots A, B, and C (black squares) reveal that the key ligand maintaining the correlation for jobs 1 and 2, is ligand 4 (the most potent ligand with pKi = 8.96). We can see that the least potent compound (ligand 7) is predicted closely for all jobs, and so are the two middle compounds (ligand 1 and 3). The most extreme compound (the most potent) ligand 4 was underestimated (less negative) in job 3, leading to complete loss of correlation versus experimental data. Finally, the other three compounds (ligands 2, 5, and 6) show similar predictions for the most part.

When compared to the 10 ns simulations, the trajectories of 1 ns displayed considerably poorer $R^2$ with experiment. $GB^{HCT}$ overall performed better than the $GB^{OBC1}$ model; however the correlations were not statistically significant (within a 5% significance level). A closer investigation (plots A, B, C) reveals that for jobs 2 and 3, again ligand 4 plays an important role in the different correlations observed between the three different protocols. In addition in the case of job 1, ligand 7 (lowest pKi) was significantly

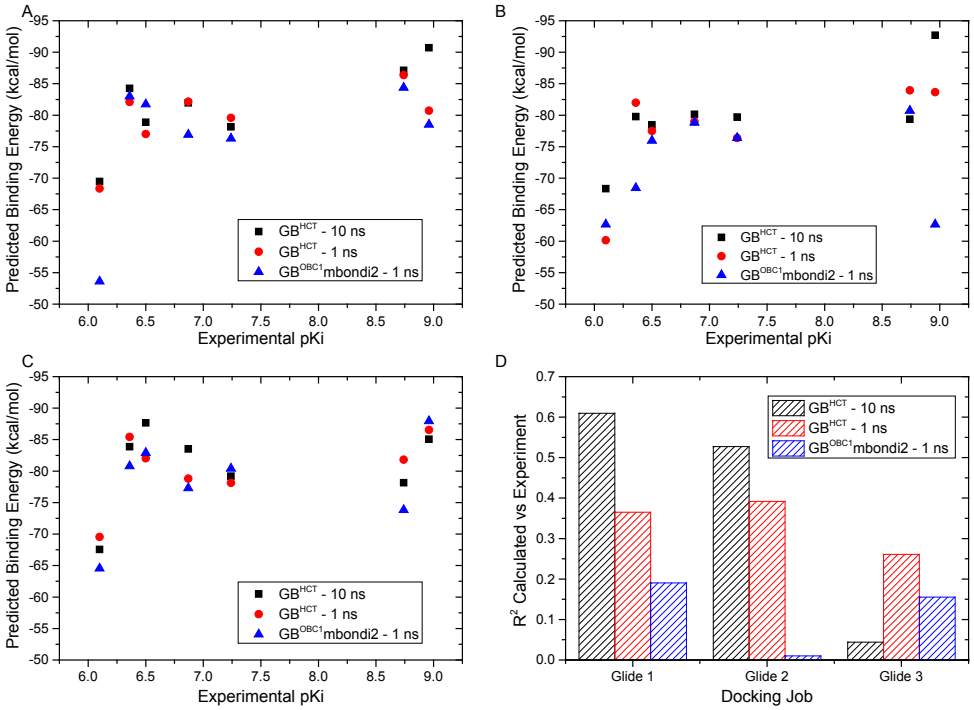


Figure 6.34: Summary of the three MD protocols (GB1 – 10ns, GB1 – 1ns, GB2mb – 1ns) versus experimental data. Glide job 1, 2, and 3 shown in plots A, B, and C respectively. Plot D: $R^2$ for each run across the three Glide jobs.

underestimated, by about 15 kcal mol$^{-1}$, when model GB$^{OBC1}$ was used (blue triangle in top left plot). Similarly, in job 2, ligand 6 (pKi = 6.36) was again underestimated by about 10 kcal mol$^{-1}$ when the same GB model was used. Glide job 3 showed large variations across all models for all ligands.

Table 6.17 shows the Kendall rank correlation coefficient ($\tau$) with the *p-values* as obtained by a two-tailed t-test. At best, half of the inhibitors were ranked according to experiment, while none showed statistical significance at the 5% level.

Table 6.17: Kendall tau ($\tau$) and the corresponding p-values for the three MD calculations versus experimental data for each Glide job.

| | Glide 1 | | Glide 2 | | Glide 3 | |
|---|---|---|---|---|---|---|
| | $\tau$ | p | $\tau$ | p | $\tau$ | p |
| $GB^{HCT}$ – 10ns | 0.52 | 0.14 | 0.43 | 0.24 | 0.05 | 1 |
| $GB^{HCT}$ – 1ns | 0.43 | 0.24 | 0.43 | 0.24 | 0.24 | 0.56 |
| $GB^{OBC1}$mbondi2 – 1ns | 0.14 | 0.77 | 0.39 | 0.22 | 0.24 | 0.56 |

Results did not change by minimising further the snapshots taken from the MD simulations, and neither did excluding snapshots from the start or end of the simulation, or both (the reasoning behind this is that the system may still be relaxing at early stages of the simulation, or drifting away at later stages).

The total energy remained stable throughout the length of the simulations for all ligands in all Glide jobs. An example is shown in the top Figure B.13. The total system energy is shown versus the simulation time along with its two components: the total kinetic energy and the total potential energy. The energies appear converged. The temperature also remained stable throughout the simulation at 300 K, indicating the use of Langevin dynamics for temperature regulation was successful. An example for this is shown for the same system in the bottom plot of Figure B.13.

The root mean squared (RMSD) fluctuations throughout the simulation were not always entirely stable. Overall protein backbone heavy atom RMSD remained below 2 Å, with minor fluctuations in loop regions, for example the

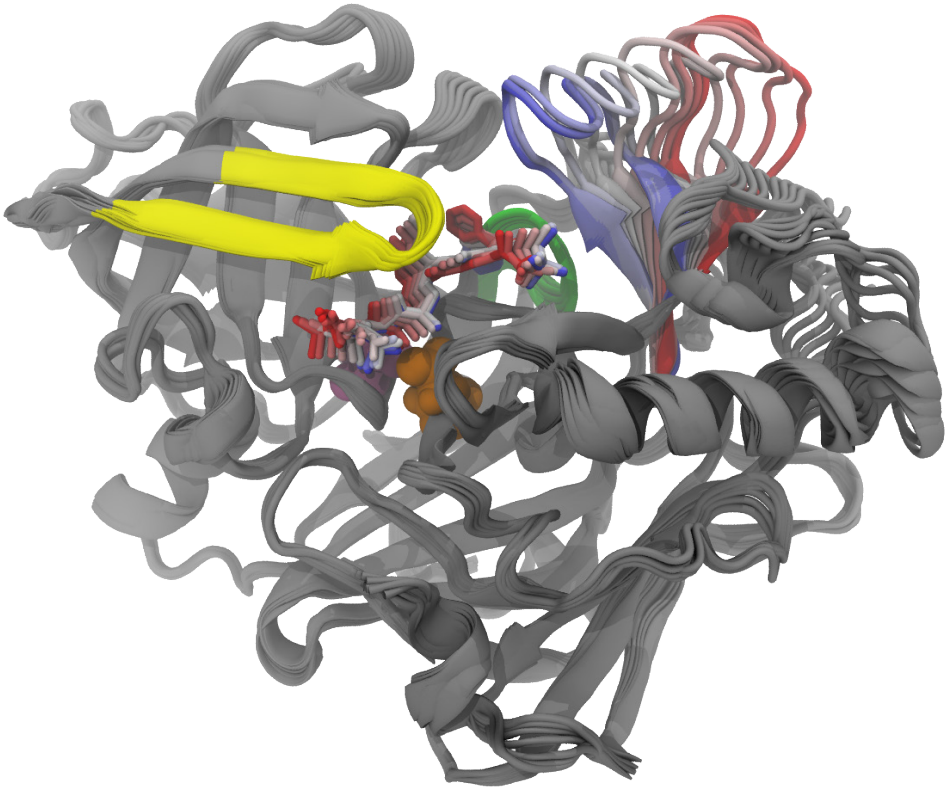

Figure 6.35: Ten equally spaced snapshots for the 10 ns trajectory of ligand 3 Glide job 1 using $GB^{HCT}$ implicit solvent smoothed with a 20-frame window. The ligand and F-loop are coloured by timestep colouring method where red is the start and blue the end of the simulation. 10s loop shown in green, the Flap region in yellow and in orange and mauve (vdW representation) the aspartate residues ASP228 and ASP32, respectively.

Flap (residues 67 through 77) region, the 10s loop (residues 9 through 14), and the F-loop (residues 311 through 318). However, there were a few cases the RMSD throughout the simulations compared to the initial structure escalated beyond the 3 Å mark. One such example was the 10 ns trajectory of ligand 3 from Glide job 1 using the $GB^{HCT}$ implicit solvent model. Ten equally spaced snapshots for the trajectory are shown in Figure 6.35. The Flap, 10s loop and Asp32 and Asp232, are shown in yellow, green mauve and

orange respectively. The ligand and F-loop are coloured accordingly indicating the progression of the simulation from red to blue. Herein large fluctuation of F-loop is shown starting form a disordered conformation to a closed conformation by the end of the simulation. More specifically, the ligand heavy atom RMSD remained at around 2 Å until the 2$^{nd}$ ns when it started to gradually increase. At the 5$^{th}$ ns there is a jump of the RMSD from around 2.5 Å to about 3.5 Å where it stabilises for the remaining of the simulation. Throughout the simulation the ligand remained hinged between the Flap and the aspartates with rotations around the ring of group R2 (Figure 4.9 and Table 4.2).

Figure 6.36 shows ten equally spaced snapshots for the 1 ns trajectory of ligand 5 Glide job 3 using the GB$^{OBC1}$mbondi2 implicit solvent. Colouring scheme is similar as in the previous examples with the difference that here the 10s loop is coloured using the timestep theme, indicating the progression throughout the trajectory with red at the start of the simulation and blue at the end. The RMSD of heavy atoms of the backbone of the protein increases in the first few picoseconds and quickly plateaus at around 1.5 Å for the remaining of the simulation. However, in comparison to the protein as a whole, loop 10s, located at S3 pocket, shows a larger movement towards the ligand from an open to a closed conformation. As this occurs, the R2 group of the ligand (see Figure 4.9 and Table 4.2) is pushed upward towards to the S1 pocket. This is indicated by a jump of the ligand heavy atom RMSD from about 1.25 Å to about 2.7 Å around the 0.5 ns mark. A similar observation was made for the same ligand during the 10 ns simulation using GB$^{HCT}$ model. The crystal structure is bound to ligand 4 which is very similar to ligand 5. It is indicated there is a crystallographic water molecule in proximity to the α-Me benzyl group of compound 4 (group R2).[16, 113] This is an example of the limitations of using implicit solvent and indicates that poor quality snapshots may be obtained, as commented by other workers.[74] This poses an interesting case for further investigation using explicit solvent.

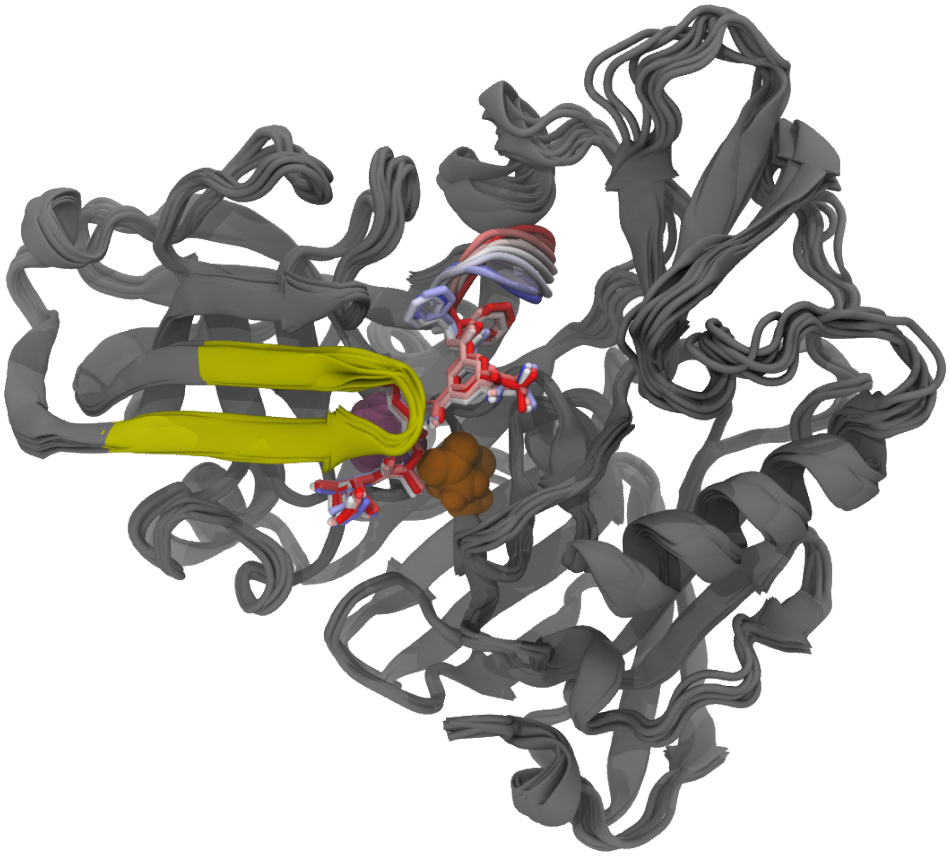

Figure 6.36: Top view of ten equally spaced snapshots for the 10 ns trajectory of ligand 5 Glide job 3 using $GB^{OBC1}$mbondi2 implicit solvent smoothed with a 20-frame window. The ligand and 10s-loop are coloured by Timestep colouring method where red is the start and blue the end of the simulation. The Flap region is shown in yellow and in orange and mauve (vdW representation) the aspartate residues ASP228 and ASP32, respectively.

### 6.4.4 Summary

In this section an assessment of the performance of a number of rescoring protocols for the target of β-Secretase with a set of seven inhibitors was carried out. Qualitative comparison with experiment showed very poor performance with zero statistically significant $R^2$ values. Ranking the compounds with experiment was also very poor as indicated by the Kendall tau statistic. Although, the size of the system and the uneven distribution of experimental binding affinities make this system a challenging case, this is a

good example of exposing the limitations of this method and the shortcomings in the setting of lead optimisation, where such small datasets could exist.

On the other hand, head to head qualitative comparison between the models showed strong correlations, but ranking was average. When compared to other systems, quantitative analysis showed that fewer differences were significant. However, we found evidence that perhaps there was type II error (false negatives) present, owing to the small size of the system. Therefore, it is more likely that in reality more differences are significant.

Finally, molecular dynamics simulations were able to improve the $R^2$ of the predicted energies versus experiment, however only for 2 out the 3 Glide sets of poses. There were cases with large movements in both ligand and protein, indicating the lack of physical waters, allows for a "frictionless" simulation and potentially the introduction of "noise" in the calculations. The examples give an indication that implicit solvent could lead to poor quality snapshots.

## 6.5 Factor Xa

### 6.5.1 System preparation

The same protein preparation and simulation protocols as described in section 6.2, were followed, using the PDB structure 1FJS (resolution = 1.92 Å)[114]. This is one of the systems discussed earlier (section 6.2.1) where complete sets of poses for all ligands for each of the three Glide jobs were not obtained. Hence here results are reported for only Glide jobs 2 and 3.

### 6.5.2 Rescoring results

***Comparison with experiment***

The results versus experiment grouped by docking run, are summarised in Table 6.18 and Figure 6.37. Results are grouped by rescoring protocol in

Table 6.18: Coefficient of determination of calculated binding energies versus experiment for each rescoring protocol. Statistically significant results based on a two tailed test, shown in bold.

| | **$R^2$ of Calculated Energies versus Experiment** | | |
|---|---|---|---|
| **Protocol** | **CDOCKER** | **Glide 2** | **Glide 3** |
| **Docking** | 0.12 | 0.18 | **0.19** |
| **E-Novo** | **0.29** | | |
| **Prime Rigid** | 0.01 | 0.06 | 0.02 |
| **Prime Flex** | 0.03 | **0.26** | **0.27** |
| **Prime Rigid L.** | | 0.17 | 0.02 |
| **Prime Flex L.** | | **0.30** | 0.14 |
| **$GB^{HCT}$ Rigid** | 0.01 | **0.49** | **0.38** |
| **$GB^{OBC1}$ bondi Rigid** | 0.08 | **0.39** | **0.32** |
| **$GB^{OBC1}$ mbondi2 Rigid** | 0.01 | **0.48** | **0.32** |
| **$GB^{OBC2}$ bondi Rigid** | 0.03 | **0.40** | **0.32** |
| **$GB^{OBC2}$ mbondi2 Rigid** | 0.01 | **0.34** | **0.31** |
| **Gbn Rigid** | 0.02 | **0.40** | **0.28** |
| **$GB^{HCT}$ Flex** | 0.00 | 0.02 | 0.03 |
| **$GB^{OBC1}$ bondi Flex** | | 0.08 | 0.08 |
| **$GB^{OBC1}$ mbondi2 Flex** | | 0.09 | 0.14 |
| **$GB^{OBC2}$ bondi Flex** | | 0.03 | 0.12 |
| **$GB^{OBC2}$ mbondi2 Flex** | | 0.00 | 0.24 |
| **Gbn Flex** | | 0.03 | 0.04 |

Figure 6.38. The black line in those figures represents a 5% significance level. In addition, statistically significant correlations are highlighted in bold in the table. Herein, due to the larger sample size (22 ligands) the significance level of $R^2$ is particularly low set at 0.18. Therefore although some correlations may be statistically significant it should be taken into account their magnitude may be low and therefore may not represent a practical

significance. Similarly as in the previous targets two sets of Prime Rigid and Flexible results are shown.

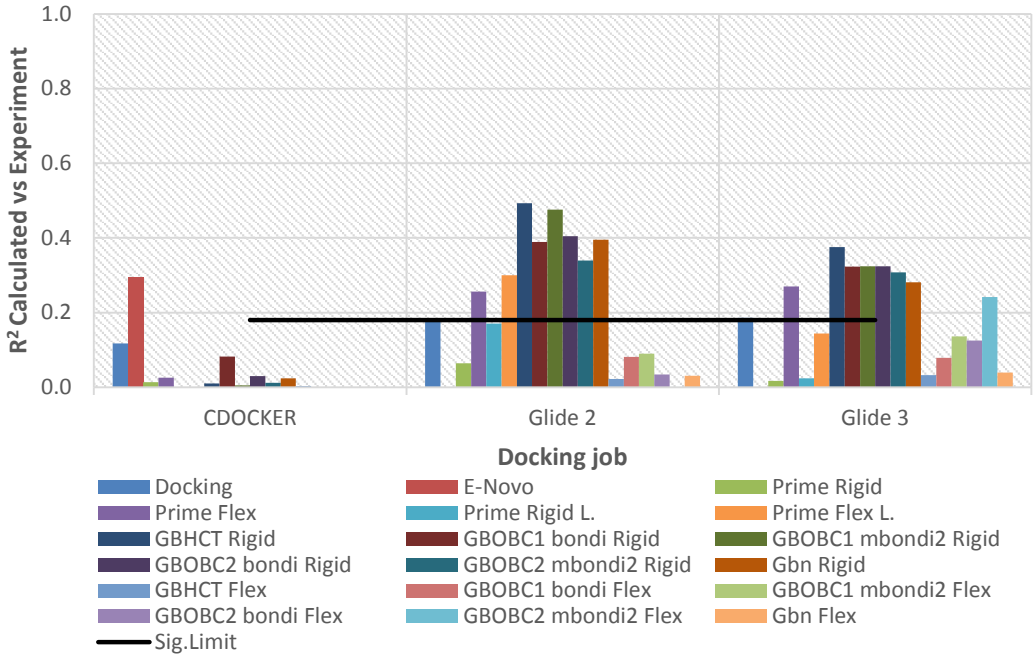


Figure 6.37: Coefficient of determination of rescoring protocols with experiment grouped by docking jobs (CDOCKER, Glide 2, Glide 3). Each rescoring protocol is shown by a differently coloured bar. The 'L.' for Prime jobs stands for the Prime score based on the lowest (more negative) docking score, in the case of two dock poses obtained for one ligand. 'Rigid' and 'Flex' refer to protein flexibility, with the latter fully flexible for Amber calculations, while only 4 Å for Prime calculations. No flexible protein calculations performed with CDOCKER poses. Glide poses not tested on Pipeline Pilot. Correlation with docking provided for comparison purposes. The black line shows the 5% significance level for the number of observations (22 ligands).

Similarly as in the two previous systems, $R^2$ with experiment for the CDOCKER poses were poor across all rescoring protocols. In fact, with the exception of the significant value obtained with E-Novo (0.29), none of the variation in the predicted energies can be explained by the linear relationship with experimental data ($R^2 \approx 0.00$).

When Glide poses are considered we find a clear trend. AMBER rigid protein minimisations provide significant and consistent $R^2$ across all GB

solvent models, which outperform the $R^2$ obtained via docking. In contrast, flexible protein simulations in AMBER, and all the Prime calculations with the exception of Prime Flex, fail to give worthy results.

Here, $R^2$ variation amongst GB solvent models for each Glide pose for AMBER rigid and flexible protein minimisations, was relatively small and therefore the RMSD analysis that was shown in the previous two protein-ligand systems, will not take be discussed here. The relevant plot, however was generated and can be found in appendix B (Figure B.6).

Figure 6.38 shows the $R^2$ versus experiment for each docking job grouped by rescoring protocol. For this dataset the $R^2$ obtained between predicted and experimental values for the same GB solvent model but with different starting conformations, was similar. For the rigid protein calculations in AMBER the input structures are the docked poses. The average ligand-ligand RMSD values calculated between the two docked poses (see RMSD comparison in Figure 6.39) would probably explain the small variations found in $R^2$.

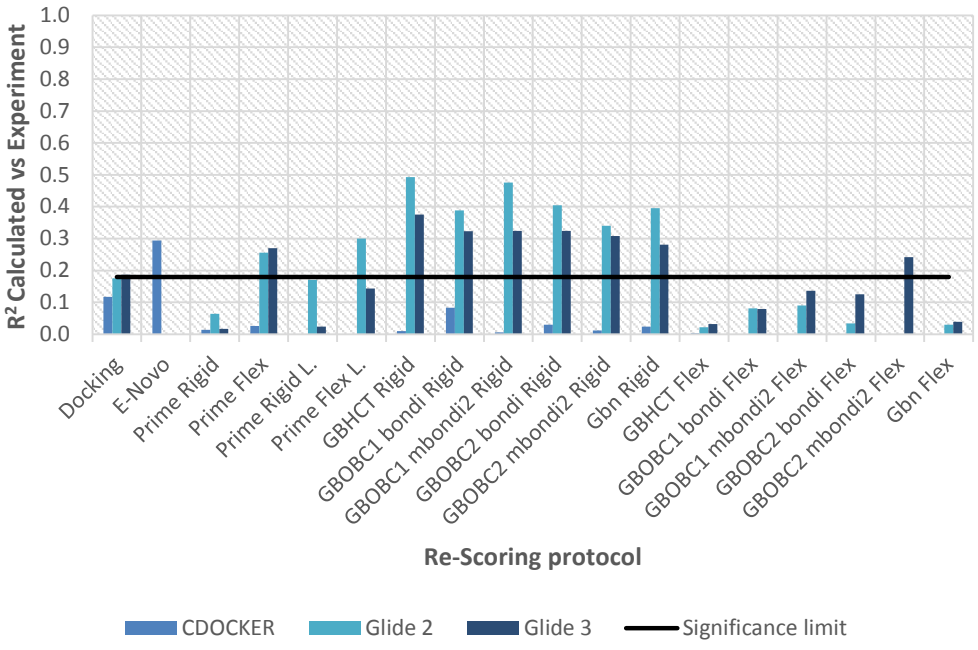


Figure 6.38: Coefficient of determination of rescoring protocols with experiment grouped by each protocol. The colour in each bar corresponds to the docking

protocol re-scored (blue for CDOCKER, light blue for Glide 2 and dark blue for Glide 3). Naming of protocols as described in Figure 6.4. No flexible protein calculations performed with CDOCKER poses. Glide poses not tested on Pipeline Pilot. Correlation with docking provided for comparison purposes. The black line shows the 5% significance level for the number of observations (22 ligands).

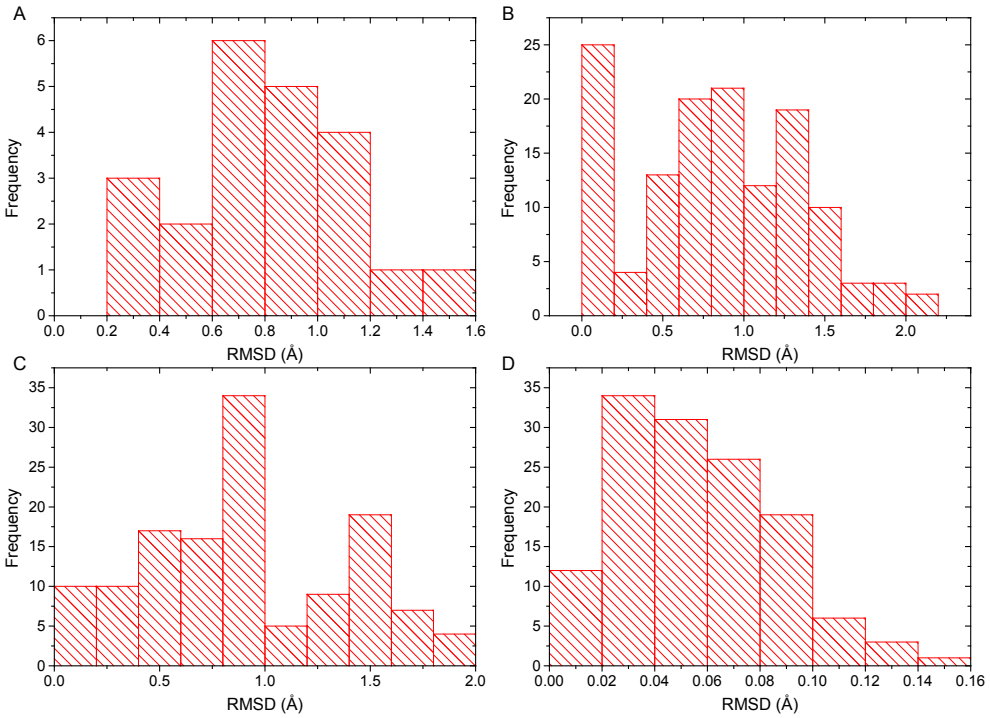


Figure 6.39: Ligand-ligand (A, B, C) and protein-protein backbone (D) RMSD distributions across between Glide 2-3 for each solvent model. Plot A: Dock poses. Plot B and C: end of rigid-protein and flexible-protein minimisations, respectively. Plot D: protein-protein backbone RMSD at end of flexible-protein minimisations. All reported RMSD are obtained using heavy atoms.

Figure 6.40 shows the $R^2$ and Kendall's rank correlation coefficient ($\tau$) along with the associated *p-values*. The ranking was random for 60% of the cases, with the ones that it was significant ranging from as low as 0.31 to a moderate 0.61. It should be noted however, that with the exception of two models, all predicted rankings for AMBER rigid protein minimisations were significant, but average. Therefore, although not a great performance, we observe a similar trend with $\tau$ as with $R^2$.

Scatter plots of the predicted versus the experimental binding affinities for the rigid and flexible protein minimisations, respectively, are shown in Figure B.15 and Figure B.16.

R^2

| | Docking | Prime R | Prime F | Prime R L | Prime F L | $GB^{HCT}$ R | $GB^{OBC1}$ B R | $GB^{OBC1}$ MB2 R | $GB^{OBC2}$ B R | $GB^{OBC2}$ MB2 R | GBn R | $GB^{HCT}$ F | $GB^{OBC1}$ B F | $GB^{OBC1}$ MB2 F | $GB^{OBC2}$ B F | $GB^{OBC2}$ MB2 F | GBn F |
|---|---|---|---|---|---|---|---|---|---|---|---|---|---|---|---|---|---|
| Glide 2 | 0.18 | 0.06 | 0.26 | 0.17 | 0.30 | 0.49 | 0.39 | 0.48 | 0.40 | 0.34 | 0.40 | 0.02 | 0.08 | 0.09 | 0.03 | 0.00 | 0.03 |
| | 0.05 | 0.26 | 0.02 | 0.06 | 0.01 | 0.00 | 0.00 | 0.00 | 0.00 | 0.00 | 0.00 | 0.51 | 0.20 | 0.17 | 0.41 | 0.94 | 0.44 |
| Glide 3 | 0.19 | 0.02 | 0.27 | 0.02 | 0.14 | 0.38 | 0.32 | 0.32 | 0.32 | 0.31 | 0.28 | 0.03 | 0.08 | 0.14 | 0.12 | 0.24 | 0.04 |
| | 0.04 | 0.57 | 0.01 | 0.49 | 0.08 | 0.00 | 0.01 | 0.01 | 0.01 | 0.01 | 0.01 | 0.42 | 0.21 | 0.09 | 0.11 | 0.02 | 0.38 |
| CDOCKER | 0.12 | 0.03 | 0.01 | | | 0.08 | 0.01 | 0.03 | 0.01 | 0.02 | 0.00 | | | | | | |
| | 0.12 | 0.48 | 0.66 | | | 0.19 | 0.75 | 0.44 | 0.63 | 0.49 | 0.80 | | | | | | |

Kendall tau

| | Docking | Prime R | Prime F | Prime R L | Prime F L | $GB^{HCT}$ R | $GB^{OBC1}$ B R | $GB^{OBC1}$ MB2 R | $GB^{OBC2}$ B R | $GB^{OBC2}$ MB2 R | GBn R | $GB^{HCT}$ F | $GB^{OBC1}$ B F | $GB^{OBC1}$ MB2 F | $GB^{OBC2}$ B F | $GB^{OBC2}$ MB2 F | GBn F |
|---|---|---|---|---|---|---|---|---|---|---|---|---|---|---|---|---|---|
| Glide 2 | 0.16 | 0.13 | 0.28 | 0.13 | 0.36 | 0.61 | 0.45 | 0.55 | 0.50 | 0.51 | 0.55 | 0.15 | 0.19 | 0.25 | 0.13 | 0.05 | 0.20 |
| | 0.30 | 0.38 | 0.07 | 0.38 | 0.02 | 0.00 | 0.00 | 0.00 | 0.00 | 0.00 | 0.00 | 0.32 | 0.22 | 0.11 | 0.41 | 0.76 | 0.18 |
| Glide 3 | 0.23 | 0.20 | 0.33 | 0.06 | 0.30 | 0.30 | 0.31 | 0.34 | 0.36 | 0.24 | 0.32 | 0.20 | 0.14 | 0.26 | 0.30 | 0.28 | 0.16 |
| | 0.13 | 0.20 | 0.03 | 0.71 | 0.05 | 0.05 | 0.05 | 0.03 | 0.02 | 0.12 | 0.04 | 0.20 | 0.35 | 0.10 | 0.05 | 0.07 | 0.30 |
| CDOCKER | 0.33 | -0.17 | -0.10 | | | 0.23 | 0.03 | 0.15 | -0.07 | 0.10 | -0.05 | | | | | | |
| | 0.03 | 0.27 | 0.52 | | | 0.13 | 0.84 | 0.32 | 0.63 | 0.52 | 0.76 | | | | | | |

Figure 6.40: The correlation of determination ($R^2$) and Kendall tau rank correlation coefficient ($\tau$) across all rescoring tests (including the docking score) for each docking protocol. The coloured boxes represent the p-values (from a two-tailed test) for each statistic ($R^2$ and Kendall's tau) with green any value below 5% (statistical significance limit), while red anything above that threshold. R, F, B, MB2 stand for Rigid, Flexible (4 Å around ligand for Prime – full flexibility for Amber), Bondi radii, and MBondi2 radii respectively. The table should be read in pairs of colourless (statistic) and coloured cells (p-value).

Table 6.19: Coefficient of determination and Kendall's tau rank correlation coefficient for heavy atoms and molecular weight with experiment. *P*-values resulting from a two tailed test.

| | $R^2$ | $P_R^2$ | Kendall tau ($\tau$) | $p_\tau$ |
|---|---|---|---|---|
| **Heavy Atoms** | 0.33 | 5.51E-3 | -0.45 | 6.05E-3 |
| **MW** | 0.28 | 1.17E-2 | -0.41 | 7.30E-3 |

For consistency, the consideration of the lowest predicted energy structure was investigated and the results are summarised in Figure B.17 and Figure B.18. Although there was a small improvement when protein flexibility

was permitted, overall performance remained poor. Similar observations were made for τ. Moreover, simply comparing number of heavy atoms (NHA) and molecular weight (MW) with experiment showed similar results to the rigid-protein protocols and considerably improved over the flexible-protein ones (Table 6.19).

In this subsection a comparison of the predicted energies versus experiment was discussed. In the next section a head-to-head comparison between the tested models is presented.

***Comparison between rescoring protocols***

To identify how the models behave, a qualitative and quantitative assessment of the models with each other was carried out and presented herein.

Table 6.20 shows descriptive statistics of $R^2$ and τ for pairwise comparisons between the 16 GB models (resulting in 120 comparisons in total). The obtained values for $R^2$ and τ shown in this table, were generally low to average, but perhaps taking into account the problematic AMBER flexible protein minimisation results, it probably explains the values of the statistics here.

Table 6.20: Descriptive statistics of $R^2$ and Kendall τ across all pairwise comparisons for each Glide job. Percentage of statistics ($R^2$, τ) with p-value below 0.05 is shown (%SIG).

| | | MIN | MAX | MEAN | STDEV | % SIG. |
|---|---|---|---|---|---|---|
| **Glide 2** | $R^2$ | 0.00 | 0.98 | 0.28 | 0.30 | 41.67 |
| | τ | -0.01 | 0.87 | 0.36 | 0.22 | 48.33 |
| **Glide 3** | $R^2$ | 0.00 | 0.98 | 0.33 | 0.30 | 62.5 |
| | τ | -0.30 | 0.92 | 0.34 | 0.30 | 61.67 |

$R^2$ and τ matrices with the corresponding *p-values* for all pairwise comparisons for each Glide job were generated and are included in appendix

B (see Table B.28 to Table B.31). Here again, an overall tendency of better correlations within rigid-protein protocols and within flexible-protein protocols was observed. Inconsistent performance between Glide jobs was also evident demonstrating some sensitivity of the method on initial poses generated by the choice of varied docking options.

To quantify the predictive performance of the models with each other, box plots were plotted of the distributions of each model for each docking job.

Figure 6.41 shows the predicted binding energies for each model when CDOCKER poses are used. E-Novo has the highest (least negative) mean and the smallest range. At -54.75 kcal$^{-1}$ mol$^{-1}$, which is more than 30 kcal mol$^{-1}$ more negative than E-Novo, GB$^{HCT}$ has the lowest median, showing just how much predictions can vary between different software for the exact equivalent poses. However, such differences are not limited to different software but also different GB models within the same software such as the HCT model that has a median of more than 10 kcal mol$^{-1}$ more negative than the median values for the OBC models.

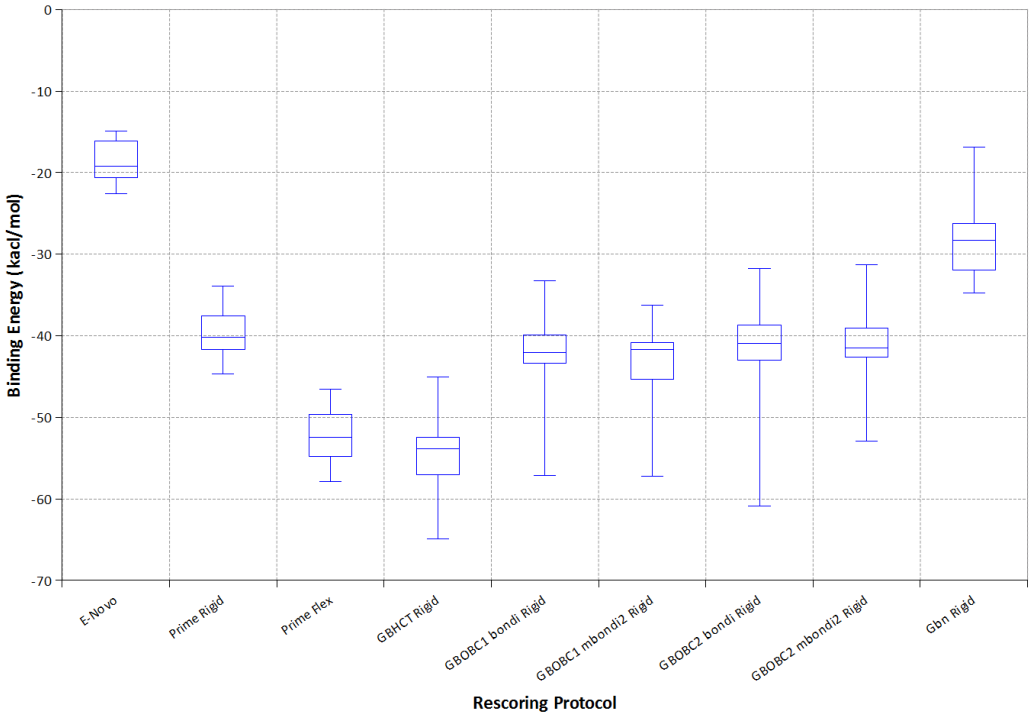

Figure 6.41: Box Plot of predicted binding free energies (kcal $mol^{-1}$) of CDOCKER poses for each rescoring protocol. The whiskers represent the minimum and maximum values, the box corresponds to the range of values between the 1st and 3rd quartiles, and the line through the box represents the median value of the binding energies.

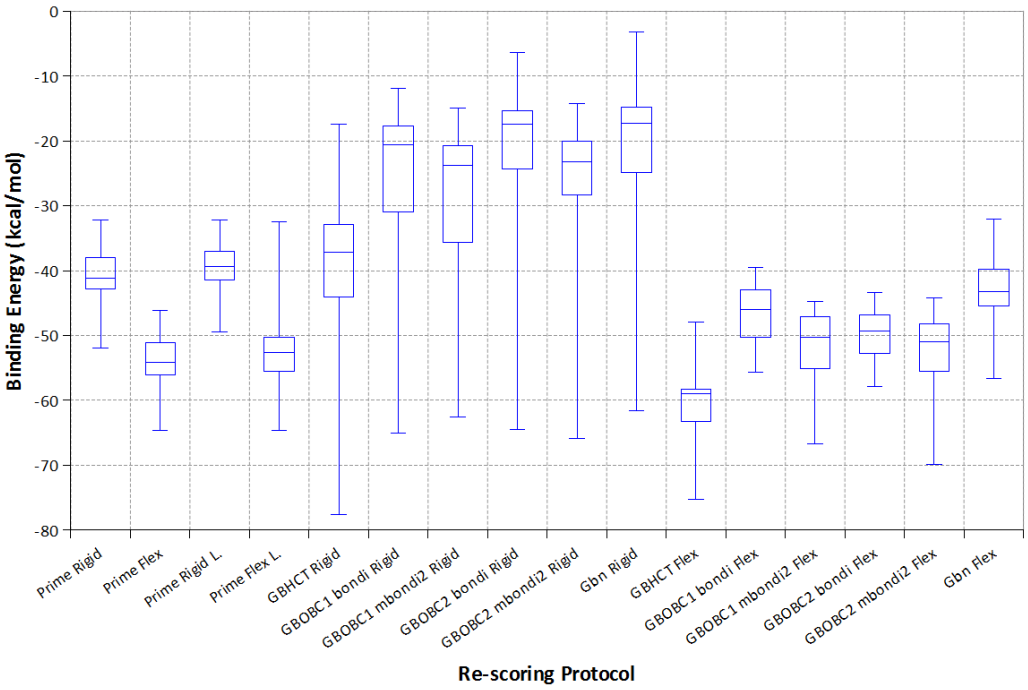


Figure 6.42: Box Plot of predicted binding free energies (kcal $mol^{-1}$) of Glide 2 poses for each rescoring protocol. The whiskers represent the minimum and maximum values, the box corresponds to the range of values between the 1st and 3rd quartiles, and the line through the box represents the median value of the binding energies.

Figure 6.42 shows the distributions of the results of rescoring the Glide 2 jobs. Similarly as in the previous datasets Prime Flexible protocols gave more negative energies than the Prime Rigid protocols. Again HCT models gave a more negative average energy compared to the rest of the AMBER models, which showed overall similar medians. What is interesting in this case is the large spread of the predictions in the case of only the AMBER rigid protein calculations. This large range is due to ligands 17 and 20 identified as outliers based on the box plot method of identifying outliers (any value above quartile 3 or below quartile 1 which is greater than the distance of 1.5 × IQR). The

experimental binding affinities for these ligands (including ligands 18 and 21) are indeed more negative than the rest of the dataset and would therefore be expected to be identified as outliers in a box plot; however, the values predicted here are far more exaggerated than one would expect. These ligands have an amine substituted in para position (group R1 in Figure 4.12 and Table 4.3) to the amidine that forms a salt bridge to the ASP189. The ligand in the crystal structure of 1FJS has a hydroxyl group in the same position that engages in a key H-bond donation with SER195.[114] Perhaps, owing to the fact the protein remains restrained throughout the calculation, this buried interaction could be highly penalised by the implicit solvent model resulting in overestimated energies for those two ligands. Such extreme values were not observed when the protein was flexible, but we see that when the bondi radii are used, the predictions for these ligands are underestimated (less negative).

Overall the same observations can be made for Glide job 3 (see Figure B.19) with the only difference that here more outliers were observed again for the case of AMBER rigid-protein minimisations. Again ligand 17 and 20 were amongst the outliers with addition of ligand 18 (only for model HCT rigid), 21 and 22. Ligands 18 and 21 have a hydroxyl moiety in the para position to the amidine, while ligand 22 has a OMe group. Again these were not outliers in the case of flexible protein minimisations.

The results from a Repeated Measures ANOVA (RM-ANOVA) are summarised in Table 6.21. The means between the models are significantly different within the 5% significance level. The two sets of dock poses gave very similar F statistics meaning that about the same amount of differences was observed for both of them.

Table 6.22 shows the percentage of significant differences following Holm-Šidák post-hoc analysis on the RM-ANOVA results. In both Glide jobs 84 out the 120 pairwise comparisons were deemed statistically different. As in the previous systems, tables with the RM-ANOVA and the effect size (d index calculated using formula (6.3.7)) are included in appendix B (Table B.34 and

Table B.35). Again, all statistically significant differences also showed a practical effect (large effect size).

Table 6.21: Repeated measures ANOVA results. $SS_b$ is the Sum of Squares between measures, df is the degrees of freedom, and $MS_b$, the Mean Square($SS_b/df\ model$).

| | $SS_b$ | df model | df error | $MS_b$ | F | p |
|---|---|---|---|---|---|---|
| Glide2 | 50736.02 | 1.57 | 32.99 | 32292.05 | 61.68 | 7.43E-11 |
| Glide 3 | 49791.56 | 1.50 | 31.40 | 33302.83 | 59.47 | 3.00E-10 |

Table 6.22: Percentage of significant differences (5% significance level) between rescoring methods, following post-hoc analysis of RM-ANOVA.

| | %Sig. Diff. |
|---|---|
| Glide 2 | 70.00 |
| Glide 3 | 70.00 |

The null hypothesis could not be rejected for 36 of the 120 pairwise differences. As in previous systems, not all of these cases had small differences in their means. The results between Glide poses were almost identical. The comparisons are shown in Table B.36, which is consistent the very similar means obtained for each model between the two poses (see Figure 6.43, and see Table B.32 and Table B.33 for descriptive statistics).

The findings of this analysis here, while there appears to be some qualitative agreement between the different models, however there is a lower quantitative agreement.

In the next section molecular dynamics simulations using implicit solvent are investigated.

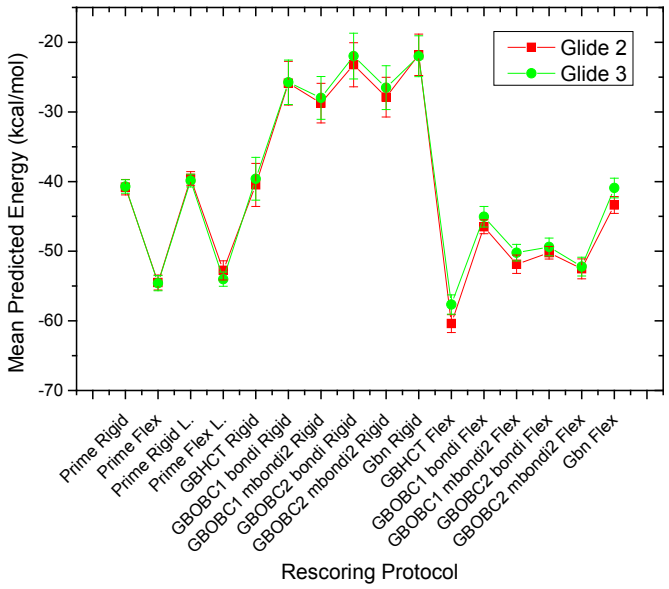


Figure 6.43: Line and symbol plot of means of each rescoring model for Glide jobs 2, and 3. Error bars correspond to the standard error of the mean$\left(s/\sqrt{n}\right)$.

### 6.5.3 Molecular dynamics results

Molecular dynamics (MD) simulations were used to investigate the effect sampling has on the results, and if there is an improvement over simply minimising a docking pose. The same MD simulations were run for this data set as for the previous ones.

Figure 6.44 shows the results of predicted binding energies from the MD simulations versus experiment for the two docking sets of poses. $R^2$ values ranged from 0.10 ($GB^{HCT}$ job3 1 ns) to 0.42 ($GB^{OBC1}$ job 3 1ns). Any value above 0.18 is considered to have not been obtained by chance (within a 5% significance level). In both docking sets (plot A and B) $GB^{OBC1}$mbondi2 gave less negative energies in accordance with the results in the previous section. It is difficult to make any conclusive inferences as to why the $R^2$ value for the OBC model nearly doubles when job 3 dock poses are used instead of job 2. The most potent and second most potent inhibitors (ligands 18 and 21) are consistently underestimated. MM-GBSA is known to be sensitive to the

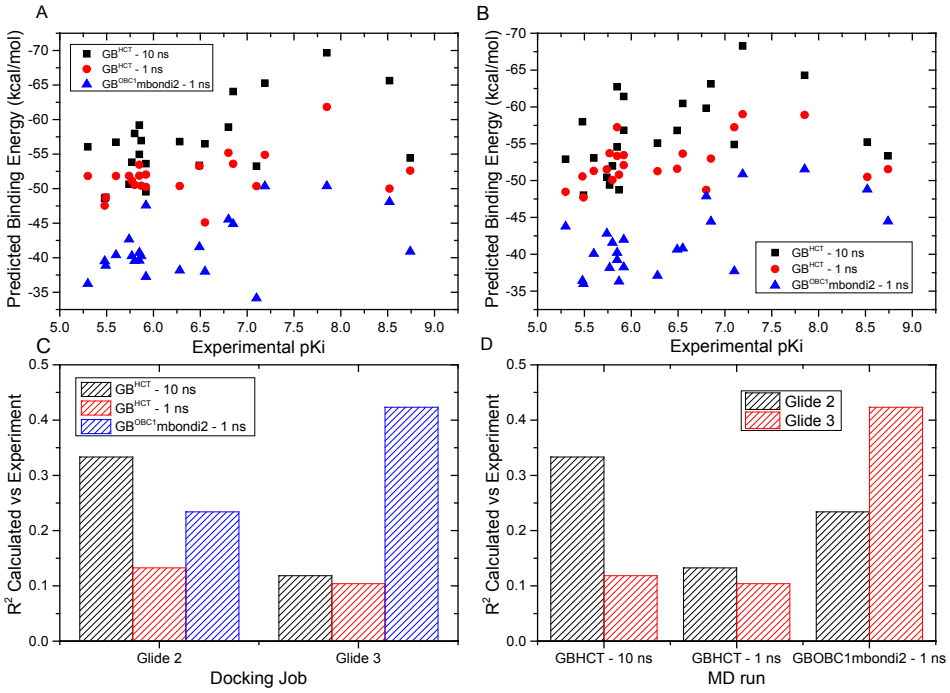


Figure 6.44: Summary of the three MD protocols (Gb1 – 10ns, GB1 – 1ns, GB2mb – 1ns) versus experimental data. Glide job 2, and 3 shown in plots A, and B respectively. Plots C and D show $R^2$ of calculated energies versus experiment grouped by docking job and my MD run respectively.

polarity of interactions[20, 67] and this is a good example of this case. As discussed earlier both these ligands have a hydroxyl group (as an R1 group) in the para position to the amidine, forming a strong hydrogen bond with Ser195. Owing to the spread of the experimental affinities, failing to correctly rank those two ligands makes it difficult to obtain decent correlations.

Table 6.23 summarises the results of Kendall tau ($\tau$) rank correlation coefficient of predicted energies with experiment. In most cases the results are significant (within a 5% significance level); however the values are low for what is expected by a model targeted towards a fast tool at the early stages of lead optimisation.

Table 6.23: Kendall tau (τ) and the corresponding p-values for the three MD calculations versus experimental data for each Glide job.

| | Glide 2 | | Glide 3 | |
|---|---|---|---|---|
| | τ | p | τ | p |
| $GB^{HCT}$ – 10ns | 0.38 | 0.01 | 0.37 | 0.02 |
| $GB^{HCT}$ – 1ns | 0.24 | 0.13 | 0.32 | 0.04 |
| $GB^{OBC1}$mbondi2 – 1ns | 0.33 | 0.03 | 0.39 | 0.01 |

Results did not change by minimising further the snapshots taken from the MD simulations, and neither did excluding snapshots from the start or the end of the simulation or both.

The energies (Kinetic, potential and total for the system – top plot) throughout the simulation were converged and the temperature (bottom plot) was kept stable at the desired 300 K, indicating the thermostat worked correctly. Data taken from ligand 3 job 2 using $GB^{OBC1}$mbondi2 were used for this example (see Figure B.20). Although in some cases energies appeared to drift a little, overall they remained constant throughout all simulations.

Figure 6.45 shows the structures of the initial and final snapshots from the 10 ns simulation of ligand 6 of Glide job 2 using $GB^{HCT}$ as a solvent. It shows that the ligand partially moves out of the S1 pocket during the course of the simulation. The aromatic ring with group R4, in this case an amine, is seen to rotate to the opposite side and form a strong hydrogen bond with the oxygen of Phe41 (see distance A in plot B in Figure 6.46). In addition a strong hydrogen bond is formed between Glu192 and the nitrogen of the central ring of the ligand (distance B, also see Figure 6.46). As this occurs, the ligand is pulled out of pocket S1 breaking the strong interactions with Asp189 as it can be seen in plot A of Figure 6.46 (distance C and D). Other

ligands in the series demonstrated similar movements. Again, the lack of water molecules in implicit solvent MD results in high mobility and potentially increased noise in the calculations.

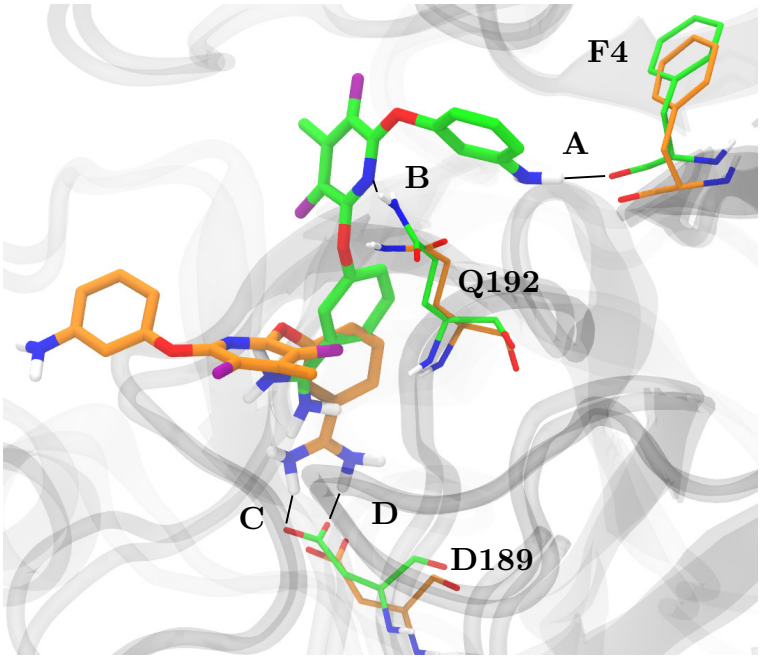


Figure 6.45: Structures of initial (orange) and final (green) snapshots of the 10 ns trajectory for ligand 6 job 2 using $GB^{HCT}$ model. Key residues are indicated using the same colour pattern. The highlighted distances correspond to the same distances in Figure 6.46. Only polar hydrogens are shown.

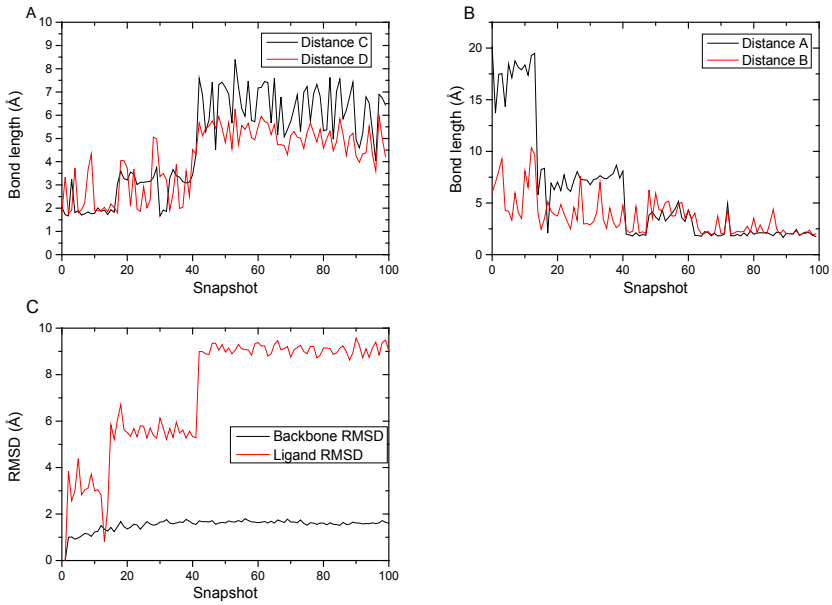


Figure 6.46: Bond lengths (Å) for distances between atoms shown in

Figure 6.45 throughout the 10 ns simulation of ligand 6 job 2 (plots A and B). Plot C shows the backbone and ligand heavy atom RMSD with respect to the initial structure in the simulation.

### 6.5.4 Summary

Results versus experiment obtained from a range of rescoring protocols were mediocre though significant. This was the case for both the coefficient of determination and Kendall tau. MM-GBSA using rigid minimisations in AMBER repeatedly and consistently outperformed to docking results. On the other hand, flexible protein minimisations performed worst although the structures pre- and post-minimisation were almost identical. Models also performed poorly when compared to each other, both qualitatively and quantitatively. The inclusion of polar R-groups for some ligands, makes for a challenging case indicating the difficulty of predicting reasonable free energy estimates for ligands which have strong polar or charged groups, and hence where a strong change in electrostatic interactions occurs.

Again, in this case a single molecular dynamics simulation was not sufficient to improve comparisons with experiment. Large ligand flexibility

was found to occur during the trajectories possibly due to lack of explicit water molecules.

However, by testing MM-GBSA on this target we found some consistent and significant results, indicating, that perhaps the method could have applications in large datasets, perhaps in virtual screening applications or enrichment studies. This however, was not in the scope of this research and nor was there time to investigate further. It is something that would be interesting to investigate further in the future.

## 6.6 HIV-1 Protease

### 6.6.1 System preparation

The same protein preparation and simulation protocols as described in section 6.2, were followed, using the PDB structure 2PQZ (resolution = 1.55 Å)[114]. Like Factor XA, complete sets of poses for all ligands for each of the three Glide jobs were not obtained. Results are reported for Glide job 2.

### 6.6.2 Rescoring results

Table 6.24 shows the correlation of determination ($R^2$) of rescored binding energies versus experiment for CDOCKER and Glide job 2 poses. Highlighted in bold are significant correlations. Figure 6.47 shows the same results in a form of a bar chart with the significance level (5%) indicated by the horizontal black line. Since here there is only one Glide job, there is only one set of Prime Rigid and Prime Flex results.

Table 6.24: Coefficient of determination of calculated binding energies versus experiment for each rescoring protocol. Statistically significant results based on a two tailed test, shown in bold.

| | **$R^2$ of Calculated Energies versus Experiment** | |
|---|---|---|
| **Protocol** | **CDOCKER** | **Glide 2** |
| **Docking** | **0.46** | **0.72** |
| **E-Novo** | 0.00 | |
| **Prime Rigid** | 0.13 | **0.38** |
| **Prime Flex** | 0.00 | **0.65** |
| **$GB^{HCT}$ Rigid** | **0.38** | **0.41** |
| **$GB^{OBC1}$ bondi Rigid** | 0.12 | **0.44** |
| **$GB^{OBC1}$ mbondi2 Rigid** | 0.28 | **0.56** |
| **$GB^{OBC2}$ bondi Rigid** | 0.29 | **0.52** |
| **$GB^{OBC2}$ mbondi2 Rigid** | 0.29 | **0.43** |
| **Gbn Rigid** | 0.15 | **0.33** |
| **$GB^{HCT}$ Flex** | | **0.57** |
| **$GB^{OBC1}$ bondi Flex** | | **0.46** |
| **$GB^{OBC1}$ mbondi2 Flex** | | **0.65** |
| **$GB^{OBC2}$ bondi Flex** | | **0.36** |
| **$GB^{OBC2}$ mbondi2 Flex** | | **0.58** |
| **Gbn Flex** | | **0.43** |

The $R^2$ of predicted binding energies with experiment ranged from 0.00 to 0.38 for CDOCKER poses and from 0.33 to 0.65 for the Glide poses. In contrast to the results obtained so far from the investigations of the other systems, all correlations obtained here are statistically significant based on a 5% threshold. However, many of these correlations are relatively low or average, with 8 out of the 14 rescoring protocols giving an $R^2$ of less than 0.5. Moreover, docking outperformed all rescoring protocols, something not surprising considering HIV-1 protease was one of the training sets used to characterise Glide XP scoring function.[139]

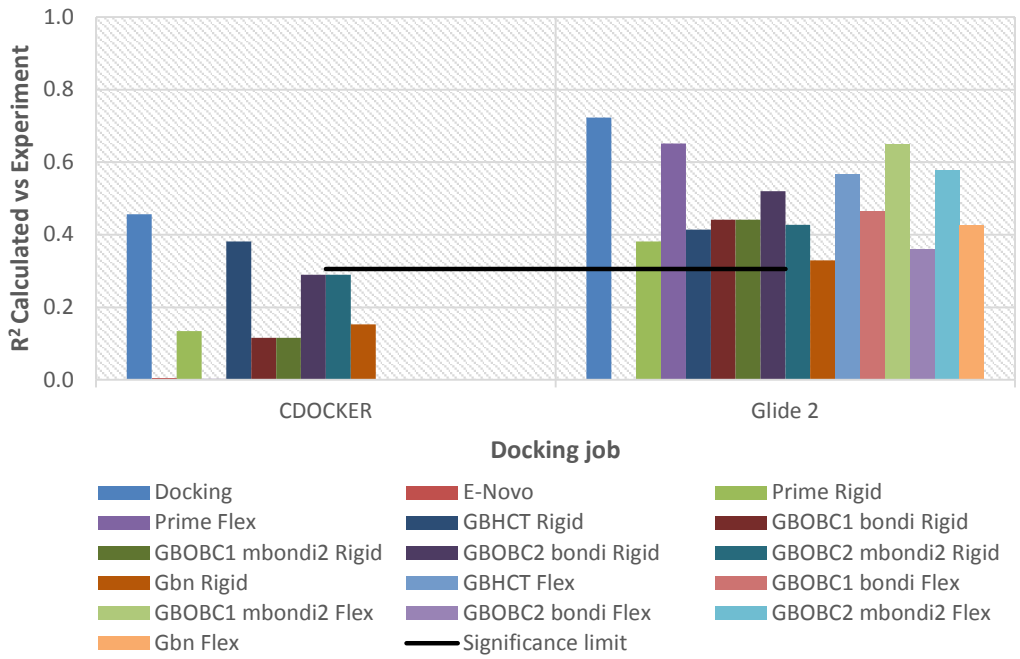


Figure 6.47: Coefficient of determination of rescoring protocols with experiment grouped by docking jobs (CDOCKER, Glide 2, Glide 3). Each rescoring protocol is shown by a differently coloured bar. The 'L.' for Prime jobs stands for the Prime score based on the lowest (more negative) docking score, in the case of two dock poses obtained for one ligand. 'Rigid' and 'Flex' refer to protein flexibility, with the latter fully flexible for Amber calculations, while only 4 Å for Prime calculations. No flexible protein calculations performed with CDOCKER poses. Glide poses not tested on Pipeline Pilot. Correlation with docking provided for comparison purposes. The black line shows the 5% significance level for the number of observations (13 ligands).

Figure 6.48 shows a root mean square deviation (RMSD) comparison between the ligands of the six different GB models used in Amber, at the end of rigid-protein minimisations, and at the end of flexible-protein minimisations. Protein backbone RMSD was also compared at the end of the flexible-protein minimisations. Again, the calculated measurements were very low averaging at 0.17, 0.35, and 0.16 Å between ligand of rigid-protein and flexible-protein calculations and between protein backbone respectively.

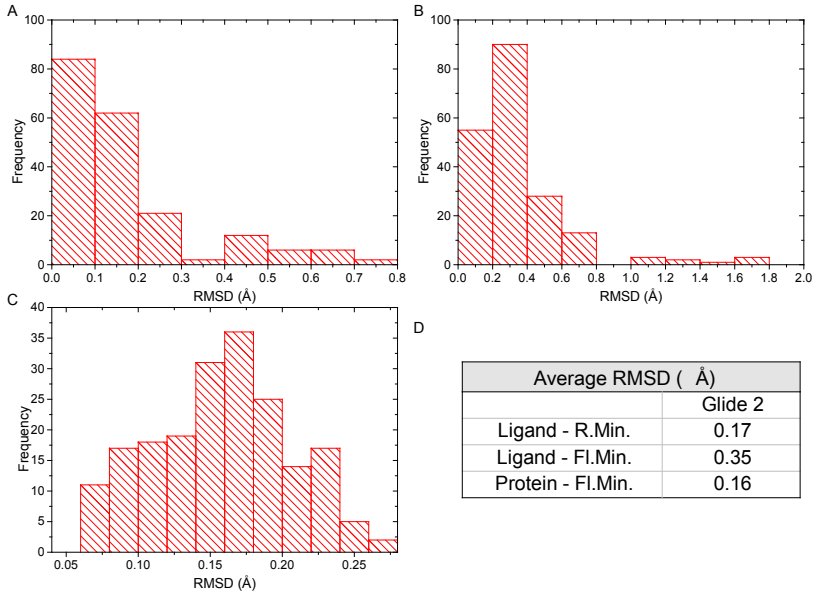


| Average RMSD ( Å) | |
|---|---|
| | Glide 2 |
| Ligand - R.Min. | 0.17 |
| Ligand - Fl.Min. | 0.35 |
| Protein - Fl.Min. | 0.16 |

Figure 6.48: Ligand-ligand (A, B) and protein-protein backbone (C) RMSD distribution between AMBER GB models in all possible combinations for each Glide job 1, prior (A) and after (B, C) protein flexible minimisations. The average RMSD values for each Glide job shown in table (D). Only heavy atoms are considered and only the backbone of the protein. R.Min. and Fl. Min., correspond to the output for rigid protein and flexible protein minimisations, respectively.

$R^2$ and Kendal tau ($\tau$) statistical measures with the matching *p-values*, are shown in Figure 6.49. Despite the significant $R^2$, more than half of the time (for 13 out of the 22 cases) ligands were not ranked correctly. This is consistent with the results from the previous three systems.

The complete data for predicted versus the experimental binding affinities for the rigid and flexible protein minimisations, respectively, are shown in the form of scatter plots in Figure B.21 and Figure B.22.

Table 6.25 shows the $R^2$ and $\tau$ with their *p-values* for the comparison of number of heavy atoms (NHA) and the molecular weight (MW) against experiment. The results obtained for the $R^2$ are on par with the top 3 out of the 22 measurement collected from the rescoring protocols, for both NHA and MW. The ranking was also significant in both cases.

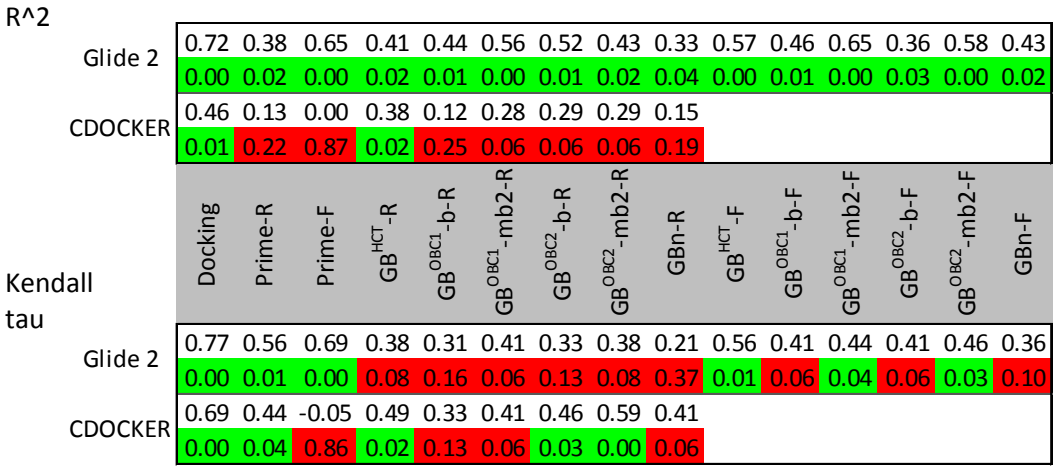


Figure 6.49: The correlation of determination ($R^2$) and Kendall tau rank correlation coefficient ($\tau$) across all rescoring tests (including the docking score) for each docking protocol. The coloured boxes represent the p-values (from a two-tailed test) for each statistic ($R^2$ and Kendall's tau) with green any value below 5% (statistical significance limit), while red anything above that threshold. R, F, B, MB2 stand for Rigid, Flexible (4 Å around ligand for Prime – full flexibility for Amber), Bondi radii, and MBondi2 radii respectively. The table should be read in pairs of colourless (statistic) and coloured cells (p-value).

Table 6.25: Coefficient of determination and Kendall's tau rank correlation coefficient for heavy atoms and molecular weight with experiment. *P*-values resulting from a two tailed test.

| | $R^2$ | $P_{R^2}$ | Kendall tau ($\tau$) | $p_\tau$ |
|---|---|---|---|---|
| **Heavy Atoms** | 0.63 | 0.00 | -0.54 | 0.01 |
| **MW** | 0.57 | 0.00 | -0.54 | 0.01 |

In this case, although the correlations are not very good, rescoring appears to work at least to the extent to give significant results consistently across all calculations; this is unique across all systems covered in this thesis. Despite this, however, only two performed similarly to the docking $R^2$, but none surpassed it. GlideScore XP, though, has been parameterised on HIV - 1 Protease, and therefore has an advantage over MM-GBSA.

Ranking on the other hand, although not always low, it gave significant results less than half of the time. Despite a few good correlations, there was no improvement over docking by any of the rescoring protocols. In the next subsection protocols are compared with each other to assess their qualitative and quantitative agreement.

**Comparison between rescoring protocols**

In this subsection rescoring protocols are compared head-to-head to ascertain how they compare with each other. First they are compared qualitatively using statistical measures including $R^2$ and $\tau$, followed by a comparison of their quantitative agreement using box plots and Repeated Measures ANOVA (RM-ANOVA) followed by post-hoc analysis and consideration of the effect size (d-index). These comparisons are performed for all 91 pairwise comparisons (resulting from 14 rescoring protocols).

Table 6.26 shows a summary of the results from the qualitative comparison of the rescoring protocols. $R^2$ was statistically significant for all pairwise comparisons. In addition, the majority of the correlations were high, averaging at 0.80. Similar observations were made for the ranking of the inhibitors. With the exception of the comparisons of Prime Rigid protocol with the AMBER protocols, the remaining comparisons gave high values for the Kendall tau rank correlation coefficient. The values for all comparisons along with reported *p-values* are shown in Table B.37 and Table B.38.

Table 6.26: Descriptive statistics of $R^2$ and Kendall $\tau$ across all pairwise comparisons for each Glide job. Percentage of statistics ($R^2$, $\tau$) with p-value below 0.05 is shown (%SIG).

| | | MIN | MAX | MEAN | STDEV | % SIG. |
|---|---|---|---|---|---|---|
| Glide 2 | $R^2$ | 0.34 | 0.98 | 0.80 | 0.15 | 100 |
| | $\tau$ | 0.23 | 0.97 | 0.68 | 0.17 | 90.83 |

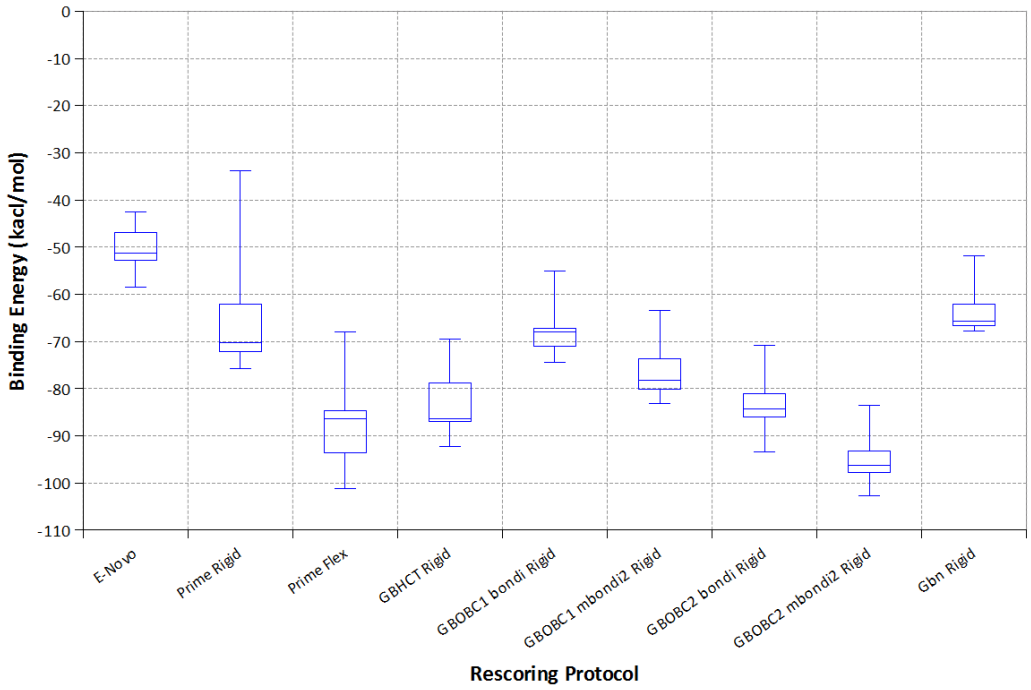


Figure 6.50: Box Plot of predicted binding free energies (kcal $mol^{-1}$) of CDOCKER poses for each rescoring protocol. The whiskers represent the minimum and maximum values, the box corresponds to the range of values between the 1st and 3rd quartiles, and the line through the box represents the median value of the binding energies.

Though qualitative agreement was confirmed between rescoring protocols, the next step is to identify whether or not the same protocols using the same structures agree quantitatively. To do this box plots are first constructed to visualise the distributions of the calculated energies.

Figure 6.50 shows the distributions of predicted energies when CDOCKER poses are used. A greater variation is observed here in comparison to what was found for Thrombin, β-Secretase, and Factor XA. It is found that the medians between AMBER models vary considerably, with box sizes (IQR) and range being similar. The trend of Prime Flex giving lower (more negative) values than Prime Rigid, observed thus far, was also noted here. The larger range obtained for Prime Rigid protocol is due to ligand 3 acting as an outlier (least negative value denoted by the top whisker).

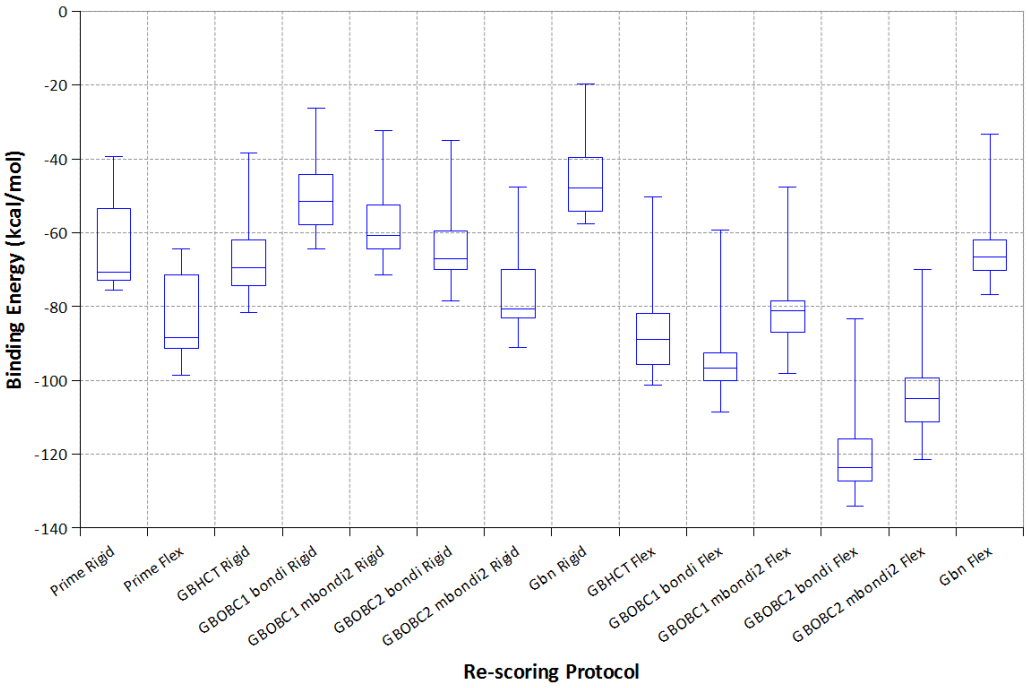


Figure 6.51: Box Plot of predicted binding free energies (kcal $mol^{-1}$) of Glide 2 poses for each rescoring protocol. The whiskers represent the minimum and maximum values, the box corresponds to the range of values between the 1st and 3rd quartiles, and the line through the box represents the median value of the binding energies.

Figure 6.51 shows the distributions of predicted energies when Glide job 2 poses are used. Similar observations as in the CDOCKER case can be made. Regarding the AMBER flexible-protein calculations, a larger variation of medians is observed. In addition, the range is large although the boxes are short indication a small spread of the data. Here ligand 3 was not an outlier, while ligand 1 and 2 in this case were, with the latter in most cases being a mild outlier. This probably to be expected as also in experiment these two ligands have the lowest binding affinity, lower than the rest of the dataset.

Table 6.27 summarises the results from RM-ANOVA analysis. As expected the differences of the means are statistically significantly different. In fact the F-statistic for this system is the largest obtained when compared to the other systems. The null hypothesis was rejected for nearly 90% (81 out of the total of 91) of the differences (see Table 6.28). Cohen's d in this case

was very high reaching values of up to 13.36. Descriptive statistics and results of the RM-ANOVA post-hoc analysis (Holm-Šidák) including *p-values* and the effect size are shown in appendix B (Table B.39 and Table B.40)

Table 6.27: Repeated measures ANOVA results. $SS_b$ is the Sum of Squares between measures, df is the degrees of freedom, and $MS_b$, the Mean Square($SS_b/df\ model$).

| | $SS_b$ | df model | df error | $MS_b$ | F | p |
|---|---|---|---|---|---|---|
| Glide2 | 74282.87 | 3.08 | 76.48 | 24147.82 | 315.75 | 1.67E-26 |

Table 6.28: Percentage of significant differences (5% significance level) between rescoring methods, following post-hoc analysis of RM-ANOVA.

| | %Sig. Diff. |
|---|---|
| Glide 2 | 89.01 |

In the next section the effect of introducing additional sampling via implicit solvent molecular dynamics is investigating. Owing to the highly flexible pocket of HIV-1 Protease, this poses an interesting case.

### 6.6.3 Molecular dynamics results

Molecular dynamics (MD) simulations were set up and run as described in section 6.2.3.

Figure 6.52 summarises the results from the three MD simulations versus experiment. The top plot shows a scattering of the predicted energies against experimentally obtained pKi. Consistently with the minimisation protocols in the previous section, $GB^{HCT}$ here, gave in general more negative results compared to model $GB^{OBC1}$. Running shorter MD simulations did not result in an improvement. All correlations were significant (within a 5% significance

level), however the OBC1 model performed worse than the HCT for this case. The latter in both cases was able to obtain almost the same $R^2$ as that obtained by docking, in which case rescoring did not add value. In fact the rank correlation coefficient for docking was higher than the ones obtained here; docking gave a $\tau$ equal to 0.77 (Figure 6.49) compared to the values obtained from MD ranging from 0.31 to 0.67 (see Table 6.29).

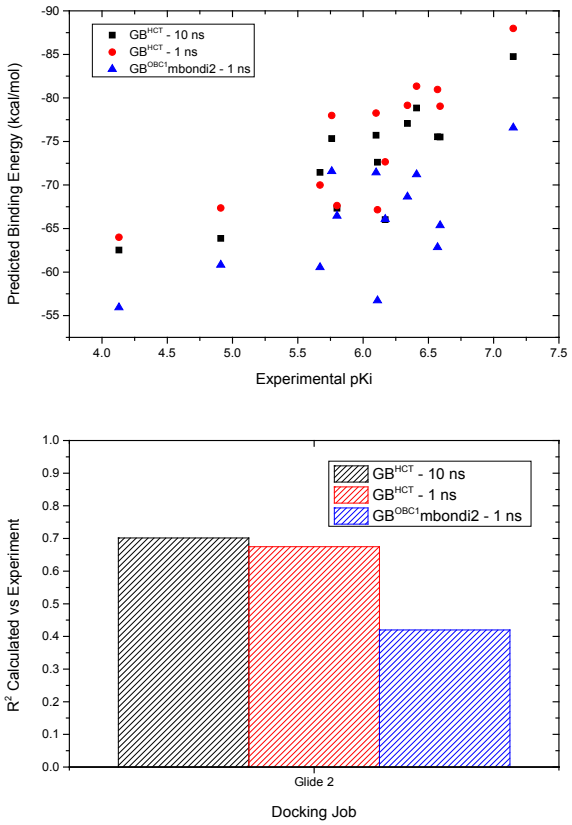


Figure 6.52: Summary of the three MD protocols (Gb1 – 10ns, GB1 – 1ns, GB2mb – 1ns) versus experimental data. Top plot: scatter plot of calculated energies versus experiment. Bottom plot: $R^2$ of calculated energies versus experiment for each MD simulation.

Table 6.29: Kendall tau (τ) and the corresponding p-values for the three MD calculations versus experimental data.

| | Glide 2 | |
|---|---|---|
| | τ | p |
| $GB^{HCT}$ – 10ns | 0.59 | 0.00 |
| $GB^{HCT}$ – 1ns | 0.67 | 0.00 |
| $GB^{OBC1}$mbondi2 – 1ns | 0.31 | 0.16 |

Simulations for this target were in general better behaved compared to Factor XA. The energy and temperature of the system remained stable throughout the simulations for all ligands. Figure 6.53 shows an example of this taken from the 10 ns MD simulation for ligand 1 Glide job2 and GB solvent $GB^{HCT}$.

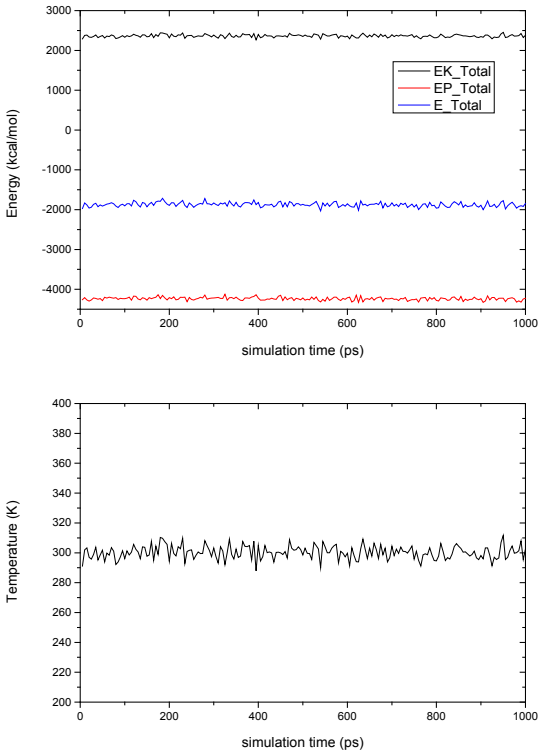


Figure 6.53: Kinetic energy (black line), potential energy (red line) and total system energy (blue line) for ligand 1 Glide job 2 during 1 ns MD using model $GB^{HCT}$. Bottom plot shows the temperature during the simulation.

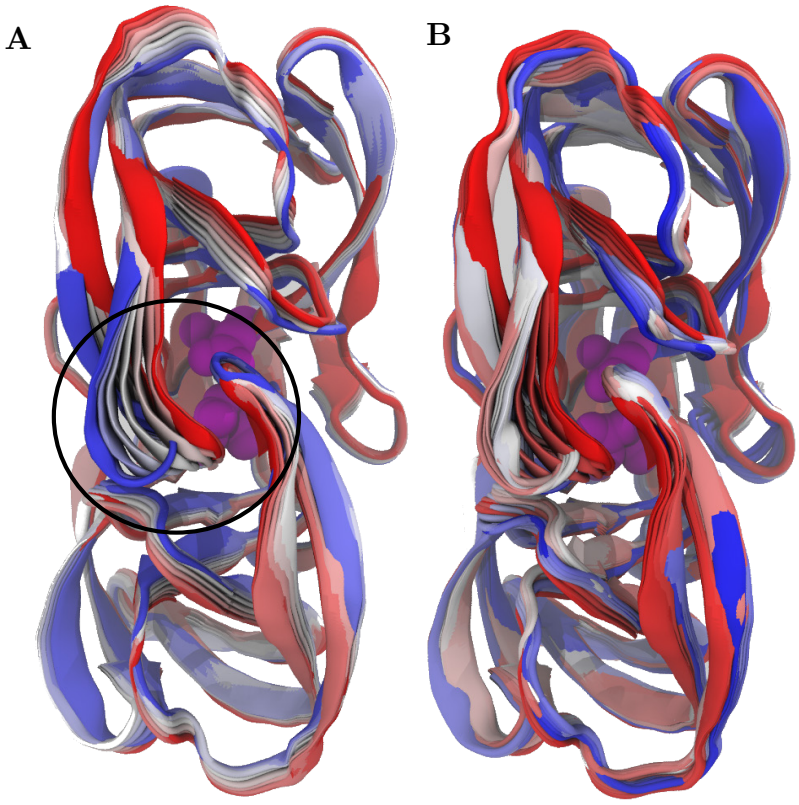


Figure 6.54: Representations of equally (every 10) spaced snapshots during the simulation of ligand 1 for (A) 10 ns and (B) 35 ns. The flap region is highlighted by the black circle. The protein is shown from the top with the catalytic dyad (D25A and D25B) shown in magenta. Figures are colour coded from red to blue corresponding from the beginning to the end of the simulation.

All simulations behaved reasonably with the ligand remaining inside the pocket throughout the length of the simulation. The central part of the ligand is held tightly due to the strong interaction between the pyrrolidine and the catalytic dyad (D25A and D25B). Electrostatic calculations indicate the nitrogen of the pyrrolidine should be protonated and both of the aspartates of the catalytic dyad deprotonated thus resulting in strong hydrogen bonds.[121, 122] The ligands were more flexible in the parts of the molecule that occupy the hydrophobic specificity pockets of the protein (S1, S2, S3 and the symmetrical, S1′, S2′, and S3′).

Overall no large structural changes were observed for the protein (backbone RMAS plateau $<$ 2.0 Å). The plasticity of the flap region was

apparent in the majority of the simulations; however some displayed larger movement with the flap resulting in one of the flaps rotating outward towards the solvent. One such case was ligand 1 when simulated for 10 ns, shown in Figure 6.54 (A). The protein is shown from the top with the catalytic dyad at the bottom (shown in magenta and vdW representation). The colouring from red to blue follows the simulation from beginning to end, respectively. The flap is seen to gradually open as the simulation progresses. At the start of the simulation a hydrogen bond between one of the inhibitor's sulphonamide oxygens and the amide of I50A of the flap region is formed, as well as between the carbonyl oxygen of I50A and the amide of I50B (shown as Dist. A in Figure 6.55 A). After the $5^{th}$ nanosecond the inhibitor changes structurally with the aromatic ring connected to the adjacent sulphonamide positioned between the now flexed configuration. The result is breakage of the aforementioned hydrogen bonds. The representation of the isoleucines at the end of the simulation is shown in Figure 6.55 B (for simplicity the ligand is excluded). At this point the carbonyl oxygen of I50A and hydrogen of amide are separated by more than 10 Å, while the amide of I50A and oxygen of I50B are closer at about 4 Å apart (Dist. B).

To investigate this further, the simulation was extended for another 25 ns to a total of 35 ns. It should be noted here that although the starting configuration of the system for this additional simulation was the output of the previous 10 ns simulation, the simulation was restarted with a new seed to the random number generator. This means there is a possibility the system would evolve to a different orientation than the one we observed, had the simulation been run continuously.

Figure 6.54 B shows the results of the 35 ns run. The plot is coloured in the same way as plot A for the 10 ns simulation. What was observed was that after the stretching of the loop the structure stabilises for about 10 ns before it retracts; however, it does not retract to the original configuration. Now, at about the $25^{th}$ ns, Dist. B has become smaller (hydrogen bond between I50B

oxygen and I50A amide hydrogen instead), and the oxygen of the previous adjacent sulphonamide's oxygen is now forming a hydrogen bond with I50B's amide hydrogen.

The orientation of the flap region isoleucines is shown in Figure 6.55 C. For this configuration the flaps are closer than at the end of the 10 ns simulation, however the I50A flap remains rotated outward towards the solvent. This is in contrast to the classic closed flap configuration obtained when an inhibitor is bound to HIV protease.[165] The system remained in this configuration for the remaining 10 ns of the simulation (i.e. from the 25$^{th}$ to the 35$^{th}$ ns). The fluctuation of the hydrogen bonds between I50A and I50B during the course of the 10 ns and 35 ns simulations, is shown in Figure 6.56. The first 10 ns overlap and hence black squares are used to highlight them.

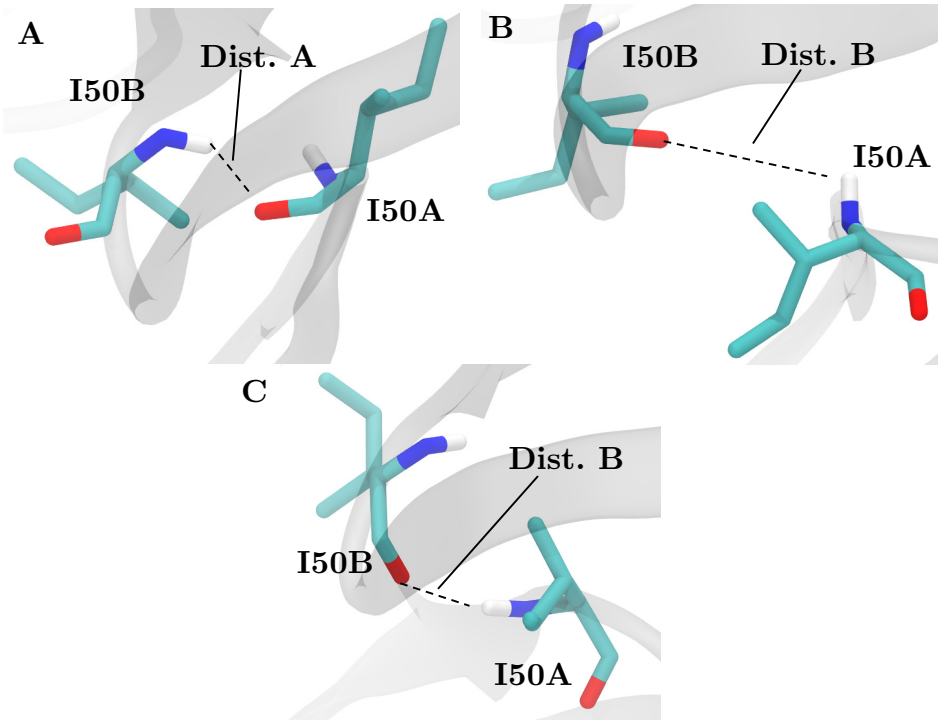


Figure 6.55: Representation of the interaction between I50A and I50B of the flap region for 35ns MD simulation of ligand 1 job 2 GB$^{HCT}$, at the start (A), 10ns mark (B) and end (C) of the simulation. Distances highlighted as in Figure 6.55. Only polar hydrogens are shown.

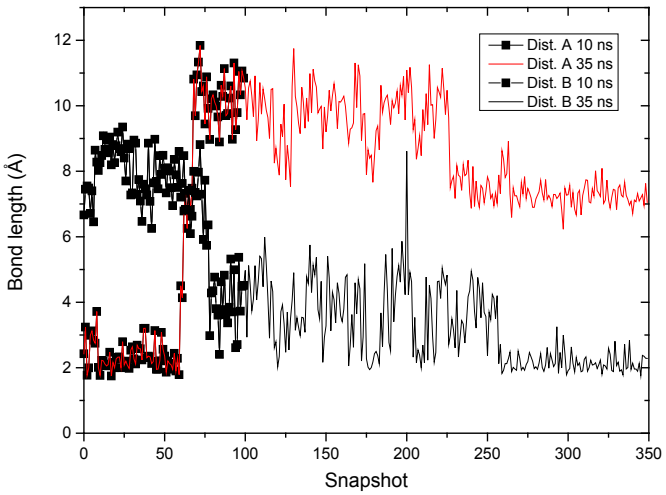


Figure 6.56: Bond distance between (A) I50A–Oxygen and I50B–Amino group, and (B) I50A-Amino group and I50B-Oxygen for 10 ns (black squares) and 35 ns (red line) MD simulation of ligand 1, job2 $GB^{HCT}$.

In their study in 2006, Hornak et al.[165] simulated a bound HIV protease for 28 ns using implicit solvent, but did not observe the structural changes reported here. In contrast they reported that the flaps remained closed throughout the simulation with all relevant flap hydrogen bonds remaining in place. According to their study, it appears our observations here are not typical on this timescale. However, large fluctuations as that observed in the example reported here were also common, although to a lesser extent, in other ligands in the series including all ligands from 2 to 9 with ligands 4, 6, 7 and 8 exhibiting larger fluctuations. In ligand 6, in particular, the flap region appeared to show a similar opening as in ligand 1 (the example reported here) towards the end of the 10 ns simulation. In contrast, the flaps for ligands 10-13 remained stable for the entirety of the simulation. The reason to this is the polar substituents at the para position of the aromatic ring attached to the sulphonamide (R3 group see Table 4.4). These groups form interactions with D29 and D30, hence keeping the ligand in place with the aromatic rings extended in parallel to the flap region. On some occasions the polar groups appear to briefly interact with the flap region, before they resume back to the

original position, precluding structural changes in the flap area. It would be interesting to investigate this further simulating at much larger timescales including explicit MD, but this is not in the scope of this work.

Further minimising MD snapshots did not result in any improvement in correlations with experiment, and neither did analysis for different parts of the trajectories (excluding initial or final parts of the simulation).

### 6.6.4 Summary

This target posed an interesting case mainly due to its highly flexible binding site. As a training data set for the Glidescore XP function, docking performed well when compared to experiment. Rescoring gave significant correlations, however with the exception of a few approaching the scoring function performance, many were considerably poorer. The same was found for the ranking correlation coefficient where only 5 out of the 14 rescoring protocols were statistically significant and from these, only two $\tau$ values were above 0.50. Simple consideration of heavy atoms or molecular weight performed equally well as the best rescoring protocols. Overall for this system, the models were found to be qualitatively but not quantitatively similar. As with previous cases, molecular dynamics results showed large fluctuations mainly due to the use of low solvent viscosity.

## 6.7 Src Tyrosine Kinase

This last dataset proved to be a special case. Owing to a number of problems encountered during the rigid-protein minimisations of Glide poses in the AMBER molecular package, it was decided not to progress further with the remaining of the testing and analysis as was performed on other targets. Therefore results from flexible protein minimisations and from MD with implicit solvent in AMBER will not be reported. In addition, the comparison and statistical analysis that was performed on all previous systems is not

included for this case. Rather, the focus will be on the issues encountered that led to the decision not to continue with the full testing and analysis for this dataset.

### 6.7.1 System preparation

As in the previous systems, the same preparation protocols as described in section 6.2 were followed for this system, using the PDB structure 2BDJ (resolution 2.50 Å). As discussed in section 4.6, in the majority of Src kinase crystal structures, the activation loop containing Tyr416 is partially disordered. This holds true for the structure used here. Specifically, the residues with numbers from 413 up to and including 423 were missing from the PDB data file. This is not a cause of concern for the industrial software used in this work; however, in the academic software AMBER the gap of 19.58 Å between the missing residues is highlighted by AMBER's LEaP program as a structural problem giving an error message. There are different ways of dealing with such a case. Typically one would use homology modelling to replace the missing residues; however, in order to remain consistent with previous work on this system, it was not deemed appropriate to proceed in this manner. Instead, the General Amber Forcefield (GAFF) parameter file (gaff.dat) was edited so that a special bond can be placed between residues Glu412 and Phe424. Then the force constant of this bond was set to zero. In this way the error was avoided, without an effect on the simulations.

### 6.7.2 Rescoring results

The correlation between estimated and experimentally determined binding affinities, grouped by docking run, are summarised in Table 6.30 and Figure 6.59. The black line in the figure represents the 5% significance level. In the table below, statistically significant correlations are highlighted in bold. The

Table 6.30: Coefficient of determination of calculated binding energies versus experiment for each rescoring protocol.

| | **$R^2$ of Calculated Energies versus Experiment** | | | |
|---|---|---|---|---|
| **Protocol** | **CDOCKER** | **Glide 1** | **Glide 2** | **Glide 3** |
| **Docking** | 0.01 | **0.48** | **0.59** | **0.54** |
| **E-Novo** | **0.56** | | | |
| **Prime Rigid** | | 0.38 | **0.55** | 0.33 |
| **Prime Flex** | | **0.44** | **0.59** | 0.27 |
| **Prime Rigid L.** | | 0.43 | **0.48** | 0.35 |
| **Prime Flex L.** | | **0.48** | **0.46** | 0.24 |
| **$GB^{HCT}$ Rigid** | | 0.02 | 0.00 | 0.07 |
| **$GB^{OBC1}$ bondi Rigid** | | 0.02 | 0.01 | 0.01 |
| **$GB^{OBC1}$ mbondi2 Rigid** | | 0.02 | 0.02 | 0.01 |
| **$GB^{OBC2}$ bondi Rigid** | | 0.00 | 0.00 | 0.01 |
| **$GB^{OBC2}$ mbondi2 Rigid** | | 0.01 | 0.01 | 0.07 |
| **Gbn Rigid** | | 0.00 | 0.04 | 0.02 |

CDOCKER poses were not used for calculations in AMBER. As in the previous systems, this was due to the questionable quality of CDOCKER poses, however additional reasons for this case are further detailed later in this section. As in previous cases, two sets of results are reported for rescoring using Prime (see second paragraph in section 6.3.2 for more details).

The $R^2$ of predicted binding free energies against experimental data was 0.56 for the CDOCKER poses, and ranged from 0.00 to 0.59 for the Glide poses (Table 6.30). Results obtained when using MM-GBSA as implemented in Prime, were statistically significant (within a 5% statistical significance) for Glide 2, but not for Glide 3. Glide 1 was found to give 2 significant measurements, both for when the protein was flexible. The Prime results ($R^2$), although in many cases significant, were only as good as the correlations of the docking results with experiment.

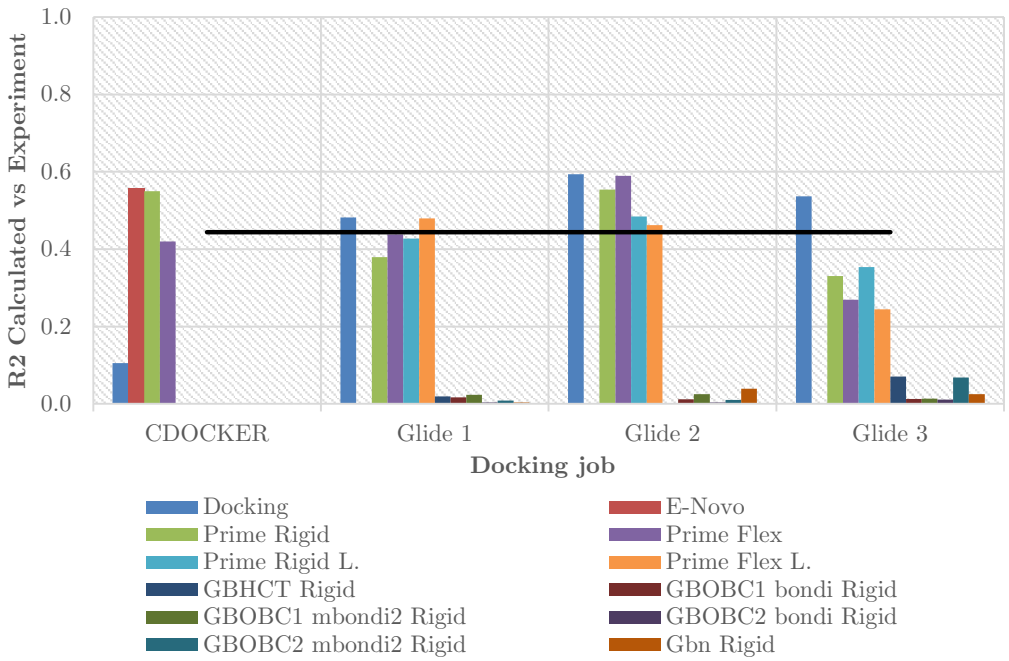


Figure 6.57: Coefficient of determination of rescoring protocols with experiment grouped by docking jobs (CDOCKER, Glide 1, Glide 2, Glide 3). Each rescoring protocol is shown by a differently coloured bar. The 'L.' for Prime jobs stands for the Prime score based on the lowest (more negative) docking score, in the case of two dock poses obtained for one ligand. 'Rigid' refers to protein flexibility, with the latter fully flexible for Amber calculations, while only 4 Å for Prime calculations. CDOCKER poses were not tested in AMBER. Glide poses not tested on Pipeline Pilot. The black line shows the 5% significance level for the number of observations (9 ligands).

On the other hand, using the AMBER implementations of MM-GBSA to rescore Glide poses, gave particularly poor results, ranging from 0.00 to 0.07. This arises from the issues associated with obtaining a binding free energy estimate for ligands 7, 8, and 9. These ligands share the same substituted group at the R4 position, which is a phosphonomethylphosphinyl (PMP) moiety (see Figure 4.19 and Table 4.5 in section 4.6). This moiety is shown, here, in Figure 6.58. As discussed in section 5.3.2, in the E-Novo publication[16] neutral charge states were chosen for all datasets except the Thrombin dataset where the contrary gave better results. Hence in this case, all three oxygens (the ones not involved in a double bond) were protonated. However this group extends out of the binding site and toward a solvent exposed area.

It would therefore be expected for this group to be charged and not neutral. The protonation state shown in Figure 6.58 is that used for the Glide poses, for all three ligands (7, 8, and 9), and determined during the ligand preparation step by the LigPrep utility included in the Maestro software.[109]

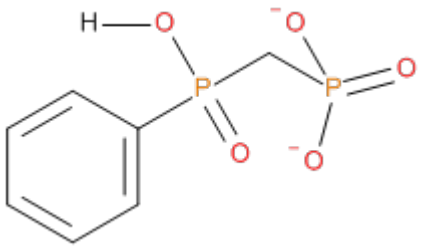


Figure 6.58: Phosphonomethylphosphinyl (PMP) attached to the benzyl ring of the ligand scaffold. Shown is the protonation state used with the Glide poses as generated by the LigPrep utility in Maestro, Schrödinger.[109]

Considering the more reasonable charge state of the Glide poses compared to the CDOCKER poses, it was decided to commence calculations in AMBER using the former. This quickly resulted in a number of problems. First, minimisations of the complex would crash. The resulting ligand geometries appeared scrambled. More specifically, the hydrogen of the protonated oxygen in the PMP group (see Figure 6.58) would collapse either onto the phosphorus atom or onto the opposite oxygen, which forms a double bond with phosphorus. This was attributed to the fact that the General Amber Forcefield (GAFF) does not include a van der Waals radius for a hydrogen bonded to a hydroxyl group. To tackle this a small van der Waals parameter was added to the hydrogen atom, and the force constant of the hydrogen-oxygen (ho-oh) bond was increased. Although this resulted in fewer minimisations to crash, there were remaining issues. Following the minimisation of the complex, the ligand and protein are post-processed in order for individual energy contributions to be obtained, and ultimately estimate the binding free energy. During the post-processing of the ligand, charges are first calculated, before the necessary parameters for obtaining the

energy, can be generated. It is at this initial charge generation step that many failed. Visualising the coordinates of some of the ligands, revealed that the hydrogen-oxygen-phosphorus (ho-oh-p) angles were skewed at around 77 degrees (according to the forcefield this angle should be 110 degrees). Minimisations were re-run using three times the force constant found in GAFF for this angle (150 kcal $mol^{-1}$ $rad^{-2}$). This resulted in no failed minimisations, however, many ligand geometries again failed at the charge generation step. In this case successfully post-processed ligand geometries differed little from the ones that failed.

A number of additional minimisations were run to investigate if a complete set of post-processed data could be obtained. This included increasing further the force constant for angle ho-oh-p to 500 kcal $mol^{-1}$ $rad^{-2}$, followed by the same increase for all angles involving the hydrogen, oxygens, and phosphorus atom. Finally a minimisation was run using a force constant of 1000 kcal $mol^{-1}$ $rad^{-2}$ on the angle ho-oh-p. This resulted in the fewest failed cases at the post-processing step. Again the poses that gave an error during the charge generation step, were near identical to the ones that did not. To obtain a complete dataset for all of these three ligands (7, 8, and 9) across all three Glide sets of poses, and the 6 different GB models, it was decided to relax the convergence criteria associated with the charge generation step in the antechamber module of AMBER (see section 6.2.2).

Although a complete series of data was eventually generated for the minimisations of Glide poses in AMBER, the estimated binding affinities could not be trusted. Some of the free energies obtained were large positive or large negative numbers. Visual inspection did not reveal any issues with the structures. In fact at a closer look, even when Prime was used to rescore the Glide poses, some of the free energies obtained for ligands 7, 8, and 9, were positive numbers. These dubious results indicate that this group (PMP) is a challenging case not only for an academic code (AMBER), but also for a professional software (Prime in Schrödinger).

The challenges discussed thus far in this section, led to the decision not to proceed with further testing and analysis on this dataset. For similar reasons, in addition to the unrealistic neutral representation of the PMP moiety, it was deemed unnecessary to commence any testing of the CDOCKER poses in AMBER.

## 6.8 Conclusions

In this chapter a range of rescoring protocols in a range of software utilising different Generalised Born (GB) models, were investigated. The aim of this chapter was to assess the performance of fast rescoring protocols versus experiment for the method to be applied at early stages of lead optimisation. Ideally the method should be able to provide a fair qualitative agreement with experiment and be able to correctly rank inhibitors according to their binding affinity. The aim is to implement this as a fast rescoring tool, meaning a minimum amount of time and effort to be spent on setting up the calculations and running them. In other words to obtain a near automated procedure. In reality this is not an easy task, and even in the implementations covered here, there was some elaborate prepearative work required; however it is far easier to set up and run these calculations compared to more rigorous methods available. In addition, short molecular dynamics simulations using implicit solvent were executed with the aim of investigating what effect additional sampling can have.

Overall the results when compared with experiment were shown to be poor, very much system dependent and highly sensitive to the system starting configuration. However, this was not always the case. All correlations obtained with rescoring on the HIV-1 Protease dataset where shown to be significant, and consistent amongst varying solvent models, though they were unable to outperform the dock scoring function (which was optimised for this target). Specific to this point, the largest dataset in this study. Factor XA,

was the only case where $R^2$ between predicted and experimental binding affinities, was higher than that of the docking scoring function, and was obtained consistently for different solvent models within the same software and with the same initial conditions (same starting poses, rigid protein). Ranking of inhibitors on the other hand, although occasionally giving good results, was on average poor.

Experimental data, on the other hand could be unreliable. For some of the systems studied here, experimental errors were not reported, and therefore one cannot be certain that the variance in experimental affinities is such that it could mask any true predictivity of the model. Comparing the methods to each other resulted in varied observations for the different systems. Overall there appeared to be some similarity between the models, in particular those of the same software implemented in the same protocol, e.g AMBER rigid protocols. Agreement was mostly on a qualitative basis, although there were cases where quantitative agreement was found. However, we found quantitative agreement for the same model between the different GIide poses, despite the poor performance between models.

The systems studied here may not be extensive, but they provide a good overview with regard the performance of the method, the limitations, and the challenges. Most of the ligands in these datasets are congeneric in which case it is expected for the method to perform well. However, some inhibitors were charged, while others contained highly polar groups, while others formed buried interactions with the protein, in which case computing the solvation free energy is a difficult task due to the dielectric inhomogeneity of the interior of the protein.[67, 70] For such systems when a strong change in polarization occurs some workers suggest increasing the dielectric constant of the solute to account for screening effects[20, 99, 149], however this was not tested here as it was not in the scope of this work. The aim is to quickly set up the calculation; hence attempting different parameters would not be consistent with a fast rescoring tool. In addition, although this intervention may yield

better results, it introduces the risk of obtaining fortuitous results, simply by attempting various values until finding one that works.

Glide 1

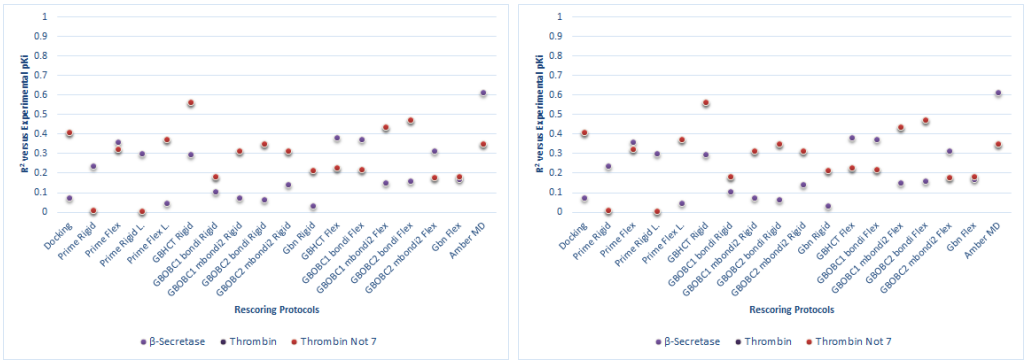


Glide 2

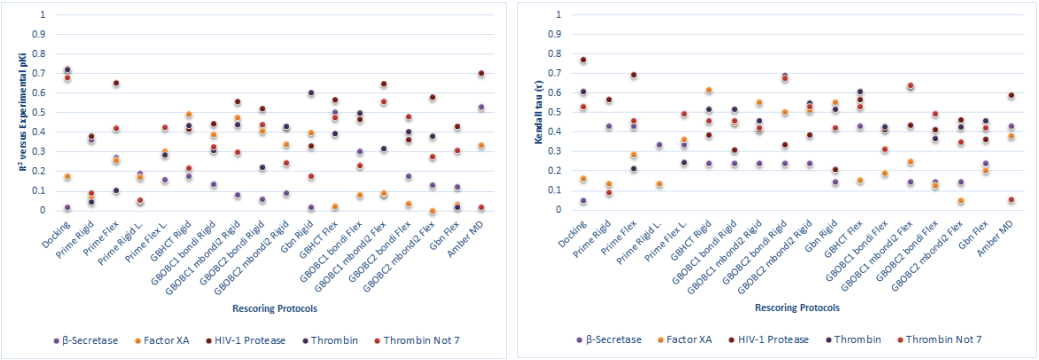


Glide 3

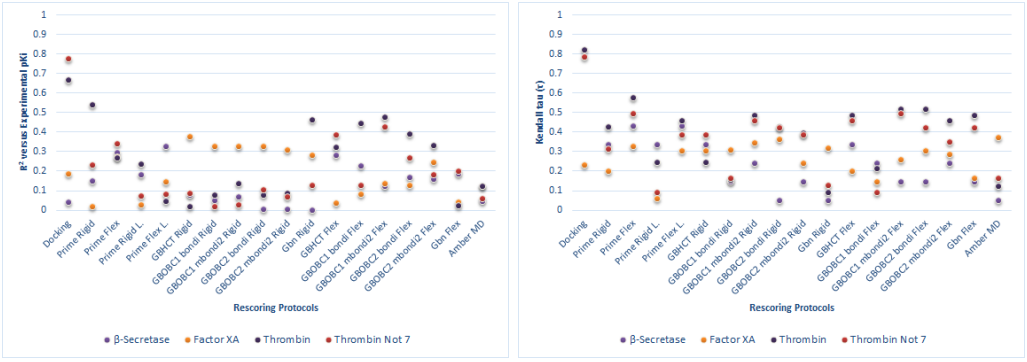


Figure 6.59: Correlation of determination ($R^2$) and Kendall tau rank correlation coefficient ($\tau$) versus experiment for each Glide job for all data sets.

Perhaps the most interesting conclusion that can be made following this thorough investigation is that: (a) for these cases studied here there does not appear to be one model that can perform well across all systems, and (b) we did not find an indication of a certain model to perform well for a system across all docked poses. In other words, there is no indication of choosing one model over another, and the results can vary vastly between them. This can be seen in Figure 6.59.

Thus far we have shown that for the cases studied here, MM-GBSA does not provide a solution as a fast rescoring tool in lead optimisation, where smaller, challenging datasets may exist. However, our results, for example better performance to large datasets (low correlations, but statistically significant), indicate that perhaps there may be applications in earlier stages of drug discovery, for example the enrichment of a lead identification screen, where larger datasets are the norm, and where the range of binding affinities is larger.

The method (MM-GBSA) suffers from many limitations, such as the approximations involved with the implicit solvent models, the quality of the underlying potential, and forcefield limitations, to name a few (see section 3.5 for more details). Besides these numerous methodological limitations, the results in this chapter indicate a significant sensitivity to the starting configuration of the system, that simple minimising prior to calculating the binding free energies does not resolve the problem. Therefore, the question arises of what an effect additional sampling would have. Using a bulk low viscosity solvent proved futile, and hence, in the next section tests will be conducted using explicit solvent instead.

# Chapter 7

# Application of MM-PBSA/GBSA using explicit solvent molecular dynamics simulations

## 7.1 Introduction

In the previous chapter we assessed and compared a large range of MM-GBSA protocols with the aim to quickly rescore docked poses. With a handful of exceptions, results were overall poor and inconsistent. Importantly, it was not possible to identify a model/protocol that on average gave better results when compared to experimental data. Amongst other issues, lack of sampling is a key limitation of fast rescoring methods.

Here the application of explicit solvent molecular dynamics (MD) simulations and averaging over three trajectories, is investigated. Do results with experiment improve for the current data sets when using explicit solvent MD? Is there any added value? How does PB compare with GB?

## 7.2 Setup of simulations

The same proteins with the same setup were used as described in Chapter 4. In this case, however, crystallographic waters were retained. The protein systems were then run through the LEaP module of AMBER Tools package to generate the necessary parameter and topology files. In the process, non-polar hydrogen atoms were added, and the system was solvated using a box consisting of TIP3P waters extending 10 Å from the surface of the protein. The systems were neutralised by adding $Na^+$ and $Cl^-$ counterions (12 $Cl^-$ were required for Thrombin, 11 $Na^+$ for β-Secretase, 2 $Cl^-$ for Factor Xa, and 5 $Cl^-$ for HIV-1 Protease). Atomic charges for the ligands were determined by the AM1-BCC[146, 147] with MOPAC via the AMBER tool Antechamber. Protein systems were described using the AMBER99 Stony Brook forcefield (ff99SB) .[145]

Once the systems were prepared, they were equilibrated. First they were subjected to an unrestrained minimisation, with 1000 steepest descent and 1500 conjugate gradient steps. This was followed by a second minimisation with a restraint of 2 kcal $mol^{-1}$ $Å^{-2}$ on all protein atoms, with 500 steepest descent and 500 conjugate gradient steps. Next, the system was gradually heated to 300 K over 500 ps, using the NVT ensemble keeping the protein restraints on. Before removing the restraints, the density is equilibrated using the NPT ensemble for another 500 ps. Finally, the restraints were removed and the system was equilibrated for yet another 500 ps.

Once the systems were equilibrated, a production run of 5 ns was performed using the PMEMD module of the AMBER software, and snapshots were saved every 5 ps (giving 1000 snapshots per simulation). To collect more valuable statistics, data was collected and averaged over three independent repeats. Each simulations was run using as starting point the equilibrated systems.

The following applied for all simulations (including equilibration steps): Hydrogen bonds were constrained using the SHAKE algorithm [33], Langevin dynamics was used to keep the temperature at 300 K with a collision frequency of 2.0 $ps^{-1}$ , long range electrostatics were treated with use of the particle mesh Ewald (PME) [166], non-bonded cut-off was set at 8 Å, and, finally, a timestep of 2 fs was employed.

To calculate the MM-GBSA binding free energies, the explicit solvent trajectories were post-processed using the mm_pbsa.pl script in AMBER, as in the implicit solvent model MD simulations in Chapter 6. Herein, post-processing was performed using three different solvent models: $GB^{HCT}$, $GB^{OBC1}$mbondi2, and Poisson Boltzmann model in AMBER. These will be referred to throughout this chapter as GB1, GB2, and PB, respectively. The first two models (the GB models) have been described earlier (section 6.2.2). For the third (PB), the PBSA program[167] in AMBER was used with the PARSE radii.[168, 169] As for the non-polar solvation term, it was calculated with the solvent accessible surface area presented in section 3.2.4, and using equation (3.2.20). The values recommended by the manual of 0.00542 and 0.92 were used for parameters $\gamma$ and b, respectively. According to AMBER developers, the results of the PBSA code are consistent with the popular *DelPhi* PB solver.[56]

## 7.3 Thrombin

The PDB structure 1ETT (resolution = 2.50 Å)[108] was used with the 12-ligand dataset as described in Chapter 4.

### 7.3.1 Explicit solvent results

The binding affinity of the 12 ligands of the dataset has been estimated by post-processing three independent 5 ns explicit MD simulations using four different implicit solvent methods: GB1, GB2, and PB (see section 7.2 for

details on the methods). The results and the corresponding errors (standard errors of the mean, i.e., the standard deviation divided by the square root of the number of observations, in this case three) for the three Glide docking jobs are collected in Table 7.1. Results without ligand 7 are also reported. The table also includes the experimental binding affinities in kcal $mol^{-1}$ calculated from the experimentally derived dissociation constants using the formula:

$$\Delta G = -RT \ln K_i \tag{7.3.1}$$

Where R is the ideal gas constant, T is the temperature, and $K_i$ is the dissociation constant.

Inherent approximations in the MM-(PB)GBSA methodology, including the continuum solvent, the lack of entropic contributions, and the omission of the 3RT term (translational/rotational term), make the relative binding free energies a much more interesting case when compared to the absolute. To investigate the relationship between predicted and experimental binding affinities the quality metrics including the range of binding free energies for each solvent model, the Mean Absolute Deviation (MAD), the correlation of determination ($R^2$), and Kendall's tau rank correlation coefficient ($\tau$), were computed , and are also shown in Table 7.1. P-values are also included for $R^2$ and $\tau$ (shown in brackets) for a significance of 5%.

The average or mean absolute difference (MD) between a theoretical estimate $(p_i)$ and the corresponding experimental $(e_i)$ value for a dataset with length $n$ (in this case equal to the number of ligands, i.e. equal to 12) is given by the following formula:

$$MD = \frac{1}{n}\sum_{i=1}^{n}|p_i - e_i| \tag{7.3.2}$$

Although this is a useful metric, it assumes that the estimates follow a regression line with a slope of one and intercept at the origin. However, with a systematic error present, as in the work here, this cannot be assumed. Therefore to overcome this, the mean signed error, or in other words the signed average of the difference between theoretical estimate and experimental measurement, can be subtracted from the MD defined in equation (7.3.2) giving a translated MD or in other words the mean absolute deviation (MAD) about the mean. In this case, the assumption remains that the estimates follow a regression curve, with slope of one, but the intercept can be different than the origin. With $x_i = p_i - e_i$ and the signed error equal to:

$$m(X) = \frac{1}{n}\sum_{i=1}^{n}(p_i - e_i) \tag{7.3.3}$$

the MAD metric is then calculated by:

$$MAD = \frac{1}{n}\sum_{i=1}^{n}|x_i - m(X)| \tag{7.3.4}$$

In this setting, this metric gives the average absolute difference between predicted and experimental values from the mean of the differences, or in simple terms, the average absolute distance from the mean. It is used here to quantify the variability of the systematic error, i.e. to evaluate the predictions in absolute terms.

Table 7.1: Predicted Binding affinities (kcal/mol) of the 12 Thrombin ligands with the various methods. Reported errors are standard errors of the mean over the three 5 ns MD trajectories.

| | GB1 | | | GB2 | | | PB | | | Exp.[a] |
|---|---|---|---|---|---|---|---|---|---|---|
| Ligand | Glide 1 | Glide 2 | Glide 3 | Glide 1 | Glide 2 | Glide 3 | Glide 1 | Glide 2 | Glide 3 | |
| 1 | -49.6 ± 1.7 | -49.8 ± 2.3 | -52.2 ± 1.7 | -36.6 ± 1.3 | -36.5 ± 2.1 | -38.6 ± 1.4 | -18.0 ± 0.9 | -21.1 ± 3.5 | -18.5 ± 1.0 | -9.99 |
| 2 | -54.5 ± 2.1 | -58.9 ± 1.9 | -59.0 ± 1.5 | -41.6 ± 1.7 | -45.6 ± 1.6 | -45.6 ± 1.4 | -24.7 ± 1.3 | -29.1 ± 1.3 | -28.3 ± 1.8 | -10.08 |
| 3 | -61.7 ± 0.8 | -63.6 ± 0.5 | -61.6 ± 0.3 | -47.7 ± 0.8 | -49.6 ± 0.4 | -47.7 ± 0.3 | -29.5 ± 1.1 | -31.9 ± 1.2 | -30.4 ± 0.4 | -12.11 |
| 4 | -57.8 ± 2.8 | -58.8 ± 2.0 | -54.8 ± 1.9 | -44.1 ± 2.8 | -45.0 ± 1.8 | -41.1 ± 2.0 | -22.7 ± 4.6 | -26.8 ± 1.9 | -18.7 ± 4.2 | -9.08 |
| 5 | -61.6 ± 0.5 | -62.8 ± 1.3 | -60.5 ± 0.3 | -47.8 ± 0.4 | -48.9 ± 1.2 | -46.7 ± 0.4 | -28.2 ± 1.6 | -27.7 ± 2.5 | -27.6 ± 1.7 | -12.23 |
| 6 | -63.4 ± 1.0 | -65.1 ± 0.3 | -62.3 ± 1.4 | -49.5 ± 0.7 | -50.9 ± 0.3 | -47.9 ± 1.5 | -30.3 ± 0.6 | -31.9 ± 0.2 | -27.4 ± 2.9 | -9.36 |
| 7 | -55.7 ± 1.5 | -56.0 ± 1.9 | -59.5 ± 4.0 | -41.7 ± 1.4 | -41.9 ± 1.8 | -45.4 ± 3.8 | -20.8 ± 3.3 | -19.8 ± 3.0 | -28.3 ± 3.2 | -7.52 |
| 8 | -62.3 ± 0.8 | -67.2 ± 1.6 | -63.9 ± 1.7 | -49.1 ± 0.8 | -53.4 ± 1.3 | -50.1 ± 1.5 | -28.7 ± 1.2 | -34.8 ± 1.3 | -29.7 ± 1.2 | -14.21 |
| 9 | -58.1 ± 3.2 | -56.4 ± 3.1 | -60.5 ± 1.8 | -44.3 ± 3.0 | -43.0 ± 2.9 | -46.7 ± 1.8 | -24.9 ± 4.0 | -25.1 ± 3.5 | -28.4 ± 2.2 | -11.12 |
| 10 | -61.2 ± 3.6 | -61.1 ± 2.2 | -57.7 ± 0.6 | -47.6 ± 3.1 | -47.8 ± 1.9 | -44.7 ± 0.5 | -29.5 ± 2.5 | -28.0 ± 1.9 | -27.2 ± 0.5 | -10.62 |
| 11 | -62.6 ± 1.8 | -61.3 ± 3.5 | -62.9 ± 2.3 | -47.8 ± 1.8 | -46.2 ± 3.5 | -47.7 ± 2.3 | -28.2 ± 2.5 | -26.0 ± 5.6 | -27.4 ± 3.4 | -13.73 |
| 12 | -62.3 ± 1.9 | -64.9 ± 0.1 | -64.9 ± 0.9 | -48.1 ± 1.6 | -50.3 ± 0.1 | -50.2 ± 0.8 | -28.6 ± 1.6 | -30.7 ± 0.3 | -31.5 ± 0.7 | -13.07 |
| Range | 13.8 | 17.4 | 12.7 | 12.9 | 16.9 | 11.6 | 12.3 | 15.0 | 13.0 | 6.69 |
| MAD | 2.3 ± 0.1 | 2.8 ± 0.1 | 2.1 ± 0.2 | 2.0 ± 0.0 | 2.8 ± 0.24 | 1.9 ± 0.3 | 2.2 ± 0.3 | 3.4 ± 0.1 | 2.8 ± 0.4 | |
| MAD* | 2.3 ± 0.1 | 2.8 ± 0.1 | 2.5 ± 0.3 | 2.0 ± 0.0 | 2.7 ± 0.23 | 2.0 ± 0.4 | 2.2 ± 0.2 | 3.0 ± 0.2 | 2.9 ± 0.5 | |
| $R^2$ | 0.3 ± 0.1 (0.06) | 0.33 ± 0.1 (0.05) | **0.4 ± 0.2 (0.034)** | 0.3 ± 0.1 (0.496) | 0.3 ± 0.1 (0.061) | **0.4 ± 0.2 (0.036)** | **0.4 ± 0.1 (0.044)** | 0.2 ± 0.1 (0.053) | 0.5 ± 0.1 (0.138) | |
| $R^{2*}$ | 0.3 ± 0.1 (0.11) | 0.3 ± 0.4 (0.10) | **0.5 ± 0.1 (0.014)** | 0.3 ± 0.1 (0.114) | 0.2 ± 0.1 (0.134) | **0.5 ± 0.1 (0.018)** | 0.2 ± 0.1 (0.148) | 0.1 ± 0.1 (0.260) | **0.4 ± 0.1 (0.042)** | |
| $\tau$ | **0.5 ± 0.1 (0.03)** | **0.5 ± 0.4 (0.03)** | **0.5 ±0.2 (0.021)** | **0.6 ± 0.1 (0.014)** | **0.5 ± 0.1 (0.045)** | **0.5 ± 0.2 (0.021)** | 0.4 ± 0.1 (0.1116) | 0.3 ± 0.1 (0.153) | 0.4 ± 0.1 (0.116) | |
| $\tau^*$ | 0.5 ± 0.1 (0.06) | 0.4 ± 0.4 (0.09) | **0.6 ± 0.1 (0.017)** | **0.5 ± 0.10 (0.026)** | 0.4 ± 0.1 (0.121) | **0.5 ± 0.1 (0.026)** | 0.3 ± 0.1 (0.283) | 0.2 ± 0.1 (0.445) | 0.5 ± 0.1 (0.060) | |

*Excluding ligand 7

[a] Experimental binding affinities in kcal mol$^{-1}$. $p$-values for $R^2$ and $\tau$ are shown in brackets. Highlighted in bold are significant measurements within a 5% significance level. MAD corresponds to the Mean Absolute Deviation (about the mean) of the differences between the predicted and experimental binding free energies

The results using model GB1 to post-process the snapshots were similar across the three Glide docking poses. Predictions were in general systematically more negative than experimental results, by 48.14, 49.40, and 48.89 kcal $mol^{-1}$ on average, for Glide 1, 2, and 3 respectively. Uncertainties (standard error of the mean, SE) were relatively high, averaging over the 12 ligands at 1.79, 1.73, and 1.53 kcal $mol^{-1}$, again for Glide 1, 2, and 3 respectively. However, the largest difference (between poses 1 and 2) amongst the three pairs is justified by what is expected from the obtained standard errors of the mean. The MAD values, although similar amongst the three sets of poses, they are high ranging from 2.06 kcal $mol^{-1}$ (Glide 3 – all ligands) to 2.84 kcal $mol^{-1}$ (Glide 2 – all ligands). This could be explained by the exaggerated range of the predicted data which took values from 12.70 kcal $mol^{-1}$ (Glide 3) to 17.41 kcal $mol^{-1}$ (Glide 2) compared to 6.69 kcal $mol^{-1}$ of the experimental results, or by remaining statistical errors. $R^2$ ranged from 0.31 (Glide 1) to 0.38 (Glide 3) when all ligands were included, and 0.26 (Glide 1) to 0.50 (Glide 3) when ligand 7 was excluded. Only the correlations obtained for Glide 3 were statistically significant (at a 5% significance level), however they were poor and moderate at best (when ligand 7 was excluded), and showed the largest standard errors (see Figure 7.1 plot A). Ranking of the ligands was better with statistically significant results for 4 out of the 6 measurements, however with the highest obtained value at 52%, the results do not give meaningful conclusions. These observations are reflected in the scatter plot shown in Figure 7.2 A. Ligand 7, which is experimentally the weakest binder, is consistently ranked wrongly. This is particularly true for Glide 3, where in contrast to the other two sets of docked poses, removal of ligand 7 improves overall correlations. As indicated by $\tau$, it can be seen that only about 50% of the inhibitors are ranked correctly. The ranking is consistent across the three Glide poses with a few exceptions, for example the most potent compound that is only correctly ranked when Glide 2 poses were used.

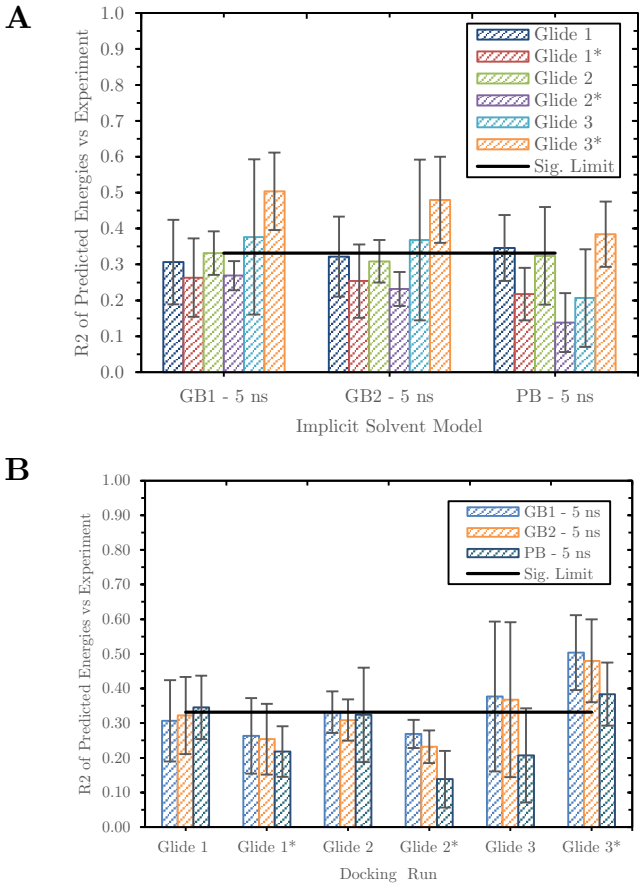


Figure 7.1: Correlation of determination ($R^2$) versus experiment. Results are grouped in Model used (A), and in docking run (B). The asterisk indicates exclusion of ligand 7. Data is shown for the entire 5 ns of MD simulations. Error bars show the standard error of the mean obtained from three independent trajectories.

The GB2 predictions show similarly large range of the theoretical estimates compared to experimental data (12.90, 16.93, and 11.65 kcal $mol^{-1}$ for Glide 1, 2, and 3 respectively), but are on average less negative (by about 14 kcal $mol^{-1}$ on average) than the estimates obtained from the GB1 method (-35.57, -35.48, -34.95 kcal $mol^{-1}$ for Glide 1, 2, and 3 respectively). With slightly lower data ranges the MAD is also slightly better than for GB1, but both correlations (coefficient of determination and Kendall tau) are similar (see Figure 7.1 B), i.e. largely poor and average for some cases with large errors. These observations are clearly reflected in the scatter plot in Figure 7.2 B,

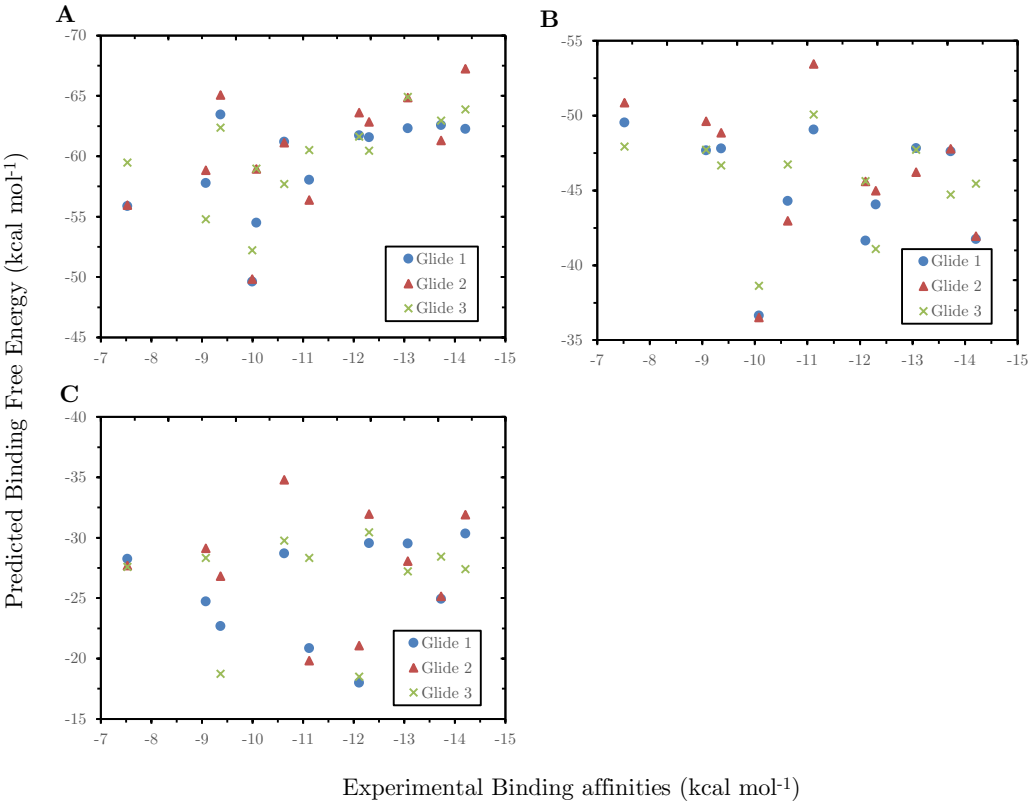


Figure 7.2: Scatter plots of the predicted and experimental binding affinities for Thrombin. Plots A to C correspond to models GB1, GB2, PB, respectively. Results are averages over three independent 5 ns MD simulations. Errors are not included for clarity, but can be seen in Table 7.1.

which appears nearly identical to Figure 7.2 A shifted by a mean signed difference of -13.86 kcal mol$^{-1}$ across all three Glide poses.

The PB results differed from the other two models. First, although the range of the predicted data was similar (with the exception of Glide 2 that was lower), the estimates were found to be closer to the experimental data. Herein, the mean signed difference between predicted estimates and experimental measurements, was on average across the three Glide poses equal to -15.87 kcal mol$^{-1}$ compared to -48.81 kcal mol$^{-1}$ (GB1) and -34.94 kcal mol$^{-1}$ (GB2). On the other hand, the uncertainties were on average greater (2.09 kcal mol$^{-1}$ for Glide 1, 2.20 kcal mol$^{-1}$ for Glide 2, and 1.95 kcal mol$^{-1}$ for Glide 3) than the ones found for models GB1 and GB2. On average,

correlations showed were poorer and again the standard errors calculated from the three repeats were very large. The ranking of inhibitors was poor and the null hypothesis (that the observed results occur at random) was not rejected at a 5% significance level for any of the 6 measurements (all ligand and excluding ligand 7 for each of the three Glide sets of poses). Kendall's tau ranged from 0.20 (job2 – excluding ligand7) to 0.45 (job3 – excluding ligand 7). It can be seen in Figure 7.2 C there is a much larger spread of the predicted estimates between the different initial starting configurations (i.e. different docked poses), when compared to the other two models.

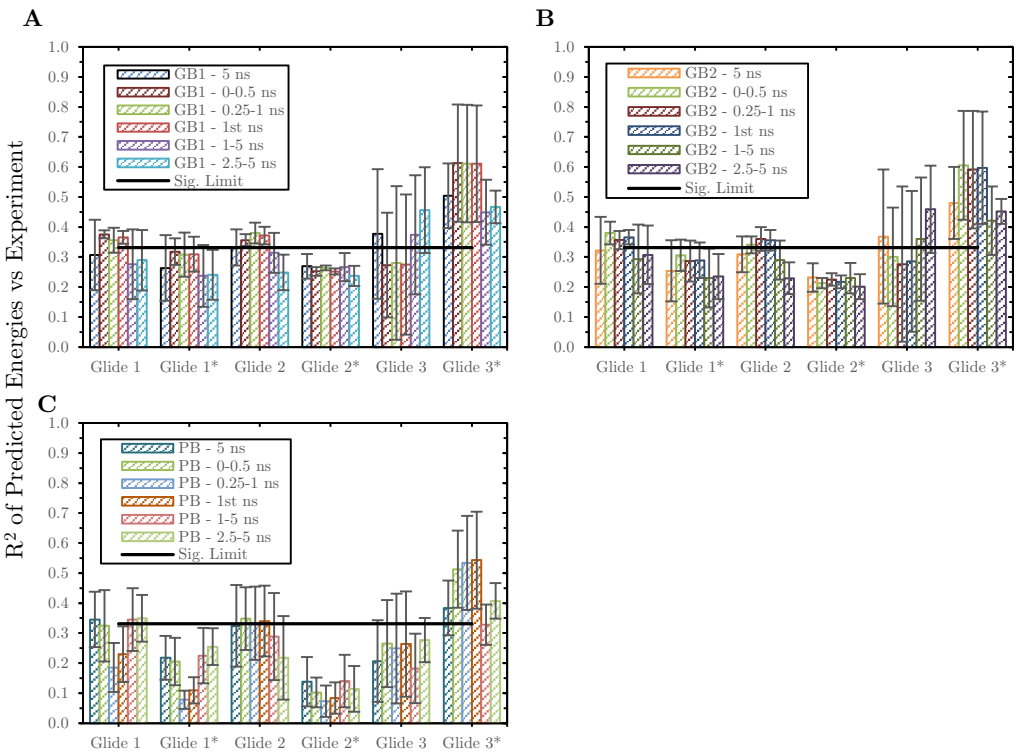


Figure 7.3: Correlation of determination ($R^2$) versus experiment for a range of intervals of the simulation (all 5 ns, 0 to 0.5 ns, 0.25 to 1 ns, 1st ns, 1 to 5 ns, and 2.5 to 5 ns) grouped by Glide docking run. Plots A to C each correspond to the different implicit models, including GB1, GB2, PB, respectively. Error bars show the standard error of the mean obtained from three independent trajectories.

A range of different lengths of the simulation taken from the 5 ns trajectories were additionally analysed. In particular, five different intervals were investigated: a) the first half nanosecond of the trajectory (energies averaged over 100 snapshots), b) 0.75 of the first nanosecond excluding the initial quarter of a nanosecond (150 snapshots), c) the entire 1st nanosecond (200 snapshots), d) from the 1st to the 5th nanosecond (800 snapshots), and e) the last 2.5 ns of the 5 ns trajectories. Figure 7.3 shows the $R^2$ for both all ligands and excluding ligand 7 with standard errors of the mean over the three trajectories as error bars. Overall the correlations appear very similar across all different lengths of analysed MD trajectories. Although, some fluctuations are seen in the PB results, the $R^2$ are so low, and the error bars so large that no conclusive observation can be made with respect to differences obtained from different simulation lengths. Perhaps the more interesting observation that can be made here, is that only running a 0.5 ns long simulation would give equivalent results to those obtained from the 5 ns simulation.

Investigating the required length of the simulation for maximising efficiency with performance has not been the scope of this investigation. In addition, the results summarised here, are from a single system with a small dataset. However, they serve as good indicator that a much shorter simulation runs can provide sufficiently similar results when compared with longer runs. This confirms the findings of other workers.[74, 101, 170]

### *Comparison with minimisation methods and implicit solvent MD*

When all the ligands and GB1 ($GB^{HCT}$) model are considered, although minor improvements in $R^2$ were found when compared with both rigid and flexible protein minimisations, such as in Glide 1 with $R^2$ equal to 0.31 in explicit MD versus 0.06 and 0.09 in the minimisation methods, these correlations are so low that the difference is not significant. This is also confirmed with a paired t-test (see Table 7.2) between the values obtained in this chapter (i.e. $R^2$ from

3 explicit MD runs) and the work done in Chapter 6, i.e. rigid-protein minimisations, flexible-protein minimisations, and implicit MD across the three Glide poses; here the data are compared to the 1 ns run only (and not the 10 ns), given that GB2 testing was not done on 10 ns simulation, and that the results between 1 ns and 10 ns for GB1 were very similar. When GB1 is compared across the different protocols, the only differences that are found to be statistically significant to within 5% significance, were flexible-protein minimisations when compared to the implicit MD simulation, and MD implicit compared to MD explicit. On both occasions implicit MD simulations performed worse. The null hypothesis was not rejected for the remaining pairwise comparisons (including with exclusion of ligand 7), meaning that the models performance with experiment across the three Glide poses did not differ significantly (at a 5% significance). The findings for GB2 were similar as is shown in Table 7.2.

Table 7.2: P-values from paired t-test comparisons of the $R^2$ between minimised (both rigid and flexible, i.e. MinR and MinF respectively), MD implicit 1ns (MDimp1ns), and MD explicit (MDexp) for model GB1 and GB2 both including all ligands and excluding ligand 7 (indicated by *). Comparisons for which the difference of the means is significant are shown in bold (for a 5% significance).

| | MinR - MDimp1ns | MinR - MinF | MinR - MDexp | MinF - MDimp1ns | MinF - MDexp | MDimp1ns - MDexp |
|---|---|---|---|---|---|---|
| GB1 | 0.149 | 0.050 | 0.132 | **0.024** | 0.772 | **0.028** |
| GB1* | 0.754 | 0.237 | 0.802 | 0.117 | 0.894 | 0.207 |
| GB2 | 0.500 | 0.489 | 0.224 | 0.344 | 0.923 | **0.015** |
| GB2* | 0.082 | 0.853 | 0.588 | **0.034** | 0.309 | 0.528 |

### 7.3.2 Summary

With the aim of identifying the effect additional sampling can have in the performance of the estimation of the binding free energy using the MM-PBSA/GBSA methodology, the results over three independent explicit solvent MD simulations was studied. Snapshots taken from each trajectory at 5 ps intervals (resulting to 1000 snapshots over the length of 5 ns) were post-processed with three different implicit solvent models (GB1, GB2, and PB), following removal of the explicit waters. The results obtained from the three trajectories were averaged and standard errors of the mean were calculated.

It was shown that in general all three models gave systematically more negative energies than experiment. PB gave results closer to experiment in absolute terms when compared to the GB models. MAD measurements for the signed error, were high but consistent across all the calculations indicating a similar performance in a relative scale. The $R^2$ with experiment was overall poor averaging below 0.4. Ranking of the inhibitors was overall slightly better but remained average at best. PB showed the worst ranking performance.

Results across different starting configurations were similar, and the obtained energies were identical to within statistical error. This was an improvement over the results presented in the previous chapter. Despite this, the results obtained for this dataset in comparison to experiment, both quantitatively and qualitatively, were not good enough to justify the additional computational cost associated with explicit solvent simulations.

Analysis for various lengths of the trajectory showed that equivalent results to the whole 5 ns simulations were obtained when only the first 0.5 ns of the trajectory were post-processed. Although not conclusive, this is an indication that perhaps shorter timescales would be sufficient to obtain similar performance.

## 7.4 β-Secretase

The PDB structure 2P4J (resolution = 2.50 Å) [113] was used with the 7-ligand dataset as described in Chapter 4.

### 7.4.1 Explicit solvent results

Similarly as in the previous subsection, three independent MD simulations using explicit solvent were performed for the 7-ligand dataset of this congeneric series and post-processed with three of the most common in literature implicit solvent models (GB1, GB2, and PB – refer to section 7.2). The results from these calculations are summarised in Table 7.3. Errors reported are standard errors of the mean (i.e. the standard deviation divided by the square root of the number of observations, in this case 3). Metrics include the range of the data, MAD about the mean of the differences between predicted estimates and experimental values (see section 7.3.1 for details), $R^2$, and $\tau$. P-values for the last two metrics are shown in brackets for a 5% significance level). Experimental data are shown in units of kcal $mol^{-1}$.

Table 7.3: Predicted Binding affinities (kcal $mol^{-1}$) of the 7 β-Secretase ligands with the various methods. Reported errors are standard errors of the mean over the three 5 ns MD trajectories.

| | GB1 | | | GB2 | | | PB | | | Exp.[a] |
|---|---|---|---|---|---|---|---|---|---|---|
| Ligand | Glide 1 | Glide 2 | Glide 3 | Glide 1 | Glide 2 | Glide 3 | Glide 1 | Glide 2 | Glide 3 | |
| 1 | -74.4 ± 1.3 | -74.7 ± 1.2 | -70.3 ± 0.5 | -69.4 ± 1.5 | -70.2 ± 1.3 | -65.3 ± 0.5 | -24.2 ± 0.3 | -26.0 ± 1.1 | -27.7 ± 0.8 | -9.94 |
| 2 | -86.2 ± 1.2 | -89.9 ± 3.1 | -91.3 ± 2.1 | -80.3 ± 0.8 | -82.5 ± 3.1 | -84.5 ± 1.7 | -33.6 ± 2.6 | -32.4 ± 4.7 | -31.9 ± 0.8 | -12.00 |
| 3 | -87.6 ± 1.5 | -87.3 ± 0.7 | -87.5 ± 0.4 | -84.5 ± 1.8 | -84.8 ± 0.9 | -84.2 ± 0.4 | -30.9 ± 0.5 | -27.8 ± 1.1 | -28.6 ± 1.4 | -9.43 |
| 4 | -85.7 ± 2.2 | -88.5 ± 0.7 | -81.8 ± 1.7 | -82.4 ± 3.2 | -86.2 ± 1.3 | -78.0 ± 1.7 | -30.6 ± 0.7 | -31.5 ± 0.6 | -29.4 ± 0.4 | -12.30 |
| 5 | -82.8 ± 2.5 | -85.0 ± 1.0 | -87.2 ± 1.0 | -79.8 ± 3.0 | -82.8 ± 1.1 | -84.6 ±1.2 | -30.2 ± 1.1 | -31.3 ± 0.2 | -30.8 ± 0.7 | -8.92 |
| 6 | -82.2 ± 2.8 | -82.3 ± 2.4 | -80.8 ± 1.2 | -78.7 ± 3.0 | -79.0 ± 2.2 | -76.3 ± 1.0 | -27.6 ± 0.34 | -27.7 ± 1.3 | -29.6 ± 1.3 | -8.73 |
| 7 | -68.2 ± 2.0 | -69.9 ± 2.3 | -68.1 ± 1.5 | -64.5 ± 2.1 | -65.8 ± 2.4 | -64.4 ± 1.4 | -29.1 ± 2.1 | -29.2 ± 2.1 | -29.1 ± 2.5 | -8.37 |
| Range | 19.4 | 20.5 | 23.2 | 20.0 | 20.4 | 20.2 | 8.5 | 6.4 | 4.2 | 3.93 |
| MAD | 5.1 ± 0.6 | 5.5 ± 0.3 | 6.7 ± 0.4 | 5.3 ± 0.7 | 5.7 ± 0.2 | 6.7 ± 0.5 | 1.9 ± 0.5 | 1.5 ± 0.6 | 1.4 ± 0.4 | |
| $R^2$ | 0.3 ± 0.1 (0.233) | 0.4 ± 0.1 (0.137) | 0.2 ± 0.1 (0.366) | 0.2 ± 0.1 (0.325) | 0.3 ± 0.1 (0.235) | 0.1 ± 0.1 (0.481) | 0.2 ± 0.1 (0.261) | 0.3 ± 0.1 (0.206) | 0.1 ± 0.1 (0.472) | |
| τ | 0.4 ± 0.1 (0.239) | 0.6 ± 0.1 (0.069) | 0.4 ±0.1 (0.239) | 0.5 ± 0.2 (0.136) | 0.5 ± 0.1 (0.136) | 0.2 ± 0.1 (0.562) | 0.2 ± 0.1 (0.381) | 0.2 ± 0.2 (0.562) | 0.1 ± 0.1 (1.000) | |

[a] Refers to Experimental energies calculated using the formula $\Delta G = -RT\ln K_i$

*p*-values for $R^2$ and τ are shown in brackets. MAD corresponds to the Mean Absolute Deviation of the differences between the predicted and experimental binding energies.

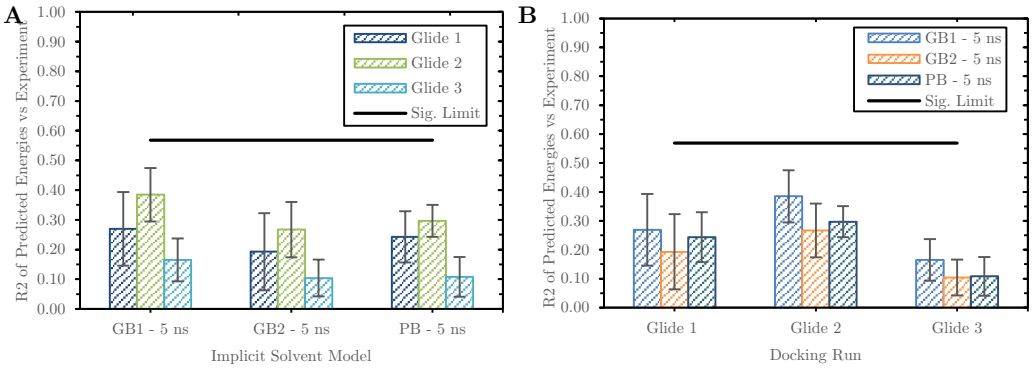


Figure 7.4: Correlation of determination ($R^2$) versus experiment. Results are grouped in Model used (A), and in docking run (B). Data is shown for the entire 5 ns of MD simulations. Error bars show the standard error of the mean obtained from three independent trajectories.

Predictions obtained using GB1 show a range of about 5 times greater than that of experiment averaging across the three poses at 21.03 kcal $mol^{-1}$ (19.38 kcal $mol^{-1}$ for Glide 1, 20.48 kcal $mol^{-1}$ for Glide 2, and 23.24 kcal $mol^{-1}$ for Glide 3), compared to the experimental 3.93 kcal $mol^{-1}$. This large range is reflected on the MAD values which are also high at 5.09, 5.49, and 6.72 kcal $mol^{-1}$ for Glide 1 to Glide 3 respectively. The predictions showed a high signed error of -71.54 kcal $mol^{-1}$ on average for the three jobs (-71.07, -72.48, and -71.05 kcal $mol^{-1}$ for Glide 1 to 3 respectively), compared to experimental data. These discrepancies of the absolute values between theoretical estimates and experimental findings, most likely come from the continuum model and the lack of the inclusion of entropic contribution. However, the interest here is on the relative performance of the model with experiment, or in other words the qualitative agreement. The performance is poor ($R^2$ of 0.16 for Glide 3) and modest at best ($R^2$ of 0.38 for Glide 2 and 0.27 for Glide 1), as shown in Table 7.3 and Figure 7.4 A. In addition the uncertainties for this metric are large. The scatter plot in Figure 7.5 A shows that ligand 7 is correctly identified as the weakest binder, while ligands 2 and 4 are also found at the correct end of the plot (highest affinity), although in the wrong order. The poor correlations appear to resonate from the incorrect prediction of ligands 3,

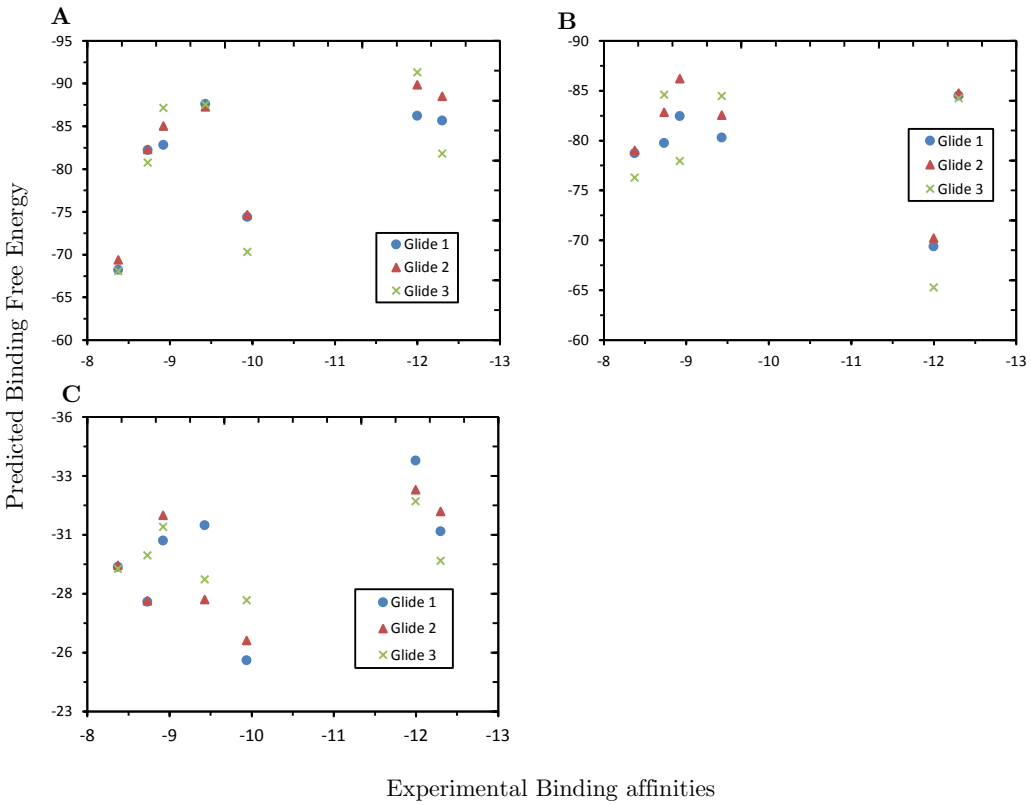


Figure 7.5: Scatter plots of the predicted and experimental binding affinities for β-Secretase. Plots A to C correspond to models GB1, GB2, PB, respectively. Results are averages over three independent 5 ns MD simulations. Errors are not included for clarity, but can be seen in Table 7.3.

5, and 6, which are predicted nearly as potent as the best two binders of the series. Ligands 4 and 5 (the best binder experimentally) only differ by the configuration of the methyl component of the α-methylbenzyl amide (group R2 in Table 4.2). Experimental observations show that the R-configuration (ligand 4) demonstrates a strong strereochemical preference at this position [112, 113], and hence a higher potency. However, it is shown that despite the stability of the structure of the ligands, obtained by the use of explicit MD simulation, the GB1 model is unable to discriminate between the two different orientations. Interestingly, in the case of Glide 3, the binding energy predicted for ligand 4 was lower than the one for ligand 5, which is reflected on the poorer $R^2$ values. The ranking was modest to average with $\tau$ values

ranging from 0.43 for Glide 1 and 3, to 0.62 for Glide 2, none of which were significant ($p - value > 0.05$).

The GB2 predictions were on average about 4 kcal mol$^{-1}$ closer to experimental energies than the GB1 predictions, with an average signed error of -67.59 kcal mol$^{-1}$ , across the three docking runs (-67.15, -68.82, and -66.79 kcal mol$^{-1}$ for Glide 1, 2, and 3 respectively). The range of the estimates was found to be similarly high at an average of 20.20 kcal mol$^{-1}$ (19.96, 20.41, 20.23 kcal mol$^{-1}$ respectively for Glide 1 through 3), reflecting similarly high MAD values (5.34, 5.69, 6.68 kcal mol$^{-1}$ for Glide 1 to 3) as model GB1. The $R^2$ (see Table 7.3 and Figure 7.4 A) in this case was lower and a similar trend across the three jobs was found, with Glide 2 giving the highest correlation (0.27) followed by Glide 1 (0.19), and finally by Glide 3 (0.10). From Figure 7.5 B similar observations as in the GB1 model can be made. Ligands 3, 5, and 6 are wrongly ranked, while in Glide 3, ligand 4 was predicted to have a lower affinity from the experimentally less potent ligand 5. In addition, the correlation here is made even worst by ligand 1 in which case is predicted to have a lower affinity than the weakest (experimentally) binder, ligand 7. As expected, Kendall's tau values were overall lower for this model (0.52 for Glide 1 and 2, and 0.24 for Glide 3).

The PB predictions, as in Thrombin, are much closer to experimental values (8.47, 6.40, 4.19 kcal mol$^{-1}$ for Glide 1 to 3) when compared to the other two models (average unsigned difference of -19.59 kcal mol$^{-1}$ across the three docking runs for GB1 and GB2). The MAD in this case was in comparison to the other solvent better with a value of 1.59 for the three jobs. On the other hand, $R^2$ was similar (0.24, 0.30, 0.11 for Glide 1 through 3) however Kendall's tau was poor (0.33, 0.34, 0.10 for Glide 1 to 3 respectively). The noise of the results obtained using this method can be seen in Figure 7.5 C.

Figure 7.4 B shows the comparison of the different models across the different docking runs. Although all correlations are poor, and some of the

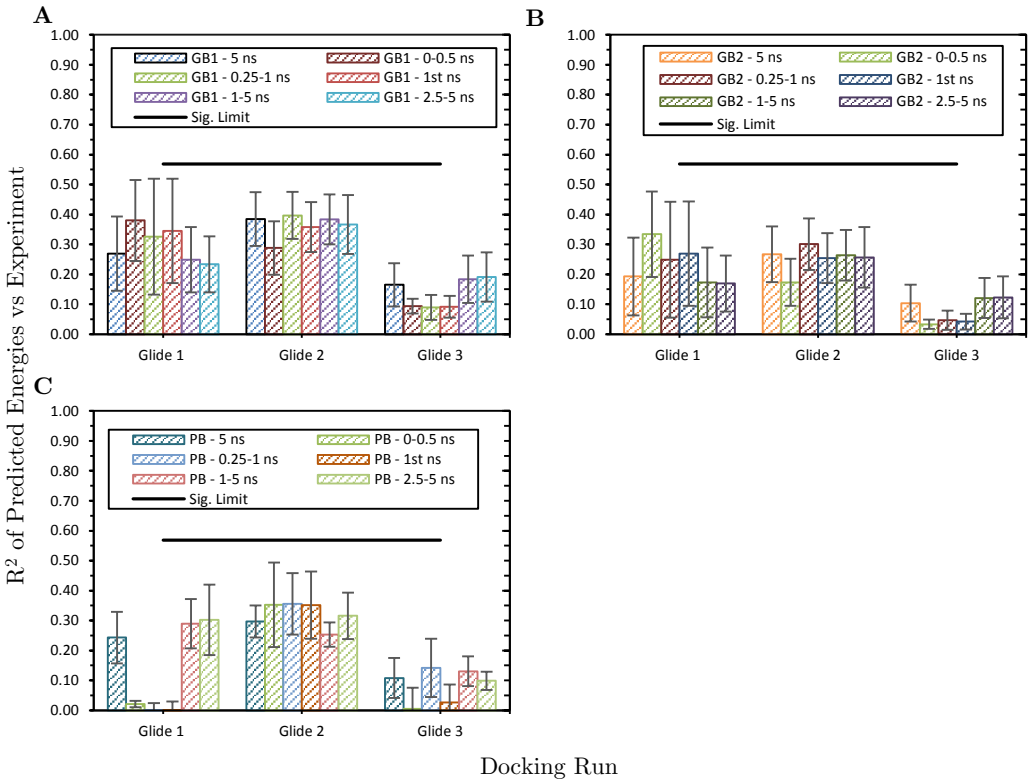


Figure 7.6: Correlation of determination ($R^2$) versus experiment for a range of intervals of the simulation (all 5 ns, 0 to 0.5 ns, 0.25 to 1 ns, 1st ns, 1 to 5 ns, and 2.5 to 5 ns) grouped by docking run. Plots A to C each correspond the different implicit models, including GB1, GB2, PB, respectively. Error bars show the standard error of the mean obtained from three independent trajectories.

error bars large, overall GB1 performed slightly better across all docking jobs for this dataset.

As in Thrombin (see relevant section in paragraph 7.3.1), a range of different intervals of the simulation were further investigated. The results of the $R^2$ of predicted versus experimental affinities with error bars, is shown in Figure 7.6. The correlations obtained were largely similar across the different intervals and were noisy. The errors are indicative of the sensitivity to structure differences amongst the snapshots analysed. Unlike all other observations, PB results show that any correlation obtained from various intervals of the 1st nanosecond give values of $R^2$ equal to zero. Owing perhaps to noise, however, considering none of the obtained correlations are

statistically significant, or in other words the null hypothesis, which assumes the observations were obtained at random, was not rejected, indicates this is likely be fortuitous.

***Comparison with minimisation methods and implicit solvent MD***

Table 7.4: P-values from paired t-test comparisons of the $R^2$ and Kendall tau ($\tau$) between minimised (both rigid and flexible, i.e. MinR and MinF respectively), MD implicit 1ns (MDimp1ns), and MD explicit (MDexp) for model GB1 and GB2. Comparisons for which the difference of the means is significant are shown in bold (for a 5% significance).

| | MinR - MDimp1ns | MinR - MinF | MinR - MDexp | MinF - MDimp1ns | MinF - MDexp | MDimp1ns - MDexp |
|---|---|---|---|---|---|---|
| GB1 – $R^2$ | 0.098 | 0.071 | 0.377 | 0.265 | **0.012** | 0.171 |
| GB1 - $\tau$ | 0.225 | 0.742 | 0.300 | 0.184 | 0.529 | 0.184 |
| GB2 – $R^2$ | 0.184 | 0.513 | 0.112 | 0.967 | 0.357 | 0.543 |
| GB2 - $\tau$ | 0.098 | 0.580 | 0.044 | 0.150 | 0.524 | 0.264 |

Considering that for this target none of the correlations (both $R^2$ and $\tau$) obtained by any of the methods used in this chapter and in Chapter 6, were statistically significant, i.e. there is a high probability they were random, a head to head comparison of the values of the metrics ($R^2$ and $\tau$) for each model and Glide set of poses, cannot provide robust insights. However, a paired t-test, as in the previous dataset, was performed for models GB1 and GB2 across the different methods for both $R^2$ and $\tau$, to assess if overall (amongst the three docking runs) any of the models performed significantly different. The results are summarised in Table 7.4. Significance was identified

for one only pair. Individual $R^2$ values show explicit MD performed worse than minimisation with flexible protein, although this is likely to be fortuitous.

### 7.4.2 Summary

The results from three independent explicit solvent molecular dynamics simulations post-processed by three commonly used MM-PBSA/GBSA implementations, were presented in this section, for the 7-ligand dataset of β-Secretase. Theoretical estimates were in poor agreement with experimental measurements. Predictions from models GB1, GB2, and PB yielded a mean signed error of -71.54 kcal $mol^{-1}$ and -67.59 kcal $mol^{-1}$, and -19.59 kcal $mol^{-1}$. The correlation coefficient ranged from as low as 0.10 (job3 using GB2) to a modest 0.38 (job2 using GB1), which was not statistically significant at a 5% significance level.

It is apparent that the results did not justify the increased computational overhead, and in this case additional sampling has not proved successful to overcome inherent methodological limitations.

## 7.5 Factor XA

The PDB structure 1FJS (resolution = 1.92 Å) [114] was used with the 22-ligand dataset as described in Chapter 4. At this stage it should be reminded to the reader that for this dataset a complete set of job 1 poses were not obtained, and therefore results are reported only for jobs 2 and 3.

### 7.5.1 Explicit solvent results

The results from three independent MD simulations using explicit waters following post-processing with three different implicit solvent models (GB1,

GB2, and PB) are shown in Table 7.5. The metrics calculated to assess the performance of the models are the same as in the previous sections of this

Table 7.5: Predicted Binding affinities (kcal mol$^{-1}$) of the 22 Factor XA ligands with the various methods. Reported errors are standard errors of the mean over the three 5 ns MD trajectories.

| | GB1 | | GB2 | | PB | | Exp.[a] |
|---|---|---|---|---|---|---|---|
| Ligand | Glide 2 | Glide 3 | Glide 2 | Glide 3 | Glide 2 | Glide 3 | |
| 1 | -51.6 ± 0.4 | -57.2 ± 0.6 | -38.8 ± 0.4 | -41.5 ± 0.5 | -18.5 ± 0.8 | -21.6 ± 0.6 | -8.99 |
| 2 | -52.9 ± 0.4 | -53.0 ± 0.6 | -40.2 ± 0.3 | -40.4 ± 0.5 | -22.0 ± 0.7 | -22.2 ± 0.3 | -8.13 |
| 3 | -53.8 ± 0.8 | -56.0 ± 0.5 | -40.5 ± 0.6 | -43.1 ± 0.4 | -21.2 ± 0.3 | -24.5 ± 0.5 | -9.75 |
| 4 | -55.3 ± 1.0 | -56.0 ± 0.6 | -42.1 ± 0.9 | -42.8 ± 0.6 | -25.6 ± 1.0 | -25.9 ± 0.5 | -8.03 |
| 5 | -52.9 ± 0.3 | -52.8 ± 0.5 | -40.4 ± 0.4 | -40.3 ± 0.4 | -22.2 ± 0.6 | -22.4 ± 0.7 | -7.69 |
| 6 | -47.1 ± 0.0 | -47.7 ± 0.4 | -35.2 ± 0.0 | -35.1 ± 0.4 | -19.3 ± 0.7 | -20.1 ± 0.5 | -7.52 |
| 7 | -54.3 ± 1.5 | -54.6 ± 0.2 | -40.9 ± 1.1 | -40.8 ± 0.3 | -25.3 ± 1.1 | -24.3 ± 0.6 | -9.33 |
| 8 | -54.2 ± 0.9 | -55.2 ± 0.3 | -41.0 ± 0.8 | -41.9 ± 0.2 | -24.5 ± 0.5 | -24.7 ± 0.4 | -8.62 |
| 9 | -53.2 ± 0.5 | -54.4 ± 0.5 | -40.6 ± 0.5 | -41.9 ± 0.4 | -23.4 ± 0.4 | -249 ± 0.4 | -8.06 |
| 10 | -52.3 ± 0.5 | -52.4 ± 0.1 | -39.4 ± 0.5 | -39.4 ± 0.1 | -22.5 ± 0.2 | -22.2 ± 0.2 | -7.88 |
| 11 | -50.4 ± 0.6 | -49.5 ± 0.3 | -38.7 ± 0.6 | -37.6 ± 0.2 | -21.8 ± 0.5 | -21.1 ± 0.2 | -7.54 |
| 12 | -52.1 ± 1.1 | -50.1 ± 0.6 | -40.2 ± 1.0 | -38.3 ± 0.6 | -21.5 ± 0.5 | -21.7 ± 0.1 | -7.92 |
| 13 | -47.4 ± 0.8 | -47.3 ± 0.5 | -35.9 ± 1.0 | -35.9 ± 0.3 | -19.5 ± 0.4 | -20.5 ± 0.6 | -7.28 |
| 14 | -52.2 ± 0.7 | -52.0 ± 0.4 | -39.5 ± 0.6 | -39.1 ± 0.4 | -21.5 ± 0.3 | -21.0 ± 0.4 | -7.96 |
| 15 | -56.2 ± 0.7 | -56.7 ± 0.4 | -43.1 ± 0.6 | -43.5 ± 0.4 | -25.0 ± 0.9 | -26.9 ± 0.1 | -9.40 |
| 16 | -57.6 ± 0.4 | -56.9 ± 0.7 | -43.7 ± 0.3 | -43.2 ± 0.7 | -28.3 ± 0.8 | -27.4 ± 0.5 | -8.91 |
| 17 | -55.6 ± 1.4 | -58.7 ± 0.6 | -41.8 ± 1.4 | -44.6 ± 0.5 | -23.0 ± 1.1 | -26.4 ± 0.6 | -10.78 |
| 18 | -55.5 ± 0.7 | -48.4 ± 1.7 | -43.6 ± 1.0 | -37.4 ± 1.5 | -23.8 ± 2.2 | -19.8 ± 1.4 | -12.00 |
| 19 | -55.0 ± 0.3 | -53.7 ± 0.1 | -41.1 ± 0.1 | -40.1 ± 0.5 | -24.8 ± 0.3 | -23.5 ± 0.6 | -8.13 |
| 20 | -59.7 ± 0.4 | -57.3 ± 0.6 | -45.0 ± 0.3 | -42.9 ± 0.7 | -27.7 ± 0.1 | -24.8 ± 0.3 | -9.87 |
| 21 | -52.0 ± 0.6 | -54.0 ± 0.3 | -38.4 ± 0.5 | -42.0 ± 0.6 | -20.5 ± 0.4 | -23.1 ± 0.5 | -11.70 |
| 22 | -57.0 ± 0.4 | -56.7 ± 0.1 | -43.1 ± 0.3 | -42.8 ± 0.1 | -22.9 ± 0.3 | -22.8 ± 0.3 | -8.03 |
| Range | 12.6 | 11.7 | 9.8 | 9.5 | 9.8 | 7.6 | 4.72 |
| MAD | 2.0 ± 0.1 | 2.4 ± 0.1 | 1.6 ± 0.1 | 1.9 ± 0.1 | 2.1 ± 0.1 | 1.7 ± 0.0 | |
| $R^2$ | **0.2 ± 0.0 (0.045)** | 0.1 ± 0.0 (0.161) | 0.2 ± 0.0 (0.056) | 0.1 ± 0.0 (0.099) | 0.0 ± 0.0 (0.410) | 0.0 ± 0.0 (0.318) | |
| $\tau$ | **0.4 ± 0.0 (0.005)** | **0.5 ± 0.0 (0.002)** | **0.4 ± 0.1 (0.009)** | **0.5 ± 0.0 (0.003)** | 0.3 ± 0.0 (0.075) | **0.3 ± 0.0 (0.026)** | |

*Excluding ligand 7

[a] Refers to Experimental energies calculated using the formula $\Delta G = -RT ln K_i$

*p*-values for $R^2$ and $\tau$ are shown in brackets. Highlighted in bold are significant measurements within a 5% significance level. ALthMAD corresponds to the Mean Absolute Deviation of the differences between the predicted and experimental binding energies.

chapter, and include the range of the estimates, the MAD of the signed error, the $R^2$, and Kendall's tau ($\tau$). Errors reported are standard errors of the mean over the three trajectories and p-values are reported for the last two metrics. Experimental measurements are converted to units of kcal $mol^{-1}$.

The GB1 predictions show a smaller range (about 2-fold of experiment) compared to the previous systems (12.59, and 11.66 kcal $mol^{-1}$ for Glide 2 and 3), but the mean signed error remained systematically large, at -44.76 and -44.70 kcal $mol^{-1}$ for Glide 2 and 3 respectively. Unlike the previous systems, uncertainties were low (in most cases below 1 kcal $mol^{-1}$). The $R^2$ was 0.19 and 0.10 for Glide and 3 respectively. Owing to the large dataset size, the former (0.2) was found to be statistically significant, though with a p-value just below 5% (0.045) it is questionable (see Figure 7.7 A). Kendall tau was better at 0.43 for Glide 2 and 0.47 for Glide 3, which shows about half of the inhibitors are ranked correctly; however this is mainly due the most potent ligands which, as shown in Figure 7.8 A, are incorrectly ranked. This also appears for to be the reason for the observed low values of $R^2$. As discussed in section 6.5.2, the common structural characteristic among these ligands is a polar substituent in the R1 position (see Figure 4.12 and Table 4.3), which is para to the amidine with the purpose to interact with Ser195. This part of the molecule is positioned in the deep S1 pocket and consequently poses a challenge for the implicit solvent. The result is an underestimated binding free energy.

The observations for the GB2 predictions were closer to experiment. Here a smaller range in the estimates was obtained (9.76 and 9.49 kcal $mol^{-1}$ respectively for Glide 2 and 3) and a lower mean signed difference of -31.82 kcal $mol^{-1}$ on average. The lower range also meant a lower MAD of 1.62 and 1.89 kcal $mol^{-1}$ for Glide 2 and 3. The $R^2$ values were all very low and statistically insignificant (see Figure 7.7 A). Kendall's tau however, was statistically significant. The scatter plot in Figure 7.8 B shows a similar distribution of the data as in GB1.

Consistent with the results presented thus far in this chapter, the PB predictions were more centred on the experimental results with a mean signed difference of -14.15 and -14.47 kcal mol$^{-1}$ for Glide 2 and 3. The average range (8.68 kcal mol$^{-1}$) and MAD (1.86 kcal mol$^{-1}$) were also lower than for GB1

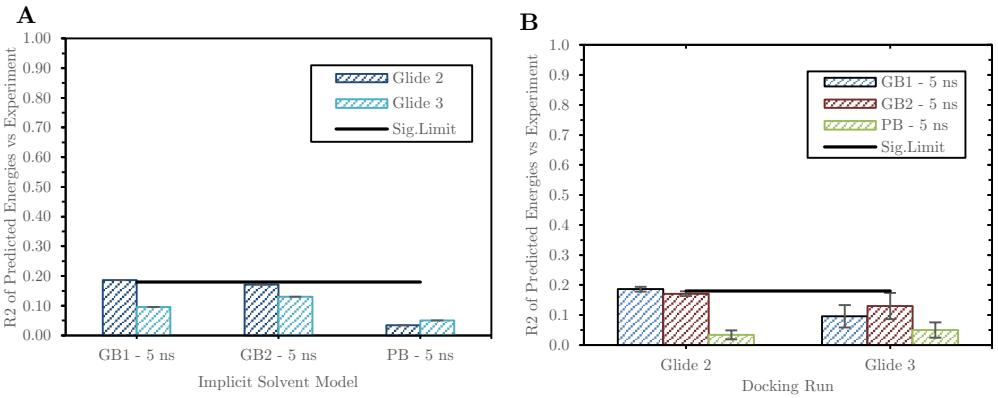


Figure 7.7: Correlation of determination ($R^2$) versus experiment. Results are grouped in Model used (A), and in docking run (B). Data is shown for the entire 5 ns of MD simulations. Error bars show the standard error of the mean obtained from three independent trajectories.

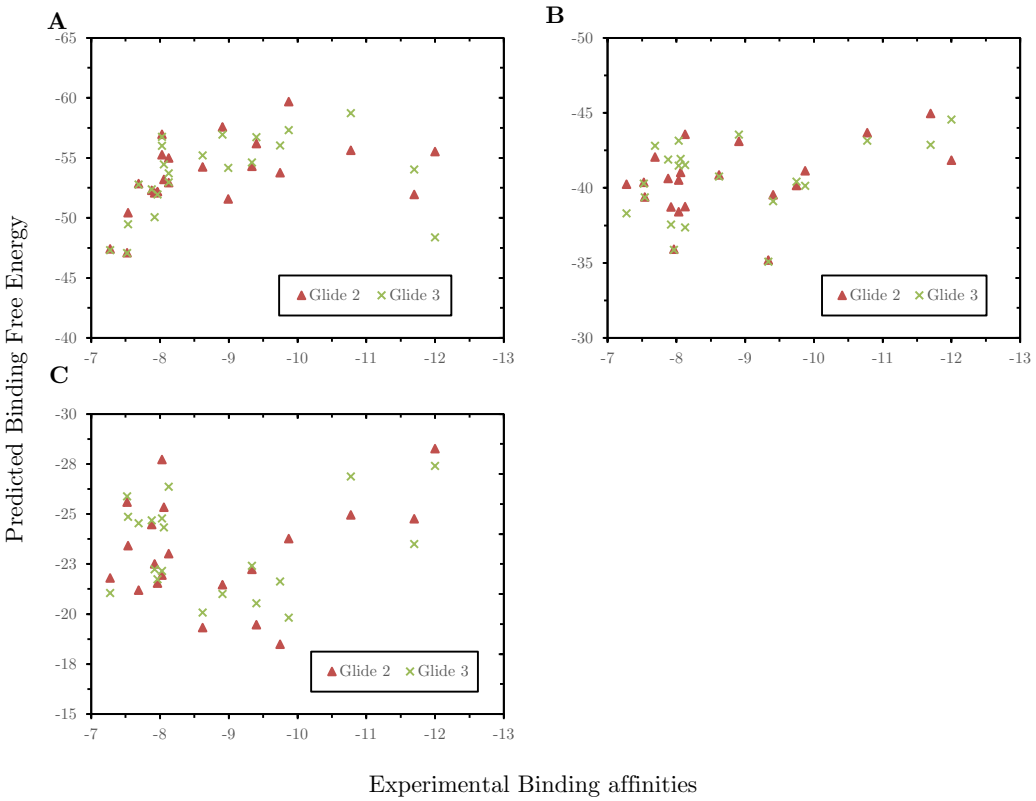


Figure 7.8: Scatter plots of the predicted and experimental binding affinities for Factor XA. Plots A through C correspond to models GB1, GB2, PB, respectively. Results are averages over three independent 5 ns MD simulations. Errors are not included for clarity, but can be seen in Table 7.5.

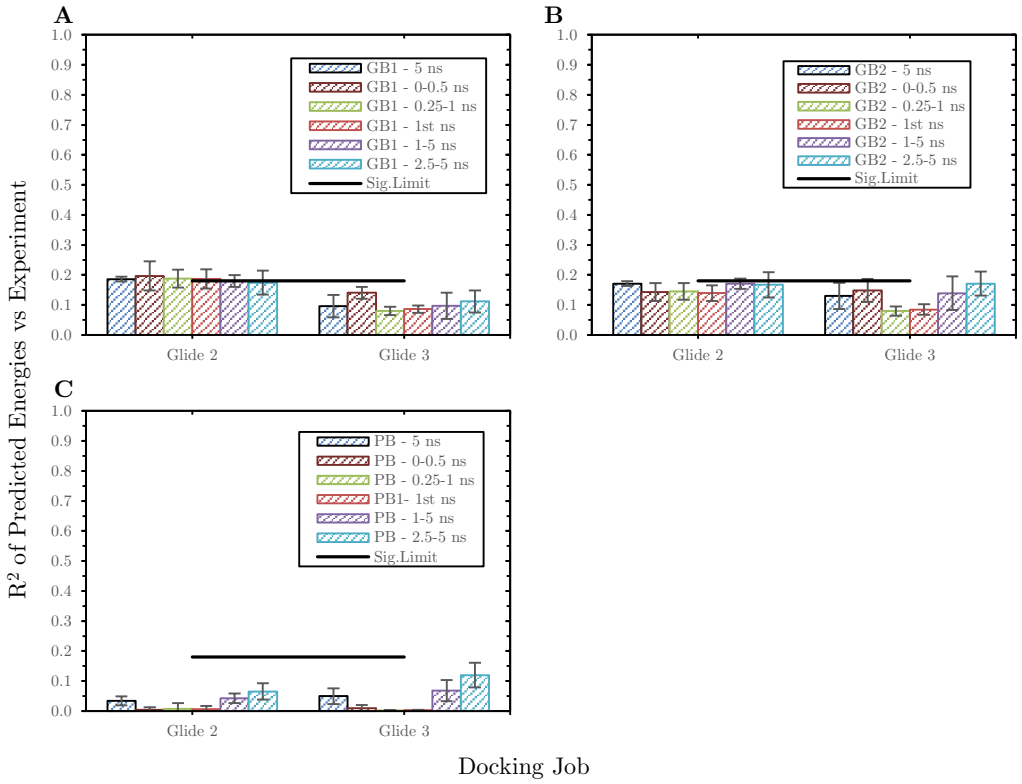


Figure 7.9: Correlation of determination ($R^2$) versus experiment for a range of intervals of the simulation (all 5 ns, 0 to 0.5 ns, 0.25 to 1 ns, 1$^{st}$ ns, 1 to 5 ns, and 2.5 to 5 ns) grouped by docking job. Plots A through each correspond the different implicit models, including GB1, GB2, PB, respectively. Error bars show the standard error of the mean obtained from three independent trajectories.

and GB2. On the other hand, both correlation metrics were worse, and are shown in Figure 7.7 A, and Figure 7.8 C.

A range of intervals of the length of the trajectory were chosen for further analysis. Figure 7.9 shows the results for the $R^2$ of predicted affinities with experimental results and the standard error of the mean as error bars. Although all the results are very poor, they are equivalent to the full 5 ns trajectory even when only the first half nanosecond is taken into account. Again this is in agreement with some recent studies where numerous short runs are preferred over longer simulations.[101, 170, 171]

### *Comparison with minimisation methods and implicit solvent MD*

Surprisingly the $R^2$ results presented in this chapter are significantly inferior to those obtained from rigid protein minimisations (0.19 vs 0.49 for job2 and GB1, 0.10 vs 0.38 for job3 and GB1, 0.17 vs 0.48 for job2 GB2, and 0.13 vs 0.32 for job3 and GB2). This could be perhaps attributed on the "rigidity" of the minimisations versus the simulations, which could have a significant effect considering the flexibility of the part of the ligand that is positioned in the highly polarizable S3 and S4 binding pockets (the aromatic box discussed in section 4.4).[117]

Both the results in this chapter and the flexible protein minimisation results ($R^2$ with experiment) performed poorly. The results presented in this chapter although they were slightly better than the flexible protein minimisation results, they were not statistically significant, hence it is likely they were fortuitous.

On the other hand Kendall tau predictions presented in this chapter were statistically significant (within a 5% significance level). Overall very similar values were obtained using explicit simulations when compared to those obtained from the rigid-protein minimisations and implicit MD, and improved from the insignificant values given by the flexible-protein minimisations. More specifically the $\tau$ for GB1 rescoring Glide 2 using explicit solvent gave 0.43 compared to 0.61, 0.15 and 0.24, obtained from rigid-protein minimisations, flexible-protein minimisations and 1 ns implicit MD simulations, respectively. In a similar manner for the same protocols (values in same order) GB1 with Glide 3 applied here gave 0.47 compared to 0.30 (not significant), 0.20 and 0.32. Similarly, for GB2 the Glide 2 and 3 $\tau$ values were respectively 0.40 and 0.46 compared to 0.55, 0.25, and 0.33 for Glide 2, and 0.34, 0.26, and 0.39 for Glide 3, when rigid-protein and flexible-protein minimisations, and 1 ns implicit MD simulations, were used respectively. All had in common the wrong prediction of the 6 most potent ligands (discussed earlier in this

chapter and Chapter 6) meaning that for larger datasets, when highly polar interactions are limited, ranking predictions can be good.

When comparing the data ($R^2$) reported in this chapter with the results from the implicit solvent MD, GB1 models performs similarly for both Glide 2 and 3; that is, 0.19 with explicit MD vs 0.13 1 ns implicit MD for Glide 2, and for Glide 3, 0.10 vs 0.10. If the GB1 explicit MD results are compared to the 10 ns implicit MD the outcome is different. In this case explicit MD performs worse (10 ns implicit MD $R^2$: 0.33 which is significant). The same was found for GB2 in which case explicit MD gave an $R^2$ of 0.13 and 0.03 for Glide docking runs 2 and 3 respectively, while the results from 1 ns MD with implicit solvent, was 0.23 and 0.42 respectively for Glide 2 and 3. Therefore, again, we found explicit MD not to be adding value to the final results.

Table 7.6: P-values from paired t-test comparisons of the $R^2$ and Kendall tau ($\tau$) between minimised (both rigid and flexible, i.e. MinR and MinF respectively), MD implicit 1ns (MDimp1ns), and MD explicit (MDexp) for model GB1 and GB2. Comparisons for which the difference of the means is significant are shown in bold (for a 5% significance).

| | MinR - MDimp1ns | MinR - MinF | MinR - MDexp | MinF - MDimp1ns | MinF - MDexp | MDimp1ns - MDexp |
|---|---|---|---|---|---|---|
| GB1 – $R^2$ | 0.100 | 0.089 | **0.030** | 0.134 | 0.264 | 0.594 |
| GB1 - $\tau$ | 0.358 | 0.529 | 0.984 | 0.119 | **7.5E-10** | 0.069 |
| GB2 – $R^2$ | 0.212 | 0.748 | 0.140 | 0.204 | 0.547 | 0.365 |
| GB2 - $\tau$ | 0.323 | 0.626 | 0.916 | 0.126 | 0.077 | **0** |

### 7.5.2 Summary

The effects of additional sampling resulting from three independent simulations of 5 ns on the calculated MM-PBSA/GBSA energy for the Factor XA dataset was investigated. Despite a reduced range and MAD, the predicted estimates of binding affinity were systematically more negative than experiment, by 44.73 kcal $mol^{-1}$ when GB1 was used, 31.82 kcal $mol^{-1}$ when GB2 was used, and 14.31 kcal $mol^{-1}$ when PB was used. Qualitatively, the performance was particularly poor across all models, with PB the worst performer. In accordance to the findings for the other targets, it was found that shorter MD trajectories yield equivalent quality metrics. On the other hand ranking was significant and with small variability consistent with results from rigid protein minimisation and implicit solvent MD simulations, serving as an indication that for large datasets there could applications of the methods (using minimisation not explicit MD) at earlier stages in the drug design process. Overall, however, again here, the expense of these calculations did not corroborate in the results.

## 7.6 HIV-1 Protease

The PDB structure 2PQZ (resolution = 1.55 Å) [122] was used with the 13-ligand dataset as described in Chapter 4. A complete set of Glide 1 and Glide 3 docked poses were not obtained, and therefore results are reported only for Glide 2 docking run.

### 7.6.1 Explicit solvent results

The same protocol of three independent explicit solvent MD simulations followed by MM-PBSA/GBSA energy calculations, was performed for this dataset. The results are shown in Table 7.7. Metrics included are the range of

predicted affinities, the MAD of the signed error, the $R^2$, and Kendall's tau (with p-values in brackets).

Table 7.7: Predicted Binding affinities (kcal $mol^{-1}$) of the 13 HIV-1 Protease ligands with the various methods. Reported errors are standard errors of the mean over the three 5 ns MD trajectories.

| | GB1 | GB2 | PB | Exp.[a] |
|---|---|---|---|---|
| Ligand | Job2 | Job2 | Job2 | |
| 1 | -57.2 ± 2.8 | -47.7 ± 2.6 | -24.7 ± 1.3 | -6.74 |
| 2 | -55.1 ± 4.6 | -46.1 ± 3.0 | -21.0 ± 3.3 | -5.67 |
| 3 | -66.7 ± 0.5 | -56.7 ± 0.6 | -27.9 ± 0.9 | -7.96 |
| 4 | -65.5 ± 1.6 | -53.3 ± 2.4 | -23.1 ± 1.4 | -7.78 |
| 5 | -71.6 ± 1.59 | -60.5 ± 2.0 | -28.7 ± 0.7 | -8.70 |
| 6 | -77.7 ± 2.9 | -67.0 ± 3.2 | -32.2 ± 0.4 | -8.80 |
| 7 | -75.5 ± 2.9 | -63.8 ± 3.2 | -28.1 ± 0.7 | -8.37 |
| 8 | -62.4 ± 1.4 | -50.0 ± 1.8 | -26.1 ± 0.5 | -8.47 |
| 9 | -61.5 ± 3.2 | -51.8 ± 2.3 | -22.3 ± 3.4 | -8.39 |
| 10 | -79.3 ± 1.1 | -67.2 ± 1.4 | -30.8 ± 1.3 | -7.91 |
| 11 | -80.5 ± 0.5 | -66.4 ± 0.5 | -23.7 ± 1.1 | -9.05 |
| 12 | -83.8 ± 3.4 | -69.5 ± 3.3 | -26.4 ± 0.6 | -9.81 |
| 13 | -78.3 ± 1.8 | -65.3 ± 1.3 | -25.7 ± 1.8 | -9.02 |
| Range | 28.7 | 23.5 | 11.36 | 4.15 |
| MAD | 7.6 ± 0.7 | 6.7 ± 0.5 | 2.5 ± 0.6 | |
| $R^2$ | **0.6 ± 0.1 (0.001)** | **0.6 ± 0.1 (0.002)** | 0.2 ± 0.1 (0.165) | |
| $\tau$ | **0.6 ± 0.1 (0.002)** | **0.5 ± 0.1 (0.010)** | 0.2 ± 0.1 (0.367) | |

*Excluding ligand 7

[a] Refers to Experimental energies calculated using the formula $\Delta G = -RT ln K_i$. *p*-values for R2 and $\tau$ are shown in brackets. Highlighted in bold are significant measurements within a 5% significance level. MAD corresponds to the Mean Absolute Deviation of the differences between the predicted and experimental binding energies.

The PB predicted energies showed the smallest mean signed error at -18 kcal $mol^{-1}$ compared to -62.18 kcal $mol^{-1}$ and -50.65 kcal $mol^{-1}$ when models GB1 and GB2 were used. PB estimates were found to be the closest to the

experimental range (11.26 kcal $mol^{-1}$ compared to 28.65 and 23.45 kcal $mol^{-1}$ for GB1 and GB2 respectively). Qualitatively however, PB estimates performed the worst. The $R^2$ for PB was not significant at 0.17 compared to the decent correlations obtained from the two GB models (0.63 with GB1 and 0.58 with GB2). Figure 7.10 shows the $R^2$ measurements between predicted affinities and experiment. Similarly a decent Kendall tau was obtained with use of the GB models (0.64 and 0.54 with GB1 and GB2 respectively). Scatter plots of the estimates versus experimental data are shown in Figure 7.11 (A for GB1, B for GB2, and C for PB).

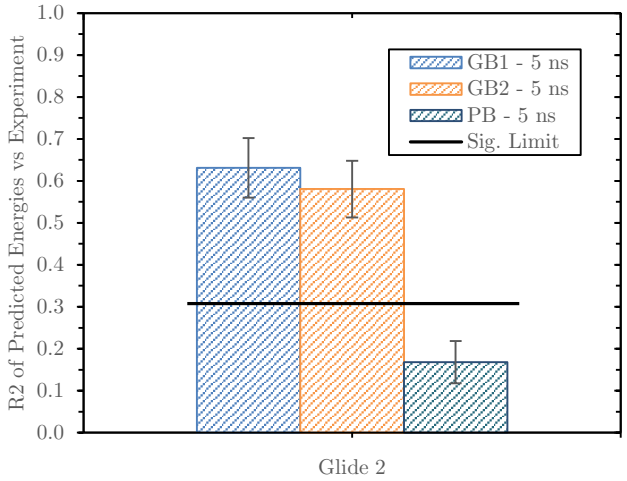


Figure 7.10: Correlation of determination ($R^2$) versus experiment. Data is shown for the entire 5 ns of MD simulations. Error bars show the standard error of the mean obtained from three independent trajectories.

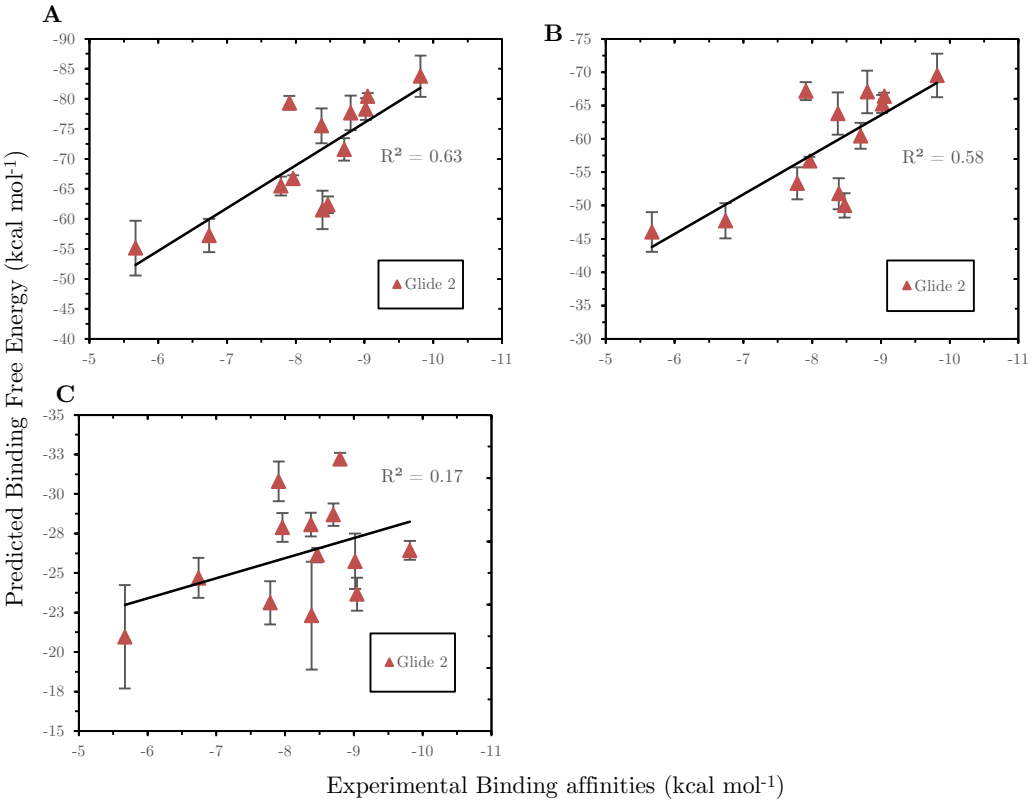


Figure 7.11: Scatter plots of the predicted and experimental binding affinities for HIV 1 Protease. Plots A through C correspond to models GB1, GB2, PB, respectively. Results are averages over three independent 5 ns MD simulations.

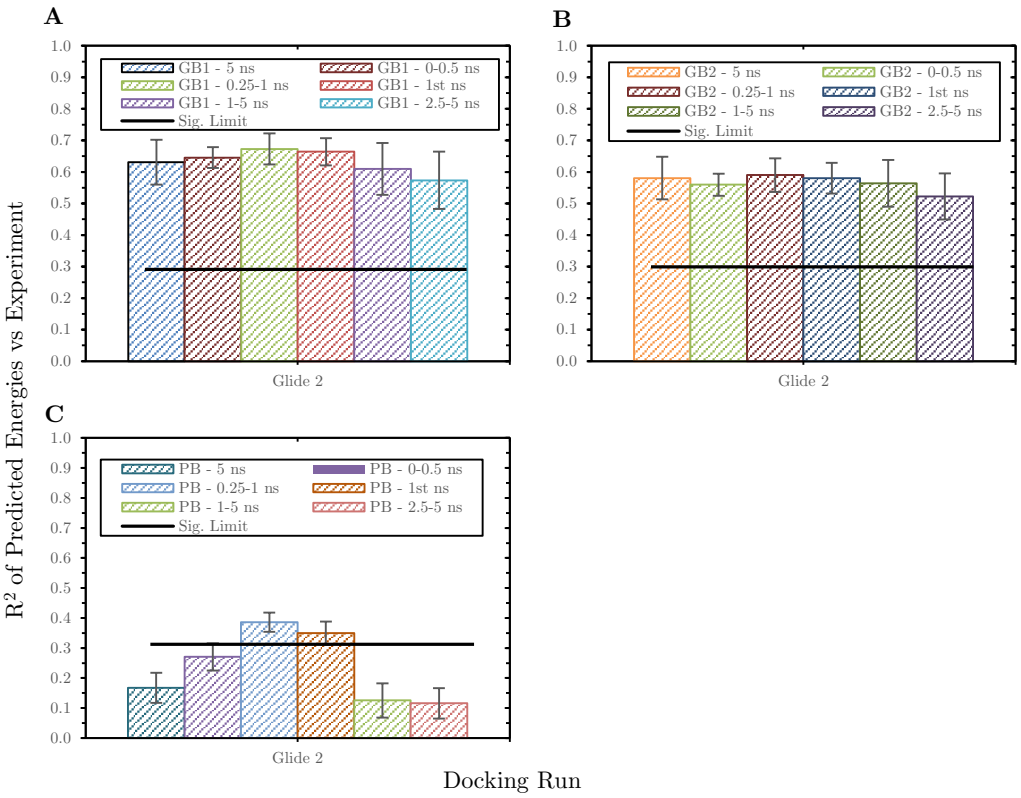


Figure 7.12: Correlation of determination ($R^2$) versus experiment for a range of intervals of the simulation (all 5 ns, 0 to 0.5 ns, 0.25 to 1 ns, 1$^{st}$ ns, 1 to 5 ns, and 2.5 to 5 ns) grouped by docking job. Plots A through each correspond the different implicit models, including GB1, GB2, PB, respectively. Error bars show the standard error of the mean obtained from three independent trajectories.

Figure 7.12 shows the $R^2$ of predicted affinities with experiment, following investigation of a range of lengths taken from the 5 ns trajectory. In agreement with the other targets, it has been shown that shorter simulations, of even a half a nanosecond, are able to give similar, or in this case, equivalent results with the 5 ns runs.

### *Comparison with minimisation methods and implicit solvent MD*

The results presented here were found to be similar to the results obtained from the minimisation protocols. Comparing the metric $R^2$, using GB1 model here ($R^2$ = 0.63), showed a 20% improvement compared to rigid-protein minimisation ($R^2$ = 0.41) and 6% against the flexible-protein minimisations

($R^2$ = 0.57). On the other hand, using GB2 model to post-process the snapshots generated with explicit MD ($R^2$ = 0.58), equivalent results were found when compared with the rigid-protein minimisations ($R^2$ = 0.56), but slightly worse when compared with flexible-protein minimisations ($R^2$ = 0.65). Ranking was also improved with explicit simulations over simple minimising of the structures. The improvements obtained ranged from 10% (GB2 from 0.44 in flexible-protein minimisations to 0.54 with explicit solvent) up to 26% (GB1 from 0.38 in rigid-protein minimisations to 0.64 using MD in with explicit solvent).

The GB1 predicted energies $R^2$ was almost identical to those obtained from implicit MD simulations (0.70 and 0.67 for 10 ns and 1 ns implicit solvent MD respectively), while there was an improvement of 16% when GB2 models were compared (0.42). Kendall tau values were equivalent and in some cases improved (GB2 from 0.31 from 1 ns implicit solvent MD to 0.54 herein).

### 7.6.2 Summary

Models GB1 and GB2 performed similarly achieving decent correlations. PB predictions however, showed a poor qualitative agreement with experiment. Comparison with minimisation protocols and implicit solvent molecular dynamics, showed similar values of $R^2$. On the other hand a slight improvement in the rank ordering of the compounds was obtained after performing explicit MD simulations. Therefore our results show that overall it is not worth it performing explicit MD simulations

Investigation of various segments of the trajectory revealed that much shorter simulation lengths can give similar or even better results.

## 7.7 Conclusions

A key limitation of fast re-scoring techniques is the dependence on the initial structure and the lack of sufficient sampling. The present study set out to

investigate the effect of sampling by performing expensive molecular dynamics simulations using explicit solvent. To allow for the calculation of statistical uncertainties the results were averaged over three independent molecular dynamics simulations. Binding energies were calculated from the same snapshots using two of the most commonly used GB models in AMBER. For comparison binding energies were also calculated using a PB implementation, also in AMBER.

The correlation between calculated and experimental binding free energies when PB was used, was poor for all the systems. The results between the two GB models were overall similar in comparison to the larger discrepancies observed in Chapter 6. Quantitatively the calculated binding free energies were systematically more negative than experiment, but GB2 energy estimates were in general slightly less negative. The magnitude of the uncertainties (standard error of the mean calculated from 3 independent repeats) indicated that perhaps a larger number of simulations would be required. Meanwhile, the energies between the three repeats differed by what was expected by the standard error.

The simulations were significantly more stable when compared to the implicit solvent simulations, with low RMSD values overall, while the large movements observed when using implicit solvent were not observed here. However, despite the stability of the structural data, the correlations with experiment did not improve significantly and in many cases were found to be the same or even worse. This was with the exception of HIV 1 Protease which showed improvement or equivalent performance in both $R^2$ and ranking ($\tau$) when compared to the protocols in Chapter 6. Ranking (Kendall's tau) generally showed some improvement over the results in the previous chapter. Statistically significant values (for a 5% significance) for ranking were found for all targets except for β-Secretase which was overall the worst performer.

Pairwise comparisons between the GB calculations in this chapter and those performed in Chapter 6, were explored using paired t-tests to identify

how the methods performed comparatively. Most results showed no statistical difference between the means of the metrics compared ($R^2$ and $\tau$), i.e. the null hypothesis (equal means) was not rejected. However, we also found that for Thrombin implicit MD results ($R^2$) were significantly different than both flexible-protein minimisations and explicit MD results; the latter, however, displayed large errors in $R^2$ and therefore the t-test results should be taken lightly. For Factor Xa, paired t-test showed that minimisations with the protein kept rigid gave statistically significantly different results from the calculations using explicit solvent MD (reported p-value = 0.03). Combining this with the values of $R^2$ it can be concluded that results using rigid-protein minimisations correlated with experiment significantly better than those following post-processing of explicit solvent MD simulations. Finally ranking of Factor Xa ligands was significantly better as obtained in this chapter when compared to the flexible-minimised calculations.

In addition, an important observation was made that across all systems equivalent results were obtained from analysis of much shorter lengths of simulation. Though this was not an in-depth study, it did highlight that perhaps increasing of the simulation length did not add any value.

Overall, it can be concluded that, although explicit solvent simulations yielded more stable results (i.e. better quality snapshots), with reduced differences in performance between the two GB models, they did not offer significant added value to justify the computational overhead, failing to overcome or reduce the effect/influence on energy estimates, of inherent methodological limitations.

# Chapter 8

# Concluding Remarks

Most drugs exert their action by binding to a macromolecule target, e.g. a protein. Hence estimating the binding affinity, using computer programs is of utmost importance in the drug design process.[5] It is commonly viewed that binding free energy calculations are too time consuming to be of practical use as a tool in drug design. The reason for this primarily lies with the requirement of multiple lengthy simulations of a large number of molecules to obtain binding free energies with a precision similar to those measured experimentally. Typically, free energy methods involve alchemical transformations of one molecule to another, to estimate the relative free energy difference between the two. This requires the simulation of many intermediate structures during the morphing of one molecule to the other.

End-point methods were developed as a way to circumvent this and reduce the computational cost by considering only the end states. The most popular of these methods is the methodology studied in this thesis: MM-PBSA/GBSA. A unified presentation of this method was published by Kollman et al. over a decade ago in a paper declaring that a new era of biomolecular simulations had begun.[7] Initially the method was applied as a simpler alternative to rigorous free energy methods to make quantitative

predictions with experiment. Owing to methodological challenges with such predictions, further approximations were soon implemented (such as a single trajectory approach, implicit MD or minimisations instead of explicit solvent, and exclusion of entropy), to be used for qualitative predictions with experiment, in earlier stages of drug design, such as high throughput screening and early stages of lead optimisation.

There is evidence in the literature that MM-PBSA/GBSA can be used as a fast rescoring tool of docked poses to improve results over docking both in terms of qualitatively estimating the binding affinity, but also improving the ranking of the affinities for a congeneric series of ligands. However, there has not been a published study to evaluate the ability and consistency of MM-PBSA/GBSA, and determine its capability as a rescoring tool of docked poses. It is therefore important to test the accuracy of the method, and compare the results obtained from various solvent models.

In Chapter 2, the underlying theoretical background of the methods used in this study were laid out. The basics of statistical mechanics was given, and the importance of the Boltzmann distribution in computational chemistry was described. Through the partition function all of the thermodynamic properties of a system can be extracted. Inter- and intramolecular interactions are calculated via a molecular mechanics force-field, which gives the potential energy of the system. Being able to calculate the interactions between and within molecules, the phase space can then be sampled. This is done using Molecular Dynamics (MD) or Monte Carlo (MC) calculations. Key thermodynamic properties can then be calculated such as the free energy of binding. A brief discussion of a number of rigorous and approximate free energy methods was given.

The theoretical background and the current state of research for the MM-PBSA/GBSA method was dealt with in Chapter 3. A description for each component of the method was given. Emphasis was given on the continuum solvent components. First, the Poisson-Boltzmann equation was defined, and

the reasons associated with its computational cost were laid out. Following this the Born equation was derived and how Still[60] extended this to the generalised Born (GB) model to be applicable for molecular systems, where it is common for radii and distances to be very small. The most challenging term to compute is the *effective* Born radii. The way this term is approximated constitutes the difference between various GB models. This was followed by a brief discussion of the nonpolar solvation term. Having described the range of ways the method has been used (use of explicit versus implicit solvent models to generate the MD trajectories, single versus three trajectory method, and use of only minimisation instead of MD simulation), its application in drug design from the origins of the methodology to the present day was laid out. Also in Chapter 3, the most major and relevant, to the work presented here, methodological limitations associated with using MM-PBSA/GBSA were covered as a basis for the challenges involved with using the method routinely in drug design.

Chapter 4 is dedicated to introducing the protein-ligand systems used in this study. For each system an overview of the biological relevance, mechanism of activity and characteristics of the ligand series is provided. In addition, the key binding site interactions between protein and ligand for each system were presented. The systems studied included 63 ligands across the following 5 proteins: Thrombin (PDB: 1ETT), β-Secretase (PDB: 2P4J), Factor Xa (PDB: 1FJS), HIV-1 Protease (PDB: 2PQZ), and Src Tyrosine Kinase (PDB: 2BDJ).

Chapter 5 details the work performed in attempting to reproduce an all-in-one published protocol for preparing, docking, and rescoring ligands to a target protein using MM-GBSA. This protocol was chosen for a number of factors including, the ease of use, its all-in-one nature, the potential applicability in the drug design process, and finally, the encouraging results. Our investigation showed it was impossible to reproduce the published results. It appears the differences were due to the different software versions used, however the 'black-box' nature of the protocol, made it impossible to pinpoint

the exact changes between software. Assessment of the individual steps of the protocol (docking and rescoring) revealed that with a few exceptions overall identical poses were generated, while the rescoring step differed considerably. The results obtained from our calculations were poor across all targets when compared with experiment. Closer investigation revealed that the published results were only marginally better than our results, with the better performance attributed mainly to the arbitrary assignment of outliers, for which poor or no explanation was provided, and to reporting results from ligand charge states that performed better despite not being physically reasonable, or in other words by manipulations of data. Although E-Novo as an idea is an attractive method, the published study is misleading, and it certainly is not an efficient structure-based lead optimisation tool, as claimed. This finding is important in its own right, and gives an indication that one should not take such encouraging results at face value; however it is not sufficient to overall denounce the performance of MM-GBSA.

In Chapter 6 we set out to investigate the performance of MM-GBSA as a fast physics-based post-docking filter. We attempted to answer questions such as, how well do different MM-GBSA implementations perform on the same input structures, or how sensitive is MM-GBSA when the input structures differ (rescoring different docked poses), or how does the method perform across a range of MM-GBSA implementations (are consistent results obtained), is there a best performer across all systems, or an indication if there is a rescoring method better for one system over another? To give answers to these questions we tested the methodology in a range of software using a range of generalised Born implementations. A total of 4 different docked poses per ligand resulting from two different docking algorithms were tested in a range of MM-GBSA methods from two software. More details on exactly the range of tests performed are shown in Figure 6.1. The tests were performed for 4 out of the 5 protein-ligand datasets. The reason why not all tests were performed for Src Kinase Tyrosine, is detailed in section 6.7.

The results, when compared to experimental binding affinities, were overall poor, system dependent and highly sensitive to the starting configuration (initial pose). HIV-1 Protease was the only case for which correlations with experiment were good and in fact statistically significant for all tests performed. Perhaps this is not surprising as previous published work has shown that scoring functions usually perform well with this target.[79] Despite this, none of the rescoring protocols were able to improve over the docking score. In relation to this, Factor Xa was the only case for which better $R^2$ between estimated and experimental binding affinities were obtained than with docking (when the protein was kept rigid). This was also the dataset with the largest number of ligands (22 ligands), which perhaps is an indicator that the method could be applicable at earlier stages of the drug discovery such as high throughput screening. The ranking of the estimated binding affinity when compared with experimental data, although occasionally gave significant results, overall it performed worse than the coefficient of determination.

Comparisons between the various solvent models were performed to ascertain how robust the methodology is, considering experimental results can potentially be wrong or have large sources of error, which for the systems used in this study are unknown. Varied results were obtained between the different systems. Overall, similarities (mostly qualitative, though in some isolated cases quantitative as well) were found between models of the same software and same setup conditions (i.e. rigid or flexible protein). However, large fluctuations were observed between models of different initial conditions and models from different codes.

The most interesting observation that this comparison study showed, was that, there does not appear to exist one model which performs overall better across all systems, and that there was no indication found for one model to perform well for each system. In simple terms, there was no trend found as to which model one should use. Choosing one model over another

can give vastly different results which in a lead optimisation experiment can prove particularly risky.

MM-GBSA suffers from a number of limitations including implicit solvent approximations resulting in difficulty dealing with charged groups or buried protein interactions, the quality of the underlying potential and forcefield approximations (for more information on methodological limitations see section 3.5). In addition to these limitations, Chapter 6 revealed the sensitivity of the method to the starting configuration of the system, and that using protocols with minimisation does not resolve the problem. This is in agreement with a published study which, amongst other things, found that minute structural changes to initial conformations, could give vastly different results.[103] Considering additional sampling using implicit MD proved futile, the question arises what effect would additional sampling using explicit MD have. This is explored in Chapter 7.

Three independent 5 ns explicit MD simulations were performed for each protein-ligand system, post-processing the generated snapshots using GBSA and PBSA before averaging the results. The findings of the investigation performed here shows that overall PB gave poorer correlations with experimental values, although the absolute difference of theoretical estimates from experimental estimates was smaller than for either the estimates obtained from models GB1 and GB2 (see section 7.2 for solvent model notation). Results also showed that in comparison to the calculations in Chapter 6, models GB1 and GB2 performed similarly (in qualitative terms) with experiment ($R^2$). The magnitude of the uncertainties indicated that a larger number of simulations is required for more accurate results to be obtained, however, the energies between the three repeats were within the standard error of the mean.

Although more stable trajectories were obtained using explicit solvent MD when compared to implicit MD simulations, overall the correlations with experiment ($R^2$) did not improve, while in some cases were even worse.

Kendall tau on the other hand showed some improvement with statistically significant values obtained for all systems with the exception of β-Secretase, which was the worst performer.

Paired t-tests between the results in Chapter 7 and the ones in Chapter 6 showed that in the majority of the cases the null hypothesis cannot be rejected, meaning the means of the observations are the same, or in other words that the observations are not statistically different (i.e. explicit MD did not add value). An exception was Factor Xa in which case the estimations obtained using rigid protein minimisations were shown to be significantly better than those obtained using explicit MD. T-tests for Thrombin showed that in this case flexible protein minimisations were significantly better than implicit MD simulations, but no difference was found with explicit MD. Finally, ranking of the compounds for Factor Xa was significantly improved when using explicit solvent MD for the generation of the trajectories.

Another interesting observation that resulted from Chapter 7, was that shorter MD simulations (in fact even only 0.5 ns) can give equivalent results to those obtained after 5 ns of explicit MD simulation. We conclude that although for Factor Xa ranking of inhibitor was improved, overall the results could not justify the additional computational overhead associated with performing explicit MD simulations.

The present study set out to investigate and critically assess the performance of MM-PBSA/GBSA as a rescoring tool in the drug design, and it can be said that this was achieved. This thesis has highlighted the challenges associated with the method, and has shown that despite some claims in literature, the method in its current state, and as applied in this particular study and systems, does not appear promising for routine use in the lead optimisation context. Most importantly we showed that large discrepancies can be obtained from different solvent models, even if they are closely related and from the same code. In addition, we were not able to identify a trend of a model that performs better for a certain system. In the literature it is usually the case that a number of solvent models are used,

however only the one that performed the best is reported. In a real-case scenario this would not be practical. Our findings from the Factor Xa dataset indicate that the method could, however, have potential applications in earlier stages of drug design, such us in high-throughput and enrichment studies, where large datasets are analysed and ranking of closely related ligands is not required. Therefore, future work should be directed towards investigating this potential applicability of the method, but perhaps more importantly at optimising current rigorous free energy methodology which feature a more physically robust theoretical background.

# Appendix A

# E-Novo Protocol Details

| Parameters | |
|---|---|
| Input Receptor | $(Receptor Source) |
| Input Ligands | $(RunDirectory)/Input/prepared_ligands_fixed_core.sdf |
| Input Site Sphere | |
| ⊟ Top Hits | $(Top Hits) |
| Pose Cluster Radius | |
| ⊟ Random Conformations | $(Random Confs) |
| Dynamics Steps | 1000 |
| Dynamics Target Temperature | 1000 |
| Include Electrostatic Interactions | True |
| ⊟ Orientations to Refine | 0 |
| Maximum Bad Orientations | 800 |
| Orientation vdW Energy Threshold | 300 |
| ⊟ Simulated Annealing | True |
| Heating Steps | 2000 |
| Heating Target Temperature | 700 |
| Cooling Steps | 5000 |
| Cooling Target Temperature | 300 |
| ⊟ Advanced | |
| Forcefield | CHARMm |
| Use Full Potential | False |
| Grid Extension | 8.0 |
| Ligand Partial Charge Method | $(Ligand Partial Charge Method) |
| Random Number Seed | 314159 |
| Final Minimization | Full Potential |
| Final Minimization Gradient Tolerance | 0 |
| ⊟ Parallel Processing | False |
| Batch Size | 25 |
| ⊟ Server | localhost |
| Processes | 2 |
| Preserve Order | True |
| CDockerConstraint | SCALAR MOVE SET 1 SELE bynum $(Fixed Core) end |

Figure A.1: Docking parameters as implemented in our assessment of E-Novo.

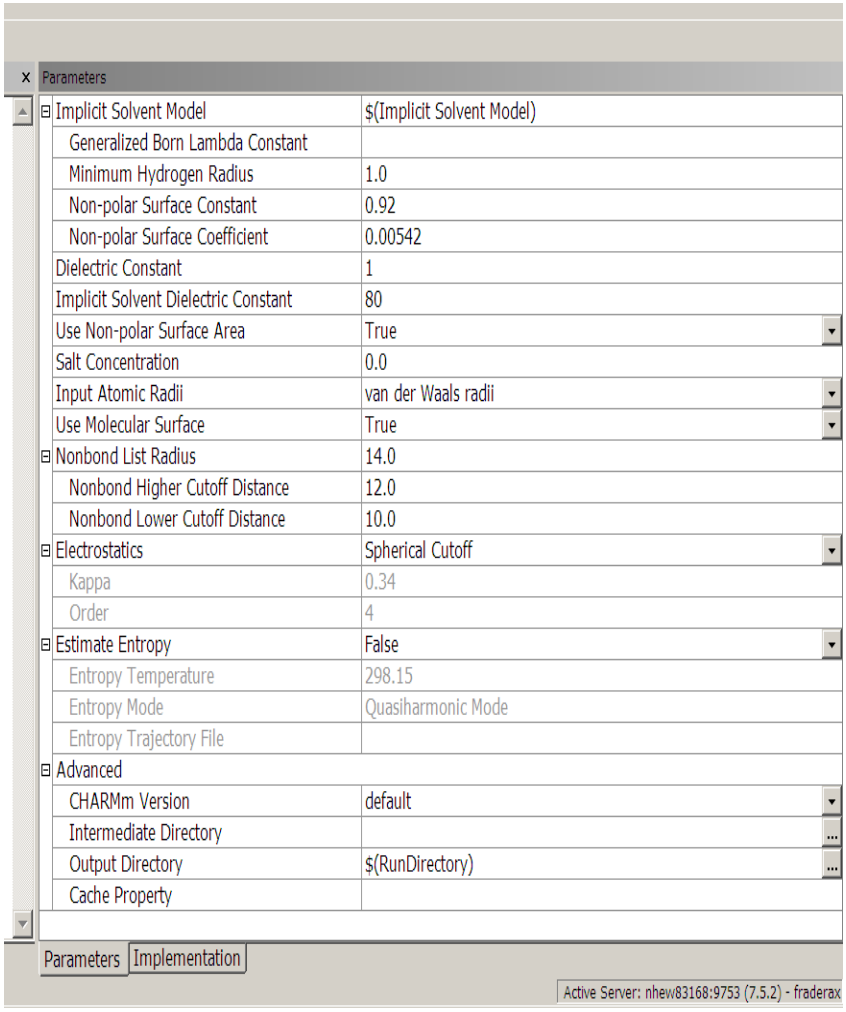


Figure A.2: Rescoring parameters as implemented in our assessment of E-Novo.

# Appendix B

# Rescoring in Range of software: Additional Analysis

Here additional analysis that would not be practical to be included in the main text of this thesis, is shown for each target. In the majority, this includes box plots and statistical analysis from the comparisons performed in Chapter 6.

## Thrombin

Table B.1: Coefficient of determination ($R^2$) matrix between rescoring models for Glide 2. P–values from a two-tailed test shown. Significant correlations highlighted in bold.

| | | Prime Rigid | Prime Flex | Prime Rigid L. | Prime Flex L. | GBHCT Rigid | GBOBC1 bondi Rigid | GBOBC1 mbondi2 Rigid | GBOBC2 bondi Rigid | GBOBC2 mbondi2 Rigid | Gbn Rigid | GBHCT Flex | GBOBC1 bondi Flex | GBOBC1 mbondi2 Flex | GBOBC2 bondi Flex | GBOBC2 mbondi2 Flex | Gbn Flex |
|---|---|---|---|---|---|---|---|---|---|---|---|---|---|---|---|---|---|
| **Prime Rigid** | $R^2$ | 1.0000 | **0.6346** | **0.9012** | **0.6313** | 0.0183 | 0.0555 | 0.0000 | 0.0001 | 0.0747 | **0.4935** | 0.0713 | 0.0578 | 0.0203 | 0.0544 | 0.0199 | 0.0282 |
| **Prime Rigid** | p | -- | **0.0019** | **0.0000** | **0.0020** | 0.6753 | 0.4611 | 0.9888 | 0.9812 | 0.3901 | **0.0108** | 0.4015 | 0.4516 | 0.6591 | 0.4659 | 0.6618 | 0.6020 |
| **Prime Flex** | $R^2$ | 1.0000 | **0.5261** | **0.9994** | **0.0000** | 0.0032 | 0.0161 | 0.0028 | 0.0194 | 0.0088 | **0.5114** | 0.0181 | 0.0248 | 0.0456 | 0.1504 | 0.0112 | 0.0031 |
| **Prime Flex** | p | -- | **0.0076** | **0.0000** | **0.5219** | 0.8624 | 0.6941 | 0.8697 | 0.6657 | 0.7713 | **0.0089** | 0.6767 | 0.6249 | 0.5051 | 0.2129 | 0.7431 | 0.8640 |
| **Prime Rigid L.** | $R^2$ | | 1.0000 | **0.5219** | **0.0080** | 0.0104 | 0.0559 | 0.0001 | 0.0000 | 0.0516 | **0.4819** | 0.1152 | 0.1055 | 0.0118 | 0.0082 | 0.0503 | 0.0795 |
| **Prime Rigid L.** | p | | -- | **0.0080** | 0.7528 | 0.4593 | 0.9710 | 0.9903 | 0.4776 | **0.0123** | 0.2805 | 0.3029 | 0.7365 | 0.7791 | 0.4837 | 0.3746 | |
| **Prime Flex L.** | $R^2$ | | | 1.0000 | 0.0033 | 0.0179 | 0.0027 | 0.0176 | 0.0075 | 0.5142 | 0.0214 | 0.0283 | 0.0400 | 0.1434 | 0.0132 | 0.0022 | |
| **Prime Flex L.** | p | | | -- | 0.8596 | 0.6781 | 0.8730 | 0.6814 | 0.7886 | 0.0087 | 0.6499 | 0.6015 | 0.5334 | 0.2248 | 0.7221 | 0.8858 | |
| **GBHCT Rigid** | $R^2$ | | | | 1.0000 | **0.3461** | **0.5240** | **0.8399** | 0.0982 | 0.1599 | 0.2776 | **0.4589** | 0.2329 | 0.1098 | **0.3286** | **0.2567** | |
| **GBHCT Rigid** | p | | | | -- | **0.0442** | **0.0078** | **0.0000** | 0.3213 | 0.1977 | 0.0784 | **0.0155** | 0.1121 | 0.2928 | **0.0514** | **0.0927** | |
| **GBOBC1 bondi Rigid** | $R^2$ | | | | | 1.0000 | **0.6162** | **0.3326** | **0.4182** | **0.4205** | 0.2242 | **0.4330** | 0.2722 | 0.2530 | **0.4034** | 0.0988 | |
| **GBOBC1 bondi Rigid** | p | | | | | -- | **0.0025** | **0.0497** | **0.0230** | **0.0226** | 0.1199 | **0.0200** | 0.0819 | 0.0955 | **0.0265** | 0.3197 | |
| **GBOBC1 mbondi2 Rigid** | $R^2$ | | | | | | 1.0000 | **0.5061** | **0.5355** | 0.2948 | 0.0653 | 0.2017 | 0.1701 | 0.1343 | 0.3247 | 0.0320 | |
| **GBOBC1 mbondi2 Rigid** | p | | | | | | -- | **0.0095** | **0.0068** | 0.0681 | 0.4229 | 0.1430 | 0.1828 | 0.2414 | 0.0531 | 0.5781 | |
| **GBOBC2 bondi Rigid** | $R^2$ | | | | | | | 1.0000 | 0.1760 | 0.1036 | **0.4683** | **0.5320** | **0.5119** | 0.3073 | **0.4693** | 0.4449 | |
| **GBOBC2 bondi Rigid** | p | | | | | | | -- | 0.1746 | 0.3076 | **0.0141** | **0.0071** | **0.0089** | 0.0614 | **0.0140** | 0.0178 | |
| **GBOBC2 mbondi2 Rigid** | $R^2$ | | | | | | | | 1.0000 | 0.1630 | 0.0446 | 0.1404 | 0.2903 | 0.2651 | 0.4640 | 0.0017 | |
| **GBOBC2 mbondi2 Rigid** | p | | | | | | | | -- | 0.1931 | 0.5097 | 0.2301 | 0.0707 | 0.0867 | 0.0147 | 0.9002 | |
| **Gbn Rigid** | $R^2$ | | | | | | | | | 1.0000 | 0.1245 | 0.1781 | 0.0171 | 0.0000 | 0.2160 | 0.0177 | |
| **Gbn Rigid** | p | | | | | | | | | -- | 0.2606 | 0.1717 | 0.6856 | 0.9946 | 0.1280 | 0.6799 | |
| **GBHCT Flex** | $R^2$ | | | | | | | | | | 1.0000 | **0.7872** | **0.7003** | **0.5457** | **0.5522** | **0.8932** | |
| **GBHCT Flex** | p | | | | | | | | | | -- | **0.0001** | **0.0007** | **0.0061** | **0.0056** | **0.0000** | |
| **GBOBC1 bondi Flex** | $R^2$ | | | | | | | | | | | 1.0000 | **0.5909** | **0.5183** | **0.7324** | **0.6960** | |
| **GBOBC1 bondi Flex** | p | | | | | | | | | | | -- | **0.0035** | **0.0083** | **0.0004** | **0.0007** | |
| **GBOBC1 mbondi2 Flex** | $R^2$ | | | | | | | | | | | | 1.0000 | **0.7982** | **0.6535** | **0.5954** | |
| **GBOBC1 mbondi2 Flex** | p | | | | | | | | | | | | -- | **0.0001** | **0.0015** | **0.0033** | |
| **GBOBC2 bondi Flex** | $R^2$ | | | | | | | | | | | | | 1.0000 | **0.5878** | **0.5585** | |
| **GBOBC2 bondi Flex** | p | | | | | | | | | | | | | -- | **0.0036** | **0.0052** | |
| **GBOBC2 mbondi2 Flex** | $R^2$ | | | | | | | | | | | | | | 1.0000 | **0.4141** | |
| **GBOBC2 mbondi2 Flex** | p | | | | | | | | | | | | | | -- | **0.0240** | |
| **Gbn Flex** | $R^2$ | | | | | | | | | | | | | | | 1.0000 | |
| **Gbn Flex** | p | | | | | | | | | | | | | | | -- | |

Table B.2: Kendall tau (τ) rank correlation coefficient matrix between rescoring models for Glide 2. P–values from a two-tailed test shown. Significant correlations highlighted in bold.

| | | Prime Rigid | Prime Flex | Prime Rigid L. | Prime Flex L. | GBHCT Rigid | GBOBC1 bondi Rigid | GBOBC1 mbondi2 Rigid | GBOBC2 bondi Rigid | GBOBC2 mbondi2 Rigid | Gbn Rigid | GBHCT Flex | GBOBC1 bondi Flex | GBOBC1 mbondi2 Flex | GBOBC2 bondi Flex | GBOBC2 mbondi2 Flex | Gbn Flex |
|---|---|---|---|---|---|---|---|---|---|---|---|---|---|---|---|---|---|
| **Prime Rigid** | τ | 1.0000 | 0.3939 | **0.8182** | 0.4242 | -0.1515 | -0.0909 | -0.0303 | -0.0153 | 0.2424 | -0.1515 | 0.0000 | 0.0606 | 0.2727 | 0.4242 | 0.0606 | 0.0303 |
| **Prime Rigid** | p | -- | 0.0746 | **0.0002** | 0.0549 | 0.4929 | 0.6808 | 0.8909 | 0.9452 | 0.2726 | 0.4929 | 1.0000 | 0.7839 | 0.2171 | 0.0549 | 0.7839 | 0.8909 |
| **Prime Flex** | τ | | 1.0000 | 0.2121 | **0.9697** | -0.0303 | 0.0303 | 0.0909 | 0.2901 | 0.1818 | -0.0909 | 0.2424 | 0.2424 | **0.4546** | **0.4849** | 0.3030 | 0.2727 |
| **Prime Flex** | p | | -- | 0.3371 | **0.0000** | 0.8909 | 0.8909 | 0.6808 | 0.1916 | 0.4106 | 0.6808 | 0.2726 | 0.2726 | **0.0397** | **0.0282** | 0.1702 | 0.2171 |
| **Prime Rigid L.** | τ | | | 1.0000 | 0.2424 | -0.0909 | -0.0303 | -0.0303 | -0.0763 | 0.1818 | -0.2121 | -0.1818 | -0.1212 | 0.0909 | 0.2424 | -0.1212 | -0.0909 |
| **Prime Rigid L.** | p | | | -- | 0.2726 | 0.6808 | 0.8909 | 0.8909 | 0.7311 | 0.4106 | 0.3371 | 0.4106 | 0.5833 | 0.6808 | 0.2726 | 0.5833 | 0.6808 |
| **Prime Flex L.** | τ | | | | 1.0000 | 0.0000 | 0.0606 | 0.1212 | 0.3206 | 0.2121 | -0.0606 | 0.2727 | 0.2121 | **0.4849** | **0.5152** | 0.3333 | 0.3030 |
| **Prime Flex L.** | p | | | | -- | 1.0000 | 0.7839 | 0.5833 | 0.1489 | 0.3371 | 0.7839 | 0.2171 | 0.3371 | **0.0282** | **0.0197** | 0.1314 | 0.1702 |
| **GBHCT Rigid** | τ | | | | | 1.0000 | **0.5152** | **0.4546** | 0.6870 | 0.6061 | 0.3333 | 0.4242 | 0.3636 | 0.3939 | 0.1212 | 0.2424 | 0.3939 |
| **GBHCT Rigid** | p | | | | | -- | **0.0197** | **0.0397** | 0.0020 | 0.0061 | 0.1314 | 0.0549 | 0.0998 | 0.0746 | 0.5833 | 0.2726 | 0.0746 |
| **GBOBC1 bondi Rigid** | τ | | | | | | 1.0000 | **0.7576** | 0.4122 | **0.5455** | **0.6364** | 0.3030 | 0.1212 | **0.5758** | 0.2424 | 0.1818 | 0.2121 |
| **GBOBC1 bondi Rigid** | p | | | | | | -- | **0.0006** | 0.0635 | **0.0136** | **0.0040** | 0.1702 | 0.5833 | **0.0092** | 0.2726 | 0.4106 | 0.3371 |
| **GBOBC1 mbondi2 Rigid** | τ | | | | | | | 1.0000 | 0.4428 | **0.6667** | **0.6970** | 0.1818 | 0.0606 | **0.5152** | 0.1818 | 0.2424 | 0.1515 |
| **GBOBC1 mbondi2 Rigid** | p | | | | | | | -- | 0.0462 | **0.0026** | **0.0016** | 0.4106 | 0.7839 | **0.0197** | 0.4106 | 0.2726 | 0.4929 |
| **GBOBC2 bondi Rigid** | τ | | | | | | | | 1.0000 | **0.5954** | 0.3817 | **0.5344** | 0.4122 | **0.5954** | 0.2596 | **0.4733** | **0.5344** |
| **GBOBC2 bondi Rigid** | p | | | | | | | | -- | **0.0074** | 0.0857 | **0.0161** | 0.0635 | **0.0074** | 0.2426 | **0.0331** | **0.0161** |
| **GBOBC2 mbondi2 Rigid** | τ | | | | | | | | | 1.0000 | **0.5455** | 0.3333 | 0.3333 | **0.6061** | 0.3939 | **0.4546** | 0.2424 |
| **GBOBC2 mbondi2 Rigid** | p | | | | | | | | | -- | **0.0136** | 0.1314 | 0.1314 | **0.0061** | 0.0746 | **0.0397** | 0.2726 |
| **Gbn Rigid** | τ | | | | | | | | | | 1.0000 | 0.1212 | 0.0000 | 0.3333 | 0.0606 | 0.1818 | -0.0303 |
| **Gbn Rigid** | p | | | | | | | | | | -- | 0.5833 | 1.0000 | 0.1314 | 0.7839 | 0.4106 | 0.8909 |
| **GBHCT Flex** | τ | | | | | | | | | | | 1.0000 | **0.6970** | 0.5455 | **0.4546** | **0.4546** | **0.7273** |
| **GBHCT Flex** | p | | | | | | | | | | | -- | **0.0016** | 0.0136 | **0.0397** | **0.0397** | **0.0010** |
| **GBOBC1 bondi Flex** | τ | | | | | | | | | | | | 1.0000 | **0.4849** | **0.5152** | **0.6364** | **0.6061** |
| **GBOBC1 bondi Flex** | p | | | | | | | | | | | | -- | **0.0282** | **0.0197** | **0.0040** | **0.0061** |
| **GBOBC1 mbondi2 Flex** | τ | | | | | | | | | | | | | 1.0000 | **0.6061** | **0.5455** | **0.6364** |
| **GBOBC1 mbondi2 Flex** | p | | | | | | | | | | | | | -- | **0.0061** | **0.0136** | **0.0040** |
| **GBOBC2 bondi Flex** | τ | | | | | | | | | | | | | | 1.0000 | **0.5152** | **0.4849** |
| **GBOBC2 bondi Flex** | p | | | | | | | | | | | | | | -- | **0.0197** | **0.0282** |
| **GBOBC2 mbondi2 Flex** | τ | | | | | | | | | | | | | | | 1.0000 | 0.3636 |
| **GBOBC2 mbondi2 Flex** | p | | | | | | | | | | | | | | | -- | 0.0998 |
| **Gbn Flex** | τ | | | | | | | | | | | | | | | | 1.0000 |
| **Gbn Flex** | p | | | | | | | | | | | | | | | | -- |

Table B.3: Coefficient of determination ($R^2$) matrix between rescoring models for Glide 3. P–values from a two-tailed test shown. Significant correlations highlighted in bold.

| | | Prime Rigid | Prime Flex | Prime Rigid L. | Prime Flex L. | GBHCT Rigid | GBOBC1 bondi Rigid | GBOBC1 mbondi2 Rigid | GBOBC2 bondi Rigid | GBOBC2 mbondi2 Rigid | Gbn Rigid | GBHCT Flex | GBOBC1 bondi Flex | GBOBC1 mbondi2 Flex | GBOBC2 bondi Flex | GBOBC2 mbondi2 Flex | Gbn Flex |
|---|---|---|---|---|---|---|---|---|---|---|---|---|---|---|---|---|---|
| **Prime Rigid** | $R^2$ | 1.0000 | **0.5732** | **0.8282** | 0.2773 | 0.0088 | 0.0394 | 0.0578 | 0.1198 | 0.0793 | 0.0804 | 0.1096 | 0.3302 | 0.0402 | **0.3668** | **0.4092** | 0.1019 |
| **Prime Rigid** | p | -- | **0.0044** | **0.0000** | 0.0786 | 0.7718 | 0.5362 | 0.4517 | 0.2705 | 0.3754 | 0.3718 | 0.2933 | 0.0507 | 0.5321 | **0.0369** | **0.0251** | 0.3118 |
| **Prime Flex** | $R^2$ | | 1.0000 | **0.3991** | **0.4000** | 0.0046 | 0.0593 | 0.1267 | 0.1036 | 0.0776 | 0.1954 | **0.6322** | **0.7413** | **0.4476** | **0.6412** | **0.7096** | **0.5854** |
| **Prime Flex** | p | | -- | **0.0276** | **0.0273** | 0.8333 | 0.4455 | 0.2561 | 0.3077 | 0.3808 | 0.1502 | **0.0020** | **0.0003** | **0.0174** | **0.0018** | **0.0006** | **0.0037** |
| **Prime Rigid L.** | $R^2$ | | | 1.0000 | 0.2852 | 0.0167 | 0.0079 | 0.0001 | 0.0160 | 0.0007 | 0.0026 | 0.0152 | 0.2022 | 0.0352 | 0.2638 | 0.2216 | 0.0639 |
| **Prime Rigid L.** | p | | | -- | 0.0737 | 0.6888 | 0.7838 | 0.9721 | 0.6950 | 0.9340 | 0.8739 | 0.7022 | 0.1425 | 0.5592 | 0.0876 | 0.1225 | 0.4278 |
| **Prime Flex L.** | $R^2$ | | | | 1.0000 | 0.0000 | 0.0042 | 0.0268 | 0.0235 | 0.0005 | 0.0069 | 0.1149 | 0.1673 | 0.1483 | 0.0335 | 0.2072 | 0.0240 |
| **Prime Flex L.** | p | | | | -- | 0.9884 | 0.8414 | 0.6113 | 0.6340 | 0.9443 | 0.7974 | 0.2811 | 0.1868 | 0.2163 | 0.5690 | 0.1371 | 0.6305 |
| **GBHCT Rigid** | $R^2$ | | | | | 1.0000 | **0.7653** | **0.7566** | **0.8560** | **0.7842** | **0.4012** | 0.0453 | 0.0321 | 0.0023 | 0.0207 | 0.0754 | 0.0028 |
| **GBHCT Rigid** | p | | | | | -- | **0.0002** | **0.0002** | **0.0000** | **0.0001** | **0.0270** | 0.5067 | 0.5772 | 0.8812 | 0.6559 | 0.3878 | 0.8711 |
| **GBOBC1 bondi Rigid** | $R^2$ | | | | | | 1.0000 | **0.7569** | **0.7779** | **0.6228** | **0.5014** | 0.0770 | 0.1524 | 0.0355 | 0.1003 | 0.1614 | 0.0774 |
| **GBOBC1 bondi Rigid** | p | | | | | | -- | **0.0002** | **0.0001** | **0.0023** | **0.0100** | 0.3825 | 0.2096 | 0.5578 | 0.3159 | 0.1955 | 0.3813 |
| **GBOBC1 mbondi2 Rigid** | $R^2$ | | | | | | | 1.0000 | **0.8935** | **0.8217** | **0.5575** | 0.2106 | 0.3031 | 0.0403 | 0.1736 | **0.3887** | 0.1016 |
| **GBOBC1 mbondi2 Rigid** | p | | | | | | | -- | **0.0000** | **0.0000** | **0.0053** | 0.1335 | 0.0636 | 0.5317 | 0.1779 | **0.0303** | 0.3127 |
| **GBOBC2 bondi Rigid** | $R^2$ | | | | | | | | 1.0000 | **0.8743** | **0.5902** | 0.1417 | 0.2161 | 0.0226 | 0.1606 | 0.3264 | 0.0522 |
| **GBOBC2 bondi Rigid** | p | | | | | | | | -- | **0.0000** | **0.0035** | 0.2277 | 0.1279 | 0.6411 | 0.1968 | 0.0523 | 0.4749 |
| **GBOBC2 mbondi2 Rigid** | $R^2$ | | | | | | | | | 1.0000 | **0.6921** | 0.1654 | 0.1914 | 0.0011 | 0.1140 | 0.2634 | 0.0308 |
| **GBOBC2 mbondi2 Rigid** | p | | | | | | | | | -- | **0.0008** | 0.1896 | 0.1550 | 0.9177 | 0.2832 | 0.0879 | 0.5856 |
| **Gbn Rigid** | $R^2$ | | | | | | | | | | 1.0000 | **0.3735** | **0.3668** | 0.0864 | 0.1857 | **0.3646** | 0.1734 |
| **Gbn Rigid** | p | | | | | | | | | | -- | **0.0348** | **0.0369** | 0.3538 | 0.1619 | **0.0376** | 0.1781 |
| **GBHCT Flex** | $R^2$ | | | | | | | | | | | 1.0000 | **0.7151** | **0.7020** | **0.5723** | **0.6104** | **0.7470** |
| **GBHCT Flex** | p | | | | | | | | | | | -- | **0.0005** | **0.0007** | **0.0044** | **0.0027** | **0.0003** |
| **GBOBC1 bondi Flex** | $R^2$ | | | | | | | | | | | | 1.0000 | **0.4330** | **0.7782** | **0.8871** | **0.6681** |
| **GBOBC1 bondi Flex** | p | | | | | | | | | | | | -- | **0.0200** | **0.0001** | **0.0000** | **0.0012** |
| **GBOBC1 mbondi2 Flex** | $R^2$ | | | | | | | | | | | | | 1.0000 | **0.4380** | 0.3086 | **0.7429** |
| **GBOBC1 mbondi2 Flex** | p | | | | | | | | | | | | | -- | **0.0191** | 0.0608 | **0.0003** |
| **GBOBC2 bondi Flex** | $R^2$ | | | | | | | | | | | | | | 1.0000 | **0.6831** | **0.7615** |
| **GBOBC2 bondi Flex** | p | | | | | | | | | | | | | | -- | **0.0009** | **0.0002** |
| **GBOBC2 mbondi2 Flex** | $R^2$ | | | | | | | | | | | | | | | 1.0000 | **0.5097** |
| **GBOBC2 mbondi2 Flex** | p | | | | | | | | | | | | | | | -- | **0.0091** |
| **Gbn Flex** | $R^2$ | | | | | | | | | | | | | | | | 1.0000 |
| **Gbn Flex** | p | | | | | | | | | | | | | | | | -- |

Table B.4: Kendall tau (τ) rank correlation coefficient matrix between rescoring models for Glide 3. P–values from a two-tailed test shown. Significant correlations highlighted in bold.

| | | Prime Rigid | Prime Flex | Prime Rigid L. | Prime Flex L. | GBHCT Rigid | GBOBC1 bondi Rigid | GBOBC1 mbondi2 Rigid | GBOBC2 bondi Rigid | GBOBC2 mbondi2 Rigid | Gbn Rigid | GBHCT Flex | GBOBC1 bondi Flex | GBOBC1 mbondi2 Flex | GBOBC2 bondi Flex | GBOBC2 mbondi2 Flex | Gbn Flex |
|---|---|---|---|---|---|---|---|---|---|---|---|---|---|---|---|---|---|
| **Prime Rigid** | τ | 1.0000 | **0.5455** | **0.7576** | 0.4242 | 0.1515 | 0.2424 | 0.2727 | 0.3333 | 0.2424 | 0.1212 | 0.2121 | 0.2424 | 0.2424 | 0.4242 | 0.3636 | 0.2121 |
| **Prime Rigid** | p | -- | **0.0136** | **0.0006** | 0.0549 | 0.4929 | 0.2726 | 0.2171 | 0.1314 | 0.2726 | 0.5833 | 0.3371 | 0.2726 | 0.2726 | 0.0549 | 0.0998 | 0.3371 |
| **Prime Flex** | τ | | 1.0000 | 0.4242 | **0.6364** | 0.1212 | 0.2121 | 0.3636 | 0.2424 | 0.3333 | 0.2121 | **0.6061** | **0.5152** | **0.4546** | **0.5152** | **0.5758** | **0.4849** |
| **Prime Flex** | p | | -- | 0.0549 | **0.0040** | 0.5833 | 0.3371 | 0.0998 | 0.2726 | 0.1314 | 0.3371 | **0.0061** | **0.0197** | **0.0397** | **0.0197** | **0.0092** | **0.0282** |
| **Prime Rigid L.** | τ | | | 1.0000 | 0.3636 | -0.0303 | 0.1818 | 0.0303 | 0.0909 | 0.0000 | -0.1212 | 0.0909 | 0.1212 | 0.1818 | 0.4242 | 0.1818 | 0.2121 |
| **Prime Rigid L.** | p | | | -- | 0.0998 | 0.8909 | 0.4106 | 0.8909 | 0.6808 | 1.0000 | 0.5833 | 0.6808 | 0.5833 | 0.4106 | 0.0549 | 0.4106 | 0.3371 |
| **Prime Flex L.** | τ | | | | 1.0000 | 0.1212 | 0.1515 | 0.2424 | 0.1212 | 0.1515 | 0.0303 | 0.3636 | 0.1515 | 0.3333 | 0.2121 | 0.2121 | 0.2424 |
| **Prime Flex L.** | p | | | | -- | 0.5833 | 0.4929 | 0.2726 | 0.5833 | 0.4929 | 0.8909 | 0.0998 | 0.4929 | 0.1314 | 0.3371 | 0.3371 | 0.2726 |
| **GBHCT Rigid** | τ | | | | | 1.0000 | **0.7273** | **0.6970** | **0.7576** | **0.7273** | **0.5455** | 0.2121 | 0.1212 | 0.1212 | 0.1212 | 0.2424 | 0.0909 |
| **GBHCT Rigid** | p | | | | | -- | **0.0010** | **0.0016** | **0.0006** | **0.0010** | **0.0136** | 0.3371 | 0.5833 | 0.5833 | 0.5833 | 0.2726 | 0.6808 |
| **GBOBC1 bondi Rigid** | τ | | | | | | 1.0000 | **0.6061** | **0.6667** | **0.6364** | **0.5152** | 0.3030 | 0.2121 | 0.3333 | 0.2727 | 0.2727 | 0.3030 |
| **GBOBC1 bondi Rigid** | p | | | | | | -- | **0.0061** | **0.0026** | **0.0040** | **0.0197** | 0.1702 | 0.3371 | 0.1314 | 0.2171 | 0.2171 | 0.1702 |
| **GBOBC1 mbondi2 Rigid** | τ | | | | | | | 1.0000 | **0.8182** | **0.8485** | **0.5455** | **0.4546** | 0.3636 | 0.3030 | 0.3030 | **0.4849** | 0.3333 |
| **GBOBC1 mbondi2 Rigid** | p | | | | | | | -- | **0.0002** | **0.0001** | **0.0136** | **0.0397** | 0.0998 | 0.1702 | 0.1702 | **0.0282** | 0.1314 |
| **GBOBC2 bondi Rigid** | τ | | | | | | | | 1.0000 | **0.9091** | **0.5455** | 0.2727 | 0.3030 | 0.1818 | 0.3636 | **0.4849** | 0.2121 |
| **GBOBC2 bondi Rigid** | p | | | | | | | | -- | **0.0000** | **0.0136** | 0.2171 | 0.1702 | 0.4106 | 0.0998 | **0.0282** | 0.3371 |
| **GBOBC2 mbondi2 Rigid** | τ | | | | | | | | | 1.0000 | **0.6364** | 0.3636 | 0.3333 | 0.2121 | 0.3333 | **0.5152** | 0.2424 |
| **GBOBC2 mbondi2 Rigid** | p | | | | | | | | | -- | **0.0040** | 0.0998 | 0.1314 | 0.3371 | 0.1314 | **0.0197** | 0.2726 |
| **Gbn Rigid** | τ | | | | | | | | | | 1.0000 | 0.2424 | 0.2121 | 0.0303 | 0.0909 | 0.2727 | 0.1212 |
| **Gbn Rigid** | p | | | | | | | | | | -- | 0.2726 | 0.3371 | 0.8909 | 0.6808 | 0.2171 | 0.5833 |
| **GBHCT Flex** | τ | | | | | | | | | | | 1.0000 | **0.5455** | **0.7273** | 0.4242 | **0.5455** | **0.7576** |
| **GBHCT Flex** | p | | | | | | | | | | | -- | **0.0136** | **0.0010** | 0.0549 | **0.0136** | **0.0006** |
| **GBOBC1 bondi Flex** | τ | | | | | | | | | | | | 1.0000 | 0.3333 | **0.4546** | **0.6364** | **0.4849** |
| **GBOBC1 bondi Flex** | p | | | | | | | | | | | | -- | 0.1314 | **0.0397** | **0.0040** | **0.0282** |
| **GBOBC1 mbondi2 Flex** | τ | | | | | | | | | | | | | 1.0000 | **0.5152** | 0.3333 | **0.8485** |
| **GBOBC1 mbondi2 Flex** | p | | | | | | | | | | | | | -- | **0.0197** | 0.1314 | **0.0001** |
| **GBOBC2 bondi Flex** | τ | | | | | | | | | | | | | | 1.0000 | **0.5758** | **0.6667** |
| **GBOBC2 bondi Flex** | p | | | | | | | | | | | | | | -- | **0.0092** | **0.0026** |
| **GBOBC2 mbondi2 Flex** | τ | | | | | | | | | | | | | | | 1.0000 | 0.4242 |
| **GBOBC2 mbondi2 Flex** | p | | | | | | | | | | | | | | | -- | 0.0549 |
| **Gbn Flex** | τ | | | | | | | | | | | | | | | | 1.0000 |
| **Gbn Flex** | p | | | | | | | | | | | | | | | | -- |

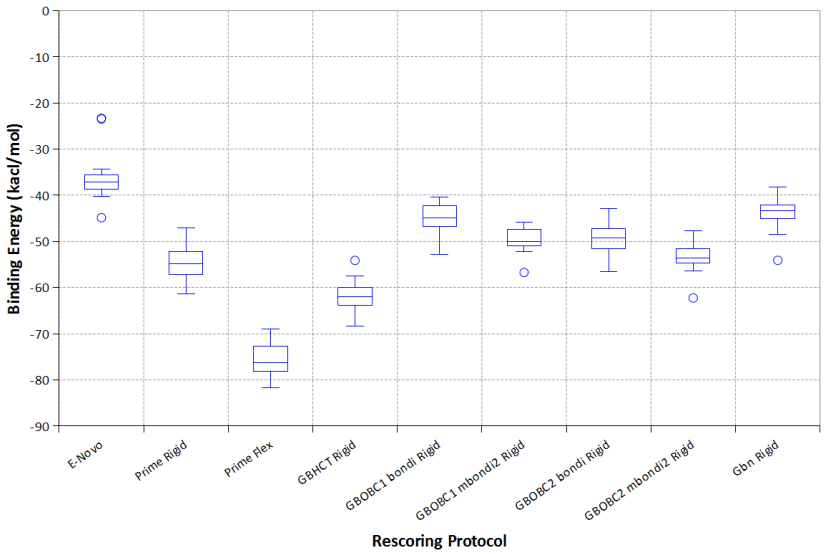


Figure B.1: Box Plot of predicted binding energies (kcal $mol^{-1}$) of CDOCKER poses for each rescoring protocol. The whiskers represent the minimum and maximum values excluding outliers (where applicable), the box corresponds to the range of values between the 1st and 3rd quartiles, and the line through the box represents the median value of the binding energies. Outliers are shown in circles for any points beyond 1.5 the interquartile range (IQR).

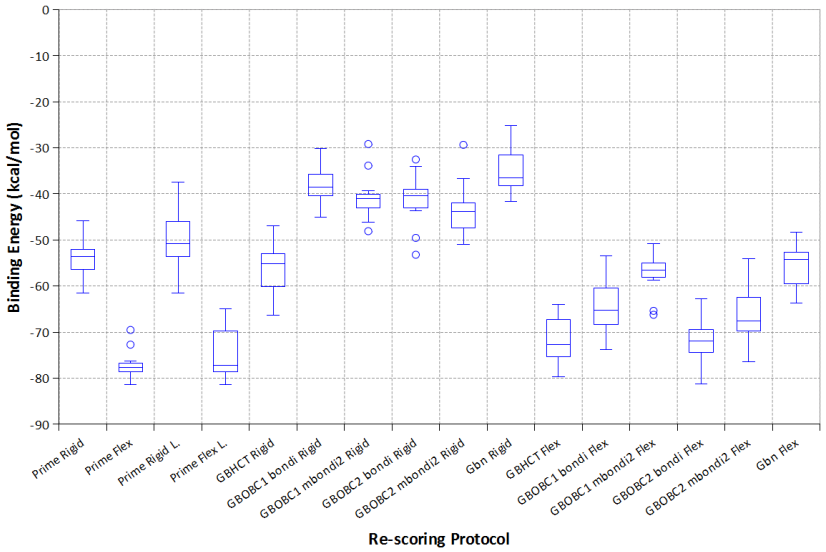


Figure B.2: Box Plot of predicted binding energies (kcal $mol^{-1}$) of Glide 1 poses for each rescoring protocol. The whiskers represent the minimum and maximum values excluding outliers (where applicable), the box corresponds to the range of values between the 1st and 3rd quartiles, and the line through the box represents the median value of the binding energies. Outliers are shown in circles for any points beyond 1.5 the interquartile range (IQR).

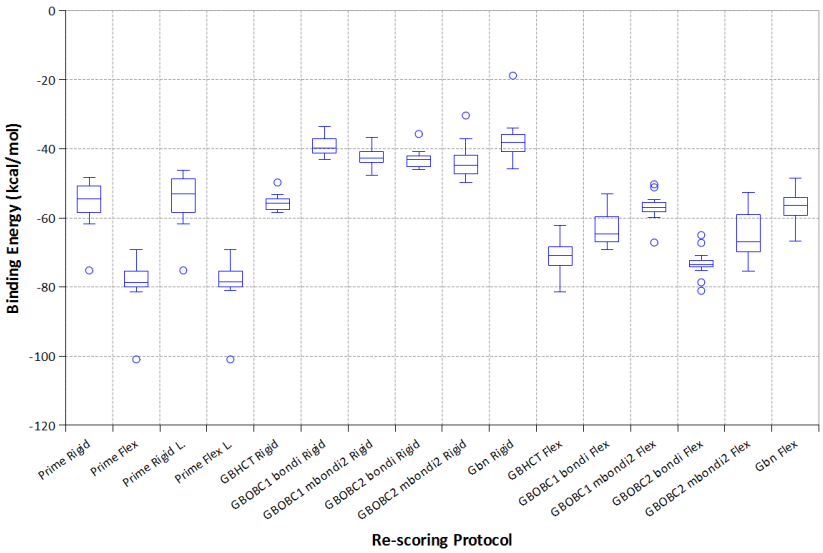


Figure B.3: Box Plot of predicted binding energies (kcal $mol^{-1}$) of Glide 2 poses for each rescoring protocol. The whiskers represent the minimum and maximum values excluding outliers (where applicable), the box corresponds to the range of values between the 1st and 3rd quartiles, and the line through the box represents the median value of the binding energies. Outliers are shown in circles for any points beyond 1.5 the interquartile range (IQR).

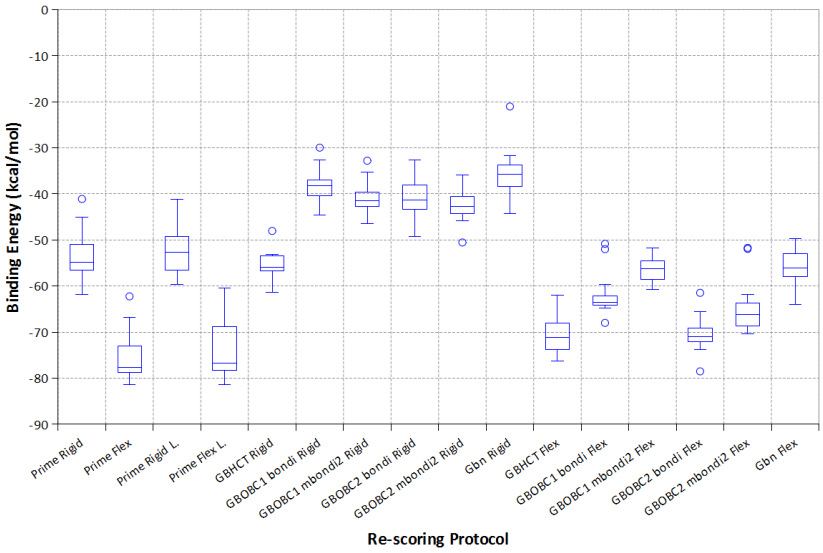


Figure B.4: Box Plot of predicted binding energies (kcal $mol^{-1}$) of Glide 3 poses for each rescoring protocol. The whiskers represent the minimum and maximum values excluding outliers (where applicable), the box corresponds to the range of values between the 1st and 3rd quartiles, and the line through the box represents the median value of the binding energies. Outliers are shown in circles for any points beyond 1.5 the interquartile range (IQR).

Table B.5: Descriptive statistics for Glide job 1 rescoring protocols.

| | All ligands | | | | Excluding Lig.7 | | | |
|---|---|---|---|---|---|---|---|---|
| **Rescoring Protocols** | **Mean** | **Std.Er.** | **95% LCL** | **95% UCL** | **Mean** | **Std.Er.** | **95% LCL** | **95% UCL** |
| Prime Rigid | -54.28 | 1.26 | -57.06 | -51.49 | -55.05 | 1.10 | -57.49 | -52.60 |
| Prime Flex | -77.02 | 0.90 | -79.01 | -75.03 | -77.01 | 0.99 | -79.22 | -74.81 |
| Prime Rigid L. | -50.00 | 2.09 | -54.60 | -45.41 | -51.14 | 1.92 | -55.41 | -46.87 |
| Prime Flex L. | -74.67 | 1.66 | -78.32 | -71.02 | -75.55 | 1.54 | -78.98 | -72.13 |
| GBHCT Rigid | -56.14 | 1.77 | -60.05 | -52.24 | -55.21 | 1.65 | -58.89 | -51.52 |
| GBOBC1 bondi Rigid | -37.87 | 1.32 | -40.77 | -34.98 | -37.53 | 1.39 | -40.62 | -34.43 |
| GBOBC1 mbondi2 Rigid | -40.77 | 1.48 | -44.01 | -37.52 | -40.66 | 1.61 | -44.25 | -37.07 |
| GBOBC2 bondi Rigid | -41.25 | 1.66 | -44.91 | -37.59 | -41.45 | 1.81 | -45.48 | -37.41 |
| GBOBC2 mbondi2 Rigid | -43.27 | 1.68 | -46.96 | -39.57 | -42.81 | 1.77 | -46.75 | -38.86 |
| Gbn Rigid | -34.82 | 1.64 | -38.43 | -31.22 | -35.50 | 1.63 | -39.14 | -31.87 |
| GBHCT Flex | -71.62 | 1.49 | -74.90 | -68.35 | -71.38 | 1.61 | -74.96 | -67.80 |
| GBOBC1 bondi Flex | -64.58 | 1.61 | -68.13 | -61.03 | -63.74 | 1.51 | -67.11 | -60.37 |
| GBOBC1 mbondi2 Flex | -57.22 | 1.33 | -60.15 | -54.29 | -56.40 | 1.15 | -58.95 | -53.85 |
| GBOBC2 bondi Flex | -71.65 | 1.66 | -75.30 | -68.00 | -70.77 | 1.54 | -74.21 | -67.34 |
| GBOBC2 mbondi2 Flex | -66.13 | 1.86 | -70.22 | -62.04 | -65.19 | 1.75 | -69.10 | -61.28 |
| Gbn Flex | -55.73 | 1.43 | -58.89 | -52.57 | -55.88 | 1.56 | -59.36 | -52.40 |

Table B.6: Descriptive statistics for Glide job 2 rescoring protocols.

| | All ligands | | | | Excluding Lig.7 | | | |
|---|---|---|---|---|---|---|---|---|
| **Rescoring Protocols** | **Mean** | **Std.Er.** | **95% LCL** | **95% UCL** | **Mean** | **Std.Er.** | **95% LCL** | **95% UCL** |
| Prime Rigid | -55.99 | 2.17 | -60.76 | -51.21 | -54.24 | 1.41 | -57.38 | -51.09 |
| Prime Flex | -78.69 | 2.34 | -83.84 | -73.54 | -76.67 | 1.29 | -79.54 | -73.80 |
| Prime Rigid L. | -55.12 | 2.33 | -60.24 | -49.99 | -53.29 | 1.58 | -56.82 | -49.76 |
| Prime Flex L. | -78.59 | 2.34 | -83.73 | -73.45 | -76.56 | 1.26 | -79.37 | -73.75 |
| GBHCT Rigid | -55.61 | 0.72 | -57.20 | -54.02 | -55.82 | 0.76 | -57.51 | -54.14 |
| GBOBC1 bondi Rigid | -39.25 | 0.85 | -41.13 | -37.38 | -39.60 | 0.85 | -41.50 | -37.69 |
| GBOBC1 mbondi2 Rigid | -42.52 | 0.87 | -44.44 | -40.61 | -42.69 | 0.93 | -44.77 | -40.62 |
| GBOBC2 bondi Rigid | -43.02 | 0.85 | -44.89 | -41.15 | -43.21 | 0.91 | -45.23 | -41.19 |
| GBOBC2 mbondi2 Rigid | -43.67 | 1.57 | -47.13 | -40.21 | -43.85 | 1.71 | -47.66 | -40.04 |
| Gbn Rigid | -37.34 | 1.96 | -41.65 | -33.04 | -39.02 | 1.09 | -41.46 | -36.59 |
| GBHCT Flex | -71.00 | 1.56 | -74.43 | -67.56 | -71.79 | 1.47 | -75.07 | -68.51 |
| GBOBC1 bondi Flex | -62.72 | 1.71 | -66.49 | -58.95 | -63.61 | 1.61 | -67.19 | -60.03 |
| GBOBC1 mbondi2 Flex | -56.95 | 1.24 | -59.67 | -54.22 | -57.16 | 1.34 | -60.13 | -54.19 |
| GBOBC2 bondi Flex | -73.19 | 1.25 | -75.94 | -70.44 | -73.15 | 1.37 | -76.20 | -70.11 |
| GBOBC2 mbondi2 Flex | -65.00 | 2.04 | -69.49 | -60.50 | -65.88 | 2.02 | -70.38 | -61.38 |
| Gbn Flex | -56.93 | 1.69 | -60.65 | -53.22 | -57.48 | 1.75 | -61.37 | -53.58 |

Table B.7: Descriptive statistics for Glide job 3 rescoring protocols.

| | All ligands | | | | Excluding Lig.7 | | | |
|---|---|---|---|---|---|---|---|---|
| **Rescoring Protocols** | **Mean** | **Std.Er.** | **95% LCL** | **95% UCL** | **Mean** | **Std.Er.** | **95% LCL** | **95% UCL** |
| Prime Rigid | -53.47 | 1.71 | -57.22 | -49.71 | -54.59 | 1.41 | -57.72 | -51.45 |
| Prime Flex | -75.20 | 1.70 | -78.94 | -71.45 | -76.38 | 1.35 | -79.38 | -73.38 |
| Prime Rigid L. | -52.27 | 1.63 | -55.86 | -48.68 | -53.29 | 1.40 | -56.40 | -50.17 |
| Prime Flex L. | -73.43 | 2.015 | -77.86 | -68.99 | -74.44 | 1.91 | -78.69 | -70.20 |
| GBHCT Rigid | -55.65 | 1.04 | -57.93 | -53.37 | -55.59 | 1.13 | -58.12 | -53.06 |
| GBOBC1 bondi Rigid | -38.16 | 1.15 | -40.70 | -35.63 | -38.19 | 1.26 | -41.00 | -35.38 |
| GBOBC1 mbondi2 Rigid | -40.74 | 1.11 | -43.19 | -38.28 | -41.03 | 1.18 | -43.65 | -38.40 |
| GBOBC2 bondi Rigid | -41.12 | 1.41 | -44.23 | -38.01 | -41.38 | 1.52 | -44.77 | -38.00 |
| GBOBC2 mbondi2 Rigid | -42.56 | 1.15 | -45.04 | -39.99 | -42.63 | 1.25 | -45.41 | -39.85 |
| Gbn Rigid | -35.59 | 1.73 | -39.40 | -31.77 | -35.56 | 1.90 | -39.79 | -31.33 |
| GBHCT Flex | -70.48 | 1.27 | -73.28 | -67.68 | -70.93 | 1.30 | -73.84 | -68.03 |
| GBOBC1 bondi Flex | -61.76 | 1.49 | -65.05 | -58.47 | -62.65 | 1.32 | -65.58 | -59.71 |
| GBOBC1 mbondi2 Flex | -56.33 | 0.85 | -58.20 | -54.46 | -56.55 | 0.90 | -58.56 | -54.54 |
| GBOBC2 bondi Flex | -70.37 | 1.23 | -73.09 | -67.65 | -71.18 | 1.02 | -73.46 | -68.90 |
| GBOBC2 mbondi2 Flex | -64.39 | 1.85 | -68.46 | -60.33 | -65.55 | 1.58 | -69.06 | -62.03 |
| Gbn Flex | -55.84 | 1.21 | -58.51 | -53.17 | -56.36 | 1.21 | -59.04 | -53.67 |

Table B.8: Holm-Šidák results for Glide job 1 excluding ligand 7. Names abbreviated for expediency. F., R., b., mb2, and d, correspond to Flexible, Rigid, bondi, mbondi2, and Cohen's d respectively. Significant differences shown in bold.

| **Compared Models** | **Index** | **Mean Diff.** | **Std.Er.** | **DF** | **\|t\|value** | **Prob>\|t\|** | **Alpha** | **d** |
|---|---|---|---|---|---|---|---|---|
| Prime F. Gbn R. | 22 | -41.51 | 1.56 | 150 | 26.55 | **1.45E-58** | 4.27E-04 | 7.11 |
| Prime F. L. Gbn R. | 47 | -40.05 | 1.56 | 150 | 25.62 | **1.20E-56** | 4.31E-04 | 7.24 |
| Prime F. GBOBC1 b. R. | 18 | -39.49 | 1.56 | 150 | 25.26 | **6.68E-56** | 4.35E-04 | 9.69 |
| Prime F. L. GBOBC1 b. R. | 43 | -38.03 | 1.56 | 150 | 24.32 | **6.36E-54** | 4.38E-04 | 9.83 |
| Prime F. GBOBC1 mb2 R. | 19 | -36.36 | 1.56 | 150 | 23.26 | **1.32E-51** | 4.42E-04 | 8.53 |
| Gbn R. GBHCT F. | 99 | 35.88 | 1.56 | 150 | 22.95 | **6.27E-51** | 4.46E-04 | 4.95 |
| Prime F. GBOBC2 b. R. | 20 | -35.57 | 1.56 | 150 | 22.75 | **1.71E-50** | 4.50E-04 | 10.75 |
| Gbn R. GBOBC2 b. F. | 102 | 35.27 | 1.56 | 150 | 22.56 | **4.58E-50** | 4.54E-04 | 6.03 |
| Prime F. L. GBOBC1 mb2 R. | 44 | -34.89 | 1.56 | 150 | 22.32 | **1.58E-49** | 4.58E-04 | 8.70 |
| Prime F. GBOBC2 mb2 R. | 21 | -34.21 | 1.56 | 150 | 21.88 | **1.55E-48** | 4.62E-04 | 5.81 |
| Prime F. L. GBOBC2 b. R. | 45 | -34.11 | 1.56 | 150 | 21.82 | **2.17E-48** | 4.66E-04 | 10.98 |
| GBOBC1 b. R. GBHCT F. | 69 | 33.85 | 1.56 | 150 | 21.66 | **5.08E-48** | 4.70E-04 | 6.80 |
| GBOBC1 b. R. GBOBC2 b. F. | 72 | 33.25 | 1.56 | 150 | 21.27 | **3.95E-47** | 4.75E-04 | 8.92 |
| Prime F. L. GBOBC2 mb2 R. | 46 | -32.75 | 1.56 | 150 | 20.95 | **2.18E-46** | 4.79E-04 | 5.80 |
| GBOBC1 mb2 R. GBHCT F. | 78 | 30.72 | 1.56 | 150 | 19.65 | **2.47E-43** | 4.84E-04 | 5.51 |
| GBOBC1 mb2 R. GBOBC2 b. F. | 81 | 30.12 | 1.56 | 150 | 19.26 | **2.12E-42** | 4.88E-04 | 6.90 |
| GBOBC2 b. R. GBHCT F. | 86 | 29.94 | 1.56 | 150 | 19.15 | **4.01E-42** | 4.93E-04 | 7.95 |

| | | | | | | | | |
|---|---|---|---|---|---|---|---|---|
| Gbn R. GBOBC2 mb2 F. | 103 | 29.68 | 1.56 | 150 | 18.99 | **9.82E-42** | 4.98E-04 | 3.87 |
| GBOBC2 b. R. GBOBC2 b. F. | 89 | 29.33 | 1.56 | 150 | 18.76 | **3.53E-41** | 5.03E-04 | 8.03 |
| GBOBC2 mb2 R. GBHCT F. | 93 | 28.57 | 1.56 | 150 | 18.28 | **5.38E-40** | 5.08E-04 | 4.12 |
| Gbn R. GBOBC1 b. F. | 100 | 28.24 | 1.56 | 150 | 18.06 | **1.85E-39** | 5.13E-04 | 3.72 |
| GBOBC2 mb2 R. GBOBC2 b. F. | 96 | 27.97 | 1.56 | 150 | 17.89 | **4.93E-39** | 5.18E-04 | 5.75 |
| GBOBC1 b. R. GBOBC2 mb2 F. | 73 | 27.66 | 1.56 | 150 | 17.69 | **1.51E-38** | 5.23E-04 | 4.67 |
| GBOBC1 b. R. GBOBC1 b. F. | 70 | 26.21 | 1.56 | 150 | 16.77 | **3.26E-36** | 5.29E-04 | 5.49 |
| Prime F. Prime R. L. | 15 | -25.87 | 1.56 | 150 | 16.55 | **1.18E-35** | 5.34E-04 | 3.74 |
| GBOBC1 mb2 R. GBOBC2 mb2 F. | 82 | 24.53 | 1.56 | 150 | 15.69 | **1.90E-33** | 5.40E-04 | 4.12 |
| Prime R. L. Prime F. L. | 29 | 24.41 | 1.56 | 150 | 15.61 | **3.00E-33** | 5.46E-04 | 3.71 |
| GBOBC2 b. R. GBOBC2 mb2 F. | 90 | 23.74 | 1.56 | 150 | 15.19 | **3.86E-32** | 5.51E-04 | 4.37 |
| GBOBC1 mb2 R. GBOBC1 b. F. | 79 | 23.08 | 1.56 | 150 | 14.76 | **4.95E-31** | 5.57E-04 | 4.24 |
| GBOBC2 mb2 R. GBOBC2 mb2 F. | 97 | 22.38 | 1.56 | 150 | 14.32 | **7.45E-30** | 5.64E-04 | 4.56 |
| GBOBC2 b. R. GBOBC1 b. F. | 87 | 22.29 | 1.56 | 150 | 14.26 | **1.05E-29** | 5.70E-04 | 5.47 |
| Prime R. Prime F. | 0 | 21.97 | 1.56 | 150 | 14.05 | **3.76E-29** | 5.76E-04 | 4.34 |
| Prime F. GBHCT R. | 17 | -21.81 | 1.56 | 150 | 13.95 | **7.02E-29** | 5.83E-04 | 5.27 |
| Prime F. Gbn F. | 28 | -21.13 | 1.56 | 150 | 13.52 | **9.82E-28** | 5.89E-04 | 4.65 |
| GBOBC2 mb2 R. GBOBC1 b. F. | 94 | 20.93 | 1.56 | 150 | 13.39 | **2.14E-27** | 5.96E-04 | 3.20 |
| Gbn R. GBOBC1 mb2 F. | 101 | 20.89 | 1.56 | 150 | 13.37 | **2.49E-27** | 6.03E-04 | 3.12 |
| Prime F. GBOBC1 mb2 F. | 25 | -20.62 | 1.56 | 150 | 13.19 | **7.44E-27** | 6.10E-04 | 6.11 |
| Prime R. Prime F. L. | 2 | 20.51 | 1.56 | 150 | 13.12 | **1.15E-26** | 6.18E-04 | 4.31 |
| Gbn R. Gbn F. | 104 | 20.38 | 1.56 | 150 | 13.04 | **1.89E-26** | 6.25E-04 | 2.40 |
| Prime F. L. GBHCT R. | 42 | -20.34 | 1.56 | 150 | 13.01 | **2.16E-26** | 6.33E-04 | 5.38 |
| Prime R. L. GBHCT F. | 36 | 20.24 | 1.56 | 150 | 12.95 | **3.30E-26** | 6.41E-04 | 2.74 |
| GBHCT R. Gbn R. | 58 | -19.70 | 1.56 | 150 | 12.60 | **2.69E-25** | 6.49E-04 | 4.49 |
| Prime F. L. Gbn F. | 53 | -19.67 | 1.56 | 150 | 12.58 | **3.08E-25** | 6.57E-04 | 4.62 |
| Prime R. L. GBOBC2 b. F. | 39 | 19.63 | 1.56 | 150 | 12.56 | **3.60E-25** | 6.66E-04 | 3.03 |
| Prime R. Gbn R. | 8 | -19.54 | 1.56 | 150 | 12.50 | **5.06E-25** | 6.75E-04 | 2.53 |
| Prime F. L. GBOBC1 mb2 F. | 50 | -19.15 | 1.56 | 150 | 12.25 | **2.35E-24** | 6.84E-04 | 6.01 |
| GBOBC1 b. R. GBOBC1 mb2 F. | 71 | 18.87 | 1.56 | 150 | 12.07 | **7.14E-24** | 6.93E-04 | 4.53 |
| GBOBC1 b. R. Gbn F. | 74 | 18.36 | 1.56 | 150 | 11.74 | **5.46E-23** | 7.02E-04 | 3.04 |
| GBHCT R. GBOBC1 b. R. | 54 | -17.68 | 1.56 | 150 | 11.31 | **7.78E-22** | 7.12E-04 | 6.27 |
| Prime R. GBOBC1 b. R. | 4 | -17.52 | 1.56 | 150 | 11.21 | **1.46E-21** | 7.22E-04 | 2.90 |
| Prime R. GBHCT F. | 9 | 16.33 | 1.56 | 150 | 10.45 | **1.54E-19** | 7.32E-04 | 3.06 |
| GBHCT R. GBHCT F. | 59 | 16.17 | 1.56 | 150 | 10.34 | **2.88E-19** | 7.43E-04 | 3.67 |
| GBOBC1 mb2 R. GBOBC1 mb2 F. | 80 | 15.74 | 1.56 | 150 | 10.07 | **1.55E-18** | 7.54E-04 | 3.37 |
| Prime R. GBOBC2 b. F. | 12 | 15.73 | 1.56 | 150 | 10.06 | **1.64E-18** | 7.65E-04 | 3.61 |
| Prime R. L. Gbn R. | 35 | -15.64 | 1.56 | 150 | 10.00 | **2.29E-18** | 7.77E-04 | 2.17 |
| GBHCT R. GBOBC2 b. F. | 62 | 15.57 | 1.56 | 150 | 9.96 | **3.05E-18** | 7.89E-04 | 4.00 |
| GBHCT F. Gbn F. | 109 | -15.50 | 1.56 | 150 | 9.91 | **3.95E-18** | 8.01E-04 | 8.02 |
| GBOBC1 mb2 R. Gbn F. | 83 | 15.22 | 1.56 | 150 | 9.74 | **1.14E-17** | 8.14E-04 | 2.38 |
| GBHCT F. GBOBC1 mb2 F. | 106 | -14.98 | 1.56 | 150 | 9.58 | **2.89E-17** | 8.27E-04 | 6.40 |
| GBOBC2 b. R. GBOBC1 mb2 F. | 88 | 14.95 | 1.56 | 150 | 9.56 | **3.23E-17** | 8.41E-04 | 4.44 |

| | | | | | | | | |
|---|---|---|---|---|---|---|---|---|
| GBOBC2 b. F. Gbn F. | 118 | -14.89 | 1.56 | 150 | 9.53 | **4.10E-17** | 8.55E-04 | 4.50 |
| GBHCT R. GBOBC1 mb2 R. | 55 | -14.55 | 1.56 | 150 | 9.31 | **1.52E-16** | 8.69E-04 | 5.97 |
| GBOBC2 b. R. Gbn F. | 91 | 14.44 | 1.56 | 150 | 9.23 | **2.33E-16** | 8.84E-04 | 3.18 |
| Prime R. GBOBC1 mb2 R. | 5 | -14.39 | 1.56 | 150 | 9.20 | **2.79E-16** | 8.99E-04 | 2.39 |
| GBOBC1 mb2 F. GBOBC2 b. F. | 114 | 14.37 | 1.56 | 150 | 9.19 | **2.95E-16** | 9.16E-04 | 8.51 |
| Prime R. L. GBOBC2 mb2 F. | 40 | 14.05 | 1.56 | 150 | 8.98 | **1.03E-15** | 9.32E-04 | 1.66 |
| GBHCT R. GBOBC2 b. R. | 56 | -13.76 | 1.56 | 150 | 8.80 | **2.99E-15** | 9.49E-04 | 10.08 |
| Prime R. L. GBOBC1 b. R. | 31 | -13.62 | 1.56 | 150 | 8.71 | **5.16E-15** | 9.67E-04 | 2.44 |
| Prime R. GBOBC2 b. R. | 6 | -13.60 | 1.56 | 150 | 8.70 | **5.45E-15** | 9.86E-04 | 2.33 |
| GBOBC2 mb2 R. GBOBC1 mb2 F. | 95 | 13.59 | 1.56 | 150 | 8.69 | **5.65E-15** | 0.00101 | 2.65 |
| Prime F. GBOBC1 b. F. | 24 | -13.27 | 1.56 | 150 | 8.49 | **1.85E-14** | 0.00103 | 3.26 |
| GBOBC2 mb2 R. Gbn F. | 98 | 13.08 | 1.56 | 150 | 8.36 | **3.86E-14** | 0.00105 | 1.68 |
| Prime R. L. GBOBC1 b. F. | 37 | 12.60 | 1.56 | 150 | 8.06 | **2.25E-13** | 0.00107 | 1.90 |
| GBHCT R. GBOBC2 mb2 R. | 57 | -12.40 | 1.56 | 150 | 7.93 | **4.57E-13** | 0.00109 | 2.18 |
| Prime R. GBOBC2 mb2 R. | 7 | -12.24 | 1.56 | 150 | 7.83 | **8.17E-13** | 0.00111 | 2.25 |
| Prime F. GBOBC2 mb2 F. | 27 | -11.83 | 1.56 | 150 | 7.56 | **3.63E-12** | 0.00114 | 2.17 |
| Prime F. L. GBOBC1 b. F. | 49 | -11.81 | 1.56 | 150 | 7.56 | **3.80E-12** | 0.00117 | 3.23 |
| Prime R. L. GBOBC1 mb2 R. | 32 | -10.48 | 1.56 | 150 | 6.71 | **3.81E-10** | 0.00119 | 1.95 |
| Prime F. L. GBOBC2 mb2 F. | 52 | -10.36 | 1.56 | 150 | 6.63 | **5.71E-10** | 0.00122 | 2.14 |
| Prime R. GBOBC2 mb2 F. | 13 | 10.14 | 1.56 | 150 | 6.49 | **1.20E-09** | 0.00125 | 1.79 |
| GBHCT R. GBOBC2 mb2 F. | 63 | 9.98 | 1.56 | 150 | 6.38 | **2.04E-09** | 0.00128 | 1.73 |
| Prime R. L. GBOBC2 b. R. | 33 | -9.70 | 1.56 | 150 | 6.20 | **5.13E-09** | 0.00131 | 1.92 |
| GBOBC2 mb2 F. Gbn F. | 119 | -9.31 | 1.56 | 150 | 5.95 | **1.79E-08** | 0.00135 | 2.60 |
| GBOBC1 mb2 F. GBOBC2 mb2 F. | 115 | 8.79 | 1.56 | 150 | 5.62 | **8.93E-08** | 0.00139 | 2.22 |
| Prime R. GBOBC1 b. F. | 10 | 8.69 | 1.56 | 150 | 5.56 | **1.20E-07** | 0.00142 | 2.24 |
| GBHCT R. GBOBC1 b. F. | 60 | 8.53 | 1.56 | 150 | 5.46 | **1.95E-07** | 0.00146 | 1.86 |
| Prime R. L. GBOBC2 mb2 R. | 34 | -8.34 | 1.56 | 150 | 5.33 | **3.49E-07** | 0.00151 | 1.74 |
| GBOBC1 b. F. Gbn F. | 113 | -7.86 | 1.56 | 150 | 5.03 | **1.41E-06** | 0.00155 | 1.84 |
| GBHCT F. GBOBC1 b. F. | 105 | -7.64 | 1.56 | 150 | 4.89 | **2.60E-06** | 0.0016 | 2.87 |
| GBOBC1 b. F. GBOBC1 mb2 F. | 110 | -7.34 | 1.56 | 150 | 4.70 | **5.94E-06** | 0.00165 | 2.04 |
| GBOBC2 mb2 R. Gbn R. | 92 | -7.30 | 1.56 | 150 | 4.67 | **6.62E-06** | 0.00171 | 1.74 |
| GBOBC1 b. F. GBOBC2 b. F. | 111 | 7.03 | 1.56 | 150 | 4.50 | **1.36E-05** | 0.00177 | 3.50 |
| Prime F. GBOBC2 b. F. | 26 | -6.24 | 1.56 | 150 | 3.99 | **1.02E-04** | 0.00183 | 2.02 |
| GBHCT F. GBOBC2 mb2 F. | 108 | -6.19 | 1.56 | 150 | 3.96 | **1.15E-04** | 0.0019 | 1.23 |
| GBOBC2 b. R. Gbn R. | 85 | -5.94 | 1.56 | 150 | 3.80 | **2.10E-04** | 0.00197 | 1.31 |
| Prime F. GBHCT F. | 23 | -5.63 | 1.56 | 150 | 3.60 | **4.26E-04** | 0.00205 | 1.70 |
| GBOBC2 b. F. GBOBC2 mb2 F. | 117 | -5.58 | 1.56 | 150 | 3.57 | **4.76E-04** | 0.00213 | 2.03 |
| GBOBC1 b. R. GBOBC2 mb2 R. | 67 | 5.28 | 1.56 | 150 | 3.38 | **9.32E-04** | 0.00223 | 2.27 |
| Prime R. L. GBOBC1 mb2 F. | 38 | 5.26 | 1.56 | 150 | 3.36 | **9.82E-04** | 0.00233 | 1.77 |
| GBOBC1 mb2 R. Gbn R. | 77 | -5.15 | 1.56 | 150 | 3.30 | **0.00122** | 0.00244 | 2.05 |
| Prime F. L. GBOBC2 b. F. | 51 | -4.78 | 1.56 | 150 | 3.06 | **0.00265** | 0.00256 | 1.99 |
| Prime R. L. Gbn F. | 41 | 4.74 | 1.56 | 150 | 3.03 | 0.00287 | 0 | 1.15 |
| Prime F. L. GBHCT F. | 48 | -4.17 | 1.56 | 150 | 2.67 | 0.00845 | 0 | 1.73 |

| | | | | | | | | |
|---|---|---|---|---|---|---|---|---|
| Prime R. L. GBHCT R. | 30 | 4.07 | 1.56 | 150 | 2.60 | 0.01025 | 0 | 1.35 |
| GBOBC1 b. R. GBOBC2 b. R. | 66 | 3.92 | 1.56 | 150 | 2.51 | 0.01324 | 0 | 1.58 |
| Prime R. Prime R. L. | 1 | -3.90 | 1.56 | 150 | 2.50 | 0.01358 | 0 | 0.36 |
| GBOBC1 b. R. GBOBC1 mb2 R. | 65 | 3.13 | 1.56 | 150 | 2.00 | 0.04691 | 0 | 1.71 |
| GBOBC1 mb2 R. GBOBC2 mb2 R. | 76 | 2.15 | 1.56 | 150 | 1.37 | 0.17157 | 0 | 1.00 |
| GBOBC1 b. R. Gbn R. | 68 | -2.02 | 1.56 | 150 | 1.29 | 0.19787 | 0 | 1.39 |
| Prime F. Prime F. L. | 16 | -1.46 | 1.56 | 150 | 0.94 | 0.35122 | 0 | 0.58 |
| GBOBC1 b. F. GBOBC2 mb2 F. | 112 | 1.45 | 1.56 | 150 | 0.93 | 0.35561 | 0 | 1.31 |
| GBOBC2 b. R. GBOBC2 mb2 R. | 84 | 1.36 | 1.56 | 150 | 0.87 | 0.38548 | 0 | 0.85 |
| Prime R. GBOBC1 mb2 F. | 11 | 1.35 | 1.56 | 150 | 0.86 | 0.38894 | 0 | 1.80 |
| GBHCT R. GBOBC1 mb2 F. | 61 | 1.19 | 1.56 | 150 | 0.76 | 0.4475 | 0 | 0.76 |
| Prime R. Gbn F. | 14 | 0.83 | 1.56 | 150 | 0.53 | 0.59422 | 0 | 1.23 |
| GBOBC1 mb2 R. GBOBC2 b. R. | 75 | 0.79 | 1.56 | 150 | 0.50 | 0.61545 | 0 | 0.84 |
| GBHCT R. Gbn F. | 64 | 0.67 | 1.56 | 150 | 0.43 | 0.66678 | 0 | 0.99 |
| GBHCT F. GBOBC2 b. F. | 107 | -0.61 | 1.56 | 150 | 0.39 | 0.69833 | 0 | 1.62 |
| GBOBC1 mb2 F. Gbn F. | 116 | -0.52 | 1.56 | 150 | 0.33 | 0.74173 | 0 | 0.93 |
| Prime R. GBHCT R. | 3 | 0.16 | 1.56 | 150 | 0.10 | 0.91853 | 0 | 1.06 |

Table B.9: Holm-Šidák results for Glide job 2 Names abbreviated for expediency. F., R., b., mb2, and d, correspond to Flexible, Rigid, bondi, mbondi2, and Cohen's d respectively. Significant differences shown in bold.

| **Compared Models** | **Index** | **Mean Diff.** | **Std.Er.** | **DF** | **\|t\|value** | **Prob>\|t\|** | **Alpha** | **d** |
|---|---|---|---|---|---|---|---|---|
| Prime F. Gbn R. | 22 | -41.35 | 2.10 | 165 | 19.65 | **4.64E-45** | 4.27E-04 | 3.00 |
| Prime F. L. Gbn R. | 47 | -41.25 | 2.10 | 165 | 19.60 | **6.21E-45** | 4.31E-04 | 2.99 |
| Prime F. GBOBC1 b. R. | 18 | -39.44 | 2.10 | 165 | 18.74 | **1.03E-42** | 4.35E-04 | 4.40 |
| Prime F. L. GBOBC1 b. R. | 43 | -39.34 | 2.10 | 165 | 18.69 | **1.39E-42** | 4.38E-04 | 4.38 |
| Prime F. GBOBC1 mb2 R. | 19 | -36.17 | 2.10 | 165 | 17.18 | **1.34E-38** | 4.42E-04 | 4.26 |
| Prime F. L. GBOBC1 mb2 R. | 44 | -36.07 | 2.10 | 165 | 17.14 | **1.82E-38** | 4.46E-04 | 4.25 |
| Gbn R. GBOBC2 b. F. | 102 | 35.85 | 2.10 | 165 | 17.03 | **3.47E-38** | 4.50E-04 | 4.46 |
| Prime F. GBOBC2 b. R. | 20 | -35.67 | 2.10 | 165 | 16.95 | **5.77E-38** | 4.54E-04 | 4.33 |
| Prime F. L. GBOBC2 b. R. | 45 | -35.57 | 2.10 | 165 | 16.90 | **7.84E-38** | 4.58E-04 | 4.32 |
| Prime F. GBOBC2 mb2 R. | 21 | -35.02 | 2.10 | 165 | 16.64 | **3.99E-37** | 4.62E-04 | 3.75 |
| Prime F. L. GBOBC2 mb2 R. | 46 | -34.92 | 2.10 | 165 | 16.59 | **5.43E-37** | 4.66E-04 | 3.73 |
| GBOBC1 b. R. GBOBC2 b. F. | 72 | 33.94 | 2.10 | 165 | 16.12 | **1.00E-35** | 4.70E-04 | 8.89 |
| Gbn R. GBHCT F. | 99 | 33.66 | 2.10 | 165 | 15.99 | **2.32E-35** | 4.75E-04 | 4.79 |
| GBOBC1 b. R. GBHCT F. | 69 | 31.74 | 2.10 | 165 | 15.08 | **7.29E-33** | 4.79E-04 | 6.64 |
| GBOBC1 mb2 R. GBOBC2 b. F. | 81 | 30.67 | 2.10 | 165 | 14.57 | **1.92E-31** | 4.84E-04 | 7.18 |
| GBOBC2 b. R. GBOBC2 b. F. | 89 | 30.17 | 2.10 | 165 | 14.33 | **8.71E-31** | 4.88E-04 | 8.28 |
| GBOBC2 mb2 R. GBOBC2 b. F. | 96 | 29.52 | 2.10 | 165 | 14.02 | **6.41E-30** | 4.93E-04 | 6.01 |
| GBOBC1 mb2 R. GBHCT F. | 78 | 28.47 | 2.10 | 165 | 13.53 | **1.55E-28** | 4.98E-04 | 5.20 |
| GBOBC2 b. R. GBHCT F. | 86 | 27.98 | 2.10 | 165 | 13.29 | **7.10E-28** | 5.03E-04 | 6.97 |
| Gbn R. GBOBC2 mb2 F. | 103 | 27.65 | 2.10 | 165 | 13.14 | **1.92E-27** | 5.08E-04 | 3.86 |

| | | | | | | | | |
|---|---|---|---|---|---|---|---|---|
| GBOBC2 mb2 R. GBHCT F. | 93 | 27.32 | 2.10 | 165 | 12.98 | **5.28E-27** | 5.13E-04 | 4.01 |
| GBOBC1 b. R. GBOBC2 mb2 F. | 73 | 25.74 | 2.10 | 165 | 12.23 | **6.76E-25** | 5.18E-04 | 4.53 |
| Gbn R. GBOBC1 b. F. | 100 | 25.38 | 2.10 | 165 | 12.06 | **2.07E-24** | 5.23E-04 | 3.69 |
| Prime F. Prime R. L. | 15 | -23.58 | 2.10 | 165 | 11.20 | **5.10E-22** | 5.29E-04 | 3.93 |
| Prime R. L. Prime F. L. | 29 | 23.47 | 2.10 | 165 | 11.15 | **7.01E-22** | 5.34E-04 | 3.90 |
| GBOBC1 b. R. GBOBC1 b. F. | 70 | 23.47 | 2.10 | 165 | 11.15 | **7.12E-22** | 5.40E-04 | 5.13 |
| Prime F. GBHCT R. | 17 | -23.08 | 2.10 | 165 | 10.97 | **2.29E-21** | 5.46E-04 | 2.68 |
| Prime F. L. GBHCT R. | 42 | -22.98 | 2.10 | 165 | 10.92 | **3.14E-21** | 5.51E-04 | 2.67 |
| Prime R. Prime F. | 0 | 22.71 | 2.10 | 165 | 10.79 | **7.13E-21** | 5.57E-04 | 4.53 |
| Prime R. Prime F. L. | 2 | 22.60 | 2.10 | 165 | 10.74 | **9.78E-21** | 5.64E-04 | 4.49 |
| GBOBC1 mb2 R. GBOBC2 mb2 F. | 82 | 22.47 | 2.10 | 165 | 10.68 | **1.46E-20** | 5.70E-04 | 3.80 |
| GBOBC2 b. R. GBOBC2 mb2 F. | 90 | 21.98 | 2.10 | 165 | 10.44 | **6.53E-20** | 5.76E-04 | 4.00 |
| Prime F. Gbn F. | 28 | -21.76 | 2.10 | 165 | 10.34 | **1.25E-19** | 5.83E-04 | 2.24 |
| Prime F. GBOBC1 mb2 F. | 25 | -21.75 | 2.10 | 165 | 10.33 | **1.30E-19** | 5.89E-04 | 2.61 |
| Prime F. L. Gbn F. | 53 | -21.65 | 2.10 | 165 | 10.29 | **1.71E-19** | 5.96E-04 | 2.22 |
| Prime F. L. GBOBC1 mb2 F. | 50 | -21.64 | 2.10 | 165 | 10.28 | **1.78E-19** | 6.03E-04 | 2.59 |
| GBOBC2 mb2 R. GBOBC2 mb2 F. | 97 | 21.32 | 2.10 | 165 | 10.13 | **4.66E-19** | 6.10E-04 | 4.08 |
| GBOBC1 mb2 R. GBOBC1 b. F. | 79 | 20.20 | 2.10 | 165 | 9.60 | **1.33E-17** | 6.18E-04 | 3.80 |
| GBOBC2 b. R. GBOBC1 b. F. | 87 | 19.70 | 2.10 | 165 | 9.36 | **5.74E-17** | 6.25E-04 | 4.59 |
| Gbn R. GBOBC1 mb2 F. | 101 | 19.61 | 2.10 | 165 | 9.31 | **7.58E-17** | 6.33E-04 | 2.60 |
| Gbn R. Gbn F. | 104 | 19.59 | 2.10 | 165 | 9.31 | **7.86E-17** | 6.41E-04 | 2.35 |
| GBOBC2 mb2 R. GBOBC1 b. F. | 94 | 19.05 | 2.10 | 165 | 9.05 | **3.88E-16** | 6.49E-04 | 2.99 |
| Prime R. Gbn R. | 8 | -18.64 | 2.10 | 165 | 8.86 | **1.25E-15** | 6.57E-04 | 1.41 |
| GBHCT R. Gbn R. | 58 | -18.27 | 2.10 | 165 | 8.68 | **3.66E-15** | 6.66E-04 | 2.94 |
| Prime R. L. GBOBC2 b. F. | 39 | 18.07 | 2.10 | 165 | 8.59 | **6.44E-15** | 6.75E-04 | 2.25 |
| Prime R. L. Gbn R. | 35 | -17.78 | 2.10 | 165 | 8.45 | **1.50E-14** | 6.84E-04 | 1.30 |
| GBOBC1 b. R. GBOBC1 mb2 F. | 71 | 17.69 | 2.10 | 165 | 8.41 | **1.88E-14** | 6.93E-04 | 4.75 |
| GBOBC1 b. R. Gbn F. | 74 | 17.68 | 2.10 | 165 | 8.40 | **1.95E-14** | 7.02E-04 | 3.13 |
| GBHCT R. GBOBC2 b. F. | 62 | 17.58 | 2.10 | 165 | 8.35 | **2.61E-14** | 7.12E-04 | 4.16 |
| Prime R. GBOBC2 b. F. | 12 | 17.20 | 2.10 | 165 | 8.17 | **7.52E-14** | 7.22E-04 | 2.47 |
| Prime R. GBOBC1 b. R. | 4 | -16.73 | 2.10 | 165 | 7.95 | **2.79E-13** | 7.32E-04 | 1.92 |
| GBHCT R. GBOBC1 b. R. | 54 | -16.36 | 2.10 | 165 | 7.77 | **7.86E-13** | 7.43E-04 | 6.52 |
| GBOBC2 b. F. Gbn F. | 118 | -16.25 | 2.10 | 165 | 7.72 | **1.04E-12** | 7.54E-04 | 4.19 |
| GBOBC1 mb2 F. GBOBC2 b. F. | 114 | 16.24 | 2.10 | 165 | 7.72 | **1.08E-12** | 7.65E-04 | 8.17 |
| Prime F. GBOBC1 b. F. | 24 | -15.97 | 2.10 | 165 | 7.59 | **2.24E-12** | 7.77E-04 | 1.48 |
| Prime R. L. GBHCT F. | 36 | 15.88 | 2.10 | 165 | 7.54 | **2.90E-12** | 7.89E-04 | 2.72 |
| Prime F. L. GBOBC1 b. F. | 49 | -15.87 | 2.10 | 165 | 7.54 | **2.97E-12** | 8.01E-04 | 1.47 |
| Prime R. L. GBOBC1 b. R. | 31 | -15.86 | 2.10 | 165 | 7.54 | **3.02E-12** | 8.14E-04 | 1.72 |
| GBHCT R. GBHCT F. | 59 | 15.39 | 2.10 | 165 | 7.31 | **1.09E-11** | 8.27E-04 | 3.34 |
| Prime R. GBHCT F. | 9 | 15.01 | 2.10 | 165 | 7.13 | **2.95E-11** | 8.41E-04 | 3.05 |
| GBOBC1 mb2 R. GBOBC1 mb2 F. | 80 | 14.42 | 2.10 | 165 | 6.85 | **1.37E-10** | 8.55E-04 | 3.52 |
| GBOBC1 mb2 R. Gbn F. | 83 | 14.41 | 2.10 | 165 | 6.85 | **1.42E-10** | 8.69E-04 | 2.37 |
| GBHCT F. Gbn F. | 109 | -14.06 | 2.10 | 165 | 6.68 | **3.47E-10** | 8.84E-04 | 7.36 |

| | | | | | | | | |
|---|---|---|---|---|---|---|---|---|
| GBHCT F. GBOBC1 mb2 F. | 106 | -14.05 | 2.10 | 165 | 6.68 | **3.58E-10** | 8.99E-04 | 4.73 |
| GBOBC2 b. R. GBOBC1 mb2 F. | 88 | 13.93 | 2.10 | 165 | 6.62 | **4.89E-10** | 9.16E-04 | 4.65 |
| GBOBC2 b. R. Gbn F. | 91 | 13.92 | 2.10 | 165 | 6.61 | **5.05E-10** | 9.32E-04 | 3.13 |
| Prime F. GBOBC2 mb2 F. | 27 | -13.70 | 2.10 | 165 | 6.51 | **8.73E-10** | 9.49E-04 | 1.24 |
| Prime F. L. GBOBC2 mb2 F. | 52 | -13.59 | 2.10 | 165 | 6.46 | **1.13E-09** | 9.67E-04 | 1.23 |
| Prime R. GBOBC1 mb2 R. | 5 | -13.46 | 2.10 | 165 | 6.40 | **1.58E-09** | 9.86E-04 | 1.66 |
| GBOBC2 mb2 R. GBOBC1 mb2 F. | 95 | 13.27 | 2.10 | 165 | 6.31 | **2.52E-09** | 1.01E-03 | 2.78 |
| GBOBC2 mb2 R. Gbn F. | 98 | 13.26 | 2.10 | 165 | 6.30 | **2.60E-09** | 1.03E-03 | 1.70 |
| GBHCT R. GBOBC1 mb2 R. | 55 | -13.09 | 2.10 | 165 | 6.22 | **3.99E-09** | 1.05E-03 | 6.22 |
| Prime R. GBOBC2 b. R. | 6 | -12.97 | 2.10 | 165 | 6.16 | **5.36E-09** | 1.07E-03 | 1.60 |
| Prime R. L. GBOBC1 mb2 R. | 32 | -12.59 | 2.10 | 165 | 5.98 | **1.32E-08** | 1.09E-03 | 1.46 |
| GBHCT R. GBOBC2 b. R. | 56 | -12.59 | 2.10 | 165 | 5.98 | **1.33E-08** | 1.11E-03 | 10.53 |
| Prime R. GBOBC2 mb2 R. | 7 | -12.31 | 2.10 | 165 | 5.85 | **2.58E-08** | 1.14E-03 | 1.54 |
| Prime R. L. GBOBC2 b. R. | 33 | -12.10 | 2.10 | 165 | 5.75 | **4.27E-08** | 1.17E-03 | 1.41 |
| GBHCT R. GBOBC2 mb2 R. | 57 | -11.94 | 2.10 | 165 | 5.67 | **6.21E-08** | 1.19E-03 | 2.28 |
| Prime R. L. GBOBC2 mb2 R. | 34 | -11.44 | 2.10 | 165 | 5.44 | **1.92E-07** | 1.22E-03 | 1.32 |
| GBOBC1 b. F. GBOBC2 b. F. | 111 | 10.47 | 2.10 | 165 | 4.97 | **1.63E-06** | 1.25E-03 | 2.54 |
| Prime R. L. GBOBC2 mb2 F. | 40 | 9.88 | 2.10 | 165 | 4.69 | **5.62E-06** | 1.28E-03 | 1.75 |
| GBHCT R. GBOBC2 mb2 F. | 63 | 9.39 | 2.10 | 165 | 4.46 | **1.52E-05** | 1.31E-03 | 1.56 |
| Prime R. GBOBC2 mb2 F. | 13 | 9.01 | 2.10 | 165 | 4.28 | **3.15E-05** | 1.35E-03 | 1.85 |
| GBHCT F. GBOBC1 b. F. | 105 | -8.28 | 2.10 | 165 | 3.93 | **1.23E-04** | 1.39E-03 | 3.02 |
| GBOBC2 b. F. GBOBC2 mb2 F. | 117 | -8.19 | 2.10 | 165 | 3.89 | **1.44E-04** | 1.42E-03 | 1.75 |
| GBOBC2 mb2 F. Gbn F. | 119 | -8.06 | 2.10 | 165 | 3.83 | **1.82E-04** | 1.46E-03 | 2.39 |
| GBOBC1 mb2 F. GBOBC2 mb2 F. | 115 | 8.05 | 2.10 | 165 | 3.82 | **1.86E-04** | 1.51E-03 | 1.82 |
| Prime F. GBHCT F. | 23 | -7.70 | 2.10 | 165 | 3.66 | **3.43E-04** | 1.55E-03 | 0.79 |
| Prime R. L. GBOBC1 b. F. | 37 | 7.60 | 2.10 | 165 | 3.61 | **4.03E-04** | 1.60E-03 | 1.86 |
| Prime F. L. GBHCT F. | 48 | -7.59 | 2.10 | 165 | 3.61 | **4.10E-04** | 1.65E-03 | 0.79 |
| GBHCT R. GBOBC1 b. F. | 60 | 7.11 | 2.10 | 165 | 3.38 | **9.12E-04** | 1.71E-03 | 1.58 |
| Prime R. GBOBC1 b. F. | 10 | 6.73 | 2.10 | 165 | 3.20 | **1.65E-03** | 1.77E-03 | 1.99 |
| GBOBC2 mb2 R. Gbn R. | 92 | -6.33 | 2.10 | 165 | 3.01 | 3.04E-03 | 1.83E-03 | 1.21 |
| GBHCT F. GBOBC2 mb2 F. | 108 | -6.00 | 2.10 | 165 | 2.85 | 4.91E-03 | 0.00E+00 | 1.31 |
| GBOBC1 b. F. Gbn F. | 113 | -5.79 | 2.10 | 165 | 2.75 | 6.65E-03 | 0.00E+00 | 1.71 |
| GBOBC1 b. F. GBOBC1 mb2 F. | 110 | -5.77 | 2.10 | 165 | 2.74 | 6.77E-03 | 0.00E+00 | 1.82 |
| GBOBC2 b. R. Gbn R. | 85 | -5.68 | 2.10 | 165 | 2.70 | 7.71E-03 | 0.00E+00 | 1.01 |
| Prime F. GBOBC2 b. F. | 26 | -5.51 | 2.10 | 165 | 2.62 | 9.74E-03 | 0.00E+00 | 0.89 |
| Prime F. L. GBOBC2 b. F. | 51 | -5.40 | 2.10 | 165 | 2.57 | 1.12E-02 | 0.00E+00 | 0.87 |
| GBOBC1 mb2 R. Gbn R. | 77 | -5.18 | 2.10 | 165 | 2.46 | 1.49E-02 | 0.00E+00 | 0.99 |
| GBOBC1 b. R. GBOBC2 mb2 R. | 67 | 4.42 | 2.10 | 165 | 2.10 | 3.72E-02 | 0.00E+00 | 2.39 |
| GBOBC1 b. R. GBOBC2 b. R. | 66 | 3.77 | 2.10 | 165 | 1.79 | 7.54E-02 | 0.00E+00 | 1.68 |
| GBOBC1 b. R. GBOBC1 mb2 R. | 65 | 3.27 | 2.10 | 165 | 1.55 | 1.22E-01 | 0.00E+00 | 1.80 |
| GBOBC1 b. F. GBOBC2 mb2 F. | 112 | 2.28 | 2.10 | 165 | 1.08 | 2.81E-01 | 0.00E+00 | 1.33 |
| GBHCT F. GBOBC2 b. F. | 107 | 2.19 | 2.10 | 165 | 1.04 | 2.99E-01 | 0.00E+00 | 1.03 |
| GBOBC1 b. R. Gbn R. | 68 | -1.91 | 2.10 | 165 | 0.91 | 3.65E-01 | 0.00E+00 | 0.78 |

| | | | | | | | | |
|---|---|---|---|---|---|---|---|---|
| Prime R. L. GBOBC1 mb2 F. | 38 | 1.83 | 2.10 | 165 | 0.87 | 3.86E-01 | 0.00E+00 | 1.30 |
| Prime R. L. Gbn F. | 41 | 1.82 | 2.10 | 165 | 0.86 | 3.89E-01 | 0.00E+00 | 1.08 |
| GBHCT R. GBOBC1 mb2 F. | 61 | 1.34 | 2.10 | 165 | 0.64 | 5.26E-01 | 0.00E+00 | 0.76 |
| GBHCT R. Gbn F. | 64 | 1.32 | 2.10 | 165 | 0.63 | 5.30E-01 | 0.00E+00 | 1.00 |
| GBOBC1 mb2 R. GBOBC2 mb2 R. | 76 | 1.15 | 2.10 | 165 | 0.55 | 5.86E-01 | 0.00E+00 | 0.97 |
| Prime R. GBOBC1 mb2 F. | 11 | 0.96 | 2.10 | 165 | 0.46 | 6.48E-01 | 0.00E+00 | 1.15 |
| Prime R. Gbn F. | 14 | 0.95 | 2.10 | 165 | 0.45 | 6.53E-01 | 0.00E+00 | 1.05 |
| Prime R. Prime R. L. | 1 | -0.87 | 2.10 | 165 | 0.41 | 6.81E-01 | 0.00E+00 | 0.34 |
| GBOBC2 b. R. GBOBC2 mb2 R. | 84 | 0.65 | 2.10 | 165 | 0.31 | 7.56E-01 | 0.00E+00 | 0.82 |
| GBOBC1 mb2 R. GBOBC2 b. R. | 75 | 0.50 | 2.10 | 165 | 0.24 | 8.14E-01 | 0.00E+00 | 0.80 |
| Prime R. L. GBHCT R. | 30 | 0.49 | 2.10 | 165 | 0.23 | 8.15E-01 | 0.00E+00 | 1.01 |
| Prime R. GBHCT R. | 3 | -0.38 | 2.10 | 165 | 0.18 | 8.59E-01 | 0.00E+00 | 0.83 |
| Prime F. Prime F. L. | 16 | -0.10 | 2.10 | 165 | 0.05 | 9.61E-01 | 0.00E+00 | 0.55 |
| GBOBC1 mb2 F. Gbn F. | 116 | -0.01 | 2.10 | 165 | 0.01 | 9.95E-01 | 0.00E+00 | 1.00 |

Table B.10: Holm-Šidák results for Glide job 2 excluding ligand 7. Names abbreviated for expediency. F., R., b., mb2, and d, correspond to Flexible, Rigid, bondi, mbondi2, and Cohen's d respectively. Significant differences shown in bold.

| **Compared Models** | **Index** | **Mean Diff.** | **Std.Er.** | **DF** | **\|t\|value** | **Prob>\|t\|** | **Alpha** | **d** |
|---|---|---|---|---|---|---|---|---|
| Prime F. Gbn R. | 22 | -37.65 | 1.45 | 150 | 25.98 | **2.11E-57** | 4.27E-04 | 7.11 |
| Prime F. L. Gbn R. | 47 | -37.53 | 1.45 | 150 | 25.90 | **3.06E-57** | 4.31E-04 | 7.24 |
| Prime F. GBOBC1 b. R. | 18 | -37.07 | 1.45 | 150 | 25.59 | **1.38E-56** | 4.35E-04 | 9.69 |
| Prime F. L. GBOBC1 b. R. | 43 | -36.96 | 1.45 | 150 | 25.51 | **2.00E-56** | 4.38E-04 | 9.83 |
| Gbn R. GBOBC2 b. F. | 102 | 34.13 | 1.45 | 150 | 23.56 | **2.91E-52** | 4.42E-04 | 6.03 |
| Prime F. GBOBC1 mb2 R. | 19 | -33.98 | 1.45 | 150 | 23.45 | **4.94E-52** | 4.46E-04 | 8.53 |
| Prime F. L. GBOBC1 mb2 R. | 44 | -33.86 | 1.45 | 150 | 23.37 | **7.34E-52** | 4.50E-04 | 8.70 |
| GBOBC1 b. R. GBOBC2 b. F. | 72 | 33.56 | 1.45 | 150 | 23.16 | **2.13E-51** | 4.54E-04 | 8.92 |
| Prime F. GBOBC2 b. R. | 20 | -33.46 | 1.45 | 150 | 23.09 | **3.01E-51** | 4.58E-04 | 10.75 |
| Prime F. L. GBOBC2 b. R. | 45 | -33.34 | 1.45 | 150 | 23.01 | **4.49E-51** | 4.62E-04 | 10.98 |
| Prime F. GBOBC2 mb2 R. | 21 | -32.82 | 1.45 | 150 | 22.65 | **2.86E-50** | 4.66E-04 | 5.81 |
| Gbn R. GBHCT F. | 99 | 32.77 | 1.45 | 150 | 22.62 | **3.43E-50** | 4.70E-04 | 4.95 |
| Prime F. L. GBOBC2 mb2 R. | 46 | -32.71 | 1.45 | 150 | 22.57 | **4.28E-50** | 4.75E-04 | 5.80 |
| GBOBC1 b. R. GBHCT F. | 69 | 32.20 | 1.45 | 150 | 22.22 | **2.63E-49** | 4.79E-04 | 6.80 |
| GBOBC1 mb2 R. GBOBC2 b. F. | 81 | 30.46 | 1.45 | 150 | 21.02 | **1.45E-46** | 4.84E-04 | 6.90 |
| GBOBC2 b. R. GBOBC2 b. F. | 89 | 29.94 | 1.45 | 150 | 20.66 | **9.89E-46** | 4.88E-04 | 8.03 |
| GBOBC2 mb2 R. GBOBC2 b. F. | 96 | 29.30 | 1.45 | 150 | 20.22 | **1.07E-44** | 4.93E-04 | 5.75 |
| GBOBC1 mb2 R. GBHCT F. | 78 | 29.10 | 1.45 | 150 | 20.08 | **2.31E-44** | 4.98E-04 | 5.51 |
| GBOBC2 b. R. GBHCT F. | 86 | 28.58 | 1.45 | 150 | 19.73 | **1.64E-43** | 5.03E-04 | 7.95 |
| GBOBC2 mb2 R. GBHCT F. | 93 | 27.94 | 1.45 | 150 | 19.29 | **1.87E-42** | 5.08E-04 | 4.12 |
| Gbn R. GBOBC2 mb2 F. | 103 | 26.86 | 1.45 | 150 | 18.54 | **1.24E-40** | 5.13E-04 | 3.87 |
| GBOBC1 b. R. GBOBC2 mb2 F. | 73 | 26.28 | 1.45 | 150 | 18.14 | **1.17E-39** | 5.18E-04 | 4.67 |
| Gbn R. GBOBC1 b. F. | 100 | 24.58 | 1.45 | 150 | 16.97 | **1.02E-36** | 5.23E-04 | 3.72 |

| | | | | | | | | |
|---|---|---|---|---|---|---|---|---|
| GBOBC1 b. R. GBOBC1 b. F. | 70 | 24.01 | 1.45 | 150 | 16.57 | **1.03E-35** | 5.29E-04 | 5.49 |
| Prime F. Prime R. L. | 15 | -23.38 | 1.45 | 150 | 16.14 | **1.34E-34** | 5.34E-04 | 3.74 |
| Prime R. L. Prime F. L. | 29 | 23.27 | 1.45 | 150 | 16.06 | **2.13E-34** | 5.40E-04 | 3.71 |
| GBOBC1 mb2 R. GBOBC2 mb2 F. | 82 | 23.19 | 1.45 | 150 | 16.00 | **2.96E-34** | 5.46E-04 | 4.12 |
| GBOBC2 b. R. GBOBC2 mb2 F. | 90 | 22.67 | 1.45 | 150 | 15.65 | **2.48E-33** | 5.51E-04 | 4.37 |
| Prime R. Prime F. | 0 | 22.43 | 1.45 | 150 | 15.48 | **6.56E-33** | 5.57E-04 | 4.34 |
| Prime R. Prime F. L. | 2 | 22.32 | 1.45 | 150 | 15.40 | **1.05E-32** | 5.64E-04 | 4.31 |
| GBOBC2 mb2 R. GBOBC2 mb2 F. | 97 | 22.03 | 1.45 | 150 | 15.21 | **3.47E-32** | 5.70E-04 | 4.56 |
| GBOBC1 mb2 R. GBOBC1 b. F. | 79 | 20.91 | 1.45 | 150 | 14.43 | **3.68E-30** | 5.76E-04 | 4.24 |
| Prime F. GBHCT R. | 17 | -20.85 | 1.45 | 150 | 14.39 | **4.85E-30** | 5.83E-04 | 5.27 |
| Prime F. L. GBHCT R. | 42 | -20.73 | 1.45 | 150 | 14.31 | **7.81E-30** | 5.89E-04 | 5.38 |
| GBOBC2 b. R. GBOBC1 b. F. | 87 | 20.39 | 1.45 | 150 | 14.08 | **3.24E-29** | 5.96E-04 | 5.47 |
| Prime R. L. GBOBC2 b. F. | 39 | 19.86 | 1.45 | 150 | 13.71 | **3.04E-28** | 6.03E-04 | 3.03 |
| GBOBC2 mb2 R. GBOBC1 b. F. | 94 | 19.76 | 1.45 | 150 | 13.64 | **4.77E-28** | 6.10E-04 | 3.20 |
| Prime F. GBOBC1 mb2 F. | 25 | -19.51 | 1.45 | 150 | 13.47 | **1.34E-27** | 6.18E-04 | 6.11 |
| Prime F. L. GBOBC1 mb2 F. | 50 | -19.40 | 1.45 | 150 | 13.39 | **2.18E-27** | 6.25E-04 | 6.01 |
| Prime F. Gbn F. | 28 | -19.19 | 1.45 | 150 | 13.25 | **5.19E-27** | 6.33E-04 | 4.65 |
| Prime F. L. Gbn F. | 53 | -19.08 | 1.45 | 150 | 13.17 | **8.41E-27** | 6.41E-04 | 4.62 |
| Prime R. GBOBC2 b. F. | 12 | 18.92 | 1.45 | 150 | 13.06 | **1.67E-26** | 6.49E-04 | 3.61 |
| Prime R. L. GBHCT F. | 36 | 18.50 | 1.45 | 150 | 12.77 | **9.67E-26** | 6.57E-04 | 2.74 |
| Gbn R. Gbn F. | 104 | 18.45 | 1.45 | 150 | 12.74 | **1.18E-25** | 6.66E-04 | 2.40 |
| Gbn R. GBOBC1 mb2 F. | 101 | 18.14 | 1.45 | 150 | 12.52 | **4.59E-25** | 6.75E-04 | 3.12 |
| GBOBC1 b. R. Gbn F. | 74 | 17.88 | 1.45 | 150 | 12.34 | **1.35E-24** | 6.84E-04 | 3.04 |
| GBOBC1 b. R. GBOBC1 mb2 F. | 71 | 17.56 | 1.45 | 150 | 12.12 | **5.23E-24** | 6.93E-04 | 4.53 |
| Prime R. GBHCT F. | 9 | 17.56 | 1.45 | 150 | 12.12 | **5.42E-24** | 7.02E-04 | 3.06 |
| GBHCT R. GBOBC2 b. F. | 62 | 17.33 | 1.45 | 150 | 11.96 | **1.42E-23** | 7.12E-04 | 4.00 |
| GBHCT R. Gbn R. | 58 | -16.80 | 1.45 | 150 | 11.60 | **1.35E-22** | 7.22E-04 | 4.49 |
| GBHCT R. GBOBC1 b. R. | 54 | -16.23 | 1.45 | 150 | 11.20 | **1.53E-21** | 7.32E-04 | 6.27 |
| GBOBC1 mb2 F. GBOBC2 b. F. | 114 | 15.99 | 1.45 | 150 | 11.04 | **4.14E-21** | 7.43E-04 | 8.51 |
| GBHCT R. GBHCT F. | 59 | 15.97 | 1.45 | 150 | 11.02 | **4.60E-21** | 7.54E-04 | 3.67 |
| GBOBC2 b. F. Gbn F. | 118 | -15.67 | 1.45 | 150 | 10.82 | **1.60E-20** | 7.65E-04 | 4.50 |
| Prime R. Gbn R. | 8 | -15.21 | 1.45 | 150 | 10.50 | **1.12E-19** | 7.77E-04 | 2.53 |
| GBOBC1 mb2 R. Gbn F. | 83 | 14.78 | 1.45 | 150 | 10.20 | **6.78E-19** | 7.89E-04 | 2.38 |
| Prime R. GBOBC1 b. R. | 4 | -14.64 | 1.45 | 150 | 10.11 | **1.24E-18** | 8.01E-04 | 2.90 |
| GBHCT F. GBOBC1 mb2 F. | 106 | -14.63 | 1.45 | 150 | 10.10 | **1.28E-18** | 8.14E-04 | 6.40 |
| GBOBC1 mb2 R. GBOBC1 mb2 F. | 80 | 14.47 | 1.45 | 150 | 9.98 | **2.58E-18** | 8.27E-04 | 3.37 |
| GBHCT F. Gbn F. | 109 | -14.31 | 1.45 | 150 | 9.88 | **4.86E-18** | 8.41E-04 | 8.02 |
| GBOBC2 b. R. Gbn F. | 91 | 14.27 | 1.45 | 150 | 9.85 | **5.92E-18** | 8.55E-04 | 3.18 |
| Prime R. L. Gbn R. | 35 | -14.27 | 1.45 | 150 | 9.85 | **5.93E-18** | 8.69E-04 | 2.17 |
| GBOBC2 b. R. GBOBC1 mb2 F. | 88 | 13.95 | 1.45 | 150 | 9.63 | **2.23E-17** | 8.84E-04 | 4.44 |
| Prime R. L. GBOBC1 b. R. | 31 | -13.69 | 1.45 | 150 | 9.45 | **6.37E-17** | 8.99E-04 | 2.44 |
| GBOBC2 mb2 R. Gbn F. | 98 | 13.63 | 1.45 | 150 | 9.41 | **8.36E-17** | 9.16E-04 | 1.68 |
| GBOBC2 mb2 R. GBOBC1 mb2 F. | 95 | 13.31 | 1.45 | 150 | 9.19 | **3.11E-16** | 9.32E-04 | 2.65 |

| | | | | | | | | |
|---|---|---|---|---|---|---|---|---|
| GBHCT R. GBOBC1 mb2 R. | 55 | -13.13 | 1.45 | 150 | 9.06 | **6.48E-16** | 9.49E-04 | 5.97 |
| Prime F. GBOBC1 b. F. | 24 | -13.06 | 1.45 | 150 | 9.02 | **8.48E-16** | 9.67E-04 | 3.26 |
| Prime F. L. GBOBC1 b. F. | 49 | -12.95 | 1.45 | 150 | 8.94 | **1.35E-15** | 9.86E-04 | 3.23 |
| GBHCT R. GBOBC2 b. R. | 56 | -12.61 | 1.45 | 150 | 8.70 | **5.33E-15** | 0.00101 | 10.08 |
| Prime R. L. GBOBC2 mb2 F. | 40 | 12.59 | 1.45 | 150 | 8.69 | **5.81E-15** | 0.00103 | 1.66 |
| GBHCT R. GBOBC2 mb2 R. | 57 | -11.97 | 1.45 | 150 | 8.26 | **6.88E-14** | 0.00105 | 2.18 |
| Prime R. GBOBC2 mb2 F. | 13 | 11.64 | 1.45 | 150 | 8.04 | **2.54E-13** | 0.00107 | 1.79 |
| Prime R. GBOBC1 mb2 R. | 5 | -11.54 | 1.45 | 150 | 7.97 | **3.77E-13** | 0.00109 | 2.39 |
| Prime R. GBOBC2 b. R. | 6 | -11.02 | 1.45 | 150 | 7.61 | **2.83E-12** | 0.00111 | 2.33 |
| Prime F. GBOBC2 mb2 F. | 27 | -10.79 | 1.45 | 150 | 7.45 | **6.97E-12** | 0.00114 | 2.17 |
| Prime F. L. GBOBC2 mb2 F. | 52 | -10.68 | 1.45 | 150 | 7.37 | **1.07E-11** | 0.00117 | 2.14 |
| Prime R. L. GBOBC1 mb2 R. | 32 | -10.60 | 1.45 | 150 | 7.31 | **1.45E-11** | 0.00119 | 1.95 |
| Prime R. GBOBC2 mb2 R. | 7 | -10.39 | 1.45 | 150 | 7.17 | **3.20E-11** | 0.00122 | 2.25 |
| Prime R. L. GBOBC1 b. F. | 37 | 10.32 | 1.45 | 150 | 7.12 | **4.18E-11** | 0.00125 | 1.90 |
| Prime R. L. GBOBC2 b. R. | 33 | -10.08 | 1.45 | 150 | 6.96 | **1.01E-10** | 0.00128 | 1.92 |
| GBHCT R. GBOBC2 mb2 F. | 63 | 10.06 | 1.45 | 150 | 6.94 | **1.10E-10** | 0.00131 | 1.73 |
| GBOBC1 b. F. GBOBC2 b. F. | 111 | 9.55 | 1.45 | 150 | 6.59 | **7.06E-10** | 0.00135 | 3.50 |
| Prime R. L. GBOBC2 mb2 R. | 34 | -9.44 | 1.45 | 150 | 6.52 | **1.04E-09** | 0.00139 | 1.74 |
| Prime R. GBOBC1 b. F. | 10 | 9.37 | 1.45 | 150 | 6.47 | **1.33E-09** | 0.00142 | 2.24 |
| GBOBC1 mb2 F. GBOBC2 mb2 F. | 115 | 8.72 | 1.45 | 150 | 6.02 | **1.29E-08** | 0.00146 | 2.22 |
| GBOBC2 mb2 F. Gbn F. | 119 | -8.40 | 1.45 | 150 | 5.80 | **3.81E-08** | 0.00151 | 2.60 |
| GBHCT F. GBOBC1 b. F. | 105 | -8.19 | 1.45 | 150 | 5.65 | **7.82E-08** | 0.00155 | 2.87 |
| GBHCT R. GBOBC1 b. F. | 60 | 7.78 | 1.45 | 150 | 5.37 | **2.93E-07** | 0.0016 | 1.86 |
| GBOBC2 b. F. GBOBC2 mb2 F. | 117 | -7.27 | 1.45 | 150 | 5.02 | **1.45E-06** | 0.00165 | 2.03 |
| GBOBC1 b. F. GBOBC1 mb2 F. | 110 | -6.45 | 1.45 | 150 | 4.45 | **1.67E-05** | 0.00171 | 2.04 |
| GBOBC1 b. F. Gbn F. | 113 | -6.13 | 1.45 | 150 | 4.23 | **4.07E-05** | 0.00177 | 1.84 |
| GBHCT F. GBOBC2 mb2 F. | 108 | -5.91 | 1.45 | 150 | 4.08 | **7.28E-05** | 0.00183 | 1.23 |
| Prime F. GBHCT F. | 23 | -4.88 | 1.45 | 150 | 3.37 | **9.67E-04** | 0.0019 | 1.70 |
| GBOBC2 mb2 R. Gbn R. | 92 | -4.83 | 1.45 | 150 | 3.33 | **0.00109** | 0.00197 | 1.74 |
| Prime F. L. GBHCT F. | 48 | -4.76 | 1.45 | 150 | 3.29 | **0.00126** | 0.00205 | 1.73 |
| GBOBC1 b. R. GBOBC2 mb2 R. | 67 | 4.25 | 1.45 | 150 | 2.94 | **0.00384** | 0.00213 | 2.27 |
| Prime R. L. Gbn F. | 41 | 4.19 | 1.45 | 150 | 2.89 | 0.00441 | 0 | 1.15 |
| GBOBC2 b. R. Gbn R. | 85 | -4.19 | 1.45 | 150 | 2.89 | 0.00442 | 0 | 1.31 |
| Prime R. L. GBOBC1 mb2 F. | 38 | 3.87 | 1.45 | 150 | 2.67 | 0.00841 | 0 | 1.77 |
| GBOBC1 mb2 R. Gbn R. | 77 | -3.67 | 1.45 | 150 | 2.53 | 0.01234 | 0 | 2.05 |
| GBOBC1 b. R. GBOBC2 b. R. | 66 | 3.62 | 1.45 | 150 | 2.50 | 0.01364 | 0 | 1.58 |
| Prime F. GBOBC2 b. F. | 26 | -3.52 | 1.45 | 150 | 2.43 | 0.01637 | 0 | 2.02 |
| Prime F. L. GBOBC2 b. F. | 51 | -3.40 | 1.45 | 150 | 2.35 | 0.02011 | 0 | 1.99 |
| Prime R. Gbn F. | 14 | 3.24 | 1.45 | 150 | 2.24 | 0.02674 | 0 | 1.23 |
| GBOBC1 b. R. GBOBC1 mb2 R. | 65 | 3.10 | 1.45 | 150 | 2.14 | 0.03411 | 0 | 1.71 |
| Prime R. GBOBC1 mb2 F. | 11 | 2.92 | 1.45 | 150 | 2.02 | 0.04547 | 0 | 1.80 |
| Prime R. L. GBHCT R. | 30 | 2.53 | 1.45 | 150 | 1.75 | 0.08235 | 0 | 1.35 |
| GBOBC1 b. F. GBOBC2 mb2 F. | 112 | 2.27 | 1.45 | 150 | 1.57 | 0.11855 | 0 | 1.31 |

| | | | | | | | | |
|---|---|---|---|---|---|---|---|---|
| GBHCT R. Gbn F. | 64 | 1.65 | 1.45 | 150 | 1.14 | 0.25529 | 0 | 0.99 |
| Prime R. GBHCT R. | 3 | 1.59 | 1.45 | 150 | 1.10 | 0.27512 | 0 | 1.06 |
| GBHCT F. GBOBC2 b. F. | 107 | 1.36 | 1.45 | 150 | 0.94 | 0.34941 | 0 | 1.62 |
| GBHCT R. GBOBC1 mb2 F. | 61 | 1.34 | 1.45 | 150 | 0.92 | 0.35815 | 0 | 0.76 |
| GBOBC1 mb2 R. GBOBC2 mb2 R. | 76 | 1.16 | 1.45 | 150 | 0.80 | 0.42606 | 0 | 1.00 |
| Prime R. Prime R. L. | 1 | -0.95 | 1.45 | 150 | 0.65 | 0.5144 | 0 | 0.36 |
| GBOBC2 b. R. GBOBC2 mb2 R. | 84 | 0.64 | 1.45 | 150 | 0.44 | 0.66023 | 0 | 0.85 |
| GBOBC1 b. R. Gbn R. | 68 | -0.57 | 1.45 | 150 | 0.39 | 0.69365 | 0 | 1.39 |
| GBOBC1 mb2 R. GBOBC2 b. R. | 75 | 0.52 | 1.45 | 150 | 0.36 | 0.72111 | 0 | 0.84 |
| GBOBC1 mb2 F. Gbn F. | 116 | 0.32 | 1.45 | 150 | 0.22 | 0.82599 | 0 | 0.93 |
| Prime F. Prime F. L. | 16 | -0.11 | 1.45 | 150 | 0.08 | 0.93754 | 0 | 0.58 |

Table B.11: Holm-Šidák results for Glide job 3. Names abbreviated for expediency. F., R., b., mb2, and d, correspond to Flexible, Rigid, bondi, mbondi2, and Cohen's d respectively. Significant differences shown in bold.

| **Compared Models** | **Index** | **Mean Diff.** | **Std.Er.** | **DF** | **\|t\|value** | **Prob>\|t\|** | **Alpha** | **d** |
|---|---|---|---|---|---|---|---|---|
| Prime F. Gbn R. | 22 | -39.61 | 1.52 | 165 | 25.98 | **3.35E-60** | 4.27E-04 | 6.30 |
| Prime F. L. Gbn R. | 47 | -37.84 | 1.52 | 165 | 24.82 | **1.38E-57** | 4.31E-04 | 4.29 |
| Prime F. GBOBC1 b. R. | 18 | -37.03 | 1.52 | 165 | 24.29 | **2.27E-56** | 4.35E-04 | 5.91 |
| Prime F. L. GBOBC1 b. R. | 43 | -35.26 | 1.52 | 165 | 23.13 | **1.19E-53** | 4.38E-04 | 4.51 |
| Gbn R. GBHCT F. | 99 | 34.90 | 1.52 | 165 | 22.89 | **4.41E-53** | 4.42E-04 | 7.25 |
| Gbn R. GBOBC2 b. F. | 102 | 34.79 | 1.52 | 165 | 22.82 | **6.60E-53** | 4.46E-04 | 6.13 |
| Prime F. GBOBC1 mb2 R. | 19 | -34.46 | 1.52 | 165 | 22.60 | **2.12E-52** | 4.50E-04 | 5.96 |
| Prime F. GBOBC2 b. R. | 20 | -34.08 | 1.52 | 165 | 22.35 | **8.56E-52** | 4.54E-04 | 5.38 |
| Prime F. L. GBOBC1 mb2 R. | 44 | -32.69 | 1.52 | 165 | 21.44 | **1.42E-49** | 4.58E-04 | 4.42 |
| Prime F. GBOBC2 mb2 R. | 21 | -32.68 | 1.52 | 165 | 21.44 | **1.47E-49** | 4.62E-04 | 5.34 |
| GBOBC1 b. R. GBHCT F. | 69 | 32.32 | 1.52 | 165 | 21.20 | **5.75E-49** | 4.66E-04 | 6.39 |
| Prime F. L. GBOBC2 b. R. | 45 | -32.31 | 1.52 | 165 | 21.19 | **5.96E-49** | 4.70E-04 | 4.10 |
| GBOBC1 b. R. GBOBC2 b. F. | 72 | 32.21 | 1.52 | 165 | 21.12 | **8.72E-49** | 4.75E-04 | 6.66 |
| Prime F. L. GBOBC2 mb2 R. | 46 | -30.91 | 1.52 | 165 | 20.27 | **1.17E-46** | 4.79E-04 | 3.89 |
| GBOBC1 mb2 R. GBHCT F. | 78 | 29.75 | 1.52 | 165 | 19.51 | **1.03E-44** | 4.84E-04 | 6.87 |
| GBOBC1 mb2 R. GBOBC2 b. F. | 81 | 29.64 | 1.52 | 165 | 19.44 | **1.59E-44** | 4.88E-04 | 6.72 |
| GBOBC2 b. R. GBHCT F. | 86 | 29.36 | 1.52 | 165 | 19.26 | **4.60E-44** | 4.93E-04 | 5.64 |
| GBOBC2 b. R. GBOBC2 b. F. | 89 | 29.25 | 1.52 | 165 | 19.19 | **7.10E-44** | 4.98E-04 | 5.79 |
| Gbn R. GBOBC2 mb2 F. | 103 | 28.81 | 1.52 | 165 | 18.90 | **4.02E-43** | 5.03E-04 | 5.21 |
| GBOBC2 mb2 R. GBHCT F. | 93 | 27.97 | 1.52 | 165 | 18.34 | **1.12E-41** | 5.08E-04 | 6.11 |
| GBOBC2 mb2 R. GBOBC2 b. F. | 96 | 27.86 | 1.52 | 165 | 18.27 | **1.75E-41** | 5.13E-04 | 5.86 |
| GBOBC1 b. R. GBOBC2 mb2 F. | 73 | 26.23 | 1.52 | 165 | 17.20 | **1.19E-38** | 5.18E-04 | 4.35 |
| Gbn R. GBOBC1 b. F. | 100 | 26.17 | 1.52 | 165 | 17.17 | **1.49E-38** | 5.23E-04 | 5.21 |
| GBOBC1 mb2 R. GBOBC2 mb2 F. | 82 | 23.66 | 1.52 | 165 | 15.52 | **4.58E-34** | 5.29E-04 | 4.73 |
| GBOBC1 b. R. GBOBC1 b. F. | 70 | 23.60 | 1.52 | 165 | 15.48 | **5.98E-34** | 5.34E-04 | 4.58 |
| GBOBC2 b. R. GBOBC2 mb2 F. | 90 | 23.28 | 1.52 | 165 | 15.27 | **2.26E-33** | 5.40E-04 | 4.32 |

| | | | | | | | | |
|---|---|---|---|---|---|---|---|---|
| Prime F. Prime R. L. | 15 | -22.93 | 1.52 | 165 | 15.04 | **9.73E-33** | 5.46E-04 | 4.62 |
| GBOBC2 mb2 R. GBOBC2 mb2 F. | 97 | 21.88 | 1.52 | 165 | 14.35 | **7.85E-31** | 5.51E-04 | 3.96 |
| Prime R. Prime F. | 0 | 21.73 | 1.52 | 165 | 14.25 | **1.45E-30** | 5.57E-04 | 5.28 |
| Prime R. L. Prime F. L. | 29 | 21.15 | 1.52 | 165 | 13.87 | **1.66E-29** | 5.64E-04 | 3.41 |
| GBOBC1 mb2 R. GBOBC1 b. F. | 79 | 21.02 | 1.52 | 165 | 13.79 | **2.88E-29** | 5.70E-04 | 4.74 |
| Gbn R. GBOBC1 mb2 F. | 101 | 20.75 | 1.52 | 165 | 13.61 | **9.32E-29** | 5.76E-04 | 3.54 |
| GBOBC2 b. R. GBOBC1 b. F. | 87 | 20.64 | 1.52 | 165 | 13.54 | **1.46E-28** | 5.83E-04 | 3.96 |
| Gbn R. Gbn F. | 104 | 20.26 | 1.52 | 165 | 13.29 | **7.44E-28** | 5.89E-04 | 3.54 |
| GBHCT R. Gbn R. | 58 | -20.07 | 1.52 | 165 | 13.16 | **1.63E-27** | 5.96E-04 | 4.31 |
| Prime R. Prime F. L. | 2 | 19.96 | 1.52 | 165 | 13.09 | **2.58E-27** | 6.03E-04 | 3.15 |
| Prime F. GBHCT R. | 17 | -19.54 | 1.52 | 165 | 12.82 | **1.51E-26** | 6.10E-04 | 2.92 |
| Prime F. Gbn F. | 28 | -19.36 | 1.52 | 165 | 12.70 | **3.32E-26** | 6.18E-04 | 5.08 |
| GBOBC2 mb2 R. GBOBC1 b. F. | 94 | 19.24 | 1.52 | 165 | 12.62 | **5.40E-26** | 6.25E-04 | 3.88 |
| Prime F. GBOBC1 mb2 F. | 25 | -18.87 | 1.52 | 165 | 12.38 | **2.66E-25** | 6.33E-04 | 4.20 |
| Prime R. L. GBHCT F. | 36 | 18.21 | 1.52 | 165 | 11.94 | **4.31E-24** | 6.41E-04 | 2.71 |
| GBOBC1 b. R. GBOBC1 mb2 F. | 71 | 18.17 | 1.52 | 165 | 11.92 | **5.18E-24** | 6.49E-04 | 4.04 |
| Prime R. L. GBOBC2 b. F. | 39 | 18.10 | 1.52 | 165 | 11.87 | **6.90E-24** | 6.57E-04 | 3.59 |
| Prime R. Gbn R. | 8 | -17.88 | 1.52 | 165 | 11.73 | **1.73E-23** | 6.66E-04 | 2.51 |
| Prime F. L. GBHCT R. | 42 | -17.77 | 1.52 | 165 | 11.66 | **2.73E-23** | 6.75E-04 | 2.27 |
| GBOBC1 b. R. Gbn F. | 74 | 17.68 | 1.52 | 165 | 11.59 | **4.12E-23** | 6.84E-04 | 3.59 |
| Prime F. L. Gbn F. | 53 | -17.59 | 1.52 | 165 | 11.54 | **5.98E-23** | 6.93E-04 | 3.11 |
| GBHCT R. GBOBC1 b. R. | 54 | -17.49 | 1.52 | 165 | 11.47 | **9.03E-23** | 7.02E-04 | 9.03 |
| Prime F. L. GBOBC1 mb2 F. | 50 | -17.10 | 1.52 | 165 | 11.21 | **4.73E-22** | 7.12E-04 | 2.65 |
| Prime R. GBHCT F. | 9 | 17.02 | 1.52 | 165 | 11.16 | **6.59E-22** | 7.22E-04 | 2.79 |
| Prime R. GBOBC2 b. F. | 12 | 16.91 | 1.52 | 165 | 11.09 | **1.05E-21** | 7.32E-04 | 3.56 |
| Prime R. L. Gbn R. | 35 | -16.69 | 1.52 | 165 | 10.95 | **2.63E-21** | 7.43E-04 | 2.08 |
| GBOBC1 mb2 R. GBOBC1 mb2 F. | 80 | 15.60 | 1.52 | 165 | 10.23 | **2.50E-19** | 7.54E-04 | 3.58 |
| Prime R. GBOBC1 b. R. | 4 | -15.30 | 1.52 | 165 | 10.04 | **8.47E-19** | 7.65E-04 | 2.38 |
| GBOBC2 b. R. GBOBC1 mb2 F. | 88 | 15.21 | 1.52 | 165 | 9.98 | **1.22E-18** | 7.77E-04 | 2.86 |
| GBOBC1 mb2 R. Gbn F. | 83 | 15.11 | 1.52 | 165 | 9.91 | **1.90E-18** | 7.89E-04 | 3.20 |
| GBHCT R. GBOBC1 mb2 R. | 55 | -14.92 | 1.52 | 165 | 9.79 | **4.07E-18** | 8.01E-04 | 7.77 |
| GBHCT R. GBHCT F. | 59 | 14.83 | 1.52 | 165 | 9.73 | **5.89E-18** | 8.14E-04 | 2.93 |
| GBOBC2 b. R. Gbn F. | 91 | 14.72 | 1.52 | 165 | 9.66 | **9.15E-18** | 8.27E-04 | 2.59 |
| GBHCT R. GBOBC2 b. F. | 62 | 14.72 | 1.52 | 165 | 9.65 | **9.30E-18** | 8.41E-04 | 2.84 |
| GBHCT F. Gbn F. | 109 | -14.64 | 1.52 | 165 | 9.60 | **1.26E-17** | 8.55E-04 | 6.50 |
| GBHCT R. GBOBC2 b. R. | 56 | -14.54 | 1.52 | 165 | 9.53 | **1.95E-17** | 8.69E-04 | 6.99 |
| GBOBC2 b. F. Gbn F. | 118 | -14.53 | 1.52 | 165 | 9.53 | **1.99E-17** | 8.84E-04 | 6.78 |
| GBHCT F. GBOBC1 mb2 F. | 106 | -14.15 | 1.52 | 165 | 9.28 | **9.27E-17** | 8.99E-04 | 5.61 |
| Prime R. L. GBOBC1 b. R. | 31 | -14.11 | 1.52 | 165 | 9.25 | **1.11E-16** | 9.16E-04 | 2.13 |
| GBOBC1 mb2 F. GBOBC2 b. F. | 114 | 14.04 | 1.52 | 165 | 9.21 | **1.45E-16** | 9.32E-04 | 4.38 |
| GBOBC2 mb2 R. GBOBC1 mb2 F. | 95 | 13.82 | 1.52 | 165 | 9.06 | **3.60E-16** | 9.49E-04 | 2.84 |
| Prime F. GBOBC1 b. F. | 24 | -13.44 | 1.52 | 165 | 8.81 | **1.62E-15** | 9.67E-04 | 4.48 |
| GBOBC2 mb2 R. Gbn F. | 98 | 13.32 | 1.52 | 165 | 8.74 | **2.55E-15** | 9.86E-04 | 2.54 |

| | | | | | | | | | |
|---|---|---|---|---|---|---|---|---|---|
| GBHCT R. GBOBC2 mb2 R. | 57 | -13.14 | 1.52 | 165 | 8.62 | **5.33E-15** | 1.01E-03 | 7.12 |
| Prime R. GBOBC1 mb2 R. | 5 | -12.73 | 1.52 | 165 | 8.35 | **2.65E-14** | 1.03E-03 | 2.04 |
| Prime R. GBOBC2 b. R. | 6 | -12.35 | 1.52 | 165 | 8.10 | **1.17E-13** | 1.05E-03 | 1.98 |
| Prime R. L. GBOBC2 mb2 F. | 40 | 12.12 | 1.52 | 165 | 7.95 | **2.79E-13** | 1.07E-03 | 1.95 |
| Prime F. L. GBOBC1 b. F. | 49 | -11.67 | 1.52 | 165 | 7.65 | **1.56E-12** | 1.09E-03 | 3.73 |
| Prime R. L. GBOBC1 mb2 R. | 32 | -11.54 | 1.52 | 165 | 7.57 | **2.54E-12** | 1.11E-03 | 1.70 |
| Prime R. L. GBOBC2 b. R. | 33 | -11.15 | 1.52 | 165 | 7.32 | **1.06E-11** | 1.14E-03 | 1.61 |
| Prime R. GBOBC2 mb2 R. | 7 | -10.95 | 1.52 | 165 | 7.18 | **2.24E-11** | 1.17E-03 | 1.81 |
| Prime R. GBOBC2 mb2 F. | 13 | 10.93 | 1.52 | 165 | 7.17 | **2.42E-11** | 1.19E-03 | 2.09 |
| Prime F. GBOBC2 mb2 F. | 27 | -10.80 | 1.52 | 165 | 7.09 | **3.81E-11** | 1.22E-03 | 3.10 |
| Prime R. L. GBOBC2 mb2 R. | 34 | -9.76 | 1.52 | 165 | 6.40 | **1.55E-09** | 1.25E-03 | 1.62 |
| Prime R. L. GBOBC1 b. F. | 37 | 9.49 | 1.52 | 165 | 6.22 | **3.90E-09** | 1.28E-03 | 1.67 |
| Prime F. L. GBOBC2 mb2 F. | 52 | -9.03 | 1.52 | 165 | 5.92 | **1.77E-08** | 1.31E-03 | 2.97 |
| GBHCT R. GBOBC2 mb2 F. | 63 | 8.74 | 1.52 | 165 | 5.73 | **4.60E-08** | 1.35E-03 | 2.10 |
| GBHCT F. GBOBC1 b. F. | 105 | -8.72 | 1.52 | 165 | 5.72 | **4.86E-08** | 1.39E-03 | 3.16 |
| GBOBC1 b. F. GBOBC2 b. F. | 111 | 8.61 | 1.52 | 165 | 5.65 | **6.94E-08** | 1.42E-03 | 3.51 |
| GBOBC2 mb2 F. Gbn F. | 119 | -8.55 | 1.52 | 165 | 5.61 | **8.34E-08** | 1.46E-03 | 1.91 |
| Prime R. GBOBC1 b. F. | 10 | 8.29 | 1.52 | 165 | 5.44 | **1.89E-07** | 1.51E-03 | 1.61 |
| GBOBC1 mb2 F. GBOBC2 mb2 F. | 115 | 8.06 | 1.52 | 165 | 5.29 | **3.86E-07** | 1.55E-03 | 1.80 |
| GBOBC2 mb2 R. Gbn R. | 92 | -6.93 | 1.52 | 165 | 4.55 | **1.05E-05** | 1.60E-03 | 1.99 |
| GBHCT R. GBOBC1 b. F. | 60 | 6.11 | 1.52 | 165 | 4.00 | **9.38E-05** | 1.65E-03 | 1.76 |
| GBHCT F. GBOBC2 mb2 F. | 108 | -6.09 | 1.52 | 165 | 3.99 | **9.79E-05** | 1.71E-03 | 1.51 |
| GBOBC2 b. F. GBOBC2 mb2 F. | 117 | -5.98 | 1.52 | 165 | 3.92 | **1.29E-04** | 1.77E-03 | 1.60 |
| GBOBC1 b. F. Gbn F. | 113 | -5.92 | 1.52 | 165 | 3.88 | **1.49E-04** | 1.83E-03 | 1.99 |
| GBOBC2 b. R. Gbn R. | 85 | -5.53 | 1.52 | 165 | 3.63 | **3.78E-04** | 1.90E-03 | 1.44 |
| GBOBC1 b. F. GBOBC1 mb2 F. | 110 | -5.43 | 1.52 | 165 | 3.56 | **4.84E-04** | 1.97E-03 | 1.92 |
| GBOBC1 mb2 R. Gbn R. | 77 | -5.15 | 1.52 | 165 | 3.38 | **9.11E-04** | 2.05E-03 | 1.27 |
| Prime F. GBOBC2 b. F. | 26 | -4.83 | 1.52 | 165 | 3.17 | **1.84E-03** | 2.13E-03 | 1.58 |
| Prime F. GBHCT F. | 23 | -4.72 | 1.52 | 165 | 3.09 | 2.33E-03 | 2.23E-03 | 2.00 |
| GBOBC1 b. R. GBOBC2 mb2 R. | 67 | 4.35 | 1.52 | 165 | 2.85 | 4.87E-03 | 0.00E+00 | 1.68 |
| Prime R. L. GBOBC1 mb2 F. | 38 | 4.06 | 1.52 | 165 | 2.66 | 8.55E-03 | 0.00E+00 | 1.10 |
| Prime R. L. Gbn F. | 41 | 3.57 | 1.52 | 165 | 2.34 | 2.05E-02 | 0.00E+00 | 1.04 |
| Prime R. L. GBHCT R. | 30 | 3.38 | 1.52 | 165 | 2.22 | 2.79E-02 | 0.00E+00 | 1.25 |
| Prime F. L. GBOBC2 b. F. | 51 | -3.06 | 1.52 | 165 | 2.00 | 4.67E-02 | 0.00E+00 | 1.34 |
| GBOBC1 b. R. GBOBC2 b. R. | 66 | 2.95 | 1.52 | 165 | 1.94 | 5.44E-02 | 0.00E+00 | 1.48 |
| Prime F. L. GBHCT F. | 48 | -2.94 | 1.52 | 165 | 1.93 | 5.52E-02 | 0.00E+00 | 1.54 |
| Prime R. GBOBC1 mb2 F. | 11 | 2.87 | 1.52 | 165 | 1.88 | 6.19E-02 | 0.00E+00 | 0.94 |
| GBOBC1 b. F. GBOBC2 mb2 F. | 112 | 2.63 | 1.52 | 165 | 1.73 | 8.58E-02 | 0.00E+00 | 1.74 |
| GBOBC1 b. R. Gbn R. | 68 | -2.58 | 1.52 | 165 | 1.69 | 9.25E-02 | 0.00E+00 | 1.36 |
| GBOBC1 b. R. GBOBC1 mb2 R. | 65 | 2.57 | 1.52 | 165 | 1.69 | 9.37E-02 | 0.00E+00 | 1.37 |
| Prime R. Gbn F. | 14 | 2.37 | 1.52 | 165 | 1.56 | 1.21E-01 | 0.00E+00 | 1.01 |
| Prime R. GBHCT R. | 3 | 2.19 | 1.52 | 165 | 1.44 | 1.53E-01 | 0.00E+00 | 1.21 |
| GBOBC1 mb2 R. GBOBC2 mb2 R. | 76 | 1.78 | 1.52 | 165 | 1.17 | 2.45E-01 | 0.00E+00 | 1.86 |

| | | | | | | | | |
|---|---|---|---|---|---|---|---|---|
| Prime F. Prime F. L. | 16 | -1.77 | 1.52 | 165 | 1.16 | 2.47E-01 | 0.00E+00 | 0.32 |
| GBOBC2 b. R. GBOBC2 mb2 R. | 84 | 1.40 | 1.52 | 165 | 0.92 | 3.61E-01 | 0.00E+00 | 1.84 |
| Prime R. Prime R. L. | 1 | -1.19 | 1.52 | 165 | 0.78 | 4.35E-01 | 0.00E+00 | 0.48 |
| GBHCT R. GBOBC1 mb2 F. | 61 | 0.68 | 1.52 | 165 | 0.44 | 6.58E-01 | 0.00E+00 | 0.92 |
| GBOBC1 mb2 F. Gbn F. | 116 | -0.49 | 1.52 | 165 | 0.32 | 7.48E-01 | 0.00E+00 | 0.94 |
| GBOBC1 mb2 R. GBOBC2 b. R. | 75 | 0.38 | 1.52 | 165 | 0.25 | 8.02E-01 | 0.00E+00 | 0.93 |
| GBHCT R. Gbn F. | 64 | 0.19 | 1.52 | 165 | 0.12 | 9.03E-01 | 0.00E+00 | 1.38 |
| GBHCT F. GBOBC2 b. F. | 107 | -0.11 | 1.52 | 165 | 0.07 | 9.42E-01 | 0.00E+00 | 1.91 |

Table B.12: Holm-Šidák results for Glide job 2 excluding ligand 7. Names abbreviated for expediency. F., R., b., mb2, and d, correspond to Flexible, Rigid, bondi, mbondi2, and Cohen's d respectively. Significant differences shown in bold.

| **Compared Models** | **Index** | **Mean Diff.** | **Std.Er.** | **DF** | **\|t\|value** | **Prob>\|t\|** | **Alpha** | **d** |
|---|---|---|---|---|---|---|---|---|
| Prime F. Gbn R. | 22 | -40.82 | 1.51 | 150 | 26.98 | 1.95E-59 | 4.27E-04 | 8.25 |
| Prime F. L. Gbn R. | 47 | -38.88 | 1.51 | 150 | 25.71 | 7.81E-57 | 4.31E-04 | 4.60 |
| Prime F. GBOBC1 b. R. | 18 | -38.18 | 1.51 | 150 | 25.24 | 7.16E-56 | 4.35E-04 | 7.53 |
| Prime F. L. GBOBC1 b. R. | 43 | -36.25 | 1.51 | 150 | 23.97 | 3.72E-53 | 4.38E-04 | 4.92 |
| Gbn R. GBOBC2 b. F. | 102 | 35.62 | 1.51 | 150 | 23.55 | 3.00E-52 | 4.42E-04 | 6.94 |
| Gbn R. GBHCT F. | 99 | 35.37 | 1.51 | 150 | 23.39 | 6.80E-52 | 4.46E-04 | 7.46 |
| Prime F. GBOBC1 mb2 R. | 19 | -35.35 | 1.51 | 150 | 23.37 | 7.40E-52 | 4.50E-04 | 6.87 |
| Prime F. GBOBC2 b. R. | 20 | -34.99 | 1.51 | 150 | 23.14 | 2.42E-51 | 4.54E-04 | 6.08 |
| Prime F. GBOBC2 mb2 R. | 21 | -33.75 | 1.51 | 150 | 22.31 | 1.65E-49 | 4.58E-04 | 6.58 |
| Prime F. L. GBOBC1 mb2 R. | 44 | -33.41 | 1.51 | 150 | 22.09 | 5.16E-49 | 4.62E-04 | 4.57 |
| Prime F. L. GBOBC2 b. R. | 45 | -33.06 | 1.51 | 150 | 21.86 | 1.75E-48 | 4.66E-04 | 4.23 |
| GBOBC1 b. R. GBOBC2 b. F. | 72 | 32.99 | 1.51 | 150 | 21.81 | 2.26E-48 | 4.70E-04 | 7.84 |
| GBOBC1 b. R. GBHCT F. | 69 | 32.74 | 1.51 | 150 | 21.65 | 5.31E-48 | 4.75E-04 | 6.45 |
| Prime F. L. GBOBC2 mb2 R. | 46 | -31.81 | 1.51 | 150 | 21.03 | 1.36E-46 | 4.79E-04 | 4.15 |
| GBOBC1 mb2 R. GBOBC2 b. F. | 81 | 30.15 | 1.51 | 150 | 19.93 | 5.21E-44 | 4.84E-04 | 7.13 |
| Gbn R. GBOBC2 mb2 F. | 103 | 29.99 | 1.51 | 150 | 19.83 | 9.49E-44 | 4.88E-04 | 7.64 |
| GBOBC1 mb2 R. GBHCT F. | 78 | 29.91 | 1.51 | 150 | 19.77 | 1.27E-43 | 4.93E-04 | 6.64 |
| GBOBC2 b. R. GBOBC2 b. F. | 89 | 29.80 | 1.51 | 150 | 19.70 | 1.89E-43 | 4.98E-04 | 6.07 |
| GBOBC2 b. R. GBHCT F. | 86 | 29.55 | 1.51 | 150 | 19.54 | 4.63E-43 | 5.03E-04 | 5.45 |
| GBOBC2 mb2 R. GBOBC2 b. F. | 96 | 28.55 | 1.51 | 150 | 18.88 | 1.83E-41 | 5.08E-04 | 6.64 |
| GBOBC2 mb2 R. GBHCT F. | 93 | 28.30 | 1.51 | 150 | 18.71 | 4.57E-41 | 5.13E-04 | 6.10 |
| GBOBC1 b. R. GBOBC2 mb2 F. | 73 | 27.35 | 1.51 | 150 | 18.08 | 1.61E-39 | 5.18E-04 | 5.67 |
| Gbn R. GBOBC1 b. F. | 100 | 27.09 | 1.51 | 150 | 17.91 | 4.45E-39 | 5.23E-04 | 6.61 |
| GBOBC1 mb2 R. GBOBC2 mb2 F. | 82 | 24.52 | 1.51 | 150 | 16.21 | 8.68E-35 | 5.29E-04 | 5.82 |
| GBOBC1 b. R. GBOBC1 b. F. | 70 | 24.45 | 1.51 | 150 | 16.17 | 1.12E-34 | 5.34E-04 | 5.54 |
| GBOBC2 b. R. GBOBC2 mb2 F. | 90 | 24.16 | 1.51 | 150 | 15.98 | 3.48E-34 | 5.40E-04 | 5.20 |
| Prime F. Prime R. L. | 15 | -23.09 | 1.51 | 150 | 15.26 | 2.42E-32 | 5.46E-04 | 4.47 |
| GBOBC2 mb2 R. GBOBC2 mb2 F. | 97 | 22.92 | 1.51 | 150 | 15.15 | 4.77E-32 | 5.51E-04 | 5.21 |
| Prime R. Prime F. | 0 | 21.79 | 1.51 | 150 | 14.41 | 4.36E-30 | 5.57E-04 | 5.05 |

| | | | | | | | | |
|---|---|---|---|---|---|---|---|---|
| GBOBC1 mb2 R. GBOBC1 b. F. | 79 | 21.62 | 1.51 | 150 | 14.29 | 8.66E-30 | 5.64E-04 | 5.24 |
| GBOBC2 b. R. GBOBC1 b. F. | 87 | 21.26 | 1.51 | 150 | 14.06 | 3.61E-29 | 5.70E-04 | 4.27 |
| Prime R. L. Prime F. L. | 29 | 21.16 | 1.51 | 150 | 13.99 | 5.55E-29 | 5.76E-04 | 3.25 |
| Gbn R. GBOBC1 mb2 F. | 101 | 20.99 | 1.51 | 150 | 13.88 | 1.09E-28 | 5.83E-04 | 3.45 |
| Gbn R. Gbn F. | 104 | 20.79 | 1.51 | 150 | 13.75 | 2.39E-28 | 5.89E-04 | 3.66 |
| Prime F. GBHCT R. | 17 | -20.79 | 1.51 | 150 | 13.74 | 2.44E-28 | 5.96E-04 | 3.87 |
| GBHCT R. Gbn R. | 58 | -20.03 | 1.51 | 150 | 13.24 | 5.37E-27 | 6.03E-04 | 4.10 |
| Prime F. Gbn F. | 28 | -20.02 | 1.51 | 150 | 13.24 | 5.49E-27 | 6.10E-04 | 6.28 |
| GBOBC2 mb2 R. GBOBC1 b. F. | 94 | 20.02 | 1.51 | 150 | 13.23 | 5.57E-27 | 6.18E-04 | 4.58 |
| Prime R. Prime F. L. | 2 | 19.86 | 1.51 | 150 | 13.13 | 1.07E-26 | 6.25E-04 | 2.99 |
| Prime F. GBOBC1 mb2 F. | 25 | -19.83 | 1.51 | 150 | 13.11 | 1.21E-26 | 6.33E-04 | 6.24 |
| Prime R. Gbn R. | 8 | -19.03 | 1.51 | 150 | 12.58 | 3.12E-25 | 6.41E-04 | 3.06 |
| Prime F. L. GBHCT R. | 42 | -18.86 | 1.51 | 150 | 12.47 | 6.26E-25 | 6.49E-04 | 2.61 |
| GBOBC1 b. R. GBOBC1 mb2 F. | 71 | 18.36 | 1.51 | 150 | 12.14 | 4.79E-24 | 6.57E-04 | 3.94 |
| GBOBC1 b. R. Gbn F. | 74 | 18.16 | 1.51 | 150 | 12.01 | 1.06E-23 | 6.66E-04 | 3.74 |
| Prime F. L. Gbn F. | 53 | -18.09 | 1.51 | 150 | 11.96 | 1.43E-23 | 6.75E-04 | 3.23 |
| Prime F. L. GBOBC1 mb2 F. | 50 | -17.89 | 1.51 | 150 | 11.83 | 3.16E-23 | 6.84E-04 | 2.93 |
| Prime R. L. GBOBC2 b. F. | 39 | 17.89 | 1.51 | 150 | 11.83 | 3.18E-23 | 6.93E-04 | 3.42 |
| Prime R. L. Gbn R. | 35 | -17.73 | 1.51 | 150 | 11.72 | 6.25E-23 | 7.02E-04 | 2.35 |
| Prime R. L. GBHCT F. | 36 | 17.65 | 1.51 | 150 | 11.67 | 8.67E-23 | 7.12E-04 | 2.62 |
| GBHCT R. GBOBC1 b. R. | 54 | -17.39 | 1.51 | 150 | 11.50 | 2.42E-22 | 7.22E-04 | 8.69 |
| Prime R. GBOBC2 b. F. | 12 | 16.59 | 1.51 | 150 | 10.97 | 6.31E-21 | 7.32E-04 | 3.42 |
| Prime R. GBOBC1 b. R. | 4 | -16.40 | 1.51 | 150 | 10.84 | 1.40E-20 | 7.43E-04 | 3.00 |
| Prime R. GBHCT F. | 9 | 16.35 | 1.51 | 150 | 10.81 | 1.71E-20 | 7.54E-04 | 2.77 |
| GBHCT R. GBOBC2 b. F. | 62 | 15.59 | 1.51 | 150 | 10.31 | 3.58E-19 | 7.65E-04 | 3.54 |
| GBOBC1 mb2 R. GBOBC1 mb2 F. | 80 | 15.52 | 1.51 | 150 | 10.26 | 4.77E-19 | 7.77E-04 | 3.40 |
| GBHCT R. GBHCT F. | 59 | 15.35 | 1.51 | 150 | 10.15 | 9.64E-19 | 7.89E-04 | 3.09 |
| GBOBC1 mb2 R. Gbn F. | 83 | 15.33 | 1.51 | 150 | 10.13 | 1.04E-18 | 8.01E-04 | 3.14 |
| GBOBC2 b. R. GBOBC1 mb2 F. | 88 | 15.17 | 1.51 | 150 | 10.03 | 1.98E-18 | 8.14E-04 | 2.72 |
| Prime R. L. GBOBC1 b. R. | 31 | -15.09 | 1.51 | 150 | 9.98 | 2.64E-18 | 8.27E-04 | 2.54 |
| GBOBC2 b. R. Gbn F. | 91 | 14.97 | 1.51 | 150 | 9.90 | 4.32E-18 | 8.41E-04 | 2.54 |
| GBOBC2 b. F. Gbn F. | 118 | -14.82 | 1.51 | 150 | 9.80 | 7.79E-18 | 8.55E-04 | 7.49 |
| GBOBC1 mb2 F. GBOBC2 b. F. | 114 | 14.63 | 1.51 | 150 | 9.67 | 1.69E-17 | 8.69E-04 | 5.63 |
| GBHCT F. Gbn F. | 109 | -14.58 | 1.51 | 150 | 9.64 | 2.08E-17 | 8.84E-04 | 6.20 |
| GBHCT R. GBOBC1 mb2 R. | 55 | -14.56 | 1.51 | 150 | 9.63 | 2.24E-17 | 8.99E-04 | 9.52 |
| GBHCT F. GBOBC1 mb2 F. | 106 | -14.38 | 1.51 | 150 | 9.51 | 4.49E-17 | 9.16E-04 | 5.74 |
| GBHCT R. GBOBC2 b. R. | 56 | -14.20 | 1.51 | 150 | 9.39 | 9.16E-17 | 9.32E-04 | 7.81 |
| GBOBC2 mb2 R. GBOBC1 mb2 F. | 95 | 13.92 | 1.51 | 150 | 9.20 | 2.79E-16 | 9.49E-04 | 2.74 |
| Prime F. GBOBC1 b. F. | 24 | -13.73 | 1.51 | 150 | 9.08 | 5.92E-16 | 9.67E-04 | 4.63 |
| GBOBC2 mb2 R. Gbn F. | 98 | 13.73 | 1.51 | 150 | 9.08 | 5.99E-16 | 9.86E-04 | 2.58 |
| Prime R. GBOBC1 mb2 R. | 5 | -13.56 | 1.51 | 150 | 8.96 | 1.15E-15 | 0.00101 | 2.34 |
| Prime R. GBOBC2 b. R. | 6 | -13.20 | 1.51 | 150 | 8.73 | 4.58E-15 | 0.00103 | 2.30 |
| GBHCT R. GBOBC2 mb2 R. | 57 | -12.96 | 1.51 | 150 | 8.57 | 1.19E-14 | 0.00105 | 7.11 |

| | | | | | | | | |
|---|---|---|---|---|---|---|---|---|
| Prime R. L. GBOBC2 mb2 F. | 40 | 12.26 | 1.51 | 150 | 8.11 | 1.72E-13 | 0.00107 | 1.88 |
| Prime R. L. GBOBC1 mb2 R. | 32 | -12.26 | 1.51 | 150 | 8.10 | 1.72E-13 | 0.00109 | 1.85 |
| Prime R. GBOBC2 mb2 R. | 7 | -11.96 | 1.51 | 150 | 7.91 | 5.30E-13 | 0.00111 | 2.27 |
| Prime R. L. GBOBC2 b. R. | 33 | -11.90 | 1.51 | 150 | 7.87 | 6.51E-13 | 0.00114 | 1.76 |
| Prime F. L. GBOBC1 b. F. | 49 | -11.80 | 1.51 | 150 | 7.80 | 9.70E-13 | 0.00117 | 3.73 |
| Prime R. GBOBC2 mb2 F. | 13 | 10.96 | 1.51 | 150 | 7.25 | 2.11E-11 | 0.00119 | 1.99 |
| Prime F. GBOBC2 mb2 F. | 27 | -10.83 | 1.51 | 150 | 7.16 | 3.36E-11 | 0.00122 | 2.97 |
| Prime R. L. GBOBC2 mb2 R. | 34 | -10.66 | 1.51 | 150 | 7.05 | 6.19E-11 | 0.00125 | 1.95 |
| GBHCT R. GBOBC2 mb2 F. | 63 | 9.96 | 1.51 | 150 | 6.58 | 7.22E-10 | 0.00128 | 2.24 |
| Prime R. L. GBOBC1 b. F. | 37 | 9.36 | 1.51 | 150 | 6.19 | 5.55E-09 | 0.00131 | 1.57 |
| GBOBC2 mb2 F. Gbn F. | 119 | -9.19 | 1.51 | 150 | 6.08 | 9.68E-09 | 0.00135 | 2.24 |
| GBOBC1 mb2 F. GBOBC2 mb2 F. | 115 | 9.00 | 1.51 | 150 | 5.95 | 1.83E-08 | 0.00139 | 2.01 |
| Prime F. L. GBOBC2 mb2 F. | 52 | -8.90 | 1.51 | 150 | 5.88 | 2.54E-08 | 0.00142 | 2.84 |
| GBOBC1 b. F. GBOBC2 b. F. | 111 | 8.53 | 1.51 | 150 | 5.64 | 8.14E-08 | 0.00146 | 3.34 |
| GBHCT F. GBOBC1 b. F. | 105 | -8.29 | 1.51 | 150 | 5.48 | 1.76E-07 | 0.00151 | 3.42 |
| Prime R. GBOBC1 b. F. | 10 | 8.06 | 1.51 | 150 | 5.33 | 3.58E-07 | 0.00155 | 1.51 |
| GBOBC2 mb2 R. Gbn R. | 92 | -7.07 | 1.51 | 150 | 4.67 | 6.56E-06 | 0.0016 | 1.95 |
| GBHCT R. GBOBC1 b. F. | 60 | 7.06 | 1.51 | 150 | 4.67 | 6.72E-06 | 0.00165 | 1.79 |
| GBOBC1 b. F. Gbn F. | 113 | -6.29 | 1.51 | 150 | 4.16 | 5.36E-05 | 0.00171 | 2.23 |
| GBOBC1 b. F. GBOBC1 mb2 F. | 110 | -6.10 | 1.51 | 150 | 4.03 | 8.82E-05 | 0.00177 | 2.13 |
| GBOBC2 b. R. Gbn R. | 85 | -5.82 | 1.51 | 150 | 3.85 | 1.75E-04 | 0.00183 | 1.49 |
| GBOBC2 b. F. GBOBC2 mb2 F. | 117 | -5.63 | 1.51 | 150 | 3.72 | 2.77E-04 | 0.0019 | 1.52 |
| GBOBC1 mb2 R. Gbn R. | 77 | -5.47 | 1.51 | 150 | 3.61 | 4.09E-04 | 0.00197 | 1.34 |
| Prime F. GBHCT F. | 23 | -5.44 | 1.51 | 150 | 3.60 | 4.35E-04 | 0.00205 | 2.03 |
| GBHCT F. GBOBC2 mb2 F. | 108 | -5.39 | 1.51 | 150 | 3.56 | 4.94E-04 | 0.00213 | 1.60 |
| Prime F. GBOBC2 b. F. | 26 | -5.20 | 1.51 | 150 | 3.44 | 7.65E-04 | 0.00223 | 1.79 |
| GBOBC1 b. R. GBOBC2 mb2 R. | 67 | 4.44 | 1.51 | 150 | 2.93 | 0.00389 | 0.00233 | 1.65 |
| Prime F. L. GBHCT F. | 48 | -3.51 | 1.51 | 150 | 2.32 | 0.02166 | 0 | 1.57 |
| Prime F. L. GBOBC2 b. F. | 51 | -3.26 | 1.51 | 150 | 2.16 | 0.03253 | 0 | 1.49 |
| Prime R. L. GBOBC1 mb2 F. | 38 | 3.26 | 1.51 | 150 | 2.16 | 0.03261 | 0 | 1.05 |
| GBOBC1 b. R. GBOBC2 b. R. | 66 | 3.19 | 1.51 | 150 | 2.11 | 0.03657 | 0 | 1.68 |
| Prime R. L. Gbn F. | 41 | 3.07 | 1.51 | 150 | 2.03 | 0.0443 | 0 | 0.95 |
| GBOBC1 b. F. GBOBC2 mb2 F. | 112 | 2.90 | 1.51 | 150 | 1.92 | 0.05705 | 0 | 2.06 |
| GBOBC1 b. R. GBOBC1 mb2 R. | 65 | 2.84 | 1.51 | 150 | 1.87 | 0.06275 | 0 | 1.52 |
| GBOBC1 b. R. Gbn R. | 68 | -2.63 | 1.51 | 150 | 1.74 | 0.0839 | 0 | 1.39 |
| Prime R. L. GBHCT R. | 30 | 2.30 | 1.51 | 150 | 1.52 | 0.1305 | 0 | 1.29 |
| Prime R. GBOBC1 mb2 F. | 11 | 1.96 | 1.51 | 150 | 1.30 | 0.19664 | 0 | 0.89 |
| Prime F. Prime F. L. | 16 | -1.93 | 1.51 | 150 | 1.28 | 0.20333 | 0 | 0.33 |
| Prime R. Gbn F. | 14 | 1.77 | 1.51 | 150 | 1.17 | 0.24453 | 0 | 0.92 |
| GBOBC1 mb2 R. GBOBC2 mb2 R. | 76 | 1.60 | 1.51 | 150 | 1.06 | 0.29181 | 0 | 1.84 |
| Prime R. Prime R. L. | 1 | -1.30 | 1.51 | 150 | 0.86 | 0.39118 | 0 | 0.51 |
| GBOBC2 b. R. GBOBC2 mb2 R. | 84 | 1.25 | 1.51 | 150 | 0.82 | 0.41162 | 0 | 1.76 |
| Prime R. GBHCT R. | 3 | 1.00 | 1.51 | 150 | 0.66 | 0.50993 | 0 | 1.38 |

| | | | | | | | | |
|---|---|---|---|---|---|---|---|---|
| GBHCT R. GBOBC1 mb2 F. | 61 | 0.96 | 1.51 | 150 | 0.64 | 0.52547 | 0 | 0.89 |
| GBHCT R. Gbn F. | 64 | 0.77 | 1.51 | 150 | 0.51 | 0.61234 | 0 | 1.29 |
| GBOBC1 mb2 R. GBOBC2 b. R. | 75 | 0.35 | 1.51 | 150 | 0.23 | 0.81489 | 0 | 0.93 |
| GBHCT F. GBOBC2 b. F. | 107 | 0.25 | 1.51 | 150 | 0.16 | 0.87102 | 0 | 1.84 |
| GBOBC1 mb2 F. Gbn F. | 116 | -0.19 | 1.51 | 150 | 0.13 | 0.89783 | 0 | 0.86 |

Table B.13: Models for which the null hypothesis was not rejected (means not significantly different) across Glide jobs. Names abbreviated for expediency. F., R., b., and mb2, correspond to Flexible, Rigid, bondi and mbondi2, respectively. The * indicates exclusion of ligand 7.

| **Compared Models** | **Glide 1** | **Glide 1*** | **Glide2** | **Glide 2*** | **Glide 3** | **Glide 3*** |
|---|---|---|---|---|---|---|
| Prime R. - Prime R. L. | ✓ | ✓ | ✓ | ✓ | ✓ | ✓ |
| Prime R. - $GB^{HCT}$ R. | ✓ | ✓ | ✓ | ✓ | ✓ | ✓ |
| Prime R. - $GB^{OBC1}$ mb2 F. | ✓ | ✓ | ✓ | ✓ | ✓ | ✓ |
| Prime R. - Gbn F. | ✓ | ✓ | ✓ | ✓ | ✓ | ✓ |
| Prime F. - Prime F. L. | ✓ | ✓ | ✓ | ✓ | ✓ | ✓ |
| Prime F. - $GB^{OBC2}$ b. F. | | | ✓ | ✓ | | |
| Prime R. L. - $GB^{HCT}$ R. | | ✓ | ✓ | ✓ | ✓ | |
| Prime R. L. - $GB^{OBC1}$ mb2 F. | | | ✓ | ✓ | ✓ | ✓ |
| Prime R. L. - Gbn F. | | ✓ | ✓ | ✓ | ✓ | ✓ |
| Prime F. L. – $GB^{HCT}$ F. | ✓ | ✓ | | | ✓ | ✓ |
| Prime F. L. - $GB^{OBC2}$ b. F. | ✓ | ✓ | ✓ | ✓ | ✓ | ✓ |
| $GB^{HCT}$ R. - $GB^{OBC1}$ mb2 F. | ✓ | ✓ | ✓ | ✓ | ✓ | ✓ |
| $GB^{HCT}$ R. - Gbn F. | ✓ | ✓ | ✓ | ✓ | ✓ | ✓ |
| $GB^{OBC1}$ b. R. - $GB^{OBC1}$ mb2 R. | ✓ | ✓ | ✓ | ✓ | ✓ | ✓ |
| $GB^{OBC1}$ b. R. - $GB^{OBC2}$ b. R. | ✓ | ✓ | ✓ | ✓ | ✓ | ✓ |
| $GB^{OBC1}$ b. R. - $GB^{OBC2}$ mb2 R. | | | ✓ | ✓ | ✓ | ✓ |
| $GB^{OBC1}$ b. R. - Gbn R. | ✓ | ✓ | ✓ | ✓ | ✓ | ✓ |
| $GB^{OBC1}$ mb2 R. - $GB^{OBC2}$ b. R. | ✓ | ✓ | ✓ | ✓ | ✓ | ✓ |
| $GB^{OBC1}$ mb2 R. - $GB^{OBC2}$ mb2 R. | ✓ | ✓ | ✓ | ✓ | ✓ | ✓ |
| $GB^{OBC1}$ mb2 R. - Gbn R. | | | ✓ | ✓ | | |
| $GB^{OBC2}$ b. R. - $GB^{OBC2}$ mb2 R. | ✓ | ✓ | ✓ | ✓ | ✓ | ✓ |
| $GB^{OBC2}$ b. R. - Gbn R. | | | ✓ | ✓ | | |
| $GB^{OBC2}$ mb2 R. - Gbn R. | | | ✓ | | | |
| $GB^{HCT}$ F. - $GB^{OBC2}$ b. F. | ✓ | ✓ | ✓ | ✓ | ✓ | ✓ |
| $GB^{HCT}$ F. - $GB^{OBC2}$ mb2 F. | | | ✓ | | | |
| $GB^{OBC1}$ b. F. - $GB^{OBC1}$ mb2 F. | | | ✓ | | | |
| $GB^{OBC1}$ b. F. - $GB^{OBC2}$ mb2 F. | ✓ | ✓ | ✓ | ✓ | ✓ | ✓ |
| $GB^{OBC1}$ b. F. - Gbn F. | | | ✓ | | | |
| $GB^{OBC1}$ mb2 F. - Gbn F. | ✓ | ✓ | ✓ | ✓ | ✓ | ✓ |

# β-Secretase

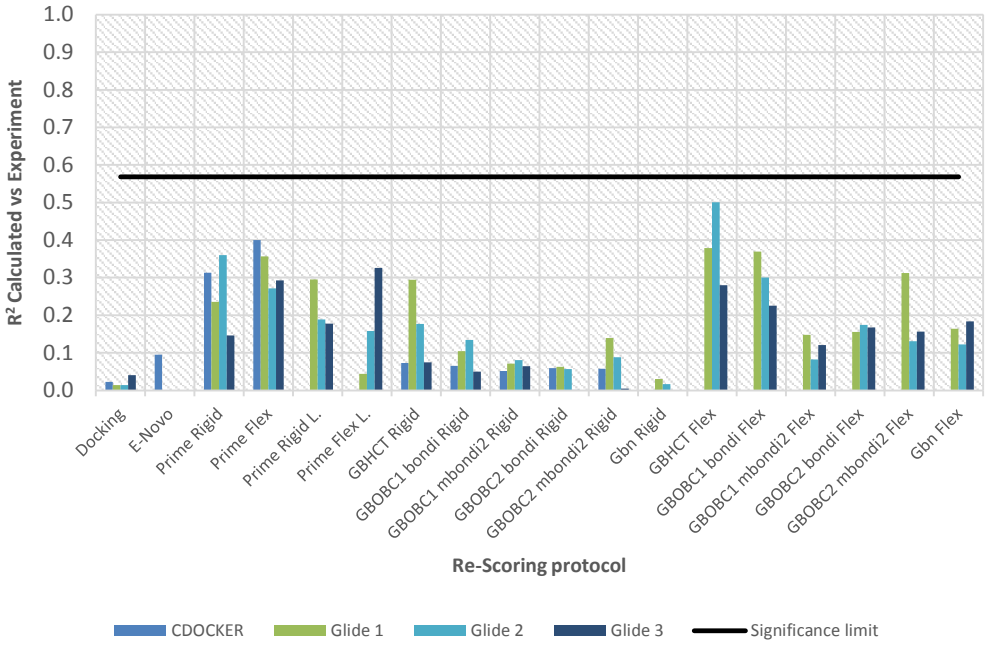


Figure B.5: Coefficient of determination of rescoring protocols with experiment grouped by each protocol. The colour in each bar corresponds to the docking protocol re-scored (blue for CDOCKER, green for Glide 1, light blue for Glide 2 and dark blue for Glide 3). Naming of protocols as described in Figure 6.4. No flexible protein calculations performed with CDOCKER poses. Glide poses not tested on Pipeline Pilot. Correlation with docking provided for comparison purposes. The black line shows the 5% significance level for the number of observations (7 ligands).

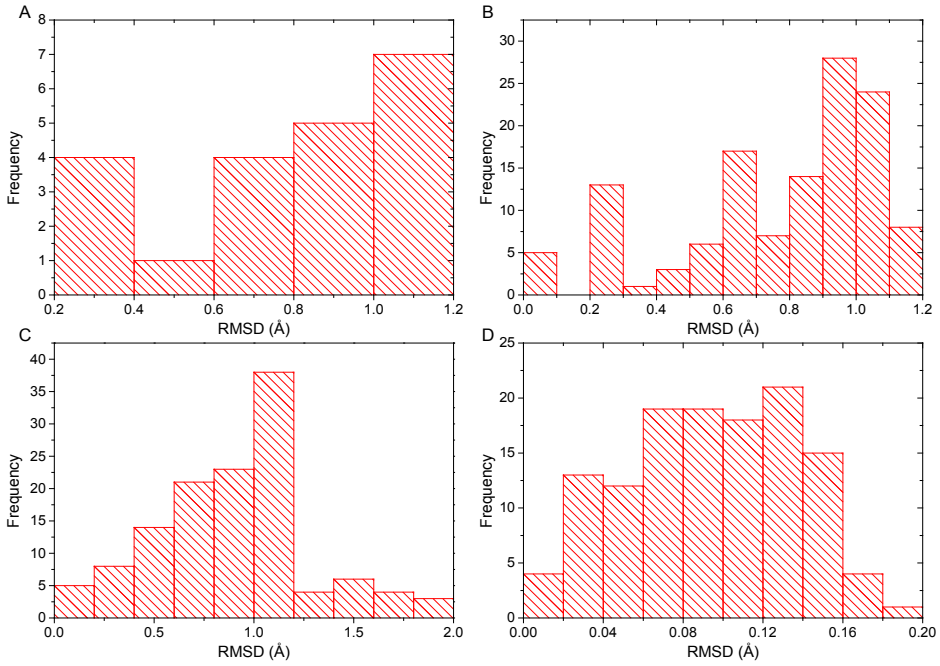


Figure B.6: Ligand-ligand (A, B, C) and protein-protein backbone (D) RMSD distributions across the different Glide poses in all possible combinations (Glide 1-2, 1-3, and 2-3) for each solvent model. Plot A: Dock poses. Plot B and C: end of rigid-protein and flexible-protein minimisations, respectively. Plot D: protein-protein backbone RMSD at end of flexible-protein minimisations. All reported RMSD are obtained using heavy atoms.

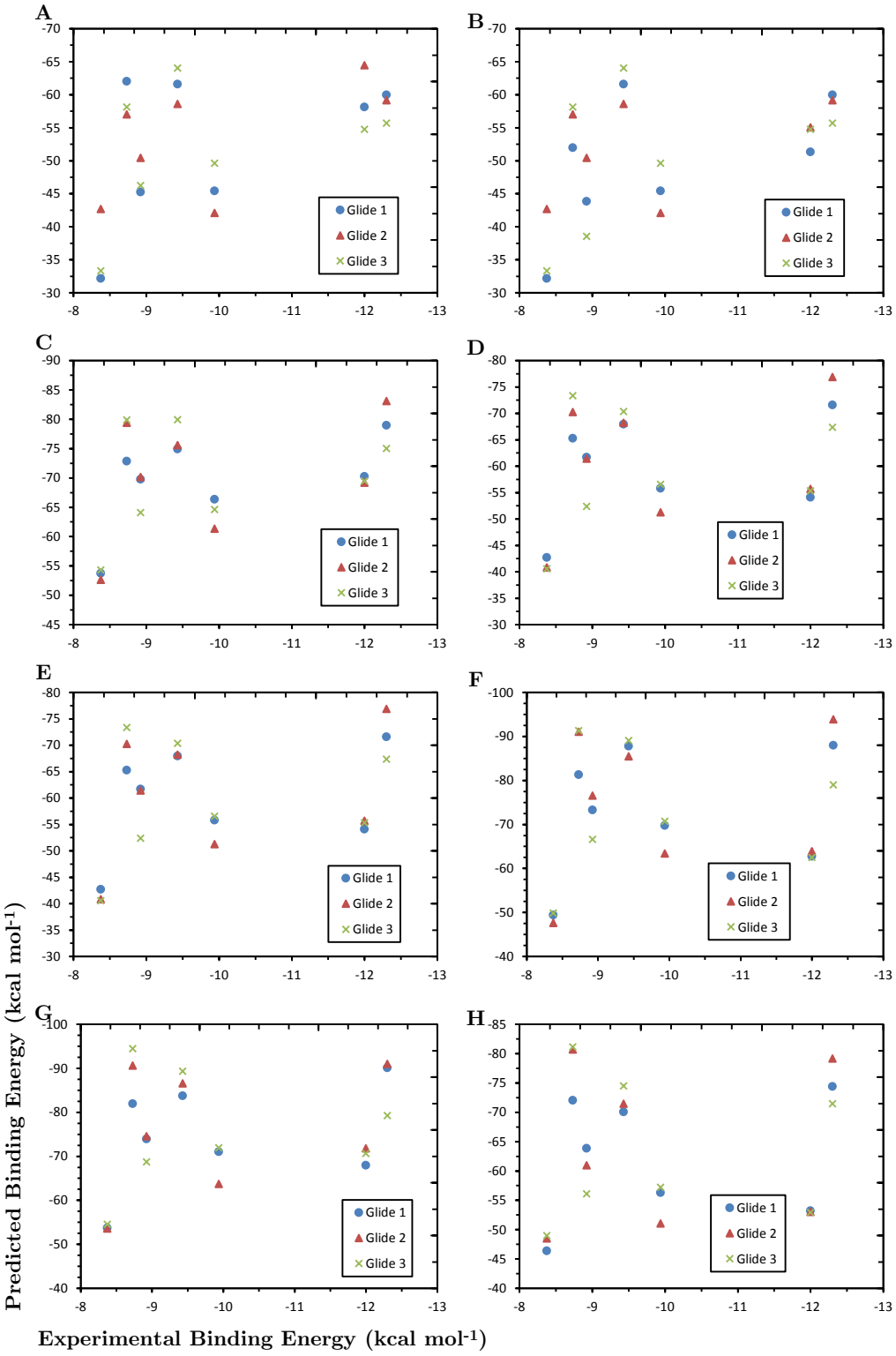


Figure B.7: Scatter plots of the predicted and experimental binding affinities for Thrombin. The plots correspond to the solvent models, A: Prime Rigid, B: Prime Rigid L., C: $GB^{HCT}$ Rigid, D: $GB^{OBC1}$ bondi Rigid, E: $GB^{OBC1}$ mbondi2 Rigid, F: $GB^{OBC2}$ bondi Rigid, G: $GB^{OBC2}$ mbondi2 Rigid, H: Gbn Rigid.

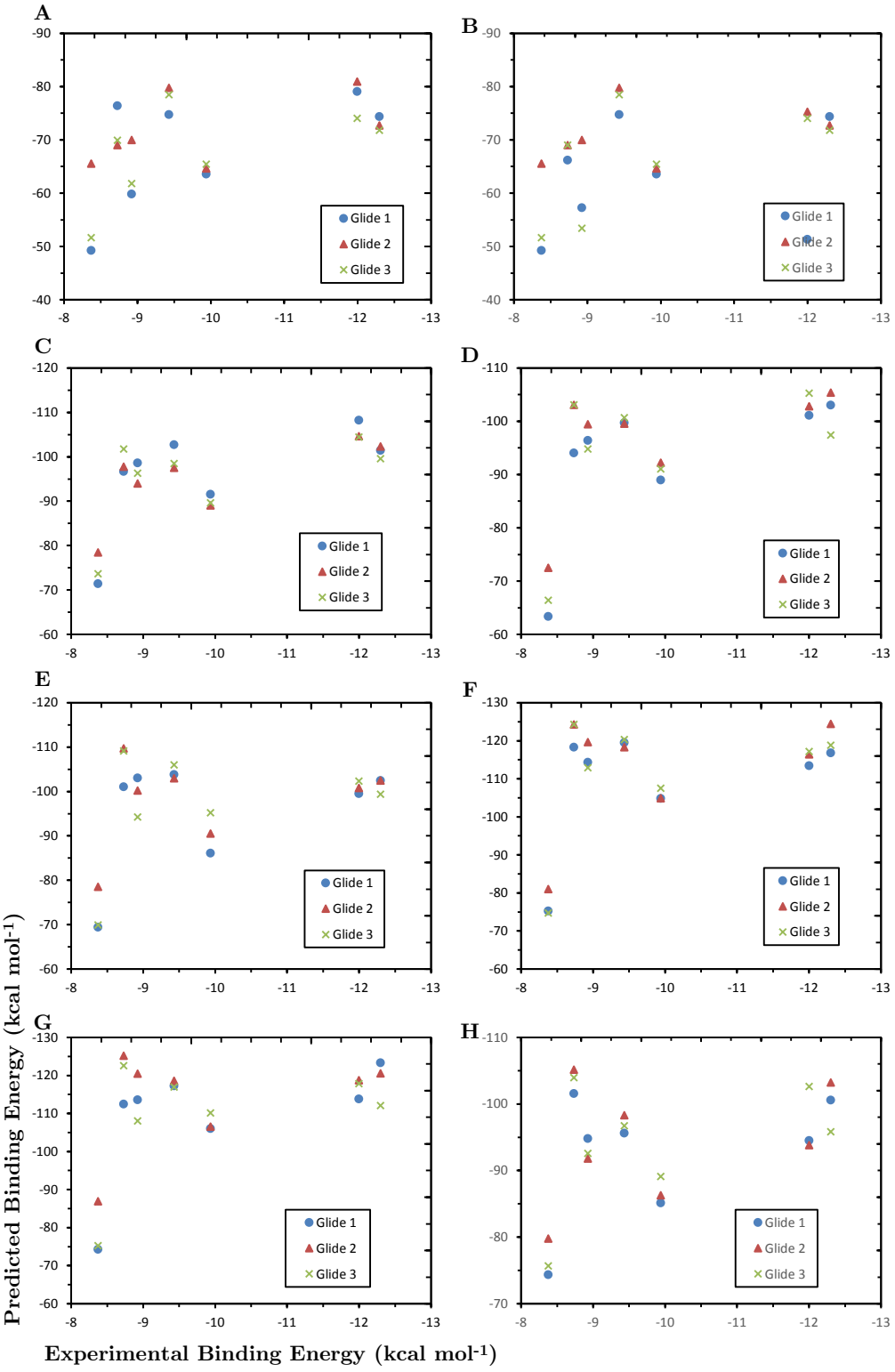


Figure B.8: Scatter plots of the predicted and experimental binding affinities for Thrombin. The plots correspond to the solvent models, A: Prime Flex, B: Prime Flex L., C: $GB^{HCT}$ Flex, D: $GB^{OBC1}$ bondi Flex, E: $GB^{OBC1}$ mbondi2 Flex, F: $GB^{OBC2}$ bondi Flex, G: $GB^{OBC2}$ mbondi2 Flex, H: Gbn Flex.

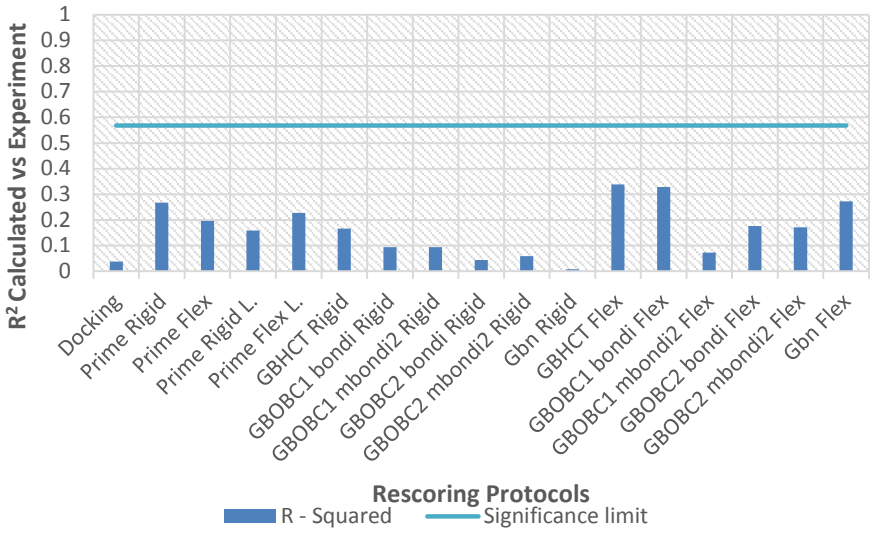


Figure B.9: Summary of $R^2$ with experiment for each protocol when the lowest poses from the three Glide jobs is considered.

| R^2 | Docking | Prime R | Prime F | Prime R L | Prime F L | $GB^{HCT}$ R | $GB^{OBC1}$ B R | $GB^{OBC1}$ MB2 R | $GB^{OBC2}$ B R | $GB^{OBC2}$ MB2 R | GBn R | $GB^{HCT}$ F | $GB^{OBC1}$ B F | $GB^{OBC1}$ MB2 F | $GB^{OBC2}$ B F | $GB^{OBC2}$ MB2 F | GBn F |
|---|---|---|---|---|---|---|---|---|---|---|---|---|---|---|---|---|---|
| All Ligands | 0.04 | 0.27 | 0.20 | 0.16 | 0.23 | 0.17 | 0.09 | 0.09 | 0.04 | 0.06 | 0.01 | 0.34 | 0.33 | 0.07 | 0.18 | 0.17 | 0.27 |
| | 0.68 | 0.23 | 0.32 | 0.38 | 0.28 | 0.36 | 0.50 | 0.50 | 0.65 | 0.60 | 0.85 | 0.17 | 0.18 | 0.56 | 0.35 | 0.36 | 0.23 |
| Kendall tau | | | | | | | | | | | | | | | | | |
| All Ligands | 0.14 | 0.33 | 0.24 | 0.33 | 0.33 | 0.43 | 0.14 | 0.24 | 0.14 | 0.05 | 0.05 | 0.43 | 0.52 | -0.05 | 0.24 | 0.14 | 0.33 |
| | 0.77 | 0.38 | 0.56 | 0.38 | 0.38 | 0.24 | 0.77 | 0.56 | 0.77 | 1.00 | 1.00 | 0.24 | 0.14 | 1.00 | 0.56 | 0.77 | 0.38 |

Figure B.10: The correlation of determination ($R^2$) and Kendall tau rank correlation coefficient ($\tau$) across of the lowest predicted energy for all rescoring tests (including the docking score).

Table B.14: Coefficient of determination and Kendall's tau rank correlation coefficient for heavy atoms and molecular weight with experiment.

| | $R^2$ | $p_{R^2}$ | Kendall tau ($\tau$) | $p_\tau$ |
|---|---|---|---|---|
| **Heavy Atoms** | 0.17 | 0.36 | -0.10 | 0.75 |
| **MW** | 0.18 | 0.34 | -0.10 | 0.76 |

Table B. 15: Coefficient of determination ($R^2$) matrix between rescoring models for Glide 1. P–values from a two-tailed test shown. Significant correlations highlighted in bold.

| | | Prime Rigid | Prime Flex | Prime Rigid L. | Prime Flex L. | GBHCT Rigid | GBOBC1 bondi Rigid | GBOBC1 mbondi2 Rigid | GBOBC2 bondi Rigid | GBOBC2 mbondi2 Rigid | Gbn Rigid | GBHCT Flex | GBOBC1 bondi Flex | GBOBC1 mbondi2 Flex | GBOBC2 bondi Flex | GBOBC2 mbondi2 Flex | Gbn Flex |
|---|---|---|---|---|---|---|---|---|---|---|---|---|---|---|---|---|---|
| **Prime Rigid** | R2 | 1.0000 | **0.9414** | **0.8710** | 0.4548 | **0.8190** | **0.6605** | **0.6854** | **0.6440** | **0.6972** | **0.5929** | **0.7142** | **0.7321** | **0.7208** | **0.7861** | **0.7300** | **0.8169** |
| **Prime Rigid** | p | -- | **0.0003** | **0.0021** | 0.0966 | **0.0051** | **0.0263** | **0.0215** | **0.0298** | **0.0194** | **0.0429** | **0.0167** | **0.0141** | **0.0157** | **0.0078** | **0.0143** | **0.0052** |
| **Prime Flex** | R2 | | 1.0000 | **0.7599** | 0.2740 | **0.6962** | 0.4576 | 0.4690 | 0.4321 | 0.5046 | 0.3693 | **0.7551** | **0.7108** | **0.6159** | **0.6982** | **0.6627** | **0.7001** |
| **Prime Flex** | p | | -- | **0.0106** | 0.2279 | **0.0196** | 0.0952 | 0.0896 | 0.1086 | 0.0737 | 0.1477 | **0.0111** | **0.0172** | **0.0366** | **0.0192** | **0.0258** | **0.0189** |
| **Prime Rigid L.** | R2 | | | 1.0000 | **0.6851** | **0.8801** | **0.7800** | **0.7332** | **0.7893** | **0.8113** | **0.6501** | **0.6649** | **0.7435** | **0.6777** | **0.7330** | **0.7707** | **0.6808** |
| **Prime Rigid L.** | p | | | -- | **0.0215** | **0.0018** | **0.0084** | **0.0139** | **0.0075** | **0.0057** | **0.0285** | **0.0254** | **0.0125** | **0.0229** | **0.0139** | **0.0094** | **0.0223** |
| **Prime Flex L.** | R2 | | | | 1.0000 | **0.6082** | **0.7838** | **0.7671** | **0.8795** | **0.8238** | **0.7664** | 0.1892 | 0.3335 | 0.3329 | 0.4178 | 0.4503 | 0.3847 |
| **Prime Flex L.** | p | | | | -- | **0.0386** | **0.0080** | **0.0098** | **0.0018** | **0.0047** | **0.0098** | 0.3294 | 0.1746 | 0.1750 | 0.1167 | 0.0989 | 0.1373 |
| **GBHCT Rigid** | R2 | | | | | 1.0000 | **0.9074** | **0.8481** | **0.8454** | **0.9120** | **0.7796** | **0.7551** | **0.8901** | **0.8601** | **0.8906** | **0.9451** | **0.8848** |
| **GBHCT Rigid** | p | | | | | -- | **0.0009** | **0.0032** | **0.0034** | **0.0008** | **0.0085** | **0.0111** | **0.0014** | **0.0026** | **0.0014** | **0.0002** | **0.0016** |
| **GBOBC1 bondi Rigid** | R2 | | | | | | 1.0000 | **0.9648** | **0.9746** | **0.9852** | **0.9501** | 0.4961 | **0.6783** | **0.7498** | **0.7696** | **0.7931** | **0.7933** |
| **GBOBC1 bondi Rigid** | p | | | | | | -- | **0.0001** | **0.0000** | **0.0000** | **0.0002** | 0.0773 | **0.0228** | **0.0117** | **0.0095** | **0.0072** | **0.0072** |
| **GBOBC1 mbondi2 Rigid** | R2 | | | | | | | 1.0000 | **0.9432** | **0.9677** | **0.9876** | 0.4019 | **0.5696** | **0.6759** | **0.6957** | **0.6868** | **0.8070** |
| **GBOBC1 mbondi2 Rigid** | p | | | | | | | -- | **0.0003** | **0.0001** | **0.0000** | 0.1263 | **0.0499** | **0.0232** | **0.0197** | **0.0212** | **0.0060** |
| **GBOBC2 bondi Rigid** | R2 | | | | | | | | 1.0000 | **0.9706** | **0.9365** | 0.4246 | **0.5985** | **0.6628** | **0.7190** | **0.7193** | **0.6989** |
| **GBOBC2 bondi Rigid** | p | | | | | | | | -- | **0.0001** | **0.0004** | 0.1128 | **0.0413** | **0.0258** | **0.0159** | **0.0159** | **0.0191** |
| **GBOBC2 mbondi2 Rigid** | R2 | | | | | | | | | 1.0000 | **0.9383** | 0.4774 | **0.6612** | **0.6905** | **0.7421** | **0.7790** | **0.7782** |
| **GBOBC2 mbondi2 Rigid** | p | | | | | | | | | -- | **0.0003** | 0.0856 | **0.0262** | **0.0206** | **0.0127** | **0.0085** | **0.0086** |
| **Gbn Rigid** | R2 | | | | | | | | | | 1.0000 | 0.3281 | 0.4965 | **0.6332** | **0.6437** | **0.6221** | **0.7520** |
| **Gbn Rigid** | p | | | | | | | | | | -- | 0.1789 | 0.0771 | **0.0323** | **0.0299** | **0.0350** | **0.0115** |
| **GBHCT Flex** | R2 | | | | | | | | | | | 1.0000 | **0.9533** | **0.8502** | **0.8567** | **0.8721** | **0.7149** |
| **GBHCT Flex** | p | | | | | | | | | | | -- | **0.0002** | **0.0031** | **0.0028** | **0.0021** | **0.0166** |
| **GBOBC1 bondi Flex** | R2 | | | | | | | | | | | | 1.0000 | **0.9033** | **0.9265** | **0.9770** | **0.8038** |
| **GBOBC1 bondi Flex** | p | | | | | | | | | | | | -- | **0.0010** | **0.0005** | **0.0000** | **0.0063** |
| **GBOBC1 mbondi2 Flex** | R2 | | | | | | | | | | | | | 1.0000 | **0.9476** | **0.9031** | **0.9005** |
| **GBOBC1 mbondi2 Flex** | p | | | | | | | | | | | | | -- | **0.0002** | **0.0010** | **0.0011** |
| **GBOBC2 bondi Flex** | R2 | | | | | | | | | | | | | | 1.0000 | **0.9453** | **0.8864** |
| **GBOBC2 bondi Flex** | p | | | | | | | | | | | | | | -- | **0.0002** | **0.0015** |
| **GBOBC2 mbondi2 Flex** | R2 | | | | | | | | | | | | | | | 1.0000 | **0.8403** |
| **GBOBC2 mbondi2 Flex** | p | | | | | | | | | | | | | | | -- | **0.0037** |
| **Gbn Flex** | R2 | | | | | | | | | | | | | | | | 1.0000 |
| **Gbn Flex** | p | | | | | | | | | | | | | | | | -- |

Table B.16: Kendall tau (τ) rank correlation coefficient matrix between rescoring models for Glide 1. P–values from a two-tailed test shown. Significant correlations highlighted in bold.

| | | Prime Rigid | Prime Flex | Prime Rigid L. | Prime Flex L. | GBHCT Rigid | GBOBC1 bondi Rigid | GBOBC1 mbondi2 Rigid | GBOBC2 bondi Rigid | GBOBC2 mbondi2 Rigid | Gbn Rigid | GBHCT Flex | GBOBC1 bondi Flex | GBOBC1 mbondi2 Flex | GBOBC2 bondi Flex | GBOBC2 mbondi2 Flex | Gbn Flex |
|---|---|---|---|---|---|---|---|---|---|---|---|---|---|---|---|---|---|
| **Prime Rigid** | τ | 1.0000 | **0.7143** | **0.8095** | 0.6191 | 0.6191 | 0.4286 | 0.5238 | 0.4286 | 0.4286 | 0.5238 | 0.3333 | 0.3333 | 0.4286 | **0.7143** | 0.4286 | **0.7143** |
| **Prime Rigid** | p | -- | **0.0243** | **0.0107** | 0.0509 | 0.0509 | 0.1765 | 0.0985 | 0.1765 | 0.1765 | 0.0985 | 0.2931 | 0.2931 | 0.1765 | **0.0243** | 0.1765 | **0.0243** |
| **Prime Flex** | τ | | 1.0000 | 0.5238 | 0.3333 | 0.3333 | 0.1429 | 0.2381 | 0.1429 | 0.1429 | 0.2381 | 0.6191 | 0.4286 | 0.1429 | 0.4286 | 0.3333 | 0.4286 |
| **Prime Flex** | p | | -- | 0.0985 | 0.2931 | 0.2931 | 0.6523 | 0.4527 | 0.6523 | 0.6523 | 0.4527 | 0.0509 | 0.1765 | 0.6523 | 0.1765 | 0.2931 | 0.1765 |
| **Prime Rigid L.** | τ | | | 1.0000 | **0.8095** | **0.8095** | 0.6191 | 0.5238 | 0.6191 | 0.6191 | 0.5238 | 0.5238 | 0.5238 | 0.6191 | **0.7143** | 0.6191 | 0.5238 |
| **Prime Rigid L.** | p | | | -- | **0.0107** | **0.0107** | 0.0509 | 0.0985 | 0.0509 | 0.0509 | 0.0985 | 0.0985 | 0.0985 | 0.0509 | **0.0243** | 0.0509 | 0.0985 |
| **Prime Flex L.** | τ | | | | 1.0000 | 0.6191 | **0.8095** | **0.7143** | **0.8095** | **0.8095** | **0.7143** | 0.3333 | 0.3333 | 0.6191 | **0.7143** | 0.4286 | 0.5238 |
| **Prime Flex L.** | p | | | | -- | 0.0509 | **0.0107** | **0.0243** | **0.0107** | **0.0107** | **0.0243** | 0.2931 | 0.2931 | 0.0509 | **0.0243** | 0.1765 | 0.0985 |
| **GBHCT Rigid** | τ | | | | | 1.0000 | **0.8095** | **0.7143** | **0.8095** | **0.8095** | **0.7143** | 0.5238 | **0.7143** | 0.6191 | **0.7143** | **0.8095** | **0.7143** |
| **GBHCT Rigid** | p | | | | | -- | **0.0107** | **0.0243** | **0.0107** | **0.0107** | **0.0243** | 0.0985 | **0.0243** | 0.0509 | **0.0243** | **0.0107** | **0.0243** |
| **GBOBC1 bondi Rigid** | τ | | | | | | 1.0000 | **0.9048** | **1.0000** | **1.0000** | **0.9048** | 0.3333 | 0.5238 | 0.6191 | **0.7143** | 0.6191 | **0.7143** |
| **GBOBC1 bondi Rigid** | p | | | | | | -- | **0.0043** | -- | -- | **0.0043** | 0.2931 | 0.0985 | 0.0509 | **0.0243** | 0.0509 | **0.0243** |
| **GBOBC1 mbondi2 Rigid** | τ | | | | | | | 1.0000 | **0.9048** | **0.9048** | 1.0000 | 0.2381 | 0.4286 | 0.5238 | 0.6191 | 0.5238 | **0.8095** |
| **GBOBC1 mbondi2 Rigid** | p | | | | | | | -- | **0.0043** | **0.0043** | -- | 0.4527 | 0.1765 | 0.0985 | 0.0509 | 0.0985 | **0.0107** |
| **GBOBC2 bondi Rigid** | τ | | | | | | | | 1.0000 | **1.0000** | **0.9048** | 0.3333 | 0.5238 | 0.6191 | **0.7143** | 0.6191 | **0.7143** |
| **GBOBC2 bondi Rigid** | p | | | | | | | | -- | -- | **0.0043** | 0.2931 | 0.0985 | 0.0509 | **0.0243** | 0.0509 | **0.0243** |
| **GBOBC2 mbondi2 Rigid** | τ | | | | | | | | | 1.0000 | **0.9048** | 0.3333 | 0.5238 | 0.6191 | **0.7143** | 0.6191 | **0.7143** |
| **GBOBC2 mbondi2 Rigid** | p | | | | | | | | | -- | **0.0043** | 0.2931 | 0.0985 | 0.0509 | **0.0243** | 0.0509 | **0.0243** |
| **Gbn Rigid** | τ | | | | | | | | | | 1.0000 | 0.2381 | 0.4286 | 0.5238 | 0.6191 | 0.5238 | **0.8095** |
| **Gbn Rigid** | p | | | | | | | | | | -- | 0.4527 | 0.1765 | 0.0985 | 0.0509 | 0.0985 | **0.0107** |
| **GBHCT Flex** | τ | | | | | | | | | | | 1.0000 | **0.8095** | 0.5238 | 0.4286 | **0.7143** | 0.2381 |
| **GBHCT Flex** | p | | | | | | | | | | | -- | **0.0107** | 0.0985 | 0.1765 | **0.0243** | 0.4527 |
| **GBOBC1 bondi Flex** | τ | | | | | | | | | | | | 1.0000 | 0.5238 | 0.4286 | **0.9048** | 0.4286 |
| **GBOBC1 bondi Flex** | p | | | | | | | | | | | | -- | 0.0985 | 0.1765 | **0.0043** | 0.1765 |
| **GBOBC1 mbondi2 Flex** | τ | | | | | | | | | | | | | 1.0000 | **0.7143** | 0.6191 | 0.5238 |
| **GBOBC1 mbondi2 Flex** | p | | | | | | | | | | | | | -- | **0.0243** | 0.0509 | 0.0985 |
| **GBOBC2 bondi Flex** | τ | | | | | | | | | | | | | | 1.0000 | 0.5238 | **0.8095** |
| **GBOBC2 bondi Flex** | p | | | | | | | | | | | | | | -- | 0.0985 | **0.0107** |
| **GBOBC2 mbondi2 Flex** | τ | | | | | | | | | | | | | | | 1.0000 | 0.5238 |
| **GBOBC2 mbondi2 Flex** | p | | | | | | | | | | | | | | | -- | 0.0985 |
| **Gbn Flex** | τ | | | | | | | | | | | | | | | | 1.0000 |
| **Gbn Flex** | p | | | | | | | | | | | | | | | | -- |

Table B. 17: Coefficient of determination ($R^2$) matrix between rescoring models for Glide 2. P–values from a two-tailed test shown. Significant correlations highlighted in bold.

| | | Prime Rigid | Prime Flex | Prime Rigid L. | Prime Flex L. | GBHCT Rigid | GBOBC1 bondi Rigid | GBOBC1 mbondi2 Rigid | GBOBC2 bondi Rigid | GBOBC2 mbondi2 Rigid | Gbn Rigid | GBHCT Flex | GBOBC1 bondi Flex | GBOBC1 mbondi2 Flex | GBOBC2 bondi Flex | GBOBC2 mbondi2 Flex | Gbn Flex |
|---|---|---|---|---|---|---|---|---|---|---|---|---|---|---|---|---|---|
| **Prime Rigid** | $R^2$ | 1.0000 | **0.7594** | **0.8353** | **0.6746** | **0.5718** | 0.4491 | 0.4869 | 0.3477 | 0.5164 | 0.3035 | **0.8367** | **0.6045** | **0.6023** | 0.5384 | 0.5574 | **0.5857** |
| **Prime Rigid** | p | -- | **0.0106** | **0.0040** | **0.0235** | **0.0492** | 0.0995 | 0.0813 | 0.1635 | 0.0689 | 0.1999 | **0.0039** | **0.0396** | **0.0402** | 0.0605 | 0.0539 | **0.0450** |
| **Prime Flex** | $R^2$ | | 1.0000 | 0.5321 | **0.9022** | 0.2248 | 0.1631 | 0.1835 | 0.0982 | 0.2042 | 0.0536 | 0.5533 | 0.3159 | 0.2762 | 0.2496 | 0.2718 | 0.2025 |
| **Prime Flex** | p | | -- | 0.0628 | **0.0011** | 0.2824 | 0.3689 | 0.3376 | 0.4937 | 0.3088 | 0.6173 | 0.0553 | 0.1891 | 0.2257 | 0.2536 | 0.2302 | 0.3111 |
| **Prime Rigid L.** | $R^2$ | | | 1.0000 | **0.6480** | **0.8448** | **0.7791** | **0.8357** | **0.6990** | **0.8408** | **0.6777** | **0.7177** | **0.6437** | **0.7405** | **0.6723** | **0.6509** | **0.8379** |
| **Prime Rigid L.** | p | | | -- | **0.0289** | **0.0034** | **0.0085** | **0.0040** | **0.0191** | **0.0037** | **0.0229** | **0.0161** | **0.0299** | **0.0129** | **0.0239** | **0.0283** | **0.0038** |
| **Prime Flex L.** | $R^2$ | | | | 1.0000 | 0.3431 | 0.3081 | 0.3404 | 0.2369 | 0.3525 | 0.1727 | 0.4852 | 0.3306 | 0.3366 | 0.3102 | 0.3134 | 0.2967 |
| **Prime Flex L.** | p | | | | -- | 0.1670 | 0.1958 | 0.1691 | 0.2680 | 0.1599 | 0.3538 | 0.0821 | 0.1769 | 0.1721 | 0.1941 | 0.1913 | 0.2061 |
| **GBHCT Rigid** | $R^2$ | | | | | 1.0000 | **0.9777** | **0.9648** | **0.9389** | **0.9728** | **0.8426** | **0.6941** | **0.8027** | **0.8479** | **0.8653** | **0.8034** | **0.9595** |
| **GBHCT Rigid** | p | | | | | -- | **0.0000** | **0.0001** | **0.0003** | **0.0000** | **0.0035** | **0.0199** | **0.0063** | **0.0033** | **0.0024** | **0.0063** | **0.0001** |
| **GBOBC1 bondi Rigid** | $R^2$ | | | | | | 1.0000 | **0.9771** | **0.9773** | **0.9674** | **0.8801** | **0.5772** | **0.7222** | **0.7667** | **0.8094** | **0.7287** | **0.9092** |
| **GBOBC1 bondi Rigid** | p | | | | | | -- | **0.0000** | **0.0000** | **0.0001** | **0.0018** | **0.0475** | **0.0155** | **0.0098** | **0.0058** | **0.0145** | **0.0009** |
| **GBOBC1 mbondi2 Rigid** | $R^2$ | | | | | | | 1.0000 | **0.9638** | **0.9796** | **0.9211** | 0.5390 | **0.6612** | **0.7800** | **0.7683** | **0.7080** | **0.9247** |
| **GBOBC1 mbondi2 Rigid** | p | | | | | | | -- | **0.0001** | **0.0000** | **0.0006** | 0.0603 | **0.0261** | **0.0084** | **0.0096** | **0.0176** | **0.0005** |
| **GBOBC2 bondi Rigid** | $R^2$ | | | | | | | | 1.0000 | **0.9633** | **0.9175** | 0.4742 | **0.6676** | **0.7699** | **0.7838** | **0.7143** | **0.8957** |
| **GBOBC2 bondi Rigid** | p | | | | | | | | -- | **0.0001** | **0.0007** | 0.0871 | **0.0248** | **0.0094** | **0.0080** | **0.0166** | **0.0012** |
| **GBOBC2 mbondi2 Rigid** | $R^2$ | | | | | | | | | 1.0000 | **0.9104** | **0.5873** | **0.7115** | **0.8393** | **0.8012** | **0.7509** | **0.9660** |
| **GBOBC2 mbondi2 Rigid** | p | | | | | | | | | -- | **0.0008** | **0.0445** | **0.0171** | **0.0037** | **0.0065** | **0.0116** | **0.0001** |
| **Gbn Rigid** | $R^2$ | | | | | | | | | | 1.0000 | 0.3170 | 0.4445 | **0.6300** | 0.5639 | 0.5074 | **0.8678** |
| **Gbn Rigid** | p | | | | | | | | | | -- | 0.1881 | 0.1019 | **0.0331** | 0.0517 | 0.0725 | **0.0023** |
| **GBHCT Flex** | $R^2$ | | | | | | | | | | | 1.0000 | **0.8961** | **0.7423** | **0.7955** | **0.7887** | **0.6555** |
| **GBHCT Flex** | p | | | | | | | | | | | -- | **0.0012** | **0.0127** | **0.0070** | **0.0076** | **0.0273** |
| **GBOBC1 bondi Flex** | $R^2$ | | | | | | | | | | | | 1.0000 | **0.8804** | **0.9677** | **0.9516** | **0.7470** |
| **GBOBC1 bondi Flex** | p | | | | | | | | | | | | -- | **0.0018** | **0.0001** | **0.0002** | **0.0121** |
| **GBOBC1 mbondi2 Flex** | $R^2$ | | | | | | | | | | | | | 1.0000 | **0.9331** | **0.9594** | **0.8764** |
| **GBOBC1 mbondi2 Flex** | p | | | | | | | | | | | | | -- | **0.0004** | **0.0001** | **0.0019** |
| **GBOBC2 bondi Flex** | $R^2$ | | | | | | | | | | | | | | 1.0000 | **0.9835** | **0.8075** |
| **GBOBC2 bondi Flex** | p | | | | | | | | | | | | | | -- | **0.0000** | **0.0060** |
| **GBOBC2 mbondi2 Flex** | $R^2$ | | | | | | | | | | | | | | | 1.0000 | **0.7745** |
| **GBOBC2 mbondi2 Flex** | p | | | | | | | | | | | | | | | -- | **0.0090** |
| **Gbn Flex** | $R^2$ | | | | | | | | | | | | | | | | 1.0000 |
| **Gbn Flex** | p | | | | | | | | | | | | | | | | -- |

Table B.18: Kendall tau (τ) rank correlation coefficient matrix between rescoring models for Glide 2. P–values from a two-tailed test shown. Significant correlations highlighted in bold.

| | | Prime Rigid | Prime Flex | Prime Rigid L. | Prime Flex L. | GBHCT Rigid | GBOBC1 bondi Rigid | GBOBC1 mbondi2 Rigid | GBOBC2 bondi Rigid | GBOBC2 mbondi2 Rigid | Gbn Rigid | GBHCT Flex | GBOBC1 bondi Flex | GBOBC1 mbondi2 Flex | GBOBC2 bondi Flex | GBOBC2 mbondi2 Flex | Gbn Flex |
|---|---|---|---|---|---|---|---|---|---|---|---|---|---|---|---|---|---|
| **Prime Rigid** | τ | 1.0000 | **0.8095** | **0.7143** | **0.7143** | 0.4286 | 0.4286 | 0.4286 | 0.4286 | 0.4286 | 0.3333 | **0.8095** | 0.6191 | 0.3333 | 0.3333 | 0.3333 | 0.4286 |
| **Prime Rigid** | p | -- | **0.0107** | **0.0243** | **0.0243** | 0.1765 | 0.1765 | 0.1765 | 0.1765 | 0.1765 | 0.2931 | **0.0107** | 0.0509 | 0.2931 | 0.2931 | 0.2931 | 0.1765 |
| **Prime Flex** | τ | | 1.0000 | 0.5238 | **0.9048** | 0.2381 | 0.2381 | 0.2381 | 0.2381 | 0.2381 | 0.1429 | 0.6191 | 0.4286 | 0.3333 | 0.1429 | 0.1429 | 0.2381 |
| **Prime Flex** | p | | -- | 0.0985 | **0.0043** | 0.4527 | 0.4527 | 0.4527 | 0.4527 | 0.4527 | 0.6523 | 0.0509 | 0.1765 | 0.2931 | 0.6523 | 0.6523 | 0.4527 |
| **Prime Rigid L.** | τ | | | 1.0000 | 0.6191 | **0.7143** | **0.7143** | **0.7143** | **0.7143** | **0.7143** | 0.6191 | 0.5238 | **0.7143** | 0.6191 | 0.6191 | 0.4286 | **0.7143** |
| **Prime Rigid L.** | p | | | -- | 0.0509 | **0.0243** | **0.0243** | **0.0243** | **0.0243** | **0.0243** | 0.0509 | 0.0985 | **0.0243** | 0.0509 | 0.0509 | 0.1765 | **0.0243** |
| **Prime Flex L.** | τ | | | | 1.0000 | 0.3333 | 0.3333 | 0.3333 | 0.3333 | 0.3333 | 0.2381 | 0.5238 | 0.3333 | 0.4286 | 0.2381 | 0.0476 | 0.3333 |
| **Prime Flex L.** | p | | | | -- | 0.2931 | 0.2931 | 0.2931 | 0.2931 | 0.2931 | 0.4527 | 0.0985 | 0.2931 | 0.1765 | 0.4527 | 0.8806 | 0.2931 |
| **GBHCT Rigid** | τ | | | | | 1.0000 | **1.0000** | **1.0000** | **1.0000** | **1.0000** | **0.9048** | 0.6191 | **0.8095** | **0.7143** | **0.9048** | **0.7143** | **0.8095** |
| **GBHCT Rigid** | p | | | | | -- | -- | -- | -- | -- | **0.0043** | 0.0509 | **0.0107** | **0.0243** | **0.0043** | **0.0243** | **0.0107** |
| **GBOBC1 bondi Rigid** | τ | | | | | | 1.0000 | **1.0000** | **1.0000** | **1.0000** | **0.9048** | 0.6191 | **0.8095** | **0.7143** | **0.9048** | **0.7143** | **0.8095** |
| **GBOBC1 bondi Rigid** | p | | | | | | -- | -- | -- | -- | **0.0043** | 0.0509 | **0.0107** | **0.0243** | **0.0043** | **0.0243** | **0.0107** |
| **GBOBC1 mbondi2 Rigid** | τ | | | | | | | 1.0000 | **1.0000** | **1.0000** | **0.9048** | 0.6191 | **0.8095** | **0.7143** | **0.9048** | **0.7143** | **0.8095** |
| **GBOBC1 mbondi2 Rigid** | p | | | | | | | -- | -- | -- | **0.0043** | 0.0509 | **0.0107** | **0.0243** | **0.0043** | **0.0243** | **0.0107** |
| **GBOBC2 bondi Rigid** | τ | | | | | | | | 1.0000 | **1.0000** | **0.9048** | 0.6191 | **0.8095** | **0.7143** | **0.9048** | **0.7143** | **0.8095** |
| **GBOBC2 bondi Rigid** | p | | | | | | | | -- | -- | **0.0043** | 0.0509 | **0.0107** | **0.0243** | **0.0043** | **0.0243** | **0.0107** |
| **GBOBC2 mbondi2 Rigid** | τ | | | | | | | | | 1.0000 | **0.9048** | 0.6191 | **0.8095** | **0.7143** | **0.9048** | **0.7143** | **0.8095** |
| **GBOBC2 mbondi2 Rigid** | p | | | | | | | | | -- | **0.0043** | 0.0509 | **0.0107** | **0.0243** | **0.0043** | **0.0243** | **0.0107** |
| **Gbn Rigid** | τ | | | | | | | | | | 1.0000 | 0.5238 | **0.7143** | **0.8095** | **0.8095** | **0.8095** | **0.9048** |
| **Gbn Rigid** | p | | | | | | | | | | -- | 0.0985 | **0.0243** | **0.0107** | **0.0107** | **0.0107** | **0.0043** |
| **GBHCT Flex** | τ | | | | | | | | | | | 1.0000 | **0.8095** | 0.5238 | 0.5238 | 0.5238 | 0.6191 |
| **GBHCT Flex** | p | | | | | | | | | | | -- | **0.0107** | 0.0985 | 0.0985 | 0.0985 | 0.0509 |
| **GBOBC1 bondi Flex** | τ | | | | | | | | | | | | 1.0000 | **0.7143** | **0.7143** | **0.7143** | **0.8095** |
| **GBOBC1 bondi Flex** | p | | | | | | | | | | | | -- | **0.0243** | **0.0243** | **0.0243** | **0.0107** |
| **GBOBC1 mbondi2 Flex** | τ | | | | | | | | | | | | | 1.0000 | 0.6191 | 0.6191 | **0.9048** |
| **GBOBC1 mbondi2 Flex** | p | | | | | | | | | | | | | -- | 0.0509 | 0.0509 | **0.0043** |
| **GBOBC2 bondi Flex** | τ | | | | | | | | | | | | | | 1.0000 | **0.8095** | **0.7143** |
| **GBOBC2 bondi Flex** | p | | | | | | | | | | | | | | -- | **0.0107** | **0.0243** |
| **GBOBC2 mbondi2 Flex** | τ | | | | | | | | | | | | | | | 1.0000 | **0.7143** |
| **GBOBC2 mbondi2 Flex** | p | | | | | | | | | | | | | | | -- | **0.0243** |
| **Gbn Flex** | τ | | | | | | | | | | | | | | | | 1.0000 |
| **Gbn Flex** | p | | | | | | | | | | | | | | | | -- |

Table B.19: Coefficient of determination ($R^2$) matrix between rescoring models for Glide 3. P–values from a two-tailed test shown. Significant correlations highlighted in bold.

| | | Prime Rigid | Prime Flex | Prime Rigid L. | Prime Flex L. | GBHCT Rigid | GBOBC1 bondi Rigid | GBOBC1 mbondi2 Rigid | GBOBC2 bondi Rigid | GBOBC2 mbondi2 Rigid | Gbn Rigid | GBHCT Flex | GBOBC1 bondi Flex | GBOBC1 mbondi2 Flex | GBOBC2 bondi Flex | GBOBC2 mbondi2 Flex | Gbn Flex |
|---|---|---|---|---|---|---|---|---|---|---|---|---|---|---|---|---|---|
| **Prime Rigid** | $R^2$ | 1.0000 | **0.9433** | **0.9342** | **0.8299** | **0.9175** | **0.8453** | **0.8648** | **0.7664** | **0.8132** | **0.6010** | **0.7282** | **0.7953** | **0.9004** | **0.8347** | **0.8243** | **0.7328** |
| **Prime Rigid** | p | -- | **0.0003** | **0.0004** | **0.0043** | **0.0007** | **0.0034** | **0.0024** | **0.0098** | **0.0055** | **0.0406** | **0.0146** | **0.0070** | **0.0011** | **0.0040** | **0.0047** | **0.0140** |
| **Prime Flex** | $R^2$ | | 1.0000 | **0.9070** | **0.9129** | **0.7834** | **0.6665** | **0.7094** | 0.5468 | **0.6067** | 0.3941 | **0.7356** | **0.7861** | **0.8087** | **0.7543** | **0.7573** | **0.7019** |
| **Prime Flex** | p | | -- | **0.0009** | **0.0008** | **0.0081** | **0.0251** | **0.0174** | 0.0575 | **0.0390** | 0.1312 | **0.0136** | **0.0078** | **0.0059** | **0.0112** | **0.0109** | **0.0186** |
| **Prime Rigid L.** | $R^2$ | | | 1.0000 | 0.9389 | **0.8713** | **0.8113** | **0.8409** | **0.7029** | **0.7628** | **0.5883** | 0.5686 | **0.6379** | **0.7702** | **0.6562** | **0.6836** | **0.6203** |
| **Prime Rigid L.** | p | | | -- | 0.0003 | **0.0021** | **0.0057** | **0.0036** | **0.0185** | **0.0102** | **0.0442** | 0.0502 | **0.0312** | **0.0094** | **0.0272** | **0.0218** | **0.0355** |
| **Prime Flex L.** | $R^2$ | | | | 1.0000 | **0.6982** | **0.6031** | **0.6540** | 0.4656 | 0.5296 | 0.3656 | 0.5153 | 0.5691 | **0.6298** | 0.5288 | 0.5677 | 0.5350 |
| **Prime Flex L.** | p | | | | -- | **0.0192** | **0.0400** | **0.0277** | 0.0912 | 0.0637 | 0.1504 | 0.0693 | 0.0500 | **0.0331** | 0.0641 | 0.0505 | 0.0618 |
| **GBHCT Rigid** | $R^2$ | | | | | 1.0000 | **0.9596** | **0.9796** | **0.8865** | **0.9347** | **0.8289** | **0.6509** | **0.6792** | **0.8363** | **0.7759** | **0.7233** | **0.7048** |
| **GBHCT Rigid** | p | | | | | -- | **0.0001** | **0.0000** | **0.0015** | **0.0004** | **0.0044** | **0.0283** | **0.0226** | **0.0039** | **0.0088** | **0.0153** | **0.0181** |
| **GBOBC1 bondi Rigid** | $R^2$ | | | | | | 1.0000 | **0.9857** | **0.9558** | **0.9623** | **0.9060** | 0.5509 | **0.5914** | **0.7888** | **0.7370** | **0.6863** | **0.6082** |
| **GBOBC1 bondi Rigid** | p | | | | | | -- | **0.0000** | **0.0001** | **0.0001** | **0.0010** | 0.0561 | **0.0433** | **0.0076** | **0.0134** | **0.0213** | **0.0386** |
| **GBOBC1 mbondi2 Rigid** | $R^2$ | | | | | | | 1.0000 | **0.9264** | **0.9376** | **0.8969** | 0.5463 | **0.5742** | **0.7579** | **0.7067** | **0.6417** | **0.5930** |
| **GBOBC1 mbondi2 Rigid** | p | | | | | | | -- | **0.0005** | **0.0003** | **0.0012** | 0.0577 | **0.0485** | **0.0108** | **0.0178** | **0.0304** | **0.0428** |
| **GBOBC2 bondi Rigid** | $R^2$ | | | | | | | | 1.0000 | **0.9701** | **0.9246** | 0.4258 | 0.4865 | **0.7136** | **0.6538** | **0.6057** | 0.4840 |
| **GBOBC2 bondi Rigid** | p | | | | | | | | -- | **0.0001** | **0.0005** | 0.1122 | 0.0815 | **0.0168** | **0.0277** | **0.0393** | 0.0826 |
| **GBOBC2 mbondi2 Rigid** | $R^2$ | | | | | | | | | 1.0000 | **0.9016** | 0.5158 | **0.5755** | **0.7920** | **0.7047** | **0.6814** | **0.6118** |
| **GBOBC2 mbondi2 Rigid** | p | | | | | | | | | -- | **0.0011** | 0.0691 | **0.0480** | **0.0073** | **0.0182** | **0.0222** | **0.0377** |
| **Gbn Rigid** | $R^2$ | | | | | | | | | | 1.0000 | 0.3071 | 0.3248 | 0.5339 | 0.4860 | 0.4151 | 0.3816 |
| **Gbn Rigid** | p | | | | | | | | | | -- | 0.1968 | 0.1816 | 0.0621 | 0.0817 | 0.1183 | 0.1394 |
| **GBHCT Flex** | $R^2$ | | | | | | | | | | | 1.0000 | **0.9745** | **0.8750** | **0.9246** | **0.8967** | **0.9486** |
| **GBHCT Flex** | p | | | | | | | | | | | -- | **0.0000** | **0.0020** | **0.0005** | **0.0012** | **0.0002** |
| **GBOBC1 bondi Flex** | $R^2$ | | | | | | | | | | | | 1.0000 | **0.9386** | **0.9509** | **0.9628** | **0.9445** |
| **GBOBC1 bondi Flex** | p | | | | | | | | | | | | -- | **0.0003** | **0.0002** | **0.0001** | **0.0003** |
| **GBOBC1 mbondi2 Flex** | $R^2$ | | | | | | | | | | | | | 1.0000 | **0.9616** | **0.9789** | **0.9028** |
| **GBOBC1 mbondi2 Flex** | p | | | | | | | | | | | | | -- | **0.0001** | **0.0000** | **0.0010** |
| **GBOBC2 bondi Flex** | $R^2$ | | | | | | | | | | | | | | 1.0000 | **0.9624** | **0.8838** |
| **GBOBC2 bondi Flex** | p | | | | | | | | | | | | | | -- | **0.0001** | **0.0016** |
| **GBOBC2 mbondi2 Flex** | $R^2$ | | | | | | | | | | | | | | | 1.0000 | **0.9036** |
| **GBOBC2 mbondi2 Flex** | p | | | | | | | | | | | | | | | -- | **0.0010** |
| **Gbn Flex** | $R^2$ | | | | | | | | | | | | | | | | 1.0000 |
| **Gbn Flex** | p | | | | | | | | | | | | | | | | -- |

Table B.20: Kendall tau (τ) rank correlation coefficient matrix between rescoring models for Glide 3. P–values from a two-tailed test shown. Significant correlations highlighted in bold.

| | | Prime Rigid | Prime Flex | Prime Rigid L. | Prime Flex L. | GBHCT Rigid | GBOBC1 bondi Rigid | GBOBC1 mbondi2 Rigid | GBOBC2 bondi Rigid | GBOBC2 mbondi2 Rigid | Gbn Rigid | GBHCT Flex | GBOBC1 bondi Flex | GBOBC1 mbondi2 Flex | GBOBC2 bondi Flex | GBOBC2 mbondi2 Flex | Gbn Flex |
|---|---|---|---|---|---|---|---|---|---|---|---|---|---|---|---|---|---|
| **Prime Rigid** | τ | 1.0000 | **0.7143** | **1.0000** | **0.7143** | **1.0000** | **0.8095** | **0.9048** | **0.7143** | **0.8095** | **0.7143** | 0.4286 | 0.5238 | **0.8095** | **0.8095** | **0.7143** | 0.6191 |
| **Prime Rigid** | p | -- | **0.0243** | -- | **0.0243** | -- | **0.0107** | **0.0043** | **0.0243** | **0.0107** | **0.0243** | 0.1765 | 0.0985 | **0.0107** | **0.0107** | **0.0243** | 0.0509 |
| **Prime Flex** | τ | | 1.0000 | **0.7143** | **1.0000** | **0.7143** | 0.5238 | 0.6191 | 0.4286 | 0.5238 | 0.4286 | 0.5238 | 0.6191 | **0.7143** | 0.5238 | 0.6191 | 0.5238 |
| **Prime Flex** | p | | -- | **0.0243** | -- | **0.0243** | 0.0985 | 0.0509 | 0.1765 | 0.0985 | 0.1765 | 0.0985 | 0.0509 | **0.0243** | 0.0985 | 0.0509 | 0.0985 |
| **Prime Rigid L.** | τ | | | 1.0000 | **0.7143** | **1.0000** | **0.8095** | **0.9048** | **0.7143** | **0.8095** | **0.7143** | 0.4286 | 0.5238 | **0.8095** | **0.8095** | **0.7143** | 0.6191 |
| **Prime Rigid L.** | p | | | -- | **0.0243** | -- | **0.0107** | **0.0043** | **0.0243** | **0.0107** | **0.0243** | 0.1765 | 0.0985 | **0.0107** | **0.0107** | **0.0243** | 0.0509 |
| **Prime Flex L.** | τ | | | | 1.0000 | **0.7143** | 0.5238 | 0.6191 | 0.4286 | 0.5238 | 0.4286 | 0.5238 | 0.6191 | **0.7143** | 0.5238 | 0.6191 | 0.5238 |
| **Prime Flex L.** | p | | | | -- | **0.0243** | 0.0985 | 0.0509 | 0.1765 | 0.0985 | 0.1765 | 0.0985 | 0.0509 | **0.0243** | 0.0985 | 0.0509 | 0.0985 |
| **GBHCT Rigid** | τ | | | | | 1.0000 | **0.8095** | **0.9048** | **0.7143** | **0.8095** | **0.7143** | 0.4286 | 0.5238 | **0.8095** | **0.8095** | **0.7143** | 0.6191 |
| **GBHCT Rigid** | p | | | | | -- | **0.0107** | **0.0043** | **0.0243** | **0.0107** | **0.0243** | 0.1765 | 0.0985 | **0.0107** | **0.0107** | **0.0243** | 0.0509 |
| **GBOBC1 bondi Rigid** | τ | | | | | | 1.0000 | **0.9048** | **0.9048** | **1.0000** | **0.9048** | 0.4286 | 0.5238 | **0.8095** | **0.8095** | **0.7143** | 0.6191 |
| **GBOBC1 bondi Rigid** | p | | | | | | -- | **0.0043** | **0.0043** | -- | **0.0043** | 0.1765 | 0.0985 | **0.0107** | **0.0107** | **0.0243** | 0.0509 |
| **GBOBC1 mbondi2 Rigid** | τ | | | | | | | 1.0000 | **0.8095** | **0.9048** | **0.8095** | 0.5238 | 0.6191 | **0.9048** | **0.9048** | **0.8095** | **0.7143** |
| **GBOBC1 mbondi2 Rigid** | p | | | | | | | -- | **0.0107** | **0.0043** | **0.0107** | 0.0985 | 0.0509 | **0.0043** | **0.0043** | **0.0107** | **0.0243** |
| **GBOBC2 bondi Rigid** | τ | | | | | | | | 1.0000 | **0.9048** | **1.0000** | 0.3333 | 0.4286 | **0.7143** | **0.7143** | 0.6191 | 0.5238 |
| **GBOBC2 bondi Rigid** | p | | | | | | | | -- | **0.0043** | -- | 0.2931 | 0.1765 | **0.0243** | **0.0243** | 0.0509 | 0.0985 |
| **GBOBC2 mbondi2 Rigid** | τ | | | | | | | | | 1.0000 | **0.9048** | 0.4286 | 0.5238 | **0.8095** | **0.8095** | **0.7143** | 0.6191 |
| **GBOBC2 mbondi2 Rigid** | p | | | | | | | | | -- | **0.0043** | 0.1765 | 0.0985 | **0.0107** | **0.0107** | **0.0243** | 0.0509 |
| **Gbn Rigid** | τ | | | | | | | | | | 1.0000 | 0.3333 | 0.4286 | **0.7143** | **0.7143** | 0.6191 | 0.5238 |
| **Gbn Rigid** | p | | | | | | | | | | -- | 0.2931 | 0.1765 | **0.0243** | **0.0243** | 0.0509 | 0.0985 |
| **GBHCT Flex** | τ | | | | | | | | | | | 1.0000 | **0.9048** | 0.6191 | 0.6191 | **0.7143** | **0.8095** |
| **GBHCT Flex** | p | | | | | | | | | | | -- | **0.0043** | 0.0509 | 0.0509 | **0.0243** | **0.0107** |
| **GBOBC1 bondi Flex** | τ | | | | | | | | | | | | 1.0000 | **0.7143** | **0.7143** | **0.8095** | **0.9048** |
| **GBOBC1 bondi Flex** | p | | | | | | | | | | | | -- | **0.0243** | **0.0243** | **0.0107** | **0.0043** |
| **GBOBC1 mbondi2 Flex** | τ | | | | | | | | | | | | | 1.0000 | **0.8095** | **0.9048** | **0.8095** |
| **GBOBC1 mbondi2 Flex** | p | | | | | | | | | | | | | -- | **0.0107** | **0.0043** | **0.0107** |
| **GBOBC2 bondi Flex** | τ | | | | | | | | | | | | | | 1.0000 | **0.7143** | **0.8095** |
| **GBOBC2 bondi Flex** | p | | | | | | | | | | | | | | -- | **0.0243** | **0.0107** |
| **GBOBC2 mbondi2 Flex** | τ | | | | | | | | | | | | | | | 1.0000 | **0.9048** |
| **GBOBC2 mbondi2 Flex** | p | | | | | | | | | | | | | | | -- | **0.0043** |
| **Gbn Flex** | τ | | | | | | | | | | | | | | | | 1.0000 |
| **Gbn Flex** | p | | | | | | | | | | | | | | | | -- |

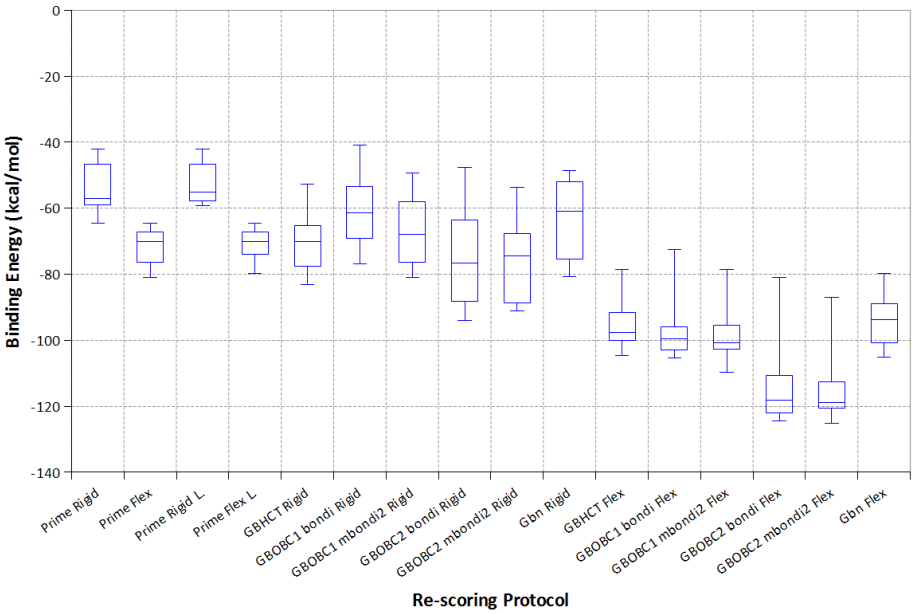


Figure B.11: Box Plot of predicted binding energies (kcal $mol^{-1}$) of Glide 2 poses for each rescoring protocol. The whiskers represent the minimum and maximum values, the box corresponds to the range of values between the 1st and 3rd quartiles, and the line through the box represents the mean value of the binding energies.

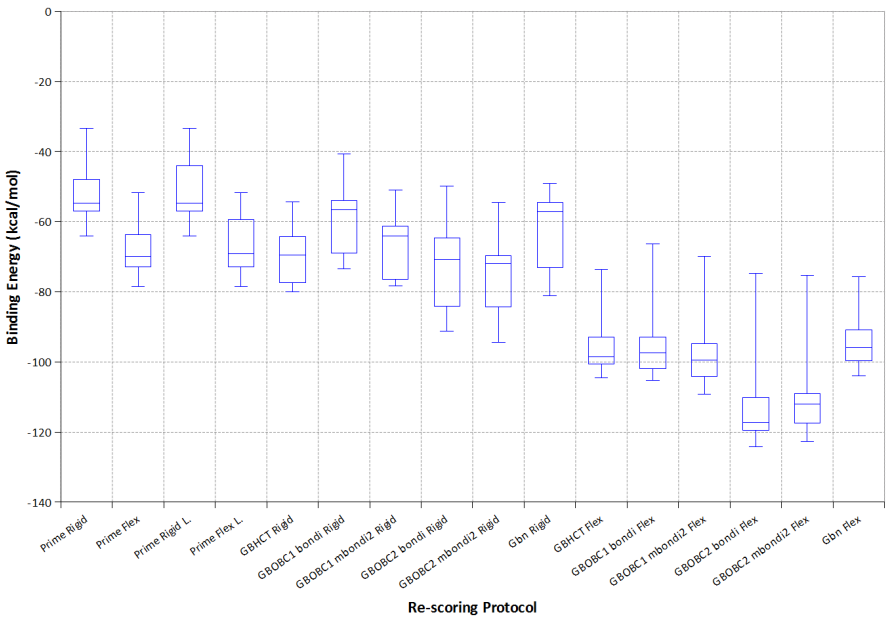


Figure B.12: Box Plot of predicted binding energies (kcal $mol^{-1}$) of Glide 3 poses for each rescoring protocol. The whiskers represent the minimum and maximum values, the box corresponds to the range of values between the 1st and 3rd quartiles, and the line through the box represents the mean value of the binding energies.

Table B.21: Descriptive statistics for Glide job 1 rescoring protocols.

| Rescoring Protocols | Mean | Std.Er. | 95% LCL | 95% UCL |
|---|---|---|---|---|
| Prime Rigid | -52.10 | 4.30 | -62.61 | -41.59 |
| Prime Flex | -68.18 | 4.14 | -78.31 | -58.06 |
| Prime Rigid L. | -49.49 | 3.83 | -58.85 | -40.13 |
| Prime Flex L. | -62.40 | 3.89 | -71.92 | -52.89 |
| GBHCT Rigid | -69.58 | 3.04 | -77.02 | -62.13 |
| GBOBC1 bondi Rigid | -59.90 | 3.71 | -68.98 | -50.82 |
| GBOBC1 mbondi2 Rigid | -66.16 | 3.69 | -75.19 | -57.12 |
| GBOBC2 bondi Rigid | -73.20 | 5.31 | -86.20 | -60.21 |
| GBOBC2 mbondi2 Rigid | -74.66 | 4.55 | -85.81 | -63.52 |
| Gbn Rigid | -62.34 | 4.01 | -72.15 | -52.53 |
| GBHCT Flex | -95.83 | 4.51 | -106.87 | -84.79 |
| GBOBC1 bondi Flex | -92.39 | 5.16 | -105.00 | -79.77 |
| GBOBC1 mbondi2 Flex | -95.07 | 4.85 | -106.94 | -83.19 |
| GBOBC2 bondi Flex | -108.92 | 5.90 | -123.35 | -94.49 |
| GBOBC2 mbondi2 Flex | -108.70 | 6.06 | -123.53 | -93.87 |
| Gbn Flex | -92.38 | 3.62 | -101.23 | -83.53 |

Table B.22: Descriptive statistics for Glide job 2 rescoring protocols.

| Rescoring Protocols | Mean | Std.Er. | 95% LCL | 95% UCL |
|---|---|---|---|---|
| Prime Rigid | -53.52 | 3.26 | -61.50 | -45.54 |
| Prime Flex | -71.82 | 2.44 | -77.79 | -65.85 |
| Prime Rigid L. | -52.18 | 2.74 | -58.89 | -45.47 |
| Prime Flex L. | -71.00 | 2.03 | -75.98 | -66.03 |
| GBHCT Rigid | -70.22 | 3.99 | -79.98 | -60.45 |
| GBOBC1 bondi Rigid | -60.67 | 4.67 | -72.11 | -49.24 |
| GBOBC1 mbondi2 Rigid | -66.74 | 4.58 | -77.95 | -55.53 |
| GBOBC2 bondi Rigid | -74.58 | 6.43 | -90.31 | -58.86 |
| GBOBC2 mbondi2 Rigid | -76.00 | 5.39 | -89.20 | -62.80 |
| Gbn Rigid | -63.57 | 5.11 | -76.09 | -51.06 |
| GBHCT Flex | -94.85 | 3.35 | -103.04 | -86.66 |
| GBOBC1 bondi Flex | -96.44 | 4.30 | -106.96 | -85.93 |
| GBOBC1 mbondi2 Flex | -97.90 | 3.88 | -107.39 | -88.42 |
| GBOBC2 bondi Flex | -112.73 | 5.83 | -127.00 | -98.47 |
| GBOBC2 mbondi2 Flex | -113.88 | 4.98 | -126.07 | -101.69 |
| Gbn Flex | -94.06 | 3.43 | -102.45 | -85.67 |

Table B.23: Descriptive statistics for Glide job 3 rescoring protocols.

| Rescoring Protocols | Mean | Std.Er. | 95% LCL | 95% UCL |
|---|---|---|---|---|
| Prime Rigid | -51.71 | 3.75 | -60.89 | -42.53 |
| Prime Flex | -67.61 | 3.37 | -75.85 | -59.37 |
| Prime Rigid L. | -50.61 | 4.16 | -60.79 | -40.44 |
| Prime Flex L. | -66.28 | 3.87 | -75.75 | -56.81 |
| GBHCT Rigid | -69.64 | 3.55 | -78.33 | -60.95 |
| GBOBC1 bondi Rigid | -59.43 | 4.38 | -70.14 | -48.72 |
| GBOBC1 mbondi2 Rigid | -66.92 | 3.94 | -76.55 | -57.29 |
| GBOBC2 bondi Rigid | -72.75 | 5.61 | -86.47 | -59.02 |
| GBOBC2 mbondi2 Rigid | -75.58 | 5.08 | -88.01 | -63.14 |
| Gbn Rigid | -63.21 | 4.66 | -74.61 | -51.81 |
| GBHCT Flex | -94.85 | 3.95 | -104.52 | -85.19 |
| GBOBC1 bondi Flex | -94.11 | 4.97 | -106.28 | -81.95 |
| GBOBC1 mbondi2 Flex | -96.62 | 4.88 | -108.57 | -84.67 |
| GBOBC2 bondi Flex | -110.83 | 6.35 | -126.38 | -95.29 |
| GBOBC2 mbondi2 Flex | -109.00 | 5.93 | -123.50 | -94.49 |
| Gbn Flex | -93.80 | 3.60 | -102.62 | -84.98 |

Table B.24: Holm-Šidák results for Glide job 1. Names abbreviated for expediency. F., R., b., mb2, and d, correspond to Flexible, Rigid, bondi, mbondi2, and Cohen's d respectively. Significant differences shown in bold.

| Compared Models | Index | Mean Diff. | Std.Er. | DF | \|t\|value | Prob>\|t\| | Alpha | d |
|---|---|---|---|---|---|---|---|---|
| Prime R. L. GBOBC2 b. F. | 39 | 59.44 | 2.72 | 90 | 21.89 | **8.35E-38** | 4.27E-04 | 6.84 |
| Prime R. L. GBOBC2 mb2 F. | 40 | 59.22 | 2.72 | 90 | 21.80 | **1.11E-37** | 4.31E-04 | 6.85 |
| Prime R. GBOBC2 b. F. | 12 | 56.82 | 2.72 | 90 | 20.92 | **2.47E-36** | 4.35E-04 | 7.45 |
| Prime R. GBOBC2 mb2 F. | 13 | 56.60 | 2.72 | 90 | 20.84 | **3.31E-36** | 4.38E-04 | 6.54 |
| GBOBC1 b. R. GBOBC2 b. F. | 72 | 49.03 | 2.72 | 90 | 18.05 | **1.16E-31** | 4.42E-04 | 5.82 |
| GBOBC1 b. R. GBOBC2 mb2 F. | 73 | 48.80 | 2.72 | 90 | 17.97 | **1.59E-31** | 4.46E-04 | 5.71 |
| Gbn R. GBOBC2 b. F. | 102 | 46.58 | 2.72 | 90 | 17.15 | **4.12E-30** | 4.50E-04 | 4.90 |
| Prime F. L. GBOBC2 b. F. | 51 | 46.52 | 2.72 | 90 | 17.13 | **4.50E-30** | 4.54E-04 | 3.91 |
| Gbn R. GBOBC2 mb2 F. | 103 | 46.36 | 2.72 | 90 | 17.07 | **5.73E-30** | 4.58E-04 | 4.61 |
| Prime R. L. GBHCT F. | 36 | 46.34 | 2.72 | 90 | 17.06 | **5.89E-30** | 4.62E-04 | 6.70 |
| Prime F. L. GBOBC2 mb2 F. | 52 | 46.30 | 2.72 | 90 | 17.05 | **6.26E-30** | 4.66E-04 | 3.89 |
| Prime R. L. GBOBC1 mb2 F. | 38 | 45.58 | 2.72 | 90 | 16.78 | **1.85E-29** | 4.70E-04 | 6.24 |
| Prime R. GBHCT F. | 9 | 43.73 | 2.72 | 90 | 16.10 | **3.05E-28** | 4.75E-04 | 6.72 |
| Prime R. GBOBC1 mb2 F. | 11 | 42.97 | 2.72 | 90 | 15.82 | **9.89E-28** | 4.79E-04 | 6.32 |
| Prime R. L. GBOBC1 b. F. | 37 | 42.90 | 2.72 | 90 | 15.80 | **1.10E-27** | 4.84E-04 | 6.04 |
| Prime R. L. Gbn F. | 41 | 42.89 | 2.72 | 90 | 15.79 | **1.11E-27** | 4.88E-04 | 7.34 |
| GBOBC1 mb2 R. GBOBC2 b. F. | 81 | 42.77 | 2.72 | 90 | 15.75 | **1.35E-27** | 4.93E-04 | 4.65 |
| GBOBC1 mb2 R. GBOBC2 mb2 F. | 82 | 42.54 | 2.72 | 90 | 15.67 | **1.90E-27** | 4.98E-04 | 4.41 |

| | | | | | | | | |
|---|---|---|---|---|---|---|---|---|
| Prime F. GBOBC2 b. F. | 26 | 40.74 | 2.72 | 90 | 15.00 | **3.23E-26** | 5.03E-04 | 4.62 |
| Prime F. GBOBC2 mb2 F. | 27 | 40.52 | 2.72 | 90 | 14.92 | **4.60E-26** | 5.08E-04 | 4.24 |
| Prime R. GBOBC1 b. F. | 10 | 40.29 | 2.72 | 90 | 14.83 | **6.65E-26** | 5.13E-04 | 5.70 |
| Prime R. Gbn F. | 14 | 40.28 | 2.72 | 90 | 14.83 | **6.72E-26** | 5.18E-04 | 8.20 |
| GBHCT R. GBOBC2 b. F. | 62 | 39.35 | 2.72 | 90 | 14.49 | **2.98E-25** | 5.23E-04 | 4.66 |
| GBHCT R. GBOBC2 mb2 F. | 63 | 39.13 | 2.72 | 90 | 14.41 | **4.26E-25** | 5.29E-04 | 4.64 |
| GBOBC1 b. R. GBHCT F. | 69 | 35.93 | 2.72 | 90 | 13.23 | **7.98E-23** | 5.34E-04 | 4.18 |
| GBOBC2 b. R. GBOBC2 b. F. | 89 | 35.72 | 2.72 | 90 | 13.15 | **1.14E-22** | 5.40E-04 | 4.30 |
| GBOBC2 b. R. GBOBC2 mb2 F. | 90 | 35.50 | 2.72 | 90 | 13.07 | **1.65E-22** | 5.46E-04 | 4.17 |
| GBOBC1 b. R. GBOBC1 mb2 F. | 71 | 35.17 | 2.72 | 90 | 12.95 | **2.86E-22** | 5.51E-04 | 5.37 |
| GBOBC2 mb2 R. GBOBC2 b. F. | 96 | 34.26 | 2.72 | 90 | 12.61 | **1.32E-21** | 5.57E-04 | 4.26 |
| GBOBC2 mb2 R. GBOBC2 mb2 F. | 97 | 34.04 | 2.72 | 90 | 12.53 | **1.92E-21** | 5.64E-04 | 4.35 |
| Gbn R. GBHCT F. | 99 | 33.49 | 2.72 | 90 | 12.33 | **4.85E-21** | 5.70E-04 | 3.19 |
| Prime F. L. GBHCT F. | 48 | 33.43 | 2.72 | 90 | 12.31 | **5.37E-21** | 5.76E-04 | 2.81 |
| Gbn R. GBOBC1 mb2 F. | 101 | 32.73 | 2.72 | 90 | 12.05 | **1.78E-20** | 5.83E-04 | 4.20 |
| Prime F. L. GBOBC1 mb2 F. | 50 | 32.67 | 2.72 | 90 | 12.03 | **1.97E-20** | 5.89E-04 | 3.00 |
| GBOBC1 b. R. GBOBC1 b. F. | 70 | 32.49 | 2.72 | 90 | 11.96 | **2.68E-20** | 5.96E-04 | 4.13 |
| GBOBC1 b. R. Gbn F. | 74 | 32.48 | 2.72 | 90 | 11.96 | **2.71E-20** | 6.03E-04 | 7.15 |
| Gbn R. GBOBC1 b. F. | 100 | 30.04 | 2.72 | 90 | 11.06 | **1.82E-18** | 6.10E-04 | 3.09 |
| Gbn R. Gbn F. | 104 | 30.04 | 2.72 | 90 | 11.06 | **1.84E-18** | 6.18E-04 | 5.67 |
| Prime F. L. GBOBC1 b. F. | 49 | 29.99 | 2.72 | 90 | 11.04 | **2.02E-18** | 6.25E-04 | 2.63 |
| Prime F. L. Gbn F. | 53 | 29.98 | 2.72 | 90 | 11.04 | **2.04E-18** | 6.33E-04 | 3.45 |
| GBOBC1 mb2 R. GBHCT F. | 78 | 29.67 | 2.72 | 90 | 10.93 | **3.47E-18** | 6.41E-04 | 3.13 |
| GBOBC1 mb2 R. GBOBC1 mb2 F. | 80 | 28.91 | 2.72 | 90 | 10.64 | **1.32E-17** | 6.49E-04 | 3.93 |
| Prime F. GBHCT F. | 23 | 27.65 | 2.72 | 90 | 10.18 | **1.21E-16** | 6.57E-04 | 4.66 |
| Prime F. GBOBC1 mb2 F. | 25 | 26.88 | 2.72 | 90 | 9.90 | **4.64E-16** | 6.66E-04 | 3.36 |
| GBHCT R. GBHCT F. | 59 | 26.26 | 2.72 | 90 | 9.67 | **1.40E-15** | 6.75E-04 | 4.14 |
| GBOBC1 mb2 R. GBOBC1 b. F. | 79 | 26.23 | 2.72 | 90 | 9.66 | **1.47E-15** | 6.84E-04 | 2.93 |
| GBOBC1 mb2 R. Gbn F. | 83 | 26.22 | 2.72 | 90 | 9.66 | **1.49E-15** | 6.93E-04 | 6.01 |
| GBHCT R. GBOBC1 mb2 F. | 61 | 25.49 | 2.72 | 90 | 9.39 | **5.41E-15** | 7.02E-04 | 4.14 |
| Prime R. L. GBOBC2 mb2 R. | 34 | 25.18 | 2.72 | 90 | 9.27 | **9.39E-15** | 7.12E-04 | 4.76 |
| Prime F. GBOBC1 b. F. | 24 | 24.20 | 2.72 | 90 | 8.91 | **5.26E-14** | 7.22E-04 | 3.29 |
| Prime F. Gbn F. | 28 | 24.19 | 2.72 | 90 | 8.91 | **5.33E-14** | 7.32E-04 | 4.03 |
| Prime R. L. GBOBC2 b. R. | 33 | 23.72 | 2.72 | 90 | 8.73 | **1.24E-13** | 7.43E-04 | 3.45 |
| GBHCT R. GBOBC1 b. F. | 60 | 22.81 | 2.72 | 90 | 8.40 | **6.10E-13** | 7.54E-04 | 3.45 |
| GBHCT R. Gbn F. | 64 | 22.80 | 2.72 | 90 | 8.40 | **6.18E-13** | 7.65E-04 | 6.73 |
| GBOBC2 b. R. GBHCT F. | 86 | 22.63 | 2.72 | 90 | 8.33 | **8.42E-13** | 7.77E-04 | 2.05 |
| Prime R. GBOBC2 mb2 R. | 7 | 22.57 | 2.72 | 90 | 8.31 | **9.37E-13** | 7.89E-04 | 3.34 |
| GBOBC2 b. R. GBOBC1 mb2 F. | 88 | 21.86 | 2.72 | 90 | 8.05 | **3.21E-12** | 8.01E-04 | 2.64 |
| GBOBC2 mb2 R. GBHCT F. | 93 | 21.17 | 2.72 | 90 | 7.79 | **1.08E-11** | 8.14E-04 | 2.25 |
| Prime R. GBOBC2 b. R. | 6 | 21.10 | 2.72 | 90 | 7.77 | **1.20E-11** | 8.27E-04 | 2.52 |
| GBOBC2 mb2 R. GBOBC1 mb2 F. | 95 | 20.40 | 2.72 | 90 | 7.51 | **4.08E-11** | 8.41E-04 | 2.80 |
| Prime R. L. GBHCT R. | 30 | 20.09 | 2.72 | 90 | 7.40 | **7.00E-11** | 8.55E-04 | 5.30 |

| | | | | | | | | |
|---|---|---|---|---|---|---|---|---|
| GBOBC2 b. R. GBOBC1 b. F. | 87 | 19.18 | 2.72 | 90 | 7.06 | **3.32E-10** | 8.69E-04 | 2.06 |
| GBOBC2 b. R. Gbn F. | 91 | 19.17 | 2.72 | 90 | 7.06 | **3.36E-10** | 8.84E-04 | 2.39 |
| Prime F. Prime R. L. | 15 | -18.70 | 2.72 | 90 | 6.88 | **7.55E-10** | 8.99E-04 | 3.47 |
| GBOBC2 mb2 R. GBOBC1 b. F. | 94 | 17.72 | 2.72 | 90 | 6.53 | **3.90E-09** | 9.16E-04 | 2.22 |
| GBOBC2 mb2 R. Gbn F. | 98 | 17.71 | 2.72 | 90 | 6.52 | **3.94E-09** | 9.32E-04 | 3.07 |
| Prime R. GBHCT R. | 3 | 17.48 | 2.72 | 90 | 6.44 | **5.85E-09** | 9.49E-04 | 3.28 |
| Prime R. L. GBOBC1 mb2 R. | 32 | 16.67 | 2.72 | 90 | 6.14 | **2.20E-08** | 9.67E-04 | 3.12 |
| GBOBC2 b. F. Gbn F. | 118 | -16.55 | 2.72 | 90 | 6.09 | **2.70E-08** | 9.86E-04 | 2.26 |
| GBOBC1 b. F. GBOBC2 b. F. | 111 | 16.54 | 2.72 | 90 | 6.09 | **2.74E-08** | 1.01E-03 | 3.72 |
| GBOBC2 mb2 F. Gbn F. | 119 | -16.32 | 2.72 | 90 | 6.01 | **3.88E-08** | 1.03E-03 | 2.00 |
| GBOBC1 b. F. GBOBC2 mb2 F. | 112 | 16.32 | 2.72 | 90 | 6.01 | **3.92E-08** | 1.05E-03 | 4.97 |
| Prime R. Prime F. | 0 | 16.08 | 2.72 | 90 | 5.92 | **5.70E-08** | 1.07E-03 | 5.85 |
| GBOBC1 b. R. GBOBC2 mb2 R. | 67 | 14.77 | 2.72 | 90 | 5.44 | **4.60E-07** | 1.09E-03 | 5.69 |
| Prime R. GBOBC1 mb2 R. | 5 | 14.06 | 2.72 | 90 | 5.18 | **1.37E-06** | 1.11E-03 | 2.20 |
| GBOBC1 mb2 F. GBOBC2 b. F. | 114 | 13.86 | 2.72 | 90 | 5.10 | **1.85E-06** | 1.14E-03 | 3.24 |
| GBOBC1 mb2 F. GBOBC2 mb2 F. | 115 | 13.64 | 2.72 | 90 | 5.02 | **2.58E-06** | 1.17E-03 | 2.46 |
| GBOBC1 b. R. GBOBC2 b. R. | 66 | 13.31 | 2.72 | 90 | 4.90 | **4.22E-06** | 1.19E-03 | 2.88 |
| GBHCT F. GBOBC2 b. F. | 107 | 13.09 | 2.72 | 90 | 4.82 | **5.77E-06** | 1.22E-03 | 2.04 |
| Prime R. L. Prime F. L. | 29 | 12.91 | 2.72 | 90 | 4.75 | **7.50E-06** | 1.25E-03 | 2.16 |
| GBHCT F. GBOBC2 mb2 F. | 108 | 12.87 | 2.72 | 90 | 4.74 | **7.97E-06** | 1.28E-03 | 1.98 |
| Prime R. L. Gbn R. | 35 | 12.85 | 2.72 | 90 | 4.73 | **8.18E-06** | 1.31E-03 | 1.99 |
| GBOBC2 mb2 R. Gbn R. | 92 | -12.32 | 2.72 | 90 | 4.54 | **1.75E-05** | 1.35E-03 | 3.88 |
| Prime F. L. GBOBC2 mb2 R. | 46 | 12.26 | 2.72 | 90 | 4.52 | **1.90E-05** | 1.39E-03 | 2.41 |
| GBOBC2 b. R. Gbn R. | 85 | -10.86 | 2.72 | 90 | 4.00 | **1.30E-04** | 1.42E-03 | 2.35 |
| Prime F. L. GBOBC2 b. R. | 45 | 10.80 | 2.72 | 90 | 3.98 | **1.40E-04** | 1.46E-03 | 1.91 |
| Prime R. L. GBOBC1 b. R. | 31 | 10.41 | 2.72 | 90 | 3.83 | **2.34E-04** | 1.51E-03 | 2.16 |
| Prime R. Prime F. L. | 2 | 10.30 | 2.72 | 90 | 3.79 | **2.69E-04** | 1.55E-03 | 2.39 |
| Prime R. Gbn R. | 8 | 10.24 | 2.72 | 90 | 3.77 | **2.90E-04** | 1.60E-03 | 2.58 |
| GBHCT R. GBOBC1 b. R. | 54 | -9.68 | 2.72 | 90 | 3.56 | **5.88E-04** | 1.65E-03 | 2.97 |
| GBOBC1 mb2 R. GBOBC2 mb2 R. | 76 | 8.51 | 2.72 | 90 | 3.13 | 2.34E-03 | 1.71E-03 | 2.83 |
| Prime F. GBOBC1 b. R. | 18 | -8.29 | 2.72 | 90 | 3.05 | 3.00E-03 | 0.00E+00 | 1.14 |
| Prime R. GBOBC1 b. R. | 4 | 7.80 | 2.72 | 90 | 2.87 | 5.09E-03 | 0.00E+00 | 1.91 |
| GBHCT R. Gbn R. | 58 | -7.23 | 2.72 | 90 | 2.66 | 9.15E-03 | 0.00E+00 | 1.40 |
| Prime F. L. GBHCT R. | 42 | 7.18 | 2.72 | 90 | 2.64 | 9.72E-03 | 0.00E+00 | 1.11 |
| GBOBC1 mb2 R. GBOBC2 b. R. | 75 | 7.05 | 2.72 | 90 | 2.59 | 1.11E-02 | 0.00E+00 | 1.65 |
| Prime F. GBOBC2 mb2 R. | 21 | 6.48 | 2.72 | 90 | 2.39 | 1.91E-02 | 0.00E+00 | 2.29 |
| GBOBC1 b. R. GBOBC1 mb2 R. | 65 | 6.26 | 2.72 | 90 | 2.30 | 2.35E-02 | 0.00E+00 | 3.39 |
| Prime F. Gbn R. | 22 | -5.84 | 2.72 | 90 | 2.15 | 3.41E-02 | 0.00E+00 | 0.82 |
| Prime F. Prime F. L. | 16 | -5.78 | 2.72 | 90 | 2.13 | 3.59E-02 | 0.00E+00 | 0.56 |
| GBHCT R. GBOBC2 mb2 R. | 57 | 5.09 | 2.72 | 90 | 1.87 | 6.42E-02 | 0.00E+00 | 1.42 |
| Prime F. GBOBC2 b. R. | 20 | 5.02 | 2.72 | 90 | 1.85 | 6.78E-02 | 0.00E+00 | 1.64 |
| GBOBC1 mb2 R. Gbn R. | 77 | -3.82 | 2.72 | 90 | 1.41 | 1.63E-01 | 0.00E+00 | 2.70 |
| Prime F. L. GBOBC1 mb2 R. | 44 | 3.76 | 2.72 | 90 | 1.38 | 1.70E-01 | 0.00E+00 | 1.48 |

| | | | | | | | | |
|---|---|---|---|---|---|---|---|---|
| GBHCT R. GBOBC2 b. R. | 56 | 3.63 | 2.72 | 90 | 1.34 | 1.85E-01 | 0.00E+00 | 2.01 |
| GBHCT F. Gbn F. | 109 | -3.45 | 2.72 | 90 | 1.27 | 2.07E-01 | 0.00E+00 | 1.38 |
| GBHCT F. GBOBC1 b. F. | 105 | -3.45 | 2.72 | 90 | 1.27 | 2.08E-01 | 0.00E+00 | 1.49 |
| GBHCT R. GBOBC1 mb2 R. | 55 | -3.42 | 2.72 | 90 | 1.26 | 2.11E-01 | 0.00E+00 | 1.22 |
| GBOBC1 mb2 F. Gbn F. | 116 | -2.69 | 2.72 | 90 | 0.99 | 3.25E-01 | 0.00E+00 | 1.30 |
| GBOBC1 b. F. GBOBC1 mb2 F. | 110 | 2.68 | 2.72 | 90 | 0.99 | 3.26E-01 | 0.00E+00 | 1.62 |
| Prime R. Prime R. L. | 1 | -2.61 | 2.72 | 90 | 0.96 | 3.39E-01 | 0.00E+00 | 0.64 |
| Prime F. L. GBOBC1 b. R. | 43 | -2.50 | 2.72 | 90 | 0.92 | 3.59E-01 | 0.00E+00 | 1.81 |
| GBOBC1 b. R. Gbn R. | 68 | 2.44 | 2.72 | 90 | 0.90 | 3.71E-01 | 0.00E+00 | 1.29 |
| Prime F. GBOBC1 mb2 R. | 19 | -2.03 | 2.72 | 90 | 0.75 | 4.58E-01 | 0.00E+00 | 0.82 |
| GBOBC2 b. R. GBOBC2 mb2 R. | 84 | 1.46 | 2.72 | 90 | 0.54 | 5.92E-01 | 0.00E+00 | 1.38 |
| Prime F. GBHCT R. | 17 | 1.39 | 2.72 | 90 | 0.51 | 6.10E-01 | 0.00E+00 | 1.44 |
| GBHCT F. GBOBC1 mb2 F. | 106 | -0.76 | 2.72 | 90 | 0.28 | 7.79E-01 | 0.00E+00 | 1.40 |
| GBOBC2 b. F. GBOBC2 mb2 F. | 117 | -0.22 | 2.72 | 90 | 0.08 | 9.35E-01 | 0.00E+00 | 1.00 |
| Prime F. L. Gbn R. | 47 | -0.06 | 2.72 | 90 | 0.02 | 9.83E-01 | 0.00E+00 | 1.56 |
| GBOBC1 b. F. Gbn F. | 113 | -0.01 | 2.72 | 90 | 0.00 | 9.98E-01 | 0.00E+00 | 1.62 |

Table B.25: Holm-Šidák results for Glide job 2. Names abbreviated for expediency. F., R., b., mb2, and d, correspond to Flexible, Rigid, bondi, mbondi2, and Cohen's d respectively. Significant differences shown in bold.

| **Compared Models** | **Index** | **Mean Diff.** | **Std.Er.** | **DF** | **\|t\|value** | **Prob>\|t\|** | **Alpha** | **d** |
|---|---|---|---|---|---|---|---|---|
| Prime R. L. GBOBC2 mb2 F. | 40 | 61.71 | 3.00 | 90 | 20.58 | **8.52E-36** | 4.27E-04 | 7.27 |
| Prime R. L. GBOBC2 b. F. | 39 | 60.56 | 3.00 | 90 | 20.20 | **3.43E-35** | 4.31E-04 | 5.85 |
| Prime R. GBOBC2 mb2 F. | 13 | 60.36 | 3.00 | 90 | 20.13 | **4.35E-35** | 4.35E-04 | 6.82 |
| Prime R. GBOBC2 b. F. | 12 | 59.21 | 3.00 | 90 | 19.75 | **1.79E-34** | 4.38E-04 | 5.47 |
| GBOBC1 b. R. GBOBC2 mb2 F. | 73 | 53.21 | 3.00 | 90 | 17.75 | **3.87E-31** | 4.42E-04 | 7.65 |
| GBOBC1 b. R. GBOBC2 b. F. | 72 | 52.06 | 3.00 | 90 | 17.36 | **1.78E-30** | 4.46E-04 | 7.54 |
| Gbn R. GBOBC2 mb2 F. | 103 | 50.31 | 3.00 | 90 | 16.78 | **1.88E-29** | 4.50E-04 | 4.96 |
| Gbn R. GBOBC2 b. F. | 102 | 49.16 | 3.00 | 90 | 16.40 | **9.06E-29** | 4.54E-04 | 4.74 |
| GBOBC1 mb2 R. GBOBC2 mb2 F. | 82 | 47.15 | 3.00 | 90 | 15.72 | **1.49E-27** | 4.58E-04 | 6.55 |
| GBOBC1 mb2 R. GBOBC2 b. F. | 81 | 46.00 | 3.00 | 90 | 15.34 | **7.56E-27** | 4.62E-04 | 6.09 |
| Prime R. L. GBOBC1 mb2 F. | 38 | 45.73 | 3.00 | 90 | 15.25 | **1.11E-26** | 4.66E-04 | 8.38 |
| Prime R. GBOBC1 mb2 F. | 11 | 44.38 | 3.00 | 90 | 14.80 | **7.63E-26** | 4.70E-04 | 6.82 |
| Prime R. L. GBOBC1 b. F. | 37 | 44.27 | 3.00 | 90 | 14.76 | **9.01E-26** | 4.75E-04 | 6.29 |
| GBHCT R. GBOBC2 mb2 F. | 63 | 43.66 | 3.00 | 90 | 14.56 | **2.16E-25** | 4.79E-04 | 7.30 |
| Prime R. GBOBC1 b. F. | 10 | 42.92 | 3.00 | 90 | 14.32 | **6.36E-25** | 4.84E-04 | 6.00 |
| Prime F. L. GBOBC2 mb2 F. | 52 | 42.88 | 3.00 | 90 | 14.30 | **6.81E-25** | 4.88E-04 | 3.86 |
| Prime R. L. GBHCT F. | 36 | 42.68 | 3.00 | 90 | 14.23 | **9.16E-25** | 4.93E-04 | 9.05 |
| GBHCT R. GBOBC2 b. F. | 62 | 42.51 | 3.00 | 90 | 14.18 | **1.16E-24** | 4.98E-04 | 6.24 |
| Prime F. GBOBC2 mb2 F. | 27 | 42.06 | 3.00 | 90 | 14.03 | **2.26E-24** | 5.03E-04 | 3.74 |
| Prime R. L. Gbn F. | 41 | 41.89 | 3.00 | 90 | 13.97 | **2.93E-24** | 5.08E-04 | 11.02 |
| Prime F. L. GBOBC2 b. F. | 51 | 41.73 | 3.00 | 90 | 13.92 | **3.70E-24** | 5.13E-04 | 3.16 |

| | | | | | | | | |
|---|---|---|---|---|---|---|---|---|
| Prime R. GBHCT F. | 9 | 41.33 | 3.00 | 90 | 13.78 | **6.66E-24** | 5.18E-04 | 11.42 |
| Prime F. GBOBC2 b. F. | 26 | 40.91 | 3.00 | 90 | 13.65 | **1.24E-23** | 5.23E-04 | 3.05 |
| Prime R. Gbn F. | 14 | 40.54 | 3.00 | 90 | 13.52 | **2.16E-23** | 5.29E-04 | 6.67 |
| GBOBC2 b. R. GBOBC2 mb2 F. | 90 | 39.30 | 3.00 | 90 | 13.11 | **1.39E-22** | 5.34E-04 | 4.29 |
| GBOBC2 b. R. GBOBC2 b. F. | 89 | 38.15 | 3.00 | 90 | 12.72 | **7.98E-22** | 5.40E-04 | 4.82 |
| GBOBC2 mb2 R. GBOBC2 mb2 F. | 97 | 37.88 | 3.00 | 90 | 12.63 | **1.21E-21** | 5.46E-04 | 5.28 |
| GBOBC1 b. R. GBOBC1 mb2 F. | 71 | 37.23 | 3.00 | 90 | 12.42 | **3.28E-21** | 5.51E-04 | 6.21 |
| GBOBC2 mb2 R. GBOBC2 b. F. | 96 | 36.73 | 3.00 | 90 | 12.25 | **7.07E-21** | 5.57E-04 | 5.33 |
| GBOBC1 b. R. GBOBC1 b. F. | 70 | 35.77 | 3.00 | 90 | 11.93 | **3.12E-20** | 5.64E-04 | 5.44 |
| Gbn R. GBOBC1 mb2 F. | 101 | 34.33 | 3.00 | 90 | 11.45 | **2.95E-19** | 5.70E-04 | 4.16 |
| GBOBC1 b. R. GBHCT F. | 69 | 34.18 | 3.00 | 90 | 11.40 | **3.75E-19** | 5.76E-04 | 4.24 |
| GBOBC1 b. R. Gbn F. | 74 | 33.39 | 3.00 | 90 | 11.14 | **1.29E-18** | 5.83E-04 | 7.23 |
| Gbn R. GBOBC1 b. F. | 100 | 32.87 | 3.00 | 90 | 10.96 | **2.92E-18** | 5.89E-04 | 3.17 |
| Gbn R. GBHCT F. | 99 | 31.28 | 3.00 | 90 | 10.43 | **3.64E-17** | 5.96E-04 | 2.78 |
| GBOBC1 mb2 R. GBOBC1 mb2 F. | 80 | 31.17 | 3.00 | 90 | 10.39 | **4.34E-17** | 6.03E-04 | 5.47 |
| Gbn R. Gbn F. | 104 | 30.49 | 3.00 | 90 | 10.17 | **1.28E-16** | 6.10E-04 | 5.03 |
| GBOBC1 mb2 R. GBOBC1 b. F. | 79 | 29.71 | 3.00 | 90 | 9.91 | **4.44E-16** | 6.18E-04 | 4.12 |
| GBOBC1 mb2 R. GBHCT F. | 78 | 28.11 | 3.00 | 90 | 9.38 | **5.66E-15** | 6.25E-04 | 3.42 |
| GBHCT R. GBOBC1 mb2 F. | 61 | 27.68 | 3.00 | 90 | 9.23 | **1.13E-14** | 6.33E-04 | 6.67 |
| GBOBC1 mb2 R. Gbn F. | 83 | 27.33 | 3.00 | 90 | 9.11 | **2.00E-14** | 6.41E-04 | 6.49 |
| Prime F. L. GBOBC1 mb2 F. | 50 | 26.90 | 3.00 | 90 | 8.97 | **3.96E-14** | 6.49E-04 | 3.21 |
| GBHCT R. GBOBC1 b. F. | 60 | 26.23 | 3.00 | 90 | 8.75 | **1.16E-13** | 6.57E-04 | 5.18 |
| Prime F. GBOBC1 mb2 F. | 25 | 26.08 | 3.00 | 90 | 8.70 | **1.45E-13** | 6.66E-04 | 2.97 |
| Prime F. L. GBOBC1 b. F. | 49 | 25.44 | 3.00 | 90 | 8.48 | **4.06E-13** | 6.75E-04 | 2.71 |
| GBHCT R. GBHCT F. | 59 | 24.63 | 3.00 | 90 | 8.22 | **1.47E-12** | 6.84E-04 | 4.22 |
| Prime F. GBOBC1 b. F. | 24 | 24.63 | 3.00 | 90 | 8.21 | **1.48E-12** | 6.93E-04 | 2.62 |
| Prime F. L. GBHCT F. | 48 | 23.85 | 3.00 | 90 | 7.95 | **5.09E-12** | 7.02E-04 | 3.72 |
| GBHCT R. Gbn F. | 64 | 23.84 | 3.00 | 90 | 7.95 | **5.12E-12** | 7.12E-04 | 9.63 |
| Prime R. L. GBOBC2 mb2 R. | 34 | 23.83 | 3.00 | 90 | 7.95 | **5.25E-12** | 7.22E-04 | 2.92 |
| GBOBC2 b. R. GBOBC1 mb2 F. | 88 | 23.32 | 3.00 | 90 | 7.78 | **1.16E-11** | 7.32E-04 | 2.48 |
| Prime F. L. Gbn F. | 53 | 23.06 | 3.00 | 90 | 7.69 | **1.77E-11** | 7.43E-04 | 3.03 |
| Prime F. GBHCT F. | 23 | 23.03 | 3.00 | 90 | 7.68 | **1.84E-11** | 7.54E-04 | 3.89 |
| Prime R. GBOBC2 mb2 R. | 7 | 22.48 | 3.00 | 90 | 7.50 | **4.35E-11** | 7.65E-04 | 2.24 |
| Prime R. L. GBOBC2 b. R. | 33 | 22.40 | 3.00 | 90 | 7.47 | **4.93E-11** | 7.77E-04 | 1.93 |
| Prime F. Gbn F. | 28 | 22.24 | 3.00 | 90 | 7.42 | **6.34E-11** | 7.89E-04 | 2.64 |
| GBOBC2 mb2 R. GBOBC1 mb2 F. | 95 | 21.90 | 3.00 | 90 | 7.30 | **1.08E-10** | 8.01E-04 | 3.43 |
| GBOBC2 b. R. GBOBC1 b. F. | 87 | 21.86 | 3.00 | 90 | 7.29 | **1.14E-10** | 8.14E-04 | 2.16 |
| Prime R. GBOBC2 b. R. | 6 | 21.06 | 3.00 | 90 | 7.02 | **3.97E-10** | 8.27E-04 | 1.57 |
| GBOBC2 mb2 R. GBOBC1 b. F. | 94 | 20.44 | 3.00 | 90 | 6.82 | **1.03E-09** | 8.41E-04 | 2.66 |
| GBOBC2 b. R. GBHCT F. | 86 | 20.27 | 3.00 | 90 | 6.76 | **1.33E-09** | 8.55E-04 | 1.60 |
| GBOBC2 mb2 F. Gbn F. | 119 | -19.82 | 3.00 | 90 | 6.61 | **2.65E-09** | 8.69E-04 | 2.94 |
| Prime F. Prime R. L. | 15 | -19.64 | 3.00 | 90 | 6.55 | **3.46E-09** | 8.84E-04 | 3.85 |
| GBOBC2 b. R. Gbn F. | 91 | 19.48 | 3.00 | 90 | 6.50 | **4.42E-09** | 8.99E-04 | 2.19 |

| | | | | | | | | |
|---|---|---|---|---|---|---|---|---|
| GBHCT F. GBOBC2 mb2 F. | 108 | 19.03 | 3.00 | 90 | 6.35 | **8.70E-09** | 9.16E-04 | 2.84 |
| GBOBC2 mb2 R. GBHCT F. | 93 | 18.85 | 3.00 | 90 | 6.29 | **1.14E-08** | 9.32E-04 | 2.00 |
| Prime R. L. Prime F. L. | 29 | 18.83 | 3.00 | 90 | 6.28 | **1.18E-08** | 9.49E-04 | 4.35 |
| GBOBC2 b. F. Gbn F. | 118 | -18.67 | 3.00 | 90 | 6.23 | **1.49E-08** | 9.67E-04 | 2.25 |
| Prime R. Prime F. | 0 | 18.30 | 3.00 | 90 | 6.10 | **2.58E-08** | 9.86E-04 | 4.20 |
| GBOBC2 mb2 R. Gbn F. | 98 | 18.06 | 3.00 | 90 | 6.02 | **3.67E-08** | 1.01E-03 | 3.22 |
| Prime R. L. GBHCT R. | 30 | 18.04 | 3.00 | 90 | 6.02 | **3.76E-08** | 1.03E-03 | 3.74 |
| GBHCT F. GBOBC2 b. F. | 107 | 17.88 | 3.00 | 90 | 5.96 | **4.76E-08** | 1.05E-03 | 2.10 |
| Prime R. Prime F. L. | 2 | 17.48 | 3.00 | 90 | 5.83 | **8.49E-08** | 1.07E-03 | 3.36 |
| GBOBC1 b. F. GBOBC2 mb2 F. | 112 | 17.44 | 3.00 | 90 | 5.82 | **9.09E-08** | 1.09E-03 | 5.35 |
| Prime R. GBHCT R. | 3 | 16.70 | 3.00 | 90 | 5.57 | **2.63E-07** | 1.11E-03 | 2.41 |
| GBOBC1 b. F. GBOBC2 b. F. | 111 | 16.29 | 3.00 | 90 | 5.43 | **4.69E-07** | 1.14E-03 | 3.46 |
| GBOBC1 mb2 F. GBOBC2 mb2 F. | 115 | 15.98 | 3.00 | 90 | 5.33 | **7.24E-07** | 1.17E-03 | 4.25 |
| GBOBC1 b. R. GBOBC2 mb2 R. | 67 | 15.33 | 3.00 | 90 | 5.11 | **1.78E-06** | 1.19E-03 | 4.99 |
| GBOBC1 mb2 F. GBOBC2 b. F. | 114 | 14.83 | 3.00 | 90 | 4.95 | **3.50E-06** | 1.22E-03 | 2.42 |
| Prime R. L. GBOBC1 mb2 R. | 32 | 14.56 | 3.00 | 90 | 4.86 | **5.02E-06** | 1.25E-03 | 2.34 |
| GBOBC1 b. R. GBOBC2 b. R. | 66 | 13.91 | 3.00 | 90 | 4.64 | **1.19E-05** | 1.28E-03 | 2.71 |
| Prime R. GBOBC1 mb2 R. | 5 | 13.22 | 3.00 | 90 | 4.41 | **2.88E-05** | 1.31E-03 | 1.92 |
| GBOBC2 mb2 R. Gbn R. | 92 | -12.43 | 3.00 | 90 | 4.15 | **7.66E-05** | 1.35E-03 | 2.91 |
| Prime R. L. Gbn R. | 35 | 11.40 | 3.00 | 90 | 3.80 | **2.62E-04** | 1.39E-03 | 1.57 |
| Prime F. GBOBC1 b. R. | 18 | -11.14 | 3.00 | 90 | 3.72 | **3.50E-04** | 1.42E-03 | 1.36 |
| GBOBC2 b. R. Gbn R. | 85 | -11.01 | 3.00 | 90 | 3.67 | **4.10E-04** | 1.46E-03 | 2.28 |
| Prime F. L. GBOBC1 b. R. | 43 | -10.33 | 3.00 | 90 | 3.45 | **8.69E-04** | 1.51E-03 | 1.44 |
| Prime R. Gbn R. | 8 | 10.05 | 3.00 | 90 | 3.35 | **1.17E-03** | 1.55E-03 | 2.12 |
| GBHCT R. GBOBC1 b. R. | 54 | -9.54 | 3.00 | 90 | 3.18 | 2.00E-03 | 1.60E-03 | 3.83 |
| GBOBC1 mb2 R. GBOBC2 mb2 R. | 76 | 9.27 | 3.00 | 90 | 3.09 | 2.66E-03 | 0.00E+00 | 3.24 |
| Prime R. L. GBOBC1 b. R. | 31 | 8.50 | 3.00 | 90 | 2.83 | 5.67E-03 | 0.00E+00 | 1.50 |
| Prime F. Gbn R. | 22 | -8.25 | 3.00 | 90 | 2.75 | 7.20E-03 | 0.00E+00 | 1.83 |
| GBOBC1 mb2 R. GBOBC2 b. R. | 75 | 7.84 | 3.00 | 90 | 2.62 | 1.04E-02 | 0.00E+00 | 1.74 |
| Prime F. L. Gbn R. | 47 | -7.43 | 3.00 | 90 | 2.48 | 1.51E-02 | 0.00E+00 | 2.28 |
| Prime R. GBOBC1 b. R. | 4 | 7.15 | 3.00 | 90 | 2.39 | 1.91E-02 | 0.00E+00 | 2.11 |
| GBHCT R. Gbn R. | 58 | -6.65 | 3.00 | 90 | 2.22 | 2.92E-02 | 0.00E+00 | 1.37 |
| GBOBC1 b. R. GBOBC1 mb2 R. | 65 | 6.06 | 3.00 | 90 | 2.02 | 4.62E-02 | 0.00E+00 | 3.23 |
| GBHCT R. GBOBC2 mb2 R. | 57 | 5.78 | 3.00 | 90 | 1.93 | 5.69E-02 | 0.00E+00 | 1.37 |
| Prime F. GBOBC1 mb2 R. | 19 | -5.08 | 3.00 | 90 | 1.70 | 9.35E-02 | 0.00E+00 | 1.67 |
| Prime F. L. GBOBC2 mb2 R. | 46 | 5.00 | 3.00 | 90 | 1.67 | 9.90E-02 | 0.00E+00 | 1.22 |
| GBHCT R. GBOBC2 b. R. | 56 | 4.36 | 3.00 | 90 | 1.45 | 1.49E-01 | 0.00E+00 | 2.06 |
| Prime F. L. GBOBC1 mb2 R. | 44 | -4.27 | 3.00 | 90 | 1.42 | 1.58E-01 | 0.00E+00 | 1.91 |
| Prime F. GBOBC2 mb2 R. | 21 | 4.18 | 3.00 | 90 | 1.40 | 1.66E-01 | 0.00E+00 | 1.41 |
| GBOBC1 mb2 F. Gbn F. | 116 | -3.84 | 3.00 | 90 | 1.28 | 2.03E-01 | 0.00E+00 | 1.60 |
| Prime F. L. GBOBC2 b. R. | 45 | 3.58 | 3.00 | 90 | 1.19 | 2.36E-01 | 0.00E+00 | 1.49 |
| GBHCT R. GBOBC1 mb2 R. | 55 | -3.48 | 3.00 | 90 | 1.16 | 2.49E-01 | 0.00E+00 | 1.32 |
| GBOBC1 mb2 R. Gbn R. | 77 | -3.16 | 3.00 | 90 | 1.05 | 2.94E-01 | 0.00E+00 | 1.38 |

| | | | | | | | | |
|---|---|---|---|---|---|---|---|---|
| GBHCT F. GBOBC1 mb2 F. | 106 | 3.05 | 3.00 | 90 | 1.02 | 3.11E-01 | 0.00E+00 | 0.98 |
| GBOBC1 b. R. Gbn R. | 68 | 2.90 | 3.00 | 90 | 0.97 | 3.36E-01 | 0.00E+00 | 1.01 |
| Prime F. GBOBC2 b. R. | 20 | 2.76 | 3.00 | 90 | 0.92 | 3.60E-01 | 0.00E+00 | 1.56 |
| GBOBC1 b. F. Gbn F. | 113 | -2.38 | 3.00 | 90 | 0.79 | 4.29E-01 | 0.00E+00 | 1.60 |
| Prime F. GBHCT R. | 17 | -1.60 | 3.00 | 90 | 0.53 | 5.95E-01 | 0.00E+00 | 1.53 |
| GBHCT F. GBOBC1 b. F. | 105 | 1.59 | 3.00 | 90 | 0.53 | 5.97E-01 | 0.00E+00 | 2.24 |
| GBOBC1 b. F. GBOBC1 mb2 F. | 110 | 1.46 | 3.00 | 90 | 0.49 | 6.28E-01 | 0.00E+00 | 1.52 |
| GBOBC2 b. R. GBOBC2 mb2 R. | 84 | 1.42 | 3.00 | 90 | 0.47 | 6.36E-01 | 0.00E+00 | 1.01 |
| Prime R. Prime R. L. | 1 | -1.34 | 3.00 | 90 | 0.45 | 6.55E-01 | 0.00E+00 | 0.38 |
| GBOBC2 b. F. GBOBC2 mb2 F. | 117 | 1.15 | 3.00 | 90 | 0.38 | 7.02E-01 | 0.00E+00 | 1.14 |
| Prime F. Prime F. L. | 16 | -0.81 | 3.00 | 90 | 0.27 | 7.87E-01 | 0.00E+00 | 0.38 |
| GBHCT F. Gbn F. | 109 | -0.79 | 3.00 | 90 | 0.26 | 7.93E-01 | 0.00E+00 | 0.97 |
| Prime F. L. GBHCT R. | 42 | -0.79 | 3.00 | 90 | 0.26 | 7.94E-01 | 0.00E+00 | 1.47 |

Table B.26: Holm-Šidák results for Glide job 3. Names abbreviated for expediency. F., R., b., mb2, and d, correspond to Flexible, Rigid, bondi, mbondi2, and Cohen's d respectively. Significant differences shown in bold.

| **Compared Models** | **Index** | **Mean Diff.** | **Std.Er.** | **DF** | **\|t\|value** | **Prob>\|t\|** | **Alpha** | **d** |
|---|---|---|---|---|---|---|---|---|
| Prime R. L. GBOBC2 b. F. | 39 | 60.22 | 2.76 | 90 | 21.84 | **9.87E-38** | 4.27E-04 | 5.91 |
| Prime R. GBOBC2 b. F. | 12 | 59.12 | 2.76 | 90 | 21.44 | **3.97E-37** | 4.31E-04 | 6.77 |
| Prime R. L. GBOBC2 mb2 F. | 40 | 58.39 | 2.76 | 90 | 21.17 | **1.02E-36** | 4.35E-04 | 6.46 |
| Prime R. GBOBC2 mb2 F. | 13 | 57.29 | 2.76 | 90 | 20.77 | **4.24E-36** | 4.38E-04 | 7.29 |
| GBOBC1 b. R. GBOBC2 b. F. | 72 | 51.40 | 2.76 | 90 | 18.64 | **1.18E-32** | 4.42E-04 | 5.66 |
| GBOBC1 b. R. GBOBC2 mb2 F. | 73 | 49.56 | 2.76 | 90 | 17.97 | **1.57E-31** | 4.46E-04 | 5.57 |
| Gbn R. GBOBC2 b. F. | 102 | 47.63 | 2.76 | 90 | 17.27 | **2.57E-30** | 4.50E-04 | 3.95 |
| Prime R. L. GBOBC1 mb2 F. | 38 | 46.01 | 2.76 | 90 | 16.68 | **2.76E-29** | 4.54E-04 | 7.42 |
| Gbn R. GBOBC2 mb2 F. | 103 | 45.79 | 2.76 | 90 | 16.60 | **3.83E-29** | 4.58E-04 | 3.75 |
| Prime R. GBOBC1 mb2 F. | 11 | 44.91 | 2.76 | 90 | 16.29 | **1.42E-28** | 4.62E-04 | 9.56 |
| Prime F. L. GBOBC2 b. F. | 51 | 44.55 | 2.76 | 90 | 16.16 | **2.45E-28** | 4.66E-04 | 3.81 |
| Prime R. L. GBHCT F. | 36 | 44.24 | 2.76 | 90 | 16.04 | **3.92E-28** | 4.70E-04 | 5.87 |
| GBOBC1 mb2 R. GBOBC2 b. F. | 81 | 43.91 | 2.76 | 90 | 15.92 | **6.45E-28** | 4.75E-04 | 4.47 |
| Prime R. L. GBOBC1 b. F. | 37 | 43.50 | 2.76 | 90 | 15.77 | **1.20E-27** | 4.79E-04 | 5.49 |
| Prime F. GBOBC2 b. F. | 26 | 43.22 | 2.76 | 90 | 15.67 | **1.84E-27** | 4.84E-04 | 4.28 |
| Prime R. L. Gbn F. | 41 | 43.18 | 2.76 | 90 | 15.66 | **1.95E-27** | 4.88E-04 | 6.32 |
| Prime R. GBHCT F. | 9 | 43.14 | 2.76 | 90 | 15.64 | **2.09E-27** | 4.93E-04 | 7.79 |
| Prime F. L. GBOBC2 mb2 F. | 52 | 42.72 | 2.76 | 90 | 15.49 | **4.00E-27** | 4.98E-04 | 4.09 |
| Prime R. GBOBC1 b. F. | 10 | 42.40 | 2.76 | 90 | 15.38 | **6.49E-27** | 5.03E-04 | 6.82 |
| Prime R. Gbn F. | 14 | 42.09 | 2.76 | 90 | 15.26 | **1.06E-26** | 5.08E-04 | 8.04 |
| GBOBC1 mb2 R. GBOBC2 mb2 F. | 82 | 42.08 | 2.76 | 90 | 15.26 | **1.08E-26** | 5.13E-04 | 4.37 |
| Prime F. GBOBC2 mb2 F. | 27 | 41.39 | 2.76 | 90 | 15.01 | **3.13E-26** | 5.18E-04 | 4.57 |
| GBHCT R. GBOBC2 b. F. | 62 | 41.20 | 2.76 | 90 | 14.94 | **4.23E-26** | 5.23E-04 | 4.28 |
| GBHCT R. GBOBC2 mb2 F. | 63 | 39.36 | 2.76 | 90 | 14.27 | **7.66E-25** | 5.29E-04 | 4.31 |

| | | | | | | | | |
|---|---|---|---|---|---|---|---|---|
| GBOBC2 b. R. GBOBC2 b. F. | 89 | 38.09 | 2.76 | 90 | 13.81 | **5.91E-24** | 5.34E-04 | 3.82 |
| GBOBC1 b. R. GBOBC1 mb2 F. | 71 | 37.19 | 2.76 | 90 | 13.49 | **2.53E-23** | 5.40E-04 | 6.26 |
| GBOBC2 b. R. GBOBC2 mb2 F. | 90 | 36.25 | 2.76 | 90 | 13.15 | **1.17E-22** | 5.46E-04 | 3.56 |
| GBOBC1 b. R. GBHCT F. | 69 | 35.42 | 2.76 | 90 | 12.84 | **4.63E-22** | 5.51E-04 | 4.44 |
| GBOBC2 mb2 R. GBOBC2 b. F. | 96 | 35.25 | 2.76 | 90 | 12.78 | **6.07E-22** | 5.57E-04 | 3.85 |
| GBOBC1 b. R. GBOBC1 b. F. | 70 | 34.68 | 2.76 | 90 | 12.58 | **1.57E-21** | 5.64E-04 | 4.06 |
| GBOBC1 b. R. Gbn F. | 74 | 34.36 | 2.76 | 90 | 12.46 | **2.67E-21** | 5.70E-04 | 4.73 |
| GBOBC2 mb2 R. GBOBC2 mb2 F. | 97 | 33.42 | 2.76 | 90 | 12.12 | **1.30E-20** | 5.76E-04 | 3.77 |
| Gbn R. GBOBC1 mb2 F. | 101 | 33.41 | 2.76 | 90 | 12.12 | **1.31E-20** | 5.83E-04 | 3.60 |
| Gbn R. GBHCT F. | 99 | 31.64 | 2.76 | 90 | 11.47 | **2.62E-19** | 5.89E-04 | 2.91 |
| Gbn R. GBOBC1 b. F. | 100 | 30.91 | 2.76 | 90 | 11.21 | **9.21E-19** | 5.96E-04 | 2.61 |
| Gbn R. Gbn F. | 104 | 30.59 | 2.76 | 90 | 11.09 | **1.59E-18** | 6.03E-04 | 3.10 |
| Prime F. L. GBOBC1 mb2 F. | 50 | 30.34 | 2.76 | 90 | 11.00 | **2.42E-18** | 6.10E-04 | 3.86 |
| GBOBC1 mb2 R. GBOBC1 mb2 F. | 80 | 29.70 | 2.76 | 90 | 10.77 | **7.28E-18** | 6.18E-04 | 4.63 |
| Prime F. GBOBC1 mb2 F. | 25 | 29.01 | 2.76 | 90 | 10.52 | **2.38E-17** | 6.25E-04 | 4.63 |
| Prime F. L. GBHCT F. | 48 | 28.57 | 2.76 | 90 | 10.36 | **5.12E-17** | 6.33E-04 | 3.68 |
| GBOBC1 mb2 R. GBHCT F. | 78 | 27.93 | 2.76 | 90 | 10.13 | **1.55E-16** | 6.41E-04 | 3.71 |
| Prime F. L. GBOBC1 b. F. | 49 | 27.83 | 2.76 | 90 | 10.09 | **1.83E-16** | 6.49E-04 | 3.22 |
| Prime F. L. Gbn F. | 53 | 27.51 | 2.76 | 90 | 9.98 | **3.18E-16** | 6.57E-04 | 3.78 |
| Prime F. GBHCT F. | 23 | 27.24 | 2.76 | 90 | 9.88 | **5.10E-16** | 6.66E-04 | 5.07 |
| GBOBC1 mb2 R. GBOBC1 b. F. | 79 | 27.19 | 2.76 | 90 | 9.86 | **5.57E-16** | 6.75E-04 | 3.16 |
| GBHCT R. GBOBC1 mb2 F. | 61 | 26.99 | 2.76 | 90 | 9.79 | **7.96E-16** | 6.84E-04 | 4.68 |
| GBOBC1 mb2 R. Gbn F. | 83 | 26.87 | 2.76 | 90 | 9.75 | **9.67E-16** | 6.93E-04 | 3.94 |
| Prime F. GBOBC1 b. F. | 24 | 26.50 | 2.76 | 90 | 9.61 | **1.84E-15** | 7.02E-04 | 3.97 |
| Prime F. Gbn F. | 28 | 26.19 | 2.76 | 90 | 9.50 | **3.19E-15** | 7.12E-04 | 4.95 |
| GBHCT R. GBHCT F. | 59 | 25.22 | 2.76 | 90 | 9.14 | **1.73E-14** | 7.22E-04 | 4.04 |
| Prime R. L. GBOBC2 mb2 R. | 34 | 24.97 | 2.76 | 90 | 9.05 | **2.66E-14** | 7.32E-04 | 3.79 |
| GBHCT R. GBOBC1 b. F. | 60 | 24.48 | 2.76 | 90 | 8.88 | **6.23E-14** | 7.43E-04 | 3.23 |
| GBHCT R. Gbn F. | 64 | 24.16 | 2.76 | 90 | 8.76 | **1.08E-13** | 7.54E-04 | 4.50 |
| GBOBC2 b. R. GBOBC1 mb2 F. | 88 | 23.88 | 2.76 | 90 | 8.66 | **1.77E-13** | 7.65E-04 | 3.00 |
| Prime R. GBOBC2 mb2 R. | 7 | 23.87 | 2.76 | 90 | 8.65 | **1.80E-13** | 7.77E-04 | 3.84 |
| Prime R. L. GBOBC2 b. R. | 33 | 22.13 | 2.76 | 90 | 8.03 | **3.60E-12** | 7.89E-04 | 2.69 |
| GBOBC2 b. R. GBHCT F. | 86 | 22.11 | 2.76 | 90 | 8.02 | **3.78E-12** | 8.01E-04 | 1.96 |
| GBOBC2 b. R. GBOBC1 b. F. | 87 | 21.37 | 2.76 | 90 | 7.75 | **1.34E-11** | 8.14E-04 | 1.94 |
| GBOBC2 b. R. Gbn F. | 91 | 21.05 | 2.76 | 90 | 7.63 | **2.31E-11** | 8.27E-04 | 1.97 |
| GBOBC2 mb2 R. GBOBC1 mb2 F. | 95 | 21.04 | 2.76 | 90 | 7.63 | **2.33E-11** | 8.41E-04 | 3.39 |
| Prime R. GBOBC2 b. R. | 6 | 21.03 | 2.76 | 90 | 7.63 | **2.37E-11** | 8.55E-04 | 2.70 |
| GBOBC2 mb2 R. GBHCT F. | 93 | 19.27 | 2.76 | 90 | 6.99 | **4.67E-10** | 8.69E-04 | 2.05 |
| Prime R. L. GBHCT R. | 30 | 19.02 | 2.76 | 90 | 6.90 | **7.08E-10** | 8.84E-04 | 4.71 |
| GBOBC2 mb2 R. GBOBC1 b. F. | 94 | 18.54 | 2.76 | 90 | 6.72 | **1.60E-09** | 8.99E-04 | 2.01 |
| GBOBC2 mb2 R. Gbn F. | 98 | 18.22 | 2.76 | 90 | 6.61 | **2.70E-09** | 9.16E-04 | 2.16 |
| Prime R. GBHCT R. | 3 | 17.92 | 2.76 | 90 | 6.50 | **4.37E-09** | 9.32E-04 | 6.28 |
| GBOBC2 b. F. Gbn F. | 118 | -17.04 | 2.76 | 90 | 6.18 | **1.85E-08** | 9.49E-04 | 2.22 |

| | | | | | | | | |
|---|---|---|---|---|---|---|---|---|
| Prime F. Prime R. L. | 15 | -17.00 | 2.76 | 90 | 6.16 | **1.97E-08** | 9.67E-04 | 4.59 |
| GBOBC1 b. F. GBOBC2 b. F. | 111 | 16.72 | 2.76 | 90 | 6.06 | **3.08E-08** | 9.86E-04 | 3.39 |
| Prime R. L. GBOBC1 mb2 R. | 32 | 16.31 | 2.76 | 90 | 5.91 | **5.92E-08** | 1.01E-03 | 3.71 |
| GBOBC1 b. R. GBOBC2 mb2 R. | 67 | 16.15 | 2.76 | 90 | 5.85 | **7.68E-08** | 1.03E-03 | 5.27 |
| GBHCT F. GBOBC2 b. F. | 107 | 15.98 | 2.76 | 90 | 5.80 | **9.93E-08** | 1.05E-03 | 2.18 |
| Prime R. Prime F. | 0 | 15.90 | 2.76 | 90 | 5.76 | **1.13E-07** | 1.07E-03 | 6.42 |
| Prime R. L. Prime F. L. | 29 | 15.67 | 2.76 | 90 | 5.68 | **1.62E-07** | 1.09E-03 | 5.69 |
| Prime R. GBOBC1 mb2 R. | 5 | 15.21 | 2.76 | 90 | 5.52 | **3.30E-07** | 1.11E-03 | 3.96 |
| GBOBC2 mb2 F. Gbn F. | 119 | -15.20 | 2.76 | 90 | 5.51 | **3.35E-07** | 1.14E-03 | 2.20 |
| GBOBC1 b. F. GBOBC2 mb2 F. | 112 | 14.88 | 2.76 | 90 | 5.40 | **5.44E-07** | 1.17E-03 | 3.95 |
| Prime R. Prime F. L. | 2 | 14.57 | 2.76 | 90 | 5.28 | **8.76E-07** | 1.19E-03 | 3.42 |
| GBOBC1 mb2 F. GBOBC2 b. F. | 114 | 14.21 | 2.76 | 90 | 5.15 | **1.50E-06** | 1.22E-03 | 2.93 |
| GBHCT F. GBOBC2 mb2 F. | 108 | 14.15 | 2.76 | 90 | 5.13 | **1.66E-06** | 1.25E-03 | 2.11 |
| GBOBC1 b. R. GBOBC2 b. R. | 66 | 13.31 | 2.76 | 90 | 4.83 | **5.63E-06** | 1.28E-03 | 3.11 |
| Prime R. L. Gbn R. | 35 | 12.60 | 2.76 | 90 | 4.57 | **1.56E-05** | 1.31E-03 | 1.87 |
| GBOBC1 mb2 F. GBOBC2 mb2 F. | 115 | 12.38 | 2.76 | 90 | 4.49 | **2.12E-05** | 1.35E-03 | 3.58 |
| GBOBC2 mb2 R. Gbn R. | 92 | -12.37 | 2.76 | 90 | 4.49 | **2.14E-05** | 1.39E-03 | 2.92 |
| Prime R. Gbn R. | 8 | 11.50 | 2.76 | 90 | 4.17 | **7.02E-05** | 1.42E-03 | 1.77 |
| GBHCT R. GBOBC1 b. R. | 54 | -10.20 | 2.76 | 90 | 3.70 | **3.71E-04** | 1.46E-03 | 3.36 |
| GBOBC2 b. R. Gbn R. | 85 | -9.54 | 2.76 | 90 | 3.46 | **8.32E-04** | 1.51E-03 | 2.11 |
| Prime F. L. GBOBC2 mb2 R. | 46 | 9.30 | 2.76 | 90 | 3.37 | **1.10E-03** | 1.55E-03 | 1.29 |
| Prime R. L. GBOBC1 b. R. | 31 | 8.82 | 2.76 | 90 | 3.20 | 1.91E-03 | 1.60E-03 | 1.74 |
| GBOBC1 mb2 R. GBOBC2 mb2 R. | 76 | 8.66 | 2.76 | 90 | 3.14 | 2.29E-03 | 0.00E+00 | 2.04 |
| Prime F. GBOBC1 b. R. | 18 | -8.18 | 2.76 | 90 | 2.96 | 3.88E-03 | 0.00E+00 | 1.83 |
| Prime F. GBOBC2 mb2 R. | 21 | 7.97 | 2.76 | 90 | 2.89 | 4.83E-03 | 0.00E+00 | 1.21 |
| Prime R. GBOBC1 b. R. | 4 | 7.72 | 2.76 | 90 | 2.80 | 6.25E-03 | 0.00E+00 | 1.67 |
| GBOBC1 b. R. GBOBC1 mb2 R. | 65 | 7.49 | 2.76 | 90 | 2.72 | 7.93E-03 | 0.00E+00 | 4.26 |
| Prime F. L. GBOBC1 b. R. | 43 | -6.85 | 2.76 | 90 | 2.48 | 1.49E-02 | 0.00E+00 | 1.40 |
| Prime F. L. GBOBC2 b. R. | 45 | 6.46 | 2.76 | 90 | 2.34 | 2.13E-02 | 0.00E+00 | 1.56 |
| GBHCT R. Gbn R. | 58 | -6.43 | 2.76 | 90 | 2.33 | 2.20E-02 | 0.00E+00 | 1.40 |
| GBHCT R. GBOBC2 mb2 R. | 57 | 5.94 | 2.76 | 90 | 2.15 | 3.38E-02 | 0.00E+00 | 1.19 |
| GBOBC1 mb2 R. GBOBC2 b. R. | 75 | 5.82 | 2.76 | 90 | 2.11 | 3.75E-02 | 0.00E+00 | 1.43 |
| Prime F. GBOBC2 b. R. | 20 | 5.14 | 2.76 | 90 | 1.86 | 6.58E-02 | 0.00E+00 | 1.39 |
| Prime F. Gbn R. | 22 | -4.40 | 2.76 | 90 | 1.60 | 1.14E-01 | 0.00E+00 | 1.09 |
| GBOBC1 b. R. Gbn R. | 68 | 3.77 | 2.76 | 90 | 1.37 | 1.74E-01 | 0.00E+00 | 1.61 |
| GBOBC1 mb2 R. Gbn R. | 77 | -3.71 | 2.76 | 90 | 1.35 | 1.81E-01 | 0.00E+00 | 1.49 |
| Prime F. L. GBHCT R. | 42 | 3.35 | 2.76 | 90 | 1.22 | 2.27E-01 | 0.00E+00 | 1.17 |
| GBHCT R. GBOBC2 b. R. | 56 | 3.11 | 2.76 | 90 | 1.13 | 2.62E-01 | 0.00E+00 | 2.05 |
| Prime F. L. Gbn R. | 47 | -3.07 | 2.76 | 90 | 1.11 | 2.68E-01 | 0.00E+00 | 1.00 |
| GBOBC2 b. R. GBOBC2 mb2 R. | 84 | 2.83 | 2.76 | 90 | 1.03 | 3.07E-01 | 0.00E+00 | 1.00 |
| GBOBC1 mb2 F. Gbn F. | 116 | -2.83 | 2.76 | 90 | 1.02 | 3.08E-01 | 0.00E+00 | 1.53 |
| GBHCT R. GBOBC1 mb2 R. | 55 | -2.71 | 2.76 | 90 | 0.98 | 3.28E-01 | 0.00E+00 | 1.56 |
| GBOBC1 b. F. GBOBC1 mb2 F. | 110 | 2.51 | 2.76 | 90 | 0.91 | 3.65E-01 | 0.00E+00 | 1.87 |

| | | | | | | | | |
|---|---|---|---|---|---|---|---|---|
| Prime F. GBHCT R. | 17 | 2.03 | 2.76 | 90 | 0.73 | 4.64E-01 | 0.00E+00 | 1.16 |
| GBOBC2 b. F. GBOBC2 mb2 F. | 117 | -1.84 | 2.76 | 90 | 0.67 | 5.07E-01 | 0.00E+00 | 1.29 |
| GBHCT F. GBOBC1 mb2 F. | 106 | 1.77 | 2.76 | 90 | 0.64 | 5.22E-01 | 0.00E+00 | 1.44 |
| Prime F. Prime F. L. | 16 | -1.33 | 2.76 | 90 | 0.48 | 6.31E-01 | 0.00E+00 | 0.42 |
| Prime R. Prime R. L. | 1 | -1.10 | 2.76 | 90 | 0.40 | 6.91E-01 | 0.00E+00 | 0.38 |
| GBHCT F. Gbn F. | 109 | -1.06 | 2.76 | 90 | 0.38 | 7.03E-01 | 0.00E+00 | 1.98 |
| GBHCT F. GBOBC1 b. F. | 105 | -0.74 | 2.76 | 90 | 0.27 | 7.90E-01 | 0.00E+00 | 1.08 |
| Prime F. GBOBC1 mb2 R. | 19 | -0.69 | 2.76 | 90 | 0.25 | 8.04E-01 | 0.00E+00 | 1.03 |
| Prime F. L. GBOBC1 mb2 R. | 44 | 0.64 | 2.76 | 90 | 0.23 | 8.17E-01 | 0.00E+00 | 1.19 |
| GBOBC1 b. F. Gbn F. | 113 | -0.32 | 2.76 | 90 | 0.12 | 9.09E-01 | 0.00E+00 | 1.14 |

Table B.27: Models for which the null hypothesis was not rejected (means not significantly different) across Glide jobs. Names abbreviated for expediency. F., R., b., and mb2, correspond to Flexible, Rigid, bondi and mbondi2, respectively.

| Compared Models | Glide 1 | Glide2 | Glide 3 |
|---|---|---|---|
| Prime R. - Prime R. L. | ✓ | ✓ | ✓ |
| Prime R. - $GB^{OBC1}$ b. R. | ✓ | ✓ | ✓ |
| Prime F. - Prime F. L. | ✓ | ✓ | ✓ |
| Prime F. - $GB^{HCT}$ R. | ✓ | ✓ | ✓ |
| Prime F. - $GB^{OBC1}$ b. R. | ✓ | | ✓ |
| Prime F. - $GB^{OBC1}$ mb2 R. | ✓ | ✓ | ✓ |
| Prime F. - $GB^{OBC2}$ b. R. | ✓ | ✓ | ✓ |
| Prime F. - $GB^{OBC2}$ mb2 R. | ✓ | ✓ | ✓ |
| Prime F. - Gbn R. | ✓ | ✓ | ✓ |
| Prime R. L. - $GB^{OBC1}$ b. R. | | ✓ | ✓ |
| Prime F. L. - $GB^{HCT}$ R. | ✓ | ✓ | ✓ |
| Prime F. L. - $GB^{OBC1}$ b. R. | ✓ | | ✓ |
| Prime F. L. - $GB^{OBC1}$ mb2 R. | ✓ | ✓ | ✓ |
| Prime F. L. - $GB^{OBC2}$ b. R. | | ✓ | ✓ |
| Prime F. L. - $GB^{OBC2}$ mb2 R. | | ✓ | |
| Prime F. L. - Gbn R. | ✓ | ✓ | ✓ |
| $GB^{HCT}$ R. - $GB^{OBC1}$ b. R. | | ✓ | |
| $GB^{HCT}$ R. - $GB^{OBC1}$ mb2 R. | ✓ | ✓ | ✓ |
| $GB^{HCT}$ R. - $GB^{OBC2}$ b. R. | ✓ | ✓ | ✓ |
| $GB^{HCT}$ R. - $GB^{OBC2}$ mb2 R. | ✓ | ✓ | ✓ |
| $GB^{HCT}$ R. - Gbn R. | ✓ | ✓ | ✓ |
| $GB^{OBC1}$ b. R. - $GB^{OBC1}$ mb2 R. | ✓ | ✓ | ✓ |

| | | | |
|---|---|---|---|
| $GB^{OBC1}$ b. R. - Gbn R. | ✓ | ✓ | ✓ |
| $GB^{OBC1}$ mb2 R. - $GB^{OBC2}$ b. R. | ✓ | ✓ | ✓ |
| $GB^{OBC1}$ mb2 R. - $GB^{OBC2}$ mb2 R. | ✓ | ✓ | ✓ |
| $GB^{OBC1}$ mb2 R. - Gbn R. | ✓ | ✓ | ✓ |
| $GB^{OBC2}$ b. R. - $GB^{OBC2}$ mb2 R. | ✓ | ✓ | ✓ |
| $GB^{HCT}$ F. - $GB^{OBC1}$ b. F. | ✓ | ✓ | ✓ |
| $GB^{HCT}$ F. - $GB^{OBC1}$ mb2 F. | ✓ | ✓ | ✓ |
| $GB^{HCT}$ F. - Gbn F. | ✓ | ✓ | ✓ |
| $GB^{OBC1}$ b. F. - $GB^{OBC1}$ mb2 F. | ✓ | ✓ | ✓ |
| $GB^{OBC1}$ b. F. - Gbn F. | ✓ | ✓ | ✓ |
| $GB^{OBC1}$ mb2 F. - Gbn F. | ✓ | ✓ | ✓ |
| $GB^{OBC2}$ b. F. - $GB^{OBC2}$ mb2 F. | ✓ | ✓ | ✓ |

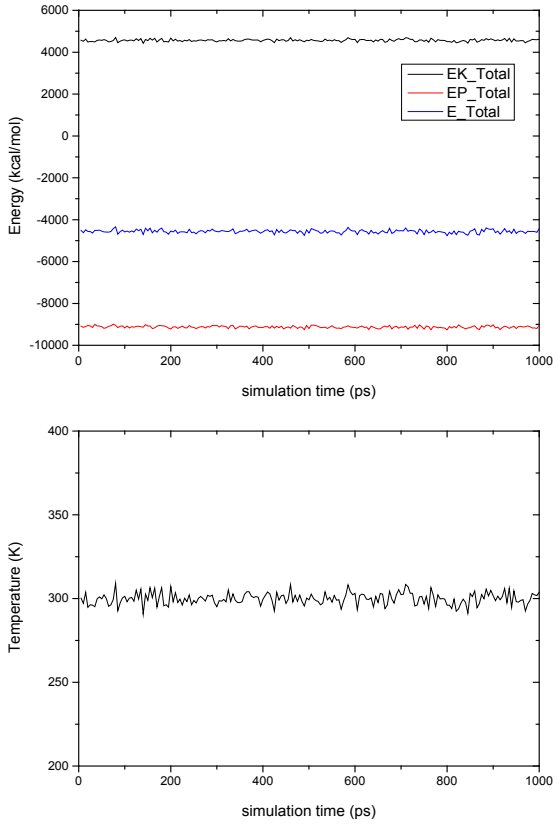


Figure B.13: Kinetic energy (black line), potential energy (red line) and total system energy (blue line) for ligand 1 Glide job 1 during 1 ns MD using model $GB^{HCT}$. Bottom plot shows the temperature during the simulation.

# Factor Xa

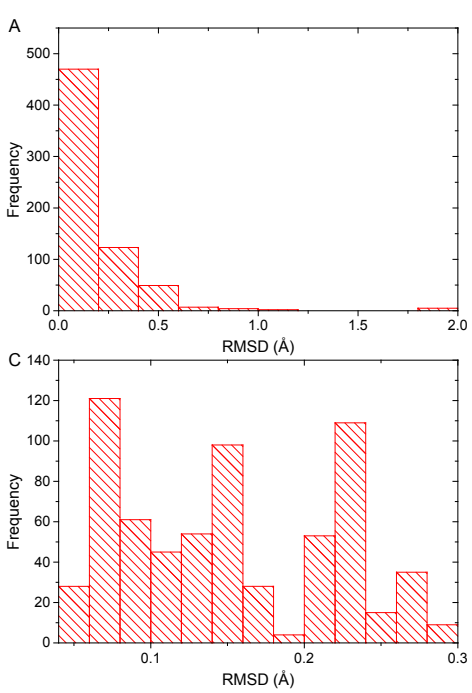


| Average RMSD ( Å) | | |
|---|---|---|
| | Glide 1 | Glide 2 |
| Ligand - R.Min. | 0.18 | 0.2 |
| Ligand - Fl.Min. | 0.27 | 0.31 |
| Protein - Fl.Min. | 0.15 | 0.15 |

Figure B.14: Ligand-ligand (A, B) and protein-protein backbone (C) RMSD distribution between AMBER GB models in all possible combinations for each Glide job 1, prior (A) and after (B, C) protein flexible minimisations. The average RMSD values for each Glide job shown in table (D). Only heavy atoms are considered and only the backbone of the protein. R.Min. and Fl. Min., correspond to the output for rigid protein and flexible protein minimisations, respectively.

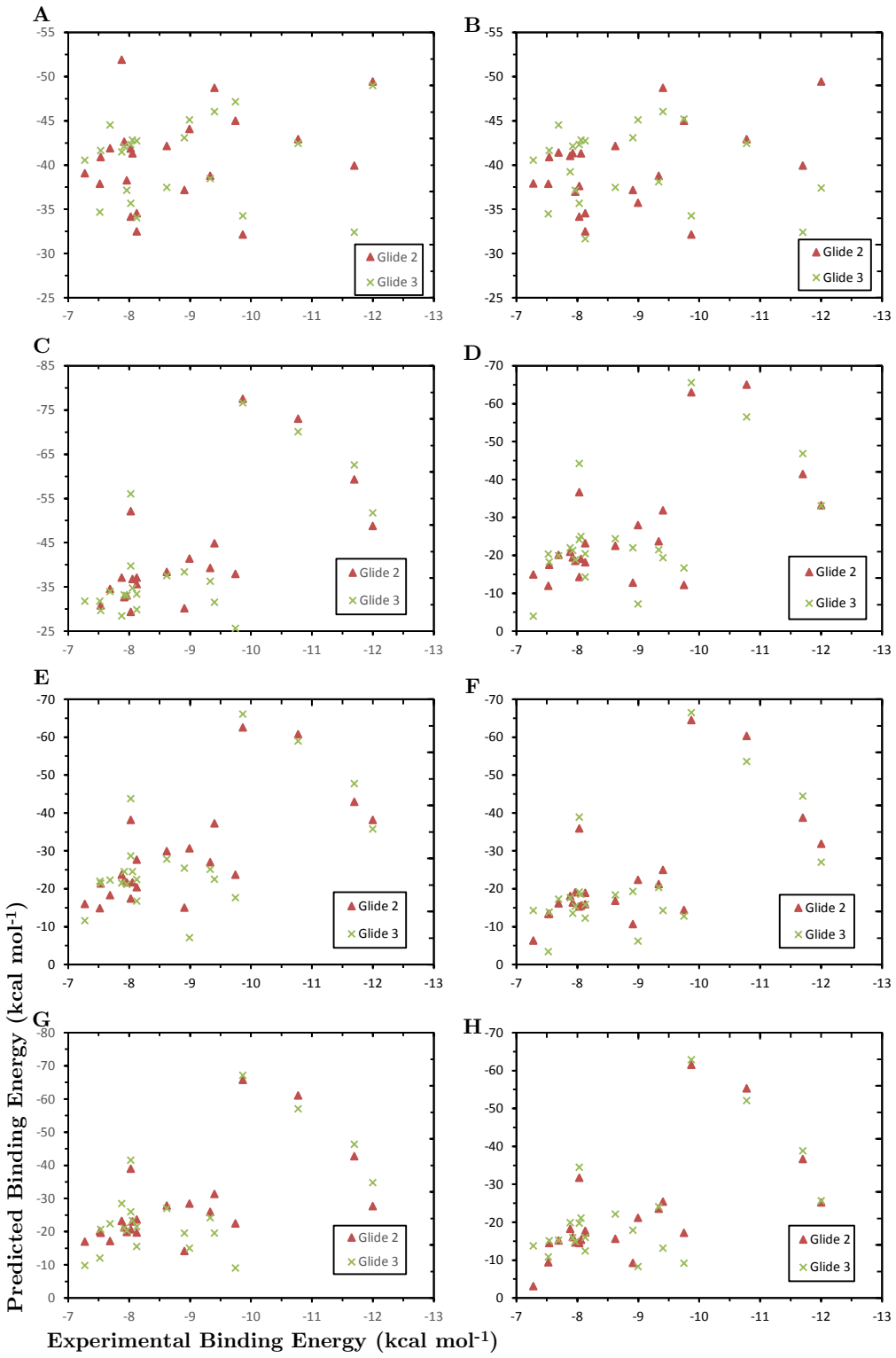


Figure B.15: Scatter plots of the predicted and experimental binding affinities for Thrombin. The plots correspond to the solvent models, A: Prime Rigid, B: Prime Rigid L., C: $GB^{HCT}$ Rigid, D: $GB^{OBC1}$ bondi Rigid, E: $GB^{OBC1}$ mbondi2 Rigid, F: $GB^{OBC2}$ bondi Rigid, G: $GB^{OBC2}$ mbondi2 Rigid, H: Gbn Rigid.

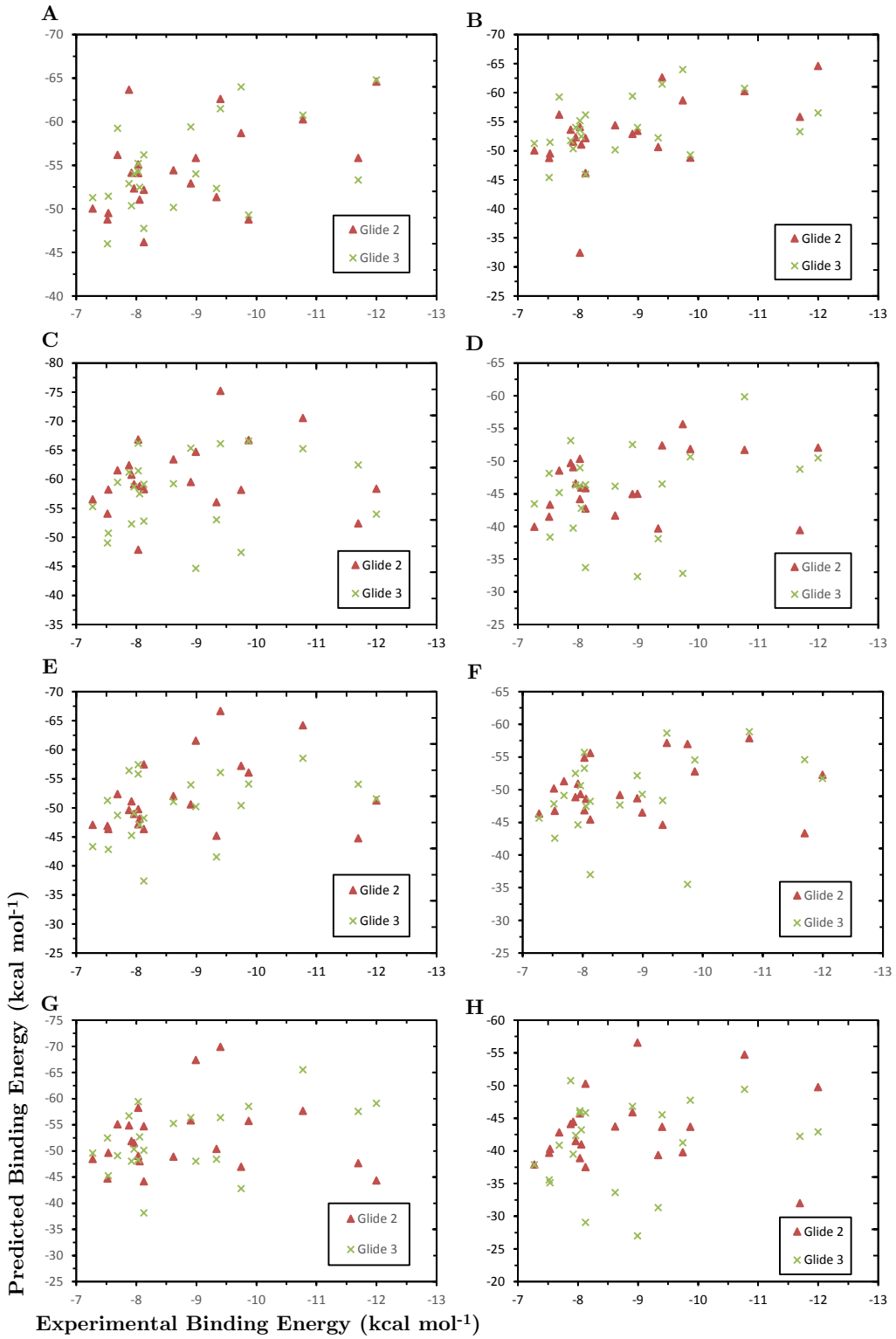


Figure B.16: Scatter plots of the predicted and experimental binding affinities for Thrombin. The plots correspond to the solvent models, A: Prime Flex, B: Prime Flex L., C: $GB^{HCT}$ Flex, D: $GB^{OBC1}$ bondi Flex, E: $GB^{OBC1}$ mbondi2 Flex, F: $GB^{OBC2}$ bondi Flex, G: $GB^{OBC2}$ mbondi2 Flex, H: Gbn Flex.

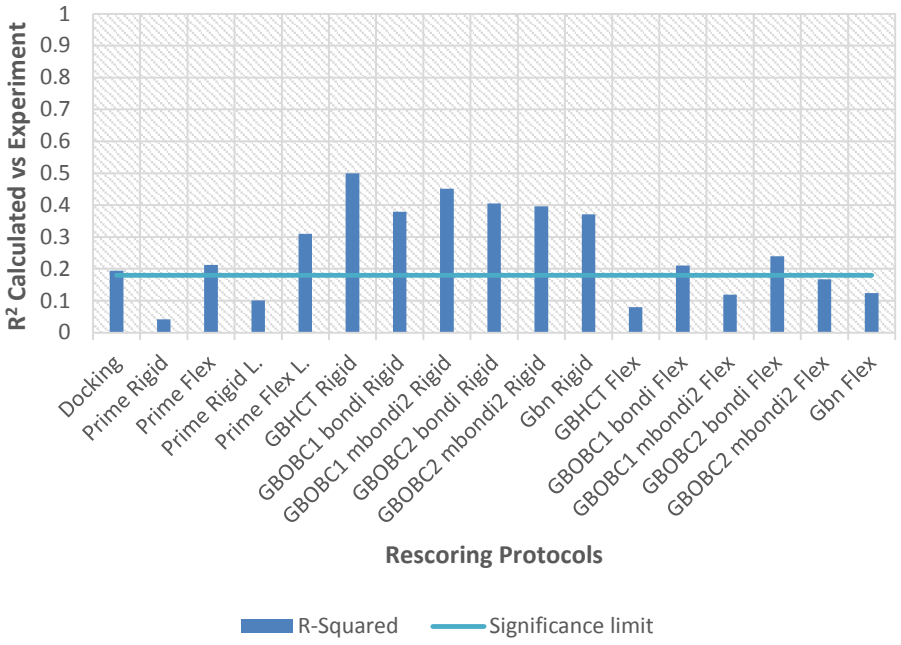


Figure B.17: Summary of $R^2$ with experiment for each protocol when the lowest poses from the two Glide jobs is considered.

| | Docking | Prime R | Prime F | Prime R L | Prime F L | $GB^{HCT}$ R | $GB^{OBC1}$ B R | $GB^{OBC1}$ MB2 R | $GB^{OBC2}$ B R | $GB^{OBC2}$ MB2 R | GBn R | $GB^{HCT}$ F | $GB^{OBC1}$ B F | $GB^{OBC1}$ MB2 F | $GB^{OBC2}$ B F | $GB^{OBC2}$ MB2 F | GBn F |
|---|---|---|---|---|---|---|---|---|---|---|---|---|---|---|---|---|---|
| R^2 | | | | | | | | | | | | | | | | | |
| All Ligands | 0.19 | 0.04 | 0.21 | 0.10 | 0.31 | 0.50 | 0.38 | 0.45 | 0.40 | 0.40 | 0.37 | 0.08 | 0.21 | 0.12 | 0.24 | 0.17 | 0.12 |
| | 0.04 | 0.36 | 0.03 | 0.15 | 0.01 | 0.00 | 0.00 | 0.00 | 0.00 | 0.00 | 0.00 | 0.20 | 0.03 | 0.12 | 0.02 | 0.06 | 0.11 |
| Kendall tau | | | | | | | | | | | | | | | | | |
| All Ligands | 0.23 | 0.18 | 0.33 | 0.27 | 0.41 | 0.64 | 0.50 | 0.58 | 0.58 | 0.47 | 0.61 | 0.26 | 0.22 | 0.27 | 0.33 | 0.34 | 0.29 |
| | 0.13 | 0.25 | 0.03 | 0.09 | 0.01 | 0.00 | 0.00 | 0.00 | 0.00 | 0.00 | 0.00 | 0.10 | 0.15 | 0.09 | 0.03 | 0.03 | 0.06 |

Figure B.18: The correlation of determination ($R^2$) and Kendall tau rank correlation coefficient ($\tau$) across of the lowest predicted energy for all rescoring tests (including the docking score).

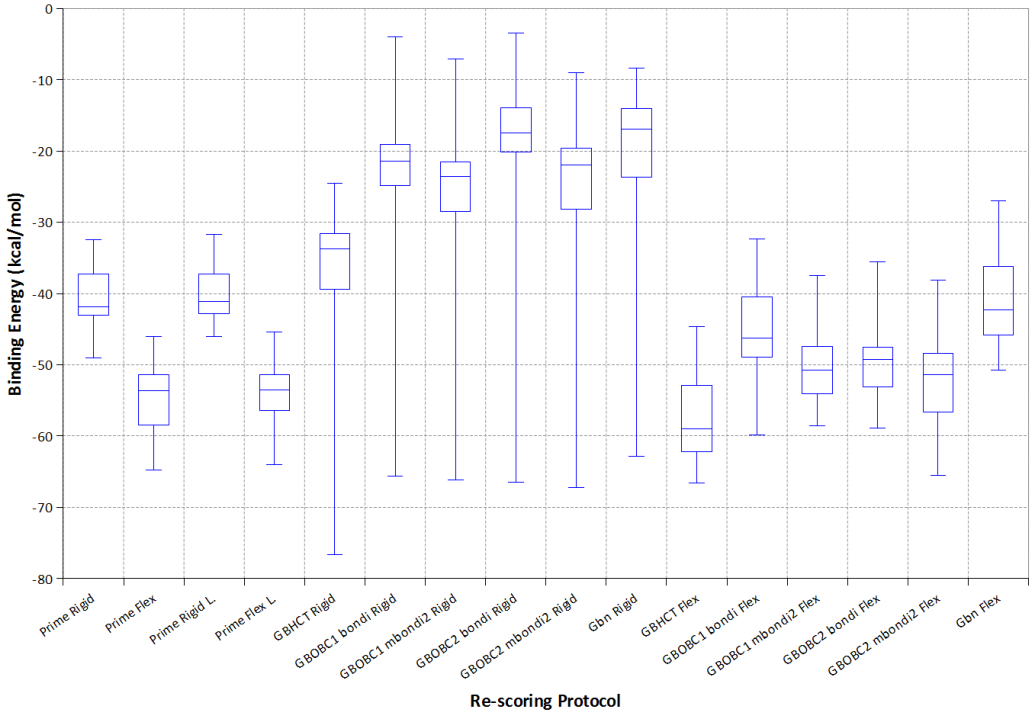


Figure B.19: Box Plot of predicted binding free energies (kcal $mol^{-1}$) of Glide 3 poses for each rescoring protocol. The whiskers represent the minimum and maximum values, the box corresponds to the range of values between the $1^{st}$ and $3^{rd}$ quartiles, and the line through the box represents the median value of the binding energies.

Table B.28: Coefficient of determination ($R^2$) matrix between rescoring models for Glide 2. P–values from a two-tailed test shown. Significant correlations highlighted in bold.

| | | Prime Rigid | Prime Flex | Prime Rigid L. | Prime Flex L. | GBHCT Rigid | GBOBC1 bondi Rigid | GBOBC1 mbondi2 Rigid | GBOBC2 bondi Rigid | GBOBC2 mbondi2 Rigid | Gbn Rigid | GBHCT Flex | GBOBC1 bondi Flex | GBOBC1 mbondi2 Flex | GBOBC2 bondi Flex | GBOBC2 mbondi2 Flex | Gbn Flex |
|---|---|---|---|---|---|---|---|---|---|---|---|---|---|---|---|---|---|
| **Prime Rigid** | $R^2$ | 1.0000 | **0.7030** | **0.6915** | **0.4744** | 0.0044 | 0.0084 | 0.0012 | 0.0189 | 0.0222 | 0.0177 | 0.0339 | 0.1337 | 0.0902 | 0.0240 | 0.0359 | 0.0465 |
| **Prime Rigid** | p | -- | **0.0000** | **0.0000** | **0.0004** | 0.7697 | 0.6849 | 0.8789 | 0.5414 | 0.5080 | 0.5547 | 0.4124 | 0.0942 | 0.1746 | 0.4915 | 0.3986 | 0.3352 |
| **Prime Flex** | $R^2$ | | 1.0000 | **0.5444** | **0.3810** | 0.0847 | 0.0576 | 0.0889 | 0.0444 | 0.0253 | 0.0376 | 0.1531 | **0.3669** | **0.2445** | **0.2103** | 0.1277 | 0.1628 |
| **Prime Flex** | p | | -- | **0.0001** | **0.0022** | 0.1890 | 0.2821 | 0.1776 | 0.3467 | 0.4798 | 0.3869 | 0.0717 | **0.0028** | **0.0193** | **0.0318** | 0.1025 | 0.0626 |
| **Prime Rigid L.** | $R^2$ | | | 1.0000 | **0.5653** | 0.0001 | 0.0004 | 0.0033 | 0.0039 | 0.0067 | 0.0042 | 0.0428 | 0.1532 | 0.0875 | 0.1096 | 0.0002 | 0.0058 |
| **Prime Rigid L.** | p | | | -- | **0.0001** | 0.9643 | 0.9275 | 0.8007 | 0.7825 | 0.7168 | 0.7745 | 0.3554 | 0.0716 | 0.1815 | 0.1323 | 0.9499 | 0.7371 |
| **Prime Flex L.** | $R^2$ | | | | 1.0000 | 0.0136 | 0.0088 | 0.0217 | 0.0032 | 0.0003 | 0.0033 | 0.0074 | 0.0791 | **0.1996** | 0.0453 | 0.0052 | 0.0362 |
| **Prime Flex L.** | p | | | | -- | 0.6049 | 0.6779 | 0.5129 | 0.8035 | 0.9353 | 0.8004 | 0.7029 | 0.2049 | **0.0371** | 0.3416 | 0.7503 | 0.3961 |
| **GBHCT Rigid** | $R^2$ | | | | | 1.0000 | **0.9224** | **0.9445** | **0.9255** | **0.8965** | **0.9466** | **0.2668** | **0.1941** | **0.1968** | 0.1350 | 0.0954 | 0.0943 |
| **GBHCT Rigid** | p | | | | | -- | **0.0000** | **0.0000** | **0.0000** | **0.0000** | **0.0000** | **0.0139** | **0.0402** | **0.0386** | 0.0926 | 0.1620 | 0.1644 |
| **GBOBC1 bondi Rigid** | $R^2$ | | | | | | 1.0000 | **0.9605** | **0.9631** | **0.9431** | **0.9393** | **0.3019** | 0.1279 | **0.2124** | 0.1343 | 0.1220 | 0.1348 |
| **GBOBC1 bondi Rigid** | p | | | | | | -- | **0.0000** | **0.0000** | **0.0000** | **0.0000** | **0.0081** | 0.1022 | **0.0309** | 0.0935 | 0.1110 | 0.0929 |
| **GBOBC1 mbondi2 Rigid** | $R^2$ | | | | | | | 1.0000 | **0.9400** | **0.9427** | **0.9334** | **0.3159** | 0.1737 | **0.2585** | **0.1795** | 0.1130 | 0.1300 |
| **GBOBC1 mbondi2 Rigid** | p | | | | | | | -- | **0.0000** | **0.0000** | **0.0000** | **0.0065** | 0.0537 | **0.0157** | **0.0495** | 0.1261 | 0.0992 |
| **GBOBC2 bondi Rigid** | $R^2$ | | | | | | | | 1.0000 | **0.9528** | **0.9753** | **0.2229** | 0.1616 | 0.1621 | 0.1438 | 0.0728 | 0.1002 |
| **GBOBC2 bondi Rigid** | p | | | | | | | | -- | **0.0000** | **0.0000** | **0.0265** | 0.0636 | 0.0632 | 0.0818 | 0.2247 | 0.1512 |
| **GBOBC2 mbondi2 Rigid** | $R^2$ | | | | | | | | | 1.0000 | **0.9529** | **0.2435** | 0.1168 | **0.1818** | 0.1341 | 0.0849 | 0.0727 |
| **GBOBC2 mbondi2 Rigid** | p | | | | | | | | | -- | **0.0000** | **0.0196** | 0.1196 | **0.0478** | 0.0937 | 0.1882 | 0.2248 |
| **Gbn Rigid** | $R^2$ | | | | | | | | | | 1.0000 | **0.2342** | 0.1662 | 0.1734 | 0.1318 | 0.0838 | 0.0750 |
| **Gbn Rigid** | p | | | | | | | | | | -- | **0.0225** | 0.0596 | 0.0539 | 0.0968 | 0.1913 | 0.2174 |
| **GBHCT Flex** | $R^2$ | | | | | | | | | | | 1.0000 | **0.3403** | **0.5944** | **0.3926** | **0.5652** | **0.3246** |
| **GBHCT Flex** | p | | | | | | | | | | | -- | **0.0044** | **0.0000** | **0.0018** | **0.0001** | **0.0056** |
| **GBOBC1 bondi Flex** | $R^2$ | | | | | | | | | | | | 1.0000 | **0.4080** | **0.6788** | 0.1286 | **0.2044** |
| **GBOBC1 bondi Flex** | p | | | | | | | | | | | | -- | **0.0014** | **0.0000** | 0.1012 | **0.0346** |
| **GBOBC1 mbondi2 Flex** | $R^2$ | | | | | | | | | | | | | 1.0000 | **0.5479** | **0.5555** | **0.4854** |
| **GBOBC1 mbondi2 Flex** | p | | | | | | | | | | | | | -- | **0.0001** | **0.0001** | **0.0003** |
| **GBOBC2 bondi Flex** | $R^2$ | | | | | | | | | | | | | | 1.0000 | 0.1438 | **0.2523** |
| **GBOBC2 bondi Flex** | p | | | | | | | | | | | | | | -- | 0.0818 | **0.0172** |
| **GBOBC2 mbondi2 Flex** | $R^2$ | | | | | | | | | | | | | | | 1.0000 | **0.3343** |
| **GBOBC2 mbondi2 Flex** | p | | | | | | | | | | | | | | | -- | **0.0048** |
| **Gbn Flex** | $R^2$ | | | | | | | | | | | | | | | | 1.0000 |
| **Gbn Flex** | p | | | | | | | | | | | | | | | | -- |

Table B.29: Kendall tau (τ) rank correlation coefficient matrix between rescoring models for Glide 2. P–values from a two-tailed test shown. Significant correlations highlighted in bold.

| | | Prime Rigid | Prime Flex | Prime Rigid L. | Prime Flex L. | GBHCT Rigid | GBOBC1 bondi Rigid | GBOBC1 mbondi2 Rigid | GBOBC2 bondi Rigid | GBOBC2 mbondi2 Rigid | Gbn Rigid | GBHCT Flex | GBOBC1 bondi Flex | GBOBC1 mbondi2 Flex | GBOBC2 bondi Flex | GBOBC2 mbondi2 Flex | Gbn Flex |
|---|---|---|---|---|---|---|---|---|---|---|---|---|---|---|---|---|---|
| **Prime Rigid** | τ | 1.0000 | **0.6191** | **0.7229** | **0.5844** | 0.1342 | 0.1082 | 0.1775 | 0.1082 | 0.1342 | 0.1342 | 0.1602 | 0.2814 | 0.2727 | 0.1515 | 0.0390 | 0.2121 |
| **Prime Rigid** | p | -- | **0.0001** | **0.0000** | **0.0001** | 0.3820 | 0.4808 | 0.2476 | 0.4808 | 0.3820 | 0.3820 | 0.2968 | 0.0668 | 0.0757 | 0.3237 | 0.7997 | 0.1671 |
| **Prime Flex** | τ | | 1.0000 | **0.4805** | **0.7576** | **0.3420** | 0.2987 | **0.3680** | 0.2987 | 0.2900 | 0.2900 | **0.3333** | **0.4026** | **0.4286** | **0.3074** | 0.2468 | **0.3333** |
| **Prime Flex** | p | | -- | **0.0018** | **0.0000** | **0.0259** | 0.0517 | **0.0165** | 0.0517 | 0.0589 | 0.0589 | **0.0299** | **0.0087** | **0.0052** | **0.0453** | 0.1080 | **0.0299** |
| **Prime Rigid L.** | τ | | | 1.0000 | **0.5844** | 0.0996 | 0.0736 | 0.1255 | 0.0043 | 0.0649 | 0.0476 | 0.1082 | 0.1775 | 0.2035 | 0.2381 | -0.0996 | 0.0909 |
| **Prime Rigid L.** | p | | | -- | **0.0001** | 0.5166 | 0.6317 | 0.4135 | 0.9775 | 0.6723 | 0.7564 | 0.4808 | 0.2476 | 0.1851 | 0.1209 | 0.5166 | 0.5538 |
| **Prime Flex L.** | τ | | | | 1.0000 | 0.2554 | 0.1775 | 0.2641 | 0.1775 | 0.1688 | 0.1515 | 0.1602 | 0.2468 | **0.3939** | 0.2381 | 0.0909 | 0.1948 |
| **Prime Flex L.** | p | | | | -- | 0.0962 | 0.2476 | 0.0854 | 0.2476 | 0.2715 | 0.3237 | 0.2968 | 0.1080 | **0.0103** | 0.1209 | 0.5538 | 0.2045 |
| **GBHCT Rigid** | τ | | | | | 1.0000 | **0.8009** | **0.8701** | **0.7662** | **0.7749** | **0.8442** | **0.3853** | 0.2987 | **0.3074** | 0.2381 | 0.2294 | 0.2468 |
| **GBHCT Rigid** | p | | | | | -- | **0.0000** | **0.0000** | **0.0000** | **0.0000** | **0.0000** | **0.0121** | 0.0517 | **0.0453** | 0.1209 | 0.1351 | 0.1080 |
| **GBOBC1 bondi Rigid** | τ | | | | | | 1.0000 | **0.8095** | **0.8442** | **0.7316** | **0.7662** | **0.4805** | 0.2208 | 0.2814 | 0.1948 | 0.3420 | 0.3420 |
| **GBOBC1 bondi Rigid** | p | | | | | | -- | **0.0000** | **0.0000** | **0.0000** | **0.0000** | **0.0018** | 0.1504 | 0.0668 | 0.2045 | 0.0259 | 0.0259 |
| **GBOBC1 mbondi2 Rigid** | τ | | | | | | | 1.0000 | **0.7749** | **0.8355** | **0.8009** | **0.3766** | **0.3247** | **0.3507** | 0.2468 | 0.2208 | **0.3074** |
| **GBOBC1 mbondi2 Rigid** | p | | | | | | | -- | **0.0000** | **0.0000** | **0.0000** | **0.0142** | **0.0344** | **0.0224** | 0.1080 | 0.1504 | **0.0453** |
| **GBOBC2 bondi Rigid** | τ | | | | | | | | 1.0000 | **0.7489** | **0.8009** | **0.3939** | 0.2900 | 0.2468 | 0.2294 | 0.2727 | **0.3074** |
| **GBOBC2 bondi Rigid** | p | | | | | | | | -- | **0.0000** | **0.0000** | **0.0103** | 0.0589 | 0.1080 | 0.1351 | 0.0757 | **0.0453** |
| **GBOBC2 mbondi2 Rigid** | τ | | | | | | | | | 1.0000 | **0.7576** | **0.3333** | 0.2294 | **0.3074** | 0.2381 | 0.1948 | 0.2468 |
| **GBOBC2 mbondi2 Rigid** | p | | | | | | | | | -- | **0.0000** | **0.0299** | 0.1351 | **0.0453** | 0.1209 | 0.2045 | 0.1080 |
| **Gbn Rigid** | τ | | | | | | | | | | 1.0000 | **0.3333** | **0.3160** | 0.2554 | 0.2208 | 0.2121 | 0.2468 |
| **Gbn Rigid** | p | | | | | | | | | | -- | **0.0299** | **0.0396** | 0.0962 | 0.1504 | 0.1671 | 0.1080 |
| **GBHCT Flex** | τ | | | | | | | | | | | 1.0000 | **0.4978** | **0.5584** | **0.4199** | **0.5671** | **0.5152** |
| **GBHCT Flex** | p | | | | | | | | | | | -- | **0.0012** | **0.0003** | **0.0062** | **0.0002** | **0.0008** |
| **GBOBC1 bondi Flex** | τ | | | | | | | | | | | | 1.0000 | **0.5758** | **0.6450** | **0.3247** | **0.3939** |
| **GBOBC1 bondi Flex** | p | | | | | | | | | | | | -- | **0.0002** | **0.0000** | **0.0344** | **0.0103** |
| **GBOBC1 mbondi2 Flex** | τ | | | | | | | | | | | | | 1.0000 | **0.6710** | **0.4546** | **0.5758** |
| **GBOBC1 mbondi2 Flex** | p | | | | | | | | | | | | | -- | 0.0000 | 0.0031 | 0.0002 |
| **GBOBC2 bondi Flex** | τ | | | | | | | | | | | | | | 1.0000 | 0.2814 | **0.4372** |
| **GBOBC2 bondi Flex** | p | | | | | | | | | | | | | | -- | 0.0668 | **0.0044** |
| **GBOBC2 mbondi2 Flex** | τ | | | | | | | | | | | | | | | 1.0000 | **0.4978** |
| **GBOBC2 mbondi2 Flex** | p | | | | | | | | | | | | | | | -- | **0.0012** |
| **Gbn Flex** | τ | | | | | | | | | | | | | | | | 1.0000 |
| **Gbn Flex** | p | | | | | | | | | | | | | | | | -- |

Table B.30: Coefficient of determination ($R^2$) matrix between rescoring models for Glide 3. P–values from a two-tailed test shown. Significant correlations highlighted in bold.

| | | Prime Rigid | Prime Flex | Prime Rigid L. | Prime Flex L. | GBHCT Rigid | GBOBC1 bondi Rigid | GBOBC1 mbondi2 Rigid | GBOBC2 bondi Rigid | GBOBC2 mbondi2 Rigid | Gbn Rigid | GBHCT Flex | GBOBC1 bondi Flex | GBOBC1 mbondi2 Flex | GBOBC2 bondi Flex | GBOBC2 mbondi2 Flex | Gbn Flex |
|---|---|---|---|---|---|---|---|---|---|---|---|---|---|---|---|---|---|
| **Prime Rigid** | $R^2$ | 1.0000 | **0.5625** | **0.7082** | **0.4604** | 0.1206 | 0.1189 | 0.1175 | 0.1078 | 0.1025 | 0.1367 | 0.0231 | 0.0054 | 0.0162 | 0.0015 | 0.0077 | 0.0279 |
| **Prime Rigid** | p | -- | **0.0001** | **0.0000** | **0.0005** | 0.1133 | 0.1161 | 0.1183 | 0.1357 | 0.1463 | 0.0904 | 0.4998 | 0.7444 | 0.5724 | 0.8620 | 0.6978 | 0.4571 |
| **Prime Flex** | $R^2$ | | 1.0000 | **0.3045** | **0.8778** | 0.0086 | 0.0068 | 0.0070 | 0.0104 | 0.0025 | 0.0000 | 0.0348 | 0.0423 | 0.1719 | 0.0580 | 0.0727 | **0.1897** |
| **Prime Flex** | p | | -- | **0.0078** | **0.0000** | 0.6822 | 0.7159 | 0.7104 | 0.6510 | 0.8241 | 0.9992 | 0.4061 | 0.3582 | 0.0551 | 0.2802 | 0.2249 | **0.0427** |
| **Prime Rigid L.** | $R^2$ | | | 1.0000 | **0.4529** | 0.1747 | 0.1511 | 0.1490 | 0.1243 | 0.1360 | 0.1483 | 0.0020 | 0.0154 | 0.0204 | 0.0000 | 0.0008 | 0.0244 |
| **Prime Rigid L.** | p | | | -- | **0.0006** | 0.0529 | 0.0737 | 0.0760 | 0.1075 | 0.0913 | 0.0768 | 0.8422 | 0.5827 | 0.5263 | 0.9971 | 0.8990 | 0.4874 |
| **Prime Flex L.** | $R^2$ | | | | 1.0000 | 0.0028 | 0.0045 | 0.0044 | 0.0109 | 0.0006 | 0.0000 | 0.0633 | 0.0274 | **0.1958** | 0.0640 | 0.0494 | **0.2075** |
| **Prime Flex L.** | p | | | | -- | 0.8135 | 0.7672 | 0.7700 | 0.6435 | 0.9107 | 0.9916 | 0.2585 | 0.4613 | **0.0392** | 0.2561 | 0.3203 | **0.0331** |
| **GBHCT Rigid** | $R^2$ | | | | | 1.0000 | **0.9203** | **0.9509** | **0.9369** | **0.9069** | **0.9284** | **0.3318** | **0.3765** | **0.2333** | **0.3647** | **0.3870** | **0.2220** |
| **GBHCT Rigid** | p | | | | | -- | **0.0000** | **0.0000** | **0.0000** | **0.0000** | **0.0000** | **0.0050** | **0.0024** | **0.0228** | **0.0029** | **0.0020** | **0.0269** |
| **GBOBC1 bondi Rigid** | $R^2$ | | | | | | 1.0000 | **0.9848** | **0.9088** | **0.9345** | **0.9202** | **0.3313** | **0.3657** | **0.2930** | **0.3379** | **0.3582** | **0.2909** |
| **GBOBC1 bondi Rigid** | p | | | | | | -- | **0.0000** | **0.0000** | **0.0000** | **0.0000** | **0.0051** | **0.0029** | **0.0093** | **0.0046** | **0.0033** | **0.0096** |
| **GBOBC1 mbondi2 Rigid** | $R^2$ | | | | | | | 1.0000 | **0.9234** | **0.9297** | **0.9357** | **0.3668** | **0.3985** | **0.2721** | **0.3454** | **0.3896** | **0.2887** |
| **GBOBC1 mbondi2 Rigid** | p | | | | | | | -- | **0.0000** | **0.0000** | **0.0000** | **0.0028** | **0.0016** | **0.0128** | **0.0040** | **0.0019** | **0.0099** |
| **GBOBC2 bondi Rigid** | $R^2$ | | | | | | | | 1.0000 | **0.9357** | **0.9687** | **0.3630** | **0.3061** | **0.2107** | **0.3126** | **0.3115** | **0.2634** |
| **GBOBC2 bondi Rigid** | p | | | | | | | | -- | **0.0000** | **0.0000** | **0.0030** | **0.0076** | **0.0317** | **0.0068** | **0.0070** | **0.0146** |
| **GBOBC2 mbondi2 Rigid** | $R^2$ | | | | | | | | | 1.0000 | **0.9550** | **0.3609** | **0.3684** | **0.2616** | **0.4018** | **0.3956** | **0.2530** |
| **GBOBC2 mbondi2 Rigid** | p | | | | | | | | | -- | **0.0000** | **0.0031** | **0.0027** | **0.0150** | **0.0015** | **0.0017** | **0.0170** |
| **Gbn Rigid** | $R^2$ | | | | | | | | | | 1.0000 | **0.3333** | **0.3358** | **0.1949** | **0.3238** | **0.3565** | **0.2217** |
| **Gbn Rigid** | p | | | | | | | | | | -- | **0.0049** | **0.0047** | **0.0397** | **0.0057** | **0.0034** | **0.0270** |
| **GBHCT Flex** | $R^2$ | | | | | | | | | | | 1.0000 | **0.5937** | **0.3873** | **0.5450** | **0.4748** | **0.5768** |
| **GBHCT Flex** | p | | | | | | | | | | | -- | **0.0000** | **0.0020** | **0.0001** | **0.0004** | **0.0000** |
| **GBOBC1 bondi Flex** | $R^2$ | | | | | | | | | | | | 1.0000 | **0.5125** | **0.5995** | **0.7771** | **0.5888** |
| **GBOBC1 bondi Flex** | p | | | | | | | | | | | | -- | **0.0002** | **0.0000** | **0.0000** | **0.0000** |
| **GBOBC1 mbondi2 Flex** | $R^2$ | | | | | | | | | | | | | 1.0000 | **0.5886** | **0.6091** | **0.5157** |
| **GBOBC1 mbondi2 Flex** | p | | | | | | | | | | | | | -- | **0.0000** | **0.0000** | **0.0002** |
| **GBOBC2 bondi Flex** | $R^2$ | | | | | | | | | | | | | | 1.0000 | **0.6776** | **0.3530** |
| **GBOBC2 bondi Flex** | p | | | | | | | | | | | | | | -- | **0.0000** | **0.0036** |
| **GBOBC2 mbondi2 Flex** | $R^2$ | | | | | | | | | | | | | | | 1.0000 | **0.4125** |
| **GBOBC2 mbondi2 Flex** | p | | | | | | | | | | | | | | | -- | **0.0013** |
| **Gbn Flex** | $R^2$ | | | | | | | | | | | | | | | | 1.0000 |
| **Gbn Flex** | p | | | | | | | | | | | | | | | | -- |

Table B.31: Kendall tau (τ) rank correlation coefficient matrix between rescoring models for Glide 3. P–values from a two-tailed test shown. Significant correlations highlighted in bold.

| | | Prime Rigid | Prime Flex | Prime Rigid L. | Prime Flex L. | GBHCT Rigid | GBOBC1 bondi Rigid | GBOBC1 mbondi2 Rigid | GBOBC2 bondi Rigid | GBOBC2 mbondi2 Rigid | Gbn Rigid | GBHCT Flex | GBOBC1 bondi Flex | GBOBC1 mbondi2 Flex | GBOBC2 bondi Flex | GBOBC2 mbondi2 Flex | Gbn Flex |
|---|---|---|---|---|---|---|---|---|---|---|---|---|---|---|---|---|---|
| **Prime Rigid** | τ | 1.0000 | **0.5671** | **0.8442** | **0.5238** | -0.1515 | -0.1429 | -0.1082 | -0.1082 | -0.1948 | -0.1862 | -0.0736 | -0.0563 | 0.1082 | -0.0130 | 0.0130 | 0.0996 |
| **Prime Rigid** | p | -- | **0.0002** | **0.0000** | **0.0006** | 0.3237 | 0.3521 | 0.4808 | 0.4808 | 0.2045 | 0.2253 | 0.6317 | 0.7139 | 0.4808 | 0.9326 | 0.9326 | 0.5166 |
| **Prime Flex** | τ | | 1.0000 | **0.4286** | **0.9221** | 0.0736 | 0.0823 | 0.0996 | 0.2035 | 0.0476 | 0.0390 | 0.2381 | 0.1862 | 0.2814 | **0.3333** | 0.1862 | **0.3074** |
| **Prime Flex** | p | | -- | **0.0052** | **0.0000** | 0.6317 | 0.5921 | 0.5166 | 0.1851 | 0.7564 | 0.7997 | 0.1209 | 0.2253 | 0.0668 | **0.0299** | 0.2253 | **0.0453** |
| **Prime Rigid L.** | τ | | | 1.0000 | **0.4719** | -0.2381 | -0.2468 | -0.2121 | -0.2121 | -0.2987 | -0.2900 | -0.0217 | -0.1255 | 0.0736 | -0.0476 | -0.0736 | 0.0996 |
| **Prime Rigid L.** | p | | | -- | **0.0021** | 0.1209 | 0.1080 | 0.1671 | 0.1671 | 0.0517 | 0.0589 | 0.8879 | 0.4135 | 0.6317 | 0.7564 | 0.6317 | 0.5166 |
| **Prime Flex L.** | τ | | | | 1.0000 | 0.0476 | 0.0390 | 0.0736 | 0.1775 | -0.0130 | 0.0130 | 0.2294 | 0.1429 | 0.2554 | **0.3074** | 0.1255 | 0.2814 |
| **Prime Flex L.** | p | | | | -- | 0.7564 | 0.7997 | 0.6317 | 0.2476 | 0.9326 | 0.9326 | 0.1351 | 0.3521 | 0.0962 | **0.0453** | 0.4135 | 0.0668 |
| **GBHCT Rigid** | τ | | | | | 1.0000 | **0.7489** | **0.8182** | **0.7662** | **0.6970** | **0.7576** | **0.5238** | **0.4372** | **0.3247** | **0.4632** | **0.4546** | **0.3507** |
| **GBHCT Rigid** | p | | | | | -- | **0.0000** | **0.0000** | **0.0000** | **0.0000** | **0.0000** | **0.0006** | **0.0044** | **0.0344** | **0.0026** | **0.0031** | **0.0224** |
| **GBOBC1 bondi Rigid** | τ | | | | | | 1.0000 | **0.8442** | **0.7403** | **0.7576** | **0.8009** | **0.4805** | **0.4805** | **0.4026** | **0.4372** | **0.5152** | **0.4113** |
| **GBOBC1 bondi Rigid** | p | | | | | | -- | **0.0000** | **0.0000** | **0.0000** | **0.0000** | **0.0018** | **0.0018** | **0.0087** | **0.0044** | **0.0008** | **0.0074** |
| **GBOBC1 mbondi2 Rigid** | τ | | | | | | | 1.0000 | **0.7229** | **0.7056** | **0.7662** | **0.4978** | **0.4459** | **0.3680** | **0.4546** | **0.4978** | **0.3766** |
| **GBOBC1 mbondi2 Rigid** | p | | | | | | | -- | **0.0000** | **0.0000** | **0.0000** | **0.0012** | **0.0037** | **0.0165** | **0.0031** | **0.0012** | **0.0142** |
| **GBOBC2 bondi Rigid** | τ | | | | | | | | 1.0000 | **0.7403** | **0.8182** | **0.5671** | **0.4632** | **0.3507** | **0.5065** | **0.4978** | **0.4459** |
| **GBOBC2 bondi Rigid** | p | | | | | | | | -- | **0.0000** | **0.0000** | **0.0002** | **0.0026** | **0.0224** | **0.0010** | **0.0012** | **0.0037** |
| **GBOBC2 mbondi2 Rigid** | τ | | | | | | | | | 1.0000 | **0.8355** | **0.4805** | **0.4113** | **0.3160** | **0.4719** | **0.4459** | **0.3420** |
| **GBOBC2 mbondi2 Rigid** | p | | | | | | | | | -- | **0.0000** | **0.0018** | **0.0074** | **0.0396** | **0.0021** | **0.0037** | **0.0259** |
| **Gbn Rigid** | τ | | | | | | | | | | 1.0000 | **0.4892** | **0.4199** | 0.2900 | **0.4286** | **0.4372** | **0.3680** |
| **Gbn Rigid** | p | | | | | | | | | | -- | **0.0014** | **0.0062** | 0.0589 | **0.0052** | **0.0044** | **0.0165** |
| **GBHCT Flex** | τ | | | | | | | | | | | 1.0000 | **0.5844** | **0.5065** | **0.5931** | **0.5498** | **0.5498** |
| **GBHCT Flex** | p | | | | | | | | | | | -- | **0.0001** | **0.0010** | **0.0001** | **0.0003** | **0.0003** |
| **GBOBC1 bondi Flex** | τ | | | | | | | | | | | | 1.0000 | **0.6277** | **0.5584** | **0.7056** | **0.6537** |
| **GBOBC1 bondi Flex** | p | | | | | | | | | | | | -- | **0.0000** | **0.0003** | **0.0000** | **0.0000** |
| **GBOBC1 mbondi2 Flex** | τ | | | | | | | | | | | | | 1.0000 | **0.6883** | **0.5931** | **0.5758** |
| **GBOBC1 mbondi2 Flex** | p | | | | | | | | | | | | | -- | **0.0000** | **0.0001** | **0.0002** |
| **GBOBC2 bondi Flex** | τ | | | | | | | | | | | | | | 1.0000 | **0.5411** | **0.4546** |
| **GBOBC2 bondi Flex** | p | | | | | | | | | | | | | | -- | **0.0004** | **0.0031** |
| **GBOBC2 mbondi2 Flex** | τ | | | | | | | | | | | | | | | 1.0000 | **0.4978** |
| **GBOBC2 mbondi2 Flex** | p | | | | | | | | | | | | | | | -- | **0.0012** |
| **Gbn Flex** | τ | | | | | | | | | | | | | | | | 1.0000 |
| **Gbn Flex** | p | | | | | | | | | | | | | | | | -- |

Table B.32: Descriptive statistics for Glide job 2 rescoring protocols.

| Rescoring Protocols | Mean | Std.Er. | 95% LCL | 95% UCL |
|---|---|---|---|---|
| Prime Rigid | -40.80 | 1.11 | -43.10 | -38.50 |
| Prime Flex | -54.50 | 1.06 | -56.71 | -52.28 |
| Prime Rigid L. | -39.54 | 0.98 | -41.57 | -37.52 |
| Prime Flex L. | -52.75 | 1.37 | -55.61 | -49.90 |
| GBHCT Rigid | -40.47 | 3.09 | -46.91 | -34.04 |
| GBOBC1 bondi Rigid | -25.87 | 3.13 | -32.38 | -19.36 |
| GBOBC1 mbondi2 Rigid | -28.73 | 2.84 | -34.63 | -22.82 |
| GBOBC2 bondi Rigid | -23.22 | 3.17 | -29.82 | -16.62 |
| GBOBC2 mbondi2 Rigid | -27.87 | 2.85 | -33.80 | -21.94 |
| Gbn Rigid | -21.79 | 2.98 | -27.98 | -15.60 |
| GBHCT Flex | -60.39 | 1.28 | -63.05 | -57.72 |
| GBOBC1 bondi Flex | -46.49 | 1.00 | -48.57 | -44.40 |
| GBOBC1 mbondi2 Flex | -51.87 | 1.32 | -54.61 | -49.13 |
| GBOBC2 bondi Flex | -50.22 | 0.91 | -52.10 | -48.34 |
| GBOBC2 mbondi2 Flex | -52.53 | 1.43 | -55.50 | -49.55 |
| Gbn Flex | -43.36 | 1.21 | -45.88 | -40.84 |

Table B.33: Descriptive statistics for Glide job 3 rescoring protocols.

| Rescoring Protocols | Mean | Std.Er. | 95% LCL | 95% UCL |
|---|---|---|---|---|
| Prime Rigid | -40.70 | 0.98 | -42.73 | -38.67 |
| Prime Flex | -54.59 | 1.09 | -56.85 | -52.32 |
| Prime Rigid L. | -39.85 | 0.92 | -41.76 | -37.95 |
| Prime Flex L. | -54.01 | 1.03 | -56.14 | -51.88 |
| GBHCT Rigid | -39.60 | 3.07 | -45.99 | -33.21 |
| GBOBC1 bondi Rigid | -25.74 | 3.19 | -32.38 | -19.10 |
| GBOBC1 mbondi2 Rigid | -27.98 | 3.07 | -34.36 | -21.60 |
| GBOBC2 bondi Rigid | -21.98 | 3.29 | -28.81 | -15.14 |
| GBOBC2 mbondi2 Rigid | -26.51 | 3.15 | -33.06 | -19.97 |
| Gbn Rigid | -22.00 | 2.94 | -28.11 | -15.89 |
| GBHCT Flex | -57.65 | 1.39 | -60.54 | -54.77 |
| GBOBC1 bondi Flex | -45.05 | 1.48 | -48.13 | -41.96 |
| GBOBC1 mbondi2 Flex | -50.21 | 1.19 | -52.69 | -47.73 |
| GBOBC2 bondi Flex | -49.38 | 1.27 | -52.02 | -46.73 |
| GBOBC2 mbondi2 Flex | -52.20 | 1.34 | -55.00 | -49.41 |
| Gbn Flex | -40.92 | 1.41 | -43.85 | -38.00 |

Table B.34: Holm-Šidák results for Glide job 2. Names abbreviated for expediency. F., R., b., mb2, and d, correspond to Flexible, Rigid, bondi, mbondi2, and Cohen's d respectively. Significant differences shown in bold.

| Compared Models | Index | Mean Diff. | Std.Er. | DF | \|t\|value | Prob>\|t\| | Alpha | d |
|---|---|---|---|---|---|---|---|---|
| Gbn R. GBHCT F. | 99 | 38.60 | 2.23 | 315 | 17.29 | **1.47E-47** | 4.27E-04 | 3.15 |
| GBOBC2 b. R. GBHCT F. | 86 | 37.17 | 2.23 | 315 | 16.65 | **4.45E-45** | 4.31E-04 | 2.82 |
| GBOBC1 b. R. GBHCT F. | 69 | 34.52 | 2.23 | 315 | 15.46 | **1.63E-40** | 4.35E-04 | 2.77 |
| Prime F. Gbn R. | 22 | -32.71 | 2.23 | 315 | 14.65 | **2.04E-37** | 4.38E-04 | 3.20 |
| GBOBC2 mb2 R. GBHCT F. | 93 | 32.52 | 2.23 | 315 | 14.56 | **4.29E-37** | 4.42E-04 | 2.79 |
| GBOBC1 mb2 R. GBHCT F. | 78 | 31.66 | 2.23 | 315 | 14.18 | **1.21E-35** | 4.46E-04 | 2.85 |
| Prime F. GBOBC2 b. R. | 20 | -31.27 | 2.23 | 315 | 14.01 | **5.51E-35** | 4.50E-04 | 3.00 |
| Prime F. L. Gbn R. | 47 | -30.96 | 2.23 | 315 | 13.87 | **1.84E-34** | 4.54E-04 | 2.63 |
| Gbn R. GBOBC2 mb2 F. | 103 | 30.74 | 2.23 | 315 | 13.77 | **4.37E-34** | 4.58E-04 | 2.54 |
| Gbn R. GBOBC1 mb2 F. | 101 | 30.08 | 2.23 | 315 | 13.47 | **5.49E-33** | 4.62E-04 | 2.69 |
| Prime F. L. GBOBC2 b. R. | 45 | -29.53 | 2.23 | 315 | 13.23 | **4.62E-32** | 4.66E-04 | 2.64 |
| GBOBC2 b. R. GBOBC2 mb2 F. | 90 | 29.30 | 2.23 | 315 | 13.13 | **1.09E-31** | 4.70E-04 | 2.50 |
| GBOBC2 b. R. GBOBC1 mb2 F. | 88 | 28.65 | 2.23 | 315 | 12.83 | **1.32E-30** | 4.75E-04 | 2.50 |
| Prime F. GBOBC1 b. R. | 18 | -28.62 | 2.23 | 315 | 12.82 | **1.45E-30** | 4.79E-04 | 3.06 |
| Gbn R. GBOBC2 b. F. | 102 | 28.43 | 2.23 | 315 | 12.73 | **3.00E-30** | 4.84E-04 | 2.65 |
| GBOBC2 b. R. GBOBC2 b. F. | 89 | 27.00 | 2.23 | 315 | 12.09 | **6.56E-28** | 4.88E-04 | 2.61 |
| Prime F. L. GBOBC1 b. R. | 43 | -26.88 | 2.23 | 315 | 12.04 | **1.02E-27** | 4.93E-04 | 2.70 |
| GBOBC1 b. R. GBOBC2 mb2 F. | 73 | 26.66 | 2.23 | 315 | 11.94 | **2.34E-27** | 4.98E-04 | 2.61 |
| Prime F. GBOBC2 mb2 R. | 21 | -26.62 | 2.23 | 315 | 11.92 | **2.64E-27** | 5.03E-04 | 2.99 |
| GBOBC1 b. R. GBOBC1 mb2 F. | 71 | 26.00 | 2.23 | 315 | 11.65 | **2.63E-26** | 5.08E-04 | 2.34 |
| Prime F. GBOBC1 mb2 R. | 19 | -25.77 | 2.23 | 315 | 11.54 | **6.14E-26** | 5.13E-04 | 2.84 |
| Prime F. L. GBOBC2 mb2 R. | 46 | -24.88 | 2.23 | 315 | 11.14 | **1.56E-24** | 5.18E-04 | 2.76 |
| Gbn R. GBOBC1 b. F. | 100 | 24.70 | 2.23 | 315 | 11.06 | **3.00E-24** | 5.23E-04 | 2.60 |
| GBOBC2 mb2 R. GBOBC2 mb2 F. | 97 | 24.66 | 2.23 | 315 | 11.04 | **3.49E-24** | 5.29E-04 | 2.50 |
| GBOBC1 b. R. GBOBC2 b. F. | 72 | 24.35 | 2.23 | 315 | 10.91 | **1.04E-23** | 5.34E-04 | 2.54 |
| Prime F. L. GBOBC1 mb2 R. | 44 | -24.03 | 2.23 | 315 | 10.76 | **3.32E-23** | 5.40E-04 | 2.60 |
| GBOBC2 mb2 R. GBOBC1 mb2 F. | 95 | 24.00 | 2.23 | 315 | 10.75 | **3.63E-23** | 5.46E-04 | 2.47 |
| GBOBC1 mb2 R. GBOBC2 mb2 F. | 82 | 23.80 | 2.23 | 315 | 10.66 | **7.35E-23** | 5.51E-04 | 2.29 |
| GBOBC2 b. R. GBOBC1 b. F. | 87 | 23.26 | 2.23 | 315 | 10.42 | **4.88E-22** | 5.57E-04 | 2.67 |
| GBOBC1 mb2 R. GBOBC1 mb2 F. | 80 | 23.15 | 2.23 | 315 | 10.37 | **7.36E-22** | 5.64E-04 | 2.34 |
| GBOBC2 mb2 R. GBOBC2 b. F. | 96 | 22.35 | 2.23 | 315 | 10.01 | **1.16E-20** | 5.70E-04 | 2.60 |
| Gbn R. Gbn F. | 104 | 21.57 | 2.23 | 315 | 9.66 | **1.65E-19** | 5.76E-04 | 2.58 |
| GBOBC1 mb2 R. GBOBC2 b. F. | 81 | 21.50 | 2.23 | 315 | 9.63 | **2.12E-19** | 5.83E-04 | 2.33 |
| Prime R. L. GBHCT F. | 36 | 20.85 | 2.23 | 315 | 9.34 | **1.86E-18** | 5.89E-04 | 3.08 |
| GBOBC1 b. R. GBOBC1 b. F. | 70 | 20.62 | 2.23 | 315 | 9.23 | **3.98E-18** | 5.96E-04 | 2.61 |
| GBOBC2 b. R. Gbn F. | 91 | 20.14 | 2.23 | 315 | 9.02 | **1.90E-17** | 6.03E-04 | 2.90 |
| GBHCT R. GBHCT F. | 59 | 19.91 | 2.23 | 315 | 8.92 | **3.90E-17** | 6.10E-04 | 2.49 |
| Prime R. GBHCT F. | 9 | 19.59 | 2.23 | 315 | 8.77 | **1.12E-16** | 6.18E-04 | 2.73 |
| Prime R. Gbn R. | 8 | -19.01 | 2.23 | 315 | 8.52 | **6.88E-16** | 6.25E-04 | 2.64 |

| | | | | | | | | |
|---|---|---|---|---|---|---|---|---|
| GBHCT R. Gbn R. | 58 | -18.69 | 2.23 | 315 | 8.37 | **1.92E-15** | 6.33E-04 | 5.56 |
| GBOBC2 mb2 R. GBOBC1 b. F. | 94 | 18.62 | 2.23 | 315 | 8.34 | **2.39E-15** | 6.41E-04 | 2.77 |
| GBOBC1 mb2 R. GBOBC1 b. F. | 79 | 17.76 | 2.23 | 315 | 7.95 | **3.26E-14** | 6.49E-04 | 2.48 |
| Prime R. L. Gbn R. | 35 | -17.76 | 2.23 | 315 | 7.95 | **3.31E-14** | 6.57E-04 | 2.62 |
| Prime R. GBOBC2 b. R. | 6 | -17.58 | 2.23 | 315 | 7.87 | **5.61E-14** | 6.66E-04 | 2.59 |
| GBOBC1 b. R. Gbn F. | 74 | 17.49 | 2.23 | 315 | 7.83 | **7.37E-14** | 6.75E-04 | 3.20 |
| GBHCT R. GBOBC2 b. R. | 56 | -17.25 | 2.23 | 315 | 7.73 | **1.49E-13** | 6.84E-04 | 4.24 |
| GBHCT F. Gbn F. | 109 | -17.03 | 2.23 | 315 | 7.63 | **2.86E-13** | 6.93E-04 | 3.13 |
| Prime R. L. GBOBC2 b. R. | 33 | -16.32 | 2.23 | 315 | 7.31 | **2.22E-12** | 7.02E-04 | 2.55 |
| GBOBC2 mb2 R. Gbn F. | 98 | 15.49 | 2.23 | 315 | 6.94 | **2.28E-11** | 7.12E-04 | 2.96 |
| Prime F. Prime R. L. | 15 | -14.95 | 2.23 | 315 | 6.70 | **9.80E-11** | 7.22E-04 | 4.29 |
| Prime R. GBOBC1 b. R. | 4 | -14.93 | 2.23 | 315 | 6.69 | **1.03E-10** | 7.32E-04 | 2.48 |
| GBOBC1 mb2 R. Gbn F. | 83 | 14.63 | 2.23 | 315 | 6.55 | **2.29E-10** | 7.43E-04 | 2.69 |
| GBHCT R. GBOBC1 b. R. | 54 | -14.60 | 2.23 | 315 | 6.54 | **2.48E-10** | 7.54E-04 | 3.55 |
| Prime F. GBHCT R. | 17 | -14.02 | 2.23 | 315 | 6.28 | **1.12E-09** | 7.65E-04 | 2.44 |
| GBHCT F. GBOBC1 b. F. | 105 | -13.90 | 2.23 | 315 | 6.23 | **1.52E-09** | 7.77E-04 | 2.77 |
| Prime R. Prime F. | 0 | 13.69 | 2.23 | 315 | 6.13 | **2.58E-09** | 7.89E-04 | 4.73 |
| Prime R. L. GBOBC1 b. R. | 31 | -13.67 | 2.23 | 315 | 6.12 | **2.72E-09** | 8.01E-04 | 2.39 |
| Prime R. L. Prime F. L. | 29 | 13.21 | 2.23 | 315 | 5.92 | **8.63E-09** | 8.14E-04 | 3.61 |
| Prime R. L. GBOBC2 mb2 F. | 40 | 12.98 | 2.23 | 315 | 5.82 | **1.49E-08** | 8.27E-04 | 1.86 |
| Prime R. GBOBC2 mb2 R. | 7 | -12.93 | 2.23 | 315 | 5.79 | **1.69E-08** | 8.41E-04 | 2.61 |
| GBHCT R. GBOBC2 mb2 R. | 57 | -12.60 | 2.23 | 315 | 5.64 | **3.69E-08** | 8.55E-04 | 3.29 |
| Prime R. L. GBOBC1 mb2 F. | 38 | 12.33 | 2.23 | 315 | 5.52 | **7.04E-08** | 8.69E-04 | 1.89 |
| Prime F. L. GBHCT R. | 42 | -12.28 | 2.23 | 315 | 5.50 | **7.92E-08** | 8.84E-04 | 2.79 |
| Prime R. GBOBC1 mb2 R. | 5 | -12.08 | 2.23 | 315 | 5.41 | **1.26E-07** | 8.99E-04 | 2.30 |
| GBHCT R. GBOBC2 mb2 F. | 63 | 12.05 | 2.23 | 315 | 5.40 | **1.33E-07** | 9.16E-04 | 2.43 |
| Prime R. Prime F. L. | 2 | 11.95 | 2.23 | 315 | 5.35 | **1.68E-07** | 9.32E-04 | 2.82 |
| GBHCT R. GBOBC1 mb2 R. | 55 | -11.75 | 2.23 | 315 | 5.26 | **2.64E-07** | 9.49E-04 | 3.35 |
| Prime R. GBOBC2 mb2 F. | 13 | 11.72 | 2.23 | 315 | 5.25 | **2.79E-07** | 9.67E-04 | 1.77 |
| Prime R. L. GBOBC2 mb2 R. | 34 | -11.67 | 2.23 | 315 | 5.23 | **3.13E-07** | 9.86E-04 | 2.49 |
| GBHCT R. GBOBC1 mb2 F. | 61 | 11.40 | 2.23 | 315 | 5.10 | **5.74E-07** | 1.01E-03 | 2.29 |
| Prime F. Gbn F. | 28 | -11.14 | 2.23 | 315 | 4.99 | **1.01E-06** | 1.03E-03 | 1.96 |
| Prime R. GBOBC1 mb2 F. | 11 | 11.07 | 2.23 | 315 | 4.96 | **1.17E-06** | 1.05E-03 | 1.76 |
| Prime R. L. GBOBC1 mb2 R. | 32 | -10.82 | 2.23 | 315 | 4.85 | **1.99E-06** | 1.07E-03 | 2.22 |
| Prime R. L. GBOBC2 b. F. | 39 | 10.68 | 2.23 | 315 | 4.78 | **2.67E-06** | 1.09E-03 | 2.09 |
| GBHCT F. GBOBC2 b. F. | 107 | -10.17 | 2.23 | 315 | 4.55 | **7.54E-06** | 1.11E-03 | 2.16 |
| GBHCT R. GBOBC2 b. F. | 62 | 9.75 | 2.23 | 315 | 4.37 | **1.72E-05** | 1.14E-03 | 2.05 |
| Prime R. GBOBC2 b. F. | 12 | 9.42 | 2.23 | 315 | 4.22 | **3.22E-05** | 1.17E-03 | 1.70 |
| Prime F. L. Gbn F. | 53 | -9.39 | 2.23 | 315 | 4.21 | **3.39E-05** | 1.19E-03 | 2.05 |
| GBOBC2 mb2 F. Gbn F. | 119 | -9.17 | 2.23 | 315 | 4.11 | **5.13E-05** | 1.22E-03 | 1.99 |
| GBHCT F. GBOBC1 mb2 F. | 106 | -8.52 | 2.23 | 315 | 3.81 | **1.64E-04** | 1.25E-03 | 2.06 |
| GBOBC1 mb2 F. Gbn F. | 116 | -8.51 | 2.23 | 315 | 3.81 | **1.65E-04** | 1.28E-03 | 1.83 |
| Prime F. GBOBC1 b. F. | 24 | -8.01 | 2.23 | 315 | 3.59 | **3.87E-04** | 1.31E-03 | 2.23 |

| | | | | | | | | |
|---|---|---|---|---|---|---|---|---|
| GBHCT F. GBOBC2 mb2 F. | 108 | -7.86 | 2.23 | 315 | 3.52 | **4.93E-04** | 1.35E-03 | 2.14 |
| Prime F. L. GBHCT F. | 48 | 7.64 | 2.23 | 315 | 3.42 | **7.07E-04** | 1.39E-03 | 1.36 |
| Prime R. L. GBOBC1 b. F. | 37 | 6.94 | 2.23 | 315 | 3.11 | 2.05E-03 | 1.42E-03 | 1.41 |
| GBOBC1 mb2 R. Gbn R. | 77 | -6.94 | 2.23 | 315 | 3.11 | 2.06E-03 | 0.00E+00 | 1.92 |
| GBOBC2 b. F. Gbn F. | 118 | -6.86 | 2.23 | 315 | 3.07 | 2.30E-03 | 0.00E+00 | 2.23 |
| Prime F. L. GBOBC1 b. F. | 49 | -6.26 | 2.23 | 315 | 2.81 | 5.33E-03 | 0.00E+00 | 1.94 |
| GBOBC2 mb2 R. Gbn R. | 92 | -6.08 | 2.23 | 315 | 2.72 | 6.80E-03 | 0.00E+00 | 2.00 |
| GBOBC1 b. F. GBOBC2 mb2 F. | 112 | 6.04 | 2.23 | 315 | 2.71 | 7.19E-03 | 0.00E+00 | 1.56 |
| GBHCT R. GBOBC1 b. F. | 60 | 6.01 | 2.23 | 315 | 2.69 | 7.47E-03 | 0.00E+00 | 1.68 |
| Prime F. GBHCT F. | 23 | 5.89 | 2.23 | 315 | 2.64 | 8.71E-03 | 0.00E+00 | 1.92 |
| Prime R. GBOBC1 b. F. | 10 | 5.68 | 2.23 | 315 | 2.55 | 1.14E-02 | 0.00E+00 | 1.13 |
| GBOBC1 mb2 R. GBOBC2 b. R. | 75 | -5.50 | 2.23 | 315 | 2.46 | 1.42E-02 | 0.00E+00 | 1.61 |
| GBOBC1 b. F. GBOBC1 mb2 F. | 110 | 5.39 | 2.23 | 315 | 2.41 | 1.64E-02 | 0.00E+00 | 1.19 |
| GBOBC2 b. R. GBOBC2 mb2 R. | 84 | 4.65 | 2.23 | 315 | 2.08 | 3.82E-02 | 0.00E+00 | 1.78 |
| Prime F. GBOBC2 b. F. | 26 | -4.27 | 2.23 | 315 | 1.91 | 5.65E-02 | 0.00E+00 | 1.29 |
| GBOBC1 b. R. Gbn R. | 68 | -4.08 | 2.23 | 315 | 1.83 | 6.84E-02 | 0.00E+00 | 1.53 |
| Prime R. L. Gbn F. | 41 | 3.82 | 2.23 | 315 | 1.71 | 8.85E-02 | 0.00E+00 | 0.98 |
| GBOBC1 b. F. GBOBC2 b. F. | 111 | 3.74 | 2.23 | 315 | 1.67 | 9.53E-02 | 0.00E+00 | 1.48 |
| GBOBC1 b. F. Gbn F. | 113 | -3.13 | 2.23 | 315 | 1.40 | 1.62E-01 | 0.00E+00 | 1.42 |
| GBHCT R. Gbn F. | 64 | 2.89 | 2.23 | 315 | 1.29 | 1.97E-01 | 0.00E+00 | 1.22 |
| GBOBC1 b. R. GBOBC1 mb2 R. | 65 | 2.86 | 2.23 | 315 | 1.28 | 2.02E-01 | 0.00E+00 | 1.45 |
| GBOBC1 b. R. GBOBC2 b. R. | 66 | -2.65 | 2.23 | 315 | 1.19 | 2.36E-01 | 0.00E+00 | 1.56 |
| Prime F. GBOBC1 mb2 F. | 25 | -2.62 | 2.23 | 315 | 1.18 | 2.41E-01 | 0.00E+00 | 1.38 |
| Prime R. Gbn F. | 14 | 2.56 | 2.23 | 315 | 1.15 | 2.53E-01 | 0.00E+00 | 1.12 |
| Prime F. L. GBOBC2 b. F. | 51 | -2.53 | 2.23 | 315 | 1.13 | 2.58E-01 | 0.00E+00 | 1.09 |
| GBOBC2 b. F. GBOBC2 mb2 F. | 117 | 2.31 | 2.23 | 315 | 1.03 | 3.03E-01 | 0.00E+00 | 0.97 |
| GBOBC1 b. R. GBOBC2 mb2 R. | 67 | 2.00 | 2.23 | 315 | 0.90 | 3.71E-01 | 0.00E+00 | 1.23 |
| Prime F. GBOBC2 mb2 F. | 27 | -1.97 | 2.23 | 315 | 0.88 | 3.79E-01 | 0.00E+00 | 1.07 |
| Prime F. Prime F. L. | 16 | -1.74 | 2.23 | 315 | 0.78 | 4.35E-01 | 0.00E+00 | 0.34 |
| GBOBC1 mb2 F. GBOBC2 b. F. | 114 | -1.65 | 2.23 | 315 | 0.74 | 4.60E-01 | 0.00E+00 | 0.72 |
| GBOBC2 b. R. Gbn R. | 85 | -1.43 | 2.23 | 315 | 0.64 | 5.21E-01 | 0.00E+00 | 1.27 |
| Prime R. Prime R. L. | 1 | -1.26 | 2.23 | 315 | 0.56 | 5.73E-01 | 0.00E+00 | 0.44 |
| Prime R. L. GBHCT R. | 30 | 0.93 | 2.23 | 315 | 0.42 | 6.77E-01 | 0.00E+00 | 0.96 |
| Prime F. L. GBOBC1 mb2 F. | 50 | -0.88 | 2.23 | 315 | 0.39 | 6.94E-01 | 0.00E+00 | 1.20 |
| GBOBC1 mb2 R. GBOBC2 mb2 R. | 76 | -0.85 | 2.23 | 315 | 0.38 | 7.02E-01 | 0.00E+00 | 0.94 |
| GBOBC1 mb2 F. GBOBC2 mb2 F. | 115 | 0.66 | 2.23 | 315 | 0.29 | 7.69E-01 | 0.00E+00 | 1.43 |
| Prime R. GBHCT R. | 3 | -0.33 | 2.23 | 315 | 0.15 | 8.83E-01 | 0.00E+00 | 1.03 |
| Prime F. L. GBOBC2 mb2 F. | 52 | -0.22 | 2.23 | 315 | 0.10 | 9.20E-01 | 0.00E+00 | 0.86 |

Table B.35: Holm-Šidák results for Glide job 3. Names abbreviated for expediency. F., R., b., mb2, and d, correspond to Flexible, Rigid, bondi, mbondi2, and Cohen's d respectively. Significant differences shown in bold.

| Compared Models | Index | Mean Diff. | Std.Er. | DF | \|t\|value | Prob>\|t\| | Alpha | d |
|---|---|---|---|---|---|---|---|---|
| GBOBC2 b. R. GBHCT F. | 86 | 35.68 | 2.25 | 315 | 15.84 | **5.77E-42** | 4.27E-04 | 2.83 |
| Gbn R. GBHCT F. | 99 | 35.65 | 2.25 | 315 | 15.83 | **6.30E-42** | 4.31E-04 | 3.14 |
| Prime F. GBOBC2 b. R. | 20 | -32.61 | 2.25 | 315 | 14.48 | **9.15E-37** | 4.35E-04 | 2.90 |
| Prime F. Gbn R. | 22 | -32.59 | 2.25 | 315 | 14.47 | **9.98E-37** | 4.38E-04 | 2.96 |
| Prime F. L. GBOBC2 b. R. | 45 | -32.04 | 2.25 | 315 | 14.22 | **8.41E-36** | 4.42E-04 | 2.86 |
| Prime F. L. Gbn R. | 47 | -32.02 | 2.25 | 315 | 14.21 | **9.17E-36** | 4.46E-04 | 2.93 |
| GBOBC1 b. R. GBHCT F. | 69 | 31.91 | 2.25 | 315 | 14.17 | **1.36E-35** | 4.50E-04 | 2.57 |
| GBOBC2 mb2 R. GBHCT F. | 93 | 31.14 | 2.25 | 315 | 13.82 | **2.66E-34** | 4.54E-04 | 2.63 |
| GBOBC2 b. R. GBOBC2 mb2 F. | 90 | 30.23 | 2.25 | 315 | 13.42 | **8.72E-33** | 4.58E-04 | 2.79 |
| Gbn R. GBOBC2 mb2 F. | 103 | 30.21 | 2.25 | 315 | 13.41 | **9.49E-33** | 4.62E-04 | 3.05 |
| GBOBC1 mb2 R. GBHCT F. | 78 | 29.67 | 2.25 | 315 | 13.17 | **7.29E-32** | 4.66E-04 | 2.54 |
| Prime F. GBOBC1 b. R. | 18 | -28.85 | 2.25 | 315 | 12.81 | **1.63E-30** | 4.70E-04 | 2.51 |
| Prime F. L. GBOBC1 b. R. | 43 | -28.28 | 2.25 | 315 | 12.55 | **1.39E-29** | 4.75E-04 | 2.45 |
| GBOBC2 b. R. GBOBC1 mb2 F. | 88 | 28.23 | 2.25 | 315 | 12.53 | **1.62E-29** | 4.79E-04 | 2.66 |
| Gbn R. GBOBC1 mb2 F. | 101 | 28.21 | 2.25 | 315 | 12.52 | **1.76E-29** | 4.84E-04 | 2.82 |
| Prime F. GBOBC2 mb2 R. | 21 | -28.08 | 2.25 | 315 | 12.46 | **2.94E-29** | 4.88E-04 | 2.53 |
| Prime F. L. GBOBC2 mb2 R. | 46 | -27.50 | 2.25 | 315 | 12.21 | **2.47E-28** | 4.93E-04 | 2.45 |
| GBOBC2 b. R. GBOBC2 b. F. | 89 | 27.40 | 2.25 | 315 | 12.16 | **3.59E-28** | 4.98E-04 | 2.75 |
| Gbn R. GBOBC2 b. F. | 102 | 27.38 | 2.25 | 315 | 12.15 | **3.90E-28** | 5.03E-04 | 3.00 |
| Prime F. GBOBC1 mb2 R. | 19 | -26.61 | 2.25 | 315 | 11.81 | **6.72E-27** | 5.08E-04 | 2.44 |
| GBOBC1 b. R. GBOBC2 mb2 F. | 73 | 26.47 | 2.25 | 315 | 11.75 | **1.12E-26** | 5.13E-04 | 2.53 |
| Prime F. L. GBOBC1 mb2 R. | 44 | -26.03 | 2.25 | 315 | 11.56 | **5.43E-26** | 5.18E-04 | 2.37 |
| GBOBC2 mb2 R. GBOBC2 mb2 F. | 97 | 25.69 | 2.25 | 315 | 11.41 | **1.85E-25** | 5.23E-04 | 2.68 |
| GBOBC1 b. R. GBOBC1 mb2 F. | 71 | 24.47 | 2.25 | 315 | 10.86 | **1.46E-23** | 5.29E-04 | 2.43 |
| GBOBC1 mb2 R. GBOBC2 mb2 F. | 82 | 24.22 | 2.25 | 315 | 10.75 | **3.50E-23** | 5.34E-04 | 2.51 |
| GBOBC2 mb2 R. GBOBC1 mb2 F. | 95 | 23.70 | 2.25 | 315 | 10.52 | **2.20E-22** | 5.40E-04 | 2.44 |
| GBOBC1 b. R. GBOBC2 b. F. | 72 | 23.64 | 2.25 | 315 | 10.49 | **2.71E-22** | 5.46E-04 | 2.40 |
| GBOBC2 b. R. GBOBC1 b. F. | 87 | 23.07 | 2.25 | 315 | 10.24 | **1.93E-21** | 5.51E-04 | 2.50 |
| Gbn R. GBOBC1 b. F. | 100 | 23.05 | 2.25 | 315 | 10.23 | **2.09E-21** | 5.57E-04 | 2.84 |
| GBOBC2 mb2 R. GBOBC2 b. F. | 96 | 22.87 | 2.25 | 315 | 10.15 | **3.91E-21** | 5.64E-04 | 2.60 |
| GBOBC1 mb2 R. GBOBC1 mb2 F. | 80 | 22.23 | 2.25 | 315 | 9.87 | **3.43E-20** | 5.70E-04 | 2.33 |
| GBOBC1 mb2 R. GBOBC2 b. F. | 81 | 21.40 | 2.25 | 315 | 9.50 | **5.57E-19** | 5.76E-04 | 2.33 |
| GBOBC1 b. R. GBOBC1 b. F. | 70 | 19.31 | 2.25 | 315 | 8.57 | **4.64E-16** | 5.83E-04 | 2.18 |
| GBOBC2 b. R. Gbn F. | 91 | 18.95 | 2.25 | 315 | 8.41 | **1.43E-15** | 5.89E-04 | 2.37 |
| Gbn R. Gbn F. | 104 | 18.92 | 2.25 | 315 | 8.40 | **1.53E-15** | 5.96E-04 | 2.28 |
| Prime R. GBOBC2 b. R. | 6 | -18.73 | 2.25 | 315 | 8.31 | **2.82E-15** | 6.03E-04 | 2.97 |
| Prime R. Gbn R. | 8 | -18.70 | 2.25 | 315 | 8.30 | **3.02E-15** | 6.10E-04 | 2.52 |
| GBOBC2 mb2 R. GBOBC1 b. F. | 94 | 18.54 | 2.25 | 315 | 8.23 | **5.04E-15** | 6.18E-04 | 2.23 |
| GBHCT R. GBHCT F. | 59 | 18.05 | 2.25 | 315 | 8.01 | **2.19E-14** | 6.25E-04 | 2.06 |

| | | | | | | | | |
|---|---|---|---|---|---|---|---|---|
| Prime R. L. GBOBC2 b. R. | 33 | -17.88 | 2.25 | 315 | 7.94 | **3.69E-14** | 6.33E-04 | 2.72 |
| Prime R. L. Gbn R. | 35 | -17.85 | 2.25 | 315 | 7.93 | **3.94E-14** | 6.41E-04 | 2.38 |
| Prime R. L. GBHCT F. | 36 | 17.80 | 2.25 | 315 | 7.90 | **4.65E-14** | 6.49E-04 | 2.27 |
| GBHCT R. GBOBC2 b. R. | 56 | -17.62 | 2.25 | 315 | 7.82 | **7.80E-14** | 6.57E-04 | 4.51 |
| GBHCT R. Gbn R. | 58 | -17.60 | 2.25 | 315 | 7.81 | **8.33E-14** | 6.66E-04 | 4.56 |
| GBOBC1 mb2 R. GBOBC1 b. F. | 79 | 17.07 | 2.25 | 315 | 7.58 | **3.99E-13** | 6.75E-04 | 2.11 |
| Prime R. GBHCT F. | 9 | 16.95 | 2.25 | 315 | 7.52 | **5.59E-13** | 6.84E-04 | 2.02 |
| GBHCT F. Gbn F. | 109 | -16.73 | 2.25 | 315 | 7.43 | **1.05E-12** | 6.93E-04 | 3.68 |
| GBOBC1 b. R. Gbn F. | 74 | 15.18 | 2.25 | 315 | 6.74 | **7.52E-11** | 7.02E-04 | 2.16 |
| Prime F. GBHCT R. | 17 | -14.99 | 2.25 | 315 | 6.65 | **1.27E-10** | 7.12E-04 | 2.34 |
| Prime R. GBOBC1 b. R. | 4 | -14.96 | 2.25 | 315 | 6.64 | **1.35E-10** | 7.22E-04 | 2.80 |
| Prime F. Prime R. L. | 15 | -14.73 | 2.25 | 315 | 6.54 | **2.47E-10** | 7.32E-04 | 3.27 |
| Prime F. L. GBHCT R. | 42 | -14.41 | 2.25 | 315 | 6.40 | **5.67E-10** | 7.43E-04 | 2.14 |
| GBOBC2 mb2 R. Gbn F. | 98 | 14.41 | 2.25 | 315 | 6.40 | **5.70E-10** | 7.54E-04 | 2.07 |
| Prime R. GBOBC2 mb2 R. | 7 | -14.19 | 2.25 | 315 | 6.30 | **9.99E-10** | 7.65E-04 | 2.60 |
| Prime R. L. Prime F. L. | 29 | 14.16 | 2.25 | 315 | 6.29 | **1.08E-09** | 7.77E-04 | 3.82 |
| Prime R. L. GBOBC1 b. R. | 31 | -14.11 | 2.25 | 315 | 6.27 | **1.22E-09** | 7.89E-04 | 2.46 |
| Prime R. Prime F. | 0 | 13.88 | 2.25 | 315 | 6.16 | **2.17E-09** | 8.01E-04 | 4.01 |
| GBHCT R. GBOBC1 b. R. | 54 | -13.86 | 2.25 | 315 | 6.15 | **2.30E-09** | 8.14E-04 | 3.28 |
| Prime F. Gbn F. | 28 | -13.66 | 2.25 | 315 | 6.07 | **3.75E-09** | 8.27E-04 | 2.15 |
| Prime R. L. GBOBC2 mb2 R. | 34 | -13.34 | 2.25 | 315 | 5.92 | **8.27E-09** | 8.41E-04 | 2.28 |
| Prime R. Prime F. L. | 2 | 13.31 | 2.25 | 315 | 5.91 | **8.92E-09** | 8.55E-04 | 3.53 |
| Prime F. L. Gbn F. | 53 | -13.09 | 2.25 | 315 | 5.81 | **1.51E-08** | 8.69E-04 | 2.13 |
| GBHCT R. GBOBC2 mb2 R. | 57 | -13.09 | 2.25 | 315 | 5.81 | **1.52E-08** | 8.84E-04 | 2.91 |
| GBOBC1 mb2 R. Gbn F. | 83 | 12.94 | 2.25 | 315 | 5.74 | **2.17E-08** | 8.99E-04 | 2.13 |
| Prime R. GBOBC1 mb2 R. | 5 | -12.72 | 2.25 | 315 | 5.65 | **3.64E-08** | 9.16E-04 | 2.61 |
| GBHCT R. GBOBC2 mb2 F. | 63 | 12.60 | 2.25 | 315 | 5.60 | **4.78E-08** | 9.32E-04 | 2.54 |
| GBHCT F. GBOBC1 b. F. | 105 | -12.60 | 2.25 | 315 | 5.60 | **4.78E-08** | 9.49E-04 | 2.75 |
| Prime R. L. GBOBC2 mb2 F. | 40 | 12.35 | 2.25 | 315 | 5.48 | **8.56E-08** | 9.67E-04 | 1.76 |
| Prime R. L. GBOBC1 mb2 R. | 32 | -11.87 | 2.25 | 315 | 5.27 | **2.53E-07** | 9.86E-04 | 2.26 |
| GBHCT R. GBOBC1 mb2 R. | 55 | -11.62 | 2.25 | 315 | 5.16 | **4.42E-07** | 1.01E-03 | 3.62 |
| Prime R. GBOBC2 mb2 F. | 13 | 11.50 | 2.25 | 315 | 5.11 | **5.70E-07** | 1.03E-03 | 1.76 |
| GBOBC2 mb2 F. Gbn F. | 119 | -11.28 | 2.25 | 315 | 5.01 | **9.14E-07** | 1.05E-03 | 2.07 |
| GBHCT R. GBOBC1 mb2 F. | 61 | 10.61 | 2.25 | 315 | 4.71 | **3.71E-06** | 1.07E-03 | 1.90 |
| Prime R. L. GBOBC1 mb2 F. | 38 | 10.36 | 2.25 | 315 | 4.60 | **6.18E-06** | 1.09E-03 | 1.58 |
| GBHCT R. GBOBC2 b. F. | 62 | 9.78 | 2.25 | 315 | 4.34 | **1.92E-05** | 1.11E-03 | 1.98 |
| Prime F. GBOBC1 b. F. | 24 | -9.54 | 2.25 | 315 | 4.23 | **3.01E-05** | 1.14E-03 | 1.36 |
| Prime R. L. GBOBC2 b. F. | 39 | 9.52 | 2.25 | 315 | 4.23 | **3.09E-05** | 1.17E-03 | 1.74 |
| Prime R. GBOBC1 mb2 F. | 11 | 9.51 | 2.25 | 315 | 4.22 | **3.19E-05** | 1.19E-03 | 1.41 |
| GBOBC1 mb2 F. Gbn F. | 116 | -9.29 | 2.25 | 315 | 4.12 | **4.78E-05** | 1.22E-03 | 1.99 |
| Prime F. L. GBOBC1 b. F. | 49 | -8.97 | 2.25 | 315 | 3.98 | **8.55E-05** | 1.25E-03 | 1.33 |
| Prime R. GBOBC2 b. F. | 12 | 8.67 | 2.25 | 315 | 3.85 | **1.42E-04** | 1.28E-03 | 1.57 |
| GBOBC2 b. F. Gbn F. | 118 | -8.46 | 2.25 | 315 | 3.75 | **2.08E-04** | 1.31E-03 | 1.88 |

| | | | | | | | | |
|---|---|---|---|---|---|---|---|---|
| GBHCT F. GBOBC2 b. F. | 107 | -8.27 | 2.25 | 315 | 3.67 | **2.81E-04** | 1.35E-03 | 2.40 |
| GBHCT F. GBOBC1 mb2 F. | 106 | -7.44 | 2.25 | 315 | 3.30 | **1.06E-03** | 1.39E-03 | 2.43 |
| GBOBC1 b. F. GBOBC2 mb2 F. | 112 | 7.16 | 2.25 | 315 | 3.18 | 1.63E-03 | 1.42E-03 | 2.18 |
| GBOBC1 mb2 R. GBOBC2 b. R. | 75 | -6.01 | 2.25 | 315 | 2.67 | 8.07E-03 | 0.00E+00 | 1.64 |
| GBOBC1 mb2 R. Gbn R. | 77 | -5.98 | 2.25 | 315 | 2.66 | 8.30E-03 | 0.00E+00 | 2.05 |
| GBHCT R. GBOBC1 b. F. | 60 | 5.45 | 2.25 | 315 | 2.42 | 1.62E-02 | 0.00E+00 | 1.80 |
| GBHCT F. GBOBC2 mb2 F. | 108 | -5.45 | 2.25 | 315 | 2.42 | 1.62E-02 | 0.00E+00 | 1.92 |
| Prime F. GBOBC2 b. F. | 26 | -5.21 | 2.25 | 315 | 2.31 | 2.14E-02 | 0.00E+00 | 0.98 |
| Prime R. L. GBOBC1 b. F. | 37 | 5.19 | 2.25 | 315 | 2.31 | 2.18E-02 | 0.00E+00 | 1.34 |
| GBOBC1 b. F. GBOBC1 mb2 F. | 110 | 5.16 | 2.25 | 315 | 2.29 | 2.26E-02 | 0.00E+00 | 1.12 |
| Prime F. L. GBOBC2 b. F. | 51 | -4.64 | 2.25 | 315 | 2.06 | 4.04E-02 | 0.00E+00 | 0.95 |
| GBOBC2 b. R. GBOBC2 mb2 R. | 84 | 4.54 | 2.25 | 315 | 2.01 | 4.49E-02 | 0.00E+00 | 1.91 |
| GBOBC2 mb2 R. Gbn R. | 92 | -4.51 | 2.25 | 315 | 2.00 | 4.60E-02 | 0.00E+00 | 1.90 |
| Prime F. GBOBC1 mb2 F. | 25 | -4.38 | 2.25 | 315 | 1.94 | 5.30E-02 | 0.00E+00 | 1.60 |
| Prime R. GBOBC1 b. F. | 10 | 4.34 | 2.25 | 315 | 1.93 | 5.46E-02 | 0.00E+00 | 1.22 |
| GBOBC1 b. F. GBOBC2 b. F. | 111 | 4.33 | 2.25 | 315 | 1.92 | 5.55E-02 | 0.00E+00 | 1.08 |
| GBOBC1 b. F. Gbn F. | 113 | -4.13 | 2.25 | 315 | 1.83 | 6.80E-02 | 0.00E+00 | 1.33 |
| Prime F. L. GBOBC1 mb2 F. | 50 | -3.80 | 2.25 | 315 | 1.69 | 9.24E-02 | 0.00E+00 | 1.73 |
| GBOBC1 b. R. GBOBC2 b. R. | 66 | -3.76 | 2.25 | 315 | 1.67 | 9.59E-02 | 0.00E+00 | 1.34 |
| GBOBC1 b. R. Gbn R. | 68 | -3.74 | 2.25 | 315 | 1.66 | 9.78E-02 | 0.00E+00 | 1.88 |
| Prime F. L. GBHCT F. | 48 | 3.64 | 2.25 | 315 | 1.62 | 1.07E-01 | 0.00E+00 | 1.33 |
| Prime F. GBHCT F. | 23 | 3.07 | 2.25 | 315 | 1.36 | 1.75E-01 | 0.00E+00 | 1.38 |
| GBOBC2 b. F. GBOBC2 mb2 F. | 117 | 2.83 | 2.25 | 315 | 1.26 | 2.10E-01 | 0.00E+00 | 1.53 |
| Prime F. GBOBC2 mb2 F. | 27 | -2.38 | 2.25 | 315 | 1.06 | 2.91E-01 | 0.00E+00 | 1.42 |
| GBOBC1 b. R. GBOBC1 mb2 R. | 65 | 2.24 | 2.25 | 315 | 1.00 | 3.20E-01 | 0.00E+00 | 1.38 |
| GBOBC1 mb2 F. GBOBC2 mb2 F. | 115 | 1.99 | 2.25 | 315 | 0.89 | 3.77E-01 | 0.00E+00 | 1.36 |
| Prime F. L. GBOBC2 mb2 F. | 52 | -1.81 | 2.25 | 315 | 0.80 | 4.23E-01 | 0.00E+00 | 1.39 |
| GBOBC1 mb2 R. GBOBC2 mb2 R. | 76 | -1.47 | 2.25 | 315 | 0.65 | 5.14E-01 | 0.00E+00 | 1.00 |
| GBHCT R. Gbn F. | 64 | 1.32 | 2.25 | 315 | 0.59 | 5.58E-01 | 0.00E+00 | 1.42 |
| Prime R. GBHCT R. | 3 | -1.10 | 2.25 | 315 | 0.49 | 6.25E-01 | 0.00E+00 | 1.14 |
| Prime R. L. Gbn F. | 41 | 1.07 | 2.25 | 315 | 0.47 | 6.35E-01 | 0.00E+00 | 1.28 |
| Prime R. Prime R. L. | 1 | -0.85 | 2.25 | 315 | 0.38 | 7.06E-01 | 0.00E+00 | 0.34 |
| GBOBC1 mb2 F. GBOBC2 b. F. | 114 | -0.83 | 2.25 | 315 | 0.37 | 7.12E-01 | 0.00E+00 | 0.68 |
| GBOBC1 b. R. GBOBC2 mb2 R. | 67 | 0.77 | 2.25 | 315 | 0.34 | 7.32E-01 | 0.00E+00 | 1.13 |
| Prime F. Prime F. L. | 16 | -0.57 | 2.25 | 315 | 0.25 | 7.99E-01 | 0.00E+00 | 0.32 |
| Prime R. L. GBHCT R. | 30 | -0.25 | 2.25 | 315 | 0.11 | 9.11E-01 | 0.00E+00 | 1.17 |
| Prime R. Gbn F. | 14 | 0.22 | 2.25 | 315 | 0.10 | 9.22E-01 | 0.00E+00 | 1.36 |
| GBOBC2 b. R. Gbn R. | 85 | 0.02 | 2.25 | 315 | 0.01 | 9.92E-01 | 0.00E+00 | 1.28 |

Table B.36: Models for which the null hypothesis was not rejected across Glide jobs. Names abbreviated for expediency. F., R., b., and mb2, correspond to Flexible, Rigid, bondi and mbondi2, respectively.

| Compared Models | Glide2 | Glide 3 |
|---|---|---|
| Prime R. - Prime R. L. | ✓ | ✓ |
| Prime R. - $GB^{HCT}$ R. | ✓ | ✓ |
| Prime R. - $GB^{OBC1}$ b. F. | ✓ | ✓ |
| Prime R. - Gbn F. | ✓ | ✓ |
| Prime F. - Prime F. L. | ✓ | ✓ |
| Prime F. - $GB^{HCT}$ F. | ✓ | ✓ |
| Prime F. - $GB^{OBC1}$ mb2 F. | ✓ | ✓ |
| Prime F. - $GB^{OBC2}$ b. F. | ✓ | ✓ |
| Prime F. - $GB^{OBC2}$ mb2 F. | ✓ | ✓ |
| Prime R. L. - $GB^{HCT}$ R. | ✓ | ✓ |
| Prime R. L. - $GB^{OBC1}$ b. F. | ✓ | ✓ |
| Prime R. L. - Gbn F. | ✓ | ✓ |
| Prime F. L. - $GB^{HCT}$ F. | | ✓ |
| Prime F. L. - $GB^{OBC1}$ b. F. | ✓ | |
| Prime F. L. - $GB^{OBC1}$ mb2 F. | ✓ | ✓ |
| Prime F. L. - $GB^{OBC2}$ b. F. | ✓ | ✓ |
| Prime F. L. - $GB^{OBC2}$ mb2 F. | ✓ | ✓ |
| GBHCT R. - $GB^{OBC1}$ b. F. | ✓ | ✓ |
| $GB^{HCT}$ R. - Gbn F. | ✓ | ✓ |
| $GB^{OBC1}$ b. R. - $GB^{OBC1}$ mb2 R. | ✓ | ✓ |
| $GB^{OBC1}$ b. R. - $GB^{OBC2}$ b. R. | ✓ | ✓ |
| $GB^{OBC1}$ b. R. - $GB^{OBC2}$ mb2 R. | ✓ | ✓ |
| $GB^{OBC1}$ b. R. - Gbn R. | ✓ | ✓ |
| $GB^{OBC1}$ mb2 R. - $GB^{OBC2}$ b. R. | ✓ | ✓ |
| $GB^{OBC1}$ mb2 R. - $GB^{OBC2}$ mb2 R. | ✓ | ✓ |
| $GB^{OBC1}$ mb2 R. - Gbn R. | ✓ | ✓ |
| $GB^{OBC2}$ b. R. - $GB^{OBC2}$ mb2 R. | ✓ | ✓ |
| $GB^{OBC2}$ b. R. - Gbn R. | ✓ | ✓ |
| $GB^{OBC2}$ mb2 R. - Gbn R. | ✓ | ✓ |
| $GB^{HCT}$ F. - $GB^{OBC2}$ mb2 F. | | ✓ |
| $GB^{OBC1}$ b. F. - $GB^{OBC1}$ mb2 F. | ✓ | ✓ |
| $GB^{OBC1}$ b. F. - $GB^{OBC2}$ b. F. | ✓ | ✓ |
| $GB^{OBC1}$ b. F. - $GB^{OBC2}$ mb2 F. | ✓ | ✓ |
| $GB^{OBC1}$ b. F. - Gbn F. | ✓ | ✓ |
| $GB^{OBC1}$ mb2 F. - $GB^{OBC2}$ b. F. | ✓ | ✓ |
| $GB^{OBC1}$ mb2 F. - $GB^{OBC2}$ mb2 F. | ✓ | ✓ |
| $GB^{OBC2}$ b. F. - $GB^{OBC2}$ mb2 F. | ✓ | ✓ |
| $GB^{OBC2}$ b. F. - Gbn F. | ✓ | |

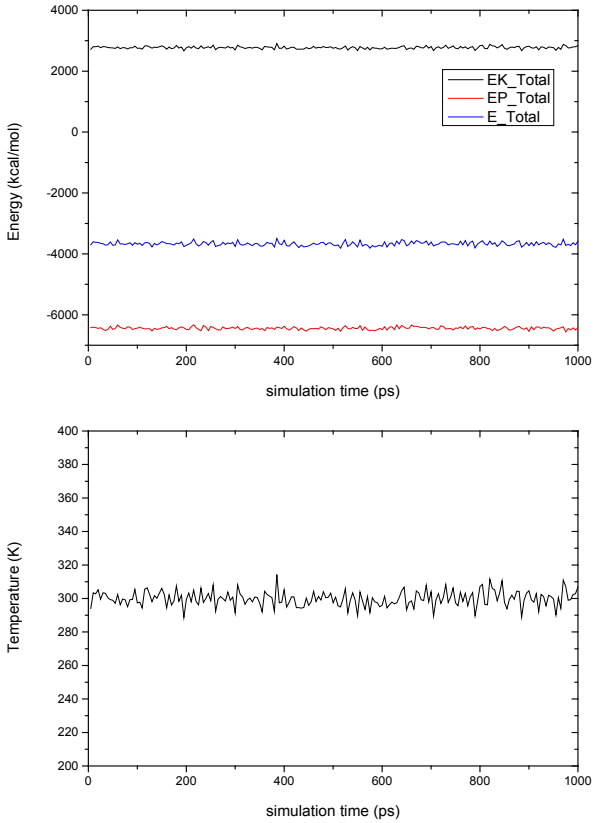


Figure B.20: Kinetic energy (black line), potential energy (red line) and total system energy (blue line) for ligand 3 Glide job 2 during 1 ns MD using model $GB^{OBC1}$mbondi2. Bottom plot shows the temperature during the simulation.

# HIV-1 Protease

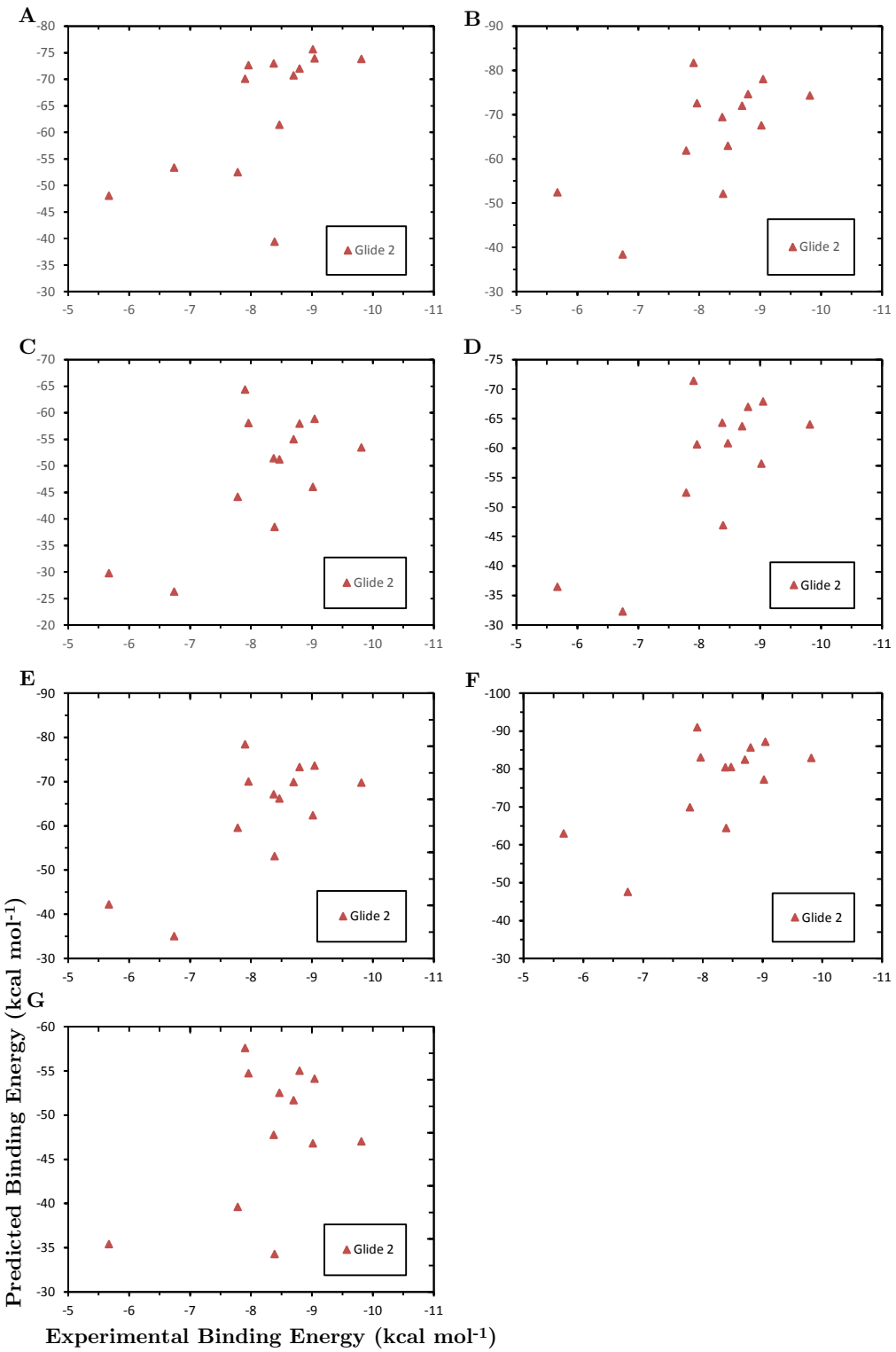


Figure B.21: Scatter plots of the predicted and experimental binding affinities for Thrombin. The plots correspond to the solvent models, A: Prime Rigid, B: Prime Rigid L., C: $GB^{HCT}$ Rigid, D: $GB^{OBC1}$ bondi Rigid, E: $GB^{OBC1}$ mbondi2 Rigid, F: $GB^{OBC2}$ bondi Rigid, G: $GB^{OBC2}$ mbondi2 Rigid, H: Gbn Rigid.

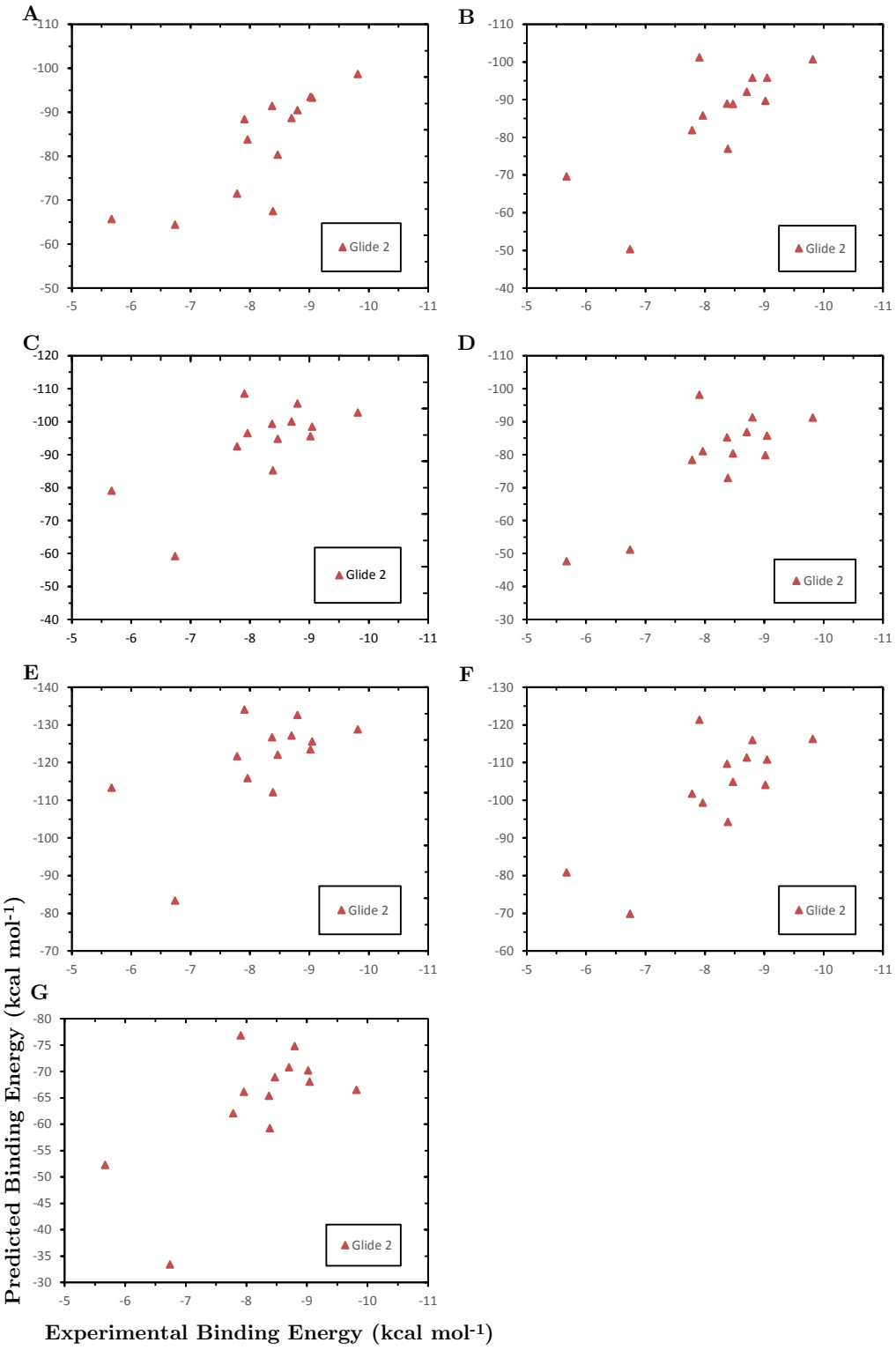


Figure B.22: Scatter plots of the predicted and experimental binding affinities for Thrombin. The plots correspond to the solvent models, A: Prime Flex, B: Prime Flex L., C: $GB^{HCT}$ Flex, D: $GB^{OBC1}$ bondi Flex, E: $GB^{OBC1}$ mbondi2 Flex, F: $GB^{OBC2}$ bondi Flex, G: $GB^{OBC2}$ mbondi2 Flex, H: Gbn Flex.

Table B.37: Coefficient of determination ($R^2$) matrix between rescoring models for Glide 2. P–values from a two-tailed test shown. Significant correlations highlighted in bold.

| | | Prime Rigid | Prime Flex | GBHCT Rigid | GBOBC1 bondi Rigid | GBOBC1 mbondi2 Rigid | GBOBC2 bondi Rigid | GBOBC2 mbondi2 Rigid | Gbn Rigid | GBHCT Flex | GBOBC1 bondi Flex | GBOBC1 mbondi2 Flex | GBOBC2 bondi Flex | GBOBC2 mbondi2 Flex | Gbn Flex |
|---|---|---|---|---|---|---|---|---|---|---|---|---|---|---|---|
| **Prime Rigid** | $R^2$ | 1.0000 | **0.8622** | **0.6457** | **0.5823** | **0.6150** | **0.5672** | **0.5974** | **0.5518** | **0.4964** | **0.4654** | **0.4854** | **0.3435** | **0.4744** | **0.3909** |
| **Prime Rigid** | p | -- | **0.0000** | **0.0009** | **0.0024** | **0.0015** | **0.0030** | **0.0020** | **0.0036** | **0.0072** | **0.0102** | **0.0081** | **0.0353** | **0.0092** | **0.0223** |
| **Prime Flex** | $R^2$ | | 1.0000 | **0.7563** | **0.6530** | **0.7598** | **0.7001** | **0.7198** | **0.6077** | **0.7445** | **0.6649** | **0.6773** | **0.5659** | **0.7111** | **0.5691** |
| **Prime Flex** | p | | -- | **0.0001** | **0.0008** | **0.0001** | **0.0004** | **0.0002** | **0.0017** | **0.0001** | **0.0007** | **0.0005** | **0.0030** | **0.0003** | **0.0029** |
| **GBHCT Rigid** | $R^2$ | | | 1.0000 | **0.9205** | **0.9174** | **0.9381** | **0.9612** | **0.8884** | **0.9083** | **0.9074** | **0.8101** | **0.7996** | **0.8688** | **0.8221** |
| **GBHCT Rigid** | p | | | -- | **0.0000** | **0.0000** | **0.0000** | **0.0000** | **0.0000** | **0.0000** | **0.0000** | **0.0000** | **0.0000** | **0.0000** | **0.0000** |
| **GBOBC1 bondi Rigid** | $R^2$ | | | | 1.0000 | **0.9550** | **0.9801** | **0.9402** | **0.9041** | **0.8308** | **0.8502** | **0.8764** | **0.6704** | **0.8424** | **0.7902** |
| **GBOBC1 bondi Rigid** | p | | | | -- | **0.0000** | **0.0000** | **0.0000** | **0.0000** | **0.0000** | **0.0000** | **0.0000** | **0.0006** | **0.0000** | **0.0000** |
| **GBOBC1 mbondi2 Rigid** | $R^2$ | | | | | 1.0000 | **0.9835** | **0.9465** | **0.8752** | **0.9028** | **0.9012** | **0.9282** | **0.7635** | **0.9313** | **0.8353** |
| **GBOBC1 mbondi2 Rigid** | p | | | | | -- | **0.0000** | **0.0000** | **0.0000** | **0.0000** | **0.0000** | **0.0000** | **0.0001** | **0.0000** | **0.0000** |
| **GBOBC2 bondi Rigid** | $R^2$ | | | | | | 1.0000 | **0.9629** | **0.9098** | **0.9095** | **0.9219** | **0.9203** | **0.7716** | **0.9172** | **0.8663** |
| **GBOBC2 bondi Rigid** | p | | | | | | -- | **0.0000** | **0.0000** | **0.0000** | **0.0000** | **0.0000** | **0.0001** | **0.0000** | **0.0000** |
| **GBOBC2 mbondi2 Rigid** | $R^2$ | | | | | | | 1.0000 | **0.9653** | **0.9246** | **0.9269** | **0.8121** | **0.8203** | **0.8769** | **0.8857** |
| **GBOBC2 mbondi2 Rigid** | p | | | | | | | -- | **0.0000** | **0.0000** | **0.0000** | **0.0000** | **0.0000** | **0.0000** | **0.0000** |
| **Gbn Rigid** | $R^2$ | | | | | | | | 1.0000 | **0.8295** | **0.8622** | **0.7103** | **0.7546** | **0.7677** | **0.8775** |
| **Gbn Rigid** | p | | | | | | | | -- | **0.0000** | **0.0000** | **0.0003** | **0.0001** | **0.0001** | **0.0000** |
| **GBHCT Flex** | $R^2$ | | | | | | | | | 1.0000 | **0.9612** | **0.8581** | **0.9077** | **0.9560** | **0.9035** |
| **GBHCT Flex** | p | | | | | | | | | -- | **0.0000** | **0.0000** | **0.0000** | **0.0000** | **0.0000** |
| **GBOBC1 bondi Flex** | $R^2$ | | | | | | | | | | 1.0000 | **0.8624** | **0.9378** | **0.9488** | **0.9431** |
| **GBOBC1 bondi Flex** | p | | | | | | | | | | -- | **0.0000** | **0.0000** | **0.0000** | **0.0000** |
| **GBOBC1 mbondi2 Flex** | $R^2$ | | | | | | | | | | | 1.0000 | **0.7050** | **0.9404** | **0.7836** |
| **GBOBC1 mbondi2 Flex** | p | | | | | | | | | | | -- | **0.0003** | **0.0000** | **0.0001** |
| **GBOBC2 bondi Flex** | $R^2$ | | | | | | | | | | | | 1.0000 | **0.8809** | **0.9036** |
| **GBOBC2 bondi Flex** | p | | | | | | | | | | | | -- | **0.0000** | **0.0000** |
| **GBOBC2 mbondi2 Flex** | $R^2$ | | | | | | | | | | | | | 1.0000 | **0.8702** |
| **GBOBC2 mbondi2 Flex** | p | | | | | | | | | | | | | -- | **0.0000** |
| **Gbn Flex** | $R^2$ | | | | | | | | | | | | | | 1.0000 |
| **Gbn Flex** | p | | | | | | | | | | | | | | -- |

Table B.38: Kendall tau (τ) rank correlation coefficient matrix between rescoring models for Glide 2. P–values from a two-tailed test shown. Significant correlations highlighted in bold.

| | | Prime Rigid | Prime Flex | GBHCT Rigid | GBOBC1 bondi Rigid | GBOBC1 mbondi2 Rigid | GBOBC2 bondi Rigid | GBOBC2 mbondi2 Rigid | Gbn Rigid | GBHCT Flex | GBOBC1 bondi Flex | GBOBC1 mbondi2 Flex | GBOBC2 bondi Flex | GBOBC2 mbondi2 Flex | Gbn Flex |
|---|---|---|---|---|---|---|---|---|---|---|---|---|---|---|---|
| **Prime Rigid** | τ | 1.0000 | **0.7692** | **0.4615** | 0.3846 | 0.3846 | 0.3590 | 0.3590 | 0.2308 | **0.4359** | 0.3333 | 0.3590 | 0.3333 | 0.3333 | 0.3333 |
| **Prime Rigid** | p | -- | **0.0003** | **0.0281** | 0.0672 | 0.0672 | 0.0876 | 0.0876 | 0.2721 | **0.0381** | 0.1127 | 0.0876 | 0.1127 | 0.1127 | 0.1127 |
| **Prime Flex** | τ | | 1.0000 | **0.5385** | **0.4615** | **0.5641** | **0.4872** | **0.4872** | 0.3077 | **0.6667** | **0.5641** | **0.5385** | **0.5128** | **0.5641** | **0.4615** |
| **Prime Flex** | p | | -- | **0.0104** | **0.0281** | **0.0073** | **0.0204** | **0.0204** | 0.1431 | **0.0015** | **0.0073** | **0.0104** | **0.0147** | **0.0073** | **0.0281** |
| **GBHCT Rigid** | τ | | | 1.0000 | **0.8718** | **0.8205** | **0.8974** | **0.8974** | **0.7692** | **0.7692** | **0.8205** | **0.7949** | **0.7692** | **0.7180** | **0.6667** |
| **GBHCT Rigid** | p | | | -- | **0.0000** | **0.0001** | **0.0000** | **0.0000** | **0.0003** | **0.0003** | **0.0001** | **0.0002** | **0.0003** | **0.0006** | **0.0015** |
| **GBOBC1 bondi Rigid** | τ | | | | 1.0000 | **0.7949** | **0.9744** | **0.9231** | **0.7949** | **0.6923** | **0.7436** | **0.7692** | **0.6410** | **0.6923** | **0.6410** |
| **GBOBC1 bondi Rigid** | p | | | | -- | **0.0002** | **0.0000** | **0.0000** | **0.0002** | **0.0010** | **0.0004** | **0.0003** | **0.0023** | **0.0010** | **0.0023** |
| **GBOBC1 mbondi2 Rigid** | τ | | | | | 1.0000 | **0.8205** | **0.8205** | **0.6923** | **0.7949** | **0.7949** | **0.8205** | **0.7436** | **0.7949** | **0.6410** |
| **GBOBC1 mbondi2 Rigid** | p | | | | | -- | **0.0001** | **0.0001** | **0.0010** | **0.0002** | **0.0002** | **0.0001** | **0.0004** | **0.0002** | **0.0023** |
| **GBOBC2 bondi Rigid** | τ | | | | | | 1.0000 | **0.9487** | **0.8205** | **0.7180** | **0.7692** | **0.7949** | **0.6667** | **0.7180** | **0.6667** |
| **GBOBC2 bondi Rigid** | p | | | | | | -- | **0.0000** | **0.0001** | **0.0006** | **0.0003** | **0.0002** | **0.0015** | **0.0006** | **0.0015** |
| **GBOBC2 mbondi2 Rigid** | τ | | | | | | | 1.0000 | **0.8205** | **0.7180** | **0.7692** | **0.7949** | **0.6667** | **0.7180** | **0.6667** |
| **GBOBC2 mbondi2 Rigid** | p | | | | | | | -- | **0.0001** | **0.0006** | **0.0003** | **0.0002** | **0.0015** | **0.0006** | **0.0015** |
| **Gbn Rigid** | τ | | | | | | | | 1.0000 | **0.5897** | **0.6410** | **0.6667** | **0.5897** | **0.5897** | **0.6410** |
| **Gbn Rigid** | p | | | | | | | | -- | **0.0050** | **0.0023** | **0.0015** | **0.0050** | **0.0050** | **0.0023** |
| **GBHCT Flex** | τ | | | | | | | | | 1.0000 | **0.8462** | **0.8205** | **0.8462** | **0.8974** | **0.7436** |
| **GBHCT Flex** | p | | | | | | | | | -- | **0.0001** | **0.0001** | **0.0001** | **0.0000** | **0.0004** |
| **GBOBC1 bondi Flex** | τ | | | | | | | | | | 1.0000 | **0.9231** | **0.8974** | **0.8462** | **0.6923** |
| **GBOBC1 bondi Flex** | p | | | | | | | | | | -- | **0.0000** | **0.0000** | **0.0001** | **0.0010** |
| **GBOBC1 mbondi2 Flex** | τ | | | | | | | | | | | 1.0000 | **0.8205** | **0.8718** | **0.6667** |
| **GBOBC1 mbondi2 Flex** | p | | | | | | | | | | | -- | **0.0001** | **0.0000** | **0.0015** |
| **GBOBC2 bondi Flex** | τ | | | | | | | | | | | | 1.0000 | **0.8974** | **0.6923** |
| **GBOBC2 bondi Flex** | p | | | | | | | | | | | | -- | **0.0000** | **0.0010** |
| **GBOBC2 mbondi2 Flex** | τ | | | | | | | | | | | | | 1.0000 | **0.6923** |
| **GBOBC2 mbondi2 Flex** | p | | | | | | | | | | | | | -- | **0.0010** |
| **Gbn Flex** | τ | | | | | | | | | | | | | | 1.0000 |
| **Gbn Flex** | p | | | | | | | | | | | | | | -- |

Table B.39: Descriptive statistics for Glide job 2 rescoring protocols.

| Rescoring Protocols | Mean | Std.Er. | 95% LCL | 95% UCL |
|---|---|---|---|---|
| Prime Rigid | -64.37 | 3.34 | -71.66 | -57.09 |
| Prime Flex | -82.91 | 3.28 | -90.05 | -75.77 |
| GBHCT Rigid | -66.03 | 3.39 | -73.42 | -58.64 |
| GBOBC1 bondi Rigid | -48.87 | 3.19 | -55.83 | -41.92 |
| GBOBC1 mbondi2 Rigid | -57.36 | 3.35 | -64.66 | -50.05 |
| GBOBC2 bondi Rigid | -63.15 | 3.53 | -70.84 | -55.45 |
| GBOBC2 mbondi2 Rigid | -76.58 | 3.37 | -83.92 | -69.25 |
| Gbn Rigid | -45.89 | 3.01 | -52.44 | -39.33 |
| GBHCT Flex | -86.00 | 3.88 | -94.45 | -77.55 |
| GBOBC1 bondi Flex | -93.69 | 3.60 | -101.53 | -85.85 |
| GBOBC1 mbondi2 Flex | -79.27 | 4.09 | -88.18 | -70.36 |
| GBOBC2 bondi Flex | -120.57 | 3.62 | -128.46 | -112.69 |
| GBOBC2 mbondi2 Flex | -103.14 | 4.03 | -111.93 | -94.35 |
| Gbn Flex | -64.22 | 3.12 | -71.02 | -57.42 |

Table B.40: Holm-Šidák results for Glide job 2. Names abbreviated for expediency. F., R., b., mb2, and d, correspond to Flexible, Rigid, bondi, mbondi2, and Cohen's d respectively. Significant differences shown in bold.

| Compared Models | Index | Mean Diff. | Std.Er. | DF | \|t\|value | Prob>\|t\| | Alpha | d |
|---|---|---|---|---|---|---|---|---|
| Gbn R. GBOBC2 b. F. | 73 | 74.69 | 1.67 | 156 | 44.76 | **6.34E-91** | 5.64E-04 | 11.52 |
| GBOBC1 b. R. GBOBC2 b. F. | 43 | 71.70 | 1.67 | 156 | 42.97 | **2.30E-88** | 5.70E-04 | 9.51 |
| GBOBC1 mb2 R. GBOBC2 b. F. | 52 | 63.22 | 1.67 | 156 | 37.89 | **1.41E-80** | 5.76E-04 | 9.90 |
| GBOBC2 b. R. GBOBC2 b. F. | 60 | 57.43 | 1.67 | 156 | 34.42 | **9.25E-75** | 5.83E-04 | 9.02 |
| Gbn R. GBOBC2 mb2 F. | 74 | 57.25 | 1.67 | 156 | 34.31 | **1.41E-74** | 5.89E-04 | 7.88 |
| GBOBC2 b. F. Gbn F. | 89 | -56.36 | 1.67 | 156 | 33.78 | **1.24E-73** | 5.96E-04 | 13.36 |
| Prime R. GBOBC2 b. F. | 10 | 56.20 | 1.67 | 156 | 33.68 | **1.80E-73** | 6.03E-04 | 4.91 |
| GBHCT R. GBOBC2 b. F. | 33 | 54.54 | 1.67 | 156 | 32.69 | **1.09E-71** | 6.10E-04 | 9.29 |
| GBOBC1 b. R. GBOBC2 mb2 F. | 44 | 54.27 | 1.67 | 156 | 32.52 | **2.17E-71** | 6.18E-04 | 8.95 |
| Gbn R. GBOBC1 b. F. | 71 | 47.81 | 1.67 | 156 | 28.65 | **4.96E-64** | 6.25E-04 | 9.64 |
| GBOBC1 mb2 R. GBOBC2 mb2 F. | 53 | 45.78 | 1.67 | 156 | 27.44 | **1.40E-61** | 6.33E-04 | 10.70 |
| GBOBC1 b. R. GBOBC1 b. F. | 41 | 44.82 | 1.67 | 156 | 26.86 | **2.16E-60** | 6.41E-04 | 8.89 |
| GBOBC2 mb2 R. GBOBC2 b. F. | 67 | 43.99 | 1.67 | 156 | 26.37 | **2.36E-59** | 6.49E-04 | 7.94 |
| GBOBC1 mb2 F. GBOBC2 b. F. | 85 | 41.31 | 1.67 | 156 | 24.76 | **6.62E-56** | 6.57E-04 | 5.14 |
| Gbn R. GBHCT F. | 70 | 40.11 | 1.67 | 156 | 24.04 | **2.49E-54** | 6.66E-04 | 6.61 |
| GBOBC2 b. R. GBOBC2 mb2 F. | 61 | 39.99 | 1.67 | 156 | 23.97 | **3.61E-54** | 6.75E-04 | 9.18 |
| GBOBC2 mb2 F. Gbn F. | 90 | -38.92 | 1.67 | 156 | 23.33 | **1.00E-52** | 6.84E-04 | 6.79 |
| Prime R. GBOBC2 mb2 F. | 11 | 38.77 | 1.67 | 156 | 23.23 | **1.61E-52** | 6.93E-04 | 3.61 |
| Prime F. GBOBC2 b. F. | 22 | 37.66 | 1.67 | 156 | 22.57 | **5.26E-51** | 7.02E-04 | 4.27 |
| GBOBC1 b. R. GBHCT F. | 40 | 37.13 | 1.67 | 156 | 22.25 | **2.90E-50** | 7.12E-04 | 6.31 |

| | | | | | | | | |
|---|---|---|---|---|---|---|---|---|
| GBHCT R. GBOBC2 mb2 F. | 34 | 37.11 | 1.67 | 156 | 22.24 | **3.09E-50** | 7.22E-04 | 6.83 |
| Prime F. Gbn R. | 18 | -37.03 | 1.67 | 156 | 22.19 | **4.00E-50** | 7.32E-04 | 4.88 |
| GBOBC1 mb2 R. GBOBC1 b. F. | 50 | 36.34 | 1.67 | 156 | 21.78 | **3.70E-49** | 7.43E-04 | 8.89 |
| GBHCT F. GBOBC2 b. F. | 78 | 34.57 | 1.67 | 156 | 20.72 | **1.19E-46** | 7.54E-04 | 8.12 |
| Prime F. GBOBC1 b. R. | 14 | -34.04 | 1.67 | 156 | 20.40 | **7.07E-46** | 7.65E-04 | 4.71 |
| Gbn R. GBOBC1 mb2 F. | 72 | 33.38 | 1.67 | 156 | 20.01 | **6.41E-45** | 7.77E-04 | 4.13 |
| GBOBC2 mb2 R. Gbn R. | 63 | -30.70 | 1.67 | 156 | 18.40 | **6.41E-41** | 7.89E-04 | 12.27 |
| GBOBC2 b. R. GBOBC1 b. F. | 58 | 30.55 | 1.67 | 156 | 18.31 | **1.08E-40** | 8.01E-04 | 8.40 |
| GBOBC1 b. R. GBOBC1 mb2 F. | 42 | 30.39 | 1.67 | 156 | 18.22 | **1.85E-40** | 8.14E-04 | 5.36 |
| GBOBC1 b. F. Gbn F. | 84 | -29.47 | 1.67 | 156 | 17.66 | **4.71E-39** | 8.27E-04 | 8.73 |
| Prime R. GBOBC1 b. F. | 8 | 29.32 | 1.67 | 156 | 17.57 | **8.10E-39** | 8.41E-04 | 2.93 |
| GBOBC1 mb2 R. GBHCT F. | 49 | 28.64 | 1.67 | 156 | 17.17 | **9.06E-38** | 8.55E-04 | 6.34 |
| GBOBC1 b. R. GBOBC2 mb2 R. | 38 | 27.71 | 1.67 | 156 | 16.61 | **2.59E-36** | 8.69E-04 | 9.30 |
| GBHCT R. GBOBC1 b. F. | 31 | 27.66 | 1.67 | 156 | 16.58 | **3.09E-36** | 8.84E-04 | 7.00 |
| GBOBC1 b. F. GBOBC2 b. F. | 82 | 26.88 | 1.67 | 156 | 16.11 | **5.21E-35** | 8.99E-04 | 8.21 |
| GBOBC2 mb2 R. GBOBC2 mb2 F. | 68 | 26.56 | 1.67 | 156 | 15.92 | **1.70E-34** | 9.16E-04 | 5.00 |
| Prime F. GBOBC1 mb2 R. | 15 | -25.56 | 1.67 | 156 | 15.32 | **6.68E-33** | 9.32E-04 | 4.22 |
| GBOBC1 mb2 F. GBOBC2 mb2 F. | 86 | 23.87 | 1.67 | 156 | 14.31 | **3.42E-30** | 9.49E-04 | 6.62 |
| GBOBC2 b. R. GBHCT F. | 57 | 22.85 | 1.67 | 156 | 13.70 | **1.53E-28** | 9.67E-04 | 5.38 |
| GBOBC1 mb2 R. GBOBC1 mb2 F. | 51 | 21.91 | 1.67 | 156 | 13.13 | **5.28E-27** | 9.86E-04 | 4.89 |
| GBHCT F. Gbn F. | 80 | -21.78 | 1.67 | 156 | 13.05 | **8.59E-27** | 1.01E-03 | 4.54 |
| Prime R. GBHCT F. | 7 | 21.63 | 1.67 | 156 | 12.96 | **1.53E-26** | 1.03E-03 | 2.45 |
| Prime F. GBOBC2 mb2 F. | 23 | 20.23 | 1.67 | 156 | 12.12 | **2.99E-24** | 1.05E-03 | 2.58 |
| GBHCT R. Gbn R. | 29 | -20.15 | 1.67 | 156 | 12.07 | **4.04E-24** | 1.07E-03 | 4.86 |
| GBHCT R. GBHCT F. | 30 | 19.97 | 1.67 | 156 | 11.97 | **7.93E-24** | 1.09E-03 | 4.57 |
| Prime F. GBOBC2 b. R. | 16 | -19.77 | 1.67 | 156 | 11.85 | **1.70E-23** | 1.11E-03 | 2.80 |
| GBOBC1 mb2 R. GBOBC2 mb2 R. | 47 | 19.23 | 1.67 | 156 | 11.52 | **1.29E-22** | 1.14E-03 | 6.81 |
| Prime F. Gbn F. | 24 | -18.69 | 1.67 | 156 | 11.20 | **9.54E-22** | 1.17E-03 | 2.31 |
| Prime R. Prime F. | 0 | 18.54 | 1.67 | 156 | 11.11 | **1.69E-21** | 1.19E-03 | 4.10 |
| Prime R. Gbn R. | 6 | -18.49 | 1.67 | 156 | 11.08 | **2.07E-21** | 1.22E-03 | 2.23 |
| Gbn R. Gbn F. | 75 | 18.33 | 1.67 | 156 | 10.99 | **3.67E-21** | 1.25E-03 | 4.64 |
| GBOBC2 b. F. GBOBC2 mb2 F. | 88 | -17.44 | 1.67 | 156 | 10.45 | **1.05E-19** | 1.28E-03 | 3.45 |
| GBOBC2 b. R. Gbn R. | 56 | -17.26 | 1.67 | 156 | 10.34 | **2.00E-19** | 1.31E-03 | 4.28 |
| GBHCT R. GBOBC1 b. R. | 25 | -17.16 | 1.67 | 156 | 10.28 | **2.91E-19** | 1.35E-03 | 4.97 |
| GBHCT F. GBOBC2 mb2 F. | 79 | 17.14 | 1.67 | 156 | 10.27 | **3.14E-19** | 1.39E-03 | 5.60 |
| GBOBC2 mb2 R. GBOBC1 b. F. | 65 | 17.11 | 1.67 | 156 | 10.25 | **3.49E-19** | 1.42E-03 | 4.85 |
| Prime F. GBHCT R. | 13 | -16.88 | 1.67 | 156 | 10.12 | **8.21E-19** | 1.46E-03 | 2.74 |
| GBOBC2 b. R. GBOBC1 mb2 F. | 59 | 16.12 | 1.67 | 156 | 9.66 | **1.34E-17** | 1.51E-03 | 3.67 |
| Prime R. GBOBC1 b. R. | 2 | -15.50 | 1.67 | 156 | 9.29 | **1.29E-16** | 1.55E-03 | 1.91 |
| GBOBC1 b. R. Gbn F. | 45 | 15.35 | 1.67 | 156 | 9.20 | **2.25E-16** | 1.60E-03 | 2.86 |
| GBOBC1 mb2 F. Gbn F. | 87 | -15.05 | 1.67 | 156 | 9.02 | **6.55E-16** | 1.65E-03 | 3.04 |
| Prime R. GBOBC1 mb2 F. | 9 | 14.90 | 1.67 | 156 | 8.93 | **1.13E-15** | 1.71E-03 | 1.51 |
| GBOBC1 b. F. GBOBC1 mb2 F. | 81 | -14.43 | 1.67 | 156 | 8.65 | **6.07E-15** | 1.77E-03 | 2.61 |

| | | | | | | | | |
|---|---|---|---|---|---|---|---|---|
| GBOBC1 b. R. GBOBC2 b. R. | 37 | 14.27 | 1.67 | 156 | 8.55 | **1.04E-14** | 1.83E-03 | 6.78 |
| GBOBC2 b. R. GBOBC2 mb2 R. | 55 | 13.44 | 1.67 | 156 | 8.05 | **1.95E-13** | 1.90E-03 | 5.42 |
| GBHCT R. GBOBC1 mb2 F. | 32 | 13.24 | 1.67 | 156 | 7.93 | **3.90E-13** | 1.97E-03 | 3.04 |
| GBOBC2 mb2 R. Gbn F. | 69 | -12.36 | 1.67 | 156 | 7.41 | **7.48E-12** | 2.05E-03 | 3.01 |
| Prime R. GBOBC2 mb2 R. | 5 | 12.21 | 1.67 | 156 | 7.32 | **1.25E-11** | 2.13E-03 | 2.02 |
| GBOBC1 mb2 R. Gbn R. | 48 | -11.47 | 1.67 | 156 | 6.88 | **1.40E-10** | 2.23E-03 | 2.67 |
| Prime F. GBOBC1 b. F. | 20 | 10.78 | 1.67 | 156 | 6.46 | **1.26E-09** | 2.33E-03 | 1.86 |
| GBHCT R. GBOBC2 mb2 R. | 28 | 10.55 | 1.67 | 156 | 6.32 | **2.58E-09** | 2.44E-03 | 4.37 |
| GBOBC1 b. F. GBOBC2 mb2 F. | 83 | 9.45 | 1.67 | 156 | 5.66 | **7.03E-08** | 2.56E-03 | 2.70 |
| GBOBC2 mb2 R. GBHCT F. | 64 | 9.42 | 1.67 | 156 | 5.64 | **7.63E-08** | 2.70E-03 | 2.32 |
| GBHCT R. GBOBC1 mb2 R. | 26 | -8.68 | 1.67 | 156 | 5.20 | **6.19E-07** | 2.85E-03 | 2.45 |
| GBOBC1 b. R. GBOBC1 mb2 R. | 36 | 8.48 | 1.67 | 156 | 5.08 | **1.04E-06** | 3.01E-03 | 3.28 |
| GBHCT F. GBOBC1 b. F. | 76 | 7.69 | 1.67 | 156 | 4.61 | **8.31E-06** | 3.20E-03 | 2.70 |
| Prime R. GBOBC1 mb2 R. | 3 | -7.01 | 1.67 | 156 | 4.20 | **4.40E-05** | 3.41E-03 | 1.32 |
| GBOBC1 mb2 R. Gbn F. | 54 | 6.86 | 1.67 | 156 | 4.11 | **6.32E-05** | 3.66E-03 | 1.40 |
| GBHCT F. GBOBC1 mb2 F. | 77 | -6.73 | 1.67 | 156 | 4.04 | **8.53E-05** | 3.94E-03 | 1.28 |
| Prime F. GBOBC2 mb2 R. | 17 | -6.33 | 1.67 | 156 | 3.79 | **2.12E-04** | 4.27E-03 | 1.10 |
| GBOBC1 mb2 R. GBOBC2 b. R. | 46 | 5.79 | 1.67 | 156 | 3.47 | **6.74E-04** | 4.65E-03 | 3.36 |
| Prime F. GBOBC1 mb2 F. | 21 | -3.64 | 1.67 | 156 | 2.18 | 3.04E-02 | 5.12E-03 | 1.34 |
| Prime F. GBHCT F. | 19 | 3.09 | 1.67 | 156 | 1.85 | 6.61E-02 | 0.00E+00 | 1.45 |
| GBOBC1 b. R. Gbn R. | 39 | -2.99 | 1.67 | 156 | 1.79 | 7.53E-02 | 0.00E+00 | 2.20 |
| GBHCT R. GBOBC2 b. R. | 27 | -2.89 | 1.67 | 156 | 1.73 | 8.57E-02 | 0.00E+00 | 1.51 |
| GBOBC2 mb2 R. GBOBC1 mb2 F. | 66 | 2.68 | 1.67 | 156 | 1.61 | 1.10E-01 | 0.00E+00 | 1.38 |
| GBHCT R. Gbn F. | 35 | -1.81 | 1.67 | 156 | 1.09 | 2.79E-01 | 0.00E+00 | 1.32 |
| Prime R. GBHCT R. | 1 | 1.66 | 1.67 | 156 | 1.00 | 3.21E-01 | 0.00E+00 | 1.14 |
| Prime R. GBOBC2 b. R. | 4 | -1.23 | 1.67 | 156 | 0.73 | 4.64E-01 | 0.00E+00 | 1.21 |
| GBOBC2 b. R. Gbn F. | 62 | 1.07 | 1.67 | 156 | 0.64 | 5.21E-01 | 0.00E+00 | 1.35 |
| Prime R. Gbn F. | 12 | -0.15 | 1.67 | 156 | 0.09 | 9.27E-01 | 0.00E+00 | 1.37 |

# Appendix C

# Application of Rigorous Free Energy methods

## Introduction

Rigorous free energy methodology (Thermodynamic Integration) is applied on two systems (Thrombin and HIV-1 Protease). The results are presented in a brief and concise manner. Setup of simulations is described in the next section.

Due to time constraints complete analysis and further investigations of results was not possible. The purpose of this appendix entry, is only to highlight some of the challenges with using rigorous free energy methodology for going from one docked pose to another. Although the majority of the docked poses for each ligands (when morphing for example from ligand A to ligand B) showed a good overlap, it was proven a difficult task to morph one ligand to another for which the initial structure differed (commonly the coordinates of ligand A and B are the same and only the groups that are different are altered). In addition, if time allowed we could have attempted intermediate perturbations, which would in theory give more accurate results.

## System setup and simulation protocols

In the present study the relative binding free energies ($\Delta\Delta$G) are calculated only for the Thrombin and HIV-1 Protease datasets; this was done due to time constraints. The reason those two datasets were chosen was based on their performance with experiment; the first performed overall poorly across the majority of the rescoring protocols, while, in contrast, the latter showed a descent performance. To obtain $\Delta\Delta$G for a protein-ligand system, two free energy calculations are required: (a) the perturbation of ligand 1 to ligand 2 alone in solution (free), and (b) morphing ligand 1 to 2 including the protein in the solvent (bound). Then $\Delta\Delta$G is calculated using the equation below.

$$\Delta\Delta G_{bind} = \Delta G_{lig2} - \Delta G_{lig1} = \Delta G_{bound} - \Delta G_{free} \tag{C.1}$$

The same protein structures as in previous chapters, with PDB codes 1ETT (resolution = 2.50 Å) and 2PQZ (resolution = 1.55 Å), were used for Thrombin and HIV-1 Protease, respectively. The inhibitors with their experimental affinities for each system can be seen in Chapter 4. All system setup information is described in section 6.2. The structures obtained following the 5000 step (1000 steps steepest descent and 4000 steps conjugate gradient) flexible protein minimisation, described in section 6.2, were used as the starting structures to construct the free energy protocols. Again, due to time constraints, free energy calculations were conducted on one of the three sets of poses (docking jobs). Considering HIV-1 Protease only consisted of docking job 2 poses, for consistency, the same set of poses (job 2) was chosen for the Thrombin dataset.

A protein scoop was generated by removal of all residues outside a radius of 24 Å from any heavy atom of the ligand (ligand 1 for Thrombin and ligand 12 for HIV-1 Protease). The bound (protein scoop and ligand) system was then solvated with a 32 Å sphere of TIP4P waters centred on the ligand. The unbound (ligand only) system was immersed in a similar sphere of water

molecules (20 Å). Crystallographic waters were converted into TIP4P waters and inserted in the solvated bound and unbound systems.

All sampling was performed using ProtoMS 2.3. Prior to simulations Grand Canonical Monte Carlo (GCMC) was applied to identify if any waters near the binding site needed adding or removing. A box was constructed to define the binding site where water molecules inserted, deleted, and translated. The box dimensions were 18.11 X 11.78 X 19.91 Å for Thrombin and 15.71 X 13.38 X 13.34 Å for HIV-1 Protease. Solute moves, insertion, deletion moves were performed in a ratio of 1-3-3. Backbone flexibility was only allowed for a radius of 12 Å around the geometric centre of the ligand. Normally GCMC is run at a range of B factors (defined by equation (C.2)) values which are used to make a free energy titration plot. The value of B can be related to the binding free energy using equation (C.3). Herein we are interested as to whether a certain water molecule is observed or not, and therefore simulations were run at the value of B factor that the free energy of binding of water is zero. Therefore setting in equation equation (C.3) $\Delta G_{bind}$ equal to zero the desired B factor with which the GCMC simulations are run is obtained. Each system was run for 40 million moves. Following visualisation of the results it was decided to remove one crystallographic water molecule from the Thrombin binding site and add a water molecule in the HIV-1 Protease binding site.

$$B = \frac{\mu_{ex}}{k_B T} + ln\bar{\rho}V \tag{C.2}$$

Where T is temperature, $k_B$ is the Boltzmann constant, $\mu_{ex}$ is the excess chemical potential, $\bar{\rho}$ is the number density of water in bulk (equal to 0.0334), and V the simulation volume (the volume of the box).

$$\Delta G_{bind} = -\Delta G_{hyd} + k_B T(B - ln\bar{\rho}V) \tag{C.3}$$

Where $\Delta G_{hyd}$ is the hydration free energy of water (equal to -6.4 kcal mol$^{-1}$).

Replica exchange thermodynamic integration (RETI)[48] was the method of choice for calculating the free energies of binding. Both single and dual topology methods were utilised. The latter was used whenever the first was not applicable, i.e. whenever a large mutation was needed. The entire backbone was kept rigid, however the sidechains of any residue within a radius of 12 Å of the centre of the ligand was sampled. Bond angles and torsion angles were sampled for the flexible side chains and the solute, while the solute and solvent were also allowed to make rotations and translations. All simulations were run with a 10 Å residue-based cutoff, a feather of 0.5 Å, and the solvent was constrained with a half-harmonic potential of 1.5 kcal mol$^{-1}$ Å$^{-1}$ applied to water molecules moving beyond 32 Å from the centre of the ligand. The simulations were performed at a temperature of 300 K. In the bound state, solute moves were attempted with a probability of 1.43%, protein side-chain moves with a probability of 12.86%, and solvent moves with a probability of 85.71%. In the unbound state, solute moves were attempted 1.64% of the time. Preferential sampling was switched on enabling solvent molecules close to the ligand to move more frequently. Bonds to dummy atoms were given a minimum length of 0.2 Å.

RETI calculations were run with 16 equally spaced lamda windows (0.00, 0.06, 0.12, 0.19, 0.26, 0.33, 0.40, 0.47, 0.54, 0.61, 0.68, 0.75, 0.82, 0.88, 0.94, 1.00), and equilibrated for 10 M moves before collecting data for 40 M moves. A replica exchange was attempted every 200000 moves. Repeats were run until the standard error was below 1 kcal mol$^{-1}$. A maximum of 16 repeats were required for Thrombin bound state of the perturbation of ligand 6 to 7 using dual topology, and 13 for HIV-1 Protease bound state of perturbing ligand 4 to 1, again using dual topology.

# Results

## *Thrombin*

Table C.1 shows RETI results of the protein-ligand ($\Delta G_{bound}$) and ligand in solvent ($\Delta G_{free}$) free energy changes which give relative binding free energy changes ($\Delta\Delta G_{bind}$). For comparison the experimental (Exp) free energies for the attempted mutations are shown. Reported errors are standard errors over a number of repeats.

Table C.1: Comparison between experimental and calculated relative binding free energies using the RETI methodology[α]

| Pert | Exp | $\Delta\Delta G_{bind}$ | $\Delta G_{bound}$ | $\Delta G_{free}$ |
|---|---|---|---|---|
| 1t2 | -0.08 | 9.03 ± 0.73 | 11.81 ± 0.45 | 2.78 ± 0.57 |
| 1t3 | -2.11 | 16.23 ± 1.13 | 14.86 ± 0.96 | -1.37 ± 0.59 |
| 2t3 | -2.03 | 4.89 ± 0.78 | 1.17 ± 0.60 | -3.73 ± 0.50 |
| 4t5 | -3.23 | -3.76 ± 0.85 | -4.57 ± 0.77 | -0.71 ± 0.35 |
| 5t6 | 2.94 | -3.33 ± 0.92 | -0.71 ± 0.86 | 2.61 ± 0.32 |
| 5t8 | -1.91 | 14.34 ± 0.73 | 16.73 ± 0.60 | 2.39 ± 0.41 |
| 5t9 | 1.18 | -6.36 ± 0.96 | -5.43 ± 0.83 | 0.94 ± 0.49 |
| 5t10 | 1.67 | -12.44 ± 1.02 | -11.83 ± 0.87 | 0.62 ± 0.53 |
| 5t12 | -0.77 | 12.75 ± 0.84 | 14.40 ± 0.70 | 1.66 ± 0.47 |
| 6t7 | 1.84 | 26.19 ± 1.24 | 17.17 ± 0.92 | -9.02 ± 0.82 |
| 6t9 | -1.76 | -3.23 ± 1.10 | -4.86 ± 0.91 | -1.63 ± 0.62 |
| 9t8 | -3.09 | 19.00 ± 1.07 | 21.36 ± 0.93 | 2.37 ± 0.53 |
| 9t11 | -2.61 | 22.35 ± 0.94 | 20.81 ± 0.76 | -1.54 ± 0.55 |

[α] Measurements in kcal $mol^{-1}$. Pert describes the mutation of one ligand to another. $\Delta\Delta G_{bind}$ the relative binding free energy. $\Delta G_{bound}$ is the free energy difference of the ligand bound to the protein. $\Delta G_{free}$ is the free energy difference in the aqueous environment.
[β] Experimental free energies are calculated using the following formula: $\Delta\Delta G = \Delta G_2 - \Delta G_1 = RT \ln(K_1/K_2)$.

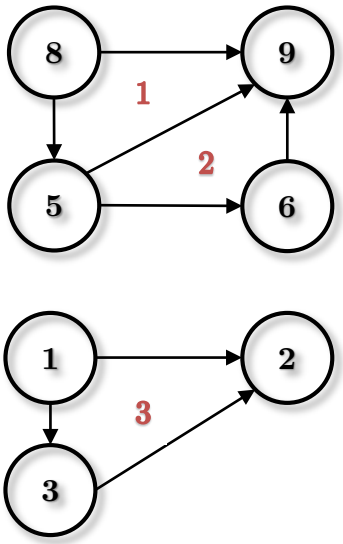


Figure C.1: Closure of thermodynamic pathways for calculation of hysteresis. Numbers in black represent ligands and in red cycle numbers.

Table C.2: Hysteresis of three thermodynamic cycles for bound ($hyst_{bound}$) and free ($hyst_{free}$) legs and the binding free energy ($hyst_{bind}$). Values shown in kcal $mol^{-1}$.

| Cycle | $hyst_{bind}$ | $hyst_{bound}$ | $hyst_{free}$ |
|---|---|---|---|
| 1 (8,9,5) | 1.71 ± 1.61 | 0.79 ± 1.38 | -0.91 ± 0.83 |
| 2 (5,9,6) | 0.20 ± 1.73 | 0.15 ± 1.50 | -0.05 ± 0.85 |
| 3 (1,2,3) | -2.31 ± 1.59 | -1.89 ± 1.22 | 0.42 ± 0.96 |

The statistical uncertainty for our calculations is shown in Table C.2. The thermodynamic cycles for which the hysteresis was calculated is shown in Figure C.1. From Table C.2 we can see that although some of the values are low, overall the statistical uncertainty of our calculations is high.

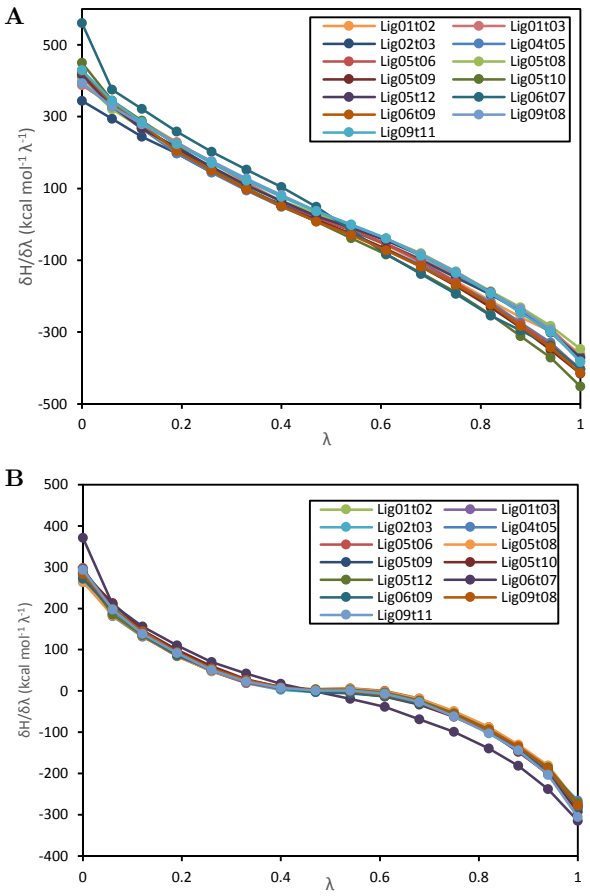


Figure C.2: Free energy gradients for all perturbations for the "bound" (A) and "free" (B) state.

Free energy gradients for our calculations are shown in Figure C.2. From this we can see that they are all smooth, however they are large. This means that even small changes, in particular in the first and last lamda values, can have a large effect in the overall calculated binding affinity.

### *HIV-1 Protease*

Table C.3 shows RETI results of the protein-ligand ($\Delta G_{bound}$) and ligand in solvent ($\Delta G_{free}$) free energy changes which give relative binding free energy changes ($\Delta\Delta G_{bind}$). For comparison the experimental (Exp) free energies for the attempted mutations are shown. Reported errors are standard errors over a number of repeats.

Table C.3: Comparison between experimental and calculated relative binding free energies using the RETI methodology[α]

| Pert | Exp | $\Delta\Delta G_{bind}$ | $\Delta G_{bound}$ | $\Delta G_{free}$ |
|---|---|---|---|---|
| 4t5 | -0.92 | 2.55 ± 0.21 | -2.28 ± 0.18 | -4.83 ± 0.09 |
| 5t6 | -010 | -1.04 ± 0.13 | -1.06 ± 0.13 | -0.02 ± 0.04 |
| 7t4 | 0.59 | -6.78 ± 0.54 | -25.37 ± 0.42 | -18.59 ± 0.35 |
| 8t4 | 0.69 | -6.06 ± 0.25 | 19.35 ± 0.23 | 25.41 ± 0.11 |
| 12t11 | 0.77 | -4.49 ± 0.67 | -28.19 ± 0.51 | -23.70 ± 0.44 |
| 13t4 | 1.24 | -1.77 ± 0.17 | 156.08 ± 0.16 | 157.86 ± 0.07 |
| 13t10 | 1.11 | -1.32 ± 0.39 | 190.43 ± 0.32 | 191.76 ± 0.21 |
| 7t6 | -0.43 | -1.20 ± 0.46 | -25.99 ± 0.40 | -24.79 ± 0.23 |
| 4t10 | -0.12 | 6.43 ± 0.53 | 39.51 ± 0.44 | 33.09 ± 0.29 |
| 02t01* | -1.07 | 32.30 ± 1.08 | 22.69 ± 0.91 | -9.61 ± 0.58 |
| 03t01* | 1.22 | 39.51 ± 1.25 | 26.89 ± 0.92 | -12.63 ± 0.85 |
| 04t01* | 1.04 | 36.07 ± 1.22 | 23.37 ± 0.99 | -12.71 ± 0.71 |
| 11t04* | 1.26 | 34.90 ± 1.26 | 10.46 ± 0.94 | -24.44 ± 0.83 |
| 03t04* | 0.18 | 6.89 ± 1.13 | 4.52 ± 0.90 | -2.37 ± 0.67 |
| 02t04* | -2.11 | -2.28 ± 0.88 | 2.36 ± 0.85 | 4.63 ± 0.22 |

[α] Measurements in kcal $mol^{-1}$. Pert describes the mutation of one ligand to another. $\Delta\Delta G_{bind}$ the relative binding free energy. $\Delta G_{bound}$ is the free energy difference of the ligand bound to the protein. $\Delta G_{free}$ is the free energy difference in the aqueous environment.

[β] Experimental free energies are calculated using the following formula: $\Delta\Delta G = \Delta G_2 - \Delta G_1 = RT \ln(K_1/K_2)$.

[*] Calculations run using dual topology; all other calculations using single topology

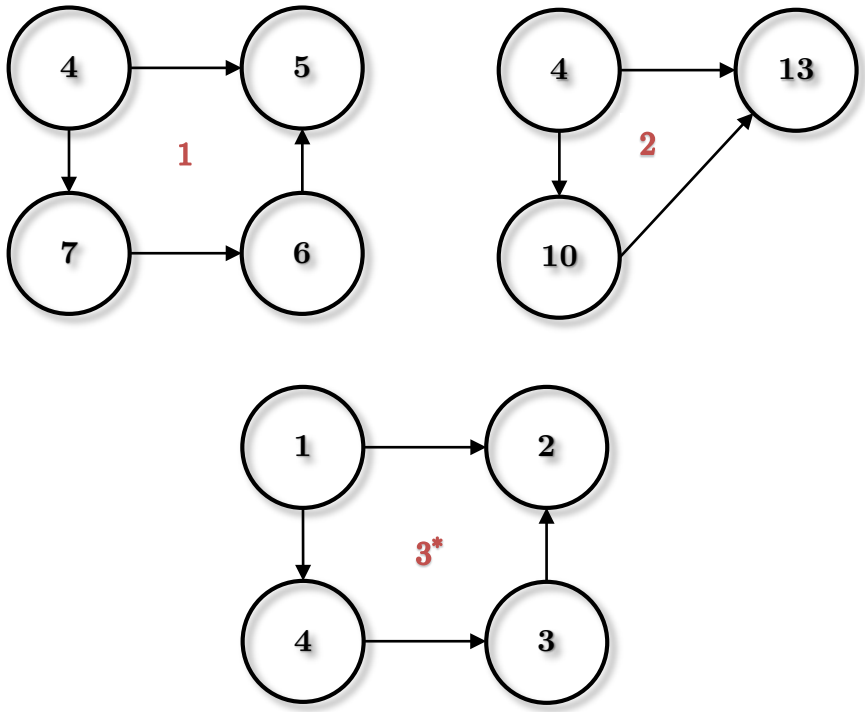


Figure C.3: Closure of thermodynamic pathways for calculation of hysteresis. Numbers in black represent ligands and in red cycle numbers. Asterisk (*) shows cycle from dual topology perturbations. All other perturbations were made using single the topology method.

Table C.4: Hysteresis of three thermodynamic cycles for bound ($hyst_{bound}$) and free ($hyst_{free}$) legs and the binding free energy ($hyst_{bind}$). Values shown in kcal $mol^{-1}$. Asterisk for dual topology calculations.

| Cycle | $hyst_{bind}$ | $hyst_{bound}$ | $hyst_{free}$ |
|---|---|---|---|
| 1 (4,5,6,7) | -4.07 ± 0.75 | -2.72 ± 0.62 | 1.35 ± 0.43 |
| 2 (4,13,10) | -5.97± 0.68 | -5.16 ± 0.57 | 0.81 ± 0.36 |
| 3 (1,2,4,3) | -1.95± 2.19 | 2.03 ± 1.79 | 3.99 ± 1.25 |

Similarly as in Thrombin the hysteris here were large. This is an indication there are large sources of error in our calculations for which further investigation is required to ascertain their origin.

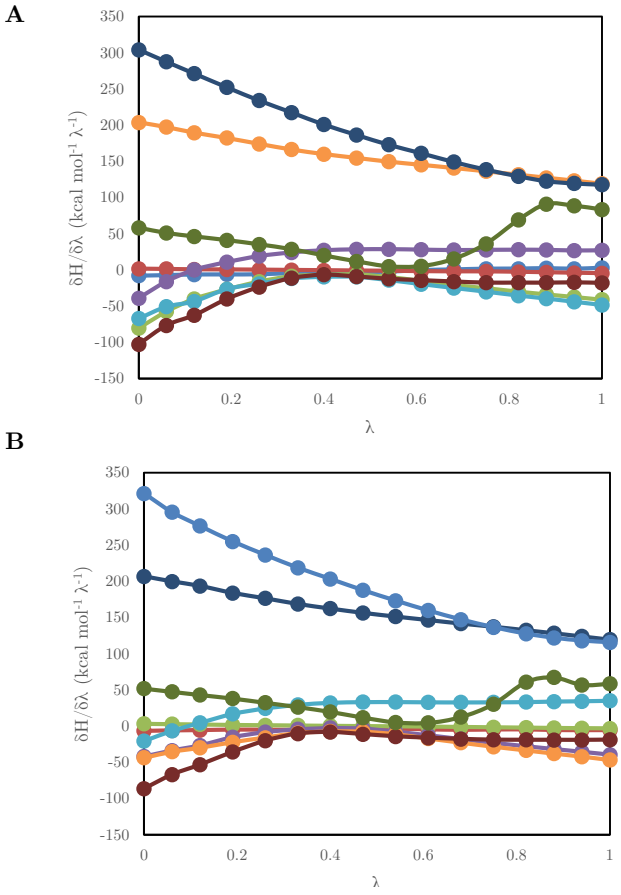


Figure C.4: Free energy gradients for all perturbations for the "bound" (A) and "free" (B) state for single topology simulations.

Figures C.4 and C.5 show the free energy gradients for the single and dual topology calculations. Gradients appear again smooth, however large. Different softcore implementations were tested, however the gradients were always high. Reasons for this could come from the different ligand poses i.e. different phase space occupied by each ligand, or that the perturbations attempted are too large. Unfortunately there was no time remaining to investigate the results further.

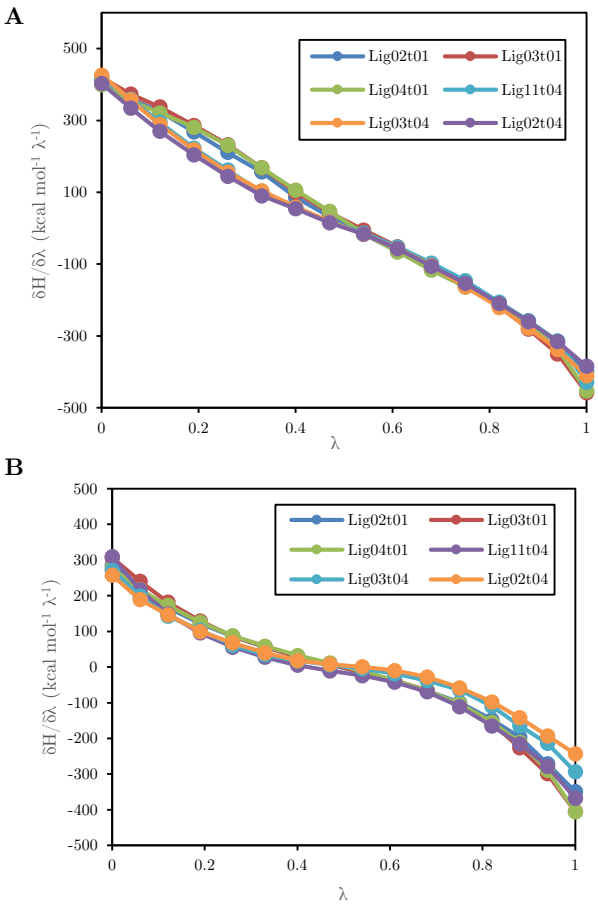


Figure C.5: Free energy gradients for all perturbations for the "bound" (A) and "free" (B) state for dual topology simulations.

# Bibliography


1. W. L. Jorgensen, *Science*, 2004, **303**, 1813-1818.

2. J. Drews, *Science*, 2000, **287**, 1960-1964.

3. M. K. Gilson and H. X. Zhou, *Annual Review of Biophysics and Biomolecular Structure*, 2007, **36**, 21-42.

4. H. Jhoti, *Structure-based Drug Discovery*, Springer, Dordrecht, 2007.

5. J. Michel, N. Foloppe and J. W. Essex, *Molecular Informatics*, 2010, **29**, 570-578.

6. I. Massova and P. A. Kollman, *Journal of the American Chemical Society*, 1999, **121**, 8133-8143.

7. P. A. Kollman, I. Massova, C. Reyes, B. Kuhn, S. H. Huo, L. Chong, M. Lee, T. Lee, Y. Duan, W. Wang, O. Donini, P. Cieplak, J. Srinivasan, D. A. Case and T. E. Cheatham, *Accounts of Chemical Research*, 2000, **33**, 889-897.

8. I. Massova and P. A. Kollman, *Perspectives in Drug Discovery and Design*, 2000, **18**, 113-135.

9. A. Suenaga, N. Okimoto, Y. Hirano and K. Fukui, *PLoS ONE*, 2012, **7**, e42846.

10. G. Rastelli, A. Del Rio, G. Degliesposti and M. Sgobba, *Journal of Computational Chemistry*, 2010, **31**, 797-810.

11. B. Kuhn, P. Gerber, T. Schulz-Gasch and M. Stahl, *Journal of Medicinal Chemistry*, 2005, **48**, 4040-4048.

12. R. C. Rizzo, S. Toba and I. D. Kuntz, *Journal of Medicinal Chemistry*, 2004, **47**, 3065-3074.

13. N. Huang, C. Kalyanaraman, K. Bernacki and M. Jacobson, *Physical Chemistry Chemical Physics*, 2006, **8**, 5166-5177.

14. N. Huang, C. Kalyanaraman, J. J. Irwin and M. P. Jacobson, *Journal of Chemical Information and Modeling*, 2006, **46**, 243-253.

15. C. R. W. Guimarães and M. Cardozo, *Journal of Chemical Information and Modeling*, 2008, **48**, 958-970.

16. B. Pearce, D. Langley, J. Kang, H. Huang and A. Kulkarni, *Journal of Chemical Information and Modeling*, 2009.

17. P. D. Lyne, M. L. Lamb and J. C. Saeh, *Journal of Medicinal Chemistry*, 2006, **49**, 4805-4808.

18. A. P. Graves, D. M. Shivakumar, S. E. Boyce, M. P. Jacobson, D. A. Case and B. K. Shoichet, *Journal of Molecular Biology*, 2008, **377**, 914-934.

19. A. M. Ferrari, G. Degliesposti, M. Sgobba and G. Rastelli, *Bioorganic & Medicinal Chemistry*, 2007, **15**, 7865-7877.

20. T. Hou, J. Wang, Y. Li and W. Wang, *Journal of Chemical Information and Modeling*, 2010, **51**, 69-82.

21. G. Degliesposti, C. Portioli, M. D. Parenti and G. Rastelli, *Journal of Biomolecular Screening*, 2011, **16**, 129-133.

22. X. Zhang, S. E. Wong and F. C. Lightstone, *Journal of Chemical Information and Modeling*, 2013, **54**, 324-337.

23. J. W. Gibbs, *Elementary prinsiples in statistical Mechanics*, Dover Publications inc., New York, USA, 1902.

24. W. J. Glazer M., *Statistical Mechanics: A survival guide*, Oxford University Press, 2001.

25. P. Atkins, *Physical Chemistry*, 8 edn., W. H. Freeman and Company, New York, NY, 2006.

26. R. Guha and R. Sardar, 2001.

27. W. L. Jorgensen and J. Tirado-Rives, *Journal of the American Chemical Society*, 1988, **110**, 1657-1666.

28. D. Case, T. Darden, T. Cheatham, C. Simmerling, J. Wang, R. Duke, R. Luo, M. Crowley, R. C. Walker and W. Zhang, *Amber 10*, University of California, 2008.

29. B. R. Brooks, R. E. Bruccoleri, B. D. Olafson, D. J. States, S. Swaminathan and M. Karplus, *Journal of Computational Chemistry*, 1983, **4**, 187-217.

30. A. R. Leach, *Molecular Modelling Modelling Principles and Applications*, Second Edition edn., Pearson Prentice Hall, 2001.

31. J. Wang, R. M. Wolf, J. W. Caldwell, P. A. Kollman and D. A. Case, *Journal of Computational Chemistry*, 2004, **25**, 1157-1174.

32. I. Muegge, *Journal of Medicinal Chemistry*, 2005, **49**, 5895-5902.

33. J.-P. Ryckaert, G. Ciccotti and H. J. C. Berendsen, *Journal of Computational Physics*, 1977, **23**, 327-341.

34. N. Metropilis, A. W. Rosenbluth, M. N. Rosenbluth, A. H. Teller and E. Teller, *J. HCem. Phys.*, 1953, **21**, 1087-1092.

35. J. Michel, University of Southampton, 2006.

36. R. D. Taylor, P. J. Jewsbury and J. W. Essex, *Journal of Computer-Aided Molecular Design*, 2002, **16**, 151-166.

37. D. B. Kitchen, H. Decornez, J. R. Furr and J. Bajorath, *Nature Reviews Drug Discovery*, 2004, **3**, 935-949.

38. B. Kramer, M. Rarey and T. Lengauer, *Proteins: Structure, Function, and Bioinformatics*, 1999, **37**, 228-241.

39. G. Jones, P. Willett, R. C. Glen, A. R. Leach and R. Taylor, *Journal of Molecular Biology*, 1997, **267**, 727-748.

40. G. M. Morris, D. S. Goodsell, R. S. Halliday, R. Huey, W. E. Hart, R. K. Belew and A. J. Olson, *Journal of Computational Chemistry*, 1998, **19**, 1639-1662.

41. M. Eldridge, C. Murray, T. Auton, G. Paolini and R. Mee, *Journal of Computer-Aided Molecular Design*, 1997, **11**, 425-445.

42. H. Gohlke, M. Hendlich and G. Klebe, *Journal of Molecular Biology*, 2000, **295**, 337-356.

43. P. S. Charifson, J. J. Corkery, M. A. Murcko and W. P. Walters, *Journal of Medicinal Chemistry*, 1999, **42**, 5100-5109.

44. J. C. Cole, C. W. Murray, J. W. M. Nissink, R. D. Taylor and R. Taylor, *Proteins-Structure Function and Bioinformatics*, 2005, **60**, 325-332.

45. D. A. Pearlman and P. S. Charifson, *Journal of Medicinal Chemistry*, 2001, **44**, 3417-3423.

46. G. L. Warren, C. W. Andrews, A. M. Capelli, B. Clarke, J. LaLonde, M. H. Lambert, M. Lindvall, N. Nevins, S. F. Semus, S. Senger, G. Tedesco, I. D. Wall, J. M. Woolven, C. E. Peishoff and M. S. Head, *Journal of Medicinal Chemistry*, 2006, **49**, 5912-5931.

47. R. W. Zwanzig, *The Journal of Chemical Physics*, 1954, **22**, 1420-1426.

48. C. J. Woods, J. W. Essex and M. A. King, *Journal of Physical Chemistry B*, 2003, **107**, 13711-13718.

49. C. J. Woods, J. W. Essex and M. A. King, *The Journal of Physical Chemistry B*, 2003, **107**, 13703-13710.

50. J. Åqvist, C. Medina and J.-E. Samuelsson, *Protein Engineering*, 1994, **7**, 385-391.

51. O. A. Adekoya, N. P. Willassen and I. Sylte, *Journal of Structural Biology*, 2006, **153**, 129-144.

52. J. Srinivasan, T. E. Cheatham, P. Cieplak, P. A. Kollman and D. A. Case, *Journal of the American Chemical Society*, 1998, **120**, 9401-9409.

53. J. Tomasi and M. Persico, *Chemical Reviews*, 1994, **94**, 2027-2094.

54. C. J. Cramer, *Essentials of Computational Chemistry - Theories and Models*, Second Edition edn., Wiley, 2004.

55. J. Warwicker and H. Watson, *Journal of Molecular Biology*, 1982, **157**, 671-679.

56. B. Honig and A. Nicholls, *SCIENCE-NEW YORK THEN WASHINGTON-*, 1995, 1144-1144.

57. M. Holst, R. E. Kozack, F. Saied and S. Subramaniam, *Proteins: Structure, Function, and Bioinformatics*, 1994, **18**, 231-245.

58. M. Born, *Zeitschrift für Physik A Hadrons and Nuclei*, 1920, **1**, 45-48.

59. J. D. Jackson, *Classical Electrodynamics*, Third Edition edn., Wiley, 1998.

60. W. C. Still, A. Tempczyk, R. C. Hawley and T. Hendrickson, *Journal of the American Chemical Society*, 1990, **112**, 6127-6129.

61. A. Onufriev, D. Bashford and D. A. Case, *Journal of Physical Chemistry B*, 2000, **104**, 3712-3720.

62. G. D. Hawkins, C. J. Cramer and D. G. Truhlar, *Chemical Physics Letters*, 1995, **246**, 122-129.

63. A. Onufriev, D. Bashford and D. A. Case, *Proteins: Structure, Function, and Bioinformatics*, 2004, **55**, 383-394.

64. D. Bashford and D. A. Case, *Annual Review of Physical Chemistry*, 2000, **51**, 129-152.

65. *SASA of a solute*, http://www.ccp4.ac.uk/html/images/areaimol_asurf.gif.

66. J. Srinivasan, T. E. Cheatham, P. Cieplak, P. A. Kollman and D. A. Case, *J Am Chem Soc*, 1998, **120**, 9401-9409.

67. N. Homeyer and H. Gohlke, *Molecular Informatics*, 2012, **31**, 114-122.

68. H. Gohlke and D. Case, *Journal of Computational Chemistry*, 2004, **25**, 238-250.

69. J. M. J. Swanson, R. H. Henchman and J. A. McCammon, *Biophysical Journal*, 2004, **86**, 67-74.

70. N. Singh and A. Warshel, *Proteins: Struct., Funct., Bioinf.*, 2010, **78**, 1705.

71. T. Hou, J. Wang, Y. Li and W. Wang, *Journal of Computational Chemistry*, 2011, **32**, 866-877.

72. A. Lindström, L. Edvinsson, A. Johansson, C. D. Andersson, I. E. Andersson, F. Raubacher and A. Linusson, *Journal of Chemical Information and Modeling*, 2011, **51**, 267-282.

73. J. Kongsted and U. Ryde, *Journal of Computer-Aided Molecular Design*, 2009, **23**, 63-71.

74. A. Weis, K. Katebzadeh, P. Soderhjelm, I. Nilsson and U. Ryde, *Journal of Medicinal Chemistry*, 2006, **49**, 6596-6606.

75. B. Kuhn and P. A. Kollman, *Journal of Medicinal Chemistry*, 2000, **43**, 3786-3791.

76. F. Fogolari, G. Esposito, P. Viglino and H. Molinari, *Journal of Computational Chemistry*, 2001, **22**, 1830-1842.

77. F. Fogolari, A. Brigo and H. Molinari, *Biophysical Journal*, 2003, **85**, 159-166.

78. Y. L. Wu, Z. J. Cao, H. Yi, D. H. Jiang, X. Mao, H. Liu and W. X. Li, *Biophysical Journal*, 2004, **87**, 105-112.

79. D. A. Pearlman, *Journal of Medicinal Chemistry*, 2005, **48**, 7796-7807.

80. N. Huang, C. Kalyanaraman, K. Bernacki and M. P. Jacobson, *Physical Chemistry Chemical Physics*, 2006, **8**, 5166-5177.

81. S. P. Brown and S. W. Muchmore, *Journal of Chemical Information and Modeling*, 2007, **47**, 1493-1503.

82. M. Jacobson, G. Kaminski, R. Friesner and C. Rapp, *Journal of Physical Chemistry B*, 2002, **106**, 11673-11680.

83. W. L. Jorgensen, D. S. Maxwell and J. Tirado-Rives, *Journal of the American Chemical Society*, 1996, **118**, 11225-11236.

84. K. Zhu, M. R. Shirts, R. A. Friesner and M. P. Jacobson, *Journal of Chemical Theory and Computation*, 2007, **3**, 640-648.

85. G. Rastelli, G. Degliesposti, A. Del Rio and M. Sgobba, *Chemical Biology & Drug Design*, 2009, **73**, 283-286.

86. W. Rocchia, E. Alexov and B. Honig, *The Journal of Physical Chemistry B*, 2001, **105**, 6507-6514.

87. D. A. Case, T. E. Cheatham, T. Darden, H. Gohlke, R. Luo, K. M. Merz, A. Onufriev, C. Simmerling, B. Wang and R. J. Woods, *Journal of Computational Chemistry*, 2005, **26**, 1668-1688.

88. MacroModel, in *Schrodinger, Inc*, New York, NY, 2005.

89. S. P. Brown and S. W. Muchmore, *Journal of Chemical Information and Modeling*, 2006, **46**, 999-1005.

90. S. P. Brown and S. W. Muchmore, *Journal of Medicinal Chemistry*, 2009, **52**, 3159-3165.

91. *OpenEye Scientific Software*, http://www.eyesopen.com/.

92. J. A. Grant, B. T. Pickup and A. Nicholls, *Journal of Computational Chemistry*, 2001, **22**, 608-640.

93. Y. Li, Z. Liu and R. Wang, *Journal of Chemical Information and Modeling*, 2010, **50**, 1682-1692.

94. W. D. Cornell, P. Cieplak, C. I. Bayly, I. R. Gould, K. M. Merz, D. M. Ferguson, D. C. Spellmeyer, T. Fox, J. W. Caldwell and P. A. Kollman, *Journal of the American Chemical Society*, 1995, **117**, 5179-5197.

95. J. Wang, P. Cieplak and P. A. Kollman, *Journal of Computational Chemistry*, 2000, **21**, 1049-1074.

96. Y. Duan, C. Wu, S. Chowdhury, M. C. Lee, G. Xiong, W. Zhang, R. Yang, P. Cieplak, R. Luo, T. Lee, J. Caldwell, J. Wang and P. Kollman, *Journal of Computational Chemistry*, 2003, **24**, 1999-2012.

97. P. Cieplak, J. Caldwell and P. Kollman, *Journal of Computational Chemistry*, 2001, **22**, 1048-1057.

98. J. M. Wang, P. Morin, W. Wang and P. A. Kollman, *Journal of the American Chemical Society*, 2001, **123**, 5221-5230.

99. T. Yang, J. C. Wu, C. Yan, Y. Wang, R. Luo, M. B. Gonzales, K. N. Dalby and P. Ren, *Proteins: Structure, Function, and Bioinformatics*, 2011, n/a-n/a.

100. I. Stoica, S. K. Sadiq and P. V. Coveney, *Journal of the American Chemical Society*, 2008, **130**, 2639-2648.

101. S. Genheden and U. Ryde, *Journal of Computational Chemistry*, 2010, **31**, 837-846.

102. N. Huang and M. P. Jacobson, *Current Opinion in Drug Discovery & Development*, 2007, **10**, 325-331.

103. M. Feher and C. I. Williams, *Journal of Chemical Information and Modeling*, 2012.

104. K. Hilpert, J. Ackermann, D. W. Banner, A. Gast, K. Gubernator, P. Hadváry, L. Labler, K. Müller, G. Schmid, T. B. Tschopp and H. Van De Waterbeemd, *Journal of Medicinal Chemistry*, 1994, **37**, 3889-3901.

105. W. Bode, *Blood Cells, Molecules, and Diseases*, 2006, **36**, 122-130.

106. WHO, *Global update on the health sector response to HIV*, Geneva, Switzerland, 2014.

107. E. Di Cera, *Molecular Aspects of Medicine*, 2008, **29**, 203-254.

108. H. Brandstetter, D. Turk, H. W. Hoeffken, D. Grosse, J. Stürzebecher, P. D. Martin, B. F. P. Edwards and W. Bode, *Journal of Molecular Biology*, 1992, **226**, 1085-1099.

109. Maestro, in *Schrodinger, Inc*, New York, NY, version 9.3.5 edn., 2012.

110. *Alzheimer's & Dementia*, 2013, **9**, 208-245.

111. S. Cole and R. Vassar, *Molecular Neurodegeneration*, 2007, **2**, 22.

112. S. J. Stachel, C. A. Coburn, T. G. Steele, K. G. Jones, E. F. Loutzenhiser, A. R. Gregro, H. A. Rajapakse, M.-T. Lai, M.-C. Crouthamel, M. Xu, K. Tugusheva, J. E. Lineberger, B. L. Pietrak, A. S. Espeseth, X.-P. Shi, E. Chen-Dodson, M. K. Holloway, S. Munshi, A. J. Simon, L. Kuo and J. P. Vacca, *Journal of Medicinal Chemistry*, 2004, **47**, 6447-6450.

113. A. K. Ghosh, N. Kumaragurubaran, L. Hong, S. S. Kulkarni, X. Xu, W. Chang, V. Weerasena, R. Turner, G. Koelsch, G. Bilcer and J. Tang, *Journal of Medicinal Chemistry*, 2007, **50**, 2399-2407.

114. M. Adler, D. D. Davey, G. B. Phillips, S.-H. Kim, J. Jancarik, G. Rumennik, D. R. Light and M. Whitlow, *Biochemistry*, 2000, **39**, 12534-12542.

115. H. Matter, E. Defossa, U. Heinelt, P.-M. Blohm, D. Schneider, A. Müller, S. Herok, H. Schreuder, A. Liesum, V. Brachvogel, P. Lönze, A. Walser, F. Al-Obeidi and P. Wildgoose, *Journal of Medicinal Chemistry*, 2002, **45**, 2749-2769.

116. S. Maignan, J.-P. Guilloteau, S. Pouzieux, Y. M. Choi-Sledeski, M. R. Becker, S. I. Klein, W. R. Ewing, H. W. Pauls, A. P. Spada and V. Mikol, *Journal of Medicinal Chemistry*, 2000, **43**, 3226-3232.

117. H. Nar, *Trends in Pharmacological Sciences*, 2012, **33**, 279-288.

118. G. Phillips, W. J. Guilford, B. O. Buckman, D. D. Davey, K. A. Eagen, S. Koovakkat, A. Liang, M. McCarrick, R. Mohan, H. P. Ng, M. Pinkerton, B. Subramanyam, E. Ho, L. Trinh, M. Whitlow, S. Wu, W. Xu and M. M. Morrissey, *Journal of Medicinal Chemistry*, 2002, **45**, 2484-2493.

119. C. Flexner, *Nat Rev Drug Discov*, 2007, **6**, 959-966.

120. A. Engelman and P. Cherepanov, *Nat Rev Micro*, 2012, **10**, 279-290.

121. P. Czodrowski, C. A. Sotriffer and G. Klebe, *Journal of Chemical Information and Modeling*, 2007, **47**, 1590-1598.

122. A. Blum, J. Bottcher, A. Heine, G. Klebe and W. E. Diederich, *Journal of Medicinal Chemistry*, 2008, **51**, 2078-2087.

123. S. R. Hubbard and J. H. Till, *Annual Review of Biochemistry*, 2000, **69**, 373-398.

124. J. Summy and G. Gallick, *Cancer Metastasis Rev*, 2003, **22**, 337-358.

125. D. Dalgarno, T. Stehle, S. Narula, P. Schelling, M. R. van Schravendijk, S. Adams, L. Andrade, J. Keats, M. Ram, L. Jin, T. Grossman, I. MacNeil, C. Metcalf, W. Shakespeare, Y. Wang, T. Keenan, R. Sundaramoorthi, R. Bohacek, M. Weigele and T. Sawyer, *Chemical Biology & Drug Design*, 2006, **67**, 46-57.

126. W. Xu, A. Doshi, M. Lei, M. J. Eck and S. C. Harrison, *Molecular Cell*, 1999, **3**, 629-638.

127. *Pipeline Pilot*, http://accelrys.com/products/pipeline-pilot/.

128. *Symyx*, http://www.symyx.com.

129. F. Milletti, L. Storchi, G. Sforna and G. Cruciani, *Journal of Chemical Information and Modeling*, 2007, **47**, 2172-2181.

130. G. S. Wu, D. H. Robertson, C. L. Brooks and M. Vieth, *Journal of Computational Chemistry*, 2003, **24**, 1549-1562.

131. F. Momany and R. Rone, *Journal of Computational Chemistry*, 1992, **13**, 888-900.

132. M. Feig, A. Onufriev, M. S. Lee, W. Im, D. A. Case and C. L. Brooks, *Journal of Computational Chemistry*, 2004, **25**, 265-284.

133. B. A. Tounge, R. Rajamani, E. W. Baxter, A. B. Reitz and C. H. Reynolds, *Journal of Molecular Graphics and Modelling*, 2006, **24**, 475-484.

134. C. R. W. Guimaraes and M. Cardozo, *Journal of Chemical Information and Modeling*, 2008, **48**, 958-970.

135. SchrodingerSuite, in *Schrodinger, Inc*, New York, NY, 2010.

136. Prime, in *Schrodinger, Inc*, New York, NY, 2010.

137. LigPrep, in *Schrodinger, Inc*, New York, NY, version 2.4 edn., 2010.

138. R. A. Friesner, J. L. Banks, R. B. Murphy, T. A. Halgren, J. J. Klicic, D. T. Mainz, M. P. Repasky, E. H. Knoll, M. Shelley, J. K. Perry, D. E. Shaw, P. Francis and P. S. Shenkin, *Journal of Medicinal Chemistry*, 2004, **47**, 1739-1749.

139. R. A. Friesner, R. B. Murphy, M. P. Repasky, L. L. Frye, J. R. Greenwood, T. A. Halgren, P. C. Sanschagrin and D. T. Mainz, *Journal of Medicinal Chemistry*, 2006, **49**, 6177-6196.

140. A. Ghosh, C. S. Rapp and R. A. Friesner, *The Journal of Physical Chemistry B*, 1998, **102**, 10983-10990.

141. E. Gallicchio, L. Y. Zhang and R. M. Levy, *Journal of Computational Chemistry*, 2002, **23**, 517-529.

142. K. Zhu, D. L. Pincus, S. Zhao and R. A. Friesner, *Proteins: Structure, Function, and Bioinformatics*, 2006, **65**, 438-452.

143. M. L. Verdonk, J. C. Cole, M. J. Hartshorn, C. W. Murray and R. D. Taylor, *Proteins: Structure, Function, and Bioinformatics*, 2003, **52**, 609-623.

144. K. Zhu, M. R. Shirts and R. A. Friesner, *Journal of Chemical Theory and Computation*, 2007, **3**, 2108-2119.

145. V. Hornak, R. Abel, A. Okur, B. Strockbine, A. Roitberg and C. Simmerling, *Proteins-Structure Function and Bioinformatics*, 2006, **65**, 712-725.

146. A. Jakalian, B. L. Bush, D. B. Jack and C. I. Bayly, *Journal of Computational Chemistry*, 2000, **21**, 132-146.

147. A. Jakalian, D. B. Jack and C. I. Bayly, *Journal of Computational Chemistry*, 2002, **23**, 1623-1641.

148. J. Mongan, C. Simmerling, J. A. McCammon, D. A. Case and A. Onufriev, *Journal of Chemical Theory and Computation*, 2006, **3**, 156-169.

149. N. Homeyer, F. Stoll, A. Hillisch and H. Gohlke, *Journal of Chemical Theory and Computation*, 2014.

150. M. G. KENDALL, *Biometrika*, 1938, **30**, 81-93.

151. T. Cheng, X. Li, Y. Li, Z. Liu and R. Wang, *Journal of Chemical Information and Modeling*, 2009, **49**, 1079-1093.

152. Y. Li, Z. Liu, J. Li, L. Han, J. Liu, Z. Zhao and R. Wang, *Journal of Chemical Information and Modeling*, 2014, **54**, 1700-1716.

153. J. W. Tukey, *Statistical science*, 1991, 100-116.

154. J. P. Shaffer, *Annual review of psychology*, 1995, **46**, 561-584.

155. C. W. Dunnett, *Biometrics*, 1964, **20**, 482-491.

156. S. W. Greenhouse, & Geisser, S., *Psychometrika*, 1959, **24**, 95-112.

157. Z. Šidák, *Journal of the American Statistical Association*, 1967, **62**, 626-633.

158. B. S. Holland and M. D. Copenhaver, *Biometrics*, 1987, 417-423.

159. A. J. Hayter, *Journal of the American Statistical Association*, 1986, **81**, 1000-1004.

160. J. W. Tukey, *Biometrics*, 1949, **5**, 99-114.

161. S. Holm, *Scandinavian journal of statistics*, 1979, 65-70.

162. J. P. Shaffer, *Journal of the American Statistical Association*, 1986, **81**, 826-831.

163. Y. Hochberg and A. C. Tamhane, *Multiple comparison procedures*, John Wiley & Sons, Inc., 1987.

164. J. Cohen, *Psychological bulletin*, 1992, **112**, 155.

165. V. Hornak, A. Okur, R. C. Rizzo and C. Simmerling, *Proceedings of the National Academy of Sciences of the United States of America*, 2006, **103**, 915-920.

166. T. Darden, D. York and L. Pedersen, *The Journal of Chemical Physics*, 1993, **98**, 10089-10092.

167. R. Luo, L. David and M. K. Gilson, *Journal of Computational Chemistry*, 2002, **23**, 1244-1253.

168. D. Sitkoff, K. A. Sharp and B. Honig, *The Journal of Physical Chemistry*, 1994, **98**, 1978-1988.

169. D. Sitkoff, N. Ben-Tal and B. Honig, *The Journal of Physical Chemistry*, 1996, **100**, 2744-2752.

170. F. Godschalk, S. Genheden, P. Soderhjelm and U. Ryde, *Physical Chemistry Chemical Physics*, 2013, **15**, 7731-7739.

171. P. Mikulskis, S. Genheden, P. Rydberg, L. Sandberg, L. Olsen and U. Ryde, *Journal of Computer-Aided Molecular Design*, 2012, **26**, 527-541.